INVESTIGATION OF HOW ENDOPLASMIC RETICULUM STRESS CAUSES INSULIN RESISTANCE AND NEUROINFLAMMATION

BROWN, MAX,ADAM

INVESTIGATION OF HOW ENDOPLASMIC RETICULUM STRESS CAUSES INSULIN RESISTANCE AND NEUROINFLAMMATION

Volume I

Max Adam Brown

This thesis is submitted as part of the requirements for the award of Degree of Doctor of Philosophy

School of Biological and Biomedical Sciences
Durham University
July 2015

ABSTRACT

Endoplasmic reticulum (ER) stress is caused by the accumulation of mis/unfolded proteins in the ER. ER stress signalling pathways termed the unfolded protein response are employed to alleviate ER stress through increasing the folding capacity and decreasing the folding demand of the ER as well as removing mis/unfolded proteins. However, ER stress signalling pathways induce diverse cellular changes beyond changes to the ER. This study aims to further investigate some of these ER stress-mediated events.

ER stress can cause activation of JNK. Prolonged ER stress-mediated JNK activation is reported to promote apoptosis whilst both acute and long-lasting JNK activation is proposed to cause insulin resistance. To begin with it is reported in this thesis that acute ER stress-induced JNK activation, which is dependent on IRE1α and TRAF2, promotes survival. In contrast to other studies, this thesis provides evidence that acute ER stress-mediated JNK activation does not inhibit insulin signalling during ER stress in several cell lines. However, prolonged ER stress, in four different cell lines, does inhibit insulin signalling in a JNK independent manner. This study argues that ER-stress-induced insulin resistance during prolonged ER stress involves inhibition of trafficking of newly synthesised insulin receptors through the secretory pathway to the plasma membrane.

Finally ER stress can activate inflammatory signalling pathways other than JNK and thus ER stress may promote inflammation. Neuroinflammation and ER stress are reported in Parkinson's disease (PD) yet a link between them has so far not been investigated. Using a cellular model of PD, it is reported in this thesis that ER stress has the potential to activate neuroinflammation in PD.

TABLE OF CONTENTS

TABLE OF TABLES

TABLE OF FIGURES

LIST OF ABBREVIATIONS

1NM-PP1	1-tert-butyl-3-naphthalen-1-ylmethyl-1H219pyrazolo[3,4-d]pyrimidin-4-ylemine
AD	Alzheimer's disease
AKT/PKB	protein kinase B
AP-1	activator protein 1
ASK	apoptosis signal-regulating kinase 1
ATF-2	activating transcription factor 2
ATF6	activating transcription factor 6
BIM	Bcl-2 interacting mediator of cell death
BP	band pass
BSA	bovine serum albumin
CAD	cath. a-differentiated
CaMKII	Ca^{2+}/calmodulin-dependent protein kinase II
CHOP	C/EBP homologous protein
CPY	carboxypeptidase yscY
dATP	deoxyadenosine triphosphate
dCTP	deoxycytidine triphosphate
DEPC	diethylpyrocarbonate
dGTP	deoxyguanosine triphosphate
DHR	dihydrorotenone
DR5	death receptor 5

DTT	dithiothreitol
dTTP	thymidine triphosphate
EDTA	ethylenediaminetetraacetic acid
eIF2α	eukaryotic initiation factor-2 α
ELISA	enzyme-linked immunosorbent assay
Endo H	endoglycosidase H
ER	endoplasmic reticulum
ERAD	endoplasmic reticulum-associated degradation
ERK	extracellular regulated kinases
Glc	glucose
GlcNAc	N-acetylglucosamine
GPT	GlcNAC phosphotransferase
GSK3	glycogen synthase kinase 3
herp	homocysteine-induced endoplasmic reticulum protein
HFD	high fat diet
HOAc	acetic acid
HRP	horseradish peroxidase
IBMX	3-Isobutyl-1-methylxanthine
IFN	interferon
IGF	insulin-like growth factor
IKK	inhibitor of kappa B kinase
IL	interleukin

INSR	insulin receptor
IRE1	inositol-requiring 1
IRS	insulin receptor substrate
IκBα	inhibitor of kappa B
JC-1	5,5′,6,6′-Tetrachloro-1,1′,3,3′-tetraethyl-imidacarbocyanine iodide
JNK	c-Jun N-terminal kinase
KLF15	Krupel-like factor 15
LLO	lipid-linked oligosaccharide
LP	long pass
LPS	lipopolysaccharide
Man	mannose
MAPK	mitogen-activated protein kinase
MAPKKK	mitogen-activated protein kinase kinase kinase
MPTP	1-methyl-4-phenyl-1, 2, 3, 6-tetrahydropyridine
mRNA	messenger RNA
NAC	non-Aβ component
NEDD	*N*-(1-Naphthyl)ethylenediamine dihydrochloride
NF-κB	nuclear factor kappa-light-chain-enhancer of activated B cells
NO	nitric oxide
NRF2	nuclear factor-erythroid-derived 2 (NF-E2)-related factor 2
NSAID	non-steroidal-anti-inflammatory drug
OST	oligosaccharyltranferase

Pael-R	Pael receptor
Pael-R	parkin-associated endothelin receptor–like receptor
p-AKT	phosphorylated AKT
PBS	phosphate-buffered saline
PCR	polymerase chain reaction
PD	Parkinson’s disease
PDI	protein disulphide isomerase
PDIp	protein disulphide isomerase specific to the pancreas
PDK	phosphoinositide-dependent kinase
p-eIF2α	phosphorylated eukaryotic initiation factor-2 α
PERK	double-stranded RNA-dependent protein kinase (PKR)-like ER kinase
PI	phosphatidylinositol
p-JNK	Phosphorylated c-Jun N-terminal kinases
PTB	phosphotyrosine binding
qPCR	quantitative polymerase chain reaction
RA	retinoic acid
rAAV	recombinant adeno-associated virus
RNA	ribonucleic acid
ROI	region of interest
ROS	reactive oxygen species
RPMI	Roswell Park Memorial institute
RT-PCR	reverse transcription PCR

RT-qPCR	reverse transcription quantitative PCR
S1P	site-1 protease
S2P	site-2 protease
SAP-1	sin1 associated protein
SDS	sodium dodecyl sulphate
SH-2	Src-homology-2
siRNA	short interfering ribonucleic acid
SNpc	substantia nigra pars compacta
$SubA_{A272}B$	catalytically inactive SubAB
SubAB	subtilase cytotoxin AB
T2D	type-II-diabetes
TAK1	transforming growth factor β activator kinase 1
Tg	thapsigargin
TGN	*trans*-Golgi network
TH	tyrosine hydroxylase
Tm	tunicamycin
TM	transmembrane
TNF	tumour necrosis factor
TPA	12-*O*-tetradecanoyl-phorbol-13-acetate
TRAF2	TNF receptor-associated factor 2
TRB3	tribbles homolog 3
Tris	tris(hydroxymethyl) methylamine

TUDCA	tauroursodeoxycholic acid
TYR	tyrosine
UPR	unfolded protein response

DECLARATION

I confirm that this thesis is my own work and that it contains no material previously submitted for a degree in this or any other institute. All data are my own other than those represented in the following figures: 3.1, 3.2, 3.4 B and E, 4.11, and 4.12. It will also be stipulated in the text where research is not my individual contribution.

STATEMENT OF COPYRIGHT

ACKNOWLEDGEMENTS

Firstly and most importantly I have to thank my supervisor; Dr Martin Schröder. I cannot stress (not involving the ER for once) how much his commitment to research and the UPR has influenced my decisions to get involved with and remain in research. Prior to working in his laboratory as an undergraduate I had no interest in becoming a researcher, but his enthusiasm, extensive knowledge, and excellent supervision changed my entire plan for the future. So without getting too emotional, it is to him whom I owe the most gratitude.

I would like to thank my grandparents and brother for providing the stability in my life which has made all the difficult times so much easier. I also wish to thank my parents who have supported me emotionally (and financially) and have never put pressure on me to do anything other than work hard and be kind. I am also grateful that they have tolerated and supported my strange activities as a child (and as an adult); especially the time I bleached an entire deer skeleton in the family bath: sorry. Supporting these strange interests has probably helped me to become the inquisitive person I am today.

I am also extremely grateful to all past and present members of the Schröder lab group, especially Dr David Cox, for showing me the importance of demonstrating patience when teaching lab novices. My gratitude also extends to all the members of the School of Biological and Biomedical Sciences at Durham University, who have made and continue to make it a great family to be part of. Although he can't read this, I want to thank my cat Hurley for keeping me company all those nights of sitting at my laptop. I am also very appreciative of Parkinson's UK who have sponsored this PhD.

Finally, I want to say thank you to Sophie Mushens, who made the unfortunate mistake of 'swiping right' for me on Tinder only a week before I started writing this thesis. Her support and love has carried me through this last year and has given me all the motivation I desperately needed. I hope she knows how important she really is.

To all those friends and family I have not mentioned I am also extremely thankful to have you in my life, I just hope you can forgive me for acknowledging my fat cat but not you.

1 INTRODUCTION

The endoplasmic reticulum (ER) is responsible for the folding of membrane and secretory proteins. When proteins are mis or unfolded they can accumulate and cause ER stress. ER stress has the potential to cause inflammation. Inflammation may contribute to the development of various diseases. In particular obesity-induced inflammation is thought to cause insulin resistance in diabetes. Neuroinflammation has been strongly implicated in the development of the neurodegenerative Parkinson's disease (PD). Inflammation is therefore an important aspect of these two diseases. Interestingly, ER stress has been implicated in both these diseases. The aim of this thesis is to investigate the role of endoplasmic reticulum stress and inflammation in the development of two age-related diseases; Parkinson's disease and type-II-diabetes (T2D). Firstly, this introduction will describe the secretory pathway with specific focus on the ER. ER stress will then be explained with reference to activation of the unfolded protein response (UPR) and its ability to activate inflammatory signalling. Then inflammation and inflammatory signalling will be explored because discussing evidence linking the UPR to inflammatory signalling and cell fate decision making. After establishing the background information to ER stress/UPR-mediated inflammation, the role of this signalling network will be explored in the context of T2D and insulin resistance. Finally, the role of the ER stress/UPR-mediated inflammatory signalling will be discussed in the context of neuroinflammation in the progress and development of PD.

1.1 The secretory pathway

In the 1960s it was discovered that in eukaryotic cells the secreted proteins are first localised to the ER before travelling within membranous structures until they reach the cell surface (Vitale and Denecke, 1999). This pathway, which involves transport of newly synthesised secretory proteins to the cell surface, is known as the secretory pathway. The secretory pathway is responsible for the synthesis and sorting of a very large class of proteins. Typically these proteins travel from the ER, through the Golgi complex, and eventually to endosomes, lysosomes or the cell surface.

1.1.1 The endoplasmic reticulum

Firstly, to understand the importance of ER stress, it is important to explain the role of the ER because ER stress is caused by a build-up of mis and unfolded proteins in the ER. The ER is the first compartment in the secretory pathway. The ER is unique in that it is responsible for the folding of both its own resident proteins and all other proteins entering the secretory pathway. This is because most proteins which enter the secretory pathway only have to undergo one translocation event- they are co-translationally translocated into the ER lumen and can therefore remain folded for the rest of the pathway. Whereas proteins not entering the secretory pathway may have to be unfolded to cross membranes before being refolded in the compartment they are destined for. All proteins entering the secretory pathway contain an ER signal sequence. The transmembrane domain of transmembrane proteins acts as the signal peptide. This signal peptide directs the ribosome synthesising the protein to the membrane of the ER. Synthesis of the polypeptide chain continues so that the protein is cotranslationally translocated into the lumen of the ER. As the polypeptide enters the ER lumen the ER signal peptide is removed by signal peptidases (Paetzel et al., 2002).

After being inserted into the ER, the polypeptide chains undergo folding and modification. The ER is therefore the site of the earliest steps in the maturation of secretory proteins. These steps include the folding of nascent polypeptide chains and posttranslational modifications. There are many proteins in the ER responsible for protein folding, including foldases, chaperones and cochaperones, lectins, glycan-modifying enzymes and oxidoreductases (Braakman and Hebert, 2013). An important part of protein folding involves molecular chaperones. Molecular chaperones are present in all cellular compartments where protein folding occurs (Hartl et al., 2011). Molecular chaperones provide the cell with a means to prevent the interactions of hydrophobic residues present in polypeptides. This is important because hydrophobic regions can interact and cause aggregation of newly synthesised polypeptides (Schroder and Kaufman, 2005b). The most well studied ER resident chaperone is Grp78/BiP. Foldases such as protein disulphide isomerase (PDI) and peptidyl-prolyl *cis-trans* isomerases are responsible for catalysing steps in protein folding.

Various posttranslational modifications occur in the ER, but the two most common are disulphide bond formation and asparagine (*N*)-linked glycosylation. The formation of disulphide bonds occurs between thiol groups of the cysteine residues in a polypeptide.

The function of a disulphide bond is to stabilise the protein into its folded topology. PDIs are responsible for the catalysis of disulphide bond formation in the ER. Recycling of the disulphide bonds is maintained by the FAD-dependent oxidases Erv2p and Ero1p (Ellgaard, 2004).

N-linked glycosylation involves the attachment of an oligosaccharide to a polypeptide chain. Once translocated into the ER, proteins with the consensus sequence N-X-S/T are acceptors for *N*-linked glycosylation (Marshall, 1974). Transfer of the oligosaccharide to the asparagine residue in the glycosylation sequence is catalysed by the oligosaccharyltranferase (OST) (Weerapana and Imperiali, 2006). Once attached to the protein these hydrophilic carbohydrate glycans alter the biophysical properties of that protein which in turn affects the folding of the protein (Hanson et al., 2009). Before the carbohydrate is attached to a protein it exists as a lipid-linked oligosaccharide (LLO). The three carbohydrate building blocks of the LLO substrate are N-acetylglucosamine (GlcNAc), mannose (Man) and glucose (Glc) (Aebi, 2013). In the first steps of glycan synthesis the enzyme GlcNAC phosphotransferase (GPT) catalyses the transfer of GlcNAc-1-phosphate from UDP-N-GlcNAc to dolichol phosphate, which is embedded in the ER membrane producing a GlcNAc disaccharide. The isoprenoid lipid dolichol serves as a carrier of the oligosaccharide. Five GDP-Man residues are subsequently attached to the disaccharide. This product is then translocated into the ER, via a poorly understood mechanism, where a further four Man and three Glc molecules are attached to form the product dolichol-$GlcNAc_2$-Man_9-Glc_3 (Welti, 2013). Subsequent processing of the oligosaccharide occurs in the Golgi apparatus.

1.1.2 The Golgi apparatus

Once correctly folded, proteins are transported from the ER to the Golgi for protein modification, including the modification of glycans. The Golgi is a highly organised structure. It is made up of various compartments or cisternae, which include: *cis* Golgi network and the *trans* Golgi network consisting of *ci*, *medial* and *trans* cisternae. Each of the individual compartments in the cisternae contain a distinct set of enzymes to allow further modification of proteins in a step wise manner. The Golgi complex is responsible for the modification of *N*-linked glycans of proteins which have been transported from the ER.

Due to removal of Glc molecules during protein folding in the ER, the glycan structure for properly folded glycoproteins entering the Golgi is $Man_9GlcNac_2$ in higher eukaryotes (Ellgaard and Helenius, 2003). After trafficking of a protein to the Golgi, mannosidase I removes multiple mannose sugars from glycans present on that protein. If further modification of this glycan does not occur then it is considered to be a high mannose oligosaccharide. Further trimming of glycans by mannosidase I and II and additional glycosylation by GlcNAc transferase produces a common core region (Trombetta and Parodi, 2003). However, additional sugars may be added to the common core region in the Golgi yielding a complex oligosaccharide. Glycans can be high-mannose, complex or a combination of both, which are known as hybrid glycans. Processing beyond the common core region stage of a glycan provides Endoglycosidase H (Endo H) insensitivity (Maley et al., 1989). For this reason Endo H can be used as a tool for assessing the glycosylation state and thus is useful for identifying the location of a protein in the secretory pathway.

The insulin receptor is an example of a transmembrane glycoprotein which traffics through the secretory pathway to the plasma membrane (Figure 1.1). The monomers of the dimeric insulin receptor consist of an extracellular α and β chain harbouring a transmembrane and intracellular tyrosine protein kinase domain. The α and β chains are linked via a disulphide bond between C647 and C872 (Sparrow et al., 1997). The α and β chains contain 14 and 4 *N*-linked oligosaccharides, respectively. The insulin receptor is first synthesised as a single polypeptide chain which subsequently undergoes: maturation of the insulin binding domain, dimerization, *N*-linked glycosylation and disulphide bond formation, all of which occurs in the ER. The insulin receptor is then trafficked to the *trans*-Golgi network where is cleaved by proprotein convertases, including furin, carboxyterminal to the basic sequence RKRR to liberate the mature α and β chains (Robertson et al., 1993). The mature receptor is then delivered to the plasma membrane.

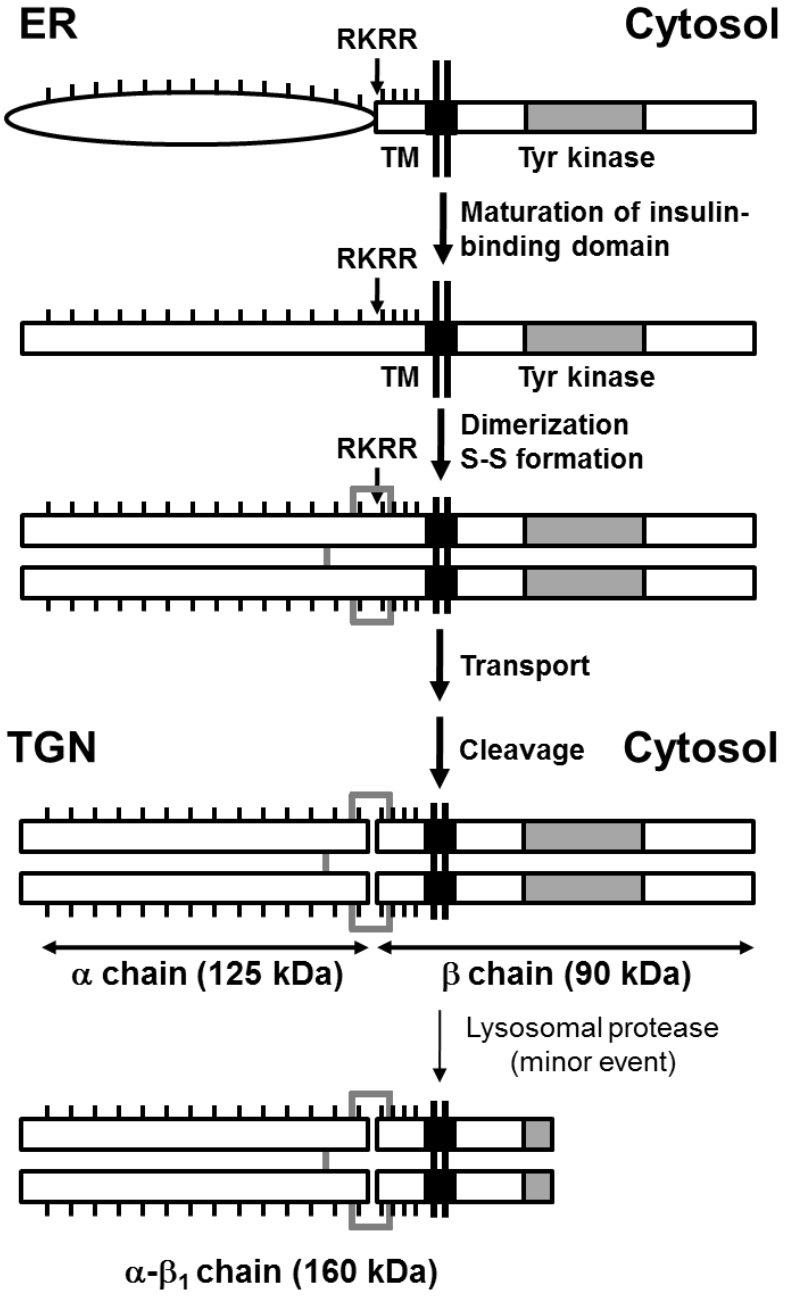

Figure 1.1. Schematic of trafficking of newly synthesised insulin receptors from the ER to the plasma membrane.

In the insulin proreceptor the α and β chains are joined via a peptide bond. The α chain harbours the extracellular, insulin-binding domain, while the β chain harbours the transmembrane (TM) and cytosolic tyrosine (TYR) protein kinase domain. The α chain carries 14 and the β chain four *N*-linked oligosaccharides (indicated by sticks). In the ER the insulin-binding domain matures, disulphide bonds are formed and insulin proreceptor dimers are formed before transport to the *trans*-Golgi network (TGN). In the TGN the proreceptor is cleaved by proprotein convertases including furin to liberate the mature α and β chains carboxyterminal to the basic amino acid sequence RKRR. Further post-translational modifications are produced by a less well characterised lysosomal event (Massague et al., 1981).

1.2 Endoplasmic reticulum stress

Because the ER is the first compartment in the secretory pathway its functional capacity is the rate limiting step. It is therefore important that proper ER function is maintained. As a consequence the disruption of protein folding homeostasis in the ER activates several signalling cascades and causes both direct and indirect changes to other cellular pathways.

1.2.1 The unfolded protein response

In all eukaryotic organisms the ER is the site of transmembrane and secretory protein folding (Schroder, 2006). In the ER, homeostasis is defined as maintaining a balance between protein folding demand and protein folding capacity (Schroder and Kaufman, 2005b). If homeostasis is not maintained then the result is ER stress and cellular damage. The unfolded protein response (UPR) is an ER stress signalling cascade, ultimately leading to the transcription of genes which prevent cellular accumulation of unfolded proteins by either degradation (ERAD) or repair and therefore functions to maintain ER homeostasis. The UPR restores homeostasis by both increasing folding capacity and reducing folding demand. It increases the folding capacity via increasing the expression of molecular chaperones and protein foldases (Schroder, 2006). The UPR also increases phospholipid production in order to expand the ER allowing its contents to be diluted. The UPR attenuates general translation as well as transcription of secretory protein genes to prevent further increase of folding demand (Schroder, 2006). The UPR also enhances ER-associated degradation (ERAD) which involves targeting of unfolded proteins to be degraded by the proteasome.

Non-drug induced activators of the UPR include viral infection, bacterial infection and wound healing. Wound healing requires the synthesis of many proteins which traffic through the secretory pathway. This increased demand on folding capacity can sometimes overwhelm the ER to induce the UPR (Wang et al., 2010). Viral infection can induce the UPR because viruses, which do not have an ER, ‘hijack’ the ER of the host cell for the synthesis of viral glycoproteins (Zhang and Wang, 2012). The additional folding of viral proteins increases the folding demand in the ER and causes ER stress and activation of the UPR. Bacterial infection has only recently been implicated in the activation of the UPR (Cho et al., 2013, Celli and Tsolis, 2015). It was shown that bacterial proteins can activate the UPR causing induction of the innate immune response (Cho et al., 2013). Therefore it

is likely that the UPR can signal the innate immune response as a protective mechanism against both viral and bacterial infection.

There are at least three branches to the UPR (Figure 1.2), in higher eukaryotes, consisting of three well-studied ER stress sensing transmembrane proteins; IRE1 (inositol-requiring 1), PERK (double-stranded RNA-dependent protein kinase (PKR)-like ER kinase), and ATF6 (activating transcription factor 6). It is thought that in a non-stressed ER all three transmembrane proteins are maintained in an inactive state through the binding of the molecular chaperone BiP to the lumenal domains of these proteins. Once unfolded proteins accumulate BiP is sequestered from the lumenal domains due to the affinity of BiP to the exposed hydrophobic regions of an unfolded protein (Schroder and Kaufman, 2005a, Gething, 1999).

1.2.1.1 IRE1

In the case of the transmembrane endoribonuclease kinase IRE1 the release of BiP from its lumenal domain allows IRE1 to either dimerise or oligomerise resulting in its activation (Bertolotti et al., 2000). However, more recent studies have suggested that direct binding between IRE1 and unfolded proteins may also account for its activation (Promlek et al., 2011) (Credle, 2005) Once activated IRE1 cleaves and together with a ligase (Jurkin et al., 2014) they splice (in a spliceosome independent manner) the mRNA encoding the bZIP transcription factor *XBP-1* in metazoans and Hac1p in yeast. Splicing of *XBP-1* mRNA via the removal of a 26 base intron introduces an alternative C terminus resulting in a transcription factor with increased activity (Ron and Walter, 2007). Active *XBP-1* is a transcription factor for various UPR target genes encoding proteins involved in ERAD, protein folding (protein foldases) and for ER chaperones such as BiP (Figure 1.2). In mammals there are two known isoforms of IRE1, IRE1α and IRE1β. IRE1α is ubiquitously expressed throughout the body whereas IRE1β is expressed selectively in the digestive tract (Wang et al., 1998).

1.2.1.2 PERK

Dimerisation (Liu et al., 2000) or oligomerisation (Carrara et al., 2015) of PERK causes *trans*-phosphorylation and allows PERK to phosphorylate eukaryotic initiation factor-2 α

(eIF2α). PERK to eIF2α signalling is responsible for the UPR mediated inhibition of general translation as eIF2α activation blocks assembly of the 43 S preinitiation complex, which is responsible for recognition of the cap structure of mRNA (Zhang and Kaufman, 2008, Harding et al., 2000, Harding et al., 1999). Activated eIF2α also allows the translation of the transcription factor ATF4. ATF4 acts as a transcription factor for various UPR target genes including those involved in ERAD, metabolism and apoptosis. PERK is also capable of inducing an antioxidant response by activating activating transcription factor 4 (ATF4) and the nuclear factor-erythroid-derived 2 (NF-E2)-related factor 2 (NRF2). Both ATF and NRF2 help maintain levels of the redox buffer glutathione via transcription of genes encoding proteins responsible for glutathione maintenance (Zhang and Kaufman, 2008, Cullinan and Diehl, 2006). NRF2 activates the transcription of various antioxidant genes (Zhang, 2006).

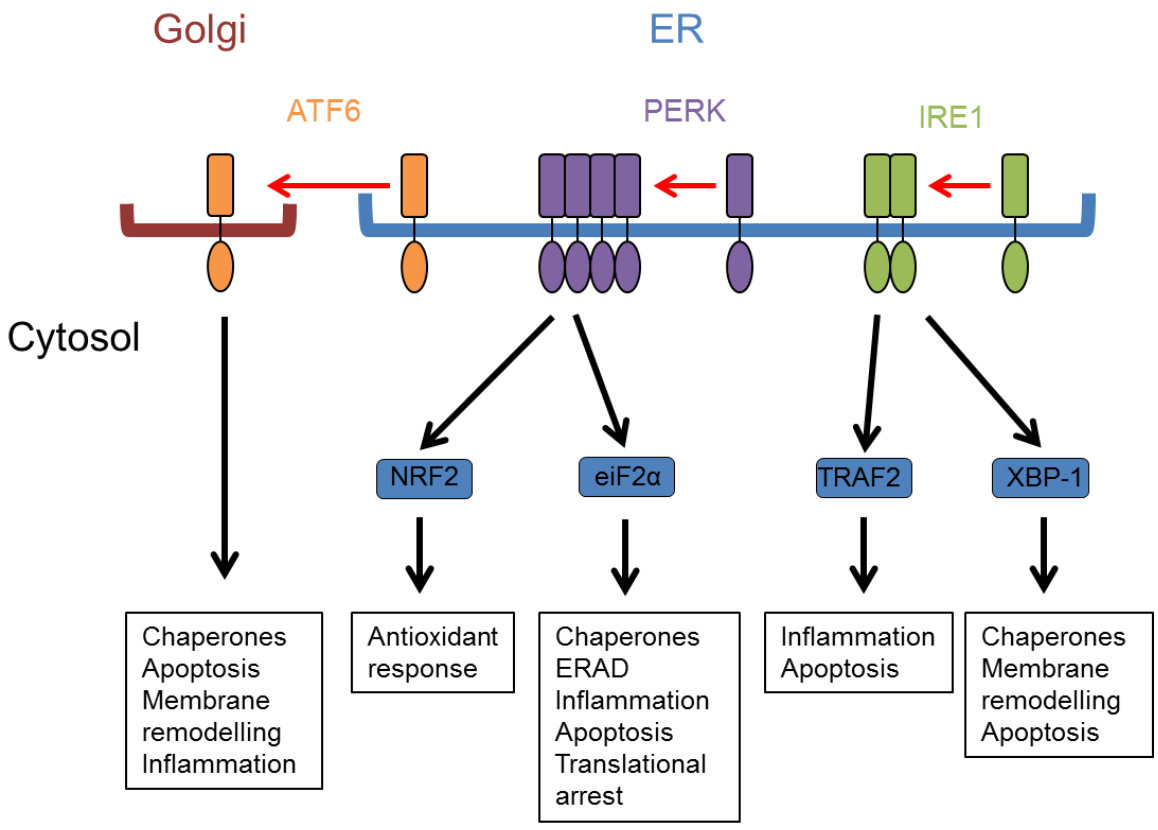

Figure 1.2. Pathways of the unfolded protein response.

The three major sensors of ER stress contribute to initiation of the UPR through upregulation of genes encoding proteins involved in ERAD, membrane remodelling, antioxidant response, protein folding (protein foldases) and for ER chaperones such as BiP. All three sensors are also responsible for initiation of inflammation and apoptosis.

1.2.1.3 ATF6

ATF6 is a bZIP domain-containing transcription factor and is part of the ATF transcription factor family (Haze et al., 1999). When unfolded proteins are detected ATF6 translocates to the Golgi apparatus where it is cleaved by proteases site-1 (S1P) and site-2 (S2P) (Schroder and Kaufman, 2005b). A bZIP-containing fragment of ATF6 is then released and migrates to the nucleus where it activates transcription of genes encoding molecular chaperones and protein foldases. Active ATF6 also activates lipogenesis (Zeng et al., 2004) which ultimately functions to expand the ER.

1.2.1.4 Activating ER stress and the UPR

N-linked glycosylation and disulphide bond formation are both posttranslational modifications of proteins in the ER which when inhibited cause ER stress and UPR signalling (Schroder and Kaufman, 2005b). Tunicamycin is a drug commonly used to induce ER stress as it inhibits *N*-linked glycosylation by blocking the transfer of *N*-acetylglucosamine 1-phosphate to dolichol monophosphate (Carrasco and Vazquez, 1984). Another drug commonly used to induce ER stress is thapsigargin. Thapsigargin is an inhibitor of the ER Ca^{2+}-ATPase and results in depletion of Ca^{2+} from the ER (Schonthal et al., 1991). As most protein folding in the ER is calcium dependent thapsigargin causes the build-up of unfolded proteins and thus ER stress. The AB5 subtilase cytotoxin (SubAB) is an infrequently used ER stressor but it is probably the most specific as it cleaves BiP to induce ER stress in a specific manner (Paton et al., 2006, Paton et al., 2004). SubAB consists of an enzymatic A subunit and a pentameric B subunit. The B subunit of AB5 toxins mediates uptake into the cell. The A unit of SubAB is a subtilase-like protease with an unusually deep active-site cleft, which creates the exquisite substrate specificity for BiP which SubAB demonstrates (Paton et al., 2006).

1.2.1.5 Severe ER stress

The UPR functions to restore protein folding homeostasis to maintain normal cellular function. However, if ER stress is too severe for the UPR-induced changes to alleviate the stress then apoptotic pathways are activated. Prolonged or severe ER stress results in the

activation of proapoptotic and inflammatory signalling pathways. UPR-induced inflammatory signalling is discussed later.

The ER membrane proteins responsible for initiating the UPR have the ability to activate both prosurvival and proapoptotic responses to ER stress. These opposing signalling outputs are exemplified by IRE1α. IRE1α promotes survival through activation of *XBP-1* and the downstream targets which function to increase ER protein folding capacity as discussed previously.

IRE1α has been shown to promote apoptosis in two ways. Firstly, the RNase domain of IRE1α can cleave several miRNAs. Cleavage of these miRNAs results in the stabilisation, and therefore promotes translation, of *TXNIP* and *caspase-2* mRNAs (Lerner et al., 2012, Oslowski et al., 2012, Upton et al., 2012). The role of caspase-2 in IRE1α-induced apoptosis has however been disputed (Sandow et al., 2014) and unmitigated ER stress may induce apoptosis through death receptor 5 (DR5) (Lu et al., 2014). IRE1α cleaves miR-17 which promotes translation of *TXNIP* mRNA, which in turn promotes apoptosis through production of IL-1β and activation of caspase-1 (Lerner et al., 2012). Sustained IRE1α RNase activation caused rapid decay of miRs -17, -34a, -96, and -125b which normally repress translation of *caspase-2* mRNA (Upton et al., 2012). Caspase-2 initiates the mitochondrial apoptotic pathway to induce cell death via release of proapoptotic proteins from the mitochondria such as cytochrome c (Guo et al., 2002). Secondly, IRE1α can promote apoptosis through its kinase activity. The kinase domain of IRE1α can activate c-Jun N-terminal kinases (JNK) through a complex with the E3 ubiquitin ligase TNF receptor-associated factor 2 (TRAF2) and the mitogen-activated protein kinase kinase kinase (MAPKKK) apoptosis signal-regulating kinase 1 (ASK1) (Nishitoh et al., 1998, Nishitoh et al., 2002). Many studies looking at prolonged ER stress-induced JNK activation have shown that it is proapoptotic (Zhang et al., 2001, Smith and Deshmukh, 2007, Chen et al., 2008, Wang et al., 2009, Jung et al., 2012, Teodoro et al., 2012, Huang et al., 2014, Jung et al., 2014, Kang et al., 2012, Arshad et al., 2013). Therefore IRE1α can promote survival through activating genes which function to increase protein folding capacity and maintain ER homeostasis, whilst also having the ability to promote apoptosis through two different mechanisms. However, not much is known about the role of JNK activation early in the ER stress response.

PERK and ATF6 also promote survival through transcriptional changes which increase protein folding capacity. However, they promote apoptosis through different mechanisms

to IRE1α. The PERK and ATF6 pathways signal apoptosis via activation of the transcription factor C/EBP homologous protein (CHOP) (Zhang and Kaufman, 2008). The importance of CHOP in ER stress induced apoptosis is demonstrated through CHOP deficient mice being resistant to apoptosis induced through ER stress (Zinszner et al., 1998). PERK-mediated phosphorylation of eIF2α activates ATF4 resulting in CHOP induction (Harding et al., 2000). Various proteins have been implicated downstream of CHOP during CHOP-mediated apoptosis including induction of proapoptotic proteins Bim (Puthalakath et al., 2007), Puma (Cazanave et al., 2010), DR5 (Yamaguchi and Wang, 2004) and Bax (Gotoh et al., 2004) as well as down-regulation of the suppressor of apoptosis protein Bcl-2 (McCullough et al., 2001).

Overall, the regulation of cell survival is an important function of the UPR. The UPR's main role is to restore ER protein folding homeostasis but ER stress which is too severe to recover from can induce severe toxicity which if left to proceed may cause necrosis, which is defined by uncontrolled and detrimental cell death. Although UPR activation ultimately functions to maintain ER homeostasis and promote cell survival, the UPR may also function to control death in cells in which ER stress is too severe to remedy.

1.3 Inflammation

As mentioned briefly, ER stress/UPR activation is believed to activate inflammation, thus it is important to describe the background to inflammation and inflammatory signalling before discussing ER stress-mediated inflammation. The following section will therefore describe inflammatory signalling and will be followed by a section detailing the links between the UPR and inflammation.

Inflammation is a reaction of multicellular organisms, which protects against a range of harmful stimuli including; viruses, bacteria, physical damage and harmful chemicals. When cells are damaged they activate inflammatory signalling pathways. This causes the cell to release cytokines which recruit various cells of the immune system. A degenerating cell is capable of initiating inflammation until it is removed by the immune system (Wyss-Coray and Mucke, 2002). Immune cells can respond to inflammatory signalling molecules by releasing further inflammatory signalling molecules to signal additional immune cells to the damaged area (Wyss-Coray and Mucke, 2002).

Inflammation has been described as a ‘double-edged sword’ (Wyss-Coray and Mucke, 2002) because in short-lasting inflammation, inflammatory mechanisms promote healing and limit injury (Tansey et al., 2007), whereas prolonged inflammation is detrimental and has been implicated as a cause for diseases such as diabetes, PD and Alzheimer’s disease (AD) (Wyss-Coray and Mucke, 2002).

Inflammatory responses differ between diseases and tissues but they all share a common spectrum of genes and endogenous mediators including; cytokines, growth factors chemokines, matrix metalloproteinases and reactive oxygen species (ROS) (Kaminska, 2005). All three branches of the UPR can induce proinflammatory transcriptional programmes which are mainly mediated through the transcription factors: nuclear factor kappa-light-chain-enhancer of activated B cells (NF-κB) and activator protein 1 (AP-1) (Garg et al., 2012, Verfaillie et al., 2013, Hotamisligil and Erbay, 2008, Zhang and Kaufman, 2008). NF-κB is one of the central mediators of proinflammatory pathways. Genes transcribed by NF-κB include many proinflammatory cytokines (Li et al., 2005b, Zhang and Kaufman, 2008, Rius et al., 2008, Pahl, 1999). NF-κB is normally held inactive within the cytoplasm in a complex with IκBα. Activation of NF-κB involves phosphorylation of IκBα at serines 32 and 36 by IκB kinase (IKK), which leads to IκBα ubiquitination and proteasomal degradation (DiDonato et al., 1996). IκBα phosphorylation and degradation can therefore be used as markers of NF-κB activation and as such IκBα degradation is used in this thesis to monitor NF-κB activation.

The following section will focus on pathways activating AP-1 and the role of inflammatory signalling pathways in activation of macrophages. This section will then be followed by a section discussing the evidence linking the UPR to these inflammatory signalling pathways.

1.3.1 MAPK Signalling pathways activating AP-1

The AP-1 transcription factor is made up of several dimeric complexes, which consist of proteins from three different families of DNA-binding proteins: Jun, Fos and ATF/CREB (Hernandez et al., 2008). The Jun family consists of: Jun, JunB, v-Jun and JunD. The Fos family consists of: Fra-1, Fra-2, c-Fos, FosB. The ATF/CREB family consists of: ATF1, ATF2, ATF3, ATF4, ATF6, B-ATF, ATFx). Mitogen-activated protein kinase (MAPK) signalling pathways are known to activate AP-1.

MAPKs are proline-directed Ser/Thr protein kinases which are activated through three-tier kinase signalling cascades (Raman et al., 2007). The MAPKs include: the p38 family, JNKs 1-3 and extracellular regulated kinases 1 and 2 (ERK1/2). As JNK and p38 signalling cascades are more significantly implicated in diabetes and PD more detail will be provided on these pathways and not ERK1/2. The MAPK signalling pathways p38 and JNK are activated during ER stress and are even considered to be part of the UPR (Darling and Cook, 2014). The MAPK signalling pathways are associated with, cell growth, cell differentiation, cell death and importantly, in the context of this thesis, inflammation (Kyriakis and Avruch, 2001). The role of the MAPKs in signalling inflammation will be the main focus of the following section.

1.3.1.1 JNK

There are three *JNK* genes in the mammalian genome; *JNK1* and *JNK2* are ubiquitously expressed, whereas *JNK3* expression is specific to the brain (Derijard et al., 1994, Kyriakis et al., 1994). JNK activation has been reported to occur during various stresses including; UV exposure, heat shock, ionising radiation and ER stress (Kyriakis et al., 1994). The dual phosphorylation of the Thr-Pro-Tyr motif by MKK4 and MKK7 is required for JNK activation (Tournier et al., 1997). Phosphorylation of JNK leads to AP-1 activation and the subsequent translocation of AP-1 to the nucleus where it initiates the transcription of its own inflammatory gene programme (Davis, 2000). JNK can activate AP-1 through activation of ATF-2 and c-Jun. AP-1 transcribes proinflammatory genes such as those encoding tumour necrosis factor (TNF), GM-CSF, interleukin (IL)-8, and cytokine receptors (Angel et al., 2001).

It is worth noting that JNK regulation is likely to be very complex especially as differentially activated alternative splice variants of MKK7 have been identified (Tournier et al., 1999). Nevertheless, JNK signalling is an important part of the cells inflammatory signalling network with the ability to activate AP-1 in response to various stress conditions.

1.3.1.1.1 JNK and apoptosis

It is widely accepted that JNK activation during stress is ultimately proapoptotic. For example, apoptosis induced through UV stimulation requires JNK as MEFs lacking both JNK1 and JNK2 are resistant to UV-induced apoptosis (Tournier et al., 2000). Apoptosis induced by exposure to an excitotoxic glutamate receptor agonist, kainic acid, is inhibited in JNK3 knockout mice (Yang et al., 1997). In another example Huang *et al.* recently demonstrated that calcium-mediated JNK and p38 activation led to apoptosis in hepatic stellate cells. The use of calcium chelators substantially inhibited JNK and p38 activation, whilst the JNK inhibiter SP600125 significantly reduced cell apoptosis (Huang et al., 2014).

JNK can also contribute to apoptosis through phosphorylation of the proapoptotic BH3-only protein Bcl-2 interacting mediator of cell death (BIM) to promote its release from the dynein motor complex, freeing it to initiate apoptosis (Lei and Davis, 2003). JNK can also promote cell death through increasing expression of death receptors and their ligands. However, JNK activation alone is not sufficient to induce apoptosis (Molton et al., 2003) suggesting that JNK can promote apoptosis but only when other signalling is activated. ER stress is also an initiator of JNK activation and is discussed further (see 1.4.1). Thus JNK can promote apoptosis through several mechanisms involving phosphorylation of BIM and increased expression of death receptors.

1.3.1.1.2 JNK prosurvival

Overall JNK activation is thought to be proapoptotic, however, evidence exists to suggest that JNK activation can also have a prosurvival role (Molton et al., 2005). JNK was shown to have a prosurvival role with antiapoptotic functions in microglia during lipopolysaccharide (LPS)-induced activation (Svensson et al., 2011). Cytokine-mediated activation of JNK has been shown to be antiapoptotic in several studies. JNK activation by TNF-α increased the expression of the mRNA for the antiapoptotic ubiquitin ligase *cIAP2/BIRC3* (Lamb et al., 2003). JNK has also been shown to induce survival in T cells through stabilisation of Mcl2, downstream of the IL-2 receptor (Hirata et al., 2013). JNK can phosphorylate BAD to suppress apoptosis during IL-3 withdrawal demonstrating that JNK contributes to cell survival (Yu et al., 2004).

Chemical induction of JNK has also been shown to promote cell survival. JNK also has a prosurvival role in bortezomib-induced toxicity. ER stress was also shown to be activated

with bortezomib treatment suggesting that ER stress-induced JNK activation may be providing prosurvival signalling in this study (Granato et al., 2013). Furthermore, Ventura *et al*. employed a chemical genetic strategy, using JNK-deficient MEFs which were reconstituted with 1-tert-butyl-3-naphthalen-1-ylmethyl-1H219pyrazolo[3,4-d]pyrimidin-4-ylemine (1NM-PP1)-sensitised alleles of JNK1 and JNK2, to causally demonstrate that the two phases of JNK activation during TNF-α treatment have two different roles in cell survival decision making. Although both the early and late phases of JNK activation contributed to TNF-α-induced gene expression the early transient phase was prosurvival whilst the late and sustained JNK activation led to proapoptotic signalling (Ventura et al., 2006).

Therefore JNK has a dual role in that it can both promote and inhibit apoptosis. This dual role is clearly demonstrated by the two phases of JNK activation which occur with treatment of TNF-α: 1) an early and transient antiapoptotic phase and 2) a late proapoptotic phase (Roulston et al., 1998, Ventura et al., 2006). Thus, JNK signalling can be both prosurvival and proapoptotic depending on the stress and duration.

1.3.1.2 p38

Another MAPK other than JNK which activates AP-1 is p38. The p38 family consists of 4 proteins; p38α, p38β, p38γ and p38σ. Both p38α and β are ubiquitously expressed whereas p38γ and σ expression is more tissue specific (Raman et al., 2007). Dual phosphorylation of the p38 Thr-Gly-Tyr motif, by MKK3, MKK4 and MKK6, is required for activation of p38 (Derijard et al., 1995, Lin et al., 1995, Raingeaud et al., 1996). Similar to JNK, p38 can also promote apoptosis through phosphorylation of BIM at the same site as JNK (Cai et al., 2006). p38 and JNK thus have some similar functions but also have divergent roles. A complex regulation of these MAPK is likely to allow appropriate cellular responses to wide-ranging stimuli.

Substrates of p38 include the transcription factors: activating transcription factor 2 (ATF-2), sin1 associated protein (SAP-1) and Elk-1 (Hardy and Chaudhri, 1997, Whitmarsh and Davis, 1996). p38 can activate AP-1 through activation of ATF-2, which in turn can lead to increased transcription of other components of the AP-1 complex: Jun and Fos. p38 has also been shown to activate AP-1 via direct phosphorylation and activation of c-Jun. Activation of AP-1 in this study was not restored by JNK during p38 inhibition, suggesting

that AP-1 activation was dependent on p38 (Humar et al., 2007). How p38 and JNK activate AP-1 is therefore complex and may depend on type, level and period of stress.

p38α is crucial to inflammatory cytokine production and signalling (Lee and Young, 1996, Lee et al., 1994). p38 is involved in the regulation and increased expression of various genes involved in inflammation including; *IL-1β*, *IL-6*, *IL-8*, *TNF-α* (Kyriakis and Avruch, 2001, Manthey et al., 1998, Lee et al., 1999b, Baldassare et al., 1999, Saccani et al., 2002). Therefore, along with JNK, p38 has an important role in contributing to inflammatory signalling through activation of AP-1 and the subsequent expression of several genes involved in inflammation.

1.3.2 Macrophage activation

Inflammatory signalling functions to recruit cells of the immune system. Macrophages are a major cell type recruited to sites of inflammation. Macrophage recruitment and activation is associated with inflammation. It is possible that ER stress-induced inflammation has the capacity to recruit and activate macrophages. This is important in disease progression and in the context of PD, microglia (which are the resident macrophages of the nervous system), have been shown to be highly activated and this activation may induce damaging levels of inflammation. In the context of T2D, macrophage activation is also a potential cause of damaging levels of inflammation which may induce cell death and ER stress.

Monocytes are precursor cells to macrophages. Monocyte development involves production of myeloid progenitor cells in the bone marrow which give rise to monoblasts. Monoblasts develop into pro-monocytes and finally into monocytes which enter the bloodstream. These monocytes can migrate to specific tissues, via the blood stream, to replenish tissue-specific macrophages such as macrophages of the liver (Kupffer cells) and central nervous system (microglia) (Gordon and Taylor, 2005). Apart from replenishment of microglia from monocytes derived from the blood stream, microglia can also increase through local proliferation of myeloid progenitor cells in the central nervous system (Ajami et al., 2007).

The main functions of macrophages are the removal of cellular debris generated during tissue remodelling and the clearing of cells that have undergone apoptosis (Mosser and Edwards, 2008). In these situations macrophages appear ‘unstimulated’ and do not produce cytokines (Kono and Rock, 2008). The phagocytic activity only is observed suggesting that

most of the macrophage-mediated phagocytosis which occurs is independent of other immune cells. However, macrophages can be activated through a number of stimuli into a more 'aggressive' physiology involving production of proinflammatory cytokines, reactive oxygen species (ROS) and nitric oxide (NO). Activation of tissue specific macrophages such as microglia in the central nervous system and macrophages in adipose tissue has been reported in PD (McGeer et al., 1988, McGeer et al., 2003, Barcia et al., 2004, Virgone-Carlotta et al. 2013) and T2D (Lee et al., 1999a, Takahashi et al., 2003, Cancello et al., 2005, Di Gregorio et al., 2005) respectively. Thus, changes in macrophage physiology may be an important step in the progression of age-related metabolic and neurodegenerative diseases.

One such stimulus which alters macrophage physiology is debris from cells which have undergone necrosis. This debris contains many endogenous danger signals which would normally be hidden from macrophages as they are normally only present within the cell (Zhang and Mosser, 2008). Upon phagocytosis of these danger signals macrophages undergo changes in their physiology resulting in increased production of proinflammatory mediators including cytokines (Mosser and Edwards, 2008). However, the response of macrophages to these danger signals is only one of the several stimuli, which can lead to the activation of macrophages.

Obesity is associated with chronic inflammation (Zeyda and Stulnig, 2007). In obesity the accumulation of macrophages has been reported and this leads to increased cytokine production and the development of insulin resistance (Lumeng et al., 2007, Zeyda and Stulnig, 2007). Adipose tissue-associated macrophages can act as sources of proinflammatory cytokines. Macrophage activation during obesity is believed to be partly mediated through the debris of necrotic cells, with necrosis of adipocytes being associated with obesity (Cinti et al., 2005). This activation of macrophages leads to production of TNF and IL-6 which can interfere with adipocyte insulin signalling (Bastard et al., 2006).

Macrophages can be classically activated and alternatively activated. Classical activation is well defined whereas alternative activation encompasses many different mechanisms which can stimulate macrophage activation. Many of these mechanisms are newly discovered and poorly understood. Classical activation of macrophages occurs via two signals. The cytokine IFNγ primes macrophages for activation but alone it is not sufficient for full classical activation of macrophages (Nathan, 1991). The final signal required to fully activate macrophages involves TNF. Exogenous TNF itself, or an inducer of

macrophage TNF production, can induce macrophage activation. The physiologically relevant second signal is most likely a molecule, such as LPS, which causes Toll-like receptor ligation and the subsequent production of endogenous TNF by the macrophage (Mosser, 2003). Activated macrophages migrate to sites of inflammation where they degrade pathogens. Activated macrophages have increased ability to kill and degrade intracellular organisms through increased production of ROS and NO (Mosser, 2003). In the murine system identification of activated macrophage cells is easily measured through their increased production of NO (Hibbs, 2002, MacMicking et al., 1997).

Along with activation of macrophages, cytokines can have an important role in inhibiting macrophage activation. Both TGFβ and IL-10 have been shown to have an important role in inhibiting macrophage activation and knockout of either of these two cytokines produces mice with increased susceptibility to develop inflammatory pathologies (Ho and Moore, 1994, Reed, 1999). Thus activation of macrophages is tightly controlled between expression of various pro- and anti-inflammatory mediators.

Overall, macrophages play an important role in maintenance of tissues as well as in the innate immune response. Activated macrophages can produce toxic molecules and further mediators of inflammation. Therefore macrophages are highly involved in inflammation of various tissues including adipose tissue and the central nervous system. They have been implicated in the progression of many diseases including PD and T2D.

1.4 The UPR and inflammation

All three branches of the UPR can contribute to inflammatory signalling (Figure 1.3). ATF6 can activate the transcription of acute phase response genes (Zhang et al., 2006). IRE1α has been shown to interact with the E3 ubiquitin ligase TRAF2 which in turn phosphorylates and activates JNK (Urano et al., 2000). Activated JNK phosphorylates and activates the transcription factor AP-1 (Davis, 2000). The IRE1α and TRAF2 interaction has also been shown to activate NF-κB suggesting a strong role for the UPR in inflammatory signalling (Kaneko et al., 2003). NF-κB can also be activated through the PERK pathway. Translation arrest mediated by PERK-dependent activation of eIF2α leads to activation of NF-κB (Jiang et al., 2003a, Deng et al., 2004, Wu et al., 2002, Wu et al., 2004).

1.4.1 The UPR and JNK

Various studies have provided evidence for JNK activation during ER stress. It is thought that the activation of IRE1α's kinase domain following ER stress results in the interaction with TRAF2 via its C-terminal domain. This interaction promotes the clustering of the N-terminal effector domain of TRAF2 (Urano et al., 2000). Interaction of TRAF2 with IRE1α during ER stress causes JNK activation and this was found to be dependent on the MAPKKK ASK1 (Nishitoh et al., 2002, Gotoh and Cooper, 1998). During oxidative stress the oligomerisation of ASK1 leads to its activation and thus the TRAF2-IRE1α interaction may also promote the oligomerisation of ASK1 (Tobiume et al., 2001). Thr845 phosphorylation in ASK1 is required for its ability to phosphorylate and activate JNK whilst ASK1 autophosphorylation of Thr845 can be a result of ASK1 oligomerisation (Tobiume et al., 2002). ASK1 phosphorylates the upstream kinases for JNK; MKK4 and MKK7 (Ichijo et al., 1997). ASK1 can also phosphorylate MKK3 and MKK6 which activate p38 (Tobiume et al., 2002). In summary, IRE1α-TRAF2 interaction activates ASK1 which in turn phosphorylates JNK and p38 (Figure 1.3).

Most studies investigating ER stress-mediated JNK activation have shown IRE1α signalling to be responsible. However, the PERK branch of the UPR may also contribute to JNK activation during ER stress. CHOP expression, which is induced by PERK signalling, can promote ER stress-induced release of Ca^{2+} from the ER lumen. It has been reported that the ER stress-induced release of Ca^{2+} causes activation of Ca^{2+}/calmodulin-dependent protein kinase II (CaMKII). Activation of the MKKKs ASK1 and transforming growth factor β activator kinase 1 (TAK1) by CaMKII promotes JNK activation (Kashiwase et al., 2005, Ishitani et al., 2003). Thus JNK can be activated during ER stress via at least two different mechanisms (Figure 1.3) which suggests it may be an important target of the UPR.

1.4.1.1 ER stress, JNK and apoptosis

ER stress has been implicated in inducing JNK activation in many studies (see above). In many of these studies ER stress-mediated JNK activation was implicated in apoptosis (Jung et al., 2014, Zhang et al., 2001, Smith and Deshmukh, 2007, Teodoro et al., 2012, Chen et al., 2008, Wang et al., 2009, Jung et al., 2012, Kang et al., 2012, Arshad et al., 2013, Nishitoh et al., 2002, Gu et al., 2009). However, most of these studies are supported

by pharmacological data. For example, ER stress through ER stress mimetic drug, tunicamycin, causes JNK activation and apoptosis. The use of resolvin D1, a potent anti-inflammatory lipid mediator (Serhan, 2010), was reported to attenuate ER stress-mediated apoptosis through inhibition of JNK signalling (Jung et al., 2014). However, rescue from ER stress-mediated apoptosis was not dependent on alleviation of ER stress. Although ER stress-dependent JNK phosphorylation was reported to be inhibited after resolvin D1 treatment it was not causally established if ER stress-mediated JNK activation was responsible for the ER stress-induced apoptosis.

The bZIP transcription factor c-jun is activated by JNK (Hibi et al., 1993). Along with JNK, c-Jun is phosphorylated during ER stress (Zhao et al., 2008). c-Jun expression can protect cells against ER stress-induced apoptosis through reduction of caspase 12 cleavage (Zhao et al., 2008). In response to ER stress, c-Jun is required for the transcription of Adapt78, which inhibits calcineurin (Zhao et al., 2008). Calcineurin is downstream of caspase 12 and its inhibition has been shown to partially attenuate thapsigargin-induced apoptosis (Mukerjee et al., 2000). How calcineurin contributes to apoptosis is not fully established but it has been proposed to, dephosphorylate BAD causing it to dimerize BCL-2 and BCL-XL, thus promoting the release of cytochrome c (Wang et al., 1999). Therefore JNK activation may mediate prosurvival signalling during ER stress through Adapt78 transcription leading to inhibition of calcineurin (Darling and Cook, 2014). However, this proposed model of ER stress-mediated JNK activation and prosurvival signalling is mostly based on circumstantial evidence and a causal link between JNK and antiapoptotic signalling during ER stress via this mechanism has not been demonstrated.

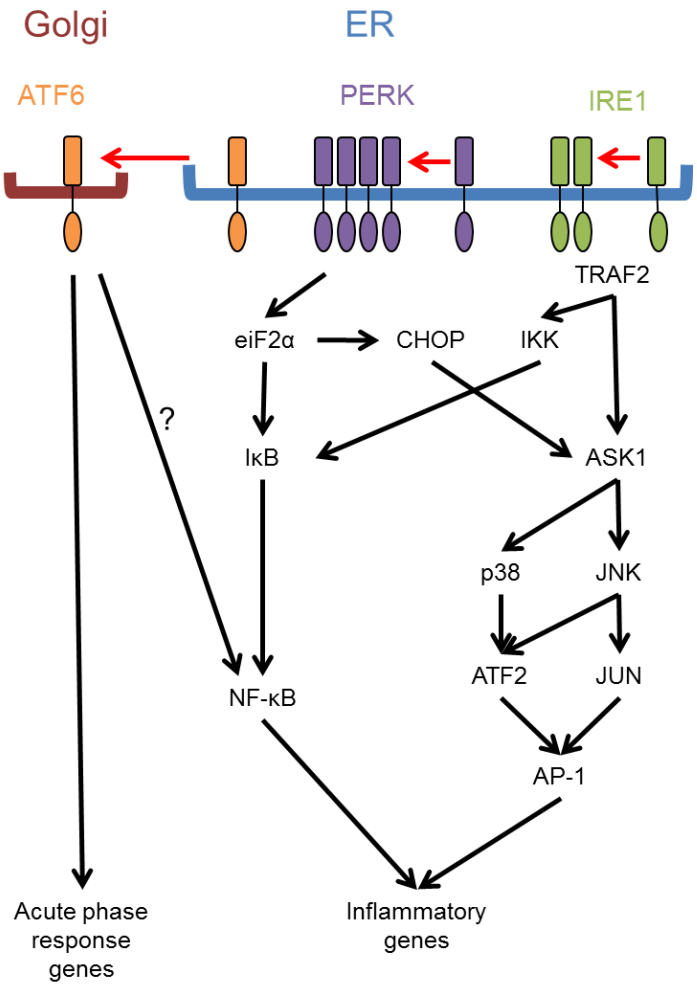

Figure 1.3. Activation of inflammatory signalling pathways by the UPR.
IRE1, PERK and ATF6 can activate inflammatory signalling pathways. IRE1 activates inflammation via interection with TRAF2 leading to either IKK or ASK1 activation to promote expression of inmflammatory genes via NF-κB or AP-1 respectively. PERK can activate either NF-κB or AP-1 through signalling downstream of eIF2α. ATF6 can activate acute phase response genes as well as NF-κB via an unknown mechanism.

1.4.2 The UPR and p38

Early evidence of p38 activation during ER stress came from a study by Hung *et al*. in which they showed that ER stress induced by tunicamycin or brefeldin A caused activation of p38 (Hung et al., 2004). Since then further studies have provided evidence that JNK is not the only MAPK activated during ER stress and that other MAPKs may also form part of the UPR during ER stress.

Using human gingival fibroblasts to study the role of ER stress in gingival tissue it was demonstrated that ER stress caused p38 activation, autophagy and cell death. Use of the

p38 inhibitor SB203580 inhibited ER stress-mediated p38 phosphorylation, autophagy and cell death (Kim et al., 2010). Another study investigating ER stress and autophagy but in fibroblasts cells from Pompe disease patients observed p38 activation. In this study ER stress activated p38 and this p38 activation was required for the increased autophagy observed with ER stress treatments (Shimada et al., 2011).

Correlative evidence using compounds which have been shown to, in addition to other effects, induce ER stress also suggest a link between ER stress and p38 activation. The natural pesticide dihydrorotenone (DHR) is believed to cause PD. DHR can induce ER stress and p38 activation (Zhang et al., 2013). However, activation of p38 in DHR treatment has so far not been shown to be dependent on ER stress and may be a product of another effect of the pesticide. As ER stress can activate p38 in other studies (Hung et al., 2004, Kim et al., 2010, Shimada et al., 2011) it is possible that ER stress induced by DHR causes phosphorylation of p38. Abrin, a toxalbumin obtained from the seeds of *Abrus precatorius*, is a potent ribosome and subsequent protein synthesis inhibitor (Benson et al., 1975). Activation of ER stress through abrin-mediated inhibition of protein synthesis was shown to activate p38 and JNK in Jurkat cells. Abrin treatment eventually led to apoptosis which was dependent of p38 but not JNK (Mishra and Karande, 2014). This recent study not only contributes to the evidence implicating ER stress in activation of p38 but also suggests that ER stress-mediated apoptosis involves p38 signalling. However, although it was demonstrated that p38 and JNK were both activated by abrin, it has not been causally proven that this p38 and JNK activation is indeed caused by ER stress as abrin may have other effects capable of activating JNK and p38 independent of ER stress.

Interestingly, activation of p38 has itself been shown to induce markers of ER stress such as upregulation of BiP and PERK signalling (Ranganathan et al., 2006). It has also been demonstrated that p38 can be involved in control of some UPR signalling pathways. For example, phosphorylation of CHOP by p38 increases its activity (Wang and Ron, 1996) and in HeLa cells apoptosis mediated by CHOP activation was found to be p38-dependent (Maytin et al., 2001). ATF6 has also been shown to be regulated by p38 (Thuerauf et al., 1998). ATF6 can be phosphorylated by and is a substrate for p38 *in vitro*. In the same study it was shown that the transactivation activity of ATF6 was promoted in primary cells transfected with ATF6 and p38α, and that sustained p38 activation caused increased activity of ATF6 at the *BiP* promoter. These studies provide evidence for a strong link between UPR signalling and p38 signalling and that these two pathways have the ability to activate each other.

Overall, there is strong evidence that p38 is another MAPK signalling pathway which can be activated through ER stress (Figure 1.3). As discussed ER stress activates ASK1-JNK through an interaction between IRE1α and TRAF2. ASK1 can activate MKK4/MKK7 and MKK3/MKK6, which are the upstream kinases for JNK and p38 respectively (Ichijo et al., 1997). It is therefore possible that ER stress-mediated ASK1 activation is a potential mechanism through which ER stress activates p38 signalling. MAPK signalling has been observed during ER stress so frequently that MAPK signalling could be considered part of the extremely complex and wide-reaching UPR.

1.4.3 The UPR and NF-κB

All three branches of the UPR can activate NF-κB signalling. The IRE1α branch of the UPR activates NF-κB via the phosphorylation and the subsequent degradation of IκBα (Hu et al., 2006b, Kaneko et al., 2003) (Figure 1.3). In a similar manner to JNK the IRE1α-TRAF2 interaction during ER stress can phosphorylate IKK which in turn phosphorylates IκBα (Hu et al., 2006b, Urano et al., 2000). Once IκBα is degraded NF-κB is free to transcribe the proinflammatory gene programme (Hu et al., 2006b, Zhang and Kaufman, 2008).

NF-κB can also be activated through the PERK pathway (Figure 1.3). As described, NF-κB is activated by the degradation of IκBα, which allows NF-κB to translocate to the nucleus where it can act as a transcription factor for various inflammatory genes. As described earlier PERK signalling inhibits translation, which means proteins with a shorter half-life will be depleted quicker. IκB has a shorter half-life than NF-κB (the protein it inhibits) so PERK signalling can directly activate NF-κB by freeing it from IκB through translational arrest (Deng et al., 2004, Wu et al., 2005). ER stress-induced activation of NF-κB should therefore allow its translocation into the nucleus. Indeed, ER stress induced by tunicamycin or brefeldin A caused translocation of NF-κB (Hung et al., 2004).

The ATF6 branch of the UPR can also activate NF-κB via a currently unknown mechanism during ER stress induced by SubAB (Hotamisligil, 2010, Yamazaki et al., 2009). Therefore, all three branches of the UPR can activate NF-κB through 2 distinct and one unknown mechanism suggesting an important role for NF-κB in ER stress-mediated inflammatory signalling.

1.4.4 The UPR, cytokine production and macrophage activation

As described ER stress can activate various inflammatory signalling pathways. These inflammatory signalling pathways ultimately lead to the increased production of proinflammatory mediators. Experimental induction of ER stress leads to the increased expression of several proinflammatory mediators such as IL-6, IL-8, MCP-1 and TNFα (Li et al., 2005b).

Experimental models of obesity have also demonstrated links between ER stress and cytokine production. For example, ER stress induced by free fatty acids caused increased ROS and cytokine production in 3T3-L1 adipocytes (Kawasaki et al., 2012). Adult derived human adipocyte stem cells exposed to ER stress, induced by thapsigargin, tunicamycin or palmitate, displayed increased *TNF-α* mRNA expression and activation of the NF-κB pathway (Mondal et al., 2012). It is therefore likely that ER stress plays an important role in inflammation originating from adipocytes. In fact, in many studies reporting inflammation and recruitment of macrophages in adipose tissue the inflammation is mediated from pathways which are also activated by the UPR (Hotamisligil, 2010). Whether or not inflammation in other tissues and disease settings is dependent on ER stress has not be extensively investigated.

Interestingly, conditioned media from cancer cells experiencing ER stress can activate macrophages and transmit ER stress (Mahadevan et al., 2011). The authors have termed this discovery as ‘transmissible’ ER stress. This study suggests an interesting phenomenon in that ER stressed cells may be able to activate macrophages through inducing ER stress in macrophages as well as inducing proinflammatory signalling. It is a possibility that macrophages activated by cancer cells secrete proteins which causes a high burden on the ER protein folding capacity of the macrophage to induce ER stress and that this is the mechanism of ‘transmissible’ ER stress.

Overall, evidence points to ER stress having an important role in transmitting a proinflammatory signal to cells of the immune system. ER stress having such a role is not entirely surprising given that ER stress occurs during wound healing (Wang et al., 2010), bacterial infection (Cho et al., 2013) and viral infection (Zhang and Wang, 2012) all three of which are likely to benefit from an immune response and inflammation.

1.5 The UPR and diabetes

1.5.1 Diabetes

Diabetes mellitus, commonly referred to as diabetes is a group metabolic disorders resulting from a defect in insulin secretion, insulin action or both. Type 2 diabetes (T2D) is one of these disorders and is different from T1D in that it begins with insulin resistance. T2D is a global health issue (Abegunde et al., 2007) as well as being an economic burden. In 2012 the cost of diabetes in the U.S. alone was estimated to be $245 billion and is expected to rise (American Diabetes, 2013) T2D is a significant risk factor for some forms of dementia, such as those observed in AD (Li and Holscher, 2007) and PD (Hu et al., 2007).

T2D is a result of both lifestyle and genetics. Several lifestyle factors are known to contribute to T2D such as: physical inactivity, excessive consumption of alcohol, having a sugar-rich diet, and being overweight (Olokoba et al., 2012). Monozygotic twins have a concordance of nearly 100% whilst almost one quarter of those with T2D have a family history of the disease (Olokoba et al., 2012). Thus evidence points to a strong genetic role in T2D. The high prevalence of T2D amongst certain ethnic groups is also evidence of the importance of genetics in development of this disease (Freeman and Cox, 2006).

It is thought that T2D arises from inheritance of a set of susceptibility genes. Numerous genes have been identified through population studies and animal models such as *PPARγ*, *KCNJ11*, *HNF4A*, and *CAPN10* (Olokoba et al., 2012). Most genes identified are associated with β-cell function but some genes are associated with the function of other tissues such as the liver and adipose tissue. Disruption of genes coding for proteins involved in the insulin signalling pathway has also been identified as being contributory to T2D (Sokhi et al., 2015). Defects in one of these genes, *INSR* (which codes for the insulin receptor), results in insulin resistance and T2D (Sesti et al., 2001), (Bodhini et al., 2012). It is possible that long lasting ER stress disrupts levels of the insulin receptor to mimic insulin resistance observed in individuals with defects in the INSR gene (see Chapter 5). Studies have also revealed that polymorphisms of the insulin receptor substrate genes are associated with development of T2D (Li et al., 2016). The current model for the development of T2D via UPR activation involves disruption of the insulin receptor substrate (discussed later) and as such links between disruption of genes and action of the UPR can be drawn.

There are some noted cases of conditions which give rise to or either contribute to T2D such as metabolic syndrome (Syndrome X), Cushing's syndrome, thyrotoxicosis, cancer, acromegaly, and chronic pancreatitis (Freeman and Cox, 2006). Thus T2D can be caused by lifestyle, genetics and pre-existing conditions. A rare disorder known as Wolcott-Rallison syndrome results in neonatal/early-onset diabetes. Wolcott-Rallison syndrome is caused by mutations in gene which codes for the ER stress-sensing protein PERK (Julier and Nicolino, 2010). It is hypothesised that loss of PERK through these mutations limits the ability of β-cells to handle a heavy protein folding load resulting in severe ER stress and apoptosis. The role for severe ER stress in β-cells is also supported by the findings that mutations in the ER Ca^{2+} channel coding gene *WFS1* cause Wolfram syndrome (Inoue et al., 1998). Wolfram syndrome is characterised by several disorders including optic atrophy, deafness and diabetes (Boutzios et al., 2011). Thus diabetes, both type I and II, can be a result of pre-existing conditions, some of which suggest a role for the UPR in the development of diabetes.

1.5.1.1 Insulin resistance

Insulin resistance is a state of weakened cellular response to the hormone insulin. Whilst insulin resistance is not recognised as a disease, it can lead to the development of T2D. Insulin resistance causes increased secretion of insulin from pancreatic β-cells in an attempt to maintain normal blood glucose levels. The resulting increased burden on pancreatic β-cells eventually causes these cells to have decreased functionality and as a result produce less insulin over time (Spielman et al., 2014). Identifying the early molecular events underlying the development of insulin resistance is therefore an important step in furthering the understanding and treatment of T2D.

1.5.1.2 The insulin signalling pathway

Pancreatic β-cells are the main cells responsible for the production of insulin (Marchetti et al., 2006). Insulin is a 51 amino acid peptide hormone belonging to the family of insulin-like hormones along with insulin-like growth factor 1 (IGF-1) and IGF-2 (Spielman et al., 2014). Insulin is most commonly known for stimulating glucose uptake but it can also stimulate cell proliferation and protein synthesis (Shulman, 1999). Insulin also has

important roles in prosurvival signalling (Kim et al., 2001) and regulating healthy neuronal function (Nistico et al., 2012).

Insulin binding to the insulin receptor induces the insulin signalling pathway (Figure 1.4). Binding of insulin to the insulin receptor causes tyrosine phosphorylation of the insulin receptor (White et al., 1988, Tornqvist et al., 1988, Tornqvist and Avruch, 1988) through activation of the protein tyrosine kinase domain and subsequent autophosphorylation (Kasuga et al., 1982, Wilden et al., 1992, Rhodes and White, 2002). Binding of insulin to the insulin receptor leads to the internalisation of the insulin receptor and insulin complex. The insulin-insulin receptor complex is then separated in endosomes prior to the degradation of insulin whilst the insulin receptor is recycled back to the plasma membrane (Foti et al., 2004). Activated insulin receptors induce the tyrosine phosphorylation of the insulin receptor substrates (IRS) 1-4, and several Shc proteins (Myers and White, 1996, Paz et al., 1996). Those proteins which are phosphorylated by the insulin receptor act as anchors for proteins containing Src-homology-2 (SH-2) domains (Cheatham and Kahn, 1995). The subunits of phosphatidylinositol (PI) 3-kinase are recruited to the cell membrane, through their SH-2 domains, by IRS and Shc proteins (Backer et al., 1992). Activated PI 3-kinase induces the recruitment to the membrane of phosphoinositide-dependent kinase (PDK 1) and PDK 2 as well as several protein kinase B (PKB/AKT) isoforms (White, 2002). Upon localisation to the membrane, PDKs can activate AKT1-2 via phosphorylation. Activated AKT1-2 are important signalling proteins for the control of various cellular events including; glucose transport, cell growth, survival, proliferation, and differentiation. AKT is involved in many signalling pathways by phosphorylating a number of nuclear and cytosolic proteins that regulate diverse cellular functions (Ahn, 2014). For example, AKT can phosphorylate ASK1 at Ser83 to decrease its activity resulting in a reduction of JNK activation (Gu et al., 2009). This inhibition of JNK activation by AKT reduces sensitivity to stress induced apoptosis (Kim et al., 2001) and is just one way in which insulin signalling promotes survival (discussed later).

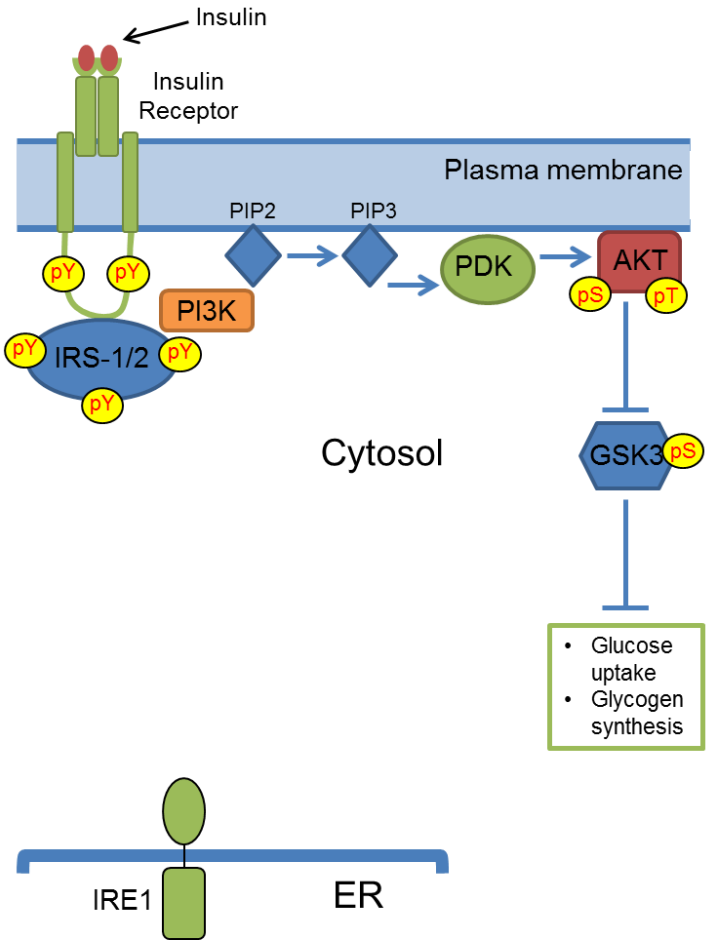

Figure 1.4. The insulin signalling pathway.

Binding of insulin to the insulin receptor induces the insulin receptor to be phosphorylated at tyrosine residues. The insulin receptor substrates (IRS) 1-4, and several Shc proteins are phosphorylated by activated insulin receptors. The subunits of phosphatidylinositol (PI) 3-kinase are recruited, through there SH-2 domains, by IRS and Shc proteins. Phosphoinositide-dependent kinase (PDK 1) and PDK 2 and several protein kinase B (PKB/AKT) isoforms are recruited to the membrane after PI 3-kinase activation. Upon localisation to the membrane, PDKs can activate AKT1-2 via phosphorylation. Phosphorylated AKT phosphorylates and inhibits glycogen synthase kinase 3 (GSK3). When AKT is not inhibiting GSK3, when insulin signalling is not occurring, GSK3 is active and inhibits glucose uptake and glycogen synthesis. Thus, during insulin signalling glucose uptake and glycogen synthesis occurs.

1.5.2 ER stress in obesity and insulin resistance

ER stress is strongly associated with obesity and insulin resistance in muscle, adipose and hepatic tissues. How ER stress affects insulin signalling varies depending on the tissue and cell type. However, there is conflicting evidence between studies on the same tissue and cell types. Nevertheless, the consensus is that ER stress inhibits normal insulin signalling. The main source of ER stress in obesity is thought to originate from free fatty acids

(Kawasaki et al., 2012, Mondal et al., 2012, Alhusaini et al., 2010). Cytokines and inflammatory signalling may also provide a mechanism for the development of ER stress in obesity and T2D. For example, cytokines are reported to induce ER stress in mouse insulinoma-derived β-cells (Hasnain et al., 2014). Regardless of the mechanisms ER stress has been observed in muscle, adipose and hepatic tissues or in cultured cells originating from these tissues.

1.5.2.1 Hepatocytes and hepatic tissue

ER-stress has been detected in the liver of both obese non-human animals (Ozcan et al., 2004) and obese humans (Puri et al., 2008, Gregor et al., 2009). Hepatic inhibition of IRE1α through overexpression of BAX inhibitor-1 has been shown to protect mice from obesity-induced insulin resistance (Bailly-Maitre et al., 2010). Transgenic mice with a constitutively active form of GADD34, which causes inhibition of the ER stress induced phosphorylation of eIF2α, have reduced gluconeogenic gene expression and consequent reduction in hepatic glucose production (Birkenfeld et al., 2011). Tunicamycin-induced ER stress caused insulin resistance in Hep G2 cells which was demonstrated through the observation that phosphorylated AKT (p-AKT) levels decreased (Achard and Laybutt, 2012). In the same study it was also reported that there was a decrease in phosphorylated AKT with palmitate-induced ER stress. The chaperone tauroursodeoxycholic acid (TUDCA), which is reported to decrease ER stress, increased insulin sensitivity in hepatic tissue of obese patients (Kars et al., 2010). Thus there is mounting evidence implicating ER stress in hepatic tissue occurring during obesity and insulin resistance.

1.5.2.2 Adipocytes and adipose tissue

ER stress has been detected in adipose tissue of obese humans (Gregor et al., 2009, Boden et al., 2008, Sharma et al., 2008) and mice (Ozcan et al., 2004). Markers of ER stress such as *BiP* and *XBP-1*s mRNA were reduced after weight loss in humans (Gregor et al., 2009). Furthermore, markers of ER stress such as *XBP-1* mRNA and PDI expression were shown to be at higher levels in adipose tissue of obese patients compared to lean (Boden et al., 2008). Chaperones which are regulated by ATF6 increase in subcutaneous fat of obese patients (Sharma et al., 2008) suggesting activation of UPR, and ATF6 specifically, in obese humans.

ER stress can be activated in adipocytes through exposure to saturated fatty acids and high glucose (Alhusaini et al., 2010). However, other investigators from the laboratory in which the data for this thesis was produced do not observe evidence of saturated fatty acid-induced ER stress in cellular models, but instead report that glucose starvation and hypoxia may be the main causes of ER stress in adipocytes (Mihai and Schröder, 2014). *Grp78* heterozygous mice which display an adaptive UPR, defined by increased expression of ER chaperones and increased folding capacity, show reduced high fat diet (HFD)-induced obesity and attenuated insulin resistance in white adipose tissue (Ye et al., 2010). Further evidence from work on murine cell lines has confirmed a role for ER stress in insulin signalling. For example, ER stress inhibited insulin signalling in 3T3 adipocytes (Xu et al., 2010).

1.5.2.3 Myotubes and muscle tissue

In a study from 2004, researchers found that obesity was associated with ER stress in liver and adipose tissue but not muscle tissue (Ozcan et al., 2004). However, a later study by the same group showed that relieving ER stress with chemical chaperones was able to improve insulin sensitivity in muscle tissue of obese mice, suggesting that ER stress is important in regulating insulin signalling in muscles cells (Ozcan et al., 2006). In agreement with this palmitate has been shown to cause ER stress in C_2C_{12} myotubes (Hage Hassan et al., 2012, Rieusset et al., 2012) as well as human myotubes (Hage Hassan et al., 2012, Peter et al., 2009). However it was found that ER stress did not mediate the palmitate-induced insulin resistance in myotubes (Hage Hassan et al., 2012). Treatment of cultured myotubes with the ER stressor tunicamycin has also been shown to reduce insulin signalling via serine phosphorylation of IRS1 (Hage Hassan et al., 2012, Rieusset et al., 2012). Finally, evidence for a role for ER stress impacting insulin signalling in muscle tissue is demonstrated through the finding that TUDCA treatment increased insulin sensitivity in muscle tissue of obese patients (Kars et al., 2010). TUDCA has been shown to alleviate ER stress (Kars et al., 2010, Rieusset et al., 2012) and thus TUDCA treatment leading to increased insulin signalling suggests, but not necessarily demonstrates, the involvement of ER stress in muscle tissue of obese patients.

1.5.2.4 Other cell types

In addition to hepatocytes, myotubes and adipocytes other cells affected by obesity and insulin resistance have also exhibited ER stress. For example accumulation of cholesterol in the ER of macrophages results in increased ordering of the ER membrane. This inhibits sarcoplasmic-endoplasmic reticulum calcium ATPase-2b activity resulting in depletion of calcium and activation of ER stress due to the calcium dependent nature of disulphide bond formation during protein folding (Li et al., 2004a).

Studies therefore suggest that ER stress plays some part in the development of insulin resistance in various tissue types. However, the addition of chemical chaperones and the subsequent inhibition of ER stress does not rescue the palmitate-induced insulin resistance in mouse and human muscle cells (Hage Hassan et al., 2012, Rieusset et al., 2012). Consistent with these data, overexpression of the ER chaperone Grp78 protein does not protect muscle cells from palmitate-induced insulin resistance (Rieusset et al., 2012). However, it is worth noting that palmitate, although reported to induce ER stress, may be causing ER stress-independent insulin resistance and chemical chaperones therefore alleviate ER stress but not insulin resistance. Thus, although studies highlight the role of ER stress in insulin resistance, the mechanism through which ER stress, or chemicals which induce ER stress cause insulin resistance, is likely to vary depending on ER stress induction and tissue or cell type.

1.5.3 How ER stress causes insulin resistance

Two mechanisms through which ER stress may cause insulin resistance have been proposed: a) activation of JNK by IRE1α-TRAF2 signalling resulting in S307 phosphorylation of IRS1 by JNK, b) induction of tribbles homolog 3 (TRB3) by the PERK pathway and the subsequent inhibition of AKT and IRS1 via formation of a complex with TRB3.

1.5.3.1 IRS1

The most common general (not necessarily involving ER stress) mechanism causing insulin resistance involves serine phosphorylation of IRS proteins. IRS serine

phosphorylation inhibits recruitment of PI 3-kinase to IRS proteins (Qiao et al., 1999, White, 2003, Um et al., 2004, Patti and Kahn, 2004, Aguirre et al., 2002, Qiao et al., 2002) as well as inhibiting the insulin receptor-mediated tyrosine phosphorylation of IRS proteins (Ozcan et al., 2006, Ozcan et al., 2004). Serine phosphorylation of IRSs is thought to interfere with the interaction between the insulin receptor and the IRSs through modification of IRS phosphotyrosine binding (PTB) domain (Tanti et al., 1994). Serine phosphorylation of IRS1 can also lead to its degradation (Shah et al., 2004) and thus may be a secondary mechanism through which serine phosphorylation of IRS1 inhibits insulin signalling. JNK is one of several protein kinases thought to be responsible for the serine phosphorylation of IRS proteins (Aguirre et al., 2000, Gao et al., 2004, Hirosumi et al., 2002, Bandyopadhyay et al., 2005). Various stresses have been shown to induce JNK-mediated S307 phosphorylation of IRS1, such as free fatty acid treatment, inflammation and ER stress (Nguyen et al., 2005, Hotamisligil et al., 1996, Hotamisligil et al., 1993, Peraldi et al., 1996, Uysal et al., 1997, Qi and Pekala, 2000, Hotamisligil and Spiegelman, 1994). Other protein kinases implicated in serine phosphorylation of IRS include; $p70^{S6K}$ (Um et al., 2004, Tremblay et al., 2005, Pende et al., 2000), IKK (Gao et al., 2002b), AKT (Ozes et al., 2001), PKCζ (Ravichandran et al., 2001, Bourbon et al., 2002, Liu et al., 2001), PKCθ (Gao et al., 2004, Li et al., 2004b), GSK 3 (Ilouz et al., 2006, Eldar-Finkelman and Krebs, 1997, Liberman and Eldar-Finkelman, 2005), ERK (Engelman et al., 2000, Rui et al., 2001, De Fea and Roth, 1997), mTOR (Ozes et al., 2001, Haruta et al., 2000) and IRAK (Kim et al., 2005). These other protein kinases have been shown to be involved in serine IRS phosphorylation under stress conditions such as free fatty acids and inflammation. However, JNK is the main protein kinase thought to lead to the inhibition of insulin signalling during ER stress.

1.5.3.2 The IRE1α-TRAF2-JNK model of ER stress-induced insulin resistance

One model of ER stress-mediated insulin resistance is that activation of JNK by IRE1α-TRAF2 signalling results in S307 phosphorylation of IRS1 by JNK (Figure 1.5). IRE1α can activate JNK by recruiting TRAF2 and ASK1 (Urano et al., 2000). The role of JNK in ER stress-mediated insulin resistance is supported by the following observational studies. The IRE1α-JNK pathway activation is elevated in obese humans compared to none obese humans (Boden et al., 2008). Markers of ER stress such as *XBP-1* mRNA and PDI were shown to be at higher levels in adipose tissue of obese patients compared to lean. JNK was

also activated at higher levels (Boden et al., 2008) demonstrating the importance of IRE1α and JNK activation in human obesity. JNK activation and markers of ER stress such as BiP and *XBP-1*s mRNA were reduced after weight loss in humans (Gregor et al., 2009). The Gregor *et al.* study also observed some increased insulin sensitivity in skeletal muscle, adipose and hepatic tissue. However, it is worth noting that these patients were not insulin resistant suggesting that the JNK and UPR activation in these obese patients, although present, was not sufficient to cause detectable insulin resistance.

Treatment of cultured myotubes with the ER stressor tunicamycin has also been shown to activate the IRE1α-JNK pathway and reduce insulin signalling via phosphorylation of IRS1 (Hage Hassan et al., 2012, Rieusset et al., 2012). However, IRE1α-JNK activation and IRS1 phosphorylation with tunicamycin is only correlative evidence and as such this inhibition of insulin signalling may not be dependent on ER-JNK signalling.

Mechanistic evidence demonstrating a link between JNK and ER stress causing insulin resistance has also been published. JNK inhibition, using the JNK inhibitor SP600125, was reported to protect cells from ER-stress induced insulin resistance (Ozcan 2004). Activated JNK is able to phosphorylate serine residues *S307/S312* of IRS1, which inhibits insulin receptor-induced tyrosine phosphorylation of IRS1 leading to insulin resistance. Consistent with JNK inhibiting IRS1 tyrosine phosphorylation, JNK inhibition rescues IRS1 tyrosine phosphorylation (Ozcan et al., 2004). In addition, mutating serine 307 of IRS1 to alanine prevents JNK-induced IRS1 serine phosphorylation and insulin resistance (Aguirre et al., 2000).

Chemical chaperones which relieve ER stress were shown to rescue insulin resistance in a mouse model of T2D (Ozcan et al., 2006). Whether or not chemical chaperone-rescued insulin resistance in obese mice is mediated via effects on IRE1α-JNK pathway remains unclear. TUDCA treatment increased insulin sensitivity in hepatic and muscle tissue of obese patients but it is not known whether this was attributable to a reduction in ER stress or other off-target effects of TUDCA (Kars et al., 2010). TUDCA treatment did not increase insulin sensitivity in adipose tissue. However, ER stress did not decrease in adipose tissue with TUDCA treatment suggesting that TUDCA treatment is not always sufficient to alleviate ER stress (Kars et al., 2010).

In conclusion it has been proposed that: 1) ER stress-induced activation of IRE1α results in an IRE1α-TRAF2 interaction, 2) the IRE1α-TRAF2 interaction causes ASK1-dependent JNK activation, 3) activated JNK phosphorylates residue S308 of IRS1, 4) S308

phosphorylation of IRS1 inhibits IR-mediated tyrosine phosphorylation of IRS1, 5) inhibition of IRS1 tyrosine phosphorylation prevents downstream insulin signalling such as phosphorylation of AKT. The IRE1α-JNK model of insulin resistance suggests that both *jnk1*$^{-/-}$ *jnk2*$^{-/-}$ and *traf2*$^{-/-}$ MEFs should be protected from ER stress-induced insulin resistance.

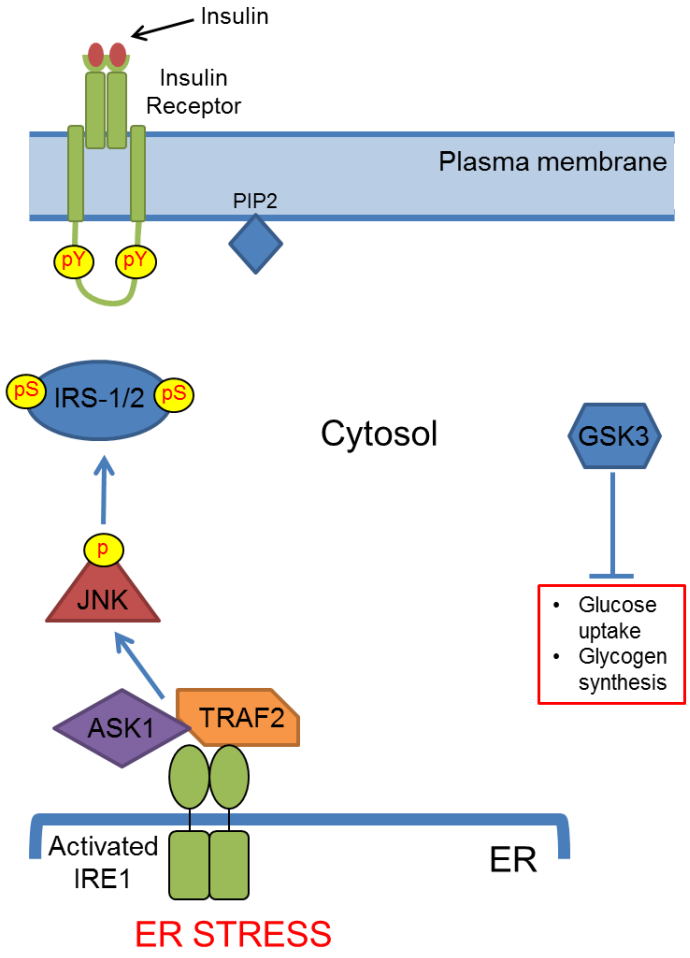

Figure 1.5. Proposed model for the disruption of the insulin signalling pathway through JNK-IRE1α.

During ER stress IRE1α is phosphorylated and interacts with TRAF2. IRE1α and TRAF2 interaction causes JNK phosphorylation in an ASK1 dependent manner. Phosphorylated JNK induces phosphorylation of IRS-1 and 2 at serine residues. The phosphorylation of serine residues on IRS1 and 2 inhibits interaction with the insulin receptor and prevents tyrosine phosphorylation of IRS1 and 2 during binding of insulin to the insulin receptor. As a result the downstream insulin signalling does not occur; leaving GSK3 to be uninhibited and in turn results in inhibition of glucose uptake and glycogen synthesis.

1.5.3.3 The PERK-TRB3 model of ER stress-induced insulin resistance

The second proposed model of ER stress-mediated insulin resistance involves induction of TRB3 by the PERK pathway and the subsequent inhibition of AKT and IRS1 via formation of a complex with TRB3. Observational evidence linking ER stress and TRB3 to insulin resistance comes from studies reporting that ER stress induces expression of TRB3 (Ohoka et al., 2005, Koh et al., 2013) whilst TRB3 is reported to inhibit insulin signalling (Figure 1.5) (Du et al., 2003, Avery et al., 2010, Koh et al., 2006, Koh et al., 2013, Liew et al., 2010).

ER stress is linked to TRB3 expression in two studies. Tunicamycin treatment enhanced *TRB3* promoter activity which could be inhibited by dominant negative forms of CHOP suggesting that there may be a role for PERK in TRB3 activation (Ohoka et al., 2005). ATF4 knockdown also inhibited tunicamycin-induced TRB3 induction providing a link between ER stress and TRB3 induction involving ATF4-CHOP signalling. ER stress increases TRB3 expression in C_2C_{12} and adult mouse skeletal muscle (Koh et al., 2013). Thus ER stress is reported to induce expression of TRB3.

TRB3 has also been shown to inhibit insulin signalling (Figure 1.6). However, the role of TRB3 in ER stress-mediated insulin resistance is controversial. TRB3 overexpression in several cell lines leads to inhibited AKT and IRS1 phosphorylation (Du et al., 2003, Avery et al., 2010, Koh et al., 2006, Koh et al., 2013, Liew et al., 2010). Conversely, two studies have shown that TRB3 expression does not cause inhibition of insulin signalling (Iynedjian, 2005, Takahashi et al., 2008). Consistent with data that TRB3 does not have a role in insulin signalling is that *TRB3*$^{-/-}$ mice show normal hepatic insulin signalling and glucose homeostasis (Okamoto et al., 2007). Therefore, the role of TRB3 in ER stress-induced insulin resistance is not straight forward.

TRB3 is thought to directly interact with both AKT and IRS1 because studies have reported that TRB3 is co-immuniprecipitated with both of these insulin signalling proteins (Du et al., 2003, Koh et al., 2006, Koh et al., 2013, Liew et al., 2010). However, it is worth noting that in these studies TRB3 has been overexpressed through viral transduction which is estimated to cause overexpression of 700-1000 fold at the mRNA level (Iynedjian, 2005). Nevertheless, TRB3 interaction with IRS1 inhibits IRS1 tyrosine 612 phosphorylation (Koh et al., 2013).

In conclusion, TRB3 is reported to have a controversial role in regulating insulin resistance. However, it may be a mechanism through which ER stress induces insulin resistance and is worthy of further study alongside JNK, which has also been shown to regulate AKT and IRS1 phosphorylation during ER stress.

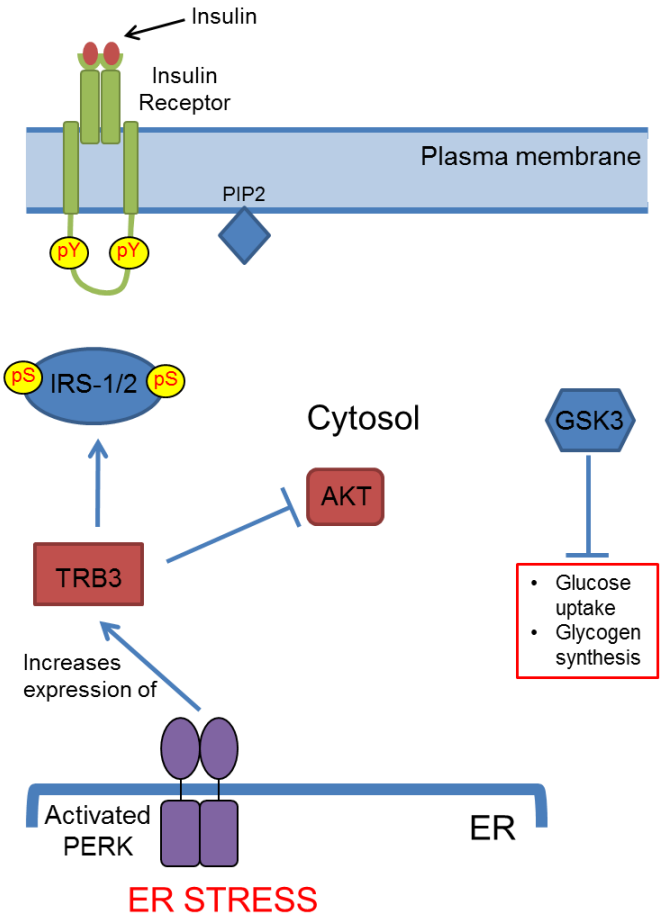

Figure 1.6. Proposed model for the disruption of the insulin signalling pathway through PERK-TRB3.

During ER stress PERK is phosphorylated and activated. Activated PERK induces the upregulation of TRB3. In a mechanism similar to JNK, TRB3 can cause phosphorylation of IRS1 and 2 at serine residues resulting in decreased interaction with the insulin receptor. TRB3 can also directly inhibit AKT. Both mechanisms prevent GSK3 from being phosphorylated during binding of insulin to the insulin receptor. Thus GSK3 is free to inhibit glucose uptake and glycogen synthesis.

1.6 The UPR and Parkinson's disease

1.6.1 Parkinson's disease

ER stress has been implicated in many diseases other than T2D. As well as T2D, ER stress has been reported in the age-related disease PD. With similarities to T2D, inflammatory signalling and ER stress have also been reported in PD. The second most common age related neurodegenerative disease was first described by James Parkinson in 1817 (Parkinson, 2002). In his monograph entitled 'Essay on the shaking palsy' he described the main features of the neurodegenerative condition, which would later be named after him; Parkinson's disease. Nearly two centuries later this disease continues to affect an estimated 1% of people over the age of 65 (Lang and Lozano, 1998, Fahn, 2003). Not all patients have the same symptoms but most suffer from rigidity, tremor, postural instability, freezing and slowness of voluntary movement (Dauer and Przedborski, 2003).

PD is characterised by the selective loss of dopaminergic neurons in the substantia nigra pars compacta (SNpc) (Warner and Schapira, 2003, Moore et al., 2005). A major pathological feature of PD is the formation of protein aggregates termed Lewy bodies in the cytosol of neurons (Moore et al., 2005). Lewy bodies are intracytoplasmic filamentous inclusions and are made up of numerous proteins including α-synuclein, ubiquitin, synphilin, tubulin and parkin (Spillantini et al., 1998, Dauer and Przedborski, 2003, Shimura et al., 2000). These protein aggregates have many detrimental effects in neurons including the poisoning and inhibition the proteasome, a large multiprotein responsible for degrading unwanted proteins (Bence et al., 2001).

How PD is caused is not known but it seems likely that several factors including genetic factors and environmental toxins contribute to the progressive loss of dopaminergic neurons in PD. More recent evidence implicates ER stress and the UPR in the pathology of PD. The following sections will look at the molecular mechanisms implicated in PD which are associated with the ER including: mitochondrial stress, inflammatory signalling, and the immune response.

1.6.2 Genetic factors

Although most forms of PD are sporadic (more than 90% (Tanner, 2003)) genetic forms do exist and their discovery has given some insight into the molecular physiology of PD.

Several genes have now been identified and the proteins they code for have been extensively investigated. Three of these proteins in particular have been linked to ER stress: α-synuclein, parkin, and DJ-1. The most well studied of these proteins is α-synuclein.

1.6.2.1 α-synuclein

Mutations in the gene for α-synuclein are responsible for dominantly inherited PD (Polymeropoulos et al., 1997). The role for α-synuclein is not fully understood but studies have shown it to be the major constituent of Lewy bodies (Tanner, 2003). Recent studies have implicated α-synuclein in the development of ER stress in PD. Various mechanisms have been suggested for α-synuclein-mediated ER stress (Figure 1.7): 1) inhibition of the proteasome, 2) inhibition of ER to Golgi transport, 3) entry of α-synuclein into the ER and disruption of protein folding. These are mechanisms involving α-synuclein only, other mechanisms not involving α-synuclein have also been shown to induce ER stress in PD (discussed later).

1.6.2.1.1 Inhibition of the proteasome

α-synuclein contains an non-Aβ component (NAC) region, which is prone to aggregate and its propensity to aggregate has been shown to increase with oxidative stress (Ostrerova-Golts et al., 2000, Dawson and Dawson, 2003). It has been demonstrated that α-synuclein aggregates poison the proteasome (Lindersson et al., 2004). It is thought that α-synuclein-mediated proteasome inhibition leads to neuronal cell death and the findings that overexpression of α-synuclein induces neuronal death supports this view (Saha et al., 2000). Evidence implicating the proteasome, UPR and PD comes from a study by Nishitoh and co-workers in which the UPR was activated in neurons by proteasome inhibition via expression of proteins with expanded glutamine repeats. This inhibition of the proteasome not only caused UPR activation but also caused UPR-induced cell death (Nishitoh et al., 2002).

Once the proteasome is compromised via Lewy bodies a build-up of mis and unfolded proteins in the ER will occur and this could further contribute to inhibition of the proteasome because the proteasome is required during ER stress to degrade unwanted

proteins. Not only that, severe ER dysfunction can lead to toxic protein aggregate formation due to accumulated unfolded proteins, which can inhibit the proteasome. Therefore, proteasome inhibition via ER stress can cause further ER stress (Paschen, 2003a). It could be possible that both build-up of accumulated proteins in the ER and proteasome inhibition lead to the UPR and that both have knock-on effects on each other increasing ER stress further.

1.6.2.1.2 Inhibition of ER to Golgi transport

Along with mammalian cells, accumulation of α-synuclein in yeast cells is also toxic. After expression of α-synuclein in yeast cells it was observed that the earliest defect was a block in ER-Golgi transport leading to the eventual development of ER stress (Cooper et al., 2006). The ERAD-mediated degradation of a misfolded carboxypeptidase yscY (CPY) protein, CPY*, which requires translocation to the Golgi before degradation was found to be inhibited suggesting that ER to Golgi transport was inhibited. There are many Rab GTPases, which function at different points of the secretory pathway. However, only the Rab GTPase Ypt1p was found to be affected by α-synuclein. Indeed overexpression of Ypt1p in yeast and the mammalian homologue Rab1 in primary rat neurons reduced α-synuclein-induced toxicity. It is therefore possible that α-synuclein inhibits transport of ER-Golgi, which in turn causes ER stress and toxicity.

Another study has also demonstrated that Rab1-mediated ER-Golgi transport is perturbed by α-synuclein (Gitler et al., 2008). However, this study went on further to demonstrate that vesicles left the ER but did not successfully fuse or dock with the Golgi showing that the *in vivo* trafficking problem is due to a direct effect of α-synuclein on the transport machinery. It is therefore not immediately obvious how blockage of transport downstream of the ER could lead to ER stress. However, ER stress was not investigated by Gitler *et al.* and inhibition of, downstream of ER, protein trafficking may have unknown knock-on effects in the ER.

1.6.2.1.3 Entry of α-synuclein into the ER and disruption of protein folding

Only three studies have reported that α-synuclein can enter the ER and disrupt protein folding machinery to induce ER stress (Colla et al., 2012a, Colla et al., 2012b, Bellucci et

al., 2011) and two of these papers originate from the same research group. Nevertheless, they suggest a novel mechanism for α-synuclein-mediated ER stress. The Colla *et al.* studies show that α-synuclein and α-synuclein aggregates are associated with ER/microsome fractions. The authors conclude that this association is not a consequence of simple membrane-binding properties of synucleins as β-synuclein does not associate with ER/microsome fractions. The study by Bellucci *et al*. reports more specifically that α-synuclein monomers interact with BiP and these were detected in ER fractions. However, the authors do not consider that ER/microsomes may contain proteasome. This is an important consideration as α-synuclein has been shown to be directed to the proteasome (Lindersson et al., 2004, Bennett et al., 1999). These Colla *et al.* papers also report that upon accumulation of α-synuclein in the ER, protein chaperones are inhibited leading to ER stress and that overexpression of α-synuclein sensitizes cells to ER stress-induced toxicity. However, further studies are yet to confirm this novel mechanism of α-synuclein-induced ER stress.

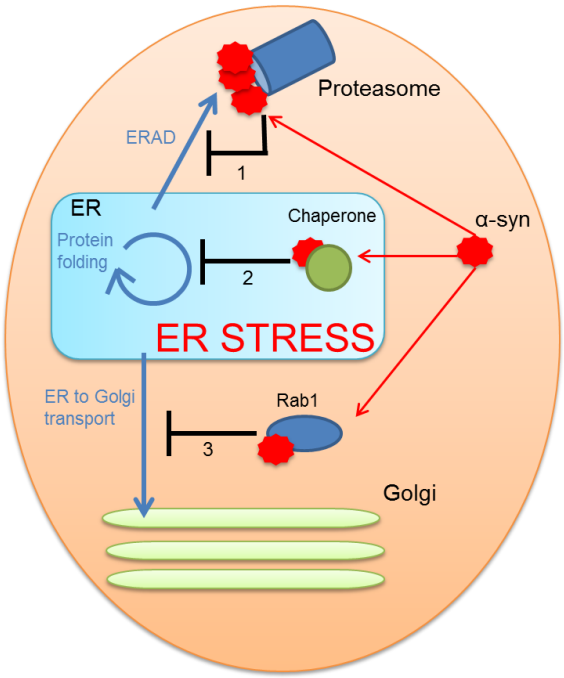

Figure 1.7. Mechanisms of α-synuclein-mediated ER stress.

Various mechanisms have been suggested for α-synuclein-mediated ER stress : 1) α-synuclein and α-synuclein–containing aggregates block and inhibit the proteasome and thus disturb ERAD 2) α-synuclein enters the ER and directly interacts with and disrupts protein folding machinery to inhibit protein folding 3) α-synuclein interacts with and inhibits Rab1 resulting in the inhibition of ER to Golgi transport,.

1.6.2.1.4 Further evidence implicating α-synuclein in ER stress

Observational evidence linking α-synuclein with ER stress comes from one study which reported that dopaminergic neurons in the brains of PD patients, containing inclusions of α-synuclein, also display markers of activation of the PERK branch of the UPR (Hoozemans et al., 2007). PERK activation in PD is also supported by mechanistic evidence linking ER stress with α-synuclein toxicity. In a rat model of PD (involving injection of an recombinant adeno-associated virus (rAAV) expressing human α-synuclein into rat SNpc), α-synuclein overexpression led to increased markers of UPR activation such as PERK and ATF6 signalling pathways (Gorbatyuk et al., 2012). In the Gorbatyuk *et al*. study the overexpression of BiP down-regulated ER stress markers which in turn diminished α-synuclein toxicity and reduced the loss of tyrosine hydroxylase positive cells. Tyrosine hydroxylase is used as a marker for dopaminergic cells and as such suggests that overexpression of BiP reduces the loss of dopaminergic cells in the above study. A link between BiP and α-synuclein has been reported in another study also. BiP was shown to bind to α-synuclein in *in vitro* and *in vivo* models displaying α-synuclein accumulation (Bellucci et al., 2011). In this study α-synuclein monomers were shown to bind BiP in ER fractions suggesting that monomeric α-synuclein can enter the ER. Further evidence supporting an involvement of the UPR in α-synuclein aggregation comes from a study by Smith and co-workers, which showed increased BiP and phospho-eIF2α levels in cells overexpressing mutant α-synuclein (Smith et al., 2005).

PERK activation with α-synuclein has been reported in other studies also. Serine 129 phosphorylation of α-synuclein causes PERK activation and UPR-mediated cell death in neuroblastoma cells (Sugeno et al., 2008) whilst overexpression of WT or mutant α-synuclein causes UPR activation in yeast (Cooper et al., 2006), via an unknown mechanism. However UPR activation in the Cooper *et al*. study may be a product of inhibited ER to Golgi transport. Thus, strong evidence implicates α-synuclein-mediated ER stress and UPR activation in the development of PD.

1.6.2.2 Parkin

Parkin has been implicated in PD ever since a mutation in the parkin gene was discovered to be responsible for a form of early onset PD (Kitada et al., 1998). Parkin is an E3 ubiquitin ligase responsible for targeting polyubiquitin chains to target substrates to be

degraded by the proteasome (Imai et al., 2000, Shimura et al., 2000). Interestingly, parkin, a protein involved in the majority of autosomal recessive Parkinsonisms (Kitada et al., 1998), has been shown to be transcriptionally regulated by ATF4, providing further evidence that the PERK branch of the UPR may play some role in PD (Bouman et al., 2011). In this study ER stress induced expression of parkin at both the mRNA and protein level. Intriguingly, the downstream target of JNK, c-Jun was also shown to be a transcriptional repressor of parkin. As JNK is considered to be part of the UPR signalling pathway this suggests a dual role for UPR signalling in that it has the potential to both upregulate and decrease the expression of parkin.

Parkin-associated endothelin receptor–like receptor (Pael-R) is a putative G-protein coupled transmembrane protein. It is a substrate for parkin and has been found in Lewy bodies (Murakami et al., 2004). Parkin can protect dopaminergic neurons from Pael-R toxicity via ubiquitination and thus signalling it to be degraded by the proteasome (Imai and Takahashi, 2004). Mutations in *PARK2*, the gene for parkin, compromise the ability of the parkin protein to function as a ubiquitin ligase (Shimura et al., 2000). In a study on juvenile onset of PD it was observed that parkin mutations led to the accumulation of parkin substrates in the ER of dopaminergic neurons in the SNpc, which in turn led to ER stress and cell death (Imai et al., 2001). Increased expression of parkin mediated through the UPR seems logical as the UPR functions to remove unfolded proteins for degradation (ERAD). Therefore inactive parkin may both directly and indirectly prevent the UPR from functioning at an optimal level thus preventing a return to homeostasis in the ER and subsequent further stress.

There is also evidence that parkin has a role in modulating DJ-1 activity (Duplan et al., 2013). Control of DJ-1 was associated with parkin-mediated upregulation of *XBP1*. The authors conclude that disrupted parkin modulation of DJ-1 may be a mechanistic explanation of the occurrence of UPR activation in PD. Overall there is a strong case for UPR involvement in the toxicity of parkin-mediated PD.

1.6.2.3 DJ-1

DJ-1 is a multifunctional protein involved in transcriptional regulation (Ishikawa et al., 2010), regulation of chaperone function (Shendelman et al., 2004), response to oxidative stress (Taira et al., 2004, Li et al., 2005a), and regulation of mitochondria (Li et al., 2005a,

Junn et al., 2009). DJ-1 is expressed in almost all cells and tissues (Ariga et al., 2013). Mutations in the DJ-1 gene cause loss of function in the DJ-1 protein and these DJ-1 mutations are linked to autosomal recessive early onset Parkinsonism. siRNA-mediated knock down of DJ-1 sensitised neuronal cells to ER stress-induced cell death (Yokota et al., 2003). However, these neuronal cells were also sensitised to cell death induced by oxidative stress and proteasome inhibition suggesting that DJ-1's role in cell death may not specifically involve the UPR, that being said, both oxidative stress and proteasome inhibition can cause UPR activation. If and how DJ-1 modulates ER stress is still to be fully established.

1.6.3 Parkinson's disease mimetic drugs and the UPR

1.6.3.1 MPP$^+$

People exposed to the neurotoxin 1-methyl-4-phenyl-1, 2, 3, 6-tetrahydropyridine (MPTP) show very similar symptoms to PD patients (Langston et al., 1983, Langston et al., 1999, Tetrud et al., 1989). MPTP is now commonly used in animal models for PD as it can induce PD-like pathological features in both mice and rats (Jackson-Lewis and Przedborski, 2007, Yazdani et al., 2006). MPTP is converted to 1-methyl-4-phenylpyridinium (MPP^+) which is the active metabolite responsible for the cellular damage. MPP^+ inhibits mitochondrial NADH dehydrogenase (complex-1 of the mitochondria) (Michel et al., 1990).

Homocysteine-induced endoplasmic reticulum protein (herp) is a stress response protein localised to the membrane of the ER. Herp knockdown renders PC-12 and MN9D cells more sensitive to MPP^+-induced cell death. Herp knockdown-induced cell death involved CHOP and depletion of ER calcium ions (Chigurupati et al., 2009). Herp overexpression blocked both the MPP^+-mediated depletion of ER calcium and the MPP^+-induced expression of CHOP suggesting that ER stress can play a strong role in MPP^+ toxicity.

1.6.3.2 6-OHDA

The dopamine derivative 6-hydroxydopamine (6-OHDA) is a neurotoxin often used as a PD mimetic drug both *in vitro* and *in vivo* (Blum et al., 2001). 6-OHDA causes the production of ROS such as hydrogen peroxide and therefore leads to oxidative stress and dopaminergic neuronal cell death (Cohen and Heikkila, 1974). 6-OHDA may also cause

toxicity through inhibition of the mitochondrial complex I (Tobon-Velasco et al., 2013) but a study using cultured neurons showed no reduction in ATP production with 6-OHDA toxicity suggesting that the mechanism of 6-OHDA toxicity may include but no necessarily require complex I inhibition (Storch et al., 2000, Blum et al., 2001). Interestingly, dopamine is also able to oxidise compounds and therefore produce ROS and thus cause toxicity in cultured neurons (Michel and Hefti, 1990). Dopamine toxicity may therefore be one of the reasons for the specificity of dopaminergic cell loss in PD and may lower the threshold for oxidative damage caused by 6-OHDA.

Importantly 6-OHDA has also been shown to induce ER stress (Ryu et al., 2002). In this study PC-12 cells were exposed to 6-OHDA for up to 8 h and it was discovered that IRE1α, PERK and eIF2α were phosphorylated indicating activation of the UPR. Many ER stress regulated genes were also shown to be upregulated after 6-OHDA exposure. Other studies have also reported UPR activation with 6-OHDA (Hu et al., 2014, Holtz and O'Malley, 2003) However, *XBP1* splicing, which is indicative of fully activated IRE1α, has so far not been fully characterised in 6-OHDA treated cells.

1.6.3.3 Other PD mimetic drugs

Another drug which causes Parkinsonism is paraquat. Paraquat is structurally similar to MPP^+ and thus is believed to act via a similar mechanism. Paraquat has been used as a herbicide giving weight to the environmental toxin hypothesis, which claims exogenous toxins are the cause of neurodegeneration in PD (Dauer and Przedborski, 2003). Further evidence to support the environmental hypothesis is the fact that the mitochondrial poison rotenone, which also causes Parkinsonism, has been used as an insecticide (Moore et al., 2005). Although paraquat is thought to cause PD through mechanisms similar to MPP^+, such as damage to mitochondrial complex I, it has also been shown to induce ER stress and subsequent ER stress-induced dopaminergic cell death (Chinta et al., 2008). It is not fully understood how paraquat triggers ER stress but the Chinta *et al*. study also reported inhibition of the proteasome which is known to induce ER stress (Nishitoh et al., 2002).

1.6.3.4 Summary

PD mimetic drugs therefore impair respiration and energy metabolism whilst causing oxidative stress and the formation of protein aggregates leading to neuronal death. Importantly, in the context of this thesis, PD mimetic drugs have also both been shown to cause ER stress and activate the UPR (Ryu et al., 2002, Holtz and O'Malley, 2003, Holtz et

al., 2006). The PD mimetic drugs paraquat, MPTP and rotenone all cause neuronal death and the formation of Lewy body-like protein aggregates (Forno et al., 1988, Manning-Bog et al., 2002, McCormack et al., 2002, Betarbet et al., 2000, Sherer et al., 2003b). As protein aggregates can cause ER stress these neurotoxins may induce ER stress through this mechanism and/or other mechanisms including oxidative stress.

1.6.4 Oxidative stress, ER stress and mitochondrial stress

It is difficult to discuss PD without mentioning mitochondria. The fact that PD mimetic drugs cause PD like symptoms via inhibiting complex I suggest a role for mitochondrial dysfunction in PD. Interestingly, some studies have shown that complex I function has been compromised in the course of PD suggesting that PD mimetic drugs could be inducing neuronal death via similar mechanisms in human PD (Parker et al., 1989, Schapira et al., 1990, Krige et al., 1992). Mitochondria are a major source of ROS, which is a by-product of the electron transport chain during respiration. Mitochondria can be signalled to produce further ROS by the cytokine TNF-α (Fernandez-Checa et al., 1997). Mitochondria are therefore of particular research interest in PD due to their potential to cause oxidative stress. Oxidative stress is defined by the accumulation of ROS because there is either a reduced antioxidant capacity or an increased ROS production (Tansey et al., 2007).

Dopaminergic neurons may be particularly sensitive to ROS as they contain high levels of oxidisable content such as dopamine (Tansey et al., 2007). Oxidatively modified α-synuclein more readily aggregates than the unmodified form so ROS may have some role in the formation of Lewy bodies (Giasson et al., 2000). ROS production in dopaminergic neurons may be a product of more than one mechanism including; ER stress, mitochondrial dysfunction, inflammation and microglial activation.

In the past mitochondria and ER have been considered to be two distinct organelles and have rarely been studied in parallel (Paschen, 2003a). However, views have changed as more and more evidence suggests a close physical and biochemical interaction of signalling between these two organelles. For example it has been shown that cells are more susceptible to initiation of the UPR when mitochondrial function is altered (Arduino et al., 2009). Both the ER and mitochondria are capable of initiating apoptosis and it seems an apoptotic crosstalk is involved.

A study by Häcki and co-workers found that ER-stress caused by treatment with the ER stressor tunicamycin resulted in the release of cytochrome *c* from the mitochondria and the subsequent activation of caspase 3. Interestingly, over-expression of a Bcl-2 chimera which has had its C- terminus exchanged with that of cytochrome b5, and thus causes it to be targeted to the ER, was able to block cytochrome *c* release suggesting that the apoptotic cross-talk between mitochondria and the ER is blocked when ER stress is reduced (Hacki et al., 2000). Stress causes release of Ca^{2+} from the ER and Ca^{2+} uptake by mitochondria (Arduino et al., 2009). As protein folding in ER is calcium dependent calcium depletion causes a build-up of unfolded proteins, ER stress and inhibition of secretory and transmembrane protein synthesis (Paschen, 2003a, Kuznetsov et al., 1992, Lodish and Kong, 1990). Disulphide bond formation during protein folding is an oxidative process and produces ROS which can target calcium channels in the membrane of the ER resulting in the release of calcium from the ER (Zhang and Kaufman, 2008). It is believed that massive uptake of calcium into mitochondria causes neuronal cell death via production of ROS, and release of cytochrome *c* to signal apoptosis (Siesjo and Siesjo, 1996, Murphy et al., 1996). Production of ROS from the mitochondria can lead to further calcium release from the ER. However, it may also be the case that depletion of ER calcium stores is an initial cause of neuronal cell death (Paschen and Doutheil, 1999, Paschen, 2003b).

Overall mitochondrial dysfunction is strongly linked to PD mainly through the ability of mitochondria to produce ROS, yet ER stress may on its own, or in combination with mitochondrial stress, lead to the production of directly or indirectly via activation of inflammation and microglia (discussed later).

1.6.5 Inflammatory signalling in PD

There is some debate as to whether the UPR in PD is neuro-protective or if it actually contributes to the progress of neuronal death in the condition. Evidence of inflammatory signalling mediated by the UPR in dopaminergic neuronal cell death may give weight to the neurotoxic role of the UPR in PD. Indeed inflammatory signalling has been detected in PD. This next section will discuss the role of inflammation in PD.

Inflammation has been described as a ‘double-edged sword’ (Wyss-Coray and Mucke, 2002) and neuroinflammation is no exception. Short-lasting inflammation promotes healing and limits injury (Tansey et al., 2007), whilst prolonged neuroinflammation is

detrimental and has been implicated as a cause for diseases such as T2D and Alzheimer's disease (AD) (Wyss-Coray and Mucke, 2002). In the case of PD, inflammation is thought to be initiated by dopaminergic neurons (though this may not actually be the case) with the initial inflammatory trigger or triggers remaining unclear.

Two epidemiological studies have provided considerable evidence to suggest an important role for inflammation in PD (Chen et al., 2003, Chen et al., 2005). One study showed that a cohort consisting of chronic users of non-steroidal-anti-inflammatory drugs (NSAIDs) had 46% less PD incidences than a control cohort (Chen et al., 2003). The same group provided further evidence for an anti-inflammatory protective role in PD using a larger cohort who frequently used the anti-inflammatory drug- ibuprofen (Chen et al., 2005). Both ibuprofen (though non-specifically) and NSAIDs inhibit COX-2, a protein responsible for catalysing the production of inflammatory signalling prostaglandins. Hence, a reduction of inflammation, possibly via COX-2 inhibition, may protect against the development of PD.

Post mortem studies have also provided molecular evidence for neuroinflammation occurring in PD. The cytokines; IL-1B, TNF-α, and interferon (IFN)-γ were detected in the SNpc of PD patients in a study by Hunot and co-workers (Hunot et al., 1999). Interestingly dopaminergic neurons in the SNpc have receptors for TNF-α, whilst the level of TNF receptor R1 is elevated in PD patients (Boka et al., 1994). It therefore seems likely that dopaminergic neurons are particularly sensitive to cytokines such as TNF-α. Neuroinflammation in the SNpc and sensitivity to inflammation and inflammatory-mediated ROS may explain the selective loss of dopaminergic neurons from the SNpc. Thus identification of events triggering or progressing inflammation may hold the key to understanding and treating PD.

Although the inflammatory triggers are unclear there is evidence that protein aggregates cause neuroinflammation in PD. Protein aggregates containing Pael receptor, which is a substrate of Parkin, have been found in patients with a recessive form of PD and aggregates have been shown to cause inflammation (Kubota et al., 2006, Su et al., 2008). α-synuclein overexpression, which causes the formation of protein aggregates induces expression of the inflammatory signalling molecules IL-1β, iNOS, IL-6, COX-2 and TNF-α (Su et al., 2008). In fact, over-expression of α-synuclein in mice leads to activation of microglia (Su et al., 2008). How protein aggregates actually cause inflammatory signalling is not currently known, but the answer may involve the UPR (discussed later). Before

exploring the evidence linking the UPR and inflammation in PD it is important to describe microglia, which are heavily involved in neuroinflammation.

1.6.5.1 Microglia

Inflammatory signalling, from damaged cells of the central nervous system, initially recruits the innate immune response, which includes microglia and astrocytes (Wyss-Coray and Mucke, 2002, Mennicken et al., 1999, Eddleston and Mucke, 1993). Microglia are the resident macrophages of the central nervous system (Wyss-Coray and Mucke, 2002). Resting microglia show little phagocytic activity but once activated the level of macrophage-like activity is high (Kreutzberg, 1996, Liu and Hong, 2003). Macrophage-like microglia have increased cell surface receptors and they also increase the production of inflammatory mediators such as ROS and NO, which can directly damage neurons (Liu and Hong, 2003).

Activated microglia have also been shown to release proinflammatory cytokines such as TNF-α, IL-1, IL-6, IFNγ and FasL (Touzani et al., 1999, Martin-Villalba et al., 1999, Barone et al., 1997, Hanisch, 2002). Microglia-mediated cytokine production may further exasperate inflammation through activation of astrocytes. Activated astrocytes can also function as sources of neurotoxic and proinflammatory cytokine production (IL-1, IL-6, TNF-α) as well as producing ROS and NO (Stoll et al., 1998). Thus a combination of proinflammatory mediators, released from microglia, can promote activation of astrocytes and vice versa whilst activation of both of these cell types induces release of neuron-damaging compounds.

Microglia activation may have even stronger implication in the SN compared to other regions of the brain because the SN is particularly rich in microglia to begin with (Kim et al., 2000, Lawson et al., 1990). LPS treatment, for example, causes activation of microglia and then specific loss of dopaminergic neurons (Gao et al., 2002a). Therefore dopaminergic neurons are particularly sensitive to microglia and this may explain how neuroinflammation in PD leads to the specific loss of mainly dopaminergic neurons. For this reason toxicity inducing activation of inflammatory signalling in cells other than dopaminergic neurons may suffice to activate microglia which in turn leads to the damage and death of dopaminergic neurons specifically. This possibly adds to the complications in

understanding dopaminergic neuronal loss in PD as the initial trigger/s may occur in other cell types.

Neuroinflammation was strongly implicated in PD in 1988 with the discovery that activated microglia were present in the SNpc in post mortem tissue from PD patients (McGeer et al., 1988). Other studies have confirmed these findings yet the role of microglia in PD is still not fully understood. PD models have also provided evidence of microglia involvement. MPTP treatment in monkeys leads to microglia activation which in fact preceded neuronal degeneration (McGeer et al., 2003, Barcia et al., 2004). In animal models the use of 6-OHDA caused microglial activation believed to contribute to the neurodegeneration in these models (Virgone-Carlotta et al. 2013). Rotenone treatment which causes parkinsonism also activates microglia in a rat model of PD (Sherer et al., 2003a).

Activated glial cells produce ROS including; NO, superoxide (O_2^-), hydrogen peroxide (H_2O_2), hydroxyl radicals (OH^-) and peroxynitrite ($ONOO^-$). All of these cause oxidative stress to the target cell and are therefore neurotoxic. Glial cells also produce neurotrophic factors to encourage the survival of neurons (Tansey et al., 2007). As with most biological systems maintaining homeostasis is important but if inflammation continues to persist then microglia may actually aid progression of neuronal degeneration by producing, once beneficial, proinflammatory molecules to such an extent that they ultimately damage neurons and induce further inflammation.

1.6.5.2 UPR and inflammatory signalling in PD

As previously discussed, the UPR is activated in PD. The UPR is also capable of activating inflammatory signalling as shown by the activation of the transcription factor NF-κB and the protein kinases JNK, p38 and IKK with ER stress (Urano et al., 2000, Hu et al., 2006b). It is possible that activation of the UPR, through a variety of mechanisms, is leading to the activation of inflammatory signalling molecules previously detected in PD neurons. In support of this idea, PD mimetic drugs 6-OHDA, paraquat, rotenone and MPP^+ activate the UPR-inducible inflammatory signalling molecules NF-κB and JNK (Ghribi et al., 2003, Boyd et al., 2007, Klintworth et al., 2007, Ouyang and Shen, 2006). As previously mentioned, PD mimetic drugs have been shown to activate UPR signalling. α-synuclein and mutations in other proteins implicated in PD lead to both ER stress and inflammation

yet the link between these two phenotypes has not been studied or reported. Linking all these well studied areas the following events are imaginable: 1) various mechanisms activate the UPR in neurons. 2) The UPR activates inflammatory signalling. 3) Neurons communicate with and activate microglia. 4) Activated microglia cause inflammation and cellular damage. 5) Cycles of cell damage, inflammation and further microglial activation lead to neuronal loss and the development of PD (Figure 1.8).

Further research into the ability of the UPR to initiate inflammatory signalling in dopaminergic neurons may provide some insight into this complex disease. It seems likely that UPR signalling is central to many pathways, which contribute to the death of dopaminergic neurons in PD. If this is true then targeting the UPR may yield the development of drugs, which may slow or even stop the neuronal degeneration in PD and other neurodegenerative diseases.

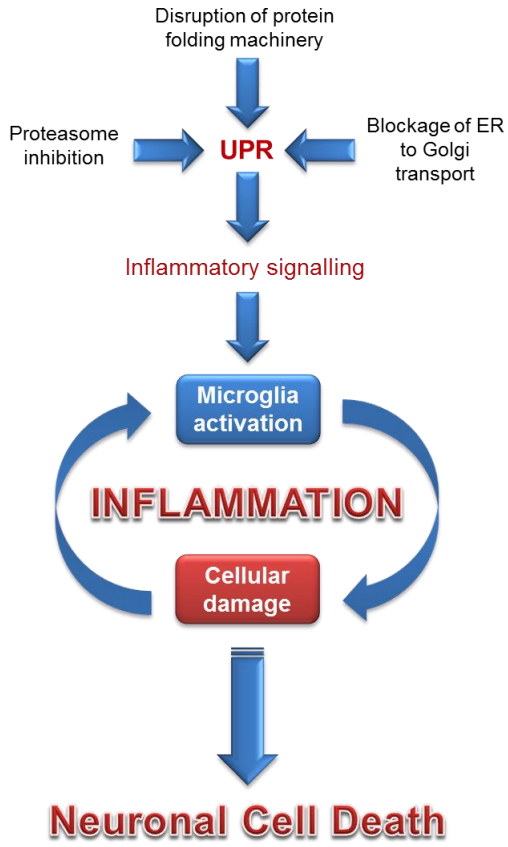

Figure 1.8. Hypothesis of how activation of UPR causes inflammation and neuronal cell death in PD.

The following series of events are proposed: 1) various mechanisms activate the UPR in neurons. 2) The UPR activates inflammatory signalling. 3) Neurons communicate with and activate microglia. 4) Activated microglia cause inflammation and cellular damage. 5) Cycles of cell damage, inflammation and further microglial activation lead to neuronal loss and the development of PD

1.6.6 Insulin signalling in PD

Insulin signalling in the brain is accepted as an important part of healthy neuronal activity (Nistico et al., 2012). Brain insulin has been proposed to promote neuronal survival during nervous system development (Recio-Pinto et al., 1986), induce neuronal protein synthesis (Schulingkamp et al., 2000), improve neurite outgrowth (Recio-Pinto et al., 1986, Song et al., 2003), increase synaptic activity and memory (Kremerskothen et al., 2002, Benedict et al., 2004) as well as increasing neuroprotection (Dudek et al., 1997, Tanaka et al., 1995). It is therefore evident that insulin has very important roles in the brain.

Increasing evidence is linking T2D and problems with insulin signalling in the brains of patients with PD. The prevalence of diabetes in patients with PD (8-30%) is in excess of the prevalence in non-PD individuals (Chalmanov and Vurbanova, 1987, Pressley et al., 2003). In a study of 800 patients with PD it was observed that those with diabetes also had accelerated progression of motor and cognitive symptoms (Schwab, 1960). In a study of Finnish males and females it was identified that both T2D (Hu et al., 2007) and excess weight (Hu et al., 2006a) were associated with an increased risk of developing PD. However, a more recent study has been unable to observe this link between T2D and PD (Palacios et al., 2011). The difference between the two studies may be due to the latter study relying of diagnosis of T2D being based on self-reporting. Nevertheless, most studies suggest that there is a link between PD and T2D. Treatment of PD may have an effect on insulin signalling (Van Woert and Mueller, 1971, Sirtori et al., 1972) and therefore may underlie the link between diabetes and PD. However, adults who have been newly diagnosed with PD and have therefore had no treatment also have increased insulin resistance (Van Woert and Mueller, 1971, Boyd et al., 1971), which suggests that the link is not dependent on medications to treat PD.

Dopaminergic neurons of the SNpc express a high level of insulin receptors (Unger et al., 1991), yet insulin receptor immunoreactivity is lost in PD (Moroo et al., 1994). Interestingly, loss of insulin receptors coincides with loss of tyrosine hydroxylase (Moroo et al., 1994). Loss of insulin receptors and insulin signalling should lead to problems with glucose utilisation. Indeed abnormal glucose utilisation in the brains of PD patients has been observed (Bowen et al., 1995, Hu et al., 2000). It was reported that in the dorsal root ganglion (DRG) of obese mice there is lower insulin receptor expression (Grote et al., 2013). Also, DRG tissue from *ob/ob* mice was less responsive to insulin (lower AKT phosphorylation) suggesting that obesity can affect insulin signalling in the brain through

reduced expression of the insulin receptor and may in part explain the links between excess weight (Hu et al., 2006a) and T2D (Hu et al., 2007) with PD.

There is evidence providing a strong link between glucose utilisation and dopamine signalling. Raising the blood glucose levels in rats supresses the firing of dopamine-containing neurons in the SNpc (Saller and Chiodo, 1980). Injecting glucose into rats also decreases the dopamine turnover in the striatum (Montefusco et al., 1983). Another study proving evidence for glucose affecting dopamine signalling showed that hyperglycaemia produced in a rat model of T1D decreases dopamine concentrations (Murzi et al., 1996). These studies further contribute to evidence linking PD with metabolic changes.

The use of PD mimetic drugs has provided further evidence linking perturbed insulin signalling in PD with ER stress is that the commonly used PD mimetic drug 6-OHDA, which causes ER stress (Ryu et al., 2002) (Figure 4.4.14) reduces insulin signalling in rat brain (Morris et al., 2008). A study by Wang *et al*. involving MPTP exposure in diabetic and obese mice also contributes to the PD and insulin resistance link. Dopamine neurons in two different mouse models of T2D (*ob/ob* and *db/db)* are more vulnerable to MPTP (Wang et al., 2014). Insulin resistance in diabetic mice was observed in the midbrain as well as the liver. It was also found that α-synuclein expression was increased, and ER stress markers were detected, in both the pancreas and midbrain, which was accompanied by increased inflammation suggesting a link between insulin signalling and inflammation. Indeed, insulin signalling has a role in inhibiting the activity of the inflammatory signalling ASK1 protein. AKT can phosphorylate ASK1 at S83 which blocks the apoptotic stimulus-induced activation of ASK1 (Kim et al., 2001). Therefore, reduced insulin signalling in dopaminergic neurons or in nearby neurons may further sensitize neurons to develop inflammatory signalling and promote detrimental inflammation.

The molecular/mechanistic link between diabetes and PD is not known. Both inflammation and inhibited insulin signalling are reported to be potential contributors to both of these diseases. A recent review article has highlighted the growing evidence suggesting insulin signalling and inflammation link neurodegeneration in obesity (Spielman et al., 2014). As discussed ER stress has been implicated strongly in both these diseases as well as being involved in insulin signalling and inflammation. It could be possible that prolonged ER stress (both mimetic and natural) mimic or even contribute to other mechanisms that have been leading to a decrease in pro-survival AKT signalling in PD. Changes in DJ-1 can cause ER stress (Yokota et al., 2003), whilst AKT phosphorylation is inhibited in cells

overexpressing DJ-1 (Wang et al., 2013). Therefore ER stress is an interesting potential phenotype linking these two age-related diseases.

1.7 Aims

This thesis aims to investigate the link between ER stress and inflammatory signalling in the context of both T2D and PD. Firstly, the ability of acutely ER-stressed cells to activate inflammatory signalling and how this affects cell fate is reported in the first results chapter (Chapter 3). Secondly, it is investigated if this early, acute ER stress activated inflammatory signalling can lead to insulin resistance (Chapter 4). Thirdly, how prolonged ER stress can lead to insulin resistance through disruption of the secretory pathway is explored (Chapter 5). Finally, the role of ER stress in PD through activation of inflammation is investigated in the final section of the results chapter (Chapter 6).

2 MATERIALS AND METHODS

2.1 Materials

The following section lists all materials used for experimentation in this thesis. Solutions are prepared in type I laboratory H_2O (resistivity 18 MΩ cm, total organic carbon < 1 ppb, microorganisms < 1 cfu/ml, particles < 0.05 µm diameter) generated by the NANOpure Diamond UV/UF TOC water purification system and sterilized by autoclaving (121°C, 20 – 30 min). If this is not possible, solutions are prepared in autoclaved type I laboratory H_2O and then filter sterilized by filtration over a 0.22 µm filter.

2.1.1 Oligodeoxynucleotides

Table 2.1 Oligodeoxynucleotides for *Homo sapiens* genes

Name	Purpose	Sequence
H8197	*TRAF2* RT-qPCR for siRNA #3, reverse	AATGGCCTTGATGAAGATGG
H8280	*TRAF2* RT-qPCR for siRNA #1, forward	CTTAGCCAAGGGCTGTGGT
H8281	*TRAF2* RT-qPCR for siRNA #1, reverse	AGGAATGCTCCCTTCTCTCC
H8282	*TRAF2* RT-qPCR for siRNA #2, forward	GTCCGCCTTGGTGAAAAG
H8283	*TRAF2* RT-qPCR for siRNA #2, reverse	TCTCACCCTCTACCGTCTCG
H8284	*TRAF2* RT-qPCR for siRNA #3, forward	ACACCAGCAGGTACGGCTAC
H8285	*GAPDH* RT-qPCR, forward	TCACCAGGGCTGCTTTTAAC
H8286	*GAPDH* RT-qPCR, reverse	GGCAGAGATGATGACCCTTT
H8287	*ACTA1* RT-qPCR, forward	CTGAGCGTGGCTACTCCTTC
H8288	*ACTA1* RT-qPCR, reverse	GGCATACAGGTCCTTCCTGA
H8289	*XBP1* PCR, forward	GAGTTAAGACAGCGCTTGGG
H8290	*XBP1* PCR, reverse	ACTGGGTCCAAGTTGTCCAG
H8293	*IRE1*α RT-qPCR, forward	TGGGACAGCTAGGCTGAGAT
H8294	*IRE1*α RT-qPCR, reverse	TGGGCACATCTGTGATCAAT
H8835	*IL-8* RT-qPCR, forward	GGACAAGAGCCAGGAAGAAA
H8836	*IL-8* RT-qPCR, reverse	AGCTGCAGAAATCAGGAAGG
H8927	*IL-6* RT-qPCR, forward	TCTCCACAAGCGCCTTCG

H8928	*IL-6* RT-qPCR, reverse	CTCAGGGCTGAGATGCCG
H8933	*TNF-α* RT-qPCR, forward	CCTGCCCCAATCCCTTTATT
H8934	*TNF-α* RT-qPCR, reverse	CCCTAAGCCCCCAATTCTCT

Table 2.2 Oligodeoxynucleotides for *Mus musculus* genes.

Name	Purpose	Sequence
H7994	*ACTB* real time PCR, forward	AGCCATGTACGTAGCCATCC
H7995	*ACTB* real time PCR, reverse	CTCTCAGCTGTGGTGGTGAA
H8962	*TRB3* real time PCR, forward	TTTGGAACGAGAGCAAGGCA
H8963	*TRB3* real time PCR, reverse	CCACATGCTGGTGGGTAGG
H9044	*INSR* real time PCR, forward	CTTCTCTTCCGTGTCTATGG
H9045	*INSR* real time PCR, reverse	GACCATCTCGAAGATAACCA
H7961	*XBP1* PCR, forward	GATCCTGACGAGGTTCCAGA
H7962	*XBP1* PCR, reverse	ACAGGGTCCAACTTGTCCAG
H7994	*ACTB* PCR, forward	AGCCATGTACGTAGCCATCC
H7995	*ACTB* PCR, reverse	CTCTCAGCTGTGGTGGTGAA
H8237	*TRAF2* RT-qPCR for siRNA #1, forward	GAACTCATCTGTCTCTCTTCTTCG
H8238	*TRAF2* RT-qPCR for siRNA #1, reverse	AGCAGGGGTGGCTAGAGTCC
H8239	TRAF2 RT-qPCR for siRNA #2, forward	CTGCAGAGCACCCTGTAGC
H824	*TRAF2* RT-qPCR for siRNA #2, reverse	CCTGCAGGTTCTCAGTCTCC

0		
H8269	*TRAF2* RT-qPCR for siRNA #3, forward	ACTGCTCCTTCTGCCTGACC
H8270	*TRAF2* RT-qPCR for siRNA #3, reverse	TTCTTTCAAGGTCCCCTTCC
H8271	*GAPDH* RT-qPCR, forward	TCGTCCCGTAGACAAAATGG
H8272	*GAPDH* RT-qPCR, reverse	CTCCTGGAAGATGGTGATGG
H9054	*cIAP1* (*BIRC2*) RT-qPCR, forward	TAGTGTTCCTGTTCAGCCCG
H9055	*cIAP1* (*BIRC2*) RT-qPCR, reverse	TCCCAACATCTCAAGCCACC
H9056	*cIAP2* (*BIRC3*) RT-qPCR, forward	ACGATTTAAAGGTATCGCGCC
H9057	*cIAP2* (*BIRC3*) RT-qPCR, reverse	CTGATACCGCAGCCCACTTC
H9076	*XIAP* (*BIRC4*) RT-qPCR, forward	ACGGAGGATGAGTCAAGTCAAA
H9077	*XIAP* (*BIRC4*) RT-qPCR, reverse	AAGTGACCAGATGTCCACAAGG
H9080	*BRUCE* (*BIRC6*) RT-qPCR, forward	CCAGTGTGAGGAGTGGATTGC
H9081	*BRUCE* (*BIRC6*) RT-qPCR, reverse	CCTCAATGTCCGGATCTAAGCC
H8756	*IL-6* RT-qPCR, forward	ACAACCACGGCCTTCCCTAC
H8757	*IL-6* RT-qPCR, reverse	ACAGGTCTGTTGGGAGTGGT
H8752	*IL-1β* RT-qPCR, forward	TGCTGGTGTGTGACGTTCCC
H8753	*IL-1β* RT-qPCR, reverse	GTCCGACAGCACGAGGCTTT
H887	*TNF-α* RT-qPCR, forward	AGCCGATGGGTTGTACCTTG

7		
H8878	*TNF-α* RT-qPCR, reverse	ATAGCAAATCGGCTGACGGT

Table 2.3 siRNAs.

Species	*Gene*	#	Sequence
H. sapiens	*IRE1α*	1	GCGUAAAUUCAGGACCUAUdTdT
H. sapiens	*IRE1α*	2	GAUAGUCUCUGCCCAUCAAdTdT
H. sapiens	*IRE1α*	3	CAUUGCACGUGAAUUGAUAdTdT
H. sapiens	*TRAF2*	1	CACUCAGAGUGGGAGCACAdTdT
H. sapiens	*TRAF2*	2	GUCAAGACUUGUGGCAAGUdTdT
H. sapiens	*TRAF2*	3	GCCUUCAGGCCCGACGUGAdTdT
M. musculus	*TRAF2*	1	GAAUUCCUAUGUGCGGGAUdTdT
M. musculus	*TRAF2*	2	GUUAGAGCAUGCAGCAAAUdTdT
M. musculus	*TRAF2*	3	CTATGAAGGCCTGTATGAAdTdT
M. musculus	*INSR*	1	GAGAUCUCCUGGGAUUCAUdTdT
M. musculus	*INSR*	2	CCUUAUCAAGGCCUGUCUAdTdT
M. musculus	*INSR*	3	GAAACUCUGCUUGUCUGAAdTdT
Aequora victoria	*eGFP*		GCAAGCUGACCCUGAAGUUCAU

2.1.2 Antibodies

Table 2.4 Antibodies for Western blotting

Name	Primary / secondary	Host	Source	Product Number
anti-phospho-JNK	Primary	Rabbit	Cell Signaling, Danvers, MA, USA	4668
anti-JNK	Primary	Rabbit	Cell Signaling	9258
anti-phospho-p38	Primary	Rabbit	Cell Signaling	9215
anti-p38	Primary	Rabbit	Cell Signaling	9212
anti-phospho-S51-eIF2α	Primary	Rabbit	Cell Signaling	9721
anti-eIF2α	Primary	Rabbit	Santa Cruz Biotechnology, Santa Cruz, CA, USA	SC-11386
anti-phospho-T308-AKT	Primary	Rabbit	Cell Signaling	4056
anti-phospho-S473-AKT	Primary	Rabbit	Cell Signaling	4060
anti-AKT	Primary	Rabbit	Cell Signaling	4691
anti-phospho-S21/9-GSK3α/β	Primary	Rabbit	Cell Signaling	9331
anti-GSK3α/β	Primary	Rabbit	Cell Signaling	5676
anti-IκBα	Primary	Rabbit	Cell Signaling	9242
anti-CD200	Primary	Rabbit	Sigma-Aldrich, Gillingham, UK	HPA031149
anti-IRS1	Primary	Rabbit	Cell Signaling	3407
anti-tyrosine hydroxylase	Primary	Rabbit	Merk Millipore, Nottingham, UK	AB152
anti-insulin receptor β chain	Primary	Rabbit	Santa Cruz Biotechnology	sc-711
anti-IGF-I receptor	Primary	Rabbit	Cell Signaling	3018

anti-rabbit IgG, HRP	Secondary	Rabbit	Cell Signaling	7074
Goat-anti-mouse	Secondary	Goat	Thermo Fisher Scientific, Loughborough, UK	31432
anti-GAPDH	Primary	Mouse	Sigma-Aldrich	G8795

2.1.3 Cell lines

Table 2.5 Mammalian cell lines

Name	Obtained from	Reference
ire1α$^{-/-}$ mouse embryonic fibroblast (MEF)	R. J. Kaufman, Sanford Burnham Medical Research Institute, La Jolla, CA, USA	(Lee et al., 2002)
traf2$^{-/-}$ MEF	T. Mak University of Toronto, Ontario Cancer Institute, Toronto, Ontario, Canada	(Yeh et al., 1997)
traf2$^{+/+}$ MEF	T. Mak University of Toronto, Ontario Cancer Institute, Toronto, Ontario, Canada	(Yeh et al., 1997)
jnk1$^{-/-}$ *jnk2*$^{-/-}$ MEF	R. Davis University of Massachusetts, Worchester, MA, USA	(Tournier et al., 2000)
WT MEF	R. J. Kaufman, Sanford Burnham Medical Research Institute, La Jolla, CA, USA	(Lee et al., 2002)
$C_2C_{12.}$ Mouse myoblast	R. Bashir, Durham University	(Blau et al., 1985)

Hep G2. Human hepatocyte carcinoma	A. Benham, Durham University	(Knowles et al., 1980)
3T3-F442A. Murine fibroblast	C. Hutchinson, Durham University	(Green and Kehinde, 1976)
Fao rat hepatoma	Public Health England, Salisbury, UK	(Deschatrette and Weiss, 1974)
N1E-115. Murine neuroblastoma	P. Chazot, Durham University	(Amano et al., 1972)
CAD (cath. a-differentiated). Murine (B6/D2 F1 hybrid) catecholaminergic neuronal tumour	P. Chazot, Durham University	(Suri et al., 1993)
SH-SY5Y. Human neuroblastoma	Public Health England, Salisbury, UK	(Ross et al., 1983)
PC-12. Rat adrenal phaeochromocytoma	Public Health England, Salisbury, UK	(Greene and Tischler, 1976)
HEK 293. Human embryonic kidney	M. Cann, Durham University	(Graham et al., 1977)
Flp-In T-Rex 293	Life Technologies, Paisley, UK	

2.1.4 Cell culture reagents

Table 2.6 Reagents used for tissue culture

Name	Supplier	Product number
Minimal essential medium	Sigma Aldrich	M2279

Dulbecco's modified Eagle's medium with pyruvate	Sigma Aldrich	D6546
Dulbecco's modified Eagle's medium without pyruvate	Sigma Aldrich	D5671
Roswell Park Memorial Institute (RPMI) 1640	Sigma Aldrich	R0883
DMEM/F-12	Life Technologies Ltd	12634-010
Neurobasal medium	Life Technologies Ltd	21103-049
Coon's modification of Ham's F12 medium	Sigma Aldrich	F6636
Fetal bovine serum	Biosera, Boussens, France	S1830
200 mM L-Glutamine solution	Sigma Aldrich	G7513
all-*trans*-retinoic acid	Sigma Aldrich	R2625
12-*O*-tetradecanoyl-phorbol-13-acetate (TPA)	Sigma Aldrich	P8139
Nerve growth factor-7S	Sigma Aldrich	N0513
B-27 supplement	Life Technologies Ltd	17504-044
Poly-L-ornithine	Sigma Aldrich	P4957
Collagen	Sigma Aldrich	C8897
Poly-L-lysine	Sigma Aldrich	P4707
Penicillin (10000 U/ml)/streptomycin(10 mg/ml)	Sigma Aldrich	P4333

Insulin (10 mg/ml) recombinant from bovine pancreas	Sigma Aldrich	I9278
6-OHDA	Sigma Aldrich	H4381
MPP^+ iodide	Sigma Aldrich	D048
Tunicamycin	Merk Millipore, Nottingham, UK	654380
Thapsigargin	Apollo Scientific, Stockport, UK	BIT4520
Dexamethasone	Sigma Aldrich	D4902
3-Isobutyl-1-methylxanthine (IBMX)	Sigma Aldrich	I5879
Trypan blue solution 0.4% (w/v) in 0.81% sodium chloride and 0.06% potassium phosphate.	Sigma Aldrich	T8154
Trypsin 0.25% (w/v)	Life Technologies Ltd	25200-056

2.1.5 Reagents

Table 2.7 Reagents

Name	Product Number	Company
5x First strand buffer	Y02321	Thermo Fisher Scientific
5x green GoTaq Flexi buffer	M891A	Promega
Acetic acid (HOAc)	A/0360/PB17	Thermo Fisher Scientific
Agarose	MB1200	Melford, Ipswich, UK
Ampicillin	BIA0104	Apollo Scientific,

		Stockport, UK
β-Mercaptoethanol	M-6250	Sigma-Aldrich
Bovine serum albumin	A2153-50G	Sigma-Aldrich
Bromophenol blue	11439	Sigma-Aldrich
CellMask deep red	C10046	Thermo Fisher Scientific
Complete mini protease inhibitors	11836 153 001	Roche
Deoxyadenosine triphosphate (dATP)	R0141	Thermo Fisher Scientific
Deoxycytidine triphosphate (dCTP)	R0151	Thermo Fisher Scientific
Diethylpyrocarbonate (DEPC)	A0300574	Acros Organics, Geel, Belgium
D-Glucose	G/0500/61	Thermo Fisher Scientific
Deoxyguanosine triphosphate (dGTP)	R0161	Thermo Fisher Scientific
Dimethyl sulfoxide	D5879-100ML	Sigma-Aldrich
Dithiothreitol (DTT)	Y00147	Thermo Fisher Scientific
Thymidine triphosphate (dTTP)	R0171	Thermo Fisher Scientific
Ethylenediaminetetraacetic acid (EDTA)	D/0700/53	Thermo Fisher Scientific
Ethidium bromide	E1510-10ML	Sigma-Aldrich
Glycerol	G/0650/17	Thermo Fisher Scientific
Glycine	BP381-1	Thermo Fisher Scientific
GoTaq Hot Start Polymerase 5 u/µl	M5001	Promega
GoTaq G2 flexi polymerase 5 u/µl	M7801	Promega
Hygromycin B	40052	Merk Millipore
JC-1 dye (5,5′,6,6′-Tetrachloro-1,1′,3,3′-tetraethyl-imidacarbocyanine	T3168	Life technologies

iodide)		
LB-Agar LENNOX	LBX0202	Formedium, King's Lynn, UK
LB-Broth LENNOX	LBX0102	Formedium
Methanol	M/4000/PC17	Thermo Fisher Scientific
Magnesium chloride	A351H	Promega
N-(1-Naphthyl)ethylenediamine dihydrochloride (NEDD)	sc-203148	Santa Cruz Biotechnology
Oligo$(dT)_{15}$ 500 µg/ml	C1101	Promega
PhosSTOP	04906837001	Roche
Potassium hydroxide pellets	P/5600/53	Thermo Fisher Scientific
Propan-2-ol	P/7490/17	Thermo Fisher Scientific
RNasin Ribonuclease Inhibitor 20-40 u/µl	N22111	Promega
Sodium carbonate	71451	Sigma-Aldrich
Sodium chloride	S/3120/65	Thermo Fisher Scientific
Sodium deoxycholate	D6750	Sigma-Aldrich
Sodium dodecyl sulphate (SDS)	BPE116-500	Thermo Fisher Scientific
Sodium hydroxide	S/4920/53	Thermo Fisher Scientific
Sodium nitrite	237213	Sigma-Aldrich
Sulphanilamide	S9251	Sigma-Aldrich
Superscript III reverse transcriptase 200 u/µl	18080044	Thermo Fisher Scientific
SybrGreen	S7563	Life Technologies
Tauroursodeoxycholic acid (TUDCA)	580549	Merk Millipore
Tetracycline	87130	Sigma-Aldrich

Thapsigargin	586005	Merk Millipore
Tris(hydroxymethyl) methylamine (Tris)	T/3710/60	Thermo Fisher Scientific
Triton X-100	282103-5G	Sigma-Aldrich
Tunicamycin	645380	Merk Millipore
Tween20	P1379-500	Sigma-Aldrich

2.1.6 Special consumables

Table 2.8 Special consumables

Name	Product Number	Company
6-well plate, adherent	83.1839	Sarstedt, Nümbrecht, Germany
Polyvinylidene difluoride (PVDF) Transfer Membrane (0.45µm pore size)	RPN303F	GE Healthcare
CL-X Posure film	34091	Thermo Fisher Scientific
Tissue culture dish 58 cm^2 Adherent	83.1802	Sarstedt
Tissue culture flask 175 cm^2 Adherent	83.1812	Sarstedt
Tissue culture flask 75 cm^2 Adherent	83.1811	Sarstedt
Tissue culture flask 25 cm^2 Adherent	83.1810	Sarstedt
Tissue culture flask 175 cm^2 Suspension	83.1812.502	Sarstedt
Tissue culture flask 75 cm^2 Suspension	83.1811.502	Sarstedt
Tissue culture flask 25 cm^2 Suspension	83.1810.502	Sarstedt
Lumox dish	94.6077.333	Sarstedt
HiTrap Q Sepharose FF	17-5053-01	GE Healthcare
Amicon Ultra-15 centrifugal filter	UFC900308	Merck Millipore

2.1.7 Commercially available kits

Table 2.9 Commercially available kits and products

Name	Product Number	Company
Amersham ECL™ Western blotting detecting reagents	RPN2009	GE Healthcare, Buckinghamshire, UK
Criterion TGX™ precast gels 4-20%	567-1094/95	BIORAD, Hemel Hemstead, UK
DC™ Protein assay reagent A	500-0113	BIORAD
DC™ Protein assay reagent B	500-0114	BIORAD
DC™ Protein assay reagent S	500-0115	BIORAD
EZ-RNA kit (solution A and B)	K1-0120	Geneflow, Lichfield, UK
GeneRuler 1 kb DNA ladder	SM0311	Thermo Fisher Scientific
GeneRuler DNA ladder mix	SM0331	Thermo Fisher Scientific
GoTaq qPCR Master Mix	A6002	Promega, Southampton, UK
STAR phospho-IRS1 (Ser307 mouse/Ser312 271 human) ELISA	17-459	Merck Millipore
Human inflammatory cytokines multi-analyte ELISArray kit	MEH-004A	Qiagen, Hilden, Germany
Mouse inflammatory cytokines multi-analyte ELISArray kit	MEM-004A	Qiagen
jetPRIME	114-07	Polyplus transfection, Illkirch, France
PageRuler Plus prestained protein ladder	26619	Thermo Fisher Scientific
Pierce ECL Western blotting substrate	32209	Thermo Fisher Scientific
Pierce ECL Plus Western blotting	32132	Thermo Fisher

substrate		Scientific
Restore Western blot stripping buffer	21059	Thermo Fisher Scientific
RunBlue SDS precast gels 4-12% 10 cm x 10 cm	NXG41212/27	Expedeon, Swavesey, UK
Tetro cDNA synthesis kit	BIO-65042	Bioline, London, UK
GenElute High Performance (HP) Plasmid Maxiprep	NA0300	Sigma-Aldrich
Complete protease inhibitors	11836153001	Roche, Basel, Switzerland

2.1.8 Solutions for protein work

Table 2.10 Solutions for protein work

Solution	Protocol
Electrotransfer buffer	4.20 g $NaHCO_3$ 1.59 g Na_2CO_3 Add 5 l H_2O
RIPA Buffer	0.5 ml 1 M Tris·HCl pH 8.0 0.3 ml 5 M NaCl 0.1 ml Triton X-100 0.5 ml 10% (w/v) sodium deoxycholate 0.1 ml 10% (w/v) sodium dodecyl sulphate (SDS) Add H_2O to 10 ml Add protease/phosphatase inhibitor as required.
10x Semi-Dry Transfer Buffer	73.19 g Glycine 60.6 g Tris-Base Dissolve in ~350 ml H_2O Add DI H_2O to 500 ml
1x Semi-Dry Transfer Buffer	50 ml 10 x semi-Dry transfer buffer 25 ml Methanol Add DI H_2O to 500 ml

TBST	24.2 g Tris base 80g NaCl 1 ml Tween 20 Dissolve in ~800 ml pH ~ 7.6 Add H_2O to 1 l
6 x SDS-PAGE sample buffer	3.50 ml 1 M Tris·HCl 3.78 g glycerol 1.00 g SDS 500 µl 10 g/l bromophenol blue 200 µl β-mercaptoethanol Add H_2O to 10 ml
10 x SDS-PAGE running buffer	144.13 g glycine 30.03 g Tris 10.00 g SDS Add H_2O to ~ 900 ml, stir until completely dissolved, then add H_2O to 1 l.
Stripping solution	1g SDS 350 µl β-mercaptoethanol Dissolve in ~40 ml H_2O Add H_2O to 50 ml
TBST + 5% (w/v) skimmed milk powder	5 g milk powder Dissolve in 100 ml TBST
TBST + 5% (w/v) BSA	0.5 g BSA Dissolve in 10 ml TBST
Griess reagent	15 mg *N*-(1-Naphthyl)ethylenediamine dihydrochloride (NEDD) 150 mg sulphanilamide 7.5 ml acetic acid 22.5 ml H_2O

2.1.9 Solutions for DNA work

Table 2.11 Solutions for DNA work.

Solution	Protocol
2 mM dNTPs	910 µl H_2O 10 µl 100 mM Tris·HCl (pH 8.0) 20 µl 100 mM dATP 20 µl 100 mM dCTP 20 µl 100 mM dGTP 20 µl 100 mM dTTP
50x TAE	242 g Tris 57.1 ml HOAc 37.2 g $Na_2EDTA·2H_2O$ Dissolve in ~800 ml H_2O Add H_2O to 1 l pH ~ 8.5
10x TE (pH 8.0)	400 ml 1 M Tris·HCl (pH 8.0) 80 ml 0.5 M EDTA Add H_2O to 4 l Autoclave

2.1.10 Solutions for RNA work

Table 2.12 Solutions for RNA work

Solution	Protocol
DEPC-H_2O	1 mL DEPC 1 l sterile H_2O Autoclave.
2 mM dNTPs	910 µl DEPC treated water 10 µl 100 mM Tris·HCl (pH 8.0) in DEPC treated water. 20 µl 100 mM dATP 20 µl 100 mM dCTP 20 µl 100 mM dGTP

	20 µl 100 mM dTTP

2.1.11 *E. coli* strains

Table 2.13 *E. coli* strains

Name	Genotype	Source
XL-10 GOLD	TetrD(mcrA)183 D(mcrCB-hsdSMR-mrr)173 endA1 supE44 thi-1 recA1 gyrA96 relA1 lac Hte [F´ proAB lacIqZDM15 Tn10 (Tetr) Amy Camr]	Agilent Technologies, Stockport, UK, cat. no. 200314(Lee et al., 2002)
Competent XL-10 GOLD	TetrD(mcrA)183 D(mcrCB-hsdSMR-mrr)173 endA1 supE44 thi-1 recA1 gyrA96 relA1 lac Hte [F´ proAB lacIqZDM15 Tn10 (Tetr) Amy Camr])	(Yeh et al., 1997) This study

2.1.12 Plasmids

Table 2.14 Plasmids

Name	Origin/Derivation	Source
pEGFP-N2-hINSR	Encodes a fusion of the human insulin receptor to eGFP	Addgene, Cambridge, MA, USA, Addgene ID 22286(Lee et al., 2002)
pcDNA5/FRT/TO-FV2E-INSR	Generated by cloning the 1,430 bp BsiWI-XmaI fragment of	Cox and Schröder, unpublished(Yeh

	pCLFv2IRE into BsiWI- and XmaI-digested pcDNA5/FRT/TO-FV2E-C'hIRE1α	et al., 1997)
pcDNA5/FRT/TO-MyrFV2E-INSR	Generated by cloning the 501 bp EcoRI-XmaI fragment of pC4M-FV2E (Arial Pharmaceuticals, Cambridge, MA, USA) into HindIII- and XmaI-digested pcDNA5/FRT/TO-FV2E-INSR after blunting the EcoRI and HindIII sites with Klenow enzyme.	Cox and Schröder, unpublished
pmaxGFP		Lonza Cologne GmbH, Cologne, Germany

2.2 Methods

2.2.1 Mammalian cell culture

2.2.1.1 Reviving cells

Cryovials were stored primarily in a liquid nitrogen tank. Backup stocks of all cell lines were stored in a -150°C freezer. The growth medium required for the cell line to be revived was added to a 75 cm^2 flask and the flask was placed in a 37°C cell culture incubator to warm the medium to 37°C. The cryovial was removed from the liquid nitrogen tank and left to gently warm for 1 min before being defrosted by placing into a 37°C water bath. The cryovial was left only partly submerged so that the water level was not high enough to reach the thread and lid of the vial to prevent contamination. The cryovial was gently

swirled in the water bath to increase even thawing of the frozen cell culture. Once the majority of the vial contents had thawed the cryovial was sterilised with 70% (v/v) EtOH. Using a 2 ml serological pipette, in the tissue culture flow hood, the contents of the cryovial was pipetted into the pre-warmed 75 cm^2 culture flask. The flask was placed in the 37°C CO_2 incubator (RS Biotech, Galaxy R+, Model Number: 170-300 PLUS) overnight before the medium was changed and new fresh medium was added.

2.2.1.2 Cell splitting

Once cells had reached high confluency the culture was split. Medium was removed from the cells before adding enough PBS to easily cover the surface of the tissue culture vessel (~0.1 ml/cm^2), in the case of a 75 cm^2 flask 10 ml of PBS was used. The tissue culture vessel was then gently rocked before removal of the PBS. After the PBS wash step ~0.01 ml/cm^2 of trypsin was added to the cells, in the case of a 75 cm^2 flask 1 ml of trypsin was added. Once again the vessel was gently rocked for approximately 5 s, ensuring that the trypsin had covered the entire bottom surface of the vessel. The trypsin was then immediately removed before moving the tissue culture vessel to the 37°C CO_2 incubator for approximately 5 min. As confluency and cell line can affect how long trypsinisation takes to detach cells, the vessel was regularly checked during the incubation period in case it had to be removed early or left longer. Once the majority of the cells had detached fresh warm media was added to the vessel. The fresh media was then pipetted several times across the growth surface of the vessel to ensure complete detachment of as many cells as possible. Once the cells had been resuspended in fresh media this was added to new tissue culture flasks accordingly depending on the seeding confluency required. If required cells were counted using a cell haemocytometer (see 'cell counting').

2.2.1.3 Cryopreservation

Cells were grown to >70% confluency. Cells were trypsinised and processed in exactly the same way as in the cell splitting protocol (2.2.1.2). After the cells had been trypsinised freeze mix containing 90% (v/v) FBS, 10% (v/v) DMSO was added to the cells. The volume of freeze mix the cells were suspended in was dependent of flask size and confluency with 1 ml of freeze mix required for each new cryovial. A 70% confluent 75 cm^2 flask was resuspended in 4 ml of freeze mix. Cryovials were then added to either a Mr Frosty (Thermo Fisher Scientific, #5100-0001) or a CoolCell LX (Biocision, San Rafael, USA #BCS-405), which both slow freezing in a -80°C freezer to 1°C/min. The container

was then put into a -80°C freezer for approximately 24 h after which cryovials were transferred to either a liquid nitrogen tank or a -150°C freezer for long term storage.

2.2.1.4 Culture conditions

2.2.1.4.1 General culture conditions

All cells were grown at 37°C in an atmosphere of 95% (v/v) air, 5% (v/v) CO_2 and 95% humidity. Cells were not left to reach high confluency (>90%) during their maintenance. All cells were maintained without the use of antibiotics, except when a new cell line was obtained, in these instances new cell lines were maintained in penicillin/streptomycin until frozen stocks had been produced. All mammalian cell culture was performed in sterile conditions in a sterile tissue culture flow hood using 70% (v/v) EtOH to sterilise all equipment entering the tissue culture hood including gloves. All cell lines except PC-12 cells were grown in cell culture plastics for adherent cells. PC-12 cells were maintained in cell culture plastics for suspension cells.

2.2.1.4.2 Culture of MEF cells

ire1α$^{+/+}$, *traf2*$^{+/+}$, *traf2*$^{-/-}$, *jnk1*$^{-/-}$ *jnk2* $^{-/-}$, *jnk1*$^{+/+}$ *jnk2*$^{+/+}$ MEF cell lines were cultured in Dulbecco's Modified Eagle's Medium with 10% (v/v) foetal bovine serum and 2 mM L-glutamine added. The medium for *ire1α*$^{-/-}$ and corresponding WT MEFs was supplemented with 110 ng/ml pyruvate (Lee et al., 2002) and with 10% (v/v) foetal bovine serum and 2 mM L-glutamine added.

2.2.1.4.3 Culture of HEK293T, C_2C_{12}, 3T3-F4421 and N1E-115 cells

HEK293T, C_2C_{12}, 3T3-F4421 and N1E-115 cells were cultured in Dulbecco's Modified Eagle's Medium with 10% (v/v) foetal bovine serum and 2 mM L-glutamine added.

2.2.1.4.4 Stably transfected Flp-In T-Rex 293

Flp-In T-Rex 293 cells stably expressing a fusion of the F_V2E drug-inducible dimerisation domain (Clackson et al., 1998) with the β chain of the human insulin receptor were maintained in Dulbecco's Modified Eagle's Medium without, and with 10% (v/v) foetal bovine serum and 2 mM L-glutamine added. 24 h after revival, hygromycin and blasticidin·HCl were added to the flask to achieve final concentrations of 100 μg/ml and 10 μg/ml, respectively.

Expression of the F_V2E insulin receptor chimera was induced for 24 h with 1 μg/ml tetracycline, where indicated. The chimera was dimerised by treating cells with 100 nM AP20187 for the times indicated in the text.

2.2.1.4.5 Culture of HepG2 cells

HepG2 cells were cultured in Modified Eagle's Medium with 10% (v/v) foetal bovine serum and 2 mM L-glutamine added.

2.2.1.4.6 Culture of CAD cells

CAD cells were cultured in Dulbecco's Modified Eagle's Medium/F12 with 10% (v/v) foetal bovine serum and 2 mM L-glutamine added.

2.2.1.4.7 Culture of BV-2 cells

BV-2 cells were cultured in DMEM/F12 with 10% (v/v) foetal bovine serum and 2 mM L-glutamine added. BV-2 cells were maintained in cell culture plastics for adherent cells.

2.2.1.4.8 Culture of SH-SY5Y cells

SH-SY5Y cells were cultured in Dulbecco's Modified Eagle's Medium/F12 with 10% (v/v) foetal bovine serum and 2 mM L-glutamine added.

2.2.1.4.9 Culture of PC-12 cells

PC-12 cells were cultured in suspension in RPMI 1640, 2 mM L-glutamine, 10% (v/v) horse serum, and 5% FBS. PC-12 cells were maintained in untreated cell culture plastics for suspension cells.

2.2.1.4.10 Culture of Fao rat hepatoma cells

Fao rat hepatoma cells were cultured in either Coon's modification of Ham's F12 or RPMI-1640 with 10% (v/v) foetal bovine serum and 2 mM L-glutamine added. Rat Fao cells were maintained in cell culture plastics for adherent cells.

2.2.1.4.11 Primary cell culture

2.2.1.4.11.1Mechanical dissociation of cells

The Brain dissection from E14-E15 Swiss mouse embryos was kindly carried out by two members of Professor Marcus Rattray's laboratory (Bradford, UK). From this dissection I was provided with foetal mouse cortices.

A Pasteur pipette was smoothed using fire (reduction 1/3 of the pipette diameter) and then coated with sterile FBS. Cortices were placed in a 15 ml sterile centrifuge tube to which 5 ml PBS (Ca^{2+}, Mg^{2+} free)/33 mM Glucose (PBS/Glucose) was added. Cells were then dissociated by slowly and gently pipetting up and down (30-40 times). PBS/Glucose was added to a final volume of 12 ml. The tube was left for 5 min so that the non-dissociated elements formed a deposit (pellet). The supernatant was then aliquoted into 2 new 15 ml tubes with 6 ml in each. 1 tube was for neurons and the other for glial cells. The tubes were centrifuged at 200 g for 5 min at RT. The supernatant was aspirated carefully so that the pellet was not disturbed. Pellets were resuspended in 10 ml of glial or neuronal medium.

The day before culture of cells, culture dishes were coated with poly-ornithine at 15 μg/ml and incubated overnight in the tissue culture incubator. Before plating, the poly-ornithine was removed and the plates were washed twice with sterile water and then finally with sterile PBS.

For selection and maintenance of primary cortical neurons, the dissociated cells were seeded at a density of 1 x 10^6 cells/ml with 2 ml in each dish of a 6-well plate coated with poly-L-ornithine in Neurobasal medium, plus 2 mM L-glutamine and B-27 supplement. Media were changed 6 d after seeding. 50% of the media was removed and replaced with fresh media leaving a 1:1 ratio of conditioned:fresh media.

2.2.1.4.11.2Primary glia culture

For selection of primary glial cells, the dissociated primary cells were seeded at a density of 0.4 x 10^6 cells /ml with 2 ml in each dish of a 6-well plate. Primary cells were grown in DMEM:F12, 2 mM L-glutamine, 33 mM glucose, 13 mM sodium bicarbonate, and 10% (v/v) FBS. On d 6 and 10 after seeding, cells were washed in PBS/Glucose and the medium changed. During the PBS wash plates were gently knocked against the floor of the tissue culture hood to loosen neurons. During the media change only 50% of the conditioned

medium was removed and replaced with fresh medium leaving a 1:1 ratio of conditioned:fresh media.

2.2.1.5 Differentiation protocols

2.2.1.5.1 Differentiation of PC-12 cells

PC-12 cells were seeded at 2 x 10^3 cells per cm^2 on 8-10 µg/cm^2 collagen-coated plates in normal PC-12 culture medium. 24 h after seeding the medium was removed and replaced with fresh differentiation media consisting of normal culture media containing 50 ng/ml 7S NGF. NGF was made up in normal PC-12 culture medium and stored at -20°C. Differentiation medium was replaced every 2 d. Cells were treated and harvested on d 7.

2.2.1.5.2 Differentiation of C_2C_{12} cells

C_2C_{12} cells were differentiated in the following way. The media was removed from 60-70% confluent cultures and replaced with low mitogen medium consisting of DMEM containing 4.5 g/l D-glucose, 2% (v/v) horse serum, and 2 mM L-glutamine. Cells were incubated in this differentiation medium for a further 7-8 d with media being replaced every 2-3 d (Bains et al., 1984). Differentiation was assessed by microscopic inspection of cultures, staining of myotubes with rhodamine-labelled phalloidin (Amato et al., 1983) and RT-PCR to monitor *AHCY*, *MYL1* and *TNNC1* gene expression.

2.2.1.5.3 Differentiation of 3T3-F442A cells

Differentiation was induced by allowing 3T3-F442A preadipocytes to grow to confluency. 2 d post-confluency the medium was removed and fresh growth medium was added with the addition of 1 µg/ml insulin, 0.5 mM 1-methyl-3-isobutylxanthine, and 0.25 µM dexamethasone. After 3 d the medium was removed and replaced with fresh medium with the addition of only 1 µg/ml insulin this time. 2 d after the medium was replaced with normal growth medium and the cells were incubated for a further 7 d (Rubin et al., 1978). Differentiation was assessed by Oil Red O staining (Hansen et al., 1999).

2.2.1.5.4 Differentiation of SH-SY5Y cells

SH-SY5Y cells were differentiated in several ways:

1. 10 µM all-*trans* retinoic acid (RA) for 3 d in normal growth medium, media was then removed and replaced with fresh 10 µM RA containing media for a further 3 d. RA was made up in DMSO and stored in brown tubes at -20 °C.
2. Normal growth medium and 20 µM all-trans retinoic acid. Cells were left without any media change for 6 d.
3. 10 µM RA for 3 d in growth medium containing 3% FBS, media removed and replaced with fresh 10 µM RA-containing medium for a further 3 d (Lopes et al., 2010, Cheung et al., 2009).
4. Growth medium containing 3% FBS and 20 µM all-trans retinoic acid. Cells were left without any media change for 6 d.
5. Cells grown in 10 µM RA for 3 d, media removed and replaced with fresh medium containing 80 nM 12-*O*-tetradecanoyl-phorbol-13-acetate (TPA) for another 3 d (Presgraves et al., 2004).

SH-SY5Y cells were seeded at 5% confluency on 8-10 µg/cm^2 collagen coated plates in normal culture medium. 24 hours after seeding media were removed and replaced with fresh differentiation media.

2.2.1.5.5 Differentiation of CAD cells

CAD cells were differentiated by seeding the cells at 5% confluency and then left for 24 h before removal of media and addition of fresh media without serum; Dulbecco's Modified Eagle's Medium/F12 with L-glutamine added. Media was changed every 3-4 d. Cells were harvested 10 d after first media change.

2.2.1.6 UV stimulation

Ultraviolet (UV) treatment was performed at 254 nm 24 J/m^2 using a Bio-Rad UV cross-linker. Medium was removed from cells and stored at room temperature. Cells were immediately transferred to the UV cross-linker for UV stimulation. After UV treatment the growth medium was added back to the cells before they were transferred to the tissue culture incubator for 30 min before harvesting of cell lysates.

2.2.1.7 Transfection of siRNAs

The INTERFERin siRNA transfection kit was used to perform siRNA transfection following the manufacturer's guidelines. Cells were seeded so that on the day of transfection they were between 60-80% confluent. Depending on the number of

transfections being performed a master mix of siRNA and serum-free medium was made consisting of siRNA to make a final concentration of 1 nM and 200 µl of serum-free medium per well of a 6-well tissue culture plate and mixed by pipetting up and down. Then 10 µl of INTERFERin reagent per well to be transfected was added to the master mix, vortexed for 10 s, spun down to collect all of the mix at the bottom of tube before being incubated at RT for 10 min. During the 10 min incubation the medium of the cells was replaced with fresh medium so that each well had 2 ml of fresh medium. After the incubation, an equal volume of transfection master mix was added to each well to be transfected. Separate master mixes were made for control plasmids. 4 h after transfection the medium was changed.

2.2.1.8 Transfection of plasmids

Plasmid transfections were performed using jetPRIME transfection kit in 6-well plates following the manufacturer's protocol. Cells were seeded so that on the day of transfection they were between 60-80% confluent. Depending on the number of transfections being performed a master mix of plasmid DNA and jetPRIME buffer was made consisting of 3 µg of plasmid DNA and 200 µl of jetPRIME buffer per well of a 6-well tissue culture. This mix was vortexed for 10 s before being spun down briefly to collect all the master mix in the bottom of the tube. For every well to be transfected 6 µl of jetPRIME reagent were added to the mix, vortexed for 10 s and then spun down briefly before being incubated for 10 min at room temperature. An equal volume of the master mix was then added to the wells to be transfected. Each well contained 2 ml of medium before the addition of the transfection mix. Separate master mixes were made for control plasmids. Transfection efficiencies were determined by transfection of 2 µg of pmaxGFP and detection of GFP-expressing cells with a Zeiss ApoTome fluorescence microscope. Transfection efficiencies were >80%. 24 h after transfection cells were analysed or time courses initiated, if not stated otherwise.

2.2.1.9 Induction of ER stress

ER stress was induced with 0.1 to 1 µM thapsigargin, 0.1 to 10 µg/ml tunicamycin, or 1 µg/ml subtilase cytotoxin AB (SubAB) or catalytically inactive $SubA_{A272}B$. SubAB and $SubA_{A272}B$ were purified as described before (Paton et al., 2004, Talbot et al., 2005).

2.2.1.10 Insulin Stimulation

Insulin stimulation was performed in the following way. Cells were serum starved for 18 h by removal of medium, washing once with PBS and addition of fresh warm medium lacking FBS. At the end of the 18 h serum starvation period insulin was added to the cells with a final concentration of 100 nM insulin, if not stated otherwise. The cells were exposed to insulin for 15 min before cells were lysed for RNA and protein extraction.

When cells were stressed for longer than 18 h they were serum-starved during the last 18 h of treatments with ER stressors. When cells were ER-stressed for shorter periods, the ER stressors were applied towards the end of the serum starvation, for example for the last 12 h of serum starvation in case of treatment with ER stressors for 12 h.

2.2.1.11 Microglia activation assay

Media from neurons were aspirated into 15 ml centrifuge tubes before being centrifuged. Medium was centrifuged at 13,000 g for 10 min at 4°C to pellet the cell debris. The supernatant was added to a fresh 15 ml centrifuge tube whilst the cell debris pellet was discarded. The supernatant was then either snap frozen in liquid nitrogen and stored at -80°C and then thawed or it was directly added used in the desalting process. HiTrap Q Sepharose FF columns were flushed with sterile PBS for 5 min at a drip rate of 5 ml/min. After flushing, 1.5 ml of sample was injected at 1 ml/min into the desalting column. 2 ml of sterile PBS was then ran through the column at 1 ml/min and collected. The column was then flushed for a further 5 min with PBS at 5 ml/min before being used again.

8 ml of PBS sample (originating from 6 ml of neuronal supernatant) from the HiTrap desalting step were concentrated to 500 µl using a 3,000 molecular weight cut-off filter by centrifugation at 4,000 g for 40 min at 4°C . As the starting volume of the samples was 6 ml then ~80 µl of the concentrated sample represented 1 ml of the original sample. Therefore 160 µl of concentrated desalted sample was added to each well containing glial cells meaning that microglia cell were exposed to a concentrated sample representing 2 ml of neuron-conditioned medium. Glial cells were incubated for a further 18 h before isolation of medium and protein lysates.

2.2.2 Molecular Biology

2.2.2.1 E. coli culture

2.2.2.1.1 Revival and Growth

LB broth was added to a 13 ml culture tube working close to the flame of a Bunsen burner. Ampicillin was added to sterile LB broth to a final concentration of 100 µg/ml. A single colony grown on an agar plate was selected using a sterile toothpick handled with a flame-sterilised pair of forceps. The toothpick was added to the 13 ml culture tube. The culture tube was then left to incubate at 37ºC overnight with shaking at 225 – 250 rpm. For growth of larger volumes a fresh saturated overnight culture was diluted 1:100 into an Erlenmeyer flask containing fresh LB-broth containing ampicillin.

2.2.2.1.2 Preparation of chemically competent *E. coli*

Preparation of chemically competent cells was performed as previously described (Chung and Miller, 1988, Chung et al., 1989).4 ml LB medium containing appropriate antibiotics was inoculated with a single colony from a fresh LB plate containing appropriate antibiotics. Cultures were grown overnight at 37°C and shaking at ~220 rpm. 1 ml of this starter culture was used to inoculate 100 ml LB medium. Cultures were grown to an A_{600} of ~0.5 at 37°C and shaking at ~220 rpm. Cultures were then incubated for 20 min on ice.

All subsequent steps were performed in a cold laboratory. All reagents and materials were chilled to 4°C.

The culture was split into four equal parts by transferring ~25 ml into four prechilled 40 ml centrifuge tubes by decanting. These were then centrifuged at 4,000 rpm for 10 min at 4°C. The supernatant was discarded. The tubes were inverted on a piece of adsorbent paper to remove traces of remaining liquid. 10 ml ice-cold 0.1 M $MgCl_2$ was added to each 40 ml centrifuge tube. The cells were completely resuspended by rolling on a roller mixer. It was made sure that all visible cell clumps had dissolved before proceeding. Cells were once again incubated on ice for 20 min followed by centrifugation at 4,000 rpm for 10 min at 4°C. Supernatant was poured off and to remove traces of liquid by the tubes were once again inverted onto adsorbent paper. Cells were washed 3 times with ice-cold 0.1 M $CaCl_2$. In each step cells were resuspended in 10 ml ice-cold 0.1 M $CaCl_2$ per 40 ml tube by rolling on a roller mixer. It was ensured that all visible cell clumps had dissolved before proceeding. Cells were incubated on ice for 30 min before centrifugation at 4,000 rpm for

10 min at 4°C. Once again supernatant was poured off and tubes inverted onto absorbent paper. Supernatant was poured off and 375 µl 0.1 M $CaCl_2$ + 15% (v/v) glycerol were added to the cell pellet in each centrifuge tube and cells resuspended by gently swirling the centrifuge tubes. It was ensured that all visible cell clumps had dissolved before proceeding. 50 µl aliquots of cells were dispensed into prechilled 1.5 ml microcentrifuge tubes using a prechilled 200 µl large orifice pipette tip. Cells were snap-frozen in liquid nitrogen before being stored at -80°C to be used as competent cells.

2.2.2.1.3 Transformation

1-5 µl solution containing the plasmid of interest or ligation mixture were added to 50 µl of competent cells. Cells were incubated on ice for 30 min. Cells were then heat-shocked for 42 s at 42°C in a water bath. After heat-shock cells were incubated on ice for 2 min. 1 ml LB medium was then added to the cell suspension and the cultures incubated for 1 h at 37°C with shaking at ~250 rpm. After incubation 100 µl of cell suspension was plated onto one LB agar plate containing appropriate antibiotics. Cells were harvested from the remaining ~900 µl by centrifugation at 12,000 g and RT for 30 s in a benchtop microcentrifuge and the supernatant aspirated. The cell pellet was then resuspended in ~100 µl LB medium and plated onto one LB agar plate containing 100 µg/ml ampicillin. Plates were incubated in a 37ºC incubator for 16 h. 5 µl 1 x TE (pH 8.0) was used as a negative control to determine if contamination of materials gives rise to undesired colonies.

2.2.2.1.4 Plasmid miniprep

Minipreps were performed as previously described (Birnboim and Doly, 1979). 1.5 ml of saturated overnight *E. coli* culture was transferred into a 1.5 ml microcentrifuge tube; the remainder of the culture was stored at 4°C. Cells were then collected by centrifugation for 1 min at 14,000 g, RT. The supernatant was aspirated leaving only the cell pellet. Tubes were centrifuged a second time for 1 min at 14,000 g, RT and the supernatant aspirated again to fully isolate cells from medium. 100 µl 50 mM D-Glucose, 25 mM Tris·HCl (pH 8.0), 10 mM EDTA were added to the cell pellet. The cells were resuspended by vortexing and pipetting up and down before being incubated for 5 min at RT. Then 200 µl 0.2 N NaOH, 1% (w/v) SDS were added following mixing by inverting tubes 4-6 times. The mixture was incubated on ice for 5 min before adding 150 µl ice-cold 5 M KOAc (pH 4.8). The contents of the tubes were mixed by inverting the tubes 4-6 times before being incubated on ice for a further 5 min. The tubes were centrifuged for 3 min at 14000 g at

4°C. The clear supernatant produced from centrifugation was carefully transferred to a new microcentrifuge tube taking care to not transfer any white precipitate. DNA was precipitated by adding 0.8 ml EtOH and mixing by inverting 2-3 times and incubating at RT for 2 min. The tubes were centrifuged for 1 min at 14000 g at RT before the supernatant was aspirated to leave the DNA pellet. 1 ml of 70% EtOH was then added to the DNA pellet and the tube centrifuged for 1 min at 14,000 g, RT. The supernatant was aspirated before a final centrifugation step for 10-15 s at 14,000 g, RT. All remaining liquid was pipetted out and the pellet left to air dry at RT. Once dry the DNA pellet was dissolved in 30 µl 1 x TE (pH 8.0), 0.3 mg/ml RNase A and stored at 4°C.

2.2.2.1.5 Plasmid Maxiprep

The GenElute High Performance (HP) Plasmid Maxiprep kit was used following the manufacturer's protocol with no changes being made.

2.2.2.2 RNA work

All RNA solutions were prepared with DEPC-treated H_2O and stored in RNase free vessels, which if were plastic were purchased as RNase free, whilst glass vessels were baked at 200 °C to eliminate RNases.

2.2.2.2.1 RNA isolation

RNA was extracted with EZ-RNA total RNA isolation kit. RNA isolation was only performed on cell grown in 6-well plates. Media was aspirated from cells and discarded. Cells were then carefully (as to not disturb cells) washed twice with ice-cold phosphate-buffered saline. Washed cells were then lysed in 500 µl of EZ-RNA solution A before being directly used or stored at -80°C. Samples were processed following the manufacturer's instructions with the exception that the isopropanol-precipitated nucleic acid was collected by centrifugation at 15000 x g for 30 min (contrasting from 12000 x g for 8 min, recommended in the manufacturer's protocol) and that the 75% EtOH wash was centrifuged at 12000 x g for 30 min (contrasting from 7500 x g for 5 min, recommended in the manufacturer's protocol). After the 75% EtOH wash and drying of the RNA pellet, 25 µl of DEPC-treated H_2O were added to the tube containing the pellet. The pellet was dissolved by playing the tube on a dry heat block at 55°C for 10 min.

2.2.2.2.2 RNA quantitation

Once dissolved in DEPC-treated H_2O (from the final stage of the RNA isolation protocol), the RNA was quantified using either a NanoDrop or SpectraMax spectrophotometer.

2.2.2.2.3 cDNA synthesis

RNA was reverse transcribed with oligo-dT primers (Promega) and Superscript III reverse transcriptase (Life Technologies).

RNA was reverse transcribed to cDNA using two different protocols.

1) cDNA was reverse transcribed from RNA using the First Strand cDNA Synthesis Kit (Invitrogen) The following reaction was set up:

   Reaction mix 1:

   1 µl of oligo$(dT)_{15}$

   11 µl of RNA/DEPC Water (up to 5 µg total RNA).

   1 µl of 100 mM RNA-safe dNTPs

   Reaction mixture 1 was heated to 65°C for 5 min and then cooled on ice to 4°C for 5 min. Reaction mixture 2 was then added to the cooled reaction mixture 1.

   Reaction mixture 2:

   4 µl 5x First Strand Buffer

   1 µl 0.1 M DTT

   1 µl RNasin

   1 µl of Superscript III reverse transcriptase

   This final reaction mixture was then incubated at 50°C for 50 min followed by inactivation at 85°C for 15 min.

2) cDNA was also reverse transcribed using a Tetro cDNA synthesis kit following the manufacturer's instructions.

2.2.2.3 DNA work

2.2.2.3.1 XBP1 splicing assay

Protocols for *XBP1* splicing assays have been described previously (Cox et al., 2011). After RT-PCR reactions for murine, human and rat *XBP1* the whole 50 µl reaction from the following sections were loaded into a well on a 2% (w/v) agarose gel containing 1 µg/ml ethidium bromide. DNA gel electrophoresis was performed at 100 V for 2 h. Bands were quantified using Image J software (Collins, 2007).

2.2.2.3.1.1 Touchdown RT-PCR for murine XBP1

The following reaction was set up:

10 µl 5x Promega GoTaq buffer

5 µl 2 mM dNTPs

0.5 µl Mouse forward primer (H7961) at 100 µM

0.5 µl Mouse reverse primer (H7962) at 100 µM

0.5 µl Promega GoTaq HotStart polymerase

3 µl 25 mM $MgCl_2$

5 µl cDNA reaction

Sterile H_2O added to 50 µl

For mouse *XBP1*, the following cycling parameters were used:

Initial denaturation	95.0°C	5 min	
Denaturation	94.0°C	30 s	
Annealing	72.0°C	30 s	x 22 cycles
Decrease annealing temperature by			

1.0°C in each cycle			
Extension	72.0°C	15 s	
Denaturation	94.0°C	30 s	
Annealing	50.0°C	30 s	x 35 cycles
Extension	72.0°C	15 s	
Final extension	72.0°C	7 min	
Hold	4.0°C	∞	

2.2.2.3.1.2 RT-PCR for human XBP1

The following reagents were added together:

10 µl 5x Promega GoTaq buffer

5 µl 2 mM dNTPs

0.5 µl Human forward primer (H8289) at 100 µM

0.5 µl Human reverse primer (H8290) at 100 µM

0.5 µl Promega GoTaq polymerase

3 µl 25mM $MgCl_2$

5 µl cDNA reaction

For human *XBP1* the following cycling parameters were used:

Initial denaturation	94.0°C	2 min	
Denaturation	94.0°C	1 min	
Annealing	59.0°C	1 min	x 35 cycles

Extension	72.0°C	30 s
Final extension	72.0°C	5 min
Hold	4.0°C	∞

2.2.2.3.2 Actin

2.2.2.3.2.1 RT-PCR for mouse and human actin

In a sterile, nuclease free PCR tube the following was added:

5.0 µl 5 x Green GoTaq flexi buffer

1.5 µl 25 mM $MgCl_2$

2.5 µl 2 mM dNTPs in 1 mM Tris·HCl, pH 8.0

2.5 µl 10 µM forward actin primer (human *ACTA1* H8287 and murine *ACTB* H7994)

2.5 µl 10 µM reverse actin primer (human *ACTA1* H8288 and murine *ACTB* H7995)

1.25 µl cDNA from above

0.25 µl 5 U/µl GoTaq hot start polymerase

Add H_2O to 25 µl.

The following cycling parameters were used:

Initial denaturation	98.0°C	2 min	
Denaturation	98.0°C	5 s	
Annealing	55.0°C	5 s	x 35 cycles
Extension	72.0°C	10 s	
Final extension	72.0°C	1 min	

Hold	4.0°C	∞

2.2.2.3.3 Gel electrophoresis

The agarose was then melted in a microwave oven at the highest power setting for 1 – 5 min with swirling every ~30 to 60 s to ensure even mixing and to avoid boiling over of the agarose solution. The agarose solution was left to cool down before addition of ethidium bromide to 0.5-1 µg/ml to the agarose solution and mixed by swirling. During the cooling of the gel the gel casting platform was sealed at both open ends using laboratory tape and the comb was inserted. The cooled, melted agarose was then poured into the gel caster, making sure that no bubbles are trapped underneath the combs and all bubbles on the surface of the agarose are removed before the gel sets. The gel was left to solidify at room temperature. After the gel had solidified, the laboratory tape was removed from the open ends of the gel caster. The gel casting platform containing the set gel was then placed in the electrophoresis tank.

0.5 µg/ml of ethidium bromide was then added to the remaining 1 x TAE to make the electrophoresis buffer. Sufficient electrophoresis buffer was then added the tank to cover the gel to a depth of about 1 mm (or just until the tops of the wells are submerged). Using a pipette, pre-prepared DNA samples were loaded into wells. An appropriate DNA molecular weight ladder was used to cover the range of the PCR products being investigated. The gel tank was assembled so that DNA will migrate toward the anode. The voltage was then set depending on the size of the gel and time required to run the gel. Separation was monitored by observing the migration of the dyes in the loading buffer. The DNA was visualized by placing the agarose gel onto a UV light source.

2.2.2.3.4 RT-qPCR

RT-qPCRs were run on a Rotorgene 3000 (Qiagen, Crawley, UK). Melt curves were monitored after each run to check for the amplification of a single product. Representative melt curves are shown in Appendix A. Amplicons were amplified with either a) 0.5 µl 5 U/µl GoTaq Flexi DNA polymerase, 2 mM $MgCl_2$, 200 µM dNTPs, and 1 µM of each primer with a 1:2,500 fold dilution of a SybrGreen stock solution or b) GoTaq qPCR Master Mix.

Using GoTaq polymerase: 2 min of denaturation at 95°C , then a subsequent 40 cycles of denaturation at 95°C for 30 s, annealing at 58°C for 30 s, primer extension at 72°C for 30 s.

Using the GoTaq Master mix: 2 min denaturation followed by 40 cycles of 95°C for 15 s, 60°C for 15 s, 72°C for 15 s for all primers except *ACTB*. Whereas denaturation was followed by 40 cycles of 95°C for 15 s, 60°C for 60 s for *ACTB*.

Fluorescence data were acquired during the annealing step for all primers. For *ACTB* data was acquired in the first 30 s of the 60°C step. To confirm amplification of only one PCR product the melting curves were recorded and analysed after every PCR run. Amplification efficiencies were between 0.6 and 0.8. These were calculated using the comparative quantitation analysis in the Rotor Gene Q software. C_T values were calculated and normalised to *GAPDH*, *ACTA1* or *ACTB* qPCR data as described by Pfaffl (Pfaffl 2001). Results represent the average and standard error of three technical repeats. These results were confirmed by at least one other biological replicate.

The murine *GAPDH* standard was used for normalising murine *ACHY*, *MYL1* and *TNNC*. The murine *ACTB* standard was used for normalising murine *BIRC6*, *CIAP1*, *CIAP2*, *TRAF2*, *XIAP*, *INSR*, *IL-6*, *TNFα* and *IL-1β*. The *GAPDH* standard was used for normalising human *IRE1α*, *IL-6*, *TNFα* and *IL-8*. The *ACTA1* standard was used for normalising human *TRAF2*.

2.2.2.4 Protein work

2.2.2.4.1 Western Blotting

2.2.2.4.1.1 Protein isolation

Media was aspirated from cells and discarded. Cells were then carefully (as to not disturb cells) washed three times with ice-cold phosphate-buffered saline (PBS). Washed cells were then lysed in RIPA buffer containing complete protease inhibitors and phosphatase inhibitors as described before (Cox et al., 2011). Protein lysates were centrifuged at 16,000 g for 10 min to remove cell debris.

2.2.2.4.1.2 Protein quantification

Protein concentrations were assessed using the DC Protein Assay following the manufacturer's instructions. Protein standards were created and added to the 96-well plate used for the protein assay. Protein standards were produced as follows:

BSA dissolved in H_2O. Adjusted to 2 mg/ml BSA and mixed well. Then a serial 1:2 dilution in 1.5 ml microcentrifuge tubes with H_2O was made to produce protein standards for a standard curve from a range of 2 to 0.0625 mg/ml. Each tube was mixed well by vortexing and pipetting up and down after each dilution step. BSA standards were subsequently stored at -20°C.

Following quantification protein samples were all diluted to the same concentration to be used in SDS-PAGE.

2.2.2.4.1.3 SDS-PAGE

Proteins were separated by SDS-PAGE using criterion precast gels. An electrophoresis unit (Bio-Rad, Hercules, CA, USA) was assembled and buffer reservoirs were filled with 1 x SDS-PAGE running buffer. 6 x SDS-PAGE sample buffer was added to each protein sample so that the sample contained 1 x SDS-PAGE sample buffer. Samples were then boiled for 5 min at 100°C or 10 min at 70°C and then centrifuged for ~15 s at 12,000 g at RT to collect the whole sample at the bottom of the tube. Using gel loading tips, protein samples were loaded onto precast SDS-PAGE gels. Gels were run at a range of voltages depending on gel type. Gels were always run until the bromophenol blue dye front had run off the bottom of the gel.

2.2.2.4.1.3.1 Electro-transfer, wet

The pre-run SDS-PAGE gel was removed from its casing and carefully transferred to a plastic container containing electrotransfer buffer at 4ºC and then incubated with gentle shaking for 1 h at 4ºC. PVDF membrane and two pieces of filter paper were cut to match the size of the gel. Whatman 3 MM filter papers were then soaked in ice-cold transfer buffer for 15 min. PVDF membrane was left to soak in methanol for 1 min before being transferred to another container containing transfer buffer for 15 min. Filter papers, gel, and membrane were placed between fibre pads in a Bio-Rad electrotransfer cassette and placed in the Bio-Rad electrotransfer unit with 2.5-3 l electrotransfer buffer. 30 mV was applied to the electrotransfer unit and the assembly was incubated overnight with stirring

in the cold After this time, the electrotransfer unit was disassembled and the membrane removed.

2.2.2.4.1.3.2 Electro-transfer, semi dry

Proteins were transferred from SDS-PAGE gels to PVDF membrane via semi-dry transfer, in the following manner:

The PVDF membrane and eight pieces of filter paper were cut to the same size to match the size of the gel. PVDF membrane was left to soak in methanol for 1 min before being transferred to another container containing semi-dry transfer buffer for 15 min. The filter paper was soaked in semi-dry transfer buffer for 15 min. The pre-run SDS-PAGE gel was removed from its casing and carefully transferred to a plastic container containing semi-dry transfer buffer, where it was left to soak for 15 min at room temperature. The surface of the anode of the semi-dry transfer unit was cleaned before assembly of the gel stack. Firstly, 4 pre-soaked pieces of filter paper where placed in a neat stack on the semi-dry transfer apparatus, a 50ml tube was then rolled over the stack to remove bubbles. Upon this stack the membrane was placed and then the gel on top of the membrane. Finally the last 4 pieces of filter paper were stacked on top of the gel. Bubbles were removed from the entire stack by rolling a 50 ml tube gently over the stack. The apparatus was then set to transfer at 2 mA/cm^2 for 60-75 min.

2.2.2.4.1.3.3 Antibody staining

Membranes were blocked in a plastic tray for 1 h RT or overnight at 4°C with gentle shaking in 5% (w/v) skimmed milk powder in TBST. The blocking solution was removed and membranes were either washed for 5 min 3 times in TBST with gentle shaking or were put directly into 50 or 15 ml centrifuge tubes without washing. Membranes were only washed at this stage if incubation with primary antibody was in 5% (w/v) bovine serum albumin (BSA) in TBST. Primary antibodies were incubated in centrifuge tubes on a roller at 4°C overnight in either 5% (w/v) skimmed milk powder or 5% (w/v) BSA in TBST. Blots were then washed for 5 min 3 times in TBST at RT with gentle agitation. Secondary antibodies were incubated in 5% (w/v) skimmed milk powder in TBST for 1h at RT in centrifuge tubes on a roller mixer.

The following primary antibodies were incubated in 5% (w/v) BSA in TBST:

Table 2.15 Primary antibodies incubated in TBST + 5% (w/v) BSA

Antibody Name	Source	Product code	Dilution
anti-JNK	Cell Signaling	9258	1 in 1000
anti-phospho-JNK	Cell Signaling	4668	1 in 1000
anti-p38	Cell Signaling	9212	1 in 1000
anti-phospho-p38	Cell Signaling	9215	1 in 1000
anti-AKT	Cell Signaling	4691	1 in 1000
anti-phospho-S473-AKT	Cell Signaling	4060	1 in 1000
anti-phospho-T308-AKT	Cell Signaling	4056	1 in 1000
anti-GSK3α/β	Cell Signaling	5676	1 in 1000
anti-phospho-S21/9-GSK3α/β	Cell Signaling	9331	1 in 1000
anti-IκBα	Cell Signaling	9242	1 in 1000
anti-IGF-I receptor	Cell Signaling	3018	1 in 1000
anti-IRS1	Cell Signaling	3407	1 in 100

The following primary antibodies were incubated in 5% (w/v) skimmed milk powder in TBST:

Table 2.16 Primary antibodies incubated in TBST + 5% (w/v) milk.

Antibody	Source	Product code	Dilution
anti-insulin receptor β chain	Santa Cruz Biotechnology	sc-711	1 in 200
anti-GAPDH	Sigma-Aldrich	G8795	1 in 30000

anti-CD200	Sigma-Aldrich	HPA031149	1 in 200
anti-tyrosine hydroxylase	Merk Millipore	AB152	1 in 200

Both secondary antibodies were incubated in 5% (w/v) skimmed milk powder in TBST:

Goat anti-rabbit-IgG (H+L)- horseradish peroxidase (HRP)-conjugated secondary antibody (1 in 1000). Goat anti-mouse IgG (H+L)-HRP-conjugated secondary antibody (1 in 20000).

2.2.2.4.1.3.4 Detection

For signal detection Pierce ECL Western Blotting Substrate or Pierce ECL Plus Western Blotting Substrate were used. Blots were exposed to CL-X Posure TM film. Exposure times were adjusted on the basis of previous exposures to obtain exposures in the linear range of the film. Films were developed through a developer (Xograph imaging systems, Compact X4, Model: X4A). Signals were quantified using ImageJ (Collins, 2007).

To reprobe blots for detection of non-phosphorylated proteins, membranes were washed twice in TBST for 5 min before they were stripped using either Restore Western Blot Stripping Buffer or stripping solution for 20 min with gentle agitation at RT before proceeding as if the membrane had just had the proteins transferred onto it.

2.2.2.4.1.4 Endoglycosidase H (Endo H) and peptide:N-glycosidase F (PNGase F) digestion

8 µg of protein were denatured in 0.5% (w/v) SDS, 40 mM DTT at 100°C for 10 min. Samples were then incubated with 1000 U of Endo H in 50 mM sodium citrate, pH 5.5 (at 25°C) at 37°C for 2 h, if not stated otherwise. For PNGase F digests denatured samples were incubated with 1000 U of PNGase F in 50 mM sodium phosphate pH 7.5 (at 25°C), 1% (v/v) NP-40 at 37°C for 2 h, if not stated otherwise.

2.2.2.4.2 ELISAs

2.2.2.4.2.1 Phospho-S307 IRS1 enzyme-linked immunosorbent assay (ELISA).

S307 phosphorylation of IRS1 was measured using the STAR phospho-IRS1 (Ser307 mouse/Ser312 271 human) ELISA following the manufacturer's instructions. S307

phosphorylation is expressed in units relative to a phospho-S307 IRS1 standard provided in the ELISA kit

2.2.2.4.2.2 Inflammatory cytokines Multi-Analyte ELISArray

Cytokine levels were measured using the Human Inflammatory Cytokines Multi-Analyte ELISArray Kit for SH-SY5Y or Mouse Inflammatory Cytokines Multi-Analyte ELISArray Kit for CAD following the manufacturer's instructions. Cell lysates were then processed and the protein concentrations were measured. Cytokine units were standardized to the protein concentration.

2.2.2.4.3 Nitric oxide assay

Nitric oxide (NO) was measured spectrophotometrically using Griess reagent as previously described (Green et al., 1982). CAD cells were exposed to ER stressors for times indicated in the text before the supernatant was removed and snap frozen in liquid nitrogen and then transferred to the -80°C freezer for storage. Supernatants from BV-2 cells and primary mouse glia were also collected in this manner. Cell lysates were also harvested for protein quantitation. Medium was centrifuged at 13,000 g for 10 min at 4 °C to pellet and then remove cell debris. Once centrifuged and cell debris removed, supernatant was either snap frozen in liquid nitrogen and stored at -80°C and then thawed or it was directly used in 96-well plates for a nitrite assay. Griess reagent was added to an equal volume of medium (100 µl) in 96-well plates. A standard curve ranging between 1-60 nmol/ml of sodium nitrite was added to plates and an equal volume of Griess reagent was added to the standard curve samples. Once Griess reagent was mixed with medium and the standard curve samples then the plate was incubated in the dark at room temperature for 10 min. The plate was then read at 540 nm in a Molecular Devices Spectramax Spectrophotometer. Protein samples isolated from the same tissue culture wells were quantified as described in the methods and then used to standardise nitrite concentrations to protein concentration.

2.2.3 Microscopy

2.2.3.1 Fluorescent monitoring of mitochondrial membrane potential with JC-1

Confocal microscopy of cells treated with JC-1 was used to monitor mitochondrial membrane potentials as a marker for ER stress. Cells were grown in Lumox dishes for 24 h before being used in experiments. Cells were then treated with 1 µM thapsigargin before incubation with 2 µg/ml JC-1 dye at 37°C for 20 min (Reers et al., 1991, Smiley et al.,

1991). After incubation with JC-1 and thapsigargin cells were washed twice with PBS. Fresh medium warmed to 37°C was added to the cells for live cell imaging on a Leica TCS SP5 II confocal microscope (Leica Microsystems, Mannheim, Germany). JC-1 fluorescence was excited at 488 nm with an argon laser set at 22% of its maximum power. Green fluorescence between 515-545 nm was collected with a photomultiplier tube and orange fluorescence between 590-620 nm 442 with a HyD 5 detector. To determine the percentage of dead cells, cells showing fluorescence emission between 515-545 nm only were counted as dead, while cells showing punctuate fluorescence emission between 590-620 nm were counted as alive.

2.2.3.2 GFP-tagged insulin receptor localisation

HEK 293 cells were first transfected with GFP-insulin receptor plasmid and then treated with tunicamycin or SubAB for 18 h. Following this, cells were stained with 5 µg/ml CellMask Deep Red (Life Technologies) for 5 min at RT to visualise the cell membrane. Images of GFP-tagged insulin receptors expressed in HEK 293 cells and cell membranes were then taken on a Zeiss ApoTome microscope (Carl Zeiss, Cambridge, UK). GFP fluorescence was observed using a band pass (BP) 450-490 filter (Carl Zeiss, FITC/GFP, filter set 9, cat. no. 488009-000) and a long pass (LP) 515 filter. CellMask Deep red fluorescence was observed using a BP546/12 filter (Carl Zeiss, Rhodamine, filter set 15, cat. no. 488015-0000) and a LP 590 filter.

To quantify colocalization of the GFP-tagged insulin receptors and CellMask Deep Red signals, individual cells were defined as regions of interest (ROI) in Image J. ROI were then background-corrected for the intracellular fluorescence of CellMask Deep Red using the Background Subtraction from ROI plug-in. The Pearson correlation coefficient between the INSR-GFP and CellMask Deep Red Fluorescence was determined in individual cells using the Colocalization Test plug-in and Costes' image randomization (Costes et al., 2004) and a point spread function (PSF) width of 0.453 µm as a quantitative measure of colocalization of both fluorescence signals (Manders et al., 1992).

2.2.4 Statistical Analysis

Experimental data are presented as the average and its standard error. Errors were propagated using the law of error propagation for random, independent errors (Ku, 1966). Two way analysis of variance (ANOVA) with Sidak's, Tukey's or Dunnet's correction for

multiple comparisons, and *t*-tests were performed in GraphPad Prism 6.04 (GraphPad Software, La Jolla, CA, USA).

3 EARLY JNK ACTIVATION BY THE ER STRESS SENSOR IRE1α INHIBITS CELL DEATH EARLY IN THE ER STRESS RESPONSE

3.1 Rationale

It is widely accepted that long-lasting JNK signalling during stress can be proapoptotic (Tournier et al., 2000, Yang et al., 1997, Lei and Davis, 2003). However, some studies have found JNK signalling to be prosurvival (Svensson et al., 2011, Lamb et al., 2003, Yu et al., 2004, Granato et al., 2013). Therefore, JNK signalling can be both prosurvival and proapoptotic depending on the stress and duration. An example of this is that two phases of JNK activation occur with treatment of TNF-α, 1) an early and transient antiapoptotic phase and 2) a late proapoptotic phase (Roulston et al., 1998).

JNK activation during ER stress is considered to be mostly proapoptotic which is in contrast to studies in which other stress situations result in acute JNK-mediated prosurvival signalling. Many studies looking at prolonged ER stress-induced JNK activation have shown that it is proapoptotic (Zhang et al., 2001, Smith and Deshmukh, 2007, Chen et al., 2008, Wang et al., 2009, Jung et al., 2012, Teodoro et al., 2012, Huang et al., 2014, Jung et al., 2014, Kang et al., 2012, Arshad et al., 2013). However, not much is known about the role of JNK activation early in the ER stress response. Data in this chapter were obtained to address that issue. This chapter contains figures from a manuscript (see appendix B) entitled 'Early JNK activation by the ER stress sensor IRE1α inhibits cell death early in the ER stress response' with the authors Max Brown, Natalie Strudwick, Monica Suwara, Louise K. Sutcliffe, Adina D. Mihai, Jamie N. Watson, and Martin Schröder.

3.2 ER stress transiently activates JNK before XBP1 splicing reaches maximal levels

In order to investigate when early JNK activation occurs during ER stress, 8 h time courses were performed with ER stress inducing drugs. The phosphorylation of JNK on T183 and Y185 in its T-loop was monitored with antibodies against phosphorylated and total JNK. Alternative splicing of *JNK* 1 and 2 produces 8 proteins, which can be grouped into two major molecular weight pools of 46 kDa and 54 kDa (Coffey, 2014). Both the JNK and

phospho-JNK antibody detect the JNK proteins in the two molecular weight groups, which most commonly results in two major bands detected during Western blotting. The splicing of *XBP1* was monitored as an indication of ER stress and more specifically activation of IRE1α.

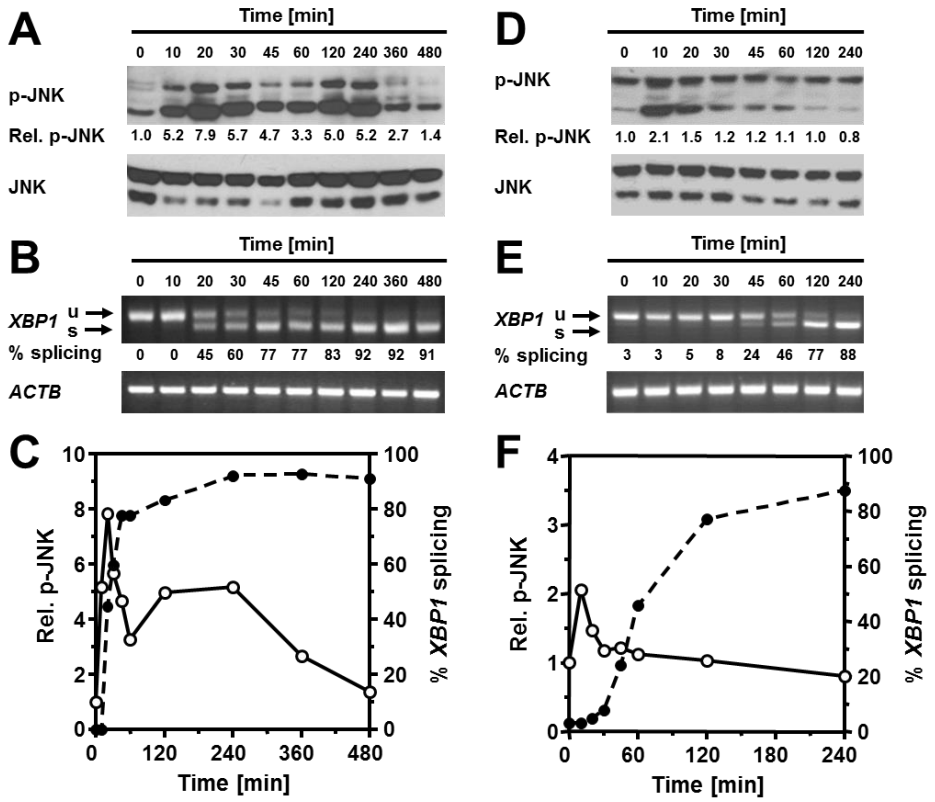

Figure 3.1. Transient JNK activation precedes activation of *XBP1* splicing in MEFs.
(A) Kinetics of JNK activation and **(B)** *XBP1* splicing in MEFs exposed to 1 μM thapsigargin. **(C)** Quantitation of the JNK phosphorylation (white circles, solid line) from panel (A) and *XBP1* splicing (black circles, dashed line) from panel (B). **(D)** Kinetics of JNK activation and **(E)** *XBP1* splicing in MEFs exposed to 10 μg/ml tunicamycin. **(F)** Quantitation of the JNK phosphorylation (white circles, solid line) from panel (D) and *XBP1* splicing (black circles, dashed line) from panel (E). All data in this figure was obtained by Monika Suwara and Natalie Strudwick.

In MEFs JNK activation occurred from as early as 10 min after treatment with the ER stressor thapsigargin and reached maximal levels after 20 min (Figure 3.1 A, data obtained by Monica Suwara and Natalie Strudwick). *XBP1* splicing was not detected until 20 min and did not reach maximal levels until 4 h (Figure 3.1 B-C). Similar kinetics were observed when using another ER stress inducing compound, tunicamycin. Tunicamycin, which induces ER stress through inhibiting *N*-linked glycosylation of newly synthesised proteins, also caused transient JNK activation as early as 10 min. As with thapsigargin,

XBP1 splicing also occurred after JNK activation when cells were exposed to tunicamycin (Figure 3.1 D-E). Thapsigargin and tunicamycin induce ER stress in biochemically distinct ways and therefore these data suggest that early JNK activation is induced by ER stress and is not a consequence of secondary effects of the drugs. ER stress-induced transient JNK activation therefore precedes *XBP1* splicing in MEFs. It is worth noting that JNK phosphorylation was observed at the 0 min time point (Figure 3.1 A and D). JNK phosphorylation at this time point should represent basal levels and therefore suggests that low levels of JNK phosphorylation occur during the culturing conditions used. Whether this basal JNK phosphorylation has any effect on the cells and interpretation of data is currently unknown. The JNK pathway is very sensitive to several stresses besides ER stress including: heat shock (Murai et al., 2010), oxidative stress (Wang et al., 2003a), and changes in pH (Xue and Lucocq, 1997). It is possible that other, unintentional, stresses during the handling of cells causes this basal JNK phosphorylation. The handling and growth conditions of cells was maintained consistent as much as possible and the 0 min time point was taken from the same 6-well plate as the 10, 20, 30, 45 and 60 min time point plate and as such any non-ER stress experienced by the 0 min time point should also have been experienced by cells at other time points which should, at least in part, control for the effect of other stresses. The phospho-JNK data is representative because biological repeats have recently confirmed this trend in all cell lines tested (data not shown). JNK phosphorylation was also observed at 0 min time points with other cell lines whilst activation of JNK higher than the basal levels after short exposures to ER stressors was observed in several cell lines suggesting that the general trend is reproducible.

To investigate if similar *XBP1* splicing and JNK phosphorylation kinetics during ER stress existed in other cell lines, Hep G2 cells were exposed to thapsigargin. Hep G2 cells are derived from human liver and were chosen because ER stress has been reported in the liver of obese humans (Puri et al., 2008, Gregor et al., 2009) and non-human animals (Ozcan et al., 2004) Treatment of Hep G2 cells with 1 µM thapsigargin led to maximal JNK phosphorylation after 30 min (Figure 3.2, data obtained by Monica Suwara and Natalie Strudwick). JNK phosphorylation then gradually decreased over the time course to below resting levels. *XBP1* splicing was at maximal levels at 8 h and in contrast only 7% of *XBP1* was spliced at 30 min which was when JNK is maximally activated. It took another 15 min after maximal JNK activation for *XBP1* splicing to reach half maximal levels (Figure 3.2 C). Similar results were also seen with 3T3-F442A adipocytes and C_2C_{12} myotubes (see manuscript in appendix B).

JNK can be activated by many different stresses. To elucidate if the early transient JNK activation is mediated by ER stress, it was investigated if JNK activation was IRE1α- and TRAF2-dependent. TRAF2 is involved in ER stress-mediated JNK activation through which it interacts with IRE1α and ASK1. Therefore, two small interfering (si)RNAs against human TRAF2 were used to knockdown TRAF2 in Hep G2 cells, whilst an siRNA against eGFP was used to control against any effects of the transfection procedure. Quantitative real time (qRT)-PCR was performed to establish efficiencies of siRNAs (Figure 3.3 A). Knock-down was most effective 24 h after transfection with both siRNAs. These conditions were therefore used to investigate if JNK activation was TRAF2-dependent. Western blotting with an antibody against TRAF2 further confirmed knock-down of TRAF2 by both siRNAs (Figure 3.3 B). Knock-down of TRAF2 decreased and delayed activation of JNK (Figure 3.3 B, C). Consistent with this finding is that C_2C_{12}, 3T3-F442A, and MEFs with knocked-down TRAF2 have disrupted early ER stress-induced JNK activation (see manuscript in appendix B, data obtained by Monica Suwara and Natalie Strudwick). In *traf2*$^{-/-}$ MEFs early JNK activation is markedly reduced and does not increase until 4 h of ER stress (Figure 3.4 D-F). Therefore activation of JNK is delayed in *traf2*$^{-/-}$ MEFs. Thapsigargin-induced early JNK activation is therefore dependent on TRAF2.

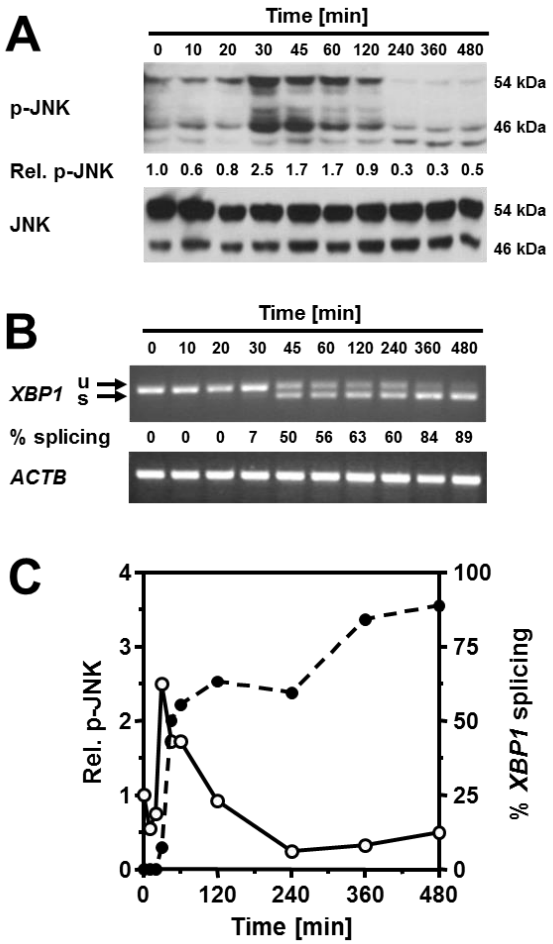

Figure 3.2. JNK activation and *XBP1* splicing kinetics in response to acute thapsigargin-induced ER stress in Hep G2 cells.

(A) Western blots for phospho-JNK (p-JNK) and total JNK (JNK) of Hep G2 cells exposed to 1 μM thapsigargin for the indicated times. **(B)** Detection of *XBP1* splicing by reverse transcriptase PCR. Hep G2 cells were exposed to 1 μM thapsigargin for the indicated times. **(C)** Quantitation of the JNK phosphorylation (white circles, solid line) from panel (A) and *XBP1* splicing (black circles, dashed line) from panel (B). All data in this figure was obtained by Monika Suwara and Natalie Strudwick.

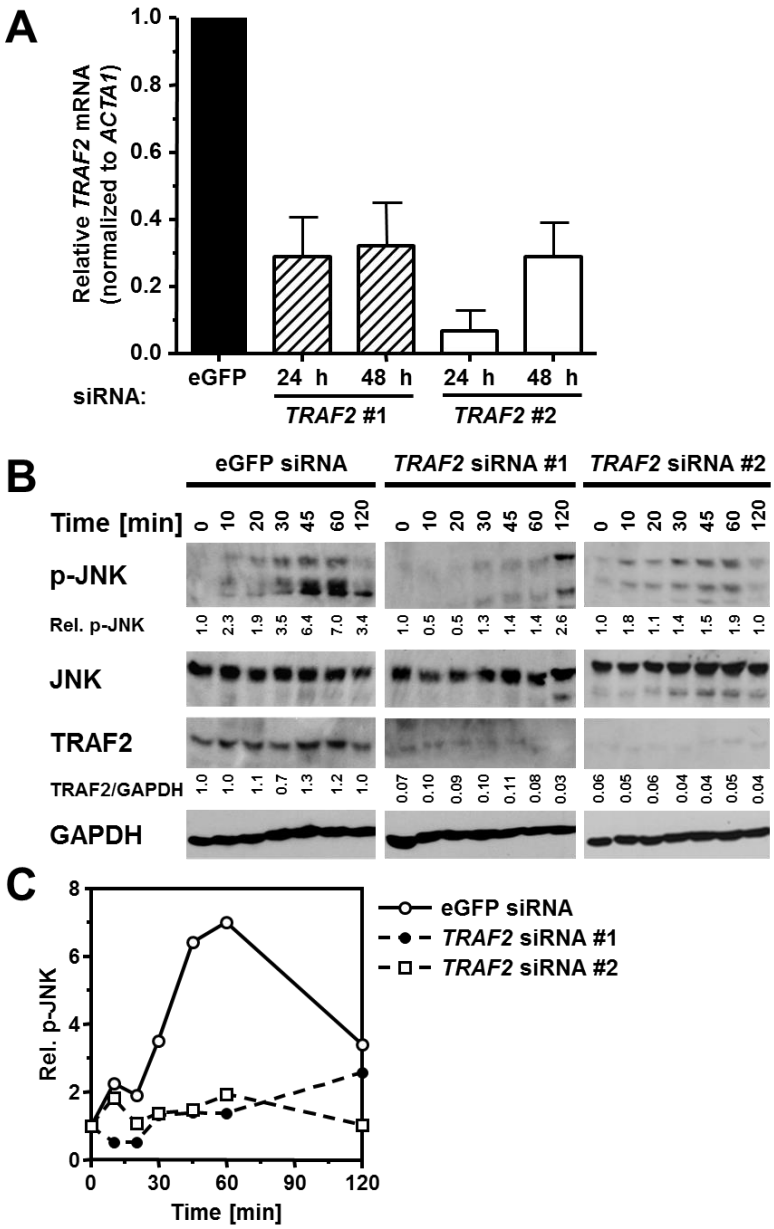

Figure 3.3. Acute JNK activation in Hep G2 cells is TRAF2 dependent.

(A) siRNA knock-down of human TRAF2 in Hep G2 cells. Relative *TRAF2* mRNA abundance (to *ACTA1*) was measured by RT-qPCR 24 or 48 h after transfection of Hep G2 cells with the indicated siRNAs (n = 3). **(B)** Knock-down of TRAF2 expression in Hep G2 cells interferes with ER stress-induced JNK phosphorylation. Hep G2 cells were treated with 1 μM thapsigargin for the times indicated before protein extraction for Western blotting with antibodies against p-JNK, total JNK, TRAF2, and GAPDH. **(C)** Quantitation of the JNK phosphorylation signals in the Western blots of panel (B).

siRNAs against human IRE1α were used to knock-down IRE1α in Hep G2 cells. RT-qPCR was performed to establish efficiencies of siRNAs (Figure 3.5 A). Knock-down was most effective 72 h after transfection with both siRNAs. These conditions were therefore used to

investigate if JNK activation was IRE1α-dependent. Knock-down of IRE1α with both siRNAs resulted in decreased activation of JNK in Hep G2 cells (Figure 3.5 B, C). Phosphorylated JNK levels were delayed in the IRE1α knock-down experiment compared to data in figures 3.3 and 3.3. Differening JNK activation kinetics may be a product of experimental variation such as changes in growth conditions (FBS batch, cell confluency, passage number) or the age of cell line stocks. Unfortuanetly, time limitations prevented this discrepancy from being understood or remedied. Consistent with this finding is that C_2C_{12} and 3T3-F442A cells with knocked-down IRE1α display disrupted early ER stress-induced JNK activation (see manuscript in appendix B, data obtained by Monica Suwara and Natalie Strudwick). In support of observations in Hep G2 cells it was also demonstrated that MEF cells without IRE1α have a delayed JNK activation phenotype with only minor activation of JNK at early time points (Figure 3.4 A-C). Therefore activation of JNK is delayed in *ire1α* $^{-/-}$ MEFs. Thapsigargin-induced early JNK activation is therefore TRAF2- and IRE1α-dependent. Overall acute ER stress transiently activates JNK before maximal *XBP1* splicing in several cell lines whilst JNK activation requires IRE1α and TRAF2.

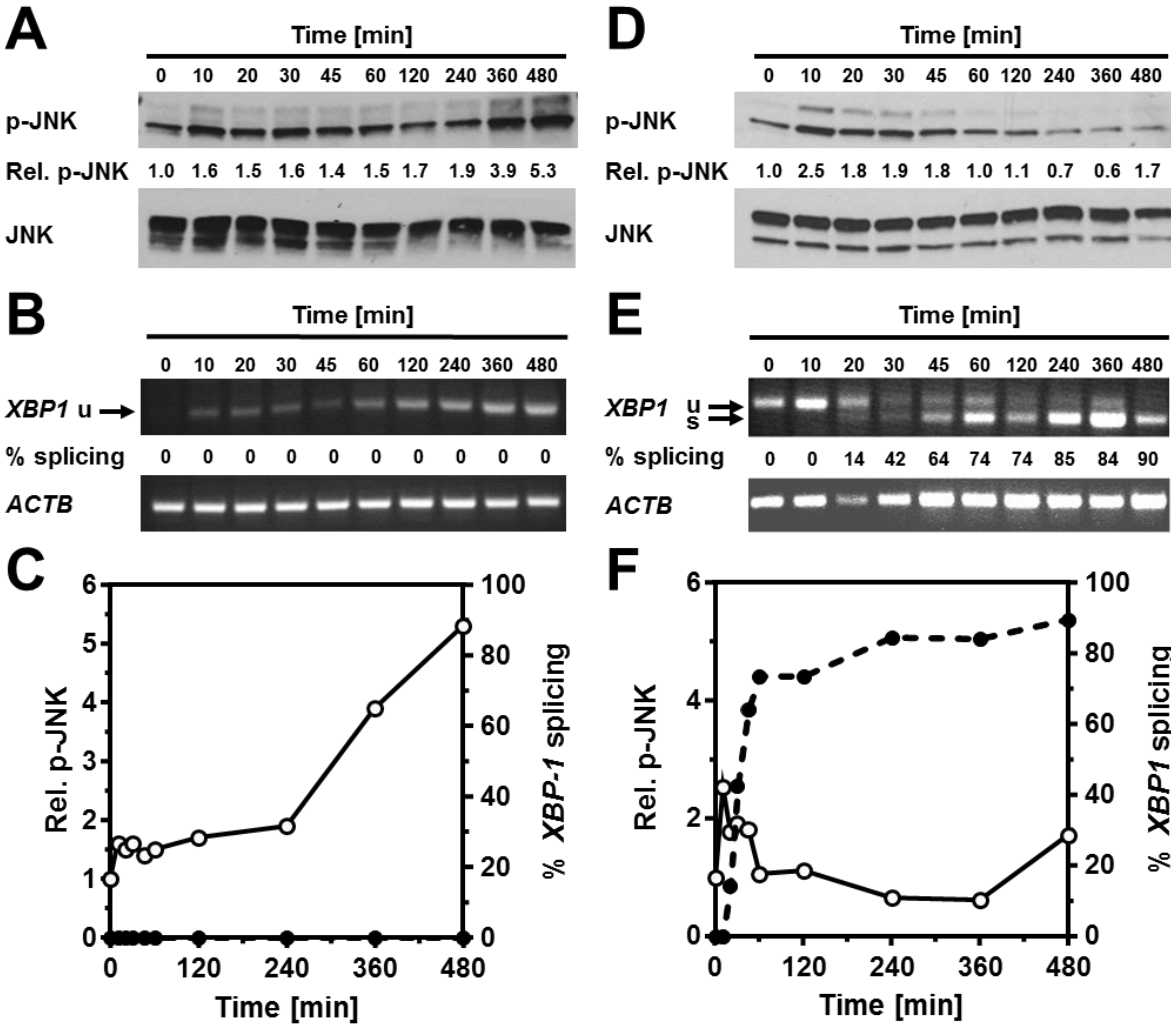

Figure 3.4. IRE1α and TRAF2 are required for the transient JNK activation in MEFs.

(A) Kinetics of JNK activation and **(B)** *XBP1* splicing in *ire1α*$^{-/-}$ MEFs exposed to 1 μM thapsigargin. **(C)** Quantitation of the JNK phosphorylation (white circles, solid line) from panel (A) and *XBP1* splicing (black circles, dashed line) from panel (B). **(D)** Kinetics of JNK activation and **(E)** *XBP1* splicing in *traf2*$^{-/-}$ MEFs exposed to 1 μM thapsigargin. **(F)** Quantitation of the JNK phosphorylation (white circles, solid line) from panel (D) and *XBP1* splicing (black circles, dashed line) from panel (E). *XBP1* splicing assay performed byMonika Suwara.

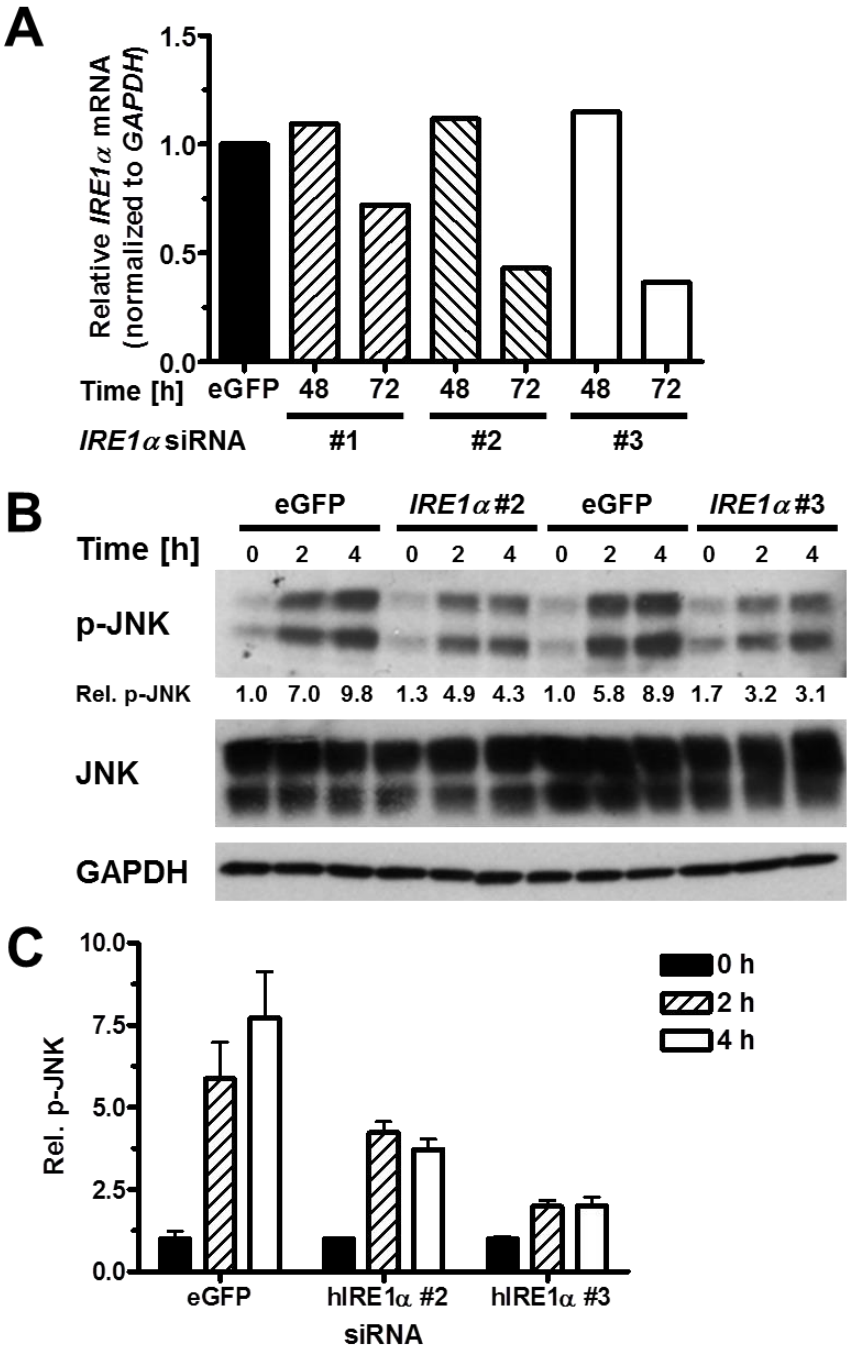

Figure 3.5. Acute JNK activation is IRE1α-dependent in Hep G2 cells.

(A) Hep G2 cells were transfected with 10 nM of the indicated siRNAs. 48 h and 72 h after transfection *IRE1α* mRNA was quantitated by quantitative reverse transcriptase (qRT)-PCR located 3' to the siRNA annealing sequences with primers H8993 and H8994. Similar knock-down efficiencies were obtained with a RT-qPCR located 5' to the siRNA annealing sequences. **(B)** siRNA knock-down of IRE1α impairs ER stress-dependent activation of JNK in Hep G2 cells. 72 h after transfection with the indicated siRNAs Hep G2 cells were stimulated for the indicated times with 1 μM thapsigargin. Cell lysates were analysed by Western blotting. **(C)** Quantitation of JNK phosphorylation in Hep G2 cells treated for the indicated times with 1 μM thapsigargin 72 h after transfection with the indicated siRNAs (n = 2).

3.3 Early transient JNK activation in ER stressed cells inhibits cell death

The early transient JNK activation during acute ER stress is interesting because JNK has a dual role in that it has been reported to both promote and inhibit apoptosis during stress. JNK's dual role in cell death making decisions is exemplified with TNF-α treatment in which early and transient JNK activation is antiapoptotic whilst late JNK activation is proapoptotic (Roulston 1998). TNF-α induces early JNK activation, which is required for increased expression of mRNA for the antiapoptotic ubiquitin ligase cIAP2/BIRC3 (Lamb et al., 2003). These findings were the motivation to investigate the expression of *cIAP2* as well as other antiapoptotic genes *cIAP1*, *XIAP* and *BIRC6* in early ER stress-mediated JNK activation. WT and *jnk1*$^{-/-}$ *jnk2*$^{-/-}$ MEFs were compared to investigate the role of JNK in the expression of these antiapoptotic genes.

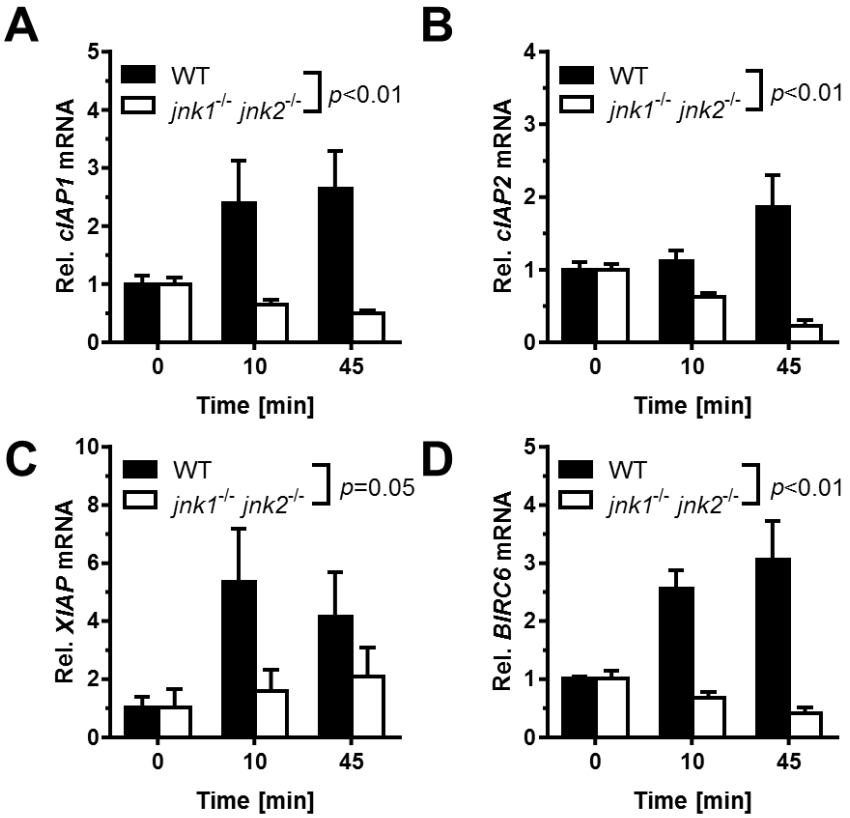

Figure 3.6. JNK is required for transcriptional induction of antiapoptotic genes early in the ER stress response.

(A) *cIAP1* (*BIRC2*), (B) *cIAP2* (*BIRC3*), (C) *XIAP* (*BIRC4*), and (D) *BIRC6* (*BRUCE, APOLLON*) steady-state mRNA levels were quantitated by RT-qPCR in WT and *jnk1*$^{-/-}$ *jnk2*$^{-/-}$ MEFs exposed to 1 μM thapsigargin for the indicated times (n = 3).

Expression of the mRNAs for *cIAP1*, *XIAP* and *BIRC6* increased as early as 10 min in WT MEFs (Figure 3.6). Expression of the mRNAs for *cIAP1*, *cIAP2*, *XIAP* and *BIRC6* increased in WT MEFs after 45 min of 1 μM thapsigargin treatment. The same was not true in *jnk1*$^{-/-}$ *jnk2*$^{-/-}$ MEFs, in fact the expression of *cIAP1*, *cIAP2* and *BIRC6* actually decreased. Although *XIAP* expression did not decrease in *jnk1*$^{-/-}$ *jnk2*$^{-/-}$ MEFs the increased expression was more pronounced in WT MEFs. These data suggest that JNK positively regulates the expression of several antiapoptotic genes early in the ER stress response.

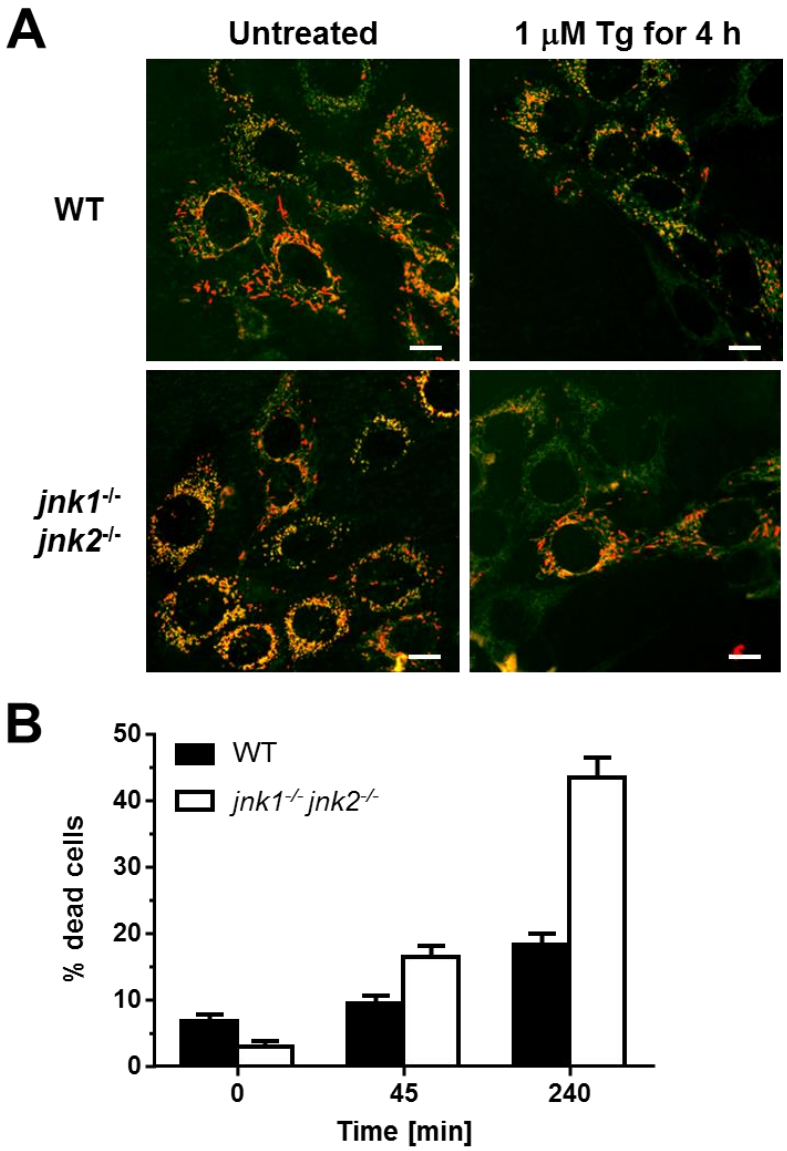

Figure 3.7. JNK inhibits loss of mitochondrial membrane potential early in the ER stress response.

(A) WT and *jnk1*$^{-/-}$ *jnk2*$^{-/-}$ were treated with 1 μM thapsigargin (Tg) for 4 h and stained with JC-1 as described in Materials and Methods. Scale bar – 10 μm. **(B)** Quantitation of the confocal fluorescence microscopy data shown in panel A. $n = 3$ experiments with at least 200 cells counted per experiment.

These data on the expression of antiapoptotic genes prompted investigation of ER stress-induced cell death between WT and *jnk1*$^{-/-}$ *jnk2*$^{-/-}$ MEFs to establish the physiological relevance of early JNK-dependent expression of antiapoptotic genes. JC-1 dye was used to monitor the depolarization of mitochondrial transmembrane potentials in order to characterise the presence of dead cells. Depolarization of mitochondrial transmembrane potentials is a distinctive feature early in programmed cell death (Ly et al., 2003). JC-1 dye can accumulate in mitochondria in a potential-dependent manner. This accumulation is indicated by a fluorescence emission shift from green (~529 nm) to red (~590 nm). Mitochondrial depolarization and cell death can therefore be characterised by a decrease in the red/green fluorescence intensity ratio. Cell death was more pronounced as early as 45 min after addition of thapsigargin to *jnk1*$^{-/-}$ *jnk2*$^{-/-}$ MEFs compared to WT MEFs (Figure 3.7). After 4 h ~40% of *jnk1*$^{-/-}$ *jnk2*$^{-/-}$ MEFs exhibited mitochondrial depolarization compared to roughly half as many in WT MEFs. Therefore, early ER stress-dependent JNK activation delays cell death early in the ER stress response.

3.4 Discussion

These results show that JNK is transiently activated early in the ER stress response (Figure 3.1 and Figure 3.2) and that JNK activation is dependent of TRAF2 and IRE1α providing evidence that early JNK activation is indeed a result of ER stress (Figure 3.3, Figure 3.4 and Figure 3.5). These results also demonstrate that JNK is required for maximal activation of several antiapoptotic genes (Figure 3.6) and that JNK deficient MEFs show a faster thapsigargin-induced depolarization of the mitochondrial transmembrane potential (Figure 3.7). These data therefore suggest that two phases of JNK activation occur during ER stress, which is similar to treatment with TNF-α, and that early JNK activation during ER stress is prosurvival. This data is consistent with reports showing that *traf2*$^{-/-}$ MEFs are more susceptible to ER stress-induced apoptosis than WT MEFs (Mauro et al., 2006) and pharmacological inhibition if JNK2 in U937 cells causes caspase 3 activation and apoptosis during ER stress (Raciti et al., 2012).

These data and other studies show biphasic activation of JNK with opposing effects on cell survival during ER stress. Other stresses have also been shown to have similar effects. For example TNF-α treatment causes biphasic JNK activation with opposing outputs (Roulston 1998). Therefore, ER stress-induced JNK activation is another example of the opposing functional outcomes of transient versus persistent JNK activation during stress. Stresses,

other that ER stress, also cause transient JNK activation (Sluss et al., 1994, Raingeaud et al., 1995, Lee et al., 1997). In one study transient activation of JNK was observed with various stressors such as cytokines (TNFα and IL-1), LPS, osmotic stress (Raingeaud et al., 1995). Other reports have also shown that JNK activation is antiapoptotic (Lee et al., 1997, Nishina et al., 1997) whilst it is also reported that long lasting JNK activation causes apoptosis (Chen et al., 1996, Guo et al., 1998, Sanchez-Perez et al., 1998).

How JNK activation switches between prosurvival and proapoptotic signalling remains poorly understood. It could be possible that the length of time JNK is phosphorylated affects its subcellular location and therefore alters the signalling output of JNK. This has been proposed for the opposing signalling outputs caused by ERKs for example (Marshall 1995). However, studies have shown that upon both early transient and prolonged JNK activation that JNK does not relocalise. Research from Martin Schröder's laboratory also suggests that JNK does not relocalise during ER stress (see manuscript in appendix B).

Another possible explanation of the opposing functions reported in JNK activation is that NF-κB signalling may alter JNK signalling outcomes. NF-κB suppresses TNF-α-induced apoptosis whilst preventing prolonged JNK activation and inhibiting caspases. Prolonged JNK activation alone was not sufficient to induce apoptosis with TNF-α but apoptosis was reported in the absence of NF-κB activation (Tang et al., 2002). JNK activation in the absence of NF-κB has also been shown to be necrotic (Ventura *et al.*, 2004). In agreement with these findings NF-κB promotes an antiapoptotic response to TNF-α (Kelliher et al., 1998, Devin et al., 2000) and this may be in part due to its ability to induce *cIAP1*, *cIAP2*, and *XIAP* (Stehlik et al., 1998). JunD is a transcription factor downstream of JNK and contributes to the induction of *cIAP2* during TNF-α induced stress (Lamb et al., 2003, Ventura et al., 2004). Interestingly, NF-κB activation during ER stress is reminiscent of JNK activation reported in this chapter, in that it is transient and displays similar kinetics (Wu et al., 2002, Jiang et al., 2003b, Deng et al., 2004, Wu et al., 2004). It could therefore be possible that the combination of NF-κB and JNK signalling is the cause of prosurvival signalling and increased expression of antiapoptotic genes identified by this research.

Another explanation for the biphasic and opposing JNK activation is that IRE1α phosphorylation may regulate JNK activation. IRE1α interacts with TRAF2 to activate JNK (Urano et al., 2000). IRE1α has ~10 phosphorylation sites (Itzhak et al., 2014) so it is possible that the level of IRE1α phosphorylation alters its affinity for TRAF2 and therefore alters its ability to activate JNK.

It is possible that the role of JNK in inducing apoptosis is more regulatory. That is to say that JNK may only contribute to apoptosis if the apoptotic process is already activated, meaning JNK activation without apoptosis being initiated is prosurvival (Liu and Lin, 2005). There could also be more subtle changes in phosphorylation between different JNK isoforms which account for the paradigm of opposing JNK signalling outcomes. For example TNF-α activates JNK1, but not JNK2 (Liu et al., 2004). This JNK1 activation is required for the TNF-α-induced apoptosis in the absence of NF-κB whilst JNK2 activation had no effect. Interestingly, JNK2 activation was reported to interfere with JNK1 activation. These differences in phosphorylation and roles of different JNKs with stress may change as JNK activation is prolonged.

In conclusion early transient, IRE1α and TRAF2-dependent, JNK activation during ER stress promotes survival through induction of antiapoptotic genes. How JNK switches from antiapoptotic signalling during early transient stress to proapoptotic signalling after chronic stress is still not fully understood but may involve NF-κB signalling. Further investigation into JNK activation and regulation during ER stress as well as other stresses is necessary to fully understand how apoptosis is regulated by JNK. Understanding how JNK regulates apoptosis during stress is important as JNK activation is reported in many stress types and in many diseases.

4 ACUTE ENDOPLASMIC RETICULUM STRESS SEPARATES JNK AND TRB3 ACTIVATION FROM INSULIN RESISTANCE

4.1 Rationale

In the previous chapter it was established that ER stress causes early transient JNK activation in Hep G2, MEF, C_2C_{12} and 3T3-F422A cells. As discussed in the introduction inhibition of insulin signalling occurs in T2D (see 1.5). A role for ER stress in the development of T2D has been strongly implicated in several studies. For example, ER stress has been detected in the liver (Puri et al., 2008, Gregor et al., 2009) and adipose tissue (Gregor et al., 2009, Boden et al., 2008, Sharma et al., 2008) of obese patients. Two mechanisms for ER stress-induced insulin resistance are proposed: JNK-mediated and TRB3-mediated.

JNK-mediated insulin resistance

JNK is reported to be involved in insulin resistance. Activated JNK can phosphorylate serine residues S307 and S312 of IRS1, which inhibits IR induced tyrosine phosphorylation of IRS1; leading to insulin resistance (Ozcan et al., 2004). Observational evidence of a physiological role for IRE1α-JNK signalling in a disease setting is that both IRE1α and JNK are activated in obese humans compared to non-obese humans (Boden et al., 2008). Ozcan *et al.* have proposed that IRE1α-JNK signalling can inhibit insulin signalling (Ozcan et al., 2004). Hence it was decided that it would be intriguing to investigate if the IRE1α-dependent JNK activation during acute ER stress which was reported in chapter 3 causes insulin resistance. Insulin resistance may reduce protein synthesis: JNK-mediated insulin resistance during acute, early ER stress may be beneficial.

TRB3-mediated insulin resistance

ER stress-mediated TRB3 expression is another mechanism through which ER stress has been implicated in causing insulin resistance. ER stress increases TRB3 expression in C_2C_{12} cells and in adult mouse skeletal muscle (Koh et al., 2013). Overexpression of TRB3 causes inhibited insulin signalling and is thought to do this through direct interaction with the insulin signalling proteins AKT and IRS1 (Du et al., 2003, Avery et al., 2010, Koh et al., 2006, Koh et al., 2013, Liew et al., 2010). TRB3-AKT interaction causes insulin resistance in HEK 293 cells (Du et al., 2003), muscle cells (Koh et al., 2006, Koh et al., 2013) and cardiac myocytes (Avery et al., 2010). In conclusion, TRB3 has a controversial

role in regulating insulin resistance. However, it may be a mechanism through which ER stress induces insulin resistance and is worthy of further study alongside JNK, which has also been shown to regulate AKT and IRS1 phosphorylation during ER stress.

Most studies looking at ER stress-induced inhibition of insulin signalling have investigated this in the context of longer lasting ER stress, with ER stress induced from 3 – 36h cells (Avery et al., 2010, Hage Hassan et al., 2012, Xu et al., 2010, Zhou et al., 2009, Tang et al., 2011, Ozcan et al., 2004). Thus it was investigated in this thesis if earlier transient JNK activation identified in Results chapter 1 can inhibit insulin signalling also.

This chapter contains figures from a manuscript (see appendix C) entitled 'Acute endoplasmic reticulum stress separates JNK and TRB3 activation from insulin resistance' with the authors Max Brown, Samantha Dainty, Natalie Strudwick, Adina D. Mihai, Jamie N. Watson, Robina Dendooven, Adrienne W. Paton, James C. Paton, and Martin Schröder.

4.2 ER stress for up to ~8 h does not inhibit insulin-stimulated AKT activation

To begin with it was investigated if ER stress up to 8 h is capable of inhibiting insulin signalling in C_2C_{12} cells. Three mechanistically different ER stressors were used, the *N*-glycosylation inhibitor tunicamycin (Carrasco and Vazquez, 1984), the SERCA pump inhibitor thapsigargin (Carrasco and Vazquez, 1984) and the BiP/GRP78 inactivating protease SubAB (Paton et al., 2006). Thapsigargin concentrations were titrated over a 10 fold concentration range whilst tunicamycin was titrated over a 100 fold concentration range. Only one concentration of SubAB was used as it is highly specific in inducing ER stress via inactivating BiP by cleaving in its hinge region (Paton et al., 2006) but this cytotoxin is also not commercially available and is of limited supply due to it being a gift from JC Paton and A Paton. Throughout experiments the catalytically inactive $SubA_{A272}B$ was used as a control for ER stress induced by SubAB. The phosphorylation of AKT at residues T308 and S473 was measured to monitor activation of insulin signalling. AKT is downstream of the insulin receptor and IRSs. Surprisingly, ER stress induced with all three ER stressors with a range of concentrations for 1, 2, 4 or 8 h did not inhibit phosphorylation of AKT in C_2C_{12} cells induced through stimulation by insulin (Figure 4.1). Insulin stimulation of C_2C_{12} cells, in the absence of ER stressors, caused a large increase in AKT-phosphorylation and thus provides evidence of activated insulin signalling in this experimental set up (Figure 4.1). *XBP1* splicing was measured to monitor if ER stress was

occurring throughout the time course with all three ER stressors. Indeed ER stress was occurring at all the time points investigated as *XBP1* splicing was recorded during the entire time course (Figure 4.2).

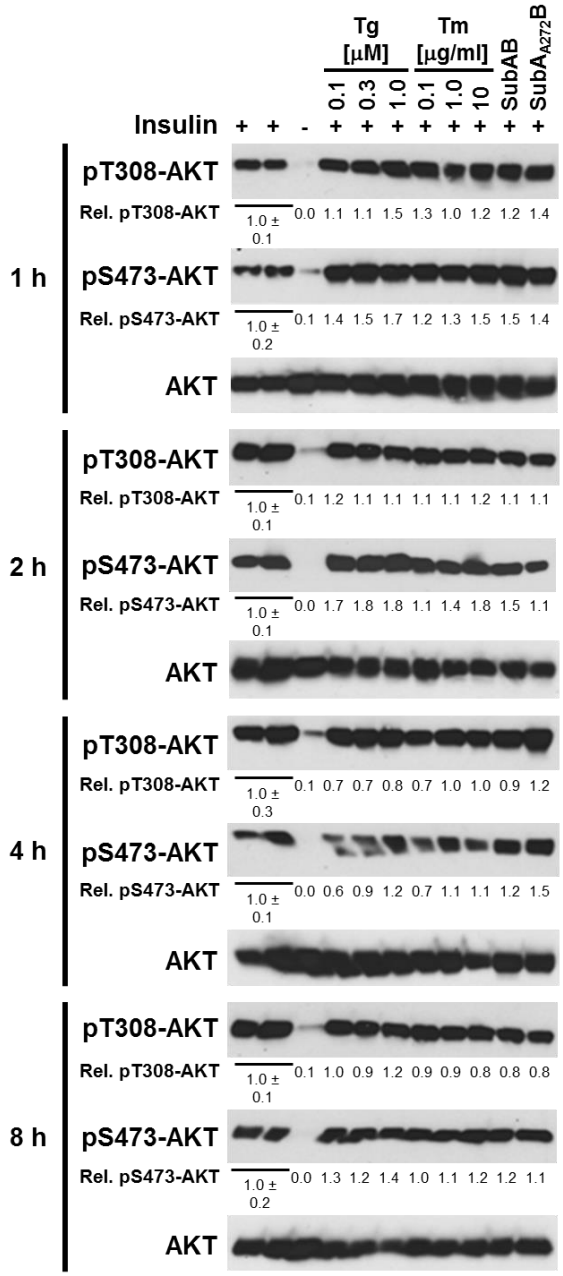

Figure 4.1. Acute ER stress does not inhibit insulin-stimulated AKT T308 or S473 phosphorylation in C_2C_{12} myotubes.

C_2C_{12} myotubes were serum-starved for 18 h and treated with the indicated concentrations of thapsigargin (Tg), tunicamycin (Tm), or 1 μg/ml SubAB or catalytically inactive $SubA_{A272}B$ during the last 1-8 h of serum starvation and then stimulated with 100 nM insulin for 15 min where indicated. Cell lysates were analysed by Western blotting.

Due to a recent study reporting strong TRB3 induction coinciding with 20-50% inhibition of insulin signalling during 4 h of ER stress, induced by thapsigargin or tunicamycin, in C_2C_{12} cells (Koh et al., 2013) the induction of *TRB3* mRNA was characterised by RT-qPCR. All three ER stressors greatly increased the expression of *TRB3* in C_2C_{12} cells (Figure 4.3). In this report the induction of TRB3 by ER stress is therefore not sufficient to inhibit insulin signalling.

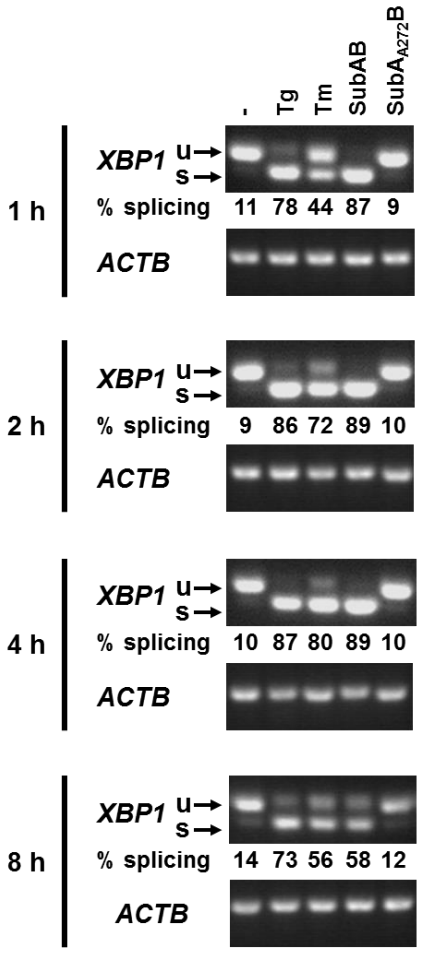

Figure 4.2. Detection of *XBP1* splicing by reverse transcriptase PCR.

PCR products were separated on a 2% (w/v) agarose gel and visualized with ethidium bromide. PCR products derived from unspliced (u) and spliced (s) *XBP1* mRNA are indicated by arrows. β-Actin (*ACTB*) was used as a loading control. Abbreviations: Tg - 300 nM thapsigargin, Tm - 1 µg/ml tunicamycin.

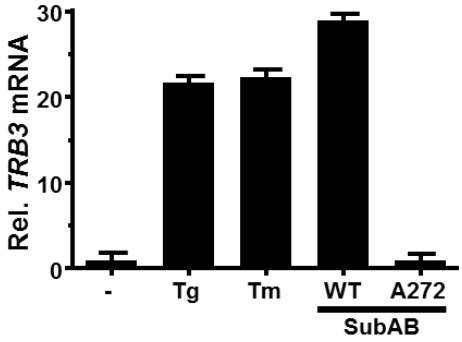

Figure 4.3. Induction of *TRB3* in C_2C_{12} cells by ER stress.

C_2C_{12} cells were treated with 300 nM thapsigargin, 1 µg/ml tunicamycin, or 1 µg/ml SubAB or $SubA_{A272}B$ for 4 h. *TRB3* mRNA levels were determined by RT-qPCR and standardised to *ACTB* (n = 3).

4.3 ER stress does not inhibit insulin-dependent AKT and GSK3α/β phosphorylation in the time window of JNK activation

The observation that ER stress does not cause insulin resistance in C_2C_{12} cells is surprising given already published data (Avery et al., 2010, Hage Hassan et al., 2012, Xu et al., 2010, Zhou et al., 2009, Tang et al., 2011, Ozcan et al., 2004). As a result, the role of ER stress in the development of insulin resistance was investigated other cell types. In chapter 3 it was demonstrated that ER stress-mediated JNK activation is early and transient (Chapter 3). Therefore it was investigated if ER stress, at the time points of early JNK activation, was sufficient to inhibit insulin signalling. 30 min of ER stress is sufficient to activate JNK in Hep G2 cells (Figure 3.2). Thus, AKT phosphorylation was monitored in Hep G2 cells after 30 min of ER stress induced by thapsigargin, tunicamycin or SubAB (Figure 4.4). Similar to data from C_2C_{12} cells stressed for 1-8 h, AKT phosphorylation at S473 was not significantly altered by any of the ER stressors in Hep G2 cells stressed for 30 min.

Maximal JNK activation with thapsigargin-induced ER stress occurs as early as 10 min and persists up to 45 min in C_2C_{12} cells (Chapter 3). Consequently, AKT phosphorylation was monitored in C_2C_{12} cells after 30 min of ER stress (Figure 4.5). ER stress induced by all three ER stressors for the earlier time point of 30 min was also not sufficient to inhibit AKT phosphorylation at either S473 or T308 in C_2C_{12} cells. GSK3 is a downstream target of AKT and its phosphorylation was therefore characterised to confirm that insulin signalling is indeed unaltered during ER stress. GSK3 phosphorylation was monitored at S21 in GSKα and S9 in GSKβ. Consistent with the phosphorylation of AKT with insulin treatment, GSK3α and β phosphorylation was also greatly increased with exposure to 100

nM insulin. In agreement with the unperturbed AKT phosphorylation observed during ER stress, insulin-induced GSK phosphorylation was also not affected by 30 min ER stress in C_2C_{12} cells.

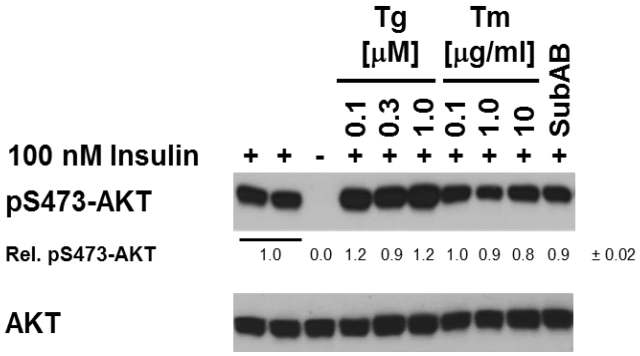

Figure 4.4. Acute ER stress does not inhibit insulin-dependent AKT activation.
Serum-starved Hep G2 cells treated with the indicated concentrations of thapsigargin, tunicamycin or 1 μg/ml SubAB for 30 min before stimulation with 100 nM insulin for 15 min. Cell lysates were analysed by Western blotting.

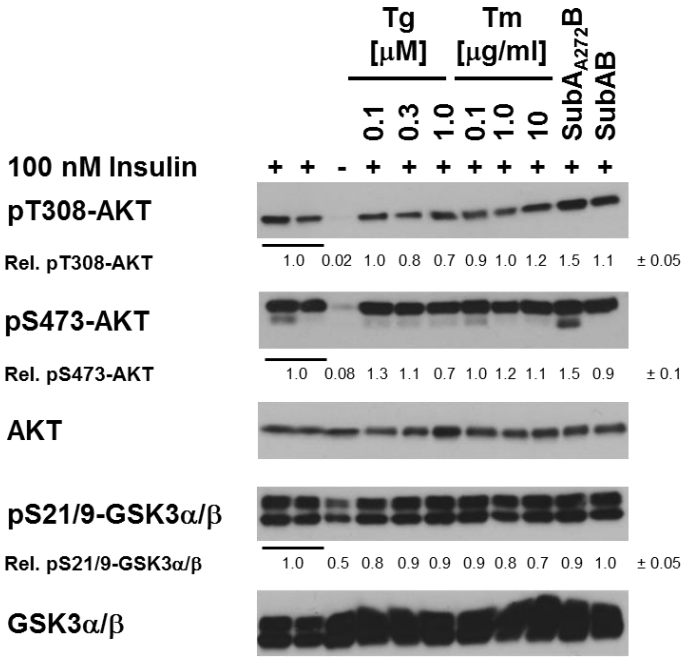

Figure 4.5. Acute ER stress does not inhibit insulin-dependent AKT activation in C_2C_{12} cells.
Serum-starved C_2C_{12} myotubes were treated for 30 min with the indicated concentrations of thapsigargin, tunicamycin or 1 μg/ml SubAB before stimulation with 100 nM insulin for 15 min. Cells were treated with 1 μg/ml catalytically inactive $SubA_{A272}B$ where indicated. Cell lysates were analysed by Western blotting.

In 3T3-F422A adipocytes JNK was activated by thapsigargin within 10 min and returned to basal levels after 1 h (Chapter 3, see manuscript in appendix B). Both S473 and T308 phosphorylation of AKT was induced with insulin treatment. However, 30 min of ER stress with thapsigargin, tunicamycin or SubAB was unable to inhibit the phosphorylation of AKT (Figure 4.6). In agreement, GSK3α/β phosphorylation was also not reduced during ER stress treatments. Insulin signalling, as indicated by AKT and GSK phosphorylation, was therefore also unaffected by 30 min ER stress in 3T3-F422A cells. Overall, acute ER stress in C_2C_{12}, Hep G2, and 3T3-F422A cells, although causing JNK activation, does not cause insulin resistance. It is surprising that insulin resistance is not induced by ER stress in all three cell types given previously reported data (Ozcan et al., 2004). However, C_2C_{12}, Hep G2, and 3T3-F422A cells were not used in the Ozcan *et al.* study, so it is possible that JNK-mediated insulin resistance is specific to the cell type previously investigated.

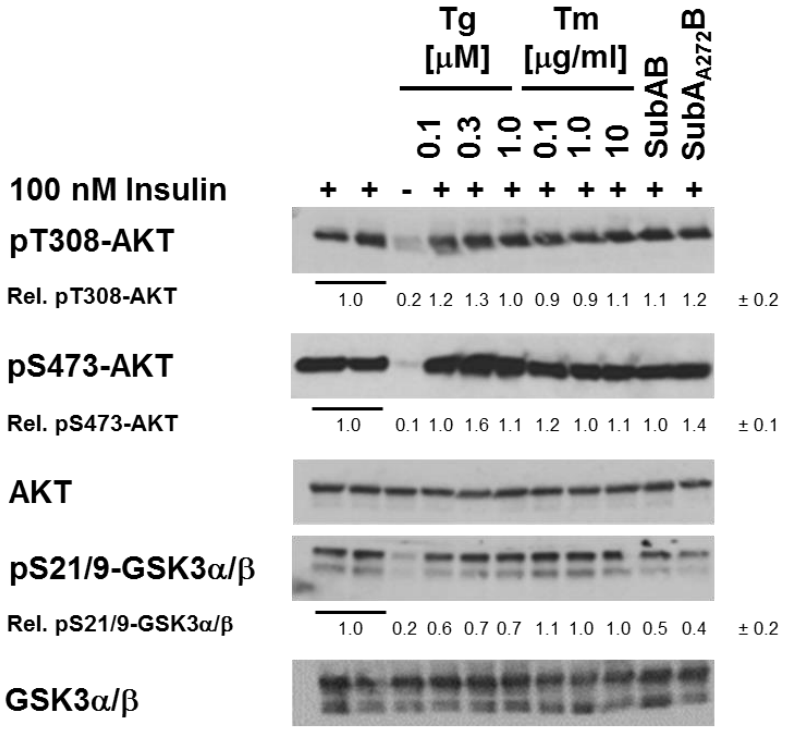

Figure 4.6. Acute ER stress does not inhibit insulin-dependent AKT activation in 3T3-F442A adipocytes.

Serum-starved 3T3-F442A adipocytes were treated for 30 min with the indicated concentrations of thapsigargin, tunicamycin or 1 μg/ml SubAB before stimulation with 100 nM insulin for 15 min. Cells were treated with 1 μg/ml catalytically inactive $SubA_{A272}B$ where indicated. Cell lysates were analysed by Western blotting.

Fao rat hepatoma cells were used in the original paper reporting that ER stress-induced JNK activation leads to inhibition of insulin signalling (Ozcan et al., 2004). To address the possibility that ER stress inhibiting insulin signalling may be cell type specific the experiments were expanded to include Fao rat hepatoma cells. Fao rat hepatoma cells were treated with all three ER stressors for 30 and 60 min (Figure 4.7). As this cell line had not been previously used in Dr Martin Schröder's laboratory ER stress-mediated JNK activation was monitored. All three ER stressors were able to activate JNK after 60 min whereas only thapsigargin and tunicamycin were able to activate JNK after 30 min of ER stress. Because ER stress activated JNK at these time points the phosphorylation of AKT and GSK3 was also monitored. Both AKT and GSK3 phosphorylation were unperturbed with 1 h of ER stress, even though JNK was highly activated at these data points in Fao rat hepatoma cells.

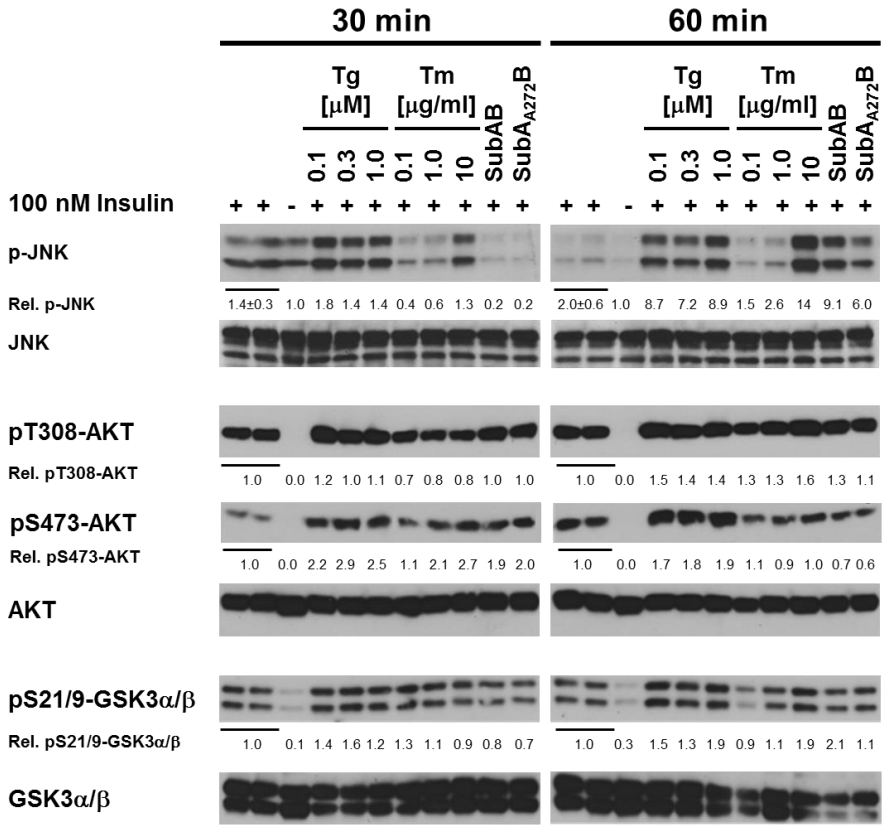

Figure 4.7. Acute ER stress activates JNK, but does not inhibit insulin-dependent AKT activation in Fao rat hepatoma cells.

Serum-starved Fao rat hepatoma cells were treated with the indicated concentrations of thapsigargin, tunicamycin or 1 μg/ml SubAB for 30 or 60 min before stimulation with 100 nM insulin for 15 min. Cell lysates were analysed by Western blotting.

This surprising result prompted further investigation and an extension of the time course of ER stress in Fao rat hepatoma cells to ensure ER stress occurred long enough to inhibit insulin signalling. Extending ER stress to 2, 3 (the same time points reported in the Ozcan et al. study (Ozcan et al., 2004)) or 4 h was still not sufficient to inhibit insulin signalling as indicated by AKT phosphorylation (Figure 4.8). In the original paper the Fao rat hepatoma cells were grown in Coon's modification of Ham's F12 medium which is in contrast to the RPMI 1640 medium recommended by the suppliers of the Fao rat hepatoma cells used in this study. To address the possibility that different media can have different effects on cells Fao rat hepatoma cells were maintained in Coon's modification of Ham's F12 medium before treating cells with ER stress for 3 h to fully recapitulate the experiment by Ozcan *et al*. (Ozcan et al., 2004). Even after changing the medium, ER stress induced by all three ER stressors, using 3 different concentrations for both thapsigargin and tunicamycin, was unable to inhibit insulin signalling as monitored by AKT phosphorylation.

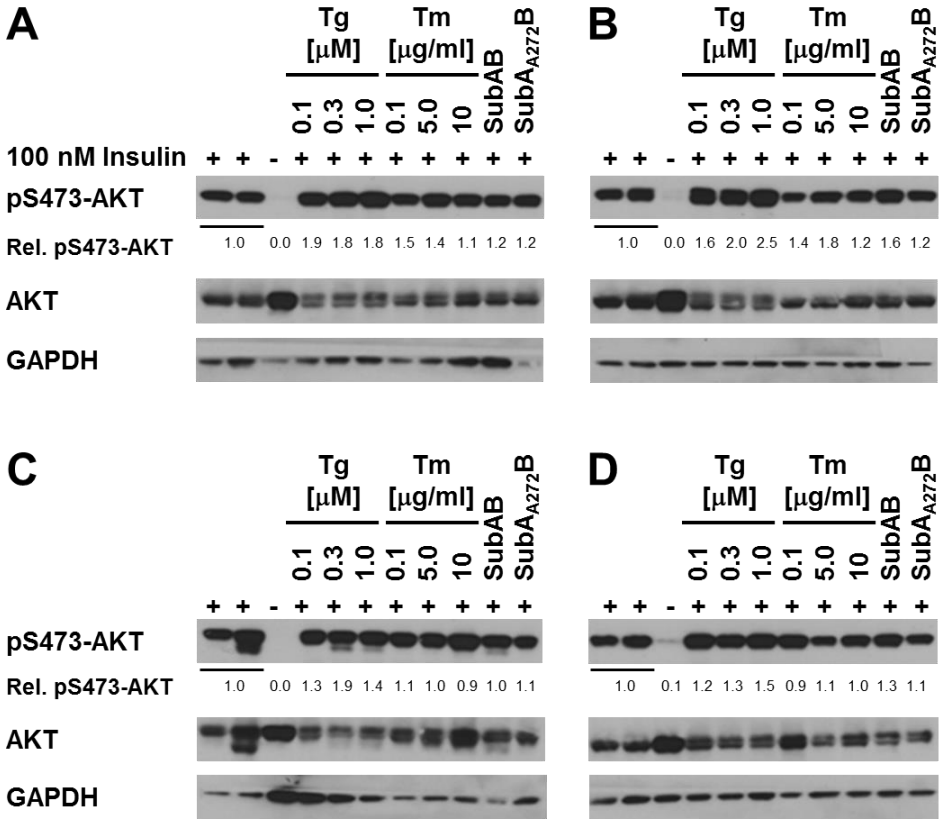

Figure 4.8. ER stress does not inhibit insulin signalling in Fao rat hepatoma cells.

Fao rat hepatoma cells were serum starved for 18 h and treated with 0.1 to 1 µM thapsigargin, 0.1 to 10 µg/ml tunicamycin, 1 µg/ml SubAB or $SubA_{A272}B$ for **(A)** 2, **(B)** and **(C)** 3 h, and **(D)** 4 h. Cells were cultured in RPMI 1640 in panels (A), (B), and (D) and in Coon's modification of Ham's F12 medium in panel (C).

Interestingly, thapsigargin consistently increases AKT phosphorylation. This may be a side-effect of the mechanism by which thapsigargin induces ER stress. Thapsigargin inhibits SERCA pumps resulting in reduced ER calcium stores causing perturbed protein folding (Schonthal et al., 1991). As a consequence the cytosolic concentration of Ca^{2+} is increased. Calmodulin is a major calcium-binding protein and is activated when the Ca^{2+} concentration is increased in the cytosol. Calmodulin has been shown to phosphorylate AKT and this may in part explain the increased phosphorylation of AKT in thapsigargin treated cells (Deb et al., 2004). However, this remains to be investigated and may not be the only explanation as calcium signalling is involved in many cellular events meaning there are many potential targets for investigation.

For investigation of insulin resistance all the cell types used were serum starved for 18 h prior to treatment with 100 nM insulin for 15 min. Serum starvation was performed to investigate and isolate the insulin signalling pathway from other growth factor pathways which may be stimulated by growth factors present in serum. To ensure that serum starvation does not induce ER stress and subsequent downstream insulin resistance, *XBP1* splicing was monitored in cells cultured in serum versus serum-free medium. Cells were either grown in normal culture media or serum starved for 18 h before treatment with 1 µM thapsigargin for 1 h. *XBP1* splicing was measured to compare the levels of ER stress induced in cells grown in serum versus serum-free media (Figure 4.9). *XBP1* splicing was comparable between cells grown in serum containing media and serum-free media in WT MEFS, *traf2*$^{-/-}$ MEFs, C_2C_{12} cells, Hep G2 cells, and 3T3-F442A cells, ruling out that serum starvation induces ER stress to detectable levels whilst suggesting that induction of ER stress is blunted by decreased protein synthesis rates in serum-starved cells.

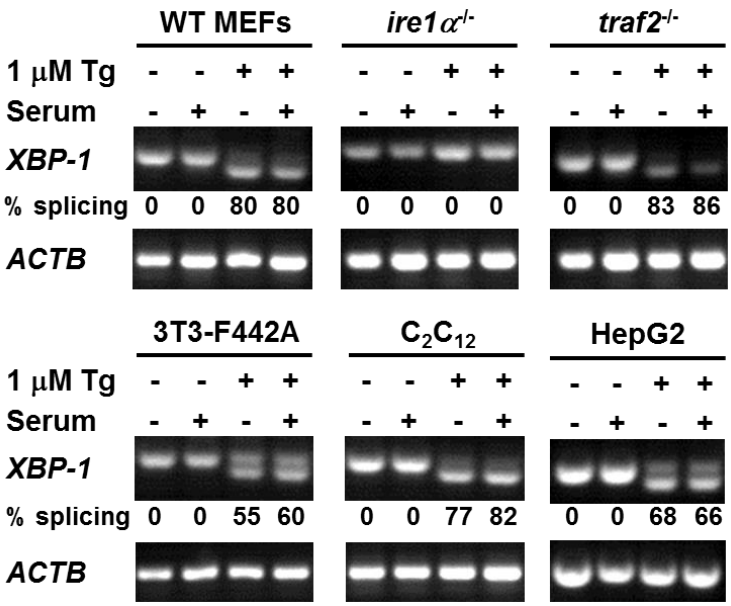

Figure 4.9. Serum starvation does not affect activation of *XBP1* splicing in MEFs, 3T3-F442A cells, C_2C_{12} cells, or Hep G2 cells.

Cells were serum-starved for 18 h and then treated with 1 μM thapsigargin for 1 h. PCR products were separated on a 2% (w/v) agarose gel and visualised with ethidium bromide. PCR products derived from unspliced (u) and spliced (s) *XBP1* mRNA are indicated by arrows. β-Actin (*ACTB*) was used as a loading control.

4.4 Acute ER stress does not inhibit IRS1 tyrosine phosphorylation

The proposed mechanism through which JNK inhibits insulin signalling has been discussed (Chapter 1). Briefly, JNK is thought to phosphorylate IRS1 at S307 (corresponding to S312 in human IRS1) and this phosphorylation event prevents the tyrosine phosphorylation of IRS1 which is required for downstream insulin signalling, including AKT activation. As this thesis has reported JNK activation but not observed insulin resistance during ER stress it would be expected that there is also no increase in IRS1 S307 or S312 phosphorylation. The phosphorylation of IRS1 at S312 in Hep G2 cells by ELISA were monitored and standardised to total IRS1 levels obtained from Western blotting. Treatment of Hep G2 cells with 1 μM thapsigargin for 30, 60 or 120 min had no effect on IRS1 S312 phosphorylation (Figure 4.10). ER stress at earlier time points of 5, 10 and 15 min in C_2C_{12} and 3T3 cells also had no effect on IRS1 S307 phosphorylation (Figure 4.11, data obtained by Monica Suwara and Natalie Strudwick).

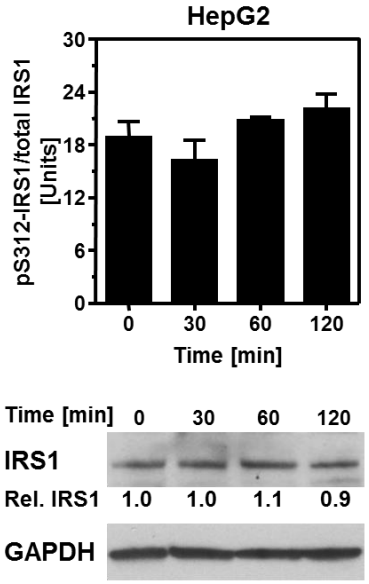

Figure 4.10. S312 phosphorylation of IRS1 during acute ER stress.

Hep G2 cells were treated with 1 μM thapsigargin for the indicated times. Cell lysates were analysed by ELISA for phosphorylation of S312 in human IRS1 by using the STAR phospho-IRS1 ELISA from Millipore. S312 phosphorylation is expressed in units relative to a phospho-S312 IRS1 standard provided in the ELISA kit. Phospho-S312-IRS1 units were standardised to the amount of total IRS1 in cell lysates determined by Western blotting (n = 3). Equal loading of all lanes in the Western blot was controlled with the GAPDH loading control.

To confirm that both the ELISA and insulin treatments were indeed working correctly C_2C_{12}, 3T3 and Hep G2 cells were treated with 100 nM insulin for 15 min and serine phosphorylation of IRS1 was monitored. Insulin elevated IRS1 S307 phosphorylation in all three cell lines (Figure 4.12, Monica Suwara and Natalie Strudwick), which is consistent with other reports (Aguirre et al., 2002, Rui et al., 2001). To confirm the above results that JNK activation during ER stress does not alter the phosphorylation of IRS1 at S307 IRS1 tyrosine phosphorylation was also monitored. In agreement with unaltered S307 phosphorylation the tyrosine phosphorylation of IRS1 was found to be unchanged in Hep G2, C_2C_{12} and 3T3 cells with ER stress (data obtained Monica Suwara and Natalie Strudwick, see manuscript in appendix C).

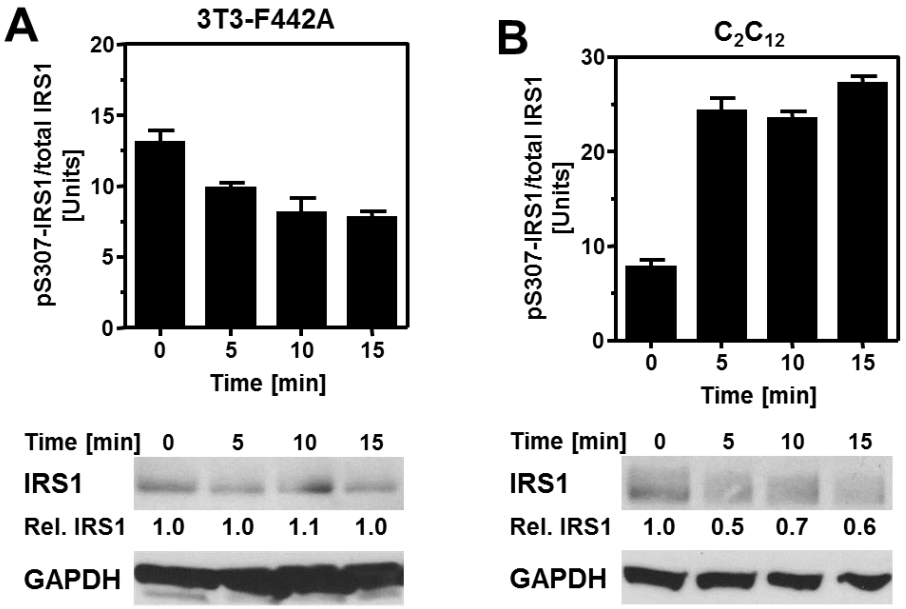

Figure 4.11. S307 phosphorylation of IRS1 during acute ER stress.

(A) 3T3-F442A and **(B)** C_2C_{12} cells were treated with 1 μM thapsigargin for the indicated times. Cell lysates were analysed by ELISA for phosphorylation of S307 in murine IRS1 by using the STAR phospho-IRS1 ELISA from Millipore. S307 phosphorylation is expressed in units relative to a phospho-S307 IRS1 standard provided in the ELISA kit. Phospho-S307 IRS1 units were standardised to the amount of total IRS1 in cell lysates determined by Western blotting (n = 3). Equal loading of all lanes in the Western blot was controlled with the GAPDH loading control. All data in this figure was obtained by Monika Suwara and Natalie Strudwick.

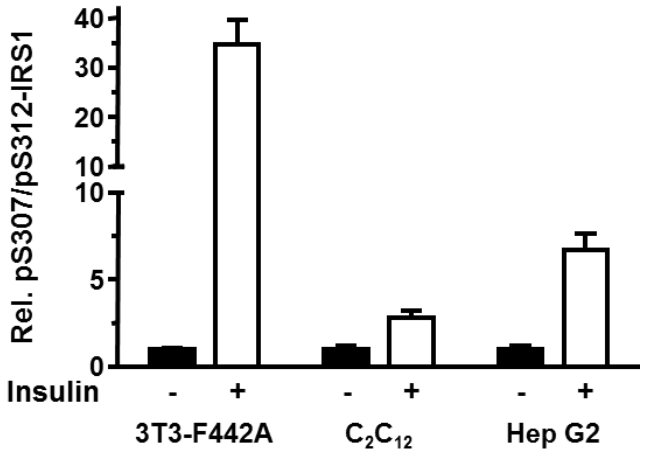

Figure 4.12. S307/S312 phosphorylation of IRS1 during acute ER stress.

IRS1 S307/S312 phosphorylation in serum-starved 3T3-F442A, C_2C_{12}, and Hep G2 cells treated with 100 nM insulin for 15 min was determined by ELISA. IRS1 phospho-S307/S312 signals in the ELISA were standardised to total protein levels (n = 3). All data in this figure was obtained by Monika Suwara and Natalie Strudwick.

4.5 Discussion

Overall data from this section suggests that ER stress-mediated JNK activation earlier that 8 h is not sufficient to inhibit insulin signalling. This has been investigated at various stages of the insulin signalling pathway from IRS1 S307 and tyrosine phosphorylation to AKT and finally GSK phosphorylation. Importantly, recapitulation of previously reported experiments did also not show ER stress-mediated JNK activation leading to inhibited insulin signalling. It is worth noting that this data has been confirmed in several cell lines over detailed time courses and with three mechanistically different ER stressors, two of which having 3 different concentrations tested.

Previously 3 h of 5 µg/ml tunicamycin has been shown to inhibit AKT S473 phosphorylation whilst inducing S307 IRS1 phosphorylation in Fao rat hepatoma cells (Ozcan et al., 2004). 1 h of 300 nM thapsigargin was also shown to induce S307 IRS1 phosphorylation in the same study but AKT phosphorylation was not investigated with thapsigargin treatment. Another study using C_2C_{12} cells reported that 4 h of 1 µg/ml tunicamycin inhibited both tyrosine phosphorylation of IRS1 and T308 phosphorylation of AKT by ~50% whilst 4 h of 2 µM thapsigargin resulted in a decrease in AKT phosphorylation by approximately 25% (Koh et al., 2013). Surprisingly, unlike both of these studies, inhibition of insulin signalling during ER stress was observed in experiments performed in this chapter, despite activation of both TRB3 and JNK. Even after extending the experiments to include several cell lines, more time points and three different ER stressors the data in this thesis chapter does not support the hypothesis that ER stress alters insulin signalling.

4.5.1 The role of JNK in ER stress-mediated insulin resistance

Whilst it has been demonstrated that IRE1α-JNK signalling can lead to insulin resistance (Ozcan et al., 2004) some studies however, have shown that JNK activation is not required for defective IRS1 phosphorylation or insulin resistance. Recently, in a mouse model of hepatic insulin resistance and ER stress, induced by a high fructose diet, there was no increase in JNK activation (Chan et al., 2013). Inhibition of AKT phosphorylation by the ER stressor tunicamycin occurred independent of JNK activation in Hep G2 cells (Achard and Laybutt, 2012). Despite activation of ER stress and JNK in a study by Jurczak *et al*, mice had increased hepatic insulin sensitivity (Jurczak et al., 2012). ER stress inhibited

insulin signalling in 3T3 adipocytes but this occurred without IRE1α-JNK signalling (Xu et al., 2010). Interestingly, Sharma *et al*. also showed that JNK is still activated by saturated free fatty acids even in the absence of IRE1α (Sharma et al., 2012a) suggesting that JNK activation in the free fatty acid model of diabetes does not necessarily require IRE1α signalling. Furthermore it was also shown that a reduction in JNK phosphorylation is not required for increased insulin sensitivity in rats (Sharma et al., 2012b).

Correlative evidence suggests that free fatty acids can lead to serine phosphorylation and reduction of IRS1 in 3T3-L1 adipocytes (Gao et al., 2004). Although both JNK and IKK were shown to be activated with free fatty acid treatment, JNK activation was detected after serine phosphorylation of IRS1 suggesting that JNK phosphorylation may not be essential for IRS1 serine phosphorylation and insulin resistance in 3T3-L1 adipocytes. Supporting this idea is the activation of IKK alongside IRS1 serine phosphorylation and prior to JNK phosphorylation. IKK deficiency in mice has previously been shown to reduce obesity and diet-induced insulin resistance (Yuan et al., 2001).

A report using *XBP1*$^{-/-}$ mice fed a fructose diet showed that ER stress and JNK activation occurred without inhibiting insulin signalling suggesting that IRE1α-mediated JNK activation can be dissociated from hepatic insulin resistance (Jurczak et al., 2012). In agreement with this Jung *et al.* show separation of JNK activation from insulin signalling. The authors report that the transcription factor Krupel-like factor 15 (KLF15) is a mediator of ER stress-induced insulin resistance in the liver. *KLF15*$^{-/-}$ mice exhibit increased hepatic ER stress and JNK activation compared to WT mice. However, *KLF15*$^{-/-}$ mice are protected from insulin resistance by both pharmacologically- and high fat diet-induced ER stress (Jung et al., 2013). Mice fed either a high fructose or high fat diet develop insulin resistance. However, only high fructose fed mice developed ER stress and this was independent of increased JNK activation. Interestingly, the high fat diet did promote JNK activation but not ER stress (Ren et al., 2012). It is possible that the IRE1α-JNK axis of insulin resistance is for some reason defective in *KLF15*$^{-/-}$ mice so this remains to be confirmed.

Studies have also struggled to provide causal evidence that JNK inhibits insulin signalling. For example, two studies have reported that the JNK inhibitor SP600125 (Bennett et al., 2001) was unable to restore normal insulin sensitivity to cells exposed to prolonged ER stress (Xu et al., 2010, Zhou et al., 2009). SP600125, although greatly reducing JNK activation, was unable to prevent thapsigargin-induced inhibition of AKT phosphorylation

in 3T3-L1 cells (Zhou et al., 2009). Also using 3T3-L1 cells it was shown that SP600125 did not significantly alleviate ER stress-induced insulin resistance (Xu et al., 2010). It should be noted that these two studies performed prolonged exposures to ER stress and as such the mechanisms of insulin resistance may differ depending on severity and duration of ER stress (discussed further in the following chapter).

Discrepancies between the data reported in this chapter and already published data could be a result of several differences. The level of AKT phosphorylation induced by insulin appears to be greater in experiments performed for this thesis. For example 100 nM insulin stimulation of C_2C_{12} cells in the Koh *et al.* paper caused a modest increase in AKT phosphorylation of ~30% in one experiment and ~80% in another (Koh et al., 2013). This modest increase of ~30% is surprising given the 100 nM insulin concentration used. 100 nM insulin stimulation of C_2C_{12} reported in this thesis caused a much greater increase in AKT phosphorylation. This raises the issue that higher levels of AKT phosphorylation may mask any inhibitory effects of ER stress. However, it was demostrated that ER stress was still not sufficient to inhibit insulin signalling when lowering insulin stimulation to a 10 nM concentration, which resulted in ~10% AKT activation (see manuscript in appendix C).

In the Ozcan *et al.* paper the conclusions regarding ER stress-mediated inhibition of insulin signalling downstream of IRS1 in *in vitro* studies rely solely on one data point: that is that 3 h of 5 µg/ml tunicamycin inhibits insulin-stimulated AKT phosphorylation at serine 473 (Ozcan et al., 2004). These data only show correlation between tunicamycin treatment and inhibited AKT phosphorylation and the study therefore lacks *in vitro* experimental data to show causation at the level of insulin signalling downstream of IRS1. Causation is only demonstrated at the level of IRS1, in which it was reported that tunicamycin-induced serine phosphorylation of IRS1 was not detected in *ire1α*$^{-/-}$ cells: no other downstream markers, such as AKT phosphorylation, were monitored. It is an important issue that there is no evidence downstream of IRS1 given that the role of IRS1 serine phosphorylation in perturbing normal insulin signalling is controversial: 1) IRS1 serine 307 to alanine knock-in mice are not protected from developing insulin resistance caused by high fat diet (White, 2002). 2) In hepatic rat Fao cells, palmitate-induced defects in AKT phosphorylation occur before defects in IRS1 phosphorylation (Ruddock et al., 2008). 3) S307 phosphorylation has been reported to promote insulin sensitivity (Copps et al., 2010).

In the Ozcan *et al.* paper the insulin signalling downstream of IRS1 is only further investigated *in vivo* (Ozcan et al., 2004). Although providing physiological relevance, *in*

vivo experiments are not as, by their nature, controlled and lack the ability to fully isolate the insulin signalling pathway experimentally as is possible in *in vitro* work. It could therefore be possible that insulin signalling inhibition reported in *in vivo* experiments may not necessarily be a direct result of ER stress-JNK signalling on insulin signalling. In support of this, *in vivo* experiments showed that inhibition of insulin signalling also occurred upstream of IRS1 as insulin receptor tyrosine phosphorylation was perturbed. This suggests that insulin signalling inhibition in these *in vivo* experiments is mechanistically different in *in vitro* experiments and may not involve ER stress-JNK signalling. As a result there is no causal evidence that ER stress-mediated JNK activation inhibits insulin signalling downstream of IRS1. However, data in this thesis do also support the findings by Ozcan *et al.* and others that ER stress-mediated JNK activation occurs, however it does not support the hypothesis that short periods of this JNK activation is sufficient to inhibit insulin signalling. Why data in this thesis chapter does not support inhibited insulin signalling during ER stress-mediated JNK activation is yet to be understood. Differences in levels of JNK phosphorylation and insulin-stimulated activation of the insulin receptor may account for the conflicting data.

4.5.2 The role of TRB3 ER stress-mediated insulin resistance

Previous studies have provided mostly correlative evidence that TRB3 overexpression induces insulin resistance (Du et al., 2003, Koh et al., 2006, Koh et al., 2013, Liew et al., 2010, Takahashi et al., 2008). In contrast to these previous reports, data in this chapter suggests that increased TRB3 expression does not necessarily result in inhibition of insulin signalling. For example, TRB3 expression was induced 20 fold with ER stress in C_2C_{12} cells yet TRB3-dependent insulin resistance is not observed (Figure 4.2.4). However, not all studies have consistently reported TRB3 expression with inhibited insulin signalling during ER stress. For example 3T3-L1 cells infected with a retroviral vector expressing TRB3 showed unaltered insulin-stimulated AKT serine phosphorylation (Takahashi et al., 2008). Also, the insulin-induced activation of AKT and GSK3 was shown to be undiminished in TRB3 transduced primary hepatocytes (Iynedjian, 2005). In these studies TRB3 has been overexpressed through viral transduction which is estimated to cause overexpression of 700-1000 fold at the mRNA level (Iynedjian, 2005). Therefore, expression levels of TRB3 in ER-stressed cells are likely to be much lower than in virally transduced cells overexpressing TRB3. Thus the expression level of TRB3 may not be high

enough to pass the threshold which overexpressing cells do to sufficiently inhibit either IRS1 or AKT phosphorylation.

A further explanation is that TRB3 may be interacting with other proteins during ER stress and therefore reducing its interaction with AKT. For example, TRB3 can interact with the ER stress-induced proteins ATF4 (Liew et al., 2010, Ord and Ord, 2003) and CHOP (Ohoka et al., 2005), which during ER stress may interact with TRB3 thus reducing its ability to interact with the insulin signalling proteins AKT and IRS1. Therefore, it is possible that reduced interaction with AKT or IRS1 explains the lack of inhibited insulin signalling during ER stress-induced TRB3 expression. Further studies are required to fully characterise the role of TRB3 during ER stress.

5 ENDOPLASMIC RETICULUM STRESS CAUSES INSULIN RESISTANCE BY INHIBITING DELIVERY OF NEWLY SYNTHESISED INSULIN RECEPTORS TO THE CELL SURFACE

5.1 Rationale

Few studies have looked at shorter periods of ER stress, such as <3 h, and these studies have not fully investigated the role of ER stress-JNK signalling on insulin signalling during these short periods of ER stress (Ozcan et al., 2004). Due to this gap in knowledge this chapter investigates if early and transient JNK activation caused by short periods of ER stress is sufficient to inhibit insulin signalling. In the previous chapter, it was reported that up to 8 h of ER stress was not sufficient to inhibit insulin stimulation-induced: GSK phosphorylation, AKT phosphorylation and IRS1 tyrosine phosphorylation. These data were observed even when the previously reported mediators of ER stress-induced inhibition of insulin signalling, JNK and TRB3, where shown to be highly activated.

Due to the surprising finding that ER stress of up to 8 h, induced by 3 mechanistically different ER stressors, was unable to inhibit insulin signalling in several cell lines it was decided to extend the time which cells were exposed to ER stressors. Previous studies have shown that ER stress for longer periods of time, 24-36 h, also leads to insulin resistance in cultured cells (Avery et al., 2010, Hage Hassan et al., 2012, Xu et al., 2010, Zhou et al., 2009, Tang et al., 2011). Therefore, it was questioned if prolonged/chronic ER stress was able to inhibit insulin signalling in a way in which short acute to ER stress was unable to.

This chapter contains figures from a manuscript (see appendix D) entitled ‘Endoplasmic reticulum stress causes insulin resistance by inhibiting delivery of newly synthesized insulin receptors to the cell surface’ with the authors Max Brown, Adina D. Mihai, Adrienne W. Paton, James C. Paton, and Martin Schröder.

5.2 Prolonged ER stress causes insulin resistance

As discussed, the majority of studies reporting ER stress-mediated insulin signalling inhibition have examined this in cultured cells experiencing long periods of ER stress (Avery et al., 2010, Hage Hassan et al., 2012, Xu et al., 2010, Zhou et al., 2009, Tang et

al., 2011). Thus the next step was to investigate if prolonged periods of ER stress, longer than the 8 h reported in the previous chapter, were sufficient to inhibit insulin signalling.

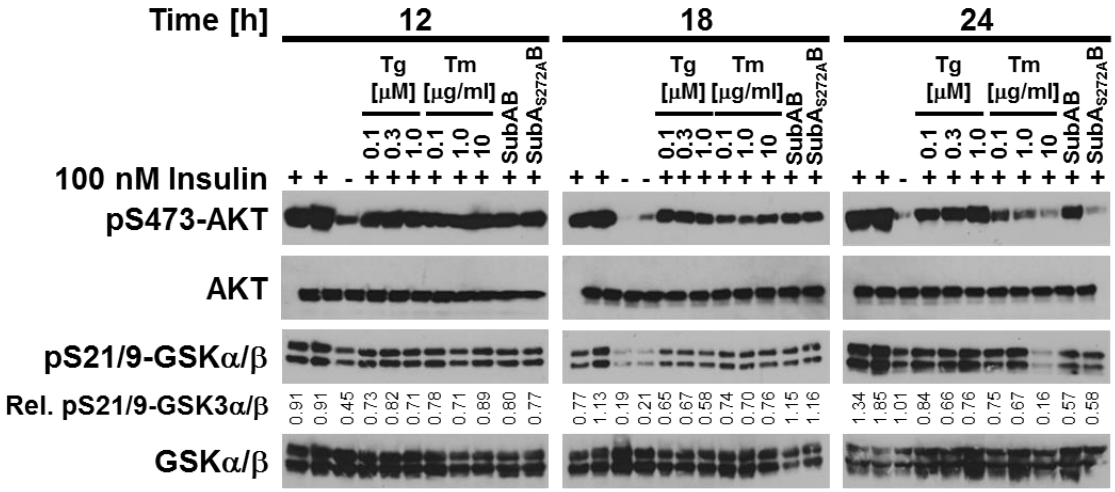

Figure 5.1. Insulin resistance develops over time in ER-stressed C_2C_{12} myoblasts.

Serum-starved C_2C_{12} cells were treated with the indicated concentrations of thapsigargin, tunicamycin, or 1 µg/ml SubAB or SubA_{A272}B for 12-24 h before stimulation with 100 nM insulin for 15 min. Cell lysates were analysed by Western blotting. Quantitation of the pS473-AKT signal relative to AKT is shown in shown in Figure 5.2.

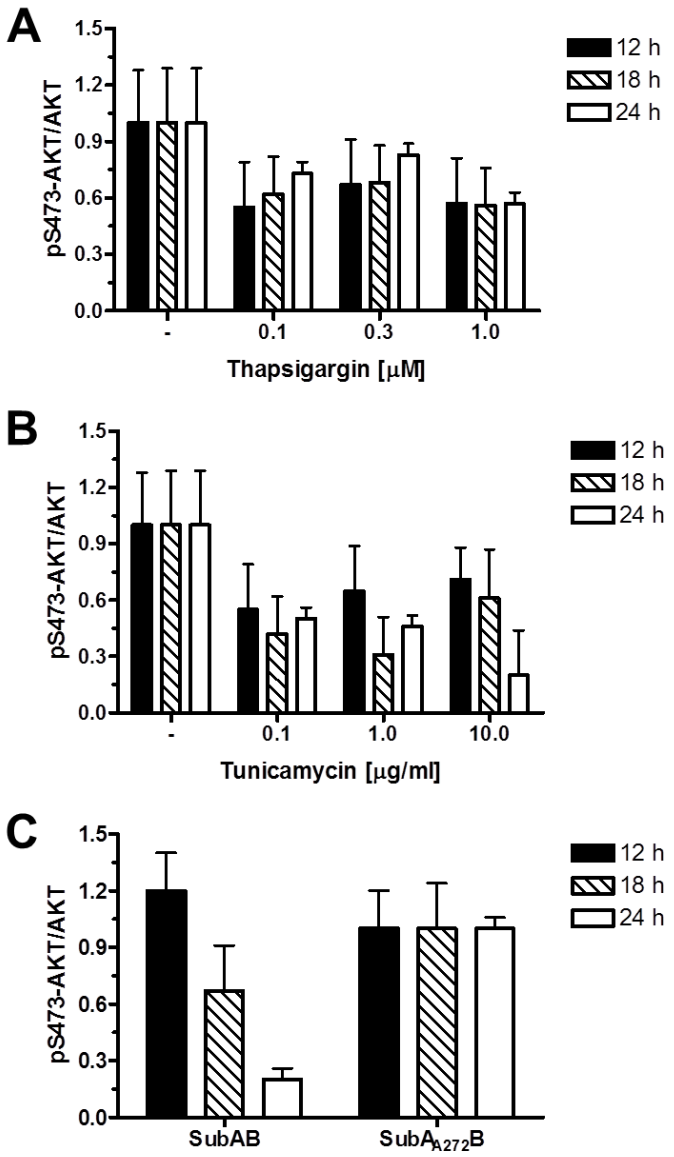

Figure 5.2. Insulin resistance develops over time in ER-stressed C_2C_{12} myoblasts: quantitation. Quantitation of the pS473-AKT signal relative to AKT from Western blots in Figure 5.1. **(A)** thapsigargin- (n = 2), **(B**) tunicamycin- (n = 2), and **(C)** SubAB-treated C_2C_{12} cells (n = 3). Bars represent standard errors.

`

Using the same wide range of ER stressors and concentrations, as used in the previous chapter, cultured C_2C_{12} cells were exposed to 12, 18 and 24 h of ER stress. Also, using the same experimental conditions as in the previous chapter, cells were serum starved for 18 h and then stimulated with 100 nM insulin for 15 min. Surprisingly, insulin-induced phosphorylation of AKT at S473 was inhibited by 12 h of both thapsigargin- and tunicamycin-induced ER stress (Figure 5.1). Inhibition of AKT activation was maintained

during 18 and 24 h of ER stress with both thapsigargin and tunicamycin exposure (Figure 5.2 A, B). Unfortunately, only one repeat was performed with thapsisgargin and tunicamycin which prevented meaningful statistical testing. SubAB-induced ER stress did not inhibit AKT phosphorylation greater than the catalytically inactive $SubA_{A272}B$ at 12 h. After 18 h of exposure a non-significant decrease in AKT phosphorylation was observed. AKT phosphorylation is significantly reduced after 24 h of SubAB-induced ER stress (Figure 5.1 and Figure 5.2 C). As an additional measure of insulin signalling to AKT activation the downstream phosphorylation of GSK3 was also monitored during prolonged ER stress (Figure 5.1). Insulin-induced GSK3 phosphorylation was also perturbed during prolonged ER stress exposure in C_2C_{12} cells. However, inhibition of GSK phosphorylation was not as obvious and consistent as perturbation of AKT phosphorylation but this may be due in part to the quality of both the antibody and Western blots. It may also be a result of secondary effects of ER stressors acting on signalling between AKT-GSK3. Overall, prolonged ER stress of 12+ h leads to insulin resistance in C_2C_{12} cells.

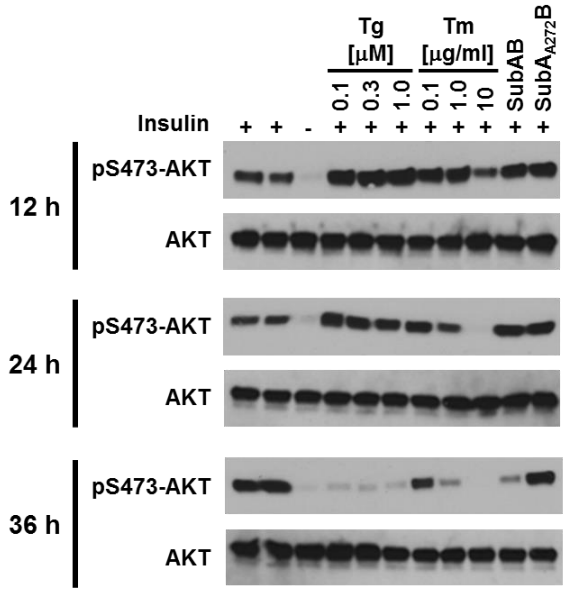

Figure 5.3. Insulin resistance develops over time in ER-stressed Hep G2 cells.

Serum-starved Hep G2 cells were treated with the indicated concentrations of thapsigargin, tunicamycin or 1 μg/ml SubAB or catalytically-inactive $SubA_{A272}B$ for 12-36 h before stimulation with 100 nM insulin for 15 min. Cell lysates were analysed by Western blotting. Quantitation of the pS473-AKT signal relative to AKT is shown in shown in Figure 5.4.

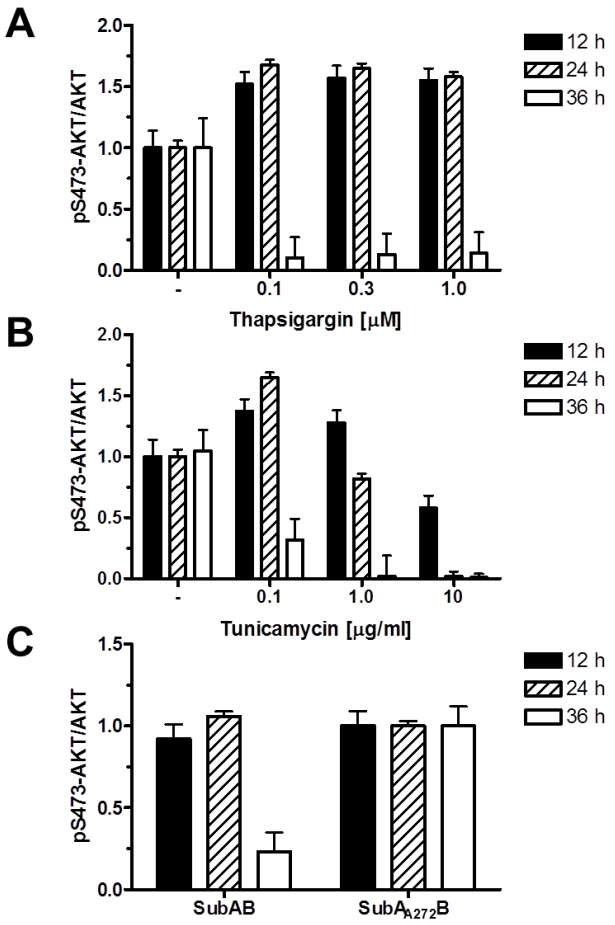

Figure 5.4. Insulin resistance develops over time in ER-stressed Hep G2 cells: quantitation. Quantitation of the pS473-AKT signal relative to AKT from Western blots in Figure 5.3. **(A)** thapsigargin- (n = 2), **(B)** tunicamycin- (n = 2), and **(C)** SubAB-treated Hep G2 cells (n = 3).

To address the question that these findings might be specific to C_2C_{12} cells, insulin signalling was investigated in other cell lines exposed to prolonged ER stress. In agreement with experiments in C_2C_{12} cells, prolonged exposure of ER stress in Hep G2 cells leads to insulin resistance (Figure 5.3 and Figure 5.4). 36 h of ER stress induced by all three ER stressors was sufficient to greatly inhibit AKT phosphorylation in Hep G2 cells. It is worth noting that Hep G2 cells require longer periods of ER stress for the manifestation of perturbed insulin signalling (discussed later). The highest concentration of tunicamycin tested was sufficient to cause perturbed insulin signalling as early as 12 h exposure, this difference may be explained by either the level of ER stress or the mechanism by which tunicamycin elicits ER stress (see discussion).

A detailed dose-response over a time course of 1-18 h with tunicamycin in 3T3-F442A cells was performed to fully characterise when insulin signalling becomes perturbed with

ER stress in these cells. Prolonged stress of 12, and to a greater degree, 18 h in 3T3-F442A cells inhibits AKT phosphorylation (Figure 5.5). Even the highest concentration of 10 µg/ml of tunicamycin was not sufficient to inhibit insulin signalling earlier than 12 h, which confirms results from the previous chapter that 8 h or less of ER stress has no effect on insulin signalling. At the latest time point of 18 h even the very low concentrations of 0.01 µg/ml tunicamycin caused insulin resistance in 3T3-F422A cells.

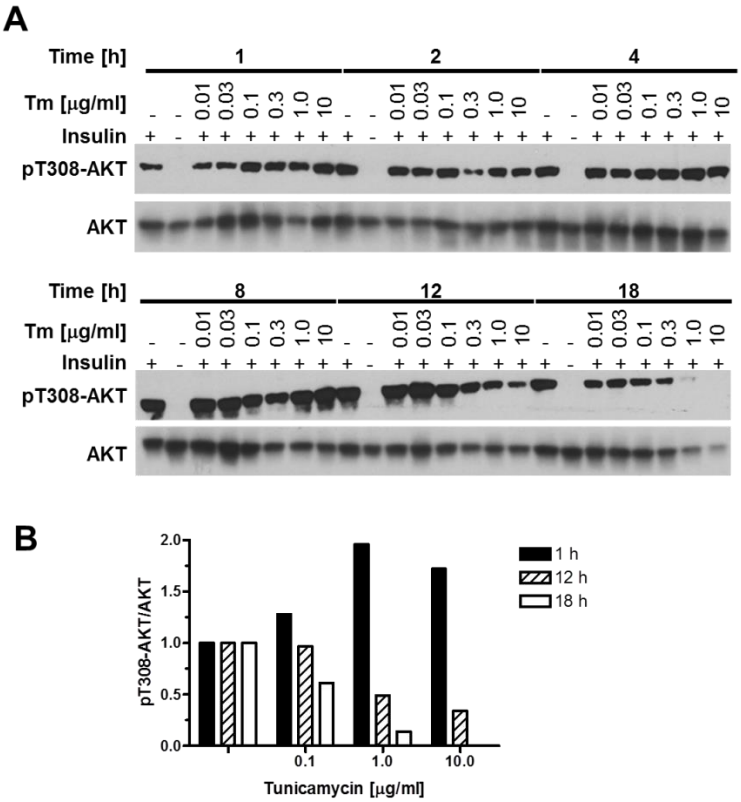

Figure 5.5. Insulin resistance develops over time in ER-stressed 3T3-F442A cells.
(A) Serum-starved 3T3-F442A cells were treated with the indicated concentrations of tunicamycin for 1-18 h before stimulation with 100 nM insulin for 15 min. **(B)** The pT308-AKT signal obtained by Western blotting was standardised to the total AKT signal to obtain the rel. pT308-AKT values.

5.3 The onset of insulin resistance caused by prolonged ER stress coincides with depletion of insulin receptors

Overall these figures suggest that prolonged ER stress is sufficient to inhibit insulin signalling in Hep G2, C_2C_{12} and 3T3-F442A. Studies investigating ER stress and insulin signalling rarely monitor the insulin signalling pathway upstream of IRS1- the insulin receptor (INSR). The insulin receptor has a half-life at the plasma membrane of 7-13 h (Reed and Lane, 1980, Reed et al., 1981a, Reed et al., 1981b, Kasuga et al., 1981, Capeau

et al., 1985, Savoie et al., 1986, Grako et al., 1992). Because loss of insulin signalling was only observed after at least 12 h of ER stress it was questioned if the onset of insulin resistance in ER-stressed cells correlates with depletion of insulin receptors.

Western blotting using the anti-INSR antibody, which recognises the C-terminus of insulin receptor β, in untreated cell lysates reveals multiple bands in different cell lines: five in murine cell lines C_2C_{12} and 3T3-F4421, and three in human Hep G2 and HEK 293 cell lines. The band migrating at ~95 kDa represents the mature insulin receptor β chain. The two bands migrating at ~210 kDa represent the α-β proreceptor and an alternatively glycosylated form of the α-β proreceptor (Hwang and Frost, 1999), this was evidenced by the appearance of an additional band in tunicamycin treated cells representing the non-glycosylated form of the α-β proreceptor (Figure 1.1). The two additional bands detected in 3T3-F442A and C_2C_{12} cells at ~130 kDa may be produced by a less well characterised lysosomal event (Massague et al., 1981).

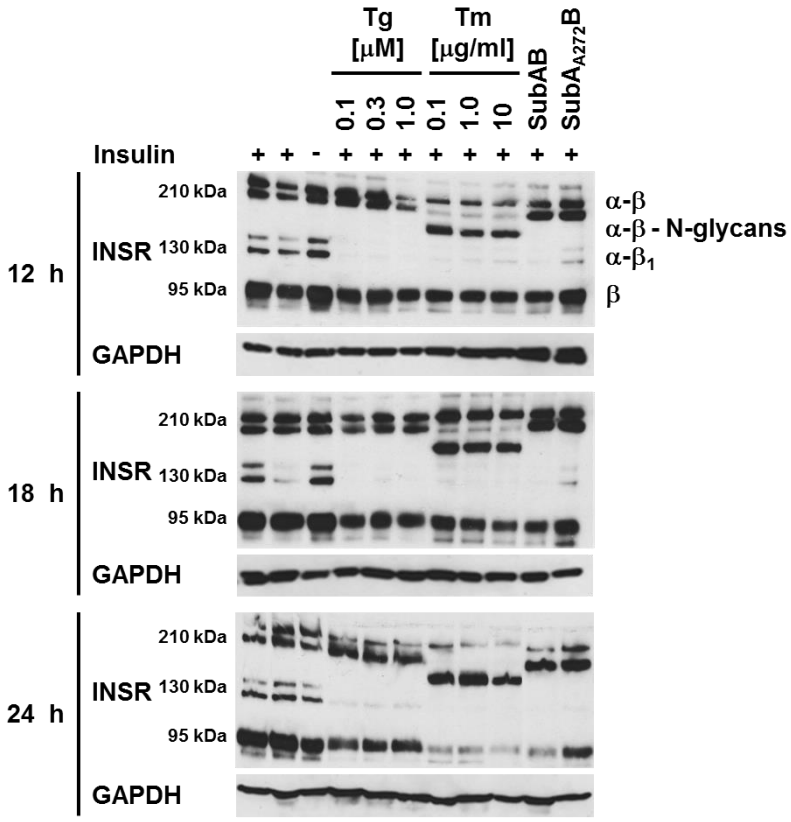

Figure 5.6. Depletion of insulin receptors in ER-stressed cells coincides with development of insulin resistance in C_2C_{12} cells.

C_2C_{12} cells were treated with the indicated ER stressors for 12-24 h before serum starvation and stimulation with 100 nM insulin for 15 min. Protein extracts were analysed by Western blotting. Quantitation of INSR β-chains is shown in Figure 5.7.

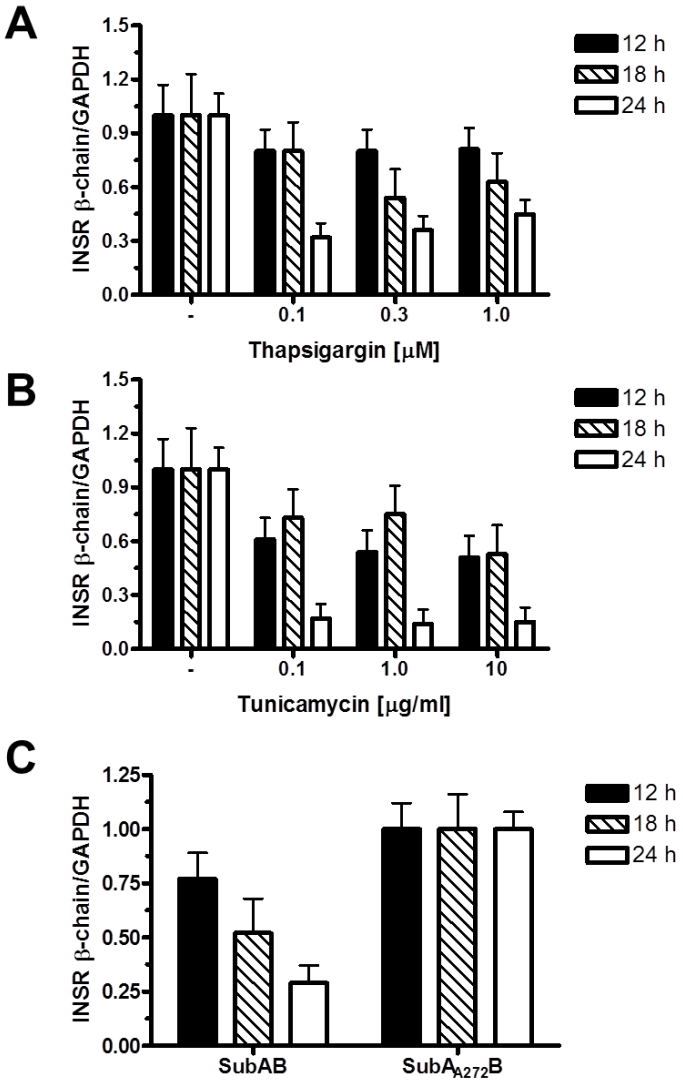

Figure 5.7. Depletion of insulin receptors in ER-stressed cells coincides with development of insulin resistance in C_2C_{12} cells: quantitation.

Quantitation of INSR β-chains from Figure 5.6 in **(A)** thapsigargin-, **(B**) tunicamycin-, and **(C)** SubAB-treated C_2C_{12} cells (n = 3).

It was observed that insulin receptor β chain levels are decreased after 12 h of ER stress in C_2C_{12} cells (Figure 5.6 and Figure 5.7). The decrease in insulin receptor β chains was exaggerated with longer periods of ER stress with the largest decrease seen at 24 h with all three ER stressors. This observed insulin receptor β chain decrease with prolonged ER stress correlates with the inhibition of insulin signalling in C_2C_{12} cells (Figure 5.1). Thus it appears that the onset of insulin resistance in ER-stressed C_2C_{12} cells correlates with depletion of insulin receptors.

Hep G2 cells differed from C_2C_{12} cells in previous experiments in that 36 h of ER stress with all three ER-stressors was required for insulin resistance (Figure 5.3). Correlating with these findings, a significant decrease in insulin receptor β chains was not observed until 36 h of ER stress with all three ER stressors in Hep G2 cells (Figure 5.8 and Figure 5.9). The highest concentration of tunicamycin was sufficient to decrease insulin receptor β levels after only 12 h and this too correlated with the faster inhibition of AKT phosphorylation observed.

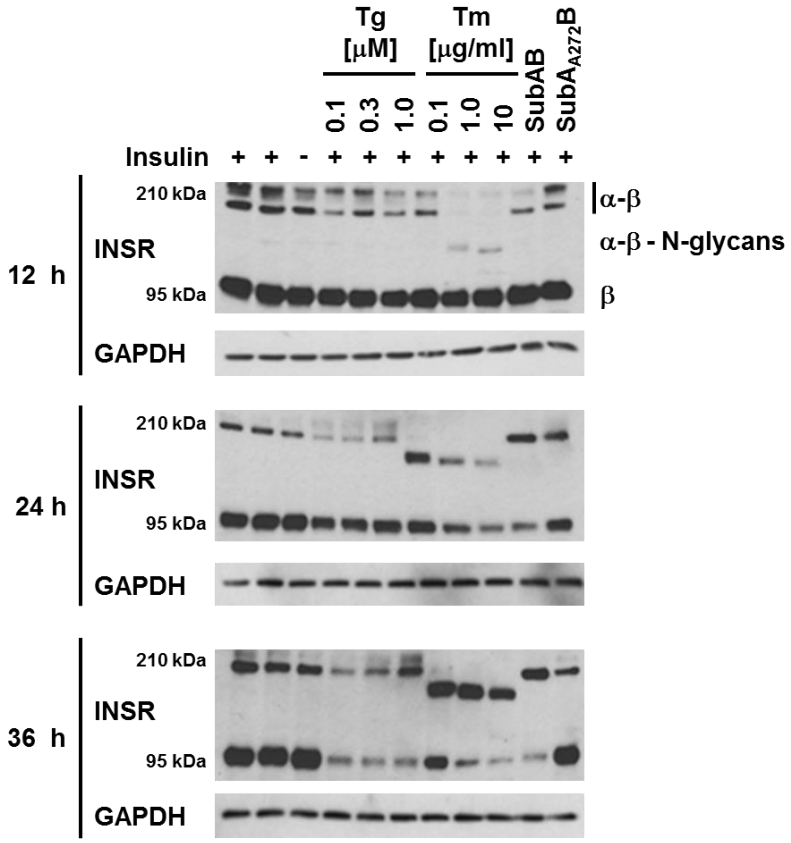

Figure 5.8. Depletion of insulin receptors in ER-stressed cells coincides with development of insulin resistance in Hep G2 cells.

Hep G2 cells were treated with the indicated ER stressors for 12-36 h times before serum starvation and stimulation with 100 nM insulin for 15 min. Protein extracts were analysed by Western blotting. Quantitation of INSR β-chains is shown in Figure 5.9.

Previously, the tunicamycin dose response experiment demonstrated that ≥12 h of tunicamycin exposure were required for insulin resistance in 3T3-F442A cells (Figure 5.5). Confirming results in both C_2C_{12} and Hep G2 cells, prolonged exposure to tunicamycin resulted in a decrease in insulin receptor β chains in 3T3-F442A (Figure 5.10). Even the lowest concentration of 0.01 μg/ml tunicamycin was previously sufficient to inhibit AKT

phosphorylation. Indeed this low tunicamycin concentration was also sufficient to lower insulin receptor β chains at 18 h but not at 12 h, which correlates with AKT phosphorylation data.

The data reported above is consistent with previous studies reporting that tunicamycin depletes insulin receptors and/or inhibits trafficking of the insulin receptor to the plasma membrane (Lane et al., 1985, Hart et al., 1988). It was proposed that inhibition of *N*-linked glycosylation, through which tunicamycin acts, was the mechanism of insulin receptor depletion. Data from this chapter extends these findings and provides evidence that other ER stressors, which do not directly inhibit *N*-linked glycosylation, also cause depletion of the insulin receptor. Hence, this data suggests that accumulation of unfolded proteins in the ER is the mechanism of insulin receptor depletion during ER stress.

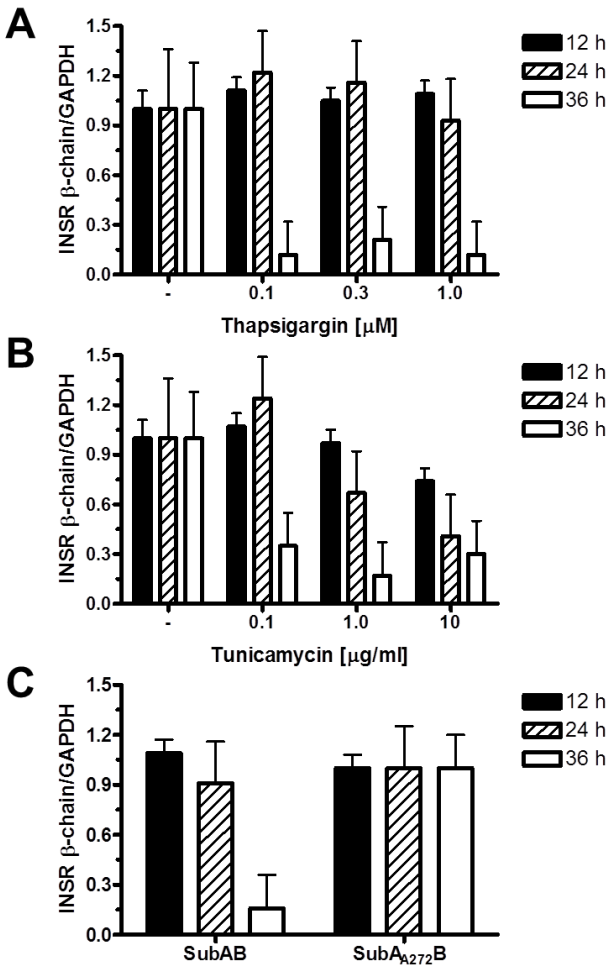

Figure 5.9. Depletion of insulin receptors in ER-stressed cells coincides with development of insulin resistance in Hep G2 cells: quantitation.

Quantitation of INSR β-chains from Figure 5.8 in **(A)** thapsigargin-, **(B**) tunicamycin-, and **(C)** SubAB-treated Hep G2 cells (n = 3).

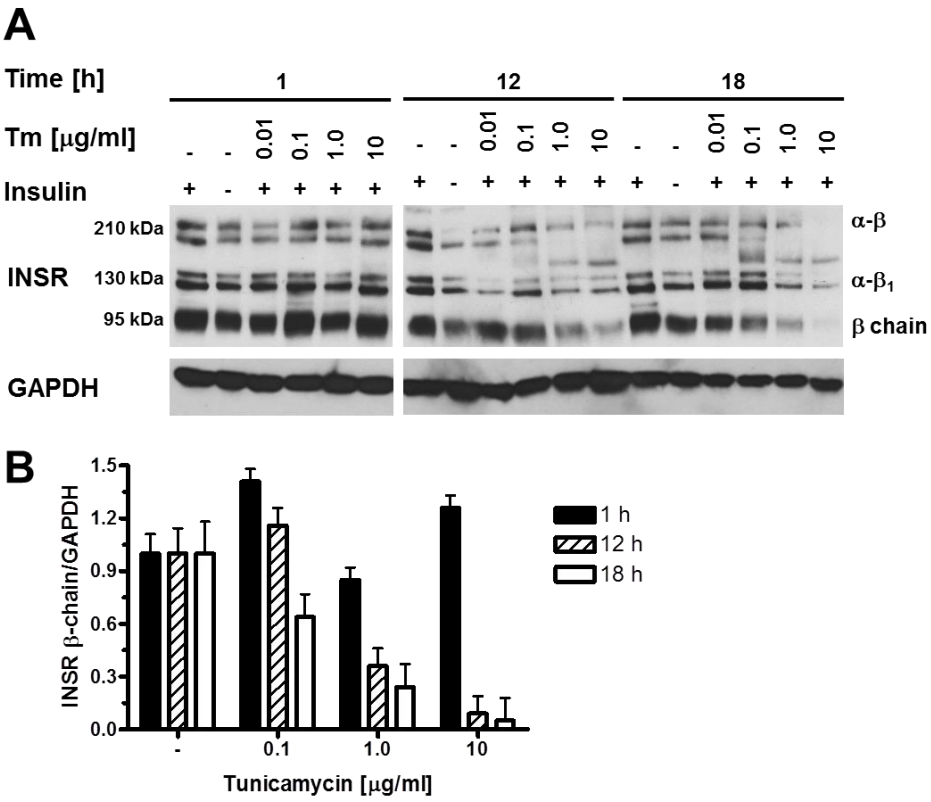

Figure 5.10. Depletion of insulin receptors in ER-stressed cells coincides with development of insulin resistance in 3T3-F442A cells.

3T3-F442A cells were treated with the indicated concentrations of tunicamycin for 1-18 h before serum starvation and stimulation with 100 nM insulin for 15 min. **(A)** Protein extracts were analysed by Western blotting. **(B)** Quantitation of INSR β-chains (n = 3).

5.4 Inhibition of transcription and translation do not account for reduced insulin receptor expression.

The UPR, which is activated during ER stress, induces several changes to cellular activity in an attempt to restore protein folding homeostasis. These changes may explain the depletion of the insulin receptor observed in cells exposed to prolonged ER stress: 1) the RIDD activity of IRE1α (Hollien and Weissman, 2006, Hollien et al., 2009) may be able to degrade insulin receptor mRNA, 2) general transcription may be repressed (Jang et al., 2010, Ord and Ord, 2003), 3) general translation of mRNA (including insulin receptor mRNA) may be inhibited by the phosphorylation of eIF2α by PERK (Harding et al., 2000, Harding et al., 1999), 4) the proper folding, maturation or trafficking of the insulin receptor may be inhibited during ER stress.

As discussed, the UPR can inhibit transcription and translation. As insulin proreceptor levels do not decrease over time with ER stress (Figure 5.6, Figure 5.8, and Figure 5.10) it is unlikely that either transcriptional or translational inhibition is responsible for depletion of the insulin receptor β chains. Nevertheless, it was investigated if the ER stress-mediated depletion of insulin receptor β chains is a result of UPR-induced inhibition of transcription or translation. RT-qPCR experiments on samples from C_2C_{12} cells exposed to 24 h of 300 nM thapsigargin, 1 µg/ml tunicamycin or 1 µg/ml SubAB reveal that there was an ~6 fold increase in steady state levels of *INSR* mRNA after prolonged ER stress (Figure 5.11). These data confirm that ER stress does not inhibit insulin receptor synthesis at the transcriptional level through general transcriptional repression or via the RIDD activity of IRE1α. An increase in *INSR* mRNA is surprising given that it could increase the burden further on the ER to maintain proper protein folding. However, it may be explained through the beneficial prosurvival signalling mediated through insulin signalling or that the *INSR* mRNA is stored in stress granules (Kedersha and Anderson, 2007). Insulin signalling can be an important prosurvival signalling pathway (Conejo and Lorenzo, 2001, Duarte et al., 2012, Duarte et al., 2008, Barber et al., 2001), meaning that increasing the mRNA for the receptor of this pathway would prioritise its synthesis during stress. For similar reasons the *INSR* mRNA may be stored in stress granules during ER stress-mediated translational inhibition (Hofmann et al., 2012) to be later released when protein folding returns to basal levels.

Evidence that translation is ongoing during ER stress was seen by the presence of nonglycosylated proreceptors in insulin receptor Western blots with lysates from cells exposed to tunicamycin (Figure 5.6, Figure 5.8, and Figure 5.10) Tunicamycin only inhibits *N*-glycosylation, it does not remove pre-existing glycans so the appearance of nonglycosylated proreceptors is indicative of continued translation of the insulin receptor during prolonged ER stress. It was also shown through experiments performed by other laboratory members that translational levels were also not significantly affected, ruling out that ER stress inhibits insulin receptor synthesis at the translational level (see manuscript in appendix D). Overall, these data show that prolonged ER stress must be causing the depletion of the synthesis of insulin receptor downstream of either transcription or translation.

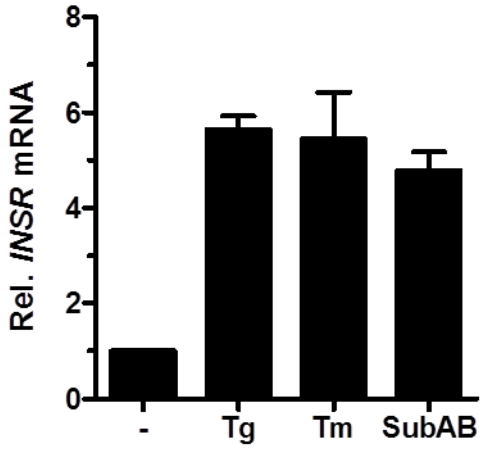

Figure 5.11. ER stress does not inhibit insulin receptor synthesis at the transcriptional level. *INSR* mRNA levels measured by RT-qPCR in C_2C_{12} cells treated with 300 nM thapsigargin, 1 µg/ml tunicamycin, or 1 µg/ml SubAB for 24 h (n = 3).

5.5 Confirmation that prolonged ER stress depletes the insulin receptor from the plasma membrane

Since transcriptional and translational effects cannot fully explain the decrease in insulin receptor levels it was characterised if ER stress was inhibiting the proper folding, maturation or transport of the insulin receptor to the cell membrane. Firstly, the ratio of proreceptors to mature insulin receptors was compared between ER stressed and untreated C_2C_{12} cells through quantification of Western blots (Figure 5.12). While mature β chains decrease in ER-stressed cells, α-β proreceptors increase relative to β chains. It is known that proprotein convertases in the *trans*-Golgi network are responsible for the cleavage of the proreceptor into α and β chains (Bravo et al., 1994, Robertson et al., 1993). It therefore stands that during prolonged ER stress proreceptors are accumulating in an earlier compartment in the secretory pathway such as the *cis*-Golgi or ER. To confirm this conclusion, protein extracts from either unstressed or ER-stressed C_2C_{12} cells were digested with endoglycosidase H (Endo H). Endo H cleaves between the two innermost *N*-acetylglucosamine units to release high mannose and some hybrid type *N*-linked oligosaccharides from glycoproteins (Maley et al., 1989). Oligosaccharide molecules are modified by a series of enzymes as a protein moves through the different compartments of the Golgi network. Mannose subunits are removed from oligosaccharides on proteins once they reach the Golgi complex by the enzyme Golgi α-mannosidase II (Trombetta and

Parodi, 2003). The presence of high mannose oligosaccharides is therefore characteristic of proteins that have not been processed in the Golgi complex.

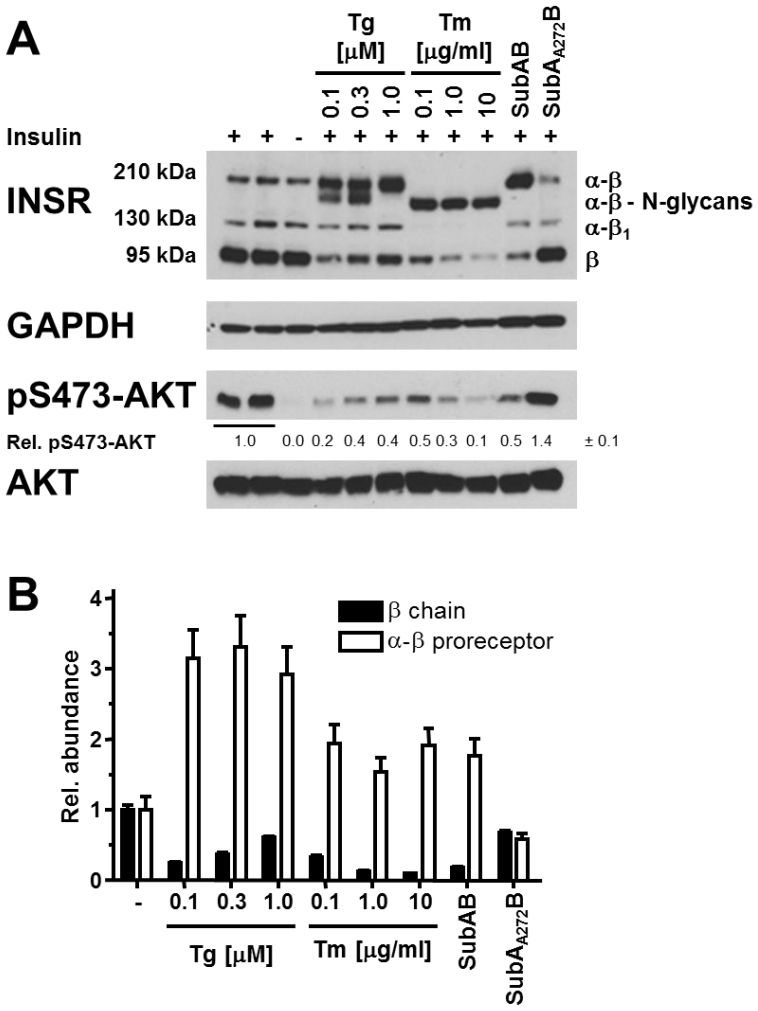

Figure 5.12. α-β Proreceptors accumulate in the ER of ER-stressed cells.

(A) Steady-state INSR levels in untreated C_2C_{12} cells or C_2C_{12} cells treated for 24 h with the indicated concentrations of thapsigargin, tunicamycin, 1 μg/ml SubAB, or 1 μg/ml $SubA_{A272}B$ and serum-starved during the last 18 h of drug treatment before stimulation with 100 nM insulin for 15 min. Cell lysates were analysed by Western blotting. **(B)** Quantitation of the results of insulin-stimulated cells from panel A (n = 2).

On SDS-PAGE gels Endo H digestion caused a shift in the band representing the proreceptors (Figure 5.13 A, B). The proreceptors migrated to the same position as fully deglycosylated proreceptors observed with PNGase F treatment (Figure 5.13 C), which removes all *N*-linked oligosaccharides regardless of a proteins location in the secretory pathway (Altmann et al., 1998). Endo H and PNGase F digested α-β proreceptors also migrate to the same position as unglycosylated α-β proreceptors synthesised in

tunicamycin treated cells, suggesting that they all represent one form of the α-β proreceptor, which lacks all the *N*-linked oligosaccharides. When digested with Endo H, the β chain, however, did not migrate to same position as the fully deglycosylated β chain (Figure 5.13 C). Consistent with a previous study this data suggests that the β chain contains only one Endo H sensitive and several Endo H resistant oligosaccharides (Hwang and Frost, 1999). This confirms that the band migrating at ~95 kDa does indeed represent the mature insulin receptor β chain found at the cell membrane. Thus, these data are consistent with the conclusion that ER stress causes accumulation of the α-β proreceptors early in the secretory pathway.

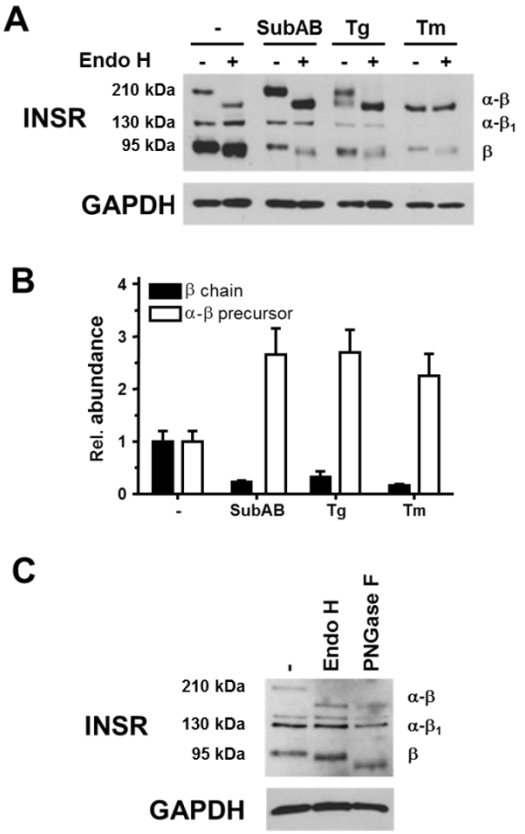

Figure 5.13. Glycosylation state of α-β proreceptors accumulating in the ER of ER-stressed cells. **(A)** Cell lysates from Figure 5.12 digested with Endo H. **(B)** Quantitation of the results of insulin-stimulated cells from panel A (n = 2). **(C)** The mature insulin receptor β chain carries an Endo H-sensitive *N*-linked oligosaccharide. Endo H and PNGase F digests of unstressed C_2C_{12} cells were Western blotted for the insulin receptor β chain.

To directly establish if the mature insulin receptor is depleted from the cell membrane during prolonged ER stress, the localisation of C-terminally GFP-tagged insulin receptors

were monitored in HEK 293 cells. It was decided that HEK 293 cells were to be used in replacement of Hep G2 cells as HEK 293 cells are: 1) more easily transfected, 2) easier to image microscopically as, in contrast to Hep G2 cells, they do not grow in clumps. Firstly, as HEK 293 cells have previously not been studied, cells were stressed with 100 ng/ml tunicamycin or 1 µg/ml SubAB for 18 h to monitor the steady state levels of the insulin receptor (Figure 5.14) 18 h of ER stress was found to be sufficient to greatly decrease the level of insulin receptor β chains in HEK 293 cells. Consequently, HEK 293 cells were transfected with C-terminally GFP-tagged insulin receptor before being treated with 100 ng/ml tunicamycin or 1 µg/ml SubAB for 18 h. It was clearly observed, through fluorescence microscopy, that after 18 h of ER stress the GFP-tagged insulin receptor redistributed from the cell membrane to intracellular compartments (Figure 5.15). This could be seen as the GFP fluorescence was localised to the fluorescence of the CellMask Deep Red plasma membrane stain in untreated cells, whereas the GFP fluorescence of cells exposed to 18 h of either tunicamycin or SubAB was more heavily concentrated to within the cell membrane defined by the CellMask Deep Red stain.

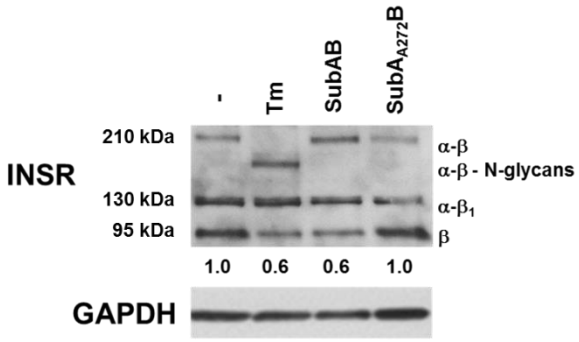

Figure 5.14. Depletion of insulin receptors in ER-stressed HEK 293 cells.
Steady-state INSR levels in untreated HEK 293 cells or HEK 293 cells treated for 18 h with 0.1 µg/ml tunicamycin, 1 µg/ml SubAB, or 1 µg/ml SubA$_{A272}$B.

To quantitatively monitor the localisation of the insulin receptor in unstressed and ER-stressed cells the Pearson's correlation coefficient, r_{obs}, was determined for the GFP and CellMask Deep Red fluorescence. An r_{obs} value of 1 suggests complete colocalisation and -1 no localisation. The average r_{obs} value for untreated cells was 0.86 whereas both tunicamycin and SubAB treatments caused a reduction in average robs values to 0.26 and 0.31 respectively (Figure 5.16). The Pearson's correlation coefficient analysis confirms the observation that in cells exposed for 18 h to either tunicamycin or SubAB there is a loss in colocalisation of the insulin receptor with the plasma membrane. Data obtained from

fluorescence microscopy therefore suggest that the mature insulin receptor is indeed depleted from the cell membrane in cells exposed to prolonged ER stress.

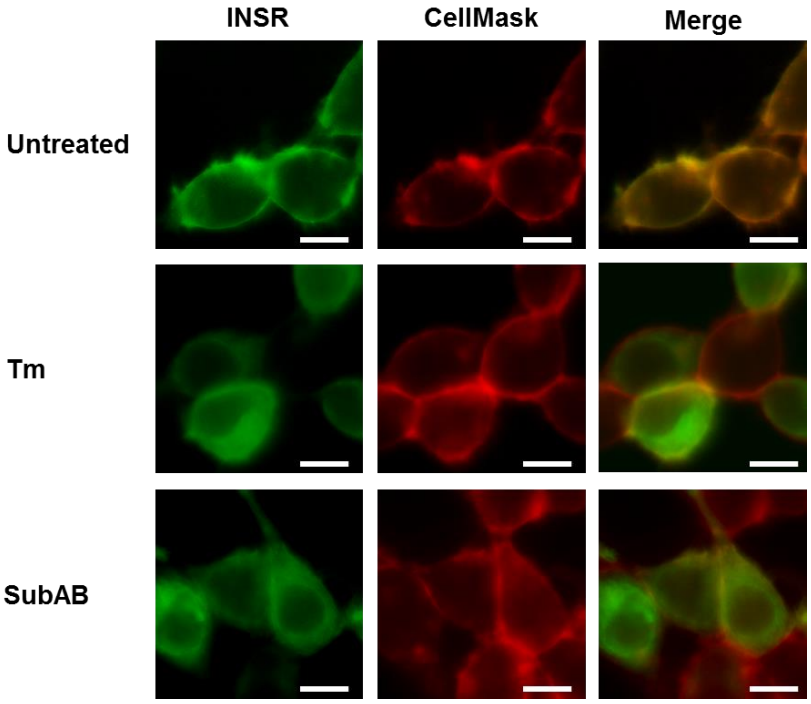

Figure 5.15. GFP-tagged INSR distribution is altered after prolonged ER stress.
(A) Localisation of GFP-tagged INSR in transiently transfected HEK 293 cells. HEK 293 cells were treated for 18 h with 1 µg/ml tunicamycin or 1 µg/ml SubAB were indicated. The scale bar is 10 µm long.

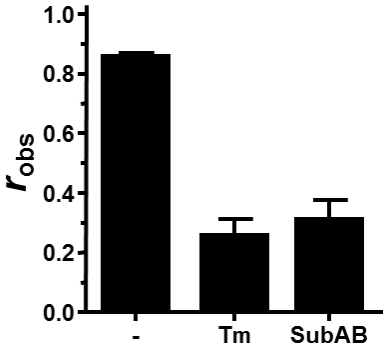

Figure 5.16. GFP-tagged INSR distribution is altered after prolonged ER stress: quantitation.
Average Pearson correlation coefficient r_{obs} between the INSR-GFP and CellMask Deep Red fluorescence determined from 11 randomly chosen cells (n = 3). The Pearson correlation coefficients for the randomised images are -0.13 ± 0.08, -0.13 ± 0.07, and -0.33 ± 0.07 for the untreated, tunicamycin-, and SubAB-treated cells, respectively.

To establish that the loss of the insulin receptor alone, without ER stress, was sufficient to inhibit insulin signalling the expression of the insulin receptor was silenced using siRNAs.

Three siRNAs against murine insulin receptor mRNA were transfected into C_2C_{12} cells before protein isolation and Western blotting to monitor AKT phosphorylation and insulin receptor protein levels. RT-qPCR was also performed to confirm knock-down of insulin receptor mRNA (Figure 5.17). All three siRNAs decreased insulin receptor mRNA steady state levels by 50-70%. The decrease in steady state levels was transient and messenger levels were highest 72 h after transfection. This is likely a result of the transient nature of siRNA mediated knockdown caused by cell division and the dilution of siRNAs below a critical threshold necessary to maintain knock-down of the gene (Dykxhoorn et al., 2003). Western blotting confirmed that reduced mRNA levels translated to a reduction in the protein level of the mature β chain. Knock-down of the insulin receptor was sufficient to inhibit insulin-stimulated AKT phosphorylation. AKT phosphorylation was reduced to a similar degree as reduced insulin receptor protein levels. Thus, loss of the insulin receptor alone is sufficient for inhibition of insulin signalling.

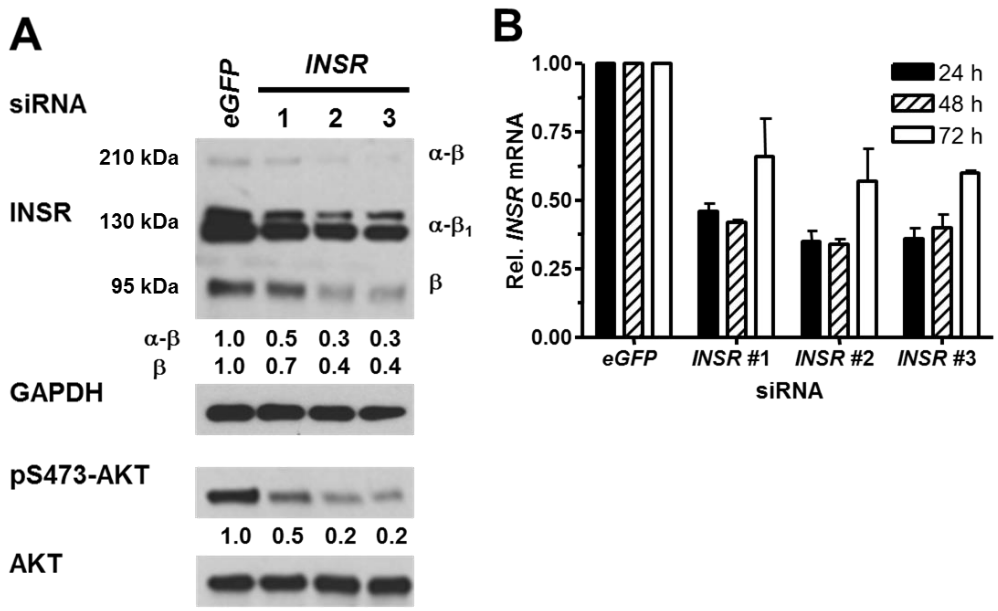

Figure 5.17. siRNA-mediated knock-down of expression of the insulin receptor inhibits insulin-stimulated phosphorylation of AKT.

(A). Serum-starved C_2C_{12} cells were stimulated with 100 nM insulin for 15 min 48 h after transfection of 50 nM of the indicated siRNAs. **(B)** Steady-state *INSR* mRNA levels standardized to *ACTB* in C_2C_{12} cells transfected with 50 nM of the indicated siRNAs for 24, 48, or 72 h (n = 2).

5.6 AKT activation by a cytosolic F_V2E-insulin receptor chimera is not affected by ER stress

Due to the accumulation of the α-β proreceptors early in the secretory pathway, as well as redistribution of the insulin receptor away from the plasma membrane in cells exposed to long-lasting ER stress, it was hypothesised that if insulin receptor synthesis bypassed the ER during long-lasting ER stress then insulin signalling would not be affected. To test this hypothesis an insulin receptor chimera was created in which the signal peptide as well as both the extracellular and transmembrane domains were replaced with an N-terminal myristoylation signal and an Fv2E domain. The myristoylation signal induces the N-terminal myristoylation of the protein resulting in it being anchored to intracellular membranes (Maurer-Stroh et al., 2002a, Maurer-Stroh et al., 2002b).

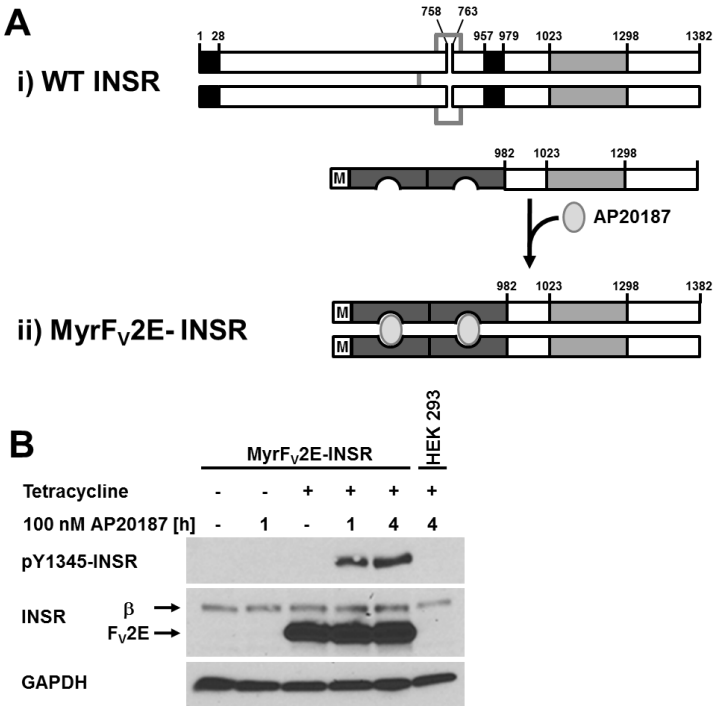

Figure 5.18. Expression and functionality of the myristoylated F_V2E-insulin receptor chimera. **(A)** Schematic of the myristoylated F_V2E-insulin receptor chimera. **(B)** Expression of the F_V2E-insulin receptor chimera was induced in Flp-In T-Rex 293 cells stably transfected with pcDNA5/FRT/TO-MyrF$_V$2E-INSR for 27 h with 1 µg/ml tetracycline, followed by dimerisation with 100 nM AP20187 for the indicated times.

Flp-In T-Rex 293 cells stably transfected with the insulin receptor chimera were treated with tetracycline and AP20187. Binding of AP20187 to the Fv2E domain mediates the dimerisation of chimeric proteins containing the Fv2E domain (Figure 5.18 A).

Dimerisation of the Fv2E-insulin receptor chimera with AP20187 resulted in increased tyrosine phosphorylation of the chimera at the Y1345 residue demonstrating that the chimera has tyrosine autophosphorylation activity (Figure 5.18 B). Treatment with AP20187 alone did not induce expression of the insulin receptor chimera and neither did it induce insulin receptor tyrosine phosphorylation. As an extra control HEK 293 cells not stably transfected were exposed to AP20187 and tetracycline and then monitored for insulin receptor expression and phosphorylation. As expected these two compounds were unable to induce expression of neither the chimeric insulin receptor nor its phosphorylation confirming that the tyrosine phosphorylation and expression of the chimeric insulin receptor is specific to the stably transfected cells and that the antibodies are detecting the correct proteins. In addition to insulin receptor phosphorylation, dimerisation in serum-starved cells caused an ~2.6 fold increase in AKT T308 phosphorylation. Treatment of cells expressing the myristoylated insulin receptor with AP20187 can therefore, at the AKT level, mimic insulin signalling mediated through insulin stimulation of the endogenous insulin receptor.

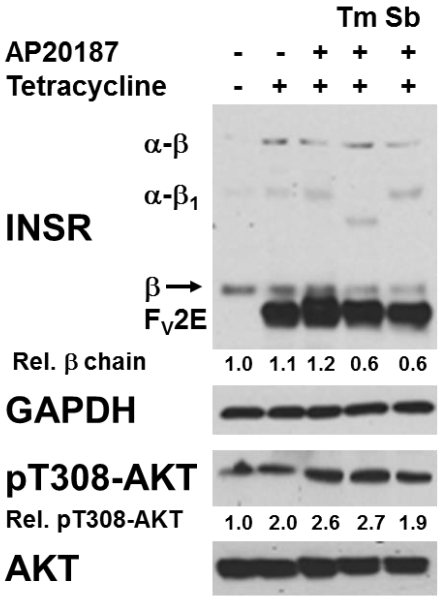

Figure 5.19. Bypass of the ER in insulin receptor synthesis abrogates ER stress-induced insulin resistance: HEK293 Flip-In T-Rex cells.

HEK293 Flp-In T-Rex cells stably transfected with pcDNA5/FRT/TO-MyrF_V2E-INSR were serum-starved during the last 18 h of a 24 h treatment with 10 μg/ml tunicamycin (Tm) or 1 μg/ml SubAB (Sb). Then, expression of the F_V2E-insulin receptor chimera was induced with 1 μg/ml tetracycline for 24 h, followed by dimerization of the construct with 100 nM AP20187 for 4 h. Western blots of total cell lysates are shown. The arrow indicates the β chain of the mature, endogenous insulin receptor.

After establishing the applicability of the insulin receptor chimera to study insulin signalling in cells not requiring trafficking of the insulin receptor through the secretory pathway, the next step was to investigate if cells ER stress-mediated depletion of the insulin receptors was dependent on inhibition of transport through the secretory pathway. To begin with, 24 h ER stress was induced in Flp-In T-Rex 293 cells stably transfected with the myristoylated insulin receptor chimera before cell lysates were Western blotted to monitor endogenous and chimeric insulin receptor levels as well as AKT phosphorylation (Figure 5.19). As expected prolonged ER stress lowered endogenous insulin receptor levels. Interestingly, although possessing the ability to autophosphorylate after dimerisation, the exposure of the chimeric insulin receptor in stably transfected Flp-In T-Rex 293 cells to AP20187 was unable to increase phosphorylation of AKT at S473 (data not shown). AKT T308 phosphorylation was instead monitored and this was modestly increased with AP20187 treatment. AKT T308 phosphorylation also increased with tetracycline suggesting that highly expressing this chimera may sometimes be sufficient to cause dimerization and autophosphorylation. Treatment with tunicamycin for 24 h was not sufficient to inhibit AKT T308 phosphorylation induced by tetracycline and AP20187. SubAB only slightly reduced the AKT T308 phosphorylation induced by a combination of AP20187 and tetracycline to the level induced by tetracycline only. The phosphorylation of both S473 and T308 was required for activation of AKT suggesting that AKT phosphorylation is defective in Flp-In T-Rex 293 cells. Because the same amount of protein was used in all Western blotting experiments (except in Endo H and PNGase F digests) it was observed that AKT S473 phosphorylation was constitutively high in Flp-In T-Rex 293 cells (data not shown) suggesting that signalling via the insulin receptor chimera may not have been sufficient to observe changes in AKT S473 phosphorylation above an already high background level.

As AKT phosphorylation in Flp-In T-Rex 293 cells appears to be overactive compared to all other cell lines investigated so far, the effect of the myristoylated insulin chimera in another cell lines was investigated. C_2C_{12} cells were chosen because: 1) transfection had previously been optimised in this cell line, and 2) the insulin receptor depletion and AKT phosphorylation have been well characterised in previous experiments. Hence, C_2C_{12} were transiently transfected with the plasmid encoding the myristoylated insulin receptor chimera before being exposed to long-lasting ER stress induced by thapsigargin, tunicamycin or SubAB (Figure 5.20). In C_2C_{12} cells AP20187 treatment increased AKT S473 phosphorylation ~3 fold. The AP20187-induced phosphorylation of AKT was

uninhibited by 24 h of ER stress and this was the same for all three mechanistically different ER stressors. The greater increase of AKT phosphorylation induced by AP20187 in C_2C_{12} versus Flp-In T-Rex 293 cells supports the idea that AKT phosphorylation was for some reason overactive or less responsive in Flp-In T-Rex 293 cells. These data therefore support the hypothesis that bypass of the ER in the synthesis of the insulin receptor prevents long-lasting ER stress-induced insulin resistance. Overall, these results support the conclusion that insulin resistance in ER-stressed cells is a result of inhibited transport of newly synthesised insulin receptors through the secretory pathway.

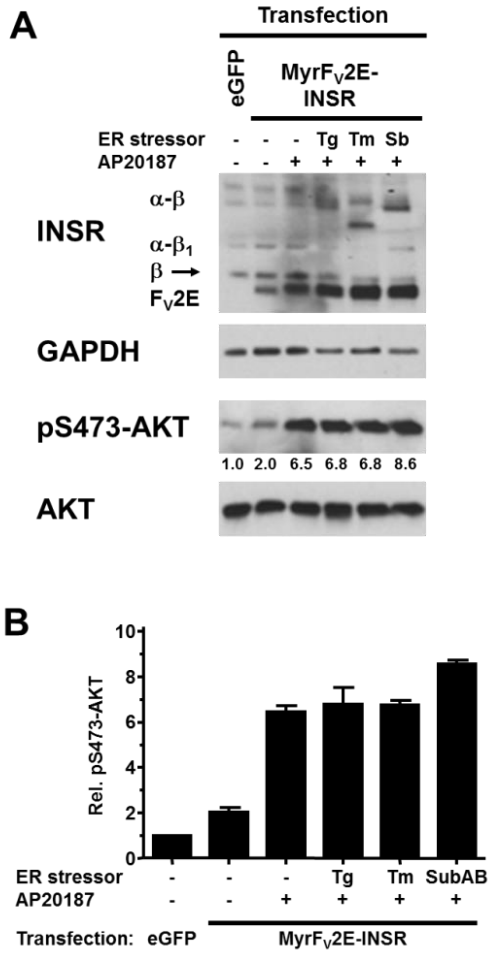

Figure 5.20. Bypass of the ER in insulin receptor synthesis abrogates ER stress-induced insulin resistance: C_2C_{12} cells.

(A) C_2C_{12} cells were transiently transfected with pmaxGFP or pcDNA5/FRT/TO-MyrF$_V$2E-INSR. 24 h after transfection ER stress was induced for 24 h with 0.1 µM thapsigargin (Tg), 0.1 µg/ml tunicamycin, or 1 µg/ml SubAB followed by dimerisation of the receptor with 100 nM AP20187 for 4 h and preparation of cell lysates for Western blotting. The arrow indicates the β chain of the mature, endogenous insulin receptor. **(B)** Quantitation of the results shown in panel (A) (n = 2).

It is worth noting that the myristoylation of the insulin receptor chimera allows its localisation to all membranes and as such it may not be entirely located at the cell membrane. However, as treatment of AP20187 was able to induce AKT phosphorylation in cells expressing the insulin receptor chimera, it would appear that either activation of the insulin signalling pathway downstream of insulin is not dependent on localisation to the plasma membrane or that the amount of chimera which is bound to plasma membrane is sufficient for activation of AKT.

5.7 JNK knock-out MEFs are not protected from ER stress-induced insulin resistance

As discussed in more detail in chapter 4, both JNK and TRB3 have been implicated in mediating insulin resistance during ER stress. In chapter 4 it was shown that ER stress up to 8 h was not sufficient to inhibit insulin signalling even when JNK was activated. Using JNK knock-out MEFs it was investigated if JNK was involved in the inhibition of insulin signalling during long-lasting ER stress. WT and *jnk1*$^{-/-}$ *jnk2*$^{-/-}$ MEF cells were exposed to thapsigargin, tunicamycin or SubAB for 24 h before protein isolation and Western blotting (Figure 5.21 and Figure 5.22). AKT phosphorylation levels were comparable between WT and *jnk1*$^{-/-}$ *jnk2*$^{-/-}$ MEF after long-lasting ER stress induced by all three ER stressors. JNK activation was also monitored at 24 h of ER stress in WT and *jnk1*$^{-/-}$ *jnk2*$^{-/-}$ MEFs to confirm that ER stress was inducing JNK phosphorylation at this time point (Figure 5.23). Unsurprisingly, total and phosphorylated JNK was not detected in *jnk1*$^{-/-}$ *jnk2*$^{-/-}$ MEFs, which confirmed that they were indeed *jnk1*$^{-/-}$ *jnk2*$^{-/-}$ MEFs (data not shown). 24 h of ER stress activated JNK 2-4 fold in WT MEFs demonstrating that JNK activation at 24 h is not involved in ER stress-dependent insulin resistance as *jnk1*$^{-/-}$ *jnk2*$^{-/-}$ MEFs also display inhibited AKT phosphorylation.

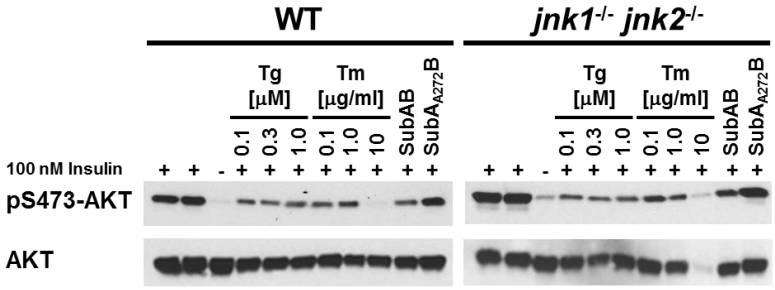

Figure 5.21. *jnk1*$^{-/-}$ *jnk2*$^{-/-}$ MEFs are not protected from developing insulin resistance when exposed to chronic ER stress.

WT and *jnk1*$^{-/-}$ *jnk2*$^{-/-}$ MEFs were treated for 24 h with the indicated concentrations of thapsigargin or tunicamycin, 1 μg/ml SubAB, or 1 μg/ml $SubA_{A272}B$ and serum-starved during the last 18 h of drug treatment before stimulation with 100 nM insulin for 15 min. Quantitation of AKT S473 phosphorylation relative to total AKT levels are shown in Figure 5.22.

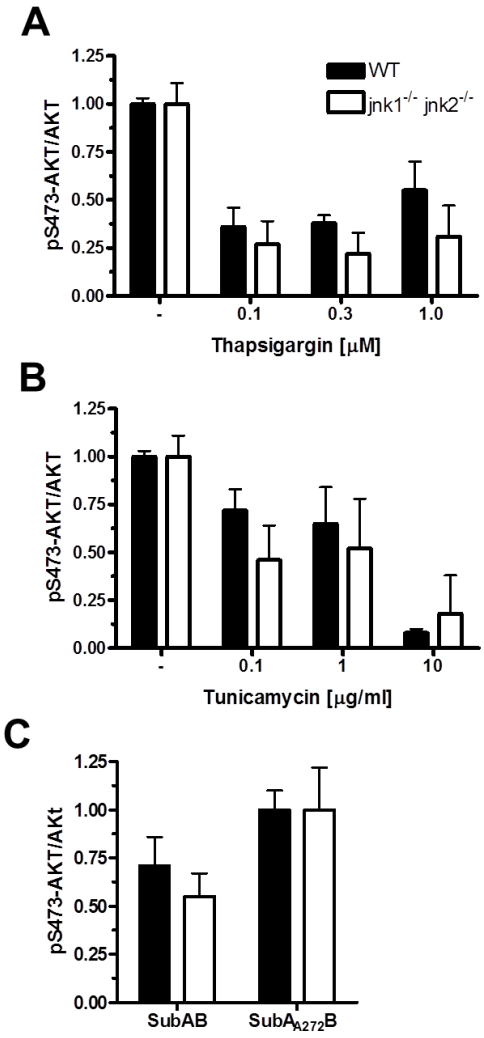

Figure 5.22. *jnk1*$^{-/-}$ *jnk2*$^{-/-}$ MEFs are not protected from developing insulin resistance when exposed to chronic ER stress: quantitation.

Quantitation of AKT S473 phosphorylation relative to total AKT levels in WT and *jnk1*$^{-/-}$ *jnk2*$^{-/-}$ MEFs exposed to **(A)** thapsigargin, **(B)** tunicamycin, and **(C)** SubAB (n = 2).

ER stress-dependent TRB3 activation is reported to mediate insulin resistance. However, in chapter 4 it was shown that ER stress up to a maximum of 8 h was not sufficient to inhibit insulin signalling even when TRB3 was highly expressed. Thus the activation of TRB3 during prolonged ER stress was investigated. Previous figures have shown that use of a myristoylated insulin receptor chimera, which bypasses the secretory pathway, prevents ER stress-induced insulin resistance in C_2C_{12} cells (Figure 5.19 and Figure 5.20). Thus experiments were performed to characterise the expression of TRB3 in C_2C_{12} cells using the same time point and ER stressor concentrations. Consistent with other reports the data suggest that long-lasting ER stress induces expression of TRB3 (Figure 5.24). TRB3, although being highly expressed during 24 h ER stress, was still not sufficient to inhibit AKT phosphorylation induced through insulin receptor chimera activation. Thus, elevated levels of TRB3 do not inhibit AKT phosphorylation during prolonged ER stress.

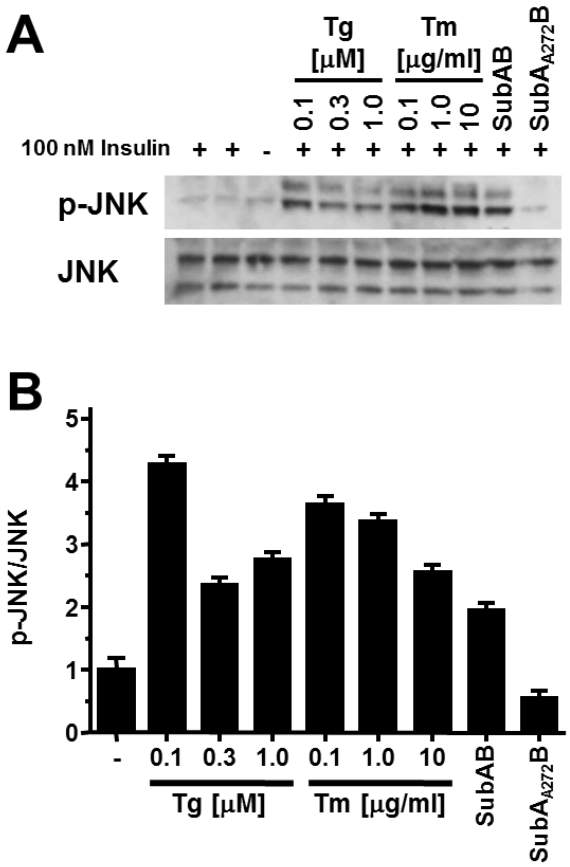

Figure 5.23. Prolonged ER stress activates JNK in WT MEFs.

(A) Activation of JNK in WT MEFs exposed to the indicated concentrations of thapsigargin or tunicamycin, 1 µg/ml SubAB, or 1 µg/ml $SubA_{A272}B$ and serum-starved during the last 18 h of drug treatment before stimulation with 100 nM insulin for 15 min. **(B)** Quantitation of the Western blots in panel (A) ($n = 2$).

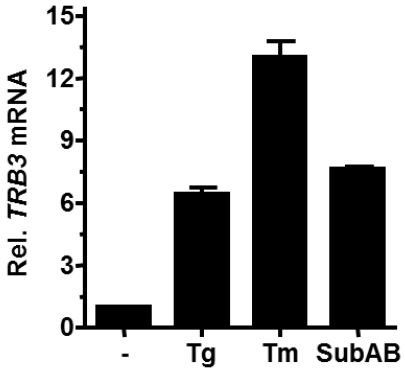

Figure 5.24. *TRB3* mRNA levels after prolonged ER stress.

TRB3 mRNA levels measured by RT-qPCR in C_2C_{12} cells treated with 300 nM thapsigargin, 1 µg/ml tunicamycin, or 1 µg/ml SubAB for 24 h (n = 3).

5.8 ER stress depletes insulin receptors in neuron-like cells

Diabetes is reported to affect neuronal tissue and as such as been implicated in neurodegenerative diseases (Wang et al., 2014, Hu et al., 2007). Previously in this chapter prolonged ER stress in cells derived from: liver, muscle and adipose tissue has been investgated. Research was therefore extended to include cells with a neuronal lineage. Differentiated human neuroblastoma SH-SY5Y (Ross et al., 1983) cells exposed to thapsigargin, tunicamycin or SubAB for 24 h showed a decrease in insulin receptor β chains to a similar extent as non-neuronal cell lines (Figure 5.25 A). Similar results were also observed in differentiated murine Cath.-a-differentiated (CAD) (Suri et al., 1993) cell line (Figure 5.25 B). 4 h of exposure to any of the three ER stressors used was not long enough to deplete insulin receptor levels and confirms the findings that ER stress over several half-lives of the insulin receptor protein is required for depletion at the plasma membrane. Thus, long-lasting ER stress also depletes insulin receptors in neuronal cell lines.

To confirm that long-lasting ER stress causing insulin resistance via depletion of insulin receptors is not specific to immortalised cell lines, mouse primary glial cultures were exposed to 24 h of SubAB (Figure 5.25 C). SubAB treatment caused a decrease in insulin receptor β chain levels whilst increasing proreceptor levels, suggesting that prolonged ER stress depletes insulin receptors at the plasma membrane by inhibiting trafficking of newly synthesised insulin receptors through the secretory pathway. During ER stress treatment, primary glial cells were serum-starved for 18 h and then stimulated with 100 nM insulin for 15 min prior to harvesting lysates to monitor insulin signalling. Insulin stimulation

resulted in increased phosphorylation of AKT at S473, demonstrating that primary glial cells are insulin sensitive. 24 h of SubAB, which lowered insulin receptor β chains, inhibited insulin-mediated phosphorylation of AKT. Thus, prolonged ER stress causes insulin resistance in primary glial cells.

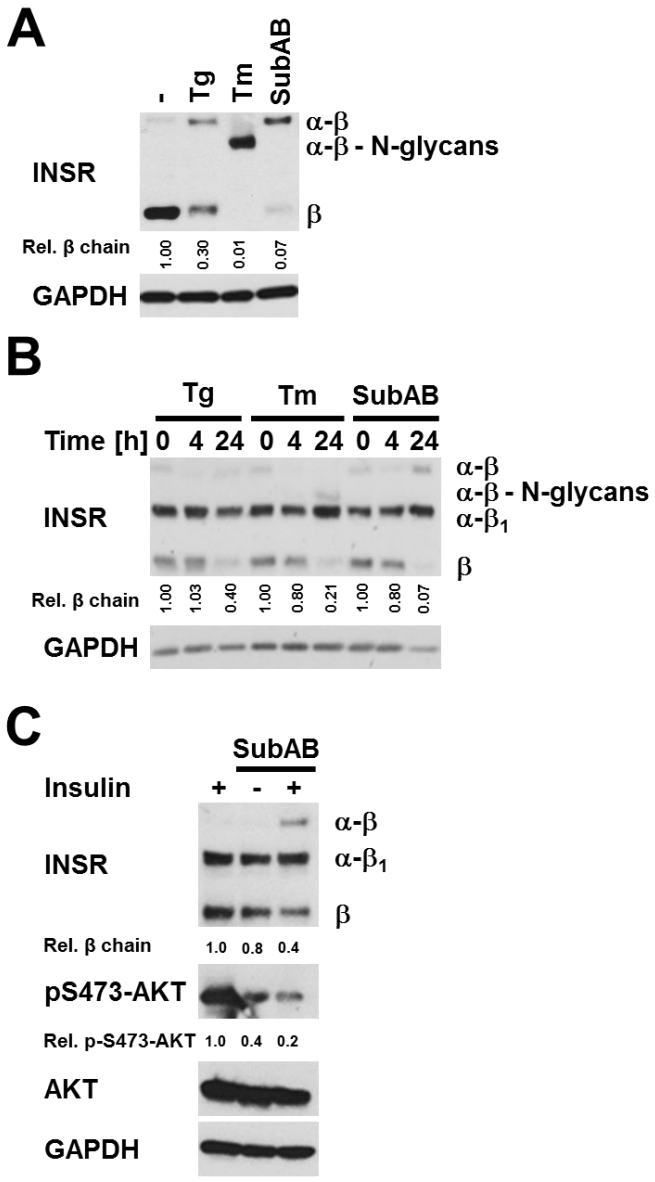

Figure 5.25. ER stress depletes insulin receptors in neuronal cell lines and primary glia.
(A-C) Depletion of the β chain of the insulin receptor by ER stress in (A) differentiated SH-SY5Y cells exposed to 24 h of 250 nM Tg, 1 µg/ml Tm or 1 µg/ml SubAB, (B) differentiated CAD cells exposed to 250 nM Tg, 1 µg/ml Tm or 1 µg/ml SubAB for the indicated times, and (C) primary mouse astrocytes exposed to 1 µg/ml SubAB for 24 h.

5.9 ER stress depletes IGF-I receptors

To investigate if the inhibited transport of newly synthesised insulin receptors from the ER to the plasma membrane is a general phenomenon affecting the majority of plasma membrane proteins during long-lasting ER stress IGF-I receptor levels were also monitored. The IGF-I receptor has a half-life of >6 h (Prager et al., 1992). With similarity to the insulin receptor, the IGF-I proreceptor is processed into α and β chains by proprotein convertases (Duguay et al., 1997). Also similar to the insulin receptor, the mature IGF-1 receptor β chain levels decreased with 18 h, and to a greater degree 24 h, of ER stress in C_2C_{12} cells (Figure 5.26 and Figure 5.27). A decrease in IGF-1 receptor levels was also observed in Hep G2 cells with prolonged ER stress (Figure 5.28 and Figure 5.29). Consistent with the insulin receptor, the IGF-I receptor levels were not greatly decreased with all three ER stressors until 36 h. Hep G2 cells are therefore more resistant to treatment with ER stressors. As well as depleting IGF-I receptor β chains, ER stress also led to an accumulation of proreceptors (Figure 5.30): suggesting a similar trafficking problem as observed with the insulin receptor during ER stress. Overall, IGF-I receptors are also depleted after prolonged ER stress.

Hep G2 cells appear to be more resistant to treatment with ER stressors as evidenced by later JNK activation and longer periods of ER stress being required to deplete both insulin receptor and IGF-I receptor levels. Several explanations are imaginable: 1) ER stressors take longer to enter Hep G2 cells 2) Hep G2 cells are more resistant to perturbations in protein folding 3) membrane protein turnover is slower in Hep G2 cells 4) Hep G2 cells have a greater protein folding capacity. Regardless of the time taken the insulin resistance induced through ER stress consistently correlates with depletion of insulin receptors in several cell lines.

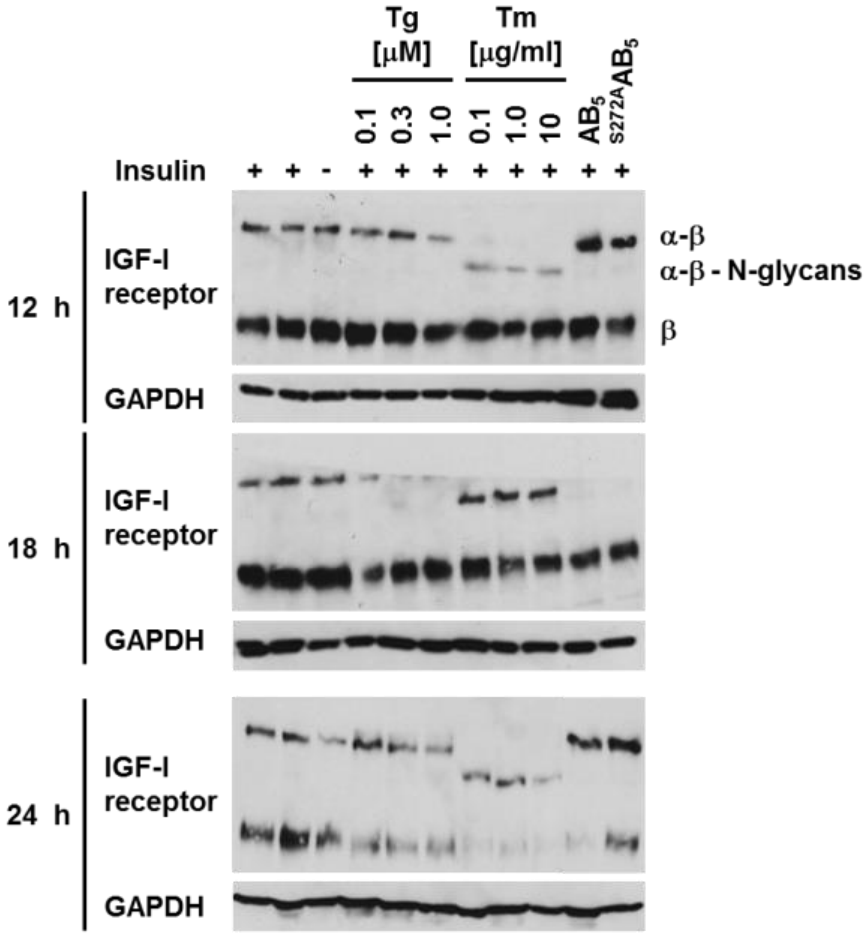

Figure 5.26. Depletion of IGF-I receptors by ER stress in C_2C_{12} cells.

C_2C_{12} cells were treated for the indicated times with the indicated concentrations of thapsigargin or tunicamycin, 1 μg/ml SubAB, or 1 μg/ml $SubA_{A272}B$ and serum-starved during the last 18 h of drug treatment before stimulation with 100 nM insulin for 15 min. Cell lysates were analysed by Western blotting. The GAPDH loading control is the same as the one shown in Figure 5.6. Quantitation of the Western blots shown in Figure 5.27.

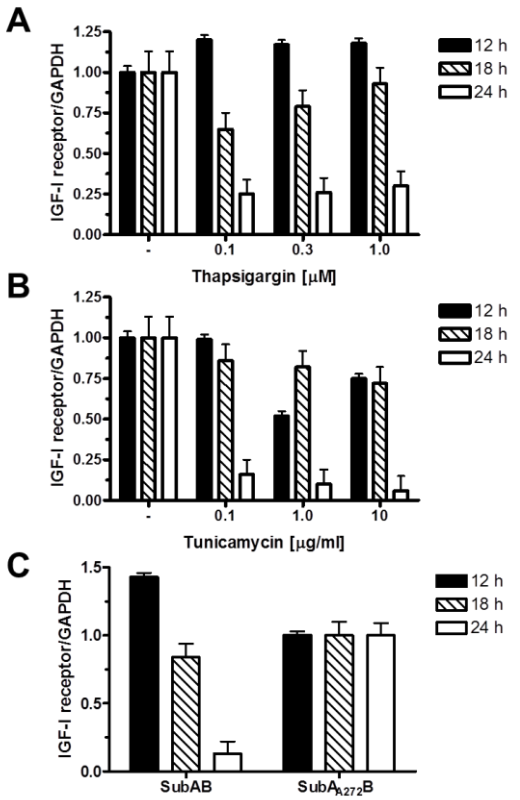

Figure 5.27. Depletion of IGF-I receptors by ER stress in C_2C_{12} cells: quantitation.

(A-C) Quantitation of the Western blots shown in Figure 5.26. Depletion of IGF-I receptors by ER stress induced in C_2C_{12} cells with (A) thapsigargin, (B) tunicamycin, and (C) SubAB ($n = 2$).

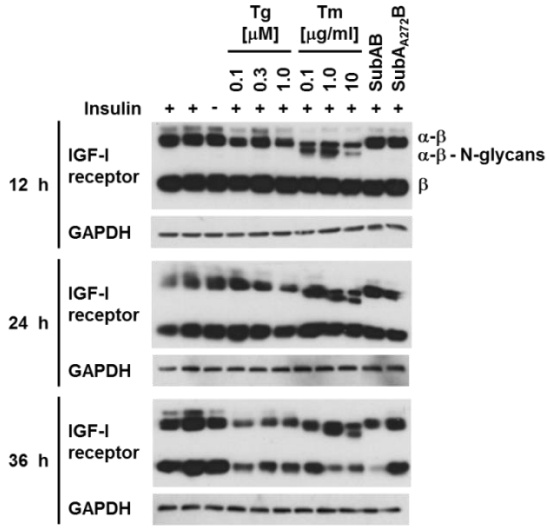

Figure 5.28. Depletion of IGF-I receptors by ER stress in Hep G2 cells.

Hep G2 cells were treated for the indicated times with the indicated concentrations of thapsigargin or tunicamycin, 1 μg/ml SubAB, or 1 μg/ml $SubA_{A272}B$ and serum-starved during the last 18 h of drug treatment before stimulation with 100 nM insulin for 15 min. Cell lysates were analysed by Western blotting. The GAPDH loading control is the same as the one shown in Figure 5.8. Quantitation of the Western blots shown are in Figure 5.29.

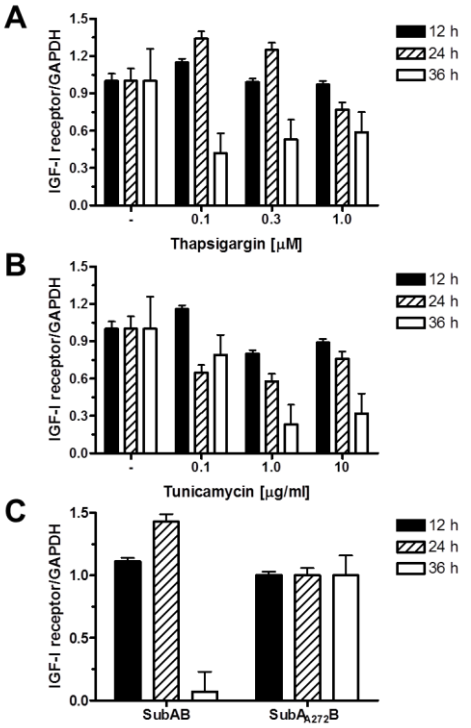

Figure 5.29. Depletion of IGF-I receptors by ER stress in Hep G2 cells: quantitation.

(A-C) Quantitation of the Western blots shown in Figure 5.28. Depletion of IGF-I receptors by ER stress induced in Hep G2 cells with (A) thapsigargin, (B) tunicamycin, and (C) SubAB (n = 2).

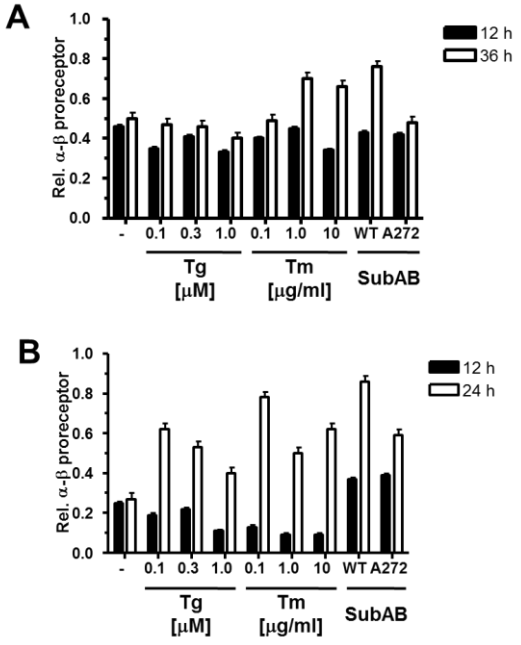

Figure 5.30. Prolonged ER stress causes accumulation of α-β IGF-I proreceptors in Hep G2 and C_2C_{12} cells.

Quantitation of IGF-I proreceptors relative to IGF-I receptors from Western blots in **(A**) HepG2 (from Figure 5.28) **(B)** C_2C_{12} cells (from Figure 5.26) (n = 2).

5.10 Discussion

Overall, the data presented in this chapter demonstrate that prolonged/chronic ER stress blocks the transport of newly synthesised insulin receptors to the plasma membrane. Without delivery of newly synthesised insulin receptors the constitutive turnover of insulin receptors in the plasma membrane results in depletion of the insulin receptor at the plasma membrane. Thus, long-lasting ER stress can inhibit insulin signalling via depletion of the insulin receptor from the cell membrane. Several lines of evidence support this conclusion. Only prolonged ER stress, which extended over several half-lives of the insulin receptor, resulted in insulin resistance, whereas shorter periods of ER stress do not cause insulin resistance. Insulin resistance occurs in parallel with depletion of mature insulin receptor β chains. Decreasing insulin receptors through siRNA-mediated knock-down was sufficient to cause insulin resistance. Prolonged ER stress causes accumulation of unprocessed proreceptors in the ER. It was shown through fluorescent microscopy that GFP-tagged insulin receptors are depleted from the cell surface and are redistributed to intracellular compartments after long-lasting ER stress. Finally, long-lasting ER stress in cells synthesising myristoylated insulin receptors, which bypass the ER, does not cause insulin resistance. It could be possible that ER stress is increasing the turn-over of the insulin receptor at the membrane and that this increased rate is sufficient to deplete the insulin receptor, whilst the insulin chimera may have not been affected by this increased turn over. Strong evidence against this is that the insulin proreceptors accumulate in the ER and that the fluorescent signal from GFP-labelled insulin receptors was lost from the cell membrane and was localised to the inside of the cell during ER stress, suggesting that the insulin receptor does indeed accumulate early in the secretory pathway such as the ER and that ER stress inhibits the transport of newly synthesised insulin receptors out of the ER and through the rest of the secretory pathway.

Two possible major implications arise from this research: 1) this research highlights the possibility that long-lasting ER stress is a potential mediator of insulin resistance in diabetes, 2) it could also be possible that the mechanism of insulin resistance established is a phenomenon of more pronounced ER stress in cultured cells. If 1 is true then this research adds to the mounting studies highlighting ER stress as a potential therapeutic target in diabetes. Whether or not more physiologically relevant levels of ER stress for long periods of time also result in insulin resistance needs to be established. If either 1 or 2 is true then this research highlights the importance of carefully considering the effect of prolonged ER stress on the depletion of membrane proteins and the subsequent effect on

downstream signalling pathways. This is extremely important because conclusions about the role of ER stress in other signalling pathways may be flawed if upstream membrane signalling proteins are not being considered.

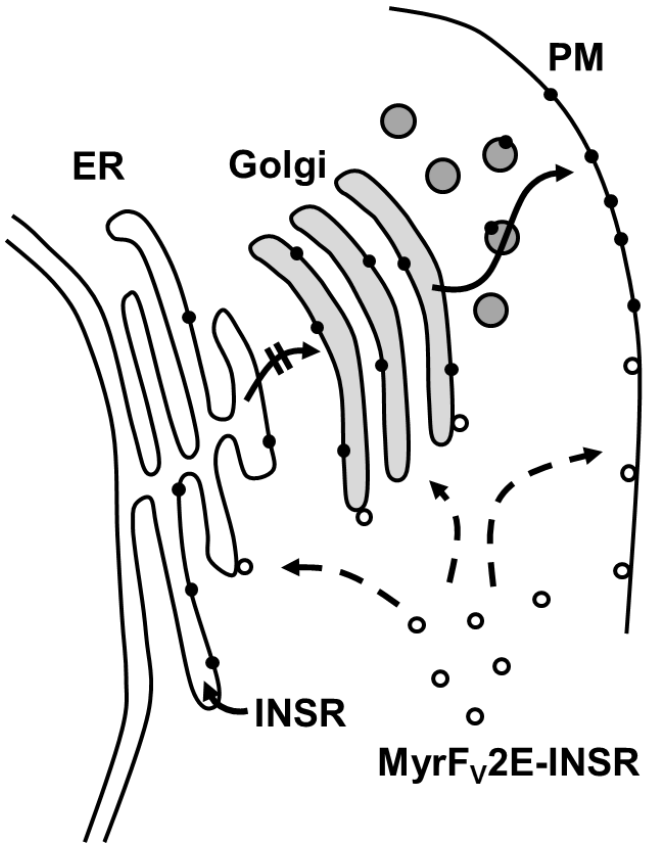

Figure 5.31. ER stress causes insulin resistance by interfering with exit of newly synthesised insulin proreceptors from the ER.

The signal peptide sequence targets ribosomes translating the insulin receptor mRNA to the ER, where the newly synthesised polypeptide chain folds into molecules with insulin binding activity. ER stress interferes with folding of newly synthesised insulin receptor molecules, preventing its transport to the Golgi complex. The Myr-F_V2R-insulin receptor chimera is not affected by ER stress because it is translated by cytoplasmic ribosomes and folds in the cytosol into active molecules thus bypassing the ER.

Although these findings contribute to the mounting evidence implicating ER stress in the development of insulin resistance, there is no evidence that UPR signalling pathways, such as IRE1α-JNK and PERK-TRB3, are involved. JNK has previously been implicated as a mediator of ER stress-dependent insulin resistance (Ozcan et al., 2004). However, this chapter reports that insulin resistance still develops in *jnk1*$^{-/-}$ *jnk2*$^{-/-}$ cells exposed to long-lasting ER stress (Figure 5.21) suggesting that JNK activation is not required for prolonged ER stress-mediated insulin resistance. These findings are consistent with two other studies

which found that the JNK selective inhibitor SP600125, although reducing JNK activation, was unable to restore insulin sensitivity in ER-stressed cells (Xu et al., 2010, Zhou et al., 2009). As JNK activation during ER stress is dependent on TRAF2 (Chapter 3), it is likely that *traf2*$^{-/-}$ MEFs are also not protected from long-lasting ER stress-induced insulin resistance but time restraints meant this was not investigated.

TRB3 has also been implicated as a mediator of insulin resistance caused by ER stress (Du et al., 2003). However, data in this thesis suggests that strong induction of TRB3 occurs without the development of insulin resistance, which provides evidence that TRB3 is also not required for the development of ER stress-dependent insulin resistance.

It was also demonstrated that not only the insulin receptor but other proteins, which traffic through the secretory pathway can be affected during long-lasting ER stress as IGF-I receptors were also depleted. Therefore, it could be possible that proteins important for vesicular trafficking and sorting are depleted after prolonged ER stress and this may contribute to depletion of the insulin receptor from the plasma membrane. Binding of insulin to the insulin receptor leads to the internalisation of the insulin receptor before the insulin-insulin receptor complex is separated in endosomes and the insulin receptor is recycled back to the plasma membrane (Foti et al., 2004). This process of internalisation and recycling of the insulin receptor downstream of insulin binding may also be disrupted through depletion of proteins which traffic through the secretory pathway. Disruption of proper vesicular trafficking and sorting may even inhibit or slow the depletion of the insulin receptor during ER stress and explain the increase in the insulin receptor's half-life in tunicamycin treated cells (Reed et al., 1981b). How long-lasting ER stress affects other proteins which move through, especially those which function within, the secretory pathway needs to be established.

The depletion of secretory and membrane proteins during prolonged ER stress may explain several observations showing that ER stress inhibits various signalling pathways. For example TNF-α induces the generation of ROS and this was shown to be inhibited by tunicamycin in L929 cells (Xue et al., 2005), however, the TNF receptor may have been depleted during the ER stress treatment as it has a short half-life of 1.5-2 h (Watanabe et al., 1988, Yoshie et al., 1986). Depletion of TNF receptors in these experiments would render cells unable to respond to TNF-α. Another study showing that cholesterol efflux in Hep G2 cells is inhibited by ER stress may also suffer from the same oversight (Rohrl et al., 2014). ER stress-mediated depletion of the ATP-binding cassette transporter A1

(ABCA1), which has a half-life of 1-2 h (Wang and Oram, 2002, Arakawa and Yokoyama, 2002, Wang et al., 2003b), at the plasma membrane may have contributed to the observed inhibition of cholesterol efflux. That being said, it is important to investigate each secretory and membrane protein during ER stress individually as tunicamycin, although inhibiting delivery of many proteins to the plasma membrane, does not affect the rate of delivery of HLA-A and HLA-B (Ploegh et al., 1981). This was also found to be the case for interferon secretion, which is not affected by tunicamycin treatment in human leukocytes (Fujisawa et al., 1978, Mizrahi et al., 1978). This work therefore highlights the need for a case-by-case analysis of every single secretory or membrane protein to understand how ER stress affects their secretion or delivery to the cell membrane. Acquiring this information is important to avoid misinterpretation of data in studies involving ER stress.

As discussed, many studies have investigated insulin signalling in the context of long-lasting ER stress (Avery et al., 2010, Hage Hassan et al., 2012, Xu et al., 2010, Zhou et al., 2009, Tang et al., 2011). However, only two reports to date have described decreased AKT phosphorylation with short lasting ER stress. The first of these studies demonstrated that Fao rat hepatoma cells had reduced AKT S473 phosphorylation when exposed to 5 µg/ml tunicamycin for 3 h (Ozcan et al., 2004). The second study showed that AKT phosphorylation is reduced by ~27% in C_2C_{12} myotubes exposed to an undocumented concentration of tunicamycin (Koh et al., 2013).

The depletion of insulin receptors reported in this results chapter may partly explain the loss of insulin signalling in various studies investigating prolonged ER stress. For example, treatment of C_2C_{12} cells with tunicamycin for 16 h caused insulin resistance (Hage Hassan et al., 2012). Insulin resistance was only shown to correlate with JNK activation in this study. In another study HL-1 atrial myocytes were exposed to 2 µM thapsigargin for 24 h, which caused insulin resistance (Avery et al., 2010). In this study TRB3 was implicated in the ER stress-mediated development of insulin resistance as siRNA-mediated knock-down of TRB3 relieved insulin resistance. However, knock-down of TRB3 only partially relieved ER stress-induced insulin resistance. In these studies the duration of ER stress may have been sufficient to deplete insulin receptors through mechanisms reported in this thesis. The fact that all of these studies did not consider the effect of ER stress on the trafficking of proteins crucial to the signalling pathways being involved highlights the importance of the findings reported in this thesis.

Trafficking of the insulin receptor through the secretory pathway has been previously well characterised (Lane et al., 1985, Hart et al., 1988). However, all of these studies have used tunicamycin to investigate how inhibiting *N*-linked glycosylation specifically affects trafficking and processing of the insulin receptor through the secretory pathway. Studies, which show that tunicamycin treatment blocks trafficking of newly synthesised insulin receptors to the plasma membrane attribute this solely to insulin receptors not being glycosylated (Kadle et al., 1984, Ercolani et al., 1984, Ronnett et al., 1984). However, as demonstrated in this chapter, two other ER stressors, thapsigargin and SubAB, which induce ER stress without directly affecting *N*-linked glycosylation, also deplete insulin receptor levels. Direct inhibition of *N*-linked glycosylation was also not required for the inhibited transport of proreceptors from the ER to the *trans*-Golgi network. It was also evident that both thapsigargin and SubAB do not inhibit the glycosylation of the insulin receptor as the glycosylated proreceptor accumulates over time suggesting that translation and glycosylation of the insulin receptor is ongoing during ER stress. Thus, ER stress-mediated depletion of insulin receptors at the plasma membrane is a result of trafficking defects through accumulation of misfolded and aggregated proteins.

It was discovered that tunicamycin caused depletion of insulin receptors earlier than the other ER stressors (Figure 5.1 and Figure 5.3). This may be due to the level of ER stress induced or the mechanism through which different ER stress mimetics cause ER stress. Another explanation is that the pharmacokinetics of tunicamycin such as: uptake rate, excretion rates, and steady state levels all contribute to early inhibition of trafficking of the insulin receptor. As tunicamycin is inhibiting the *N*-linked glycosylation of newly synthesised insulin receptors directly as well as causing ER stress it is likely that the insulin receptors are depleted quickly. Whereas the other ER stressors will take time to block trafficking of the insulin receptor as a secondary effect of long-lasting ER stress and a blockage in the secretory pathway.

The level of insulin receptors at the plasma membrane is decreased in obesity (Olefsky and Reaven, 1975, Olefsky, 1976), whilst ER stress has been reported in several tissues in both obese mice and obese patients (Ozcan et al., 2004, Ozcan et al., 2006, Sreejayan et al., 2008, Hosogai et al., 2007). Data in this reults chapter suggest that ER stress could cause less efficient trafficking of newly synthesised insulin receptors to the cell surface in obesity resulting in insulin resistance. Chemical chaperones such as TUDCA and 4-phenylbutyrate, which relieve ER stress have been shown to restore insulin sensitivity and blood glucose in models of diabetes (Ozcan et al., 2006, Ozcan et al., 2008). Relieving ER

stress is therefore a potential therapeutic target in diabetes and this may be through restoration of proper trafficking of the insulin receptor. Interestingly, diabetes is not the only disease associated with decreased insulin receptor levels. Decreased insulin receptor levels have been reported in the neurodegenerative diseases PD (Moroo et al., 1994, Moloney et al., 2010) and AD. This is of particular interest because both neurodegenerative diseases are linked to diabetes whilst ageing, which is a major risk factor for these three diseases, has been shown to involve a decrease in insulin receptor levels (Bolinder et al., 1983, Frolich et al., 1998). The role of the insulin receptor in ageing and neurodegeneration is investigated in more detail in the final discussion (Chapter 7).

In conclusion, prolonged ER stress leads to insulin resistance through inhibiting the transport of newly synthesised insulin receptors through the secretory pathway leading to the loss of insulin receptors at the cell membrane. An important question remaining is how does this apply to physiological ER stress in diabetes? Regardless of the answer, an important finding is that studying insulin signalling after ER stress for longer than 18 hours is misleading without considering the trafficking of insulin receptors. This finding also demonstrates the danger of studying and interpreting results when analysing signalling pathways affected by prolonged ER stress as results may be artefacts of protein loss through inhibition of the secretory pathway. For this reason it is important to establish how ER stress affects all proteins which traffic through the secretory pathway. This knowledge would be of significant importance for the reliable interpretation of experiments involving ER stress.

6 ER STRESS-INDUCED INFLAMMATORY SIGNALLING IN PARKINSON'S DISEASE

6.1 Rationale

The early molecular mechanisms in the development of PD are poorly understood. Activation of the UPR has been detected in various PD models (see 1.6.1-3). The UPR has also been shown to induce inflammatory signalling (see 1.4). Prolonged neuroinflammation is detrimental and has been strongly implicated in PD along with activation of the UPR (see 1.6.5). However, a link between the UPR and neuroinflammation in PD has so far not been studied. Thus, it was investigated if pathways activating the inflammatory signalling pathways; AP-1 and NF-κB are switched on during ER stress and UPR activation in cultured neuronal cell lines.

The most widely associated protein with PD is α-synuclein. Recent studies have implicated α-synuclein in the development of ER stress in PD (see 1.6.2.1). Various mechanisms have been suggested for α-synuclein-mediated ER stress: 1) inhibition of the proteasome, 2) inhibition of ER to Golgi transport, 3) entry of α-synuclein into the ER and disruption of protein folding. Not only do genetic models of PD suggest an involvement of ER stress and the UPR in PD, drugs mimicking PD can also activate the UPR. The PD mimetic drugs 6-OHDA (Ryu et al., 2002), MPP+ (Chigurupati et al., 2009, Ryu et al., 2002), rotenone (Ryu et al., 2002) and paraquat (Chinta et al., 2008) have been shown to induce ER stress. Overall there is strong evidence that ER stress can be activated in PD.

The role of ER stress in PD is not fully understood but it may involve initiation or contribution of inflammation. Epidemiological studies (Chen et al., 2003, Chen et al., 2005), post mortem studies (Hunot et al., 1999) and animal models (Su et al., 2008) have provided mounting evidence for a role for neuroinflammation in PD. As discussed, the UPR is also capable of activating inflammatory signalling pathways NF-κB, JNK and p38 (see 1.4). Also, ER stress is strongly implicated in the development of inflammation in metabolic diseases (Mondal et al., 2012, Kawasaki et al., 2012, Li and Engelhardt, 2006). It could be the case that activation of the UPR, through a variety of mechanisms, is leading to the activation of inflammatory signalling molecules previously detected in PD neurons.

Evidence of ER stress-mediated JNK activation in various cell lines has been provided (Results Chapter 3) but so far the effect of ER stress on inflammatory signalling outside of

and downstream of JNK has not been investigated. The mediator of transcription of pro-inflammatory genes AP-1 is activated downstream of JNK activation (Davis, 2000). For these reasons it was questioned if the observed ER stress-mediated JNK activation leads to pro-inflammatory signalling and if ER stress, in this research group's experimental system, activates other pro-inflammatory signalling pathways. In other studies ER stress has been able to activate the transcription factors NF-κB (Kaneko et al., 2003) and AP-1 (Urano et al., 2000), which control pro-inflammatory genes. These transcription factors have been shown to be activated by JNK, and p38.

Bringing all these molecular events together the following sequence of events may account for the loss of neurons in PD: 1) Disruption protein folding homeostasis through mechanisms discussed. 2) Accumulation of unfolded proteins in the ER and activation of the UPR. 3) The UPR activates inflammatory signalling pathways which activates and recruits microglia. 4) Activated microglia release inflammatory and neurotoxic molecules causing further damage to unhealthy neurons, possibly through further ER stress, mitochondrial stress and oxidative stress. 5) And finally both microglia and unhealthy neurons activate further microglia causing self-propelling cycles of inflammation, neuronal damage and neuronal cell death (Figure 1.8).

In the following section the role of ER stress in mediating inflammatory signalling and inflammation in cellular models of PD is investigated.

6.2 ER stress activates inflammatory signalling pathways in neuronal cells

6.2.1 Activation of inflammatory signalling in N1E-115 cells with ER stressors

To investigate if ER stress activates JNK as well as other inflammatory signalling pathways, murine neuroblastoma N1E-115 (Amano et al., 1972) cells were exposed to ER stressors. N1E-115 cells were exposed to thapsigargin at concentrations of 0.3 and 0.5 µM for up to 4 h before cells were harvested for protein and RNA extraction. Western blotting was performed to monitor the activation of the MAPK signalling pathways JNK and p38 as well as the transcription factor NF-κB. Phosphorylation of eIF2α was also investigated through Western blotting along with splicing of *XBP1* to monitor the kinetics of UPR activation in ER-stressed cultures. Both concentrations of thapsigargin resulted in increased JNK phosphorylation (Figure 6.1 A). Thapsigargin caused a drastic increase in the phosphorylation of the MAPK p38 after 2 and 4 h. The phosphorylation and

subsequent degradation of IκBα results in NF-κB activation (DiDonato et al., 1996). IκBα degradation is therefore indicative of NF-κB activation. Thus the level of IκBα protein during ER stress was investigated using Western blotting. IκBα degradation occurred in N1E-115 cells after exposure to thapsigargin suggesting that NF-κB signalling is also activated by ER stress. Interestingly, JNK activation occurred before p38 in N1E-115 cells and may suggest that p38 activation is regulated differently to JNK during ER stress in N1E-115 cells.

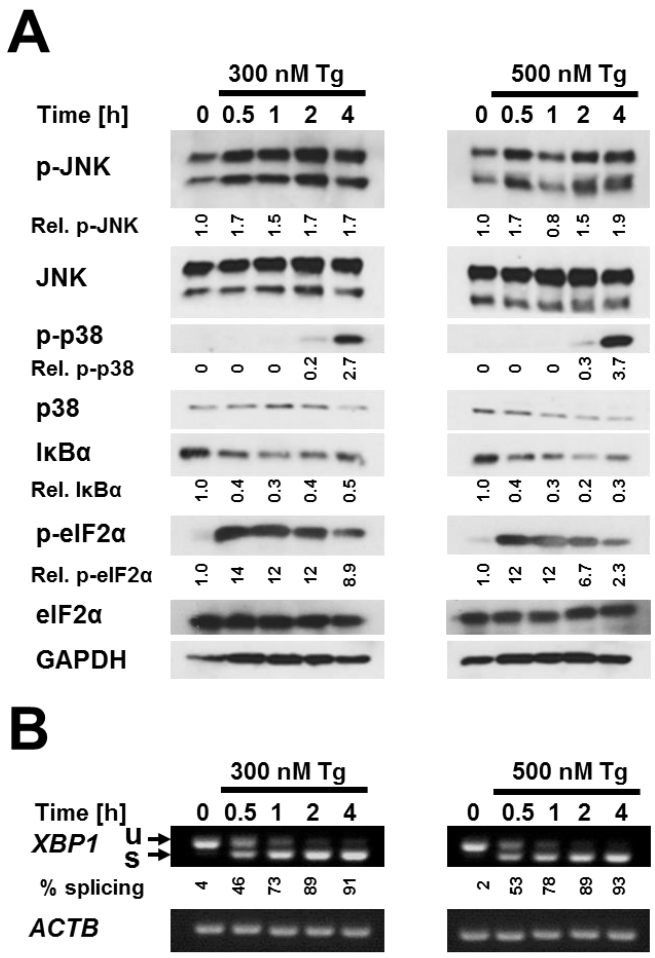

Figure 6.1. Thapsigargin activates inflammatory signalling pathways in N1E-115 cells.
Induction of ER stress with 300 or 500 nM Tg in N1E-115 cells. (A) Western blots for phospho-JNK (p-JNK), total-JNK (JNK), phospho-p38 (p-p38), total-p38 (p38), phospho-eIF2α (p-eIF2α), total-eIF2α (eIF2α), IκBα and GAPDH proteins. (B) Detection of *XBP1* splicing by RT-PCR.

Splicing of *XBP1* was measured to monitor activation of the UPR (Figure 6.1 B). A second marker of UPR activation was also employed - eIF2α phosphorylation, which occurs with

activation of the PERK branch of the UPR, was monitored alongside *XBP1* splicing. Both markers of UPR activation, *XBP1* splicing and phosphorylation of eIF2α, were observed as early as 30 min after thapsigargin treatment. Interestingly, JNK and NF-κB activation correlated with the markers of UPR activation. However, p38 phosphorylation did not occur until after 2 h of thapsigargin treatment, suggesting that different kinetics of activation of these inflammatory signalling pathways by the UPR exist in N1E-115 cells.

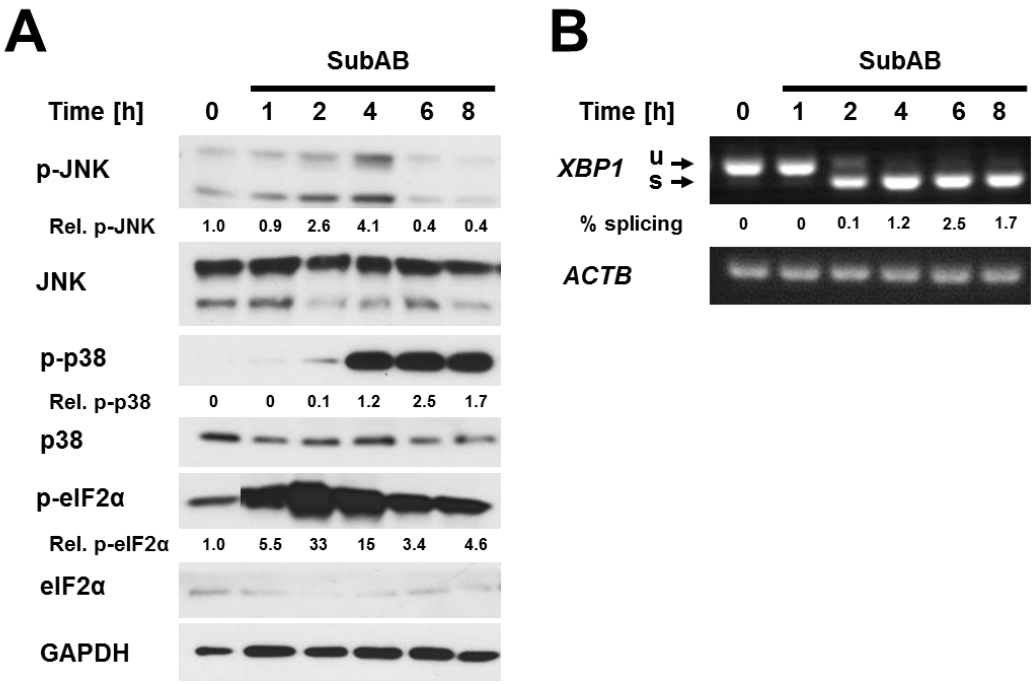

Figure 6.2. SubAB activates inflammatory signalling pathways in N1E-115 cells.
N1E-115 cells were exposed to 1 μg/ml SubAB for the 1, 2, 4, 6, and 8 h. **(A)** Western blots for phospho-JNK (p-JNK), total-JNK (JNK), phospho-p38 (p-p38), total-p38 (p38), phospho-eIF2α (p-eIF2α) , total-eIF2α (eIF2α), IκBα and GAPDH proteins. **(B)** Detection of *XBP1* splicing by RT-PCR.

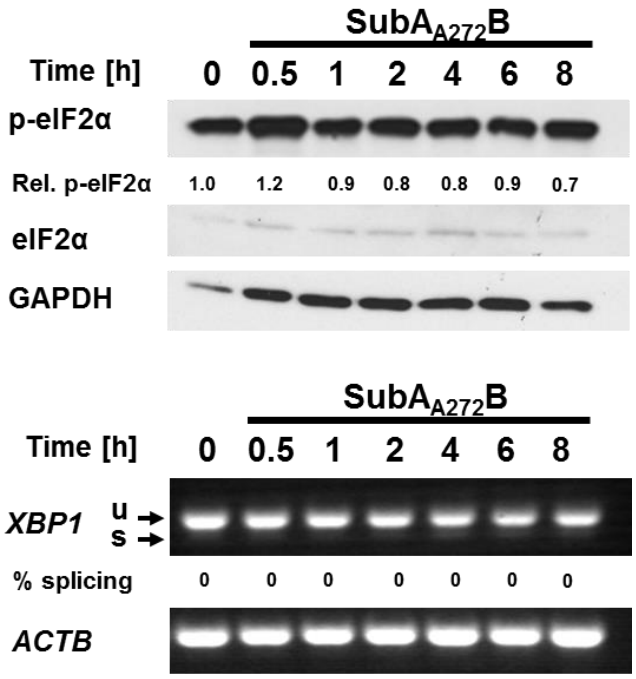

Figure 6.3. Catalytically inactive SubA$_{A272}$B does no activate the UPR in N1E-115 cells.
N1E-115 cells were exposed to 1 μg/ml SubA$_{A272}$B for the 1, 2, 4, 6, and 8 h before protein and RNA isolation. Western blots for phospho-JNK (p-JNK), total-JNK (JNK), phospho-p38 (p-p38), total-p38 (p38), phospho-eIF2α (p-eIF2α), total-eIF2α (eIF2α), IκBα and GAPDH proteins shown above. Detection of *XBP1* splicing by RT-PCR. β-Actin (*ACTB*) was used as a loading control.

A second ER stressor, SubAB, was also used to confirm results from the thapsigargin treatments (Figure 6.2). The UPR marker, phospho-eIF2α and spliced *XBP1* were not observed until 1 and 2 h after addition of SubAB, respectively. Both JNK and p38 were not activated until 2 h of exposure to SubAB, which correlates with markers of UPR activation. To ensure observations are a direct result of ER stress induced by SubAB rather than off-target effects from contaminants produced in the preparation of SubAB cells were exposed to the catalytically inactive SubA$_{A272}$B (Figure 6.3). Treatment of N1E-115 cells with SubA$_{A272}$B up to 4 h was unable to induce *XBP1* splicing or phosphorylation of eIF2α. Therefore, activation of the inflammatory signalling pathways: JNK, p38 and NF-κB correlate with UPR activation in N1E-115 cells. As with ER stress induced with thapsigargin, SubAB also caused JNK activation prior to p38 (see Discussion).

6.2.2 Activation of inflammatory signalling in differentiated SH-SY5Y cells with ER stressors

Several characteristics of the human neuroblastoma SH-SY5Y (Ross et al., 1983) cell line make it a useful tool for studying dopaminergic neurons. SH-SY5Y cells have been shown to synthesise dopamine, express tyrosine hydroxylase (TH) activity, and express dopamine transporter (Xie et al., 2010). TH is used as a marker for a dopaminergic phenotype as TH is the first rate limiting enzyme in the synthesis of dopamine. SH-SY5Y cells can also be differentiated into a more pronounced dopaminergic phenotype with differentiation induced by a combination of retinoic acid (RA) and 12-*O*-tetradecanoylphorbol-13-acetate (TPA) (Presgraves et al., 2004). RA treatment alone has also been shown to increase TH expression in SH-SY5Y cells (Lopes et al.), however, other studies using RA alone for SH-SY5Y cell differentiation have reported that differentiation does not induce expression of TH (Cheung et al., 2009, Presgraves et al., 2004). RA-induced differentiation of SH-SY5Y cells is the most common protocol used for studying PD in this cell line. TPA acts mainly through activating protein kinase C (Fagerstrom et al., 1996). RA induces differentiation through binding the RA receptors and the retinoic X receptors effecting the regulation of the transcription of neurotrophin receptor genes (Clagett-Dame et al., 2006), the Wnt signalling pathway (Uemura et al., 2003) and type II protein kinase A (Encinas et al., 2000).

Human neuroblastoma SH-SY5Y cells were differentiated by treating cells with 10 μM RA on day 1 and day 3 (Presgraves et al., 2004) After 7 days of differentiation cell lysates were harvested and processed for Western blotting. Blotting for TH revealed that differentiation with 10 μM RA on day 1 and day 3 was not sufficient to induce expression of TH expression in SH-SY5Y (data not shown). Due to the first differentiation protocol not being sufficient to induce detectable levels of TH expression at the protein level several differentiation protocols were trialled. Human neuroblastoma SH-SY5Y cells were differentiated in several ways (see Methods section for full details). After differentiation cell lysates were harvested and processed for Western blotting. Blotting for TH revealed that none of the differentiation protocols were sufficient to induce expression of TH expression in SH-SY5Y (data not shown).

TPA with RA although being reported to previously (Presgraves et al., 2004), was unable to induce expression of TH. Also, TPA is known to have oxidative effects (Datta et al., 2000). As oxidative effects may mask effects of ER stressors and PD mimetics, which can

induce oxidative stress, a differentiation protocol without TPA was chosen for further experiments. Using 10 μM RA on day 1 and day 3 for SH-SY5Y differentiation is a common protocol for inducing a neuronal phenotype including increased neurite length, which is typical of neuron-like cells. Neurites are elongated processes which extend from the cell body and serve as precursors of axons and dendrites to allow polarisation of the neuron (Clagett-Dame et al., 2006). Neurite length was measured using ImageJ software and the average neurite length was calculated. Differentiation with 10 μM all-*trans* RA on day 1 and day 3 caused a pronounced change in morphology to neuron-like cells increasing the length of neurons significantly (Figure 6.4 A, B).

Differentiation is reported to cause activation of MAPK pathways including JNK (Tiwari et al., 2012). As previous chapters have characterised the effect of ER stress on the activation of JNK in non-neuronal cells it was to decided that JNK activation, using the anti-phospho-JNK antibody, should be monitored through the differentiation process of SH-SY5Y cells (Figure 6.4 C). JNK phosphorylation did not increase through differentiation, which suggests that differentiation was not activating JNK signalling in SH-SY5Y cells. Activation of the MAPK p38 was also monitored. Phosphorylation of p38 also was not increased during differentiation. Differentiation with RA, which leads to neurite outgrowth, therefore does not activate stress signalling pathways p38 and JNK.

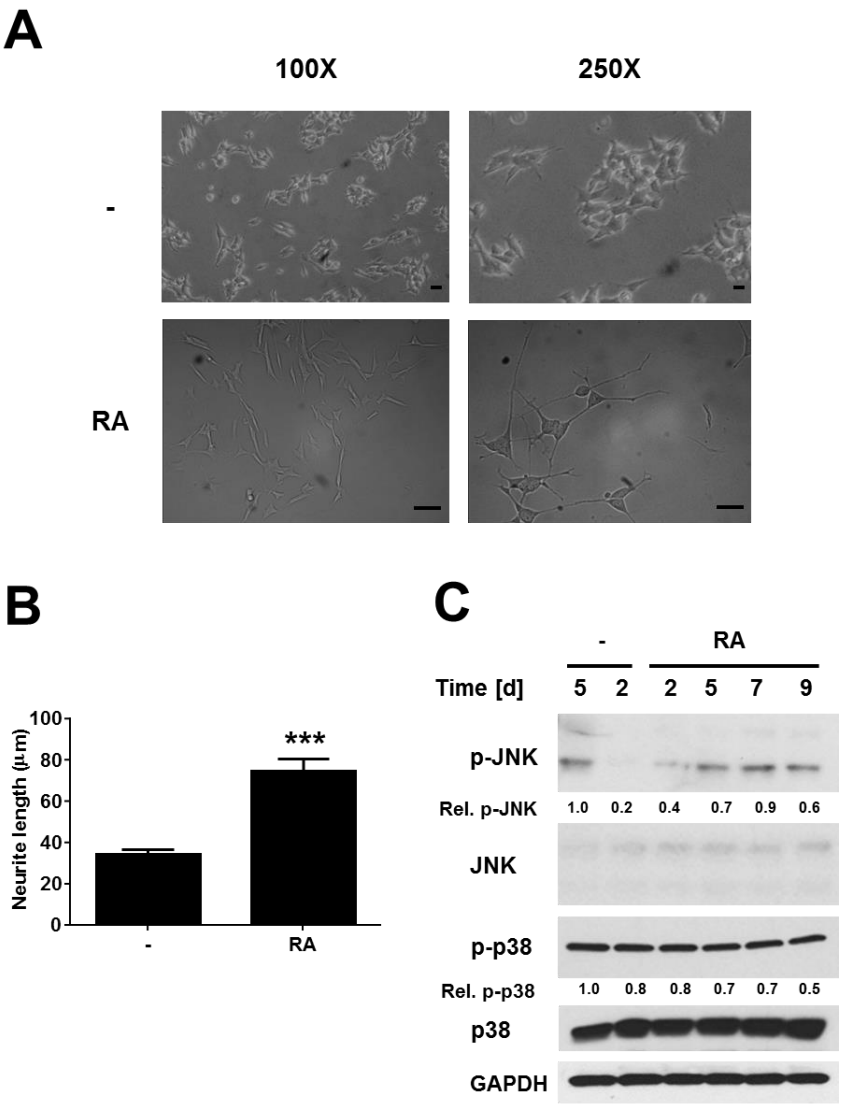

Figure 6.4. Differentiation with retinoic acid induces neuronal phenotype in SH-SY5Y cells.
(A) Microscopic images of SH-SY5Y cells with and without 10 µM retinoic acid (RA). SHS-SY5Y cells were differentiated with RA treatment on days 1 and 3. Images were taken after 7 days of differentiation. Scale bar = 50 µm **(B)** Quantitation of neurite length from images obtained as represented in (A). Error bars = SEM (n = 4). **(C)** Western blots for phospho-JNK (p-JNK), total-JNK (JNK), and GAPDH of lysates from SH-SY5Y cells which were differentiated with 10 µM RA for the number of days indicated. (–) no treatment. (*** - $p < 0.001$).

To investigate if the ER stressor-induced activation of inflammatory signalling pathways in N1E-115 is also a feature of differentiated neuron-like cells the effect of ER stress on inflammatory signalling was monitored in differentiated human SH-SY5Y cells. Differentiated SH-SY5Y cells were exposed to the ER stressor SubAB for up to 4 h before extraction of lysates for Western blotting and PCR (Figure 6.5). Both *XBP1* splicing and

eIF2α phosphorylation were observed 2 h after treatment with 1 µg/ml SubAB suggesting that the UPR was activated at this time point.

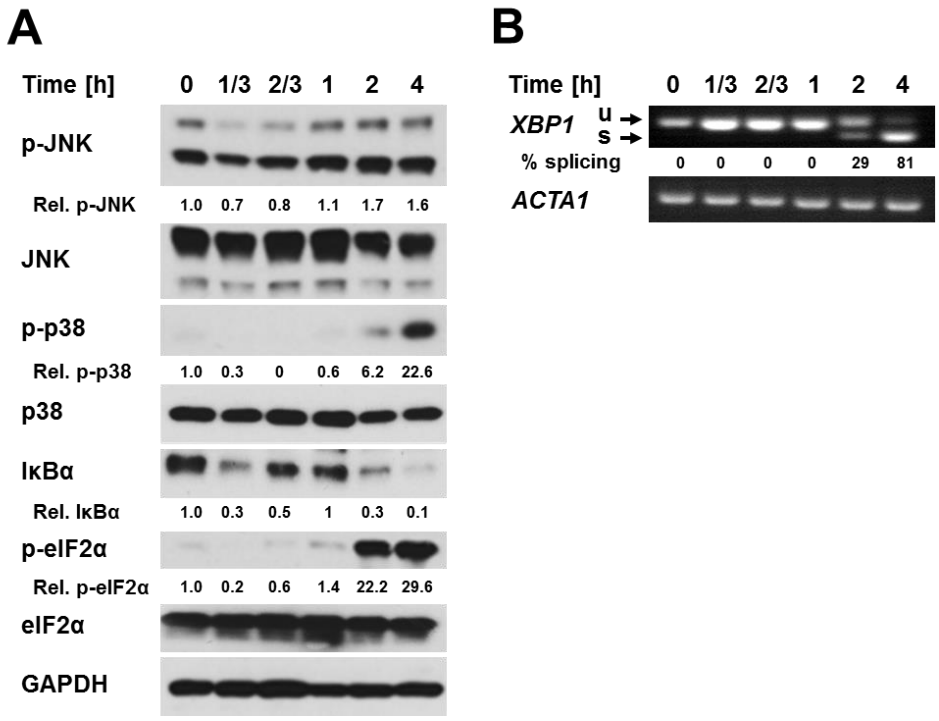

Figure 6.5. SubAB-induced ER stress activates inflammatory signalling pathways in *in vitro* differentiated human SH-SY5Y cells.

SH-SY5Y cells were exposed to 1 µg/ml SubAB before lysate collection, Western blotting (A) and RT-PCR (B). **(A)** Induction of ER stress with SubAB activates JNK, p38, and NF-κB in differentiated SH-SY5Y cells. SH-SY5Y cells were exposed to 1 µg/ml SubAB before lysate collection and Western blotting. **(B)** SubAB activates *XBP1* splicing. Detection of *XBP1* splicing by RT-PCR.

Phosphorylation of the MAPK JNK during ER stress was monitored through Western blotting and revealed that JNK phosphorylation occurred after 2 h of ER stress treatment and therefore correlates with the appearance of markers of UPR activation (Figure 6.6). After Western blotting for phosphorylated p38 it was observed that the p38 signalling pathway was also activated 2 h after ER stress treatment with SubAB. Thus, activation of both JNK and p38 signalling pathways correlated with markers of ER stress. IκBα levels dropped after 20 min, before returning to basal levels, and then dropping again at 2 and 4 h, suggesting that IκBα degradation occurred transiently (Figure 6.6 A). However the late degradation of IκBα correlates with activation of ER stress, JNK, and p38.

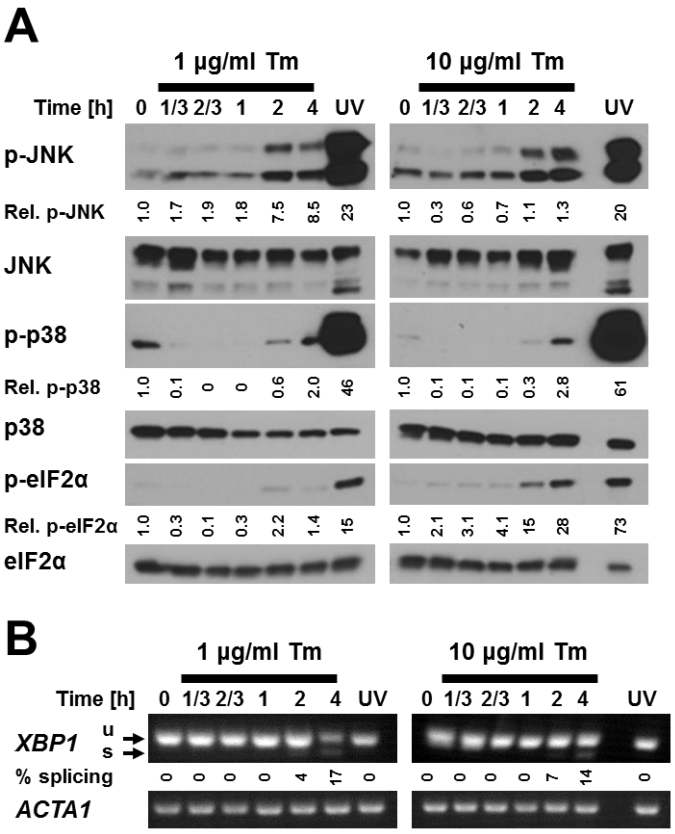

Figure 6.6. Tunicamycin-induced ER stress activates inflammatory signalling pathways in *in vitro* differentiated human SH-SY5Y cells.

Differentiated SH-SY5Y cells were exposed to 1 or 10 µg/ml Tm for the times indicated. **(A)** Western blots for phospho-JNK (p-JNK), total-JNK (JNK), phospho-p38 (p-p38), total-p38 (p38), phospho-eIF2α (p-eIF2α), total-eIF2α (eIF2α) and GAPDH of lysates from SH-SY5Y cells. **(B)** Detection of *XBP1* splicing by RT-PCR. UV stimulation was used as a positive control.

To address the question that SubAB-mediated JNK and p38 activation in SH-SY5Y cells may be specific to SubAB and not a general response to SubAB-induced ER stress SH-SY5Y cells were exposed to a second ER stressor, tunicamycin. In agreement with SubAB, tunicamycin treatment caused activation of inflammatory signalling pathways (Figure 6.6). Activation of inflammatory signalling pathways also correlated with UPR activation by tunicamycin. Thus, the ER stressors SubAB and tunicamycin cause activation of inflammatory signalling pathways in differentiated SH-SY5Y cells. The ability of two mechanistically different ER stressors to activate inflammatory signalling suggests that this was a result of ER stress and not off-target drug effects.

6.2.3 Activation of inflammatory signalling in differentiated PC-12 cells

Rat adrenal phaeochromocytoma PC-12 (Greene and Tischler, 1976) cells were differentiated through exposure to nerve growth factor (NGF) as previously described (Greene and Tischler, 1976). Differentiation caused an increase in TH expression, which increased as early as day 2 of differentiation and was maintained to day 9 (Figure 6.7). Undifferentiated PC-12 cells already have a high level of TH expression which was greatly increased with differentiation induced by NGF exposure. JNK activation was also monitored through Western blotting. Differentiation caused a large increase in the activation of JNK, which was observed as early as 2 days of differentiation and reached maximal levels after 7 days of differentiation. Phosphorylation of p38 also increased with differentiation. Due to strong activation of p38 and JNK with differentiation it was decided that PC-12 would not be used for further investigation of inflammatory signalling during ER stress.

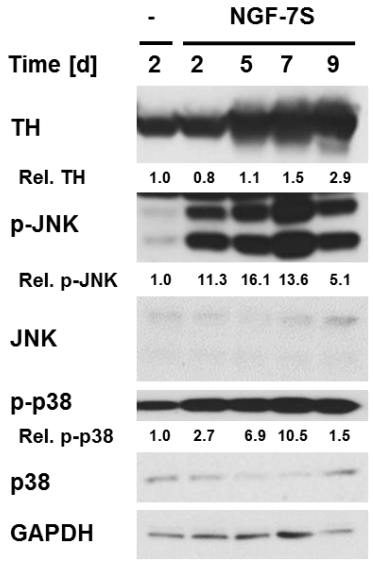

Figure 6.7. NGF induces a neuronal phenotype in PC-12 cells.
Western blots for tyrosine hydroxylase (TH), phospho-JNK (p-JNK), total-JNK (JNK), phospho-p38 (p-p38), total-p38 (p38) and GAPDH of lysates from PC-12 cells differentiated with 50 ng/ml NGF-7S for the number of days indicated. (–) no treatment.

6.2.4 Activation of inflammatory signalling in differentiated CAD cells with ER stressors

The murine Cath.-a-differentiated (CAD) (Suri et al., 1993) cell line was originally derived from TH-positive tumours in transgenic mice carrying the SV40 T antigen oncogene under the transcriptional control of the sequences from the rat TH gene (Suri et al., 1993). CAD

cells are a useful tool to study PD as they express TH, produce dopamine, express neurofilaments (NF) which are intermediate filaments characteristic of neurons (Lazarides, 1982), and express the integral membrane protein synaptophysin, which is localised to the membranes of small vesicles found only in neurons (Navone et al., 1986). CAD cells were differentiated through serum starvation. Differentiation markedly increased TH expression as detected through Western blotting (Figure 6.8 A). TH was undetectable in undifferentiated CAD cells. After 2 days of differentiation the anti-TH antibody detected TH expression. Expression increased as the time of differentiation increased. JNK and p38 activation were monitored during differentiation to establish if differentiation affected these MAPK signalling pathways (Figure 6.8 A). Indeed differentiation caused JNK activation with phospho-JNK levels being highest by day 10. Differentiation also slightly increased p38 activation. Thus differentiation, induced through serum starvation, activates the JNK and 38 signalling pathways in CAD cells. However, JNK and p38 activation was not as markedly increased through differentiation as was observed in PC-12 cells.

Neurite length was also monitored in undifferentiated and differentiated CAD cells. CAD cells were grown in either serum or serum-free medium for 10 d before images were captured using brightfield microscopy (Figure 6.8 B). Neurite length was measured using ImageJ software and the average neurite length was calculated. The average neurite length greatly increased with differentiation (Figure 6.8 C). The number of processes extending from cells did not significantly vary after differentiation (data not shown) and thus extension of processes defines the neuronal morphology induced through serum starvation.

As differentiated SH-SY5Y cells do not express TH, the ability of ER stress to induce inflammatory signalling was investigated in dopaminergic CAD cells. Differentiated CAD cells were exposed to SubAB for a maximum of 6 h (Figure 6.9). In agreement with differentiated SH-SY5Y cells, exposure for up to 2 h of SubAB was required to induce ER stress. eIF2α phosphorylation occurred after 2 h of ER stress whilst *XBP1* splicing was not observed until after 4 h of SubAB exposure.

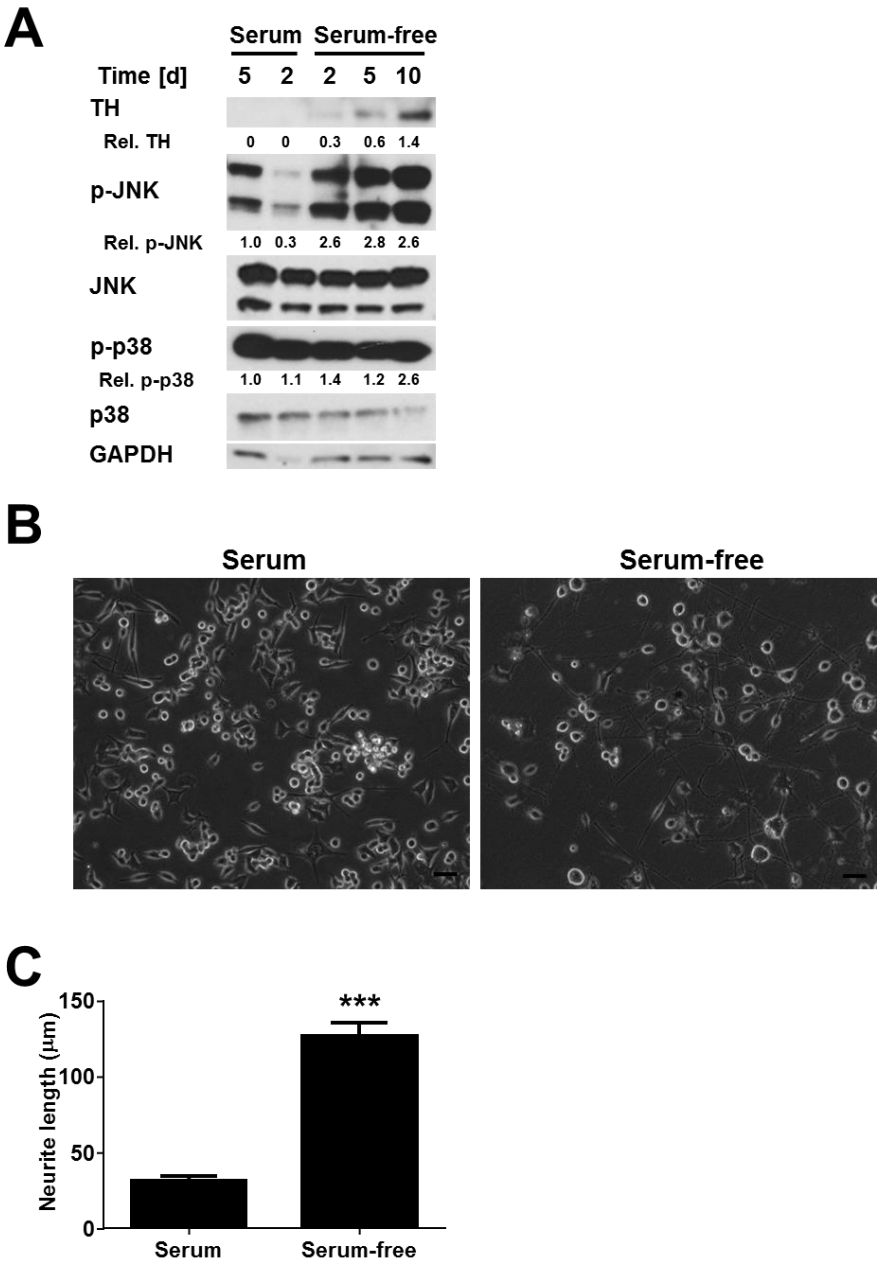

Figure 6.8. Serum starvation induces a neuronal phenotype in CAD cells.

(A) Western blots for tyrosine hydroxylase (TH), phospho-JNK (p-JNK), total-JNK (JNK), phospho-p38 (p-p38), total-p38 (p38) and GAPDH of lysates from CAD cells which were grown in either serum or serum-free medium for the indicated number of days. **(B)** Microscopic images of CAD cells grown in serum or serum-free medium for 10 d. Scale bar = 50 µm **(C)** Quantitation of neurite length from images as represented in (B). Error bars = SEM ($n = 4$). (*** - $p < 0.001$).

Correlating with ER stress activation, both JNK and p38 phosphorylation occurred after 2 h of SubAB treatment (Figure 6.9 A). p38 phosphorylation increased greatly after 2 h and was maintained for at least another 2 h. JNK phosphorylation was also maintained up to 6

h. The difference between untreated and the 6 h time point was much more striking in the p38 pathway than in the JNK pathway. After 4 h of SubAB exposure IκBα levels decrease suggesting that the NF-κB pathway was activated in differentiated CAD cells exposed to SubAB.

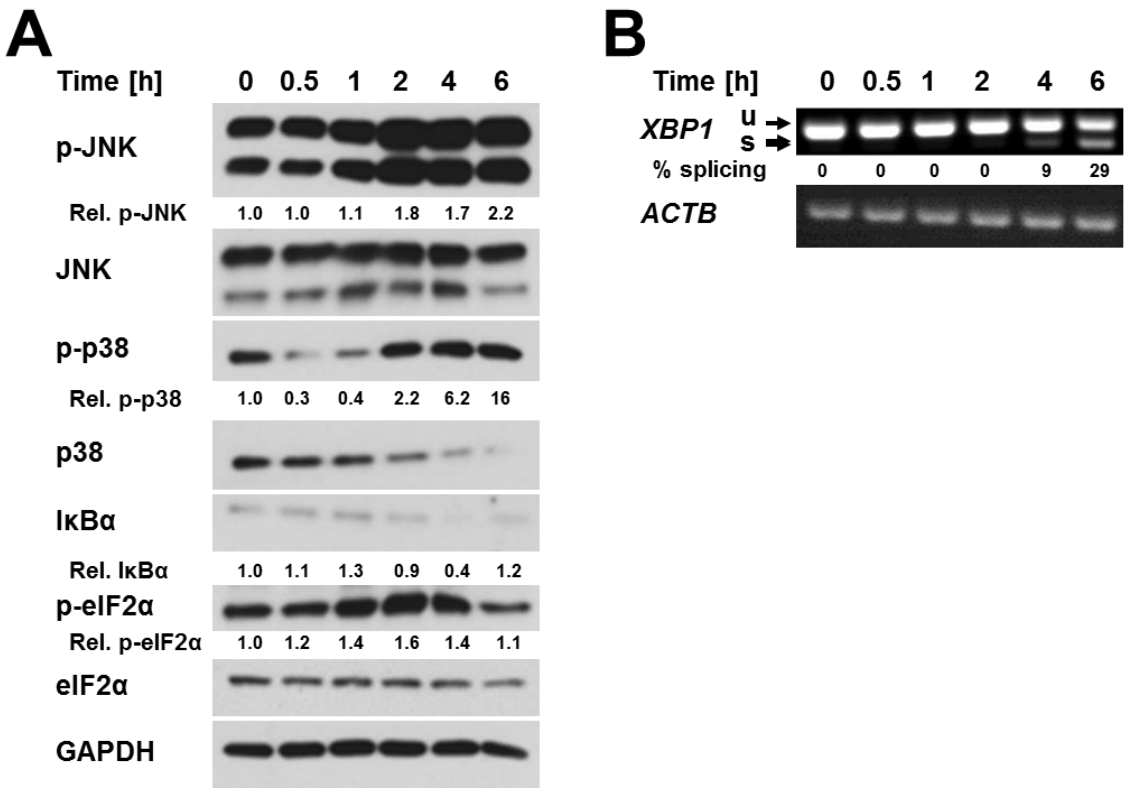

Figure 6.9. SubAB-induced ER stress activates inflammatory signalling pathways in *in vitro* differentiated CAD cells.

Induction of ER stress with 1 μg/ml SubAB in differentiated CAD cells. **(A)** Western blots for phospho-JNK (p-JNK), total-JNK (JNK), phospho-p38 (p-p38), total-p38 (p38), phospho-eIF2α (p-eIF2α) , total-eIF2α (eIF2α) and GAPDH proteins. **(B)** Detection of *XBP1* splicing by RT-PCR.

To confirm the results from SubAB treatment, CAD cells were exposed to 4 h of either thapsigargin or tunicamycin (Figure 6.10). Both ER stressors caused *XBP1* splicing and eIF2α phosphorylation demonstrating that ER stress occurs with 4 h treatment with tunicamycin and thapsigargin in differentiated CAD cells. These two treatments were also sufficient to induce the phosphorylation of p38 and JNK as well as the degradation of IκBα. Overall, these data suggest that ER stress leads to activation of inflammatory signalling in murine and human neuroblastoma cells as well as dopaminergic CAD cells.

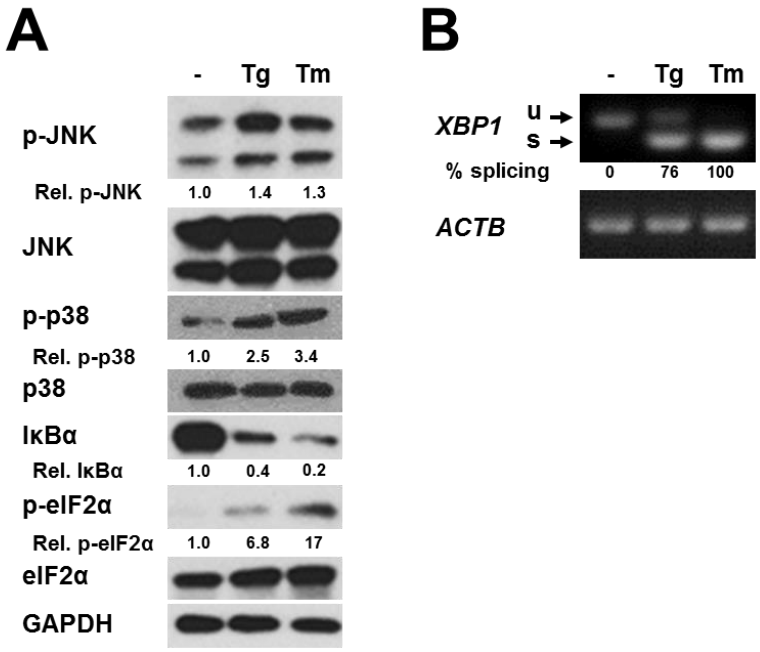

Figure 6.10. ER stressors activate inflammatory signalling pathways in *in vitro* differentiated CAD cells.

Exposure to Tg, (250 nM) and Tm, (1 μg/ml) for 4 h activates JNK, p38, and NF-κB in differentiated CAD cells. Cell lysates were analysed by **(A)** Western blotting and **(B)** and RT-PCR for *XBP1* splicing.

6.3 ER stress causes expression of pro-inflammatory cytokines

The inflammatory signalling pathways: JNK, p38 and NF-κB are involved in many cell signalling events other than inflammation. Activation of these pathways is, consequently, not entirely indicative of inflammation. To address this problem, the expression of genes, encoding pro-inflammatory proteins, were measured in ER-stressed CAD cells. Differentiated CAD cells were exposed to 4 h of thapsigargin or tunicamycin before RNA extraction and RT-qPCR. The expression of *IL-1β*, *TNF-α* and *IL-6*, which have all been implicated in neuroinflammation in PD, was measured by RT-qPCR (Figure 6.11). There was an ~7 fold increase in steady state levels of *IL-1β* mRNA after 4 h of thapsigargin exposure whereas tunicamycin induced an ~3 fold increase in *IL-1β* mRNA (Figure 6.11 A). The steady state levels of *IL-6* increased ~3 fold after treatment of both thapsigargin and tunicamycin (Figure 6.11 B). Both thapsigargin and tunicamycin treatments resulted in an increase in the steady state levels of *TNF-α* mRNA with thapsigargin having a more pronounced effect (Figure 6.11 C). Overall, the ER stressors thapsigargin and tunicamycin

induce the expression of three pro-inflammatory cytokines: *IL-1β*, *IL-6* and *TNF-α* in CAD cells.

In order to establish if the expression of genes encoding pro-inflammatory cytokines during ER stress is applicable to other neuronal cell lines, differentiated SH-SY5Y cells were also investigated. Previously, exposure of 4 h of SubAB to SH-SY5Y cells caused activation of inflammatory signalling (Figure 6.5). Hence, differentiated SH-SY5Y cells were exposed to 4 h of SubAB before harvesting of RNA. In SH-SY5Y cells 4 h of SubAB exposure resulted in increased levels of *IL-6*, *IL-8* and *TNF-α* demonstrating that ER-stressed SH-SY5Y cells also exhibit increased expression of pro-inflammatory cytokine genes (Figure 6.12).

To investigate whether ER stress-induced inflammatory signalling causes an increase in pro-inflammatory cytokine production, which could lead to microglial activation and neuroinflammation in PD, neuronal cells were exposed to ER stress and the release cytokines was monitored. Using established drug concentrations and time points for inducing both ER stress and inflammatory signalling (4 h of 250 nM thapsigargin and 1 µg/ml tunicamycin), pro-inflammatory cytokine production in differentiated CAD cells was monitored using ELISAs. 12 pro-inflammatory cytokines were investigated: TNFα, IL1A, IL2, IL1B, IL4, IL6 IL8, IL10, IL12, IL17A, GM-CSF and IFNγ. Only IL-6 was detected in CAD cell supernatant (Figure 6.13). Interestingly, IL-6 levels increased in the medium of CAD cells exposed to either thapsigargin or tunicamycin with a greater increase induced by thapsigargin. *IL-6* gene expression was also increased with thapsigargin and tunicamycin with tunicamycin causing a greater induction (Figure 6.11). Therefore, it is interesting that the gene expression data did not necessarily translate to the secreted protein level. Differences in how these two ER stressors induce ER stress and how this may impact on the transport of the newly synthesised IL-6 may account for the discrepancy in protein levels detected by ELISA. Nevertheless IL-6 was detected as being released into the media by ER stressed CAD cells.

Neurons undergoing stress can signal to neighbouring cells using various signalling molecules other than cytokines. Nitric oxide is a potent mediator of inflammation and can be released at high concentrations by macrophages but nitric oxide release can occur from other cell types such as neurons. The release of nitric oxide from ER-stressed CAD cells was monitored indirectly by measuring nitrite concentrations in medium conditioned by ER-stressed CAD cells (Figure 6.14). Nitrite concentration, which is indicative of nitric

oxide release, increased in the supernatant of cells exposed to thapsigargin for 4 h, and to an even greater extent 24 h. 4 h of tunicamycin also increased nitrite concentrations similar to thapsigargin, whereas 24 h of tunicamycin, although increasing nitrite concentration more than 4 h, was not as effective as 24 h of thapsigargin at increasing nitrite concentrations in the supernatant of CAD cells.

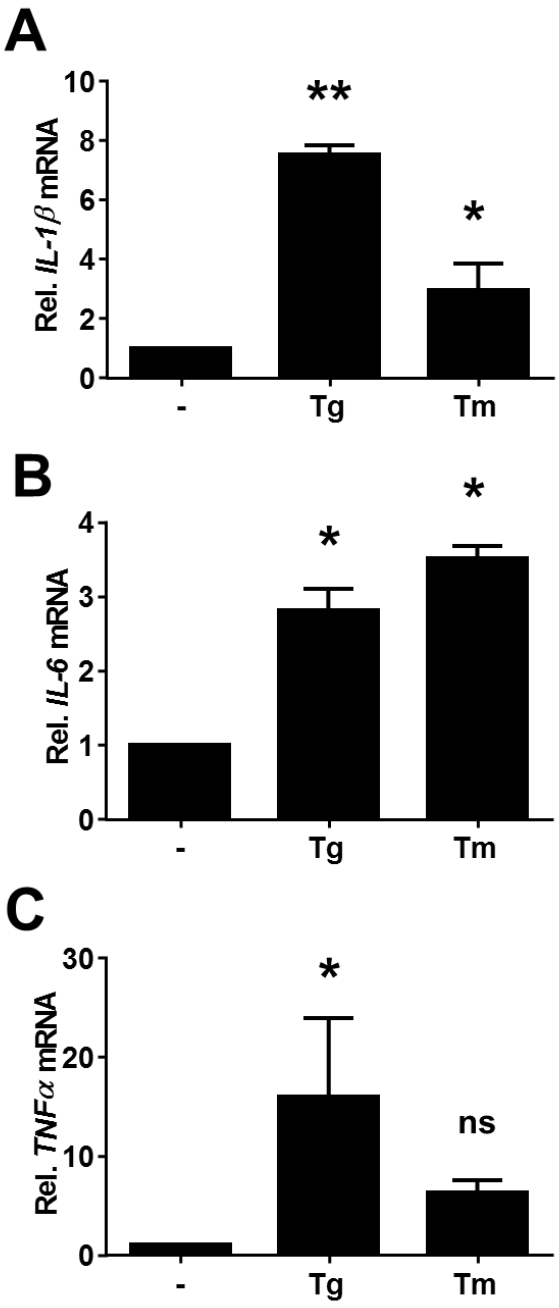

Figure 6.11. ER stress induces expression of *IL-1β*, *IL-6*, and *TNF-a* in CAD cells.

CAD cells were treated with Tg (250 nM) or Tm (1 μg/ml) for 4 h. *IL-1β*, *IL-6*, and *TNF-a* mRNA levels were measured by RT-quantitative PCR (qPCR). Measurements were normalised to *ACTB* mRNA ($n = 3$).(* - $p < 0.05$, ** - $p < 0.01$).

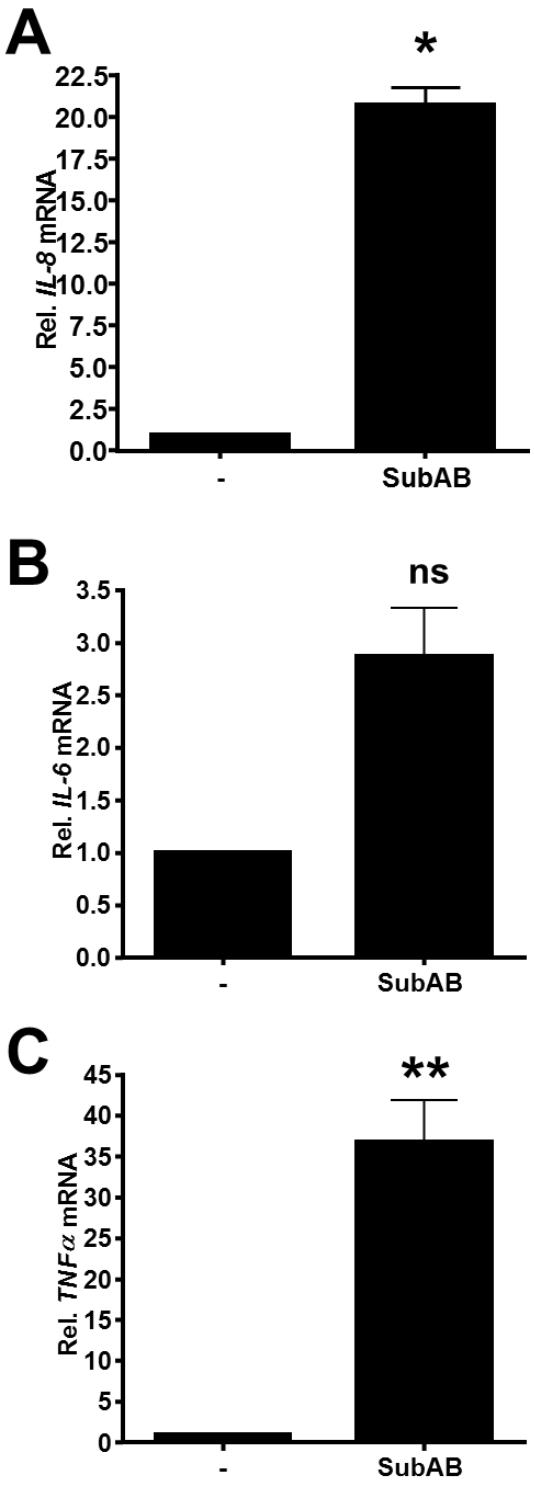

Figure 6.12. ER stress induces expression of *IL-6, IL-8,* and *TNF-a* in SH-SY5Y cells.

(A) SH-SY5Y cells were treated with 1 µg/ml SubAB for 4 h. *IL-6*, *IL-8*, and *TNF-a* mRNA levels were measured by RT-quantitative PCR (qPCR). In SH-SY5Y cells the normaliser is *GAPDH* mRNA ($n = 3$). (* - $p < 0.05$, ** - $p < 0.01$).

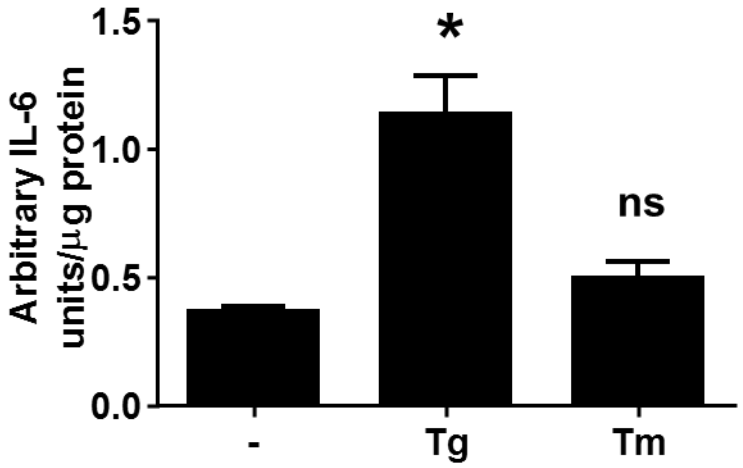

Figure 6.13. ER stress induces release of IL-6 from CAD cells.

CAD cells were treated with Tg (250 nM) or Tm (1 μg/ml) for 4 h. IL-6 levels were measured in CAD cell supernatant using a mouse cytokine ELISA. Arbitrary IL-6 units from OD readings at 450 nm were standardised to total protein from cell lysates (n = 3).

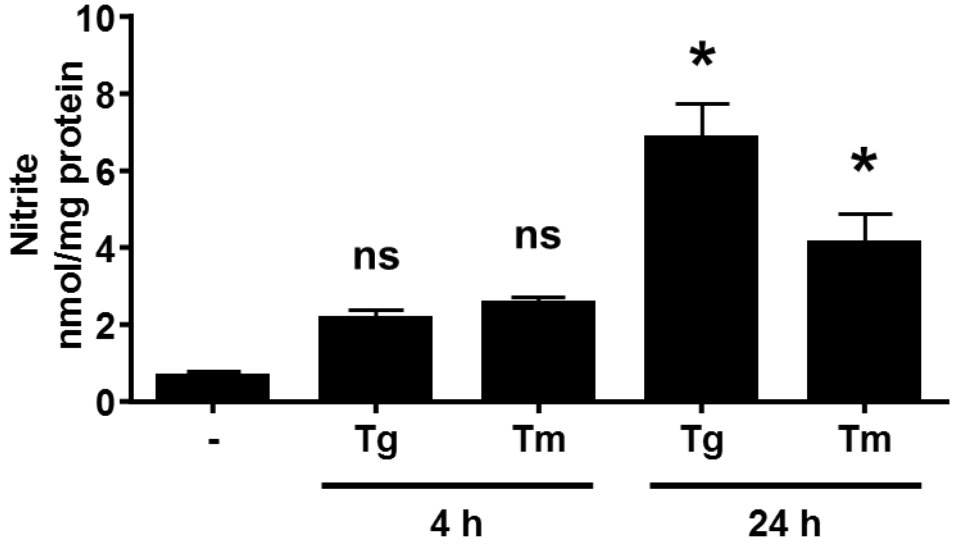

Figure 6.14. ER stress induces nitric oxide release.

CAD cells were treated with Tg (250 nM) or Tm (1 μg/ml) for 4 or 24 h. Nitrite concentration was measured in the culture supernatant and standardised to protein concentration (n = 3). (* - $p < 0.05$, ** - $p < 0.01$).

6.4 Media conditioned by ER-stressed neurons activate glial cells

Data reported above have established that, in dopaminergic CAD cells, ER stress leads to: 1) activation of inflammatory signalling pathways, 2) increased expression of pro-inflammatory genes, 3) release of IL-6, 4) nitric oxide release. Therefore, ER stress can contribute to pro-inflammatory signalling, however, whether this pro-inflammatory signalling is sufficient to amount a response has not been investigated. As discussed in the introduction chapter, inflammatory signalling from stressed neurons has been implicated in the activation of microglia in patients with PD. Microglia are the resident macrophages of the nervous system (Wyss-Coray and Mucke, 2002). Microglia activation is a well-established phenotype of PD (McGeer et al., 2003, McGeer et al., 1988, Barcia et al., 2004). Prolonged activation of microglia causes unnecessary death of healthy neurons and may cause or contribute to the progressive loss of dopaminergic neurons in PD (Gao et al., 2002a). Microglia activation involves microglia changing from a 'silent' to an 'aggressive' state following pro-inflammatory signalling. Microglia activation may contribute to detrimental neuroinflammation in PD as activated microglia release harmful molecules such as pro-inflammatory cytokines, nitric oxide and other ROS (Liu and Hong, 2003). For these reasons a microglia activation was developed assay with the intention of investigating if ER-stressed dopaminergic CAD cells can activate microglial cell line, BV-2. The BV-2 microglia cell line is a well-established cell line for the investigation of microglia activation and along with CAD cells is a murine cell line. Hence it is appropriate to use in a microglia activation assay to test CAD-conditioned medium.

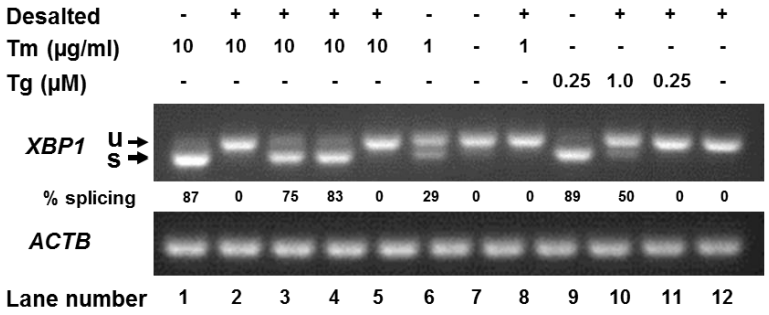

Figure 6.15. Desalting removes Tg and Tm from medium.

XBP1 splicing assay in BV-2 cells. Desalting columns were used to remove ER stressors from DMEM/F12 medium. Desalted or non-desalted supernatant were added to BV-2 cells for 24 h. Conditioned medium from non-stressed CAD cells was filtered before being dosed with either Tm or Tg at the indicated concentrations. All samples originated from DMEM/F12 medium with or without ER stressors except lane 8 which was just PBS. Lanes 2-4 represent fractions from the same original sample with lane 1 being the first fraction collected from the desalting process.

CAD cells were chosen, in addition to the reasons stated above, because differentiation is induced by serum starvation and thus media conditioned by these cells would not contain any serum. This is of practical importance as desalted medium has to be concentrated before being added to microglia and the high protein concentration of serum makes centrifugal concentration problematic. Thus, with serum-containing medium the post-concentrated sample is enriched for serum-derived proteins, which as well as producing a viscous sample difficult to process it may also affect the downstream application. CAD cells exposed to thapsigargin or tunicamycin for 4 h: 1) display markers of active inflammatory signalling pathways, 2) express genes encoding pro-inflammatory cytokines, 3) secrete IL-6. Thus ER-stressed CAD cells display a pro-inflammatory phenotype. Activation of inflammatory signalling pathways and the subsequent release of pro-inflammatory mediators is a possible cause of microglial activation and neurodegeneration in PD. Hence, to establish if activation ER stressor-mediated inflammatory signalling in neuronal cells is sufficient to signal and activate microglia it was investigated if media conditioned by ER-stressed CAD cells could activate a microglial cell line.

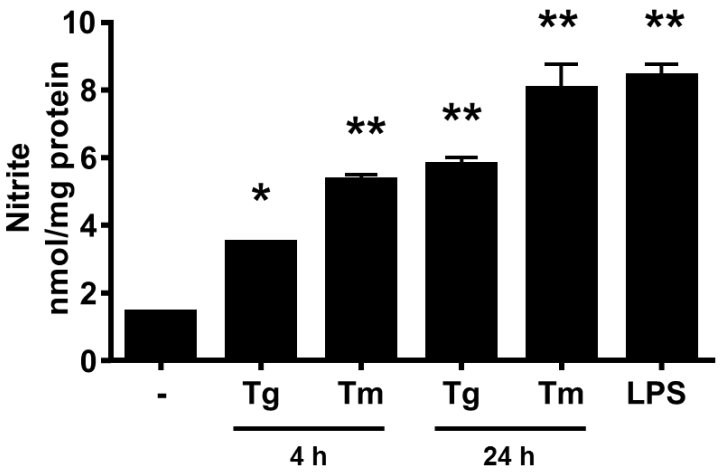

Figure 6.16. Media conditioned by ER stressed neurons activates microglia.

BV-2 microglia activation assay. ER stress was induced for either 4 or 24 h with one of three different ER stressors: 250 nM Tg, or 1 µg/ml Tm. Media conditioned from ER stressed CAD cells were added to BV-2 cells and incubated for 16 h. Nitrite concentration was measured in supernatant from BV-2 cells and standardised to protein concentration (n = 3). 100 ng/ml lipopolysaccharide (LPS) treatment was used as a positive control. (* - $p < 0.05$, ** - $p < 0.01$). '-' indicates BV-2 cells exposed to desalted medium conditioned by non-ER stressed CAD cells.

Media conditioned by CAD cells exposed to tunicamycin or thapsigargin were desalted on HiTrap desalting columns to remove any ER stressors from the medium. After desalting, the conditioned media were added to BV-2 microglia. An *XBP1* assay was performed to confirm that the desalting procedure had depleted the ER stressors from the conditioned media to levels below those which cause ER stress (Figure 6.15). *XBP1* splicing occurred in BV-2 cells exposed to 250 nM thapsigargin or 1-10 µg/ml tunicamycin showing that BV-2 cells respond to these commonly used ER stressors. The desalted media conditioned by CAD cells exposed to either 250 nM thapsigargin or 1 µg/ml tunicamycin (conditions used in Figure 6.16) did not cause *XBP1* splicing in BV-2 cells suggesting that the desalting procedure was successful in removing ER stressors from the media. The desalting of media conditioned by CAD cells exposed to a high concentration of 10 µg/ml tunicamycin was unable to remove all of the ER stressor as BV-2 cells exposed to this medium displayed splicing of *XBP1*. Exposure of CAD cells to 250 nM thapsigargin or 1 µg/ml tunicamycin for 4 h was chosen for microglial activation assays.

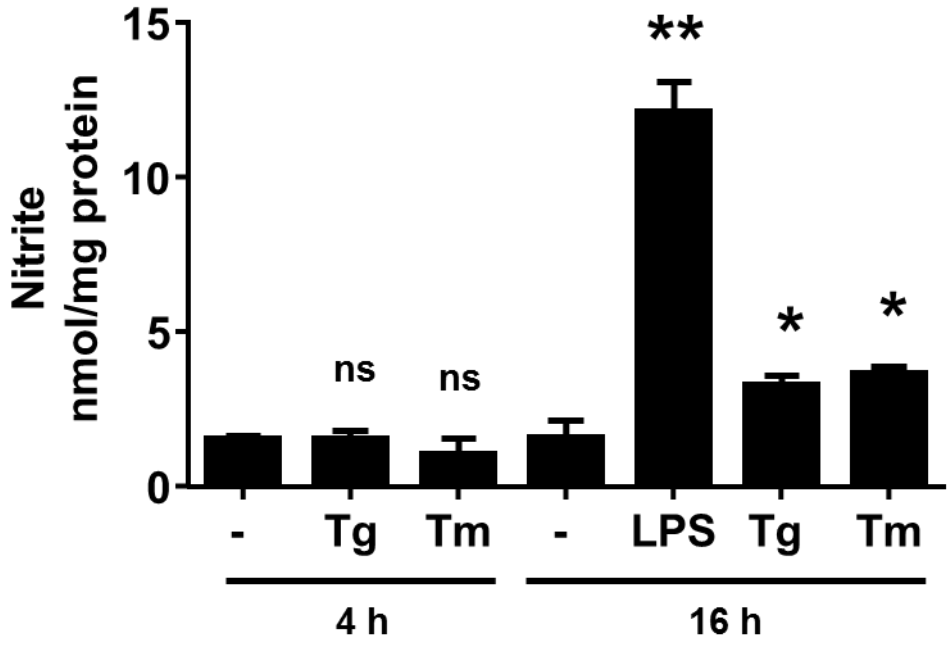

Figure 6.17. ER stress mimetic drugs mildly activate BV-2 cells.

BV-2 microglia activation assay. BV-2 cells were exposed to 250 nM Tg or 1 µg/ml Tm for either 1 or 16 h. Nitrite concentration measured in supernatant from BV-2 cells and standardised to protein concentration ($n = 3$). 100 ng/ml lipopolysaccharide (LPS) treatment was used as a positive control. (* - $p < 0.05$, ** - $p < 0.01$).

Activated microglia release NO (Liu and Hong, 2003). Nitrite concentration, which is indicative of nitric oxide release, was measured in media conditioned by BV-2 cells to monitor BV-2 microglial activation. CAD cells were exposed to either thapsigargin or tunicamycin for 4 or 24 h. Media from ER-stressed CAD cells as well as CAD cells without any treatment were desalted and then finally added to BV-2 cultures for 16 h (Figure 6.16). As a positive control, BV-2 cells were exposed to LPS for 16 h. LPS treatment caused an increase in nitrite concentration from ~1.5 (in BV-2 cells exposed to untreated CAD conditioned media) to ~8 nmol/mg protein. Media from ER-stressed CAD cells was sufficient to induce activation of BV-2 cells. 24 h of ER stress resulted in the strongest activation of BV-2 cells, which was similar to levels induced by LPS.

It could be possible that a small concentration of ER stressor, which is not sufficient to induce measurable *XBP1* splicing in BV-2 cells, remains in the media after desalting. To ascertain if ER stressors carried across from CAD conditioned media to BV-2 cells affected the microglial activation assay, BV-2 cells were exposed to 250 nM thapsigargin or 1 µg/ml tunicamycin (Figure 6.17). These concentrations of ER stressor are higher than any possible concentration carried across through the desalting protocol as demonstrated by the lack of *XBP1* splicing see in Figure 6.16. The nitrite concentration of the supernatant of BV-2 cells exposed to 250 nM thapsigargin or 1 µg/ml tunicamycin for 16 h was only moderately increased compared to untreated BV-2 cells. Higher concentrations of ER stressor therefore can activate BV-2 microglia. The activation of glial cells by ER stress has been observed before (Meares et al., 2014). However, more pronounced microglial activation was observed in BV-2 cells exposed to media conditioned by ER-stressed CAD cells, which had been desalted to remove the ER stressors. Therefore, the observed microglial activation is most likely a consequence of release of pro-inflammatory factors from ER-stressed CAD cells.

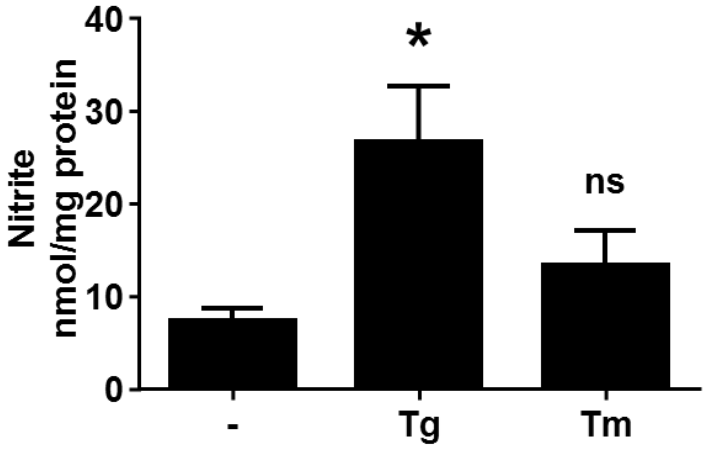

Figure 6.18. Media conditioned by ER stressed primary neurons activates primary glia.
ER stress was induced in primary cortical neurons for 4 h with one of two different ER stressors: 250 nM Tg, or 1 μg/ml Tm. Media conditioned from ER stressed primary murine cortical neurons were desalted before being added to primary murine glia cultures and incubated for 16 h. Nitrite concentration was measured in the supernatants from primary cortical neurons and standardised to protein concentration ($n = 3$). (* - $p < 0.05$, ** - $p < 0.01$).

To investigate if activation of microglia by ER-stressed neurons occurred in more physiologically relevant conditions experiments were expanded to include primary neurons and primary glia. The brain dissection from E14-E15 Swiss mouse embryos was carried out by members of Professor Marcus Rattray's group (Bradford University). Mouse primary cortical neurons were exposed to 250 nM thapsigargin or 1 μg/ml tunicamycin for 4 h before media were desalted and added to mouse primary glia cultures (Figure 6.18). Basal nitrite concentration from primary glia exposed to conditioned media from untreated primary neurons was higher than observed in BV-2 cells. Similar to experiments with CAD and BV-2 cells, conditioned media form ER-stressed primary neurons also activated primary glia with the thapsigargin treatment having a more pronounced effect than tunicamycin. Thus, ER stress-mediated pro-inflammatory signalling from neurons is sufficient to activate glia in differentiated cell lines as well as primary cultures.

6.5 The PD mimetic drug 6-OHDA induces ER stress

The PD mimetic 6-OHDA has previously been shown to cause activation of the UPR (Ryu et al., 2002); yet there is little evidence that 6-OHDA activates the IRE1α branch of the

UPR. SH-SY5Y cells display markers of ER stress when exposed to 6-OHDA such as increased expression of *CHOP* and *BiP*, which are not specific to IRE1α activation (Yamamuro et al., 2006). Also, *XBP1* splicing, a marker for IRE1α activation specifically, has so far not been reported in 6-OHDA treated SH-SY5Y cells. 6-OHDA-mediated *XBP1* splicing has been reported in MN9D cells (Holtz and O'Malley, 2003) but 6-OHDA was also reported to have no effect on *XBP1* splicing in PC-12 cells (Hu et al., 2014). Whether 6-OHDA causes *XBP1* splicing is important to know, in the context of inflammatory signalling, as *XBP1* splicing is specific to activation of IRE1α, which is implicated in the activation of JNK (Nishitoh et al., 2002), p38 (Hung et al., 2004, Ichijo et al., 1997) and NF-κB (Hu et al., 2006b). Whether 6-OHDA causes *XBP1* splicing in SH-SY5Y cells is also important to understand because *XBP1* is reported to protect against 6-OHDA in mice (Valdes et al., 2014). Differentiated SH-SY5Y cells were exposed to 10 or 100 µM 6-OHDA for 4 – 48 h before protein and RNA extraction. *XBP1* splicing assays revealed that 4 h of 10 µM 6-OHDA was sufficient to cause very low levels of *XBP1* splicing (Figure 6.19 A). Although levels of *XBP1* splicing were very low after 6-OHDA exposure, low levels of splicing are likely to be closer to physiologically relevant splicing compared to those observed after exposure to ER stress mimetic drugs. *XBP1* splicing was maintained up to 6 h and then began to decrease by 12 h and was not detectable by 24 and 48 h with 10 µM 6-OHDA. *XBP1* splicing not occurring at later time points may be a result of 6-OHDA being a fairly unstable compound (Powell and Heacock, 1973) or that SH-SY5Y cells have alleviated the low level of ER stress induced by 6-OHDA. Consistent with these explanations, 100 µM 6-OHDA resulted in more prolonged *XBP1* splicing.

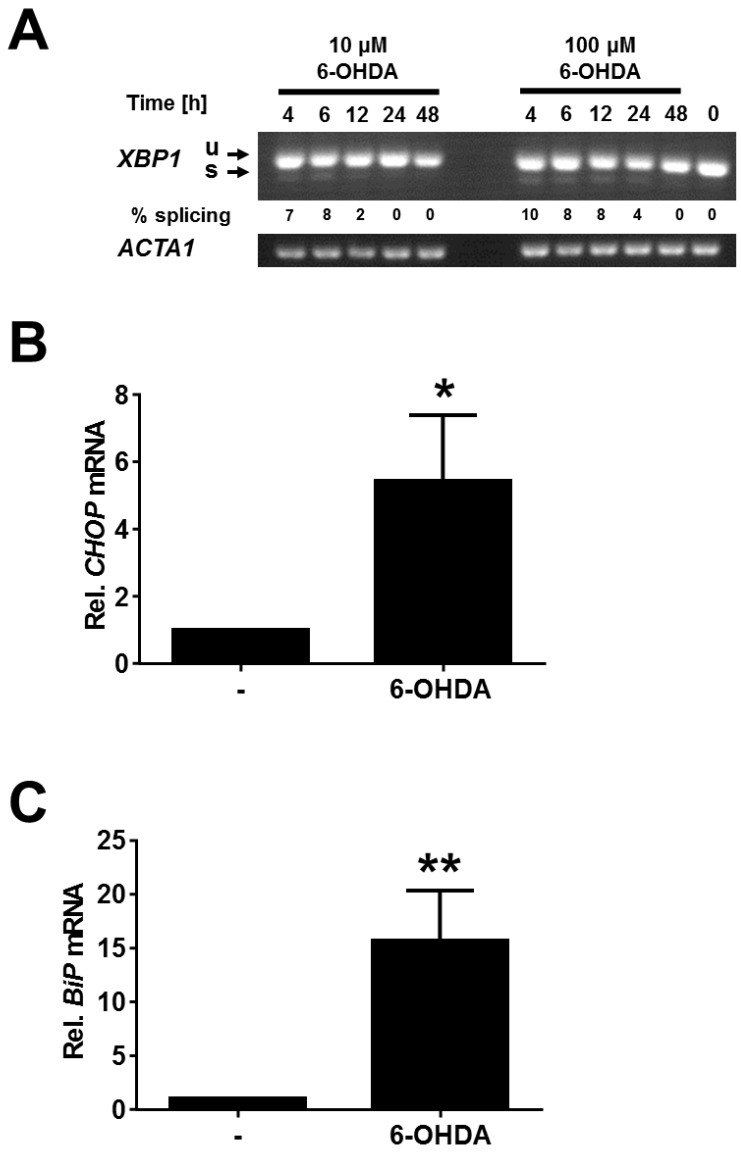

Figure 6.19. 6-OHDA induces ER stress.

(A) Differentiated SH-SY5Y cells were exposed to either 10 and 100 µM 6-OHDA for the indicated times before harvesting RNA and performing an *XBP1* splicing assay PCR. **(B)** Expression of *CHOP* and **(C)** *BiP* mRNAs in differentiated CAD cells exposed to 100 µM 6-OHDA for 2 h (n = 3). The RT-qPCR data were normalised to *ACTB*. (* - $p < 0.05$, ** - $p < 0.01$).

XBP1 splicing should result in the increased expression of ER stress response genes *BiP* and *CHOP*. Hence the expression of *BiP* and *CHOP* was monitored after ER stress. Differentiated CAD cells were exposed to 100 µM 6-OHDA for 2 h before RNA isolation. *CHOP* and *BiP* mRNAs were measured using RT-qPCR to monitor activation of the UPR (Figure 6.19 B). 6-OHDA treatment resulted in increased expression of both *CHOP* and

BiP mRNAs, suggesting that 6-OHDA causes ER stress and activates the UPR in differentiated neuron-like cells.

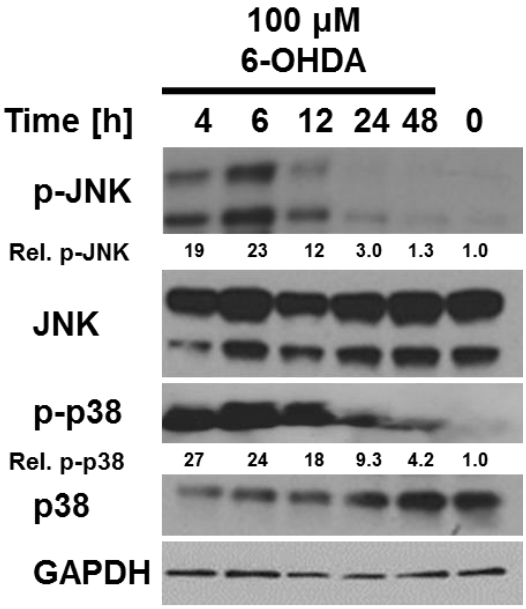

Figure 6.20. 6-OHDA activates inflammatory signalling pathways.
Differentiated SH-SY5Y cells were exposd to 100 µM 6-OHDA for the times indicated before extraction of protein and western blotting for phospho-JNK (p-JNK), total-JNK (JNK), phospho-p38 (p-p38), total-p38 (p38).

Next it was investigated if 6-OHDA, alongside activating the UPR, can also activate inflammatory signalling pathways. Hence, protein samples from SH-SY5Y cells treated with 100 µM 6-OHDA were used to investigate activation of inflammatory signalling pathways (Figure 6.20). In agreement with a recent study (Tobon-Velasco et al., 2013), both JNK and p38 signalling pathways are activated from 4 h, reaching maximal levels after 6 h and activation decreases subsequently to the lowest level at 48 h. Thus, 6-OHDA causes inflammatory signalling and activation of the UPR in SH-SY5Y cells. However, whether 6-OHDA-mediated inflammatory signalling is dependent on UPR activation is not known. Further investigation is therefore required to ascertain to what extent ER stress contributes to 6-OHDA-mediated inflammation.

6.6 Discussion

This chapter provides evidence that ER stress activates inflammatory signalling pathways, JNK, p38 and NF-κB in three different neuronal cell lines: murine neuroblastoma N1E-115, differentiated human neuroblastoma SH-SY5Y and differentiated murine

dopaminergic CAD cells. Activation of inflammatory signalling pathways largely correlates with the appearance of markers of ER stress. Three different ER stressors were used on CAD and SH-SY5Y cells with similar results and kinetics suggesting that inflammatory signalling is a product of ER stress and not secondary effects of the ER stressors used.

Activation of inflammatory signalling pathways should result in the expression of pro-inflammatory cytokines. Indeed, it has been demonstrated that pro-inflammatory cytokine gene expression is increased in ER-stressed neuronal cells. Release of nitric oxide from ER-stressed CAD cells is also observed. Nitric oxide is unlikely to contribute to the activation of BV-2 microglia as it has a very short half-life (Hakim et al., 1996), and is likely to be removed by desalting, suggesting that nitric oxide levels in conditioned media added to BV-2 cells in microglia assays is likely to be extremely low.

ER stress has been reported to cause inflammatory signalling. However, it has never been shown that ER stress-mediated release of inflammatory factors is sufficient to activate microglia. Evidence is also provided that ER-stressed neuronal cells condition growth medium to an extent that they create an environment which activates microglia. The next important questions are: 1) What factor or factors released by ER-stressed neurons are sufficient to activate microglia? 2) Can these be inhibited? Further experimentation is required to ascertain which factor/s is/are causing microglial activation. Mass spectrometry may provide a clue as to which inflammatory factors exist in the media conditioned by ER-stressed neurons. The ELISA data highlights IL-6 as a potential target in CAD neuronal cultures. Given that CAD cells release IL-6, several questions arise: 1) Does addition of IL-6 to BV-2 cells activate them? 2) Can IL-6 be removed from CAD-conditioned medium by an IL-6 antibody and will this prevent the activation of BV-2 cells by medium conditioned by ER-stressed CAD cells? 3) Does knock-down of *IL-6* in neurons prevent activation of BV-2 cells by medium conditioned by ER-stressed CAD cells? However, pro-inflammatory cytokines may not be the only mediators of inflammation during ER stress.

Along with microglia, IL-6 can also be secreted by neurons (Gadient and Otten, 1994). The role of IL-6 in the nervous system is complicated. IL-6 has a dual role in brain injury but importantly it is upregulated whenever neuroinflammation is expected (Erta et al., 2012). IL-6 is upregulated in PD (Mogi et al., 1994) but its protective effect in the MPTP model of PD implies that it may actually have a neuroprotective role (Bolin et al., 2002, Akaneya et al., 1995). However, this neuroprotective role has only been demonstrated in the MPTP

model and thus may only be specific to the action of MPTP. Further research is required to establish if IL-6 plays an important role in mediating microglial activation induced through neuronal ER stress.

It has previously been shown that 10 ng/ml IFNγ is sufficient to induce NO release by BV-2 cells (Sheng et al., 2011). In the same study it was shown that a combination of TNFα, IL-1β and IFNγ resulted in the highest induction of NO release, whereas a combination of IL-1β and TNFα alone did not induce NO release. Therefore, it is likely that activation of BV-2 microglia and NO release is dependent on a balance between different cytokines and other possible pro-inflammatory mediators. Elucidating the combination of pro-inflammatory mediators responsible for maximal induction of NO release from BV-2 cells may, therefore, require further investigation. It is also a possibility that cytokines which were not detected in the ELISA are responsible for contributing to the activation of BV-2 cells. Concentrations lower than the detection limit of the ELISA may still be sufficient to activate microglia especially if in combination with other pro-inflammatory mediators, including other cytokines. Classical activation of macrophages involves priming by IFNγ and further activation by TNFα (Nathan, 1991). Neither of these two cytokines were detected in the ELISA even though expression of the *TNFα* gene increased with ER stress (Figure 6.12). Either these cytokines are sufficient to activate BV-2 cells at levels lower than the detection limit of the ELISA or the BV-2 cells are not classically activated and are therefore activated through another signal, or more likely, combination of signals which may or may not involve IL-6 (Figure 6.21).

An interesting finding is that the various differentiation protocols for SH-SY5Y cells were all unable to induce TH expression. Regardless of this, differentiation was able to induce the neuronal phenotype of extended neurite outgrowth and reduced cell division. It has previously been published that 10 μM RA (Lopes et al., 2010) and 10 μM RA and TPA (Presgraves et al., 2004) can induce TH expression in SH-SY5Y cells. However, experiments for this thesis did not find evidence of TH expression in SH-SY5Y cells which is in agreement with other reports (Cheung et al., 2009, Presgraves et al., 2004). Differentiation with a combination of RA and TPA is reported to induce higher TH expression compared to undifferentiated, and RA-differentiated cells (Presgraves et al., 2004). However, experiments in this thesis were not sufficient to observe detectable expression of TH in undifferentiated, RA or RA and TPA differentiated SH-SY5Y cells using the anti-TH antibody. The same antibody has been shown to work with both PC-12

and CAD cells suggesting that problems in detecting TH in SH-SY5Y cell lysates is not a problem with the antibody.

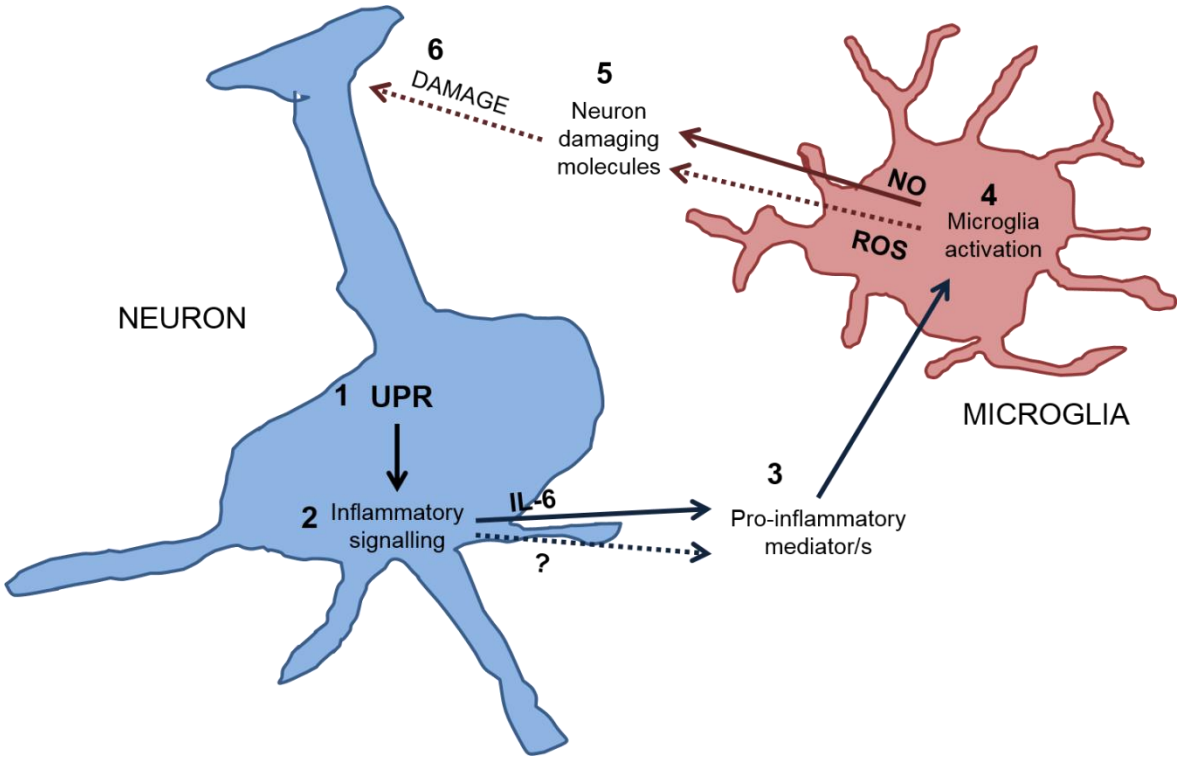

Figure 6.21 Model of how neuron-secreted IL-6 may be involved in activation of microglia.
Switching on of the UPR in neurons (1) leads to activation of inflammatory signalling pathways (2) which results in the release of IL-6 and other possible molecules to make up the pool of exogenous pro-inflammatory mediators (3). Pro-inflammatory mediators, which may include IL-6, are detected by microglia leading to microglia activation (4). Activation of microglia causes release of neuron damaging molecules such as NO and ROS (5). These molecules damage neurons and lead to further inflammation (6). Solid arrows represent events which are supported by the data. Dashed arrows represent events which no data is presented for but are supported by other studies.

Increasing passage number is known to inhibit a cell line's ability to differentiate and this may be a possible explanation for the difference in differentiation phenotype reported by different laboratories. For this reason passaging of cells was limited and new frozen stocks of cells were used when cells had been passaged more than ten times. However, the frozen stocks may already have undergone many passages meaning that freshly thawed cells may have had a reduced ability to respond to differentiation. HPA, the source of this lab's frozen stock of SH-SY5Y cells, were unable to provide the passage number of the frozen stock of cells. The different histories of cell lines belonging to each research group may

account for more than just differences in differentiation phenotypes but is likely to be a more wide reaching problem contributing to variability of data in the published literature.

PC-12 cells displayed the highest expression of TH both before and after differentiation. The murine CAD cell line was prioritised in further experiments as the dopaminergic cell line model over PC-12 cells because: differentiation was more cost effective, cells could be grown without serum which prevents issues with concentration of supernatant, differentiation induces less p38 and JNK activation than in PC-12 cells. A further important reason for prioritising CAD cells over other cell lines was that the project plan initially involved lentiviral knock-down of ER stress sensing proteins IRE1α, PERK and ATF6 to fully establish causation between ER stress and inflammation as well as identify which UPR signalling pathways were important. shRNAs were designed against mouse genes with the idea that these same lentiviruses could be used against primary mouse cells. Lentiviral transduction with GFP was indeed optimised early in the project alongside production of a plasmid encoding a GFP-tagged α-synuclein protein suitable for the lentiviral transduction system intended for this investigation. Unfortunately, failure (for one year) of the only flow hood legally suitable for lentiviral work meant this branch of the project could not be completed. Unfortunately, this branch of the project is still necessary to establish key questions in ER stress-mediated inflammatory signalling. For example: 1) Which branch or branches of the UPR is/are responsible for activation of p38, JNK and NF-κB? 2) Which UPR branch/s is/are responsible for increased expression of cytokines? 3) Is UPR activation responsible for conditioning of media capable of activating microglia?

In this results chapter it is shown that 6-OHDA can induce the UPR in neuronal cultures whilst also activating inflammatory signalling pathways. Interestingly, very low levels of *XBP1* splicing in SH-SY5Y cells was detected with 6-OHDA exposure. The IRE1α branch of the UPR specifically has so far not been shown to be activated by 6-OHDA in SH-SY5Y cells. Activation of IRE1α may be a possible mechanism through which 6-OHDA activates inflammatory signalling pathways. However, *XBP1* splicing was very low whilst inflammatory signalling markers were strongly activated, which suggest that UPR activation is not the only mechanism of inflammatory signalling activation taking place. It is necessary to elucidate to what extent, if any, the UPR contributes to activation of inflammatory signalling pathways. Hence, this branch of the investigation would also be progressed with knock-down of UPR branches to investigate causality.

Overall, strong correlative evidence is provided that ER stress activates inflammatory signalling pathways: JNK, p38 and NF-κB as well as increasing expression of genes encoding pro-inflammatory cytokines in neuron-like cell lines. It also demonstrated that medium conditioned by ER-stressed cells is sufficient to activate microglia. Bringing all this together it seems likely that ER stress has a role in activating or contributing to inflammation. However, further dissection of these signalling pathways is required to establish: 1) causation, 2) which branches of the UPR activate inflammatory signalling, 3) which inflammatory signalling pathways are responsible for pro-inflammatory gene and protein expression 3) which pro-inflammatory mediator/s is/are responsible for microglial activation.

7 FINAL DISCUSSION

7.1 The role of ER stress-mediated JNK activation

7.1.1 Early ER stress-dependent JNK activation is prosurvival

Evidence is provided in chapter 3 that early stress-mediated JNK activity can be prosurvival. Acute ER stress causing transient JNK activation is observed in several cell lines. This JNK activation was found to be IRE1α and TRAF2 dependent. Using *jnk1*$^{-/-}$ *jnk2*$^{-/-}$ MEFs it was shown that transient JNK activation during acute ER stress upregulates the expression of several antiapoptotic mediators. Not only that, but JNK is required for early protection against ER stress-induced apoptosis as *jnk1*$^{-/-}$ *jnk2*$^{-/-}$ MEFs were more susceptible to ER stress-induced cell death.

The role of JNK in apoptosis is intriguing because it can be both pro and antiapoptotic depending on the stress and even the time of stress. However, how JNK activation switches between being prosurvival and proapoptotic is poorly understood. It is very likely that this switch involves the activity of at least one other signalling pathway. The NF-κB pathway is a likely suspect because it has been previously shown to be involved in TNFα-induced cell death alongside JNK activation. In TNFα-induced cell death NF-κB had a prosurvival role whilst JNK was proapoptotic and cell death occurred only in the absence of NF-κB signalling (Tang 2002). Intriguingly, NF-κB activation during ER stress is reminiscent of the JNK activation observed during ER stress in this thesis, in that it is transient and displays similar kinetics (Wu *et al.*, 2002; Jiang *et al.*, 2003; Deng *et al.*, 2004; Wu *et al.*, 2004). Therefore the interaction between NF-κB and JNK may explain the biphasic JNK activation and the conflicting roles for JNK in apoptosis.

It has been suggested that JNK activation may not be sufficient to induce apoptosis and may only contribute to apoptosis if it has already been initiated and that JNK activation without prior apoptotic signalling is prosurvival (Liu and Lin 2005). The PERK branch of the UPR is reported to activate apoptosis whilst calcium release from the ER during ER stress is also capable of inducing cell death. It is possible that a combination of these signals regulates if ER stress-mediated JNK contributes to apoptosis. Another possible explanation is that JNK isoforms are phosphorylated differently to one another allowing tight control of the effect of JNK activation as exemplified by JNK1, but not JNK2, being required for TNFα-induced apoptosis (Liu 2004). A more specific mechanism for biphasic

JNK activation during ER stress may be through control of IRE1α phosphorylation, which in turn alters its ability to induce activation of JNK.

Regardless of the mechanism controlling biphasic JNK activation, data support that early JNK activation is prosurvival through upregulation of antiapoptotic genes. Previous antiapoptotic genes have been identified as being upregulated through prosurvival JNK activity (Lamb et al., 2003) this thesis provides evidence for addition of *cIAP1*, *XIAP* and *BIRC6* in the repertoire of antiapoptotic genes which can be controlled by JNK. The mechanism of how JNK induces anti-inflammatory genes is yet to be discovered but it may involve JunD. NF-κB cooperates with the transcription factor JunD (Rahmani et al., 2001), whilst in TNF-α-stimulated cells, JunD contributes to the transcriptional induction of *cIAP2* (Lamb et al., 2003). A co-operation between NF-κB and JNK to induce and regulate JunD may explain the JNK-dependent induction of antiapoptotic genes early in the ER stress response. There are many more anti and proapoptotic genes which have so far not been investigated during JNK activation. A larger study to characterise the expression profiles of the whole range of genes involved in cell death and survival during stress including ER stress may help provide an answer to how JNK can have two distinct roles.

7.1.2 The role of acute ER stress in the development of insulin resistance

In chapter 4 strong evidence is provided that ER stress-mediated JNK activation does not inhibit insulin signalling, which is in contrast to previously published data (Ozcan et al., 2004). The data in this thesis is comprehensive in that it includes several cell lines (ruling out cell line specific observations), uses three mechanistically different ER stressors (ruling out off target drug effects), covers a range of time points from 0.5 to 8 h and monitors insulin signalling at three distinct stages in the insulin signalling pathway.

JNK is thought to inhibit insulin signalling through the serine phosphorylation of IRS1 which prevents its interaction with, and the subsequent tyrosine phosphorylation by, the insulin receptor. Although demonstrating IRE1α- and TRAF2-dependent activation of JNK during ER stress, no significant changes in IRS1 serine or tyrosine phosphorylation was observed. More thorough investigation of downstream insulin signalling proteins: AKT and GSK, also revealed that ER stress-induced JNK activation does not inhibit insulin signalling.

Results in chapter 4 suggest that the role for JNK in inhibiting insulin resistance may not be as well established as reported. IRE1α-JNK signalling causing insulin resistance at early

time points has not been repeated since the first observation of this mechanism for ER stress-mediated insulin resistance. It could be that results from the original study are a product of a cell batch specific phenomenon or that experimental conditions have for some reason not been fully replicated in this or in other published studies. Another possible explanation is that JNK-IRS1 activity is restricted through JNK's subcellular localisation or through differences in interactions with proteins which bridge JNK to its substrates. Regulation of kinases can involve changes in subcellular localisation. For example, ERKs are reported to have opposing outputs depending on subcellular localisation (Marshall, 1995). JNK, however does not appear to relocalise after activation during transient or persistent stress (Chen et al., 1996, Sanchez-Perez et al., 1998). JNK-interacting proteins (JIPs) are reported to interact with specific parts of the JNK signalling pathway and may underlie how JNK's activity is regulated. For example, JIP1 and JIP2 have thought to be required for normal glucose homeostasis and this was explained through their ability to interact with IRS proteins (Standen et al., 2009). JIPs may be important for bridging JNK to IRS1: differences in JIP expression and regulation may explain study to study variation. However, the role of JIPs in mediating JNK activity, especially in the context of insulin signalling, is not well known. Thus, it still remains to be concluded if ER stress mediated JNK activation is responsible for insulin resistance.

7.2 The effect of ER stress on the trafficking of proteins through the secretory pathway

An important implication arising from this thesis is that prolonged/chronic ER stress, induced by three mechanistically different ER stressors, causes a block in the secretory pathway. This block may have wide ranging effects. The main potential effect is that all proteins, which are processed through or reside in the secretory pathway (a third of all proteins (Levine et al., 2005)), are over time going to be depleted. How each protein is affected over time will vary depending on several factors such as its half-life and if other proteins involved in another proteins regulation have also been affected by the block in the secretory pathway. It would therefore be difficult to predict how a secretory protein will be affected during long-lasting ER stress. Thus, it will be necessary to investigate each protein individually during prolonged ER stress to establish when ER stress causes depletion significant enough to affect cellular processes. Establishing how all proteins, which are synthesised through the secretory pathway, are affected during prolonged ER stress would provide much needed information for the planning experiments and the interpretation of data involving ER stress. It is important that future studies investigating how ER stress

affects other signalling events in the cell should take into consideration the effect of long-lasting ER stress on proteins involved in the specific signalling pathway being investigated.

7.2.1 ER stress-mediated depletion of the insulin receptor via inhibited trafficking through the secretory pathway

It was demonstrated in chapter 5 that during prolonged ER stress the insulin receptor is depleted from the plasma membrane. What's more is that data in chapter 5 provide evidence that ER stress blocks the transport of newly synthesised insulin receptors from the ER to Golgi. This block in transport over several half-lives of the membrane bound insulin receptor is sufficient to deplete the insulin receptor at the plasma membrane. Importantly this depletion of insulin receptors causes insulin resistance as demonstrated by reduced insulin mediated AKT and GSK phosphorylation. Shorter exposures of ER stress which do not extend over several half-lives of the insulin receptor are not sufficient to cause insulin resistance and the rescue of insulin signalling by an insulin receptor chimera which does not traffic through the ER suggests that blockage of the secretory pathway is the only mechanism through which ER stress-mediated insulin resistance is observed.

The UPR is known to inhibit both transcription and translation so it is interesting that both transcription and translation of the insulin receptor continued during chronic ER stress. Why cells continue to translate the insulin receptor during chronic ER stress is not known. A possible explanation is that insulin receptors promote survival through insulin-mediated activation of AKT phosphorylation (Kim et al., 2001). If or how synthesis of the insulin receptor during ER stress is prioritised over other proteins still needs to be established. Accumulation of IGF-1 proreceptors during chronic ER stress suggest that at least translation of IGF-1 is maintained. However, IGF-1 activation may also be able to promote survival through AKT phosphorylation so its synthesis may also be prioritised during ER. The monitoring of other proteins, which traffic through the secretory pathway, during chronic ER stress will establish if the continued translation of IGF-1 and the insulin receptor is specific to these proteins.

7.2.1.1 ER stress-mediated depletion of the insulin receptor: implications for type II diabetes

The mechanism for insulin resistance during ER stress reported in this thesis has serious implications for understanding of T2D. ER stress is believed to be induced in T2D as is

reported in models of T2D (Ozcan et al., 2004, Alhusaini et al., 2010, Kars et al., 2010) and in the tissues of obese patients (Puri et al., 2008, Gregor et al., 2009, Boden et al., 2008, Sharma et al., 2008). How ER stress occurs in diabetes is not fully established but increased exposure to free fatty acids and an inflammatory environment have been suggested (Alhusaini et al., 2010, Hasnain et al., 2014). Research from other members of Martin Schröder's laboratory also emphasises the role of hypoxia and glucose starvation in causing ER stress in adipocytes (Mihai and Schröder, 2014). It could be possible that ER stress-mediated depletion of the insulin receptor at the plasma membrane is a cause of, or contributory factor to, the development of insulin resistance during ER stress. However, it is worth noting that ER stress mimetics, although providing an important tool for investigating ER stress, do not accurately replicate physiological ER stress. Thus it is important to establish if more physiological ER stress levels over time are also sufficient to deplete insulin receptors and cause insulin resistance. Titrating the concentrations of ER stressors even further may provide lower and more physiological levels of ER stress. SubAB could be prioritised over other ER stressors because it is highly specific and has been used at one concentration only (1 µg/ml). Another possible way of achieving physiological ER stress may include treatment of palmitate, however, it should be stressed that palmitate-induced ER stress is not fully characterised and is controversial (Mihai and Schröder, 2014, Achard and Laybutt, 2012). Therefore providing a physiological ER stress may prove to be a difficult task, which may become more achievable upon further characterisation of the causes of ER stress in obesity and diabetes.

7.2.1.2 ER stress-mediated depletion of the insulin receptor: implications for neurodegeneration

Interestingly, insulin receptor levels were reduced in the SNpc of PD patients (Moroo et al., 1994). Insulin signalling has only recently been accepted as an important part of neuronal functioning (Nistico et al., 2012). Disrupted insulin signalling has been suggested to play a part in PD (Wang et al., 2014, Spielman et al., 2014, Van Woert and Mueller, 1971, Moroo et al., 1994, Takahashi et al., 1996, Aviles-Olmos et al., 2013, Santiago and Potashkin, 2013, Dandona et al., 2004) and even more so in AD with some researchers proposing to name AD type 3 diabetes (Frolich et al., 1998, Spielman et al., 2014, Craft et al., 2013). ER stress is a common observation in studies involving neurodegeneration and may therefore underlie a common cause of, or at least a contributory factor to, the progression of these diseases. Data in this thesis support the conclusion that long-lasting ER stress leads to insulin resistance through depletion of the insulin receptor in

hepatocytes, myocytes, adipocytes and finally neuronal and primary glial cells (Chapter 5). The observation that insulin receptor depletion and insulin resistance also occurs in primary glial cells and in two neuronal cell lines demonstrates that long-lasting ER stress-mediated insulin resistance is a potential mechanism explaining the reported depletion of insulin receptors and insulin resistance in PD and other neurodegenerative diseases. However, it is worth noting that insulin receptor depletion and insulin resistance may occur via another more specific mechanism and that long-lasting ER stress may just mimic this to produce the same end result. For this reason it is important to establish if inhibition of ER stress in a PD model is sufficient to prevent depletion of insulin receptors and insulin resistance.

7.3 Activation of inflammation during ER stress

7.3.1 ER stress-mediated activation of inflammatory signalling pathways

The UPR and inflammation have been linked in many studies with crosstalk between these two signalling events being reported. Inflammatory signalling pathways are considered to be part of the ever expanding UPR. Data from chapters 3-6 also support the view that the UPR can activate JNK, p38 and NF-κB. It has been demostrated that JNK activation during ER stress is dependent on IRE1α and TRAF2 (Chapter 3). It would be interesting to establish if p38 activation is also dependent on IRE1α and TRAF2 as the IRE1α-TRAF2 interaction is reported to activate ASK1, which is an upstream kinase of both p38 and JNK. However, in some experiments differing phosphorylation kinetics between these two MAPKs (Figures 6.1 and 6.2) is apparent, suggesting that the UPR may activate them via different mechanisms or that other regulatory proteins account for the different kinetics. However, different phosphorylation kinetics between JNK and p38 may also be an artefact of N1E-115 cells and not a general signalling event. Overall the AP-1 inflammatory signalling pathway, which is regulated by JNK and p38, is activated during ER stress.

There are two known mechanisms of ER stress-dependent NF-κB activation: PERK-mediated inhibition of translation leads to the depletion of the NF-κB regulatory protein IκBα which has a shorter half-life, and IRE1α-TRAF2 interaction activates IKK which subsequently phosphorylates IκBα and targets it for degradation. It is therefore not surprising that reduced IκBα levels during ER stress in neuronal cells is reported. The different roles of these signalling pathways in mediating inflammation during ER stress is currently not known. The next logical step would be to manipulate these pathways individually during ER stress with inhibitors and knock-down where appropriate. Knock-

down of JNK may prove difficult as it would require at least two siRNAs or shRNAs and this extra stress may complicate interpretation of results. Inhibitors have been widely used for these signalling pathways but caution should be taken as they are not necessarily specific.

7.3.2 ER stress-mediated inflammatory signalling: implications for exogenous inflammation

In chapter 6 data suggest that ER stress upregulates the expression of several pro-inflammatory cytokine genes. However, an ELISA assay was able to detect the release of IL-6 only. These results suggest that only one cytokine- IL-6- is released into the medium at a high level. Indeed, IL-6 release does increase during ER stress demonstrating that ER stress does have the potential to induce exogenous pro-inflammatory signalling in CAD cells. Interestingly, IL-6 was the only cytokine detected by the ELISA in untreated samples. Therefore it could be that cytokine levels were too low for detection by ELISA and that it is still possible that ER stress induces secretion of other cytokines. Cytokine levels being below the detection limit of the ELISA is plausible given that the expression levels of *TNFα* and *IL-1β* at the mRNA level were increased with ER stress. However, as demonstrated by the insulin receptor in Chapter 5, the occurrence of transcription and translation does not necessarily mean a protein trafficking through the secretory pathway reaches its intended destination.

The transport of proteins through the secretory pathway is a potentially complex situation in that ER stress may function to promote inflammation through increased expression of pro-inflammatory cytokines, yet secretion of cytokines may be blocked by the very same ER stress. However, it is known that cytokines may be stored in secretory vesicles or granules (Moqbel and Coughlin, 2006). Build-up and storage of cytokines prior to and during acute ER stress and then there release during chronic ER stress may be a mechanism to overcome ER-stress mediated inhibition of ER to Golgi transport. IL-6 is reported to accumulate in the Golgi complex before release (Manderson et al., 2007) and may be one explanation as to why only IL-6 is released at levels detected by the ELISA assay. Another possible mechanism of cytokines avoiding ER stress-mediated inhibition of ER-Golgi transport is that, although most cytokines are released through classical secretion, there are several cytokines which are released through non-classical secretion which avoids the ER and Golgi. One such cytokine is IL-1β which lacks the conventional hydrophobic signal sequence required for targeting it to the ER (Rubartelli et al., 1990).

Thus, cytokines which are released through non-classical secretion may not be affected by blocking ER-Golgi transport. Unfortunately, this is further complicated by the possibility that proteins involved in the release of non-classically secreted cytokines such as plasma membrane bound transporters, which do traffic through the ER, may be depleted by ER stress-dependent inhibition of ER-Golgi transport.

Although IL-6 only was detected in the supernatant of ER stressed neurons, this supernatant was sufficient to activate microglia. Microglial activation by ER stress-condition medium provides evidence that ER stress induces the release of pro-inflammatory mediators (Figure 6.21). Unfortunately, due to a lack of time, the mediator or mediators of inflammation were not identified. Profiling, via techniques such as mass spectrometry, of proteins and other compounds in media conditioned by non-stressed versus ER-stressed neuronal cultures may provide potential targets for investigation. Once identified these mediators could be depleted from the supernatant to see if microglial activation still occurred. At the same time they could be added to medium conditioned by non-stressed neurons to establish if they are sufficient to activate microglia.

It is also worth noting that most of the understanding of cytokine regulation and release comes from studies of innate immune cells whereas the mechanisms of trafficking of cytokines from other cell types are not yet understood. This may be due to limitation of assays to detect the smaller quantities of cytokines produced by non-immune cells compared to cell of the immune system.

7.3.3 Evolution

As mentioned in the introduction a naturally occurring example of ER stress takes place during viral (Zhang and Wang, 2012) and bacterial infection (Cho et al., 2013). Thus the inflammatory signalling branches of the UPR may have evolved as an early mechanism which contributes to the innate immune response to infection. Wound healing, which also induces ER stress (Wang et al., 2010), would also benefit from innate immune response and low level inflammation. It could be possible that this conditioning of the ER to induce inflammatory signalling upon ER stress induced by infection has an evolutionary advantage which outweighs the negative effects of detrimental inflammation observed in the age related diseases T2D and PD. If the negative effects of ER-stress induced inflammation are mostly manifested in aged humans then they will not be selected against through evolutionary pressures.

7.4 Does ER stress link T2D and PD?

A recent review has provided evidence that inflammation and insulin resistance may link PD and T2D (Spielman et al., 2014). This thesis provides evidence that prolonged ER stress can cause insulin resistance through the blockage of transport of newly synthesised insulin receptors through the secretory pathway. Furthermore this mechanism of insulin resistance induced by ER stress is not specific to just one cell type and occurs in adipocytes, hepatic cells and neuronal cells.

The development of insulin resistance in PD may arise from decreased expression of the insulin receptor at the plasma membrane. Indeed, insulin receptor immunoreactivity is lost from neurons of the SNpc in PD (Moroo et al., 1994). Interestingly, some drugs which have been used to treat diabetes are being trialled for the treatment of PD. The following drugs being used or tested to treat both PD and diabetes also have been shown to reduce ER stress: Exendin (Tsunekawa et al., 2007, Kwon et al., 2009), ergot-derived dopamine D2 receptor agonists (Kim et al., 2012), pioglitazone (Yoshiuchi et al., 2009), and rosiglitazone (Kim et al., 2009). Thus, the effectiveness of these drugs to treat both PD and diabetes may be through alleviating ER stress which in turn prevents progression of these diseases through various ER-related mechanisms discussed.

The effect of ER stress on insulin signalling may be applicable to neurodegenerative diseases as a whole and more specifically AD. Using a mouse model of AD it was observed that insulin receptor levels decreased but that there was an increase in more internal and nuclear localisation of the insulin receptor in neuronal cells suggesting that the insulin receptor may be accumulating in a compartment such as the ER (Moloney et al., 2010). Insulin receptor mRNA levels have also been reported to be reduced in Parkinson's brain tissues (Takahashi et al., 1996, Tong et al., 2009). It is therefore possible that ER stress is just one mechanism through which insulin resistance occurs in neurodegeneration.

Age is a common factor which increases the risk of both T2D and PD. Interestingly the expression of the insulin receptor has consistently been reported to be decreased with age in: gerbils (Park et al., 2009), adipose tissue of humans (Bolinder et al., 1983), and in obese Zucker rats (Amessou et al., 2010). However, the latter study also found that the insulin receptor expression also decreased at the mRNA level. The study also identified that increased endocytosis and degradation of the insulin receptor occurred with time. A decrease in insulin receptors in the SN specifically has also been observed with age (Frolich et al., 1998). Interestingly, the Frolich *et al*. study also demonstrated that insulin

receptors were reduced in the SN of AD patients compared to healthy age-matched controls. Consequently, age may lower the threshold required to inhibit insulin signalling through further reduction of the insulin receptor via ER stress. A further contributing factor is that ER chaperone levels are reduced with ageing (Nuss et al., 2008). Thus the threshold for the development of ER stress is also lowered during ageing. Overall, age being an important risk factor for developing T2D as well as PD may be a product of lower insulin receptor levels and a decreased capacity to maintain trafficking of proteins through the secretory pathway which may further reduce insulin receptor levels.

As covered in the review by Spielman *et al*. (Spielman et al., 2014) and this thesis inflammation is an important manifestation of PD and T2D. In addition to insulin resistance, inflammation can also be induced through ER stress. Thus, ER stress may also be the linking stress which is inducing inflammation in these two diseases. It is therefore imaginable that ER stress can cause or at least contribute to both inflammation and insulin resistance in PD and T2D and may therefore provide the hidden link between these two diseases. Further research is required to fully understand the role of ER stress in both these diseases.

Overall insulin resistance in the SNpc may play a crucial role in the development of PD. The fact that: 1) insulin receptors are depleted in PD. 2) Age, the biggest risk factor for PD, also causes a reduction in insulin receptor number. 3) Insulin signalling is important for a normal healthy neuronal environment all adds evidence to this hypothesis. Defective insulin signalling has recently been strongly linked between PD and T2D alongside inflammation (Spielman et al., 2014). What has not been considered is that ER stress has also been linked between these two diseases. Data support the conclusions that ER stress can cause both insulin resistance, through depletion of insulin receptors, and inflammatory signalling, including activation of microglia, through an unknown mechanism. ER stress may therefore be the linking pathway between these two phenotypes (insulin resistance and inflammation) and thus ER stress may also link these two diseases (T2D and PD). Further research is required to fully establish: 1) if ER stress is responsible for, or at least can contribute to, inflammation in both PD and T2D. 2) If long-lasting physiologically relevant ER stress is sufficient to inhibit transport of newly synthesised insulin receptors.

7.5 Conclusion

In conclusion strong evidence is provided for a role of ER stress in the development of two different diseases: T2D and PD. How ER stress contributes to the progression of these two

diseases may be similar. For example ER stress blocking trafficking of newly synthesised insulin receptors may be a common feature between both diseases. Indeed a reduction in insulin receptors levels has been reported in patients with diabetes and with patients with PD. Age is also reported to reduce insulin receptor levels and may therefore contribute to, over time, reducing the threshold necessary for the manifestation of these two age-related diseases. The ability of UPR to stimulate inflammatory signalling and inflammation may also contribute to cycles of detrimental inflammation in tissues which are specifically affected in these two diseases, SNPC in PD and liver in T2D. Thus, further research into ER stress in the context of both PD and T2D is warranted. Further to this, data support the conclusion that IRE1α- and TRAF2-dependent activation of JNK during acute ER stress is prosurvival; involving upregulation of several antiapoptotic genes. These data add to evidence that the UPR can contribute to cell fate decision making. This research further highlights the complexity of ER stress-mediated cellular changes whilst emphasising the importance of characterising ER stress signalling pathways.

8 BIBLIOGRAPHY

Bibliography

ABEGUNDE, D. O., MATHERS, C. D., ADAM, T., ORTEGON, M. & STRONG, K. 2007. The burden and costs of chronic diseases in low-income and middle-income countries. *Lancet,* 370**,** 1929-38.

ACHARD, C. S. & LAYBUTT, D. R. 2012. Lipid-induced endoplasmic reticulum stress in liver cells results in two distinct outcomes: adaptation with enhanced insulin signaling or insulin resistance. *Endocrinology,* 153**,** 2164-77.

AEBI, M. 2013. N-linked protein glycosylation in the ER. *Biochim Biophys Acta,* 1833**,** 2430-7.

AGUIRRE, V., UCHIDA, T., YENUSH, L., DAVIS, R. & WHITE, M. F. 2000. The c-Jun NH(2)-terminal kinase promotes insulin resistance during association with insulin receptor substrate-1 and phosphorylation of Ser(307). *J Biol Chem,* 275**,** 9047-54.

AGUIRRE, V., WERNER, E. D., GIRAUD, J., LEE, Y. H., SHOELSON, S. E. & WHITE, M. F. 2002. Phosphorylation of Ser307 in insulin receptor substrate-1 blocks interactions with the insulin receptor and inhibits insulin action. *J Biol Chem,* 277**,** 1531-7.

AHN, J. Y. 2014. Neuroprotection signaling of nuclear akt in neuronal cells. *Exp Neurobiol,* 23**,** 200-6.

AJAMI, B., BENNETT, J. L., KRIEGER, C., TETZLAFF, W. & ROSSI, F. M. 2007. Local self-renewal can sustain CNS microglia maintenance and function throughout adult life. *Nat Neurosci,* 10**,** 1538-43.

AKANEYA, Y., TAKAHASHI, M. & HATANAKA, H. 1995. Interleukin-1 beta enhances survival and interleukin-6 protects against MPP+ neurotoxicity in cultures of fetal rat dopaminergic neurons. *Exp Neurol,* 136**,** 44-52.

ALHUSAINI, S., MCGEE, K., SCHISANO, B., HARTE, A., MCTERNAN, P., KUMAR, S. & TRIPATHI, G. 2010. Lipopolysaccharide, high glucose and saturated fatty acids induce endoplasmic reticulum stress in cultured primary human adipocytes: Salicylate alleviates this stress. *Biochem Biophys Res Commun,* 397**,** 472-8.

ALTMANN, F., PASCHINGER, K., DALIK, T. & VORAUER, K. 1998. Characterisation of peptide-N4-(N-acetyl-beta-glucosaminyl)asparagine amidase A and its N-glycans. *Eur J Biochem,* 252**,** 118-23.

AMANO, T., RICHELSON, E. & NIRENBERG, M. 1972. Neurotransmitter synthesis by neuroblastoma clones (neuroblast differentiation-cell culture-choline acetyltransferase-acetylcholinesterase-tyrosine hydroxylase-axons-dendrites). *Proc Natl Acad Sci U S A,* 69**,** 258-63.

AMATO, P. A., UNANUE, E. R. & TAYLOR, D. L. 1983. Distribution of actin in spreading macrophages: a comparative study on living and fixed cells. *J Cell Biol,* 96**,** 750-61.

AMERICAN DIABETES, A. 2013. Economic costs of diabetes in the U.S. in 2012. *Diabetes Care,* 36**,** 1033-46.

AMESSOU, M., TAHIRI, K., CHAUVET, G. & DESBUQUOIS, B. 2010. Age-related changes in insulin receptor mRNA and protein expression in genetically obese Zucker rats. *Diabetes Metab,* 36**,** 120-8.

ANGEL, P., SZABOWSKI, A. & SCHORPP-KISTNER, M. 2001. Function and regulation of AP-1 subunits in skin physiology and pathology. *Oncogene,* 20**,** 2413-23.

ARAKAWA, R. & YOKOYAMA, S. 2002. Helical apolipoproteins stabilize ATP-binding cassette transporter A1 by protecting it from thiol protease-mediated degradation. *J Biol Chem,* 277**,** 22426-9.

ARDUINO, D. M., ESTEVES, A. R., CARDOSO, S. M. & OLIVEIRA, C. R. 2009. Endoplasmic reticulum and mitochondria interplay mediates apoptotic cell death: relevance to Parkinson's disease. *Neurochem Int,* 55**,** 341-8.

ARIGA, H., TAKAHASHI-NIKI, K., KATO, I., MAITA, H., NIKI, T. & IGUCHI-ARIGA, S. M. 2013. Neuroprotective function of DJ-1 in Parkinson's disease. *Oxid Med Cell Longev,* 2013**,** 683920.

ARSHAD, M., YE, Z., GU, X., WONG, C. K., LIU, Y., LI, D., ZHOU, L., ZHANG, Y., BAY, W. P., YU, V. C. & LI, P. 2013. RNF13, a RING finger protein, mediates endoplasmic reticulum stress-induced apoptosis through the inositol-requiring enzyme (IRE1alpha)/c-Jun NH2-terminal kinase pathway. *J Biol Chem,* 288**,** 8726-36.

AVERY, J., ETZION, S., DEBOSCH, B. J., JIN, X., LUPU, T. S., BEITINJANEH, B., GRAND, J., KOVACS, A., SAMBANDAM, N. & MUSLIN, A. J. 2010. TRB3 function in cardiac endoplasmic reticulum stress. *Circ Res,* 106**,** 1516-23.

AVILES-OLMOS, I., LIMOUSIN, P., LEES, A. & FOLTYNIE, T. 2013. Parkinson's disease, insulin resistance and novel agents of neuroprotection. *Brain,* 136**,** 374-84.

BACKER, J. M., MYERS, M. G., JR., SHOELSON, S. E., CHIN, D. J., SUN, X. J., MIRALPEIX, M., HU, P., MARGOLIS, B., SKOLNIK, E. Y., SCHLESSINGER, J. & ET AL. 1992. Phosphatidylinositol 3'-kinase is activated by association with IRS-1 during insulin stimulation. *EMBO J,* 11**,** 3469-79.

BAILLY-MAITRE, B., BELGARDT, B. F., JORDAN, S. D., COORNAERT, B., VON FREYEND, M. J., KLEINRIDDERS, A., MAUER, J., CUDDY, M., KRESS, C. L., WILLMES, D., ESSIG, M., HAMPEL, B., PROTZER, U., REED, J. C. & BRUNING, J. C. 2010. Hepatic Bax inhibitor-1 inhibits IRE1alpha and protects from obesity-associated insulin resistance and glucose intolerance. *J Biol Chem,* 285**,** 6198-207.

BAINS, W., PONTE, P., BLAU, H. & KEDES, L. 1984. Cardiac actin is the major actin gene product in skeletal muscle cell differentiation in vitro. *Mol Cell Biol,* 4**,** 1449-53.

BALDASSARE, J. J., BI, Y. & BELLONE, C. J. 1999. The role of p38 mitogen-activated protein kinase in IL-1 beta transcription. *J Immunol,* 162**,** 5367-73.

BANDYOPADHYAY, G. K., YU, J. G., OFRECIO, J. & OLEFSKY, J. M. 2005. Increased p85/55/50 expression and decreased phosphotidylinositol 3-kinase activity in insulin-resistant human skeletal muscle. *Diabetes,* 54**,** 2351-9.

BARBER, A. J., NAKAMURA, M., WOLPERT, E. B., REITER, C. E., SEIGEL, G. M., ANTONETTI, D. A. & GARDNER, T. W. 2001. Insulin rescues retinal neurons from apoptosis by a phosphatidylinositol 3-kinase/Akt-mediated mechanism that reduces the activation of caspase-3. *J Biol Chem,* 276**,** 32814-21.

BARCIA, C., SANCHEZ BAHILLO, A., FERNANDEZ-VILLALBA, E., BAUTISTA, V., POZA, Y. P. M., FERNANDEZ-BARREIRO, A., HIRSCH, E. C. & HERRERO, M. T. 2004. Evidence of active microglia in substantia nigra pars compacta of parkinsonian monkeys 1 year after MPTP exposure. *Glia,* 46**,** 402-9.

BARONE, F. C., ARVIN, B., WHITE, R. F., MILLER, A., WEBB, C. L., WILLETTE, R. N., LYSKO, P. G. & FEUERSTEIN, G. Z. 1997. Tumor necrosis factor-alpha. A mediator of focal ischemic brain injury. *Stroke,* 28**,** 1233-44.

BASTARD, J. P., MAACHI, M., LAGATHU, C., KIM, M. J., CARON, M., VIDAL, H., CAPEAU, J. & FEVE, B. 2006. Recent advances in the relationship between obesity, inflammation, and insulin resistance. *Eur Cytokine Netw,* 17**,** 4-12.

BELLUCCI, A., NAVARRIA, L., ZALTIERI, M., FALARTI, E., BODEI, S., SIGALA, S., BATTISTIN, L., SPILLANTINI, M., MISSALE, C. & SPANO, P. 2011. Induction of the unfolded protein response by alpha-synuclein in experimental models of Parkinson's disease. *J Neurochem,* 116**,** 588-605.

BENCE, N. F., SAMPAT, R. M. & KOPITO, R. R. 2001. Impairment of the ubiquitin-proteasome system by protein aggregation. *Science,* 292**,** 1552-5.

BENEDICT, C., HALLSCHMID, M., HATKE, A., SCHULTES, B., FEHM, H. L., BORN, J. & KERN, W. 2004. Intranasal insulin improves memory in humans. *Psychoneuroendocrinology,* 29**,** 1326-34.

BENNETT, B. L., SASAKI, D. T., MURRAY, B. W., O'LEARY, E. C., SAKATA, S. T., XU, W., LEISTEN, J. C., MOTIWALA, A., PIERCE, S., SATOH, Y., BHAGWAT, S. S., MANNING, A. M. & ANDERSON, D. W. 2001. SP600125, an anthrapyrazolone inhibitor of Jun N-terminal kinase. *Proc Natl Acad Sci U S A,* 98**,** 13681-6.

BENNETT, M. C., BISHOP, J. F., LENG, Y., CHOCK, P. B., CHASE, T. N. & MOURADIAN, M. M. 1999. Degradation of alpha-synuclein by proteasome. *J Biol Chem,* 274**,** 33855-8.

BENSON, S., OLSNES, S., PIHL, A., SKORVE, J. & ABRAHAM, A. K. 1975. On the mechanism of protein-synthesis inhibition by abrin and ricin. Inhibition of the GTP-hydrolysis site on the 60-S ribosomal subunit. *Eur J Biochem,* 59**,** 573-80.

BERTOLOTTI, A., ZHANG, Y., HENDERSHOT, L. M., HARDING, H. P. & RON, D. 2000. Dynamic interaction of BiP and ER stress transducers in the unfolded-protein response. *Nat Cell Biol,* 2**,** 326-32.

BETARBET, R., SHERER, T. B., MACKENZIE, G., GARCIA-OSUNA, M., PANOV, A. V. & GREENAMYRE, J. T. 2000. Chronic systemic pesticide exposure reproduces features of Parkinson's disease. *Nat Neurosci,* 3**,** 1301-6.

BIRKENFELD, A. L., LEE, H. Y., MAJUMDAR, S., JURCZAK, M. J., CAMPOREZ, J. P., JORNAYVAZ, F. R., FREDERICK, D. W., GUIGNI, B., KAHN, M., ZHANG, D., WEISMANN, D., ARAFAT, A. M., PFEIFFER, A. F., LIESKE, S., OYADOMARI, S., RON, D., SAMUEL, V. T. & SHULMAN, G. I. 2011. Influence of the hepatic eukaryotic initiation factor 2alpha (eIF2alpha) endoplasmic reticulum (ER) stress response pathway on insulin-mediated ER stress and hepatic and peripheral glucose metabolism. *J Biol Chem,* 286**,** 36163-70.

BIRNBOIM, H. C. & DOLY, J. 1979. A rapid alkaline extraction procedure for screening recombinant plasmid DNA. *Nucleic Acids Res,* 7**,** 1513-23.

BLAU, H. M., PAVLATH, G. K., HARDEMAN, E. C., CHIU, C. P., SILBERSTEIN, L., WEBSTER, S. G., MILLER, S. C. & WEBSTER, C. 1985. Plasticity of the differentiated state. *Science,* 230**,** 758-66.

BLUM, D., TORCH, S., LAMBENG, N., NISSOU, M., BENABID, A. L., SADOUL, R. & VERNA, J. M. 2001. Molecular pathways involved in the neurotoxicity of 6-OHDA, dopamine and MPTP: contribution to the apoptotic theory in Parkinson's disease. *Prog Neurobiol,* 65**,** 135-72.

BODEN, G., DUAN, X., HOMKO, C., MOLINA, E. J., SONG, W., PEREZ, O., CHEUNG, P. & MERALI, S. 2008. Increase in endoplasmic reticulum stress-related proteins and genes in adipose tissue of obese, insulin-resistant individuals. *Diabetes,* 57**,** 2438-44.

BODHINI, D., SANDHIYA, M., GHOSH, S., MAJUMDER, P. P., RAO, M. R., MOHAN, V. & RADHA, V. 2012. Association of His1085His INSR gene

polymorphism with type 2 diabetes in South Indians. *Diabetes Technol Ther,* 14**,** 696-700.

BOKA, G., ANGLADE, P., WALLACH, D., JAVOY-AGID, F., AGID, Y. & HIRSCH, E. C. 1994. Immunocytochemical analysis of tumor necrosis factor and its receptors in Parkinson's disease. *Neurosci Lett,* 172**,** 151-4.

BOLIN, L. M., STRYCHARSKA-ORCZYK, I., MURRAY, R., LANGSTON, J. W. & DI MONTE, D. 2002. Increased vulnerability of dopaminergic neurons in MPTP-lesioned interleukin-6 deficient mice. *J Neurochem,* 83**,** 167-75.

BOLINDER, J., OSTMAN, J. & ARNER, P. 1983. Influence of aging on insulin receptor binding and metabolic effects of insulin on human adipose tissue. *Diabetes,* 32**,** 959-64.

BOUMAN, L., SCHLIERF, A., LUTZ, A. K., SHAN, J., DEINLEIN, A., KAST, J., GALEHDAR, Z., PALMISANO, V., PATENGE, N., BERG, D., GASSER, T., AUGUSTIN, R., TRUMBACH, D., IRRCHER, I., PARK, D. S., WURST, W., KILBERG, M. S., TATZELT, J. & WINKLHOFER, K. F. 2011. Parkin is transcriptionally regulated by ATF4: evidence for an interconnection between mitochondrial stress and ER stress. *Cell Death Differ,* 18**,** 769-82.

BOURBON, N. A., SANDIRASEGARANE, L. & KESTER, M. 2002. Ceramide-induced inhibition of Akt is mediated through protein kinase Czeta: implications for growth arrest. *J Biol Chem,* 277**,** 3286-92.

BOUTZIOS, G., LIVADAS, S., MARINAKIS, E., OPIE, N., ECONOMOU, F. & DIAMANTI-KANDARAKIS, E. 2011. Endocrine and metabolic aspects of the Wolfram syndrome. *Endocrine,* 40**,** 10-3.

BOWEN, B. C., BLOCK, R. E., SANCHEZ-RAMOS, J., PATTANY, P. M., LAMPMAN, D. A., MURDOCH, J. B. & QUENCER, R. M. 1995. Proton MR spectroscopy of the brain in 14 patients with Parkinson disease. *AJNR Am J Neuroradiol,* 16**,** 61-8.

BOYD, A. E., 3RD, LEBOVITZ, H. E. & FELDMAN, J. M. 1971. Endocrine function and glucose metabolism in patients with Parkinson's disease and their alternation by L-Dopa. *J Clin Endocrinol Metab,* 33**,** 829-37.

BOYD, J. D., JANG, H., SHEPHERD, K. R., FAHERTY, C., SLACK, S., JIAO, Y. & SMEYNE, R. J. 2007. Response to 1-methyl-4-phenyl-1,2,3,6-tetrahydropyridine (MPTP) differs in mouse strains and reveals a divergence in JNK signaling and COX-2 induction prior to loss of neurons in the substantia nigra pars compacta. *Brain Res,* 1175**,** 107-16.

BRAAKMAN, I. & HEBERT, D. N. 2013. Protein folding in the endoplasmic reticulum. *Cold Spring Harb Perspect Biol,* 5**,** a013201.

BRAVO, D. A., GLEASON, J. B., SANCHEZ, R. I., ROTH, R. A. & FULLER, R. S. 1994. Accurate and efficient cleavage of the human insulin proreceptor by the human proprotein-processing protease furin. Characterization and kinetic parameters using the purified, secreted soluble protease expressed by a recombinant baculovirus. *J Biol Chem,* 269**,** 25830-7.

CAI, B., CHANG, S. H., BECKER, E. B., BONNI, A. & XIA, Z. 2006. p38 MAP kinase mediates apoptosis through phosphorylation of BimEL at Ser-65. *J Biol Chem,* 281**,** 25215-22.

CANCELLO, R., HENEGAR, C., VIGUERIE, N., TALEB, S., POITOU, C., ROUAULT, C., COUPAYE, M., PELLOUX, V., HUGOL, D., BOUILLOT, J. L., BOULOUMIE, A., BARBATELLI, G., CINTI, S., SVENSSON, P. A., BARSH, G. S., ZUCKER, J. D., BASDEVANT, A., LANGIN, D. & CLEMENT, K. 2005. Reduction of macrophage infiltration and chemoattractant gene expression changes in white adipose tissue of morbidly obese subjects after surgery-induced weight loss. *Diabetes,* 54**,** 2277-86.

CAPEAU, J., LASCOLS, O., FLAIG-STAEDEL, C., BLIVET, M. J., BECK, J. P. & PICARD, J. 1985. Degradation of insulin receptors by hepatoma cells: insulin-induced down-regulation results from an increase in the rate of basal receptor degradation. *Biochimie,* 67**,** 1133-41.

CARRARA, M., PRISCHI, F., NOWAK, P. R. & ALI, M. M. 2015. Crystal structures reveal transient PERK luminal domain tetramerization in endoplasmic reticulum stress signaling. *EMBO J,* 34**,** 1589-600.

CARRASCO, L. & VAZQUEZ, D. 1984. Molecular bases for the action and selectivity of nucleoside antibiotics. *Med Res Rev,* 4**,** 471-512.

CAZANAVE, S. C., ELMI, N. A., AKAZAWA, Y., BRONK, S. F., MOTT, J. L. & GORES, G. J. 2010. CHOP and AP-1 cooperatively mediate PUMA expression during lipoapoptosis. *Am J Physiol Gastrointest Liver Physiol,* 299**,** G236-43.

CELLI, J. & TSOLIS, R. M. 2015. Bacteria, the endoplasmic reticulum and the unfolded protein response: friends or foes? *Nat Rev Microbiol,* 13**,** 71-82.

CHALMANOV, V. & VURBANOVA, M. 1987. [Diabetes mellitus in parkinsonism patients]. *Vutr Boles,* 26**,** 68-73.

CHAN, S. M., SUN, R. Q., ZENG, X. Y., CHOONG, Z. H., WANG, H., WATT, M. J. & YE, J. M. 2013. Activation of PPARalpha ameliorates hepatic insulin resistance and steatosis in high fructose-fed mice despite increased endoplasmic reticulum stress. *Diabetes,* 62**,** 2095-105.

CHEATHAM, B. & KAHN, C. R. 1995. Insulin action and the insulin signaling network. *Endocr Rev,* 16**,** 117-42.

CHEN, C. L., LIN, C. F., CHANG, W. T., HUANG, W. C., TENG, C. F. & LIN, Y. S. 2008. Ceramide induces p38 MAPK and JNK activation through a mechanism involving a thioredoxin-interacting protein-mediated pathway. *Blood,* 111**,** 4365-74.

CHEN, H., JACOBS, E., SCHWARZSCHILD, M. A., MCCULLOUGH, M. L., CALLE, E. E., THUN, M. J. & ASCHERIO, A. 2005. Nonsteroidal antiinflammatory drug use and the risk for Parkinson's disease. *Ann Neurol,* 58**,** 963-7.

CHEN, H., ZHANG, S. M., HERNAN, M. A., SCHWARZSCHILD, M. A., WILLETT, W. C., COLDITZ, G. A., SPEIZER, F. E. & ASCHERIO, A. 2003. Nonsteroidal anti-inflammatory drugs and the risk of Parkinson disease. *Arch Neurol,* 60**,** 1059-64.

CHEN, Y. R., MEYER, C. F. & TAN, T. H. 1996. Persistent activation of c-Jun N-terminal kinase 1 (JNK1) in gamma radiation-induced apoptosis. *J Biol Chem,* 271**,** 631-4.

CHEUNG, Y. T., LAU, W. K., YU, M. S., LAI, C. S., YEUNG, S. C., SO, K. F. & CHANG, R. C. 2009. Effects of all-trans-retinoic acid on human SH-SY5Y neuroblastoma as in vitro model in neurotoxicity research. *Neurotoxicology,* 30**,** 127-35.

CHIGURUPATI, S., WEI, Z., BELAL, C., VANDERMEY, M., KYRIAZIS, G. A., ARUMUGAM, T. V. & CHAN, S. L. 2009. The homocysteine-inducible endoplasmic reticulum stress protein counteracts calcium store depletion and induction of CCAAT enhancer-binding protein homologous protein in a neurotoxin model of Parkinson disease. *J Biol Chem,* 284**,** 18323-33.

CHINTA, S. J., RANE, A., POKSAY, K. S., BREDESEN, D. E., ANDERSEN, J. K. & RAO, R. V. 2008. Coupling endoplasmic reticulum stress to the cell death program in dopaminergic cells: effect of paraquat. *Neuromolecular Med,* 10**,** 333-42.

CHO, J. A., LEE, A. H., PLATZER, B., CROSS, B. C., GARDNER, B. M., DE LUCA, H., LUONG, P., HARDING, H. P., GLIMCHER, L. H., WALTER, P., FIEBIGER, E., RON, D., KAGAN, J. C. & LENCER, W. I. 2013. The unfolded protein

response element IRE1alpha senses bacterial proteins invading the ER to activate RIG-I and innate immune signaling. *Cell Host Microbe,* 13**,** 558-69.

CHUNG, C. T. & MILLER, R. H. 1988. A rapid and convenient method for the preparation and storage of competent bacterial cells. *Nucleic Acids Res,* 16**,** 3580.

CHUNG, C. T., NIEMELA, S. L. & MILLER, R. H. 1989. One-step preparation of competent Escherichia coli: transformation and storage of bacterial cells in the same solution. *Proc Natl Acad Sci U S A,* 86**,** 2172-5.

CINTI, S., MITCHELL, G., BARBATELLI, G., MURANO, I., CERESI, E., FALOIA, E., WANG, S., FORTIER, M., GREENBERG, A. S. & OBIN, M. S. 2005. Adipocyte death defines macrophage localization and function in adipose tissue of obese mice and humans. *J Lipid Res,* 46**,** 2347-55.

CLACKSON, T., YANG, W., ROZAMUS, L. W., HATADA, M., AMARA, J. F., ROLLINS, C. T., STEVENSON, L. F., MAGARI, S. R., WOOD, S. A., COURAGE, N. L., LU, X., CERASOLI, F., JR., GILMAN, M. & HOLT, D. A. 1998. Redesigning an FKBP-ligand interface to generate chemical dimerizers with novel specificity. *Proc Natl Acad Sci U S A,* 95**,** 10437-42.

CLAGETT-DAME, M., MCNEILL, E. M. & MULEY, P. D. 2006. Role of all-trans retinoic acid in neurite outgrowth and axonal elongation. *J Neurobiol,* 66**,** 739-56.

COFFEY, E. T. 2014. Nuclear and cytosolic JNK signalling in neurons. *Nat Rev Neurosci,* 15**,** 285-99.

COHEN, G. & HEIKKILA, R. E. 1974. The generation of hydrogen peroxide, superoxide radical, and hydroxyl radical by 6-hydroxydopamine, dialuric acid, and related cytotoxic agents. *J Biol Chem,* 249**,** 2447-52.

COLLA, E., COUNE, P., LIU, Y., PLETNIKOVA, O., TRONCOSO, J. C., IWATSUBO, T., SCHNEIDER, B. L. & LEE, M. K. 2012a. Endoplasmic reticulum stress is important for the manifestations of alpha-synucleinopathy in vivo. *J Neurosci,* 32**,** 3306-20.

COLLA, E., JENSEN, P. H., PLETNIKOVA, O., TRONCOSO, J. C., GLABE, C. & LEE, M. K. 2012b. Accumulation of toxic alpha-synuclein oligomer within endoplasmic reticulum occurs in alpha-synucleinopathy in vivo. *J Neurosci,* 32**,** 3301-5.

COLLINS, T. J. 2007. ImageJ for microscopy. *Biotechniques,* 43**,** 25-30.

CONEJO, R. & LORENZO, M. 2001. Insulin signaling leading to proliferation, survival, and membrane ruffling in C2C12 myoblasts. *J Cell Physiol,* 187**,** 96-108.

COOPER, A. A., GITLER, A. D., CASHIKAR, A., HAYNES, C. M., HILL, K. J., BHULLAR, B., LIU, K., XU, K., STRATHEARN, K. E., LIU, F., CAO, S., CALDWELL, K. A., CALDWELL, G. A., MARSISCHKY, G., KOLODNER, R. D., LABAER, J., ROCHET, J. C., BONINI, N. M. & LINDQUIST, S. 2006. Alpha-synuclein blocks ER-Golgi traffic and Rab1 rescues neuron loss in Parkinson's models. *Science,* 313**,** 324-8.

COPPS, K. D., HANCER, N. J., OPARE-ADO, L., QIU, W., WALSH, C. & WHITE, M. F. 2010. Irs1 serine 307 promotes insulin sensitivity in mice. *Cell Metab,* 11**,** 84-92.

COSTES, S. V., DAELEMANS, D., CHO, E. H., DOBBIN, Z., PAVLAKIS, G. & LOCKETT, S. 2004. Automatic and quantitative measurement of protein-protein colocalization in live cells. *Biophys J,* 86**,** 3993-4003.

COX, D. J., STRUDWICK, N., ALI, A. A., PATON, A. W., PATON, J. C. & SCHRODER, M. 2011. Measuring signaling by the unfolded protein response. *Methods Enzymol,* 491**,** 261-92.

CRAFT, S., CHOLERTON, B. & BAKER, L. D. 2013. Insulin and Alzheimer's disease: untangling the web. *J Alzheimers Dis,* 33 Suppl 1**,** S263-75.

CULLINAN, S. B. & DIEHL, J. A. 2006. Coordination of ER and oxidative stress signaling: the PERK/Nrf2 signaling pathway. *Int J Biochem Cell Biol,* 38**,** 317-32.

DANDONA, P., ALJADA, A. & BANDYOPADHYAY, A. 2004. Inflammation: the link between insulin resistance, obesity and diabetes. *Trends Immunol,* 25**,** 4-7.

DARLING, N. J. & COOK, S. J. 2014. The role of MAPK signalling pathways in the response to endoplasmic reticulum stress. *Biochim Biophys Acta,* 1843**,** 2150-63.

DATTA, R., YOSHINAGA, K., KANEKI, M., PANDEY, P. & KUFE, D. 2000. Phorbol ester-induced generation of reactive oxygen species is protein kinase cbeta - dependent and required for SAPK activation. *J Biol Chem,* 275**,** 41000-3.

DAUER, W. & PRZEDBORSKI, S. 2003. Parkinson's disease: mechanisms and models. *Neuron,* 39**,** 889-909.

DAVIS, R. J. 2000. Signal transduction by the JNK group of MAP kinases. *Cell,* 103**,** 239-52.

DAWSON, T. M. & DAWSON, V. L. 2003. Molecular pathways of neurodegeneration in Parkinson's disease. *Science,* 302**,** 819-22.

DE FEA, K. & ROTH, R. A. 1997. Modulation of insulin receptor substrate-1 tyrosine phosphorylation and function by mitogen-activated protein kinase. *J Biol Chem,* 272**,** 31400-6.

DEB, T. B., COTICCHIA, C. M. & DICKSON, R. B. 2004. Calmodulin-mediated activation of Akt regulates survival of c-Myc-overexpressing mouse mammary carcinoma cells. *J Biol Chem,* 279**,** 38903-11.

DENG, J., LU, P. D., ZHANG, Y., SCHEUNER, D., KAUFMAN, R. J., SONENBERG, N., HARDING, H. P. & RON, D. 2004. Translational repression mediates activation of nuclear factor kappa B by phosphorylated translation initiation factor 2. *Mol Cell Biol,* 24**,** 10161-8.

DERIJARD, B., HIBI, M., WU, I. H., BARRETT, T., SU, B., DENG, T., KARIN, M. & DAVIS, R. J. 1994. JNK1: a protein kinase stimulated by UV light and Ha-Ras that binds and phosphorylates the c-Jun activation domain. *Cell,* 76**,** 1025-37.

DERIJARD, B., RAINGEAUD, J., BARRETT, T., WU, I. H., HAN, J., ULEVITCH, R. J. & DAVIS, R. J. 1995. Independent human MAP-kinase signal transduction pathways defined by MEK and MKK isoforms. *Science,* 267**,** 682-5.

DESCHATRETTE, J. & WEISS, M. C. 1974. Characterization of differentiated and dedifferentiated clones from a rat hepatoma. *Biochimie,* 56**,** 1603-11.

DEVIN, A., COOK, A., LIN, Y., RODRIGUEZ, Y., KELLIHER, M. & LIU, Z. 2000. The distinct roles of TRAF2 and RIP in IKK activation by TNF-R1: TRAF2 recruits IKK to TNF-R1 while RIP mediates IKK activation. *Immunity,* 12**,** 419-29.

DI GREGORIO, G. B., YAO-BORENGASSER, A., RASOULI, N., VARMA, V., LU, T., MILES, L. M., RANGANATHAN, G., PETERSON, C. A., MCGEHEE, R. E. & KERN, P. A. 2005. Expression of CD68 and macrophage chemoattractant protein-1 genes in human adipose and muscle tissues: association with cytokine expression, insulin resistance, and reduction by pioglitazone. *Diabetes,* 54**,** 2305-13.

DIDONATO, J., MERCURIO, F., ROSETTE, C., WU-LI, J., SUYANG, H., GHOSH, S. & KARIN, M. 1996. Mapping of the inducible IkappaB phosphorylation sites that signal its ubiquitination and degradation. *Mol Cell Biol,* 16**,** 1295-304.

DU, K., HERZIG, S., KULKARNI, R. N. & MONTMINY, M. 2003. TRB3: a tribbles homolog that inhibits Akt/PKB activation by insulin in liver. *Science,* 300**,** 1574-7.

DUARTE, A. I., MOREIRA, P. I. & OLIVEIRA, C. R. 2012. Insulin in central nervous system: more than just a peripheral hormone. *J Aging Res,* 2012**,** 384017.

DUARTE, A. I., SANTOS, P., OLIVEIRA, C. R., SANTOS, M. S. & REGO, A. C. 2008. Insulin neuroprotection against oxidative stress is mediated by Akt and GSK-3beta signaling pathways and changes in protein expression. *Biochim Biophys Acta,* 1783**,** 994-1002.

DUDEK, H., DATTA, S. R., FRANKE, T. F., BIRNBAUM, M. J., YAO, R., COOPER, G. M., SEGAL, R. A., KAPLAN, D. R. & GREENBERG, M. E. 1997. Regulation

of neuronal survival by the serine-threonine protein kinase Akt. *Science,* 275**,** 661-5.

DUGUAY, S. J., MILEWSKI, W. M., YOUNG, B. D., NAKAYAMA, K. & STEINER, D. F. 1997. Processing of wild-type and mutant proinsulin-like growth factor-IA by subtilisin-related proprotein convertases. *J Biol Chem,* 272**,** 6663-70.

DUPLAN, E., GIAIME, E., VIOTTI, J., SEVALLE, J., CORTI, O., BRICE, A., ARIGA, H., QI, L., CHECLER, F. & ALVES DA COSTA, C. 2013. ER-stress-associated functional link between Parkin and DJ-1 via a transcriptional cascade involving the tumor suppressor p53 and the spliced X-box binding protein XBP-1. *J Cell Sci,* 126**,** 2124-33.

DYKXHOORN, D. M., NOVINA, C. D. & SHARP, P. A. 2003. Killing the messenger: short RNAs that silence gene expression. *Nat Rev Mol Cell Biol,* 4**,** 457-67.

EDDLESTON, M. & MUCKE, L. 1993. Molecular profile of reactive astrocytes--implications for their role in neurologic disease. *Neuroscience,* 54**,** 15-36.

ELDAR-FINKELMAN, H. & KREBS, E. G. 1997. Phosphorylation of insulin receptor substrate 1 by glycogen synthase kinase 3 impairs insulin action. *Proc Natl Acad Sci U S A,* 94**,** 9660-4.

ELLGAARD, L. 2004. Catalysis of disulphide bond formation in the endoplasmic reticulum. *Biochem Soc Trans,* 32**,** 663-7.

ELLGAARD, L. & HELENIUS, A. 2003. Quality control in the endoplasmic reticulum. *Nat Rev Mol Cell Biol,* 4**,** 181-91.

ENCINAS, M., IGLESIAS, M., LIU, Y., WANG, H., MUHAISEN, A., CENA, V., GALLEGO, C. & COMELLA, J. X. 2000. Sequential treatment of SH-SY5Y cells with retinoic acid and brain-derived neurotrophic factor gives rise to fully differentiated, neurotrophic factor-dependent, human neuron-like cells. *J Neurochem,* 75**,** 991-1003.

ENGELMAN, J. A., BERG, A. H., LEWIS, R. Y., LISANTI, M. P. & SCHERER, P. E. 2000. Tumor necrosis factor alpha-mediated insulin resistance, but not dedifferentiation, is abrogated by MEK1/2 inhibitors in 3T3-L1 adipocytes. *Mol Endocrinol,* 14**,** 1557-69.

ERCOLANI, L., BROWN, T. J. & GINSBERG, B. H. 1984. Tunicamycin blocks the emergence and maintenance of insulin receptors on mitogen-activated human T lymphocytes. *Metabolism,* 33**,** 309-16.

ERTA, M., QUINTANA, A. & HIDALGO, J. 2012. Interleukin-6, a major cytokine in the central nervous system. *Int J Biol Sci,* 8**,** 1254-66.

FAGERSTROM, S., PAHLMAN, S., GESTBLOM, C. & NANBERG, E. 1996. Protein kinase C-epsilon is implicated in neurite outgrowth in differentiating human neuroblastoma cells. *Cell Growth Differ,* 7**,** 775-85.

FAHN, S. 2003. Description of Parkinson's disease as a clinical syndrome. *Ann N Y Acad Sci,* 991**,** 1-14.

FERNANDEZ-CHECA, J. C., KAPLOWITZ, N., GARCIA-RUIZ, C., COLELL, A., MIRANDA, M., MARI, M., ARDITE, E. & MORALES, A. 1997. GSH transport in mitochondria: defense against TNF-induced oxidative stress and alcohol-induced defect. *Am J Physiol,* 273**,** G7-17.

FORNO, L. S., LANGSTON, J. W., DELANNEY, L. E. & IRWIN, I. 1988. An electron microscopic study of MPTP-induced inclusion bodies in an old monkey. *Brain Res,* 448**,** 150-7.

FOTI, M., MOUKIL, M. A., DUDOGNON, P. & CARPENTIER, J. L. 2004. Insulin and IGF-1 receptor trafficking and signalling. *Novartis Found Symp,* 262**,** 125-41; discussion 141-7, 265-8.

FREEMAN, H. & COX, R. D. 2006. Type-2 diabetes: a cocktail of genetic discovery. *Hum Mol Genet,* 15 Spec No 2**,** R202-9.

FROLICH, L., BLUM-DEGEN, D., BERNSTEIN, H. G., ENGELSBERGER, S., HUMRICH, J., LAUFER, S., MUSCHNER, D., THALHEIMER, A., TURK, A., HOYER, S., ZOCHLING, R., BOISSL, K. W., JELLINGER, K. & RIEDERER, P. 1998. Brain insulin and insulin receptors in aging and sporadic Alzheimer's disease. *J Neural Transm,* 105**,** 423-38.

FUJISAWA, J., IWAKURA, Y. & KAWADE, Y. 1978. Nonglycosylated mouse L cell interferon produced by the action of tunicamycin. *J Biol Chem,* 253**,** 8677-9.

GADIENT, R. A. & OTTEN, U. 1994. Identification of interleukin-6 (IL-6)-expressing neurons in the cerebellum and hippocampus of normal adult rats. *Neurosci Lett,* 182**,** 243-6.

GAO, H. M., HONG, J. S., ZHANG, W. & LIU, B. 2002a. Distinct role for microglia in rotenone-induced degeneration of dopaminergic neurons. *J Neurosci,* 22**,** 782-90.

GAO, Z., HWANG, D., BATAILLE, F., LEFEVRE, M., YORK, D., QUON, M. J. & YE, J. 2002b. Serine phosphorylation of insulin receptor substrate 1 by inhibitor kappa B kinase complex. *J Biol Chem,* 277**,** 48115-21.

GAO, Z., ZHANG, X., ZUBERI, A., HWANG, D., QUON, M. J., LEFEVRE, M. & YE, J. 2004. Inhibition of insulin sensitivity by free fatty acids requires activation of multiple serine kinases in 3T3-L1 adipocytes. *Mol Endocrinol,* 18**,** 2024-34.

GARG, A. D., KACZMAREK, A., KRYSKO, O., VANDENABEELE, P., KRYSKO, D. V. & AGOSTINIS, P. 2012. ER stress-induced inflammation: does it aid or impede disease progression? *Trends Mol Med,* 18**,** 589-98.

GETHING, M. J. 1999. Role and regulation of the ER chaperone BiP. *Semin Cell Dev Biol,* 10**,** 465-72.

GHRIBI, O., HERMAN, M. M., PRAMOONJAGO, P. & SAVORY, J. 2003. MPP+ induces the endoplasmic reticulum stress response in rabbit brain involving activation of the ATF-6 and NF-kappaB signaling pathways. *J Neuropathol Exp Neurol,* 62**,** 1144-53.

GIASSON, B. I., DUDA, J. E., MURRAY, I. V., CHEN, Q., SOUZA, J. M., HURTIG, H. I., ISCHIROPOULOS, H., TROJANOWSKI, J. Q. & LEE, V. M. 2000. Oxidative damage linked to neurodegeneration by selective alpha-synuclein nitration in synucleinopathy lesions. *Science,* 290**,** 985-9.

GITLER, A. D., BEVIS, B. J., SHORTER, J., STRATHEARN, K. E., HAMAMICHI, S., SU, L. J., CALDWELL, K. A., CALDWELL, G. A., ROCHET, J. C., MCCAFFERY, J. M., BARLOWE, C. & LINDQUIST, S. 2008. The Parkinson's disease protein alpha-synuclein disrupts cellular Rab homeostasis. *Proc Natl Acad Sci U S A,* 105**,** 145-50.

GORBATYUK, M. S., SHABASHVILI, A., CHEN, W., MEYERS, C., SULLIVAN, L. F., SALGANIK, M., LIN, J. H., LEWIN, A. S., MUZYCZKA, N. & GORBATYUK, O. S. 2012. Glucose regulated protein 78 diminishes alpha-synuclein neurotoxicity in a rat model of Parkinson disease. *Mol Ther,* 20**,** 1327-37.

GORDON, S. & TAYLOR, P. R. 2005. Monocyte and macrophage heterogeneity. *Nat Rev Immunol,* 5**,** 953-64.

GOTOH, T., TERADA, K., OYADOMARI, S. & MORI, M. 2004. hsp70-DnaJ chaperone pair prevents nitric oxide- and CHOP-induced apoptosis by inhibiting translocation of Bax to mitochondria. *Cell Death Differ,* 11**,** 390-402.

GOTOH, Y. & COOPER, J. A. 1998. Reactive oxygen species- and dimerization-induced activation of apoptosis signal-regulating kinase 1 in tumor necrosis factor-alpha signal transduction. *J Biol Chem,* 273**,** 17477-82.

GRAHAM, F. L., SMILEY, J., RUSSELL, W. C. & NAIRN, R. 1977. Characteristics of a human cell line transformed by DNA from human adenovirus type 5. *J Gen Virol,* 36**,** 59-74.

GRAKO, K. A., OLEFSKY, J. M. & MCCLAIN, D. A. 1992. Tyrosine kinase-defective insulin receptors undergo decreased endocytosis but do not affect internalization of normal endogenous insulin receptors. *Endocrinology,* 130**,** 3441-52.

GRANATO, M., SANTARELLI, R., LOTTI, L. V., DI RENZO, L., GONNELLA, R., GARUFI, A., TRIVEDI, P., FRATI, L., D'ORAZI, G., FAGGIONI, A. & CIRONE, M. 2013. JNK and macroautophagy activation by bortezomib has a pro-survival effect in primary effusion lymphoma cells. *PLoS One,* 8**,** e75965.

GREEN, H. & KEHINDE, O. 1976. Spontaneous heritable changes leading to increased adipose conversion in 3T3 cells. *Cell,* 7**,** 105-13.

GREEN, L. C., WAGNER, D. A., GLOGOWSKI, J., SKIPPER, P. L., WISHNOK, J. S. & TANNENBAUM, S. R. 1982. Analysis of nitrate, nitrite, and [15N]nitrate in biological fluids. *Anal Biochem,* 126**,** 131-8.

GREENE, L. A. & TISCHLER, A. S. 1976. Establishment of a noradrenergic clonal line of rat adrenal pheochromocytoma cells which respond to nerve growth factor. *Proc Natl Acad Sci U S A,* 73**,** 2424-8.

GREGOR, M. F., YANG, L., FABBRINI, E., MOHAMMED, B. S., EAGON, J. C., HOTAMISLIGIL, G. S. & KLEIN, S. 2009. Endoplasmic reticulum stress is reduced in tissues of obese subjects after weight loss. *Diabetes,* 58**,** 693-700.

GROTE, C. W., GROOVER, A. L., RYALS, J. M., GEIGER, P. C., FELDMAN, E. L. & WRIGHT, D. E. 2013. Peripheral nervous system insulin resistance in ob/ob mice. *Acta Neuropathol Commun,* 1**,** 15.

GU, J. J., WANG, Z., REEVES, R. & MAGNUSON, N. S. 2009. PIM1 phosphorylates and negatively regulates ASK1-mediated apoptosis. *Oncogene,* 28**,** 4261-71.

GUO, Y., SRINIVASULA, S. M., DRUILHE, A., FERNANDES-ALNEMRI, T. & ALNEMRI, E. S. 2002. Caspase-2 induces apoptosis by releasing proapoptotic proteins from mitochondria. *J Biol Chem,* 277**,** 13430-7.

GUO, Y. L., BAYSAL, K., KANG, B., YANG, L. J. & WILLIAMSON, J. R. 1998. Correlation between sustained c-Jun N-terminal protein kinase activation and apoptosis induced by tumor necrosis factor-alpha in rat mesangial cells. *J Biol Chem,* 273**,** 4027-34.

HACKI, J., EGGER, L., MONNEY, L., CONUS, S., ROSSE, T., FELLAY, I. & BORNER, C. 2000. Apoptotic crosstalk between the endoplasmic reticulum and mitochondria controlled by Bcl-2. *Oncogene,* 19**,** 2286-95.

HAGE HASSAN, R., HAINAULT, I., VILQUIN, J. T., SAMAMA, C., LASNIER, F., FERRE, P., FOUFELLE, F. & HAJDUCH, E. 2012. Endoplasmic reticulum stress does not mediate palmitate-induced insulin resistance in mouse and human muscle cells. *Diabetologia,* 55**,** 204-14.

HAKIM, T. S., SUGIMORI, K., CAMPORESI, E. M. & ANDERSON, G. 1996. Half-life of nitric oxide in aqueous solutions with and without haemoglobin. *Physiol Meas,* 17**,** 267-77.

HANISCH, U. K. 2002. Microglia as a source and target of cytokines. *Glia,* 40**,** 140-55.

HANSEN, J. B., PETERSEN, R. K., LARSEN, B. M., BARTKOVA, J., ALSNER, J. & KRISTIANSEN, K. 1999. Activation of peroxisome proliferator-activated receptor gamma bypasses the function of the retinoblastoma protein in adipocyte differentiation. *J Biol Chem,* 274**,** 2386-93.

HANSON, S. R., CULYBA, E. K., HSU, T. L., WONG, C. H., KELLY, J. W. & POWERS, E. T. 2009. The core trisaccharide of an N-linked glycoprotein intrinsically accelerates folding and enhances stability. *Proc Natl Acad Sci U S A,* 106**,** 3131-6.

HARDING, H. P., ZHANG, Y., BERTOLOTTI, A., ZENG, H. & RON, D. 2000. Perk is essential for translational regulation and cell survival during the unfolded protein response. *Mol Cell,* 5**,** 897-904.

HARDING, H. P., ZHANG, Y. & RON, D. 1999. Protein translation and folding are coupled by an endoplasmic-reticulum-resident kinase. *Nature,* 397**,** 271-4.

HARDY, K. & CHAUDHRI, G. 1997. Activation and signal transduction via mitogen-activated protein (MAP) kinases in T lymphocytes. *Immunol Cell Biol,* 75**,** 528-45.

HART, C. B., ROTH, J. & LESNIAK, M. A. 1988. Post-translational modifications of the insulin receptor. *Adv Exp Med Biol,* 231**,** 481-94.

HARTL, F. U., BRACHER, A. & HAYER-HARTL, M. 2011. Molecular chaperones in protein folding and proteostasis. *Nature,* 475**,** 324-32.

HARUTA, T., UNO, T., KAWAHARA, J., TAKANO, A., EGAWA, K., SHARMA, P. M., OLEFSKY, J. M. & KOBAYASHI, M. 2000. A rapamycin-sensitive pathway down-regulates insulin signaling via phosphorylation and proteasomal degradation of insulin receptor substrate-1. *Mol Endocrinol,* 14**,** 783-94.

HASNAIN, S. Z., BORG, D. J., HARCOURT, B. E., TONG, H., SHENG, Y. H., NG, C. P., DAS, I., WANG, R., CHEN, A. C., LOUDOVARIS, T., KAY, T. W., THOMAS, H. E., WHITEHEAD, J. P., FORBES, J. M., PRINS, J. B. & MCGUCKIN, M. A. 2014. Glycemic control in diabetes is restored by therapeutic manipulation of cytokines that regulate beta cell stress. *Nat Med,* 20**,** 1417-26.

HAZE, K., YOSHIDA, H., YANAGI, H., YURA, T. & MORI, K. 1999. Mammalian transcription factor ATF6 is synthesized as a transmembrane protein and activated by proteolysis in response to endoplasmic reticulum stress. *Mol Biol Cell,* 10**,** 3787-99.

HERNANDEZ, J. M., FLOYD, D. H., WEILBAECHER, K. N., GREEN, P. L. & BORIS-LAWRIE, K. 2008. Multiple facets of junD gene expression are atypical among AP-1 family members. *Oncogene,* 27**,** 4757-67.

HIBBS, J. B., JR. 2002. Infection and nitric oxide. *J Infect Dis,* 185 Suppl 1**,** S9-17.

HIBI, M., LIN, A., SMEAL, T., MINDEN, A. & KARIN, M. 1993. Identification of an oncoprotein- and UV-responsive protein kinase that binds and potentiates the c-Jun activation domain. *Genes Dev,* 7**,** 2135-48.

HIRATA, Y., SUGIE, A., MATSUDA, A., MATSUDA, S. & KOYASU, S. 2013. TAK1-JNK axis mediates survival signal through Mcl1 stabilization in activated T cells. *J Immunol,* 190**,** 4621-6.

HIROSUMI, J., TUNCMAN, G., CHANG, L., GORGUN, C. Z., UYSAL, K. T., MAEDA, K., KARIN, M. & HOTAMISLIGIL, G. S. 2002. A central role for JNK in obesity and insulin resistance. *Nature,* 420**,** 333-6.

HO, A. S. & MOORE, K. W. 1994. Interleukin-10 and its receptor. *Ther Immunol,* 1**,** 173-85.

HOFMANN, S., CHERKASOVA, V., BANKHEAD, P., BUKAU, B. & STOECKLIN, G. 2012. Translation suppression promotes stress granule formation and cell survival in response to cold shock. *Mol Biol Cell,* 23**,** 3786-800.

HOLLIEN, J., LIN, J. H., LI, H., STEVENS, N., WALTER, P. & WEISSMAN, J. S. 2009. Regulated Ire1-dependent decay of messenger RNAs in mammalian cells. *J Cell Biol,* 186**,** 323-31.

HOLLIEN, J. & WEISSMAN, J. S. 2006. Decay of endoplasmic reticulum-localized mRNAs during the unfolded protein response. *Science,* 313**,** 104-7.

HOLTZ, W. A. & O'MALLEY, K. L. 2003. Parkinsonian mimetics induce aspects of unfolded protein response in death of dopaminergic neurons. *J Biol Chem,* 278**,** 19367-77.

HOLTZ, W. A., TURETZKY, J. M., JONG, Y. J. & O'MALLEY, K. L. 2006. Oxidative stress-triggered unfolded protein response is upstream of intrinsic cell death evoked by parkinsonian mimetics. *J Neurochem,* 99**,** 54-69.

HOOZEMANS, J. J., VAN HAASTERT, E. S., EIKELENBOOM, P., DE VOS, R. A., ROZEMULLER, J. M. & SCHEPER, W. 2007. Activation of the unfolded protein response in Parkinson's disease. *Biochem Biophys Res Commun,* 354**,** 707-11.

HOSOGAI, N., FUKUHARA, A., OSHIMA, K., MIYATA, Y., TANAKA, S., SEGAWA, K., FURUKAWA, S., TOCHINO, Y., KOMURO, R., MATSUDA, M. & SHIMOMURA, I. 2007. Adipose tissue hypoxia in obesity and its impact on adipocytokine dysregulation. *Diabetes,* 56**,** 901-11.

HOTAMISLIGIL, G. S. 2010. Endoplasmic reticulum stress and the inflammatory basis of metabolic disease. *Cell,* 140**,** 900-17.

HOTAMISLIGIL, G. S. & ERBAY, E. 2008. Nutrient sensing and inflammation in metabolic diseases. *Nat Rev Immunol,* 8**,** 923-34.

HOTAMISLIGIL, G. S., PERALDI, P., BUDAVARI, A., ELLIS, R., WHITE, M. F. & SPIEGELMAN, B. M. 1996. IRS-1-mediated inhibition of insulin receptor tyrosine kinase activity in TNF-alpha- and obesity-induced insulin resistance. *Science,* 271**,** 665-8.

HOTAMISLIGIL, G. S., SHARGILL, N. S. & SPIEGELMAN, B. M. 1993. Adipose expression of tumor necrosis factor-alpha: direct role in obesity-linked insulin resistance. *Science,* 259**,** 87-91.

HOTAMISLIGIL, G. S. & SPIEGELMAN, B. M. 1994. Tumor necrosis factor alpha: a key component of the obesity-diabetes link. *Diabetes,* 43**,** 1271-8.

HU, G., JOUSILAHTI, P., BIDEL, S., ANTIKAINEN, R. & TUOMILEHTO, J. 2007. Type 2 diabetes and the risk of Parkinson's disease. *Diabetes Care,* 30**,** 842-7.

HU, G., JOUSILAHTI, P., NISSINEN, A., ANTIKAINEN, R., KIVIPELTO, M. & TUOMILEHTO, J. 2006a. Body mass index and the risk of Parkinson disease. *Neurology,* 67**,** 1955-9.

HU, L. W., YEN, J. H., SHEN, Y. T., WU, K. Y. & WU, M. J. 2014. Luteolin modulates 6-hydroxydopamine-induced transcriptional changes of stress response pathways in PC12 cells. *PLoS One,* 9**,** e97880.

HU, M. T., TAYLOR-ROBINSON, S. D., CHAUDHURI, K. R., BELL, J. D., LABBE, C., CUNNINGHAM, V. J., KOEPP, M. J., HAMMERS, A., MORRIS, R. G., TURJANSKI, N. & BROOKS, D. J. 2000. Cortical dysfunction in non-demented Parkinson's disease patients: a combined (31)P-MRS and (18)FDG-PET study. *Brain,* 123 (Pt 2)**,** 340-52.

HU, P., HAN, Z., COUVILLON, A. D., KAUFMAN, R. J. & EXTON, J. H. 2006b. Autocrine tumor necrosis factor alpha links endoplasmic reticulum stress to the membrane death receptor pathway through IRE1alpha-mediated NF-kappaB activation and down-regulation of TRAF2 expression. *Mol Cell Biol,* 26**,** 3071-84.

HUANG, Y., LI, X., WANG, Y., WANG, H., HUANG, C. & LI, J. 2014. Endoplasmic reticulum stress-induced hepatic stellate cell apoptosis through calcium-mediated JNK/P38 MAPK and Calpain/Caspase-12 pathways. *Mol Cell Biochem,* 394**,** 1-12.

HUMAR, M., LOOP, T., SCHMIDT, R., HOETZEL, A., ROESSLEIN, M., ANDRIOPOULOS, N., PAHL, H. L., GEIGER, K. K. & PANNEN, B. H. 2007. The mitogen-activated protein kinase p38 regulates activator protein 1 by direct phosphorylation of c-Jun. *Int J Biochem Cell Biol,* 39**,** 2278-88.

HUNG, J. H., SU, I. J., LEI, H. Y., WANG, H. C., LIN, W. C., CHANG, W. T., HUANG, W., CHANG, W. C., CHANG, Y. S., CHEN, C. C. & LAI, M. D. 2004. Endoplasmic reticulum stress stimulates the expression of cyclooxygenase-2 through activation of NF-kappaB and pp38 mitogen-activated protein kinase. *J Biol Chem,* 279**,** 46384-92.

HUNOT, S., DUGAS, N., FAUCHEUX, B., HARTMANN, A., TARDIEU, M., DEBRE, P., AGID, Y., DUGAS, B. & HIRSCH, E. C. 1999. FcepsilonRII/CD23 is

expressed in Parkinson's disease and induces, in vitro, production of nitric oxide and tumor necrosis factor-alpha in glial cells. *J Neurosci,* 19**,** 3440-7.

HWANG, J. B. & FROST, S. C. 1999. Effect of alternative glycosylation on insulin receptor processing. *J Biol Chem,* 274**,** 22813-20.

ICHIJO, H., NISHIDA, E., IRIE, K., TEN DIJKE, P., SAITOH, M., MORIGUCHI, T., TAKAGI, M., MATSUMOTO, K., MIYAZONO, K. & GOTOH, Y. 1997. Induction of apoptosis by ASK1, a mammalian MAPKKK that activates SAPK/JNK and p38 signaling pathways. *Science,* 275**,** 90-4.

ILOUZ, R., KOWALSMAN, N., EISENSTEIN, M. & ELDAR-FINKELMAN, H. 2006. Identification of novel glycogen synthase kinase-3beta substrate-interacting residues suggests a common mechanism for substrate recognition. *J Biol Chem,* 281**,** 30621-30.

IMAI, Y., SODA, M., INOUE, H., HATTORI, N., MIZUNO, Y. & TAKAHASHI, R. 2001. An unfolded putative transmembrane polypeptide, which can lead to endoplasmic reticulum stress, is a substrate of Parkin. *Cell,* 105**,** 891-902.

IMAI, Y., SODA, M. & TAKAHASHI, R. 2000. Parkin suppresses unfolded protein stress-induced cell death through its E3 ubiquitin-protein ligase activity. *J Biol Chem,* 275**,** 35661-4.

IMAI, Y. & TAKAHASHI, R. 2004. How do Parkin mutations result in neurodegeneration? *Curr Opin Neurobiol,* 14**,** 384-9.

INOUE, H., TANIZAWA, Y., WASSON, J., BEHN, P., KALIDAS, K., BERNAL-MIZRACHI, E., MUECKLER, M., MARSHALL, H., DONIS-KELLER, H., CROCK, P., ROGERS, D., MIKUNI, M., KUMASHIRO, H., HIGASHI, K., SOBUE, G., OKA, Y. & PERMUTT, M. A. 1998. A gene encoding a transmembrane protein is mutated in patients with diabetes mellitus and optic atrophy (Wolfram syndrome). *Nat Genet,* 20**,** 143-8.

ISHIKAWA, S., TAIRA, T., TAKAHASHI-NIKI, K., NIKI, T., ARIGA, H. & IGUCHI-ARIGA, S. M. 2010. Human DJ-1-specific transcriptional activation of tyrosine hydroxylase gene. *J Biol Chem,* 285**,** 39718-31.

ISHITANI, T., KISHIDA, S., HYODO-MIURA, J., UENO, N., YASUDA, J., WATERMAN, M., SHIBUYA, H., MOON, R. T., NINOMIYA-TSUJI, J. & MATSUMOTO, K. 2003. The TAK1-NLK mitogen-activated protein kinase cascade functions in the Wnt-5a/Ca(2+) pathway to antagonize Wnt/beta-catenin signaling. *Mol Cell Biol,* 23**,** 131-9.

ITZHAK, D., BRIGHT, M., MCANDREW, P., MIRZA, A., NEWBATT, Y., STROVER, J., WIDYA, M., THOMPSON, A., MORGAN, G., COLLINS, I. & DAVIES, F. 2014. Multiple autophosphorylations significantly enhance the endoribonuclease activity of human inositol requiring enzyme 1alpha. *BMC Biochem,* 15**,** 3.

IYNEDJIAN, P. B. 2005. Lack of evidence for a role of TRB3/NIPK as an inhibitor of PKB-mediated insulin signalling in primary hepatocytes. *Biochem J,* 386**,** 113-8.

JACKSON-LEWIS, V. & PRZEDBORSKI, S. 2007. Protocol for the MPTP mouse model of Parkinson's disease. *Nat Protoc,* 2**,** 141-51.

JANG, Y. Y., KIM, N. K., KIM, M. K., LEE, H. Y., KIM, S. J., KIM, H. S., SEO, H. Y., LEE, I. K. & PARK, K. G. 2010. The Effect of Tribbles-Related Protein 3 on ER Stress-Suppressed Insulin Gene Expression in INS-1 Cells. *Korean Diabetes J,* 34**,** 312-9.

JIANG, H. Y., WEK, S. A., MCGRATH, B. C., SCHEUNER, D., KAUFMAN, R. J., CAVENER, D. R. & WEK, R. C. 2003a. Phosphorylation of the Subunit of Eukaryotic Initiation Factor 2 Is Required for Activation of NF- B in Response to Diverse Cellular Stresses. *Molecular and Cellular Biology,* 23**,** 5651-5663.

JIANG, H. Y., WEK, S. A., MCGRATH, B. C., SCHEUNER, D., KAUFMAN, R. J., CAVENER, D. R. & WEK, R. C. 2003b. Phosphorylation of the alpha subunit of

eukaryotic initiation factor 2 is required for activation of NF-kappaB in response to diverse cellular stresses. *Mol Cell Biol,* 23**,** 5651-63.

JULIER, C. & NICOLINO, M. 2010. Wolcott-Rallison syndrome. *Orphanet J Rare Dis,* 5**,** 29.

JUNG, D. Y., CHALASANI, U., PAN, N., FRIEDLINE, R. H., PROSDOCIMO, D. A., NAM, M., AZUMA, Y., MAGANTI, R., YU, K., VELAGAPUDI, A., O'SULLIVAN-MURPHY, B., SARTORETTO, J. L., JAIN, M. K., COOPER, M. P., URANO, F., KIM, J. K. & GRAY, S. 2013. KLF15 is a molecular link between endoplasmic reticulum stress and insulin resistance. *PLoS One,* 8**,** e77851.

JUNG, T. W., HWANG, H. J., HONG, H. C., CHOI, H. Y., YOO, H. J., BAIK, S. H. & CHOI, K. M. 2014. Resolvin D1 reduces ER stress-induced apoptosis and triglyceride accumulation through JNK pathway in HepG2 cells. *Mol Cell Endocrinol,* 391**,** 30-40.

JUNG, T. W., LEE, M. W., LEE, Y. J. & KIM, S. M. 2012. Metformin prevents endoplasmic reticulum stress-induced apoptosis through AMPK-PI3K-c-Jun NH2 pathway. *Biochem Biophys Res Commun,* 417**,** 147-52.

JUNN, E., JANG, W. H., ZHAO, X., JEONG, B. S. & MOURADIAN, M. M. 2009. Mitochondrial localization of DJ-1 leads to enhanced neuroprotection. *J Neurosci Res,* 87**,** 123-9.

JURCZAK, M. J., LEE, A. H., JORNAYVAZ, F. R., LEE, H. Y., BIRKENFELD, A. L., GUIGNI, B. A., KAHN, M., SAMUEL, V. T., GLIMCHER, L. H. & SHULMAN, G. I. 2012. Dissociation of inositol-requiring enzyme (IRE1alpha)-mediated c-Jun N-terminal kinase activation from hepatic insulin resistance in conditional X-box-binding protein-1 (XBP1) knock-out mice. *J Biol Chem,* 287**,** 2558-67.

JURKIN, J., HENKEL, T., NIELSEN, A. F., MINNICH, M., POPOW, J., KAUFMANN, T., HEINDL, K., HOFFMANN, T., BUSSLINGER, M. & MARTINEZ, J. 2014. The mammalian tRNA ligase complex mediates splicing of XBP1 mRNA and controls antibody secretion in plasma cells. *EMBO J,* 33**,** 2922-36.

KADLE, R., FELLOWS, R. E. & RAIZADA, M. K. 1984. The effects of insulin and tunicamycin on insulin receptors of cultured fibroblasts. *Exp Cell Res,* 151**,** 533-41.

KAMINSKA, B. 2005. MAPK signalling pathways as molecular targets for anti-inflammatory therapy--from molecular mechanisms to therapeutic benefits. *Biochim Biophys Acta,* 1754**,** 253-62.

KANEKO, M., NIINUMA, Y. & NOMURA, Y. 2003. Activation signal of nuclear factor-kappa B in response to endoplasmic reticulum stress is transduced via IRE1 and tumor necrosis factor receptor-associated factor 2. *Biol Pharm Bull,* 26**,** 931-5.

KANG, M. J., CHUNG, J. & RYOO, H. D. 2012. CDK5 and MEKK1 mediate pro-apoptotic signalling following endoplasmic reticulum stress in an autosomal dominant retinitis pigmentosa model. *Nat Cell Biol,* 14**,** 409-15.

KARS, M., YANG, L., GREGOR, M. F., MOHAMMED, B. S., PIETKA, T. A., FINCK, B. N., PATTERSON, B. W., HORTON, J. D., MITTENDORFER, B., HOTAMISLIGIL, G. S. & KLEIN, S. 2010. Tauroursodeoxycholic Acid may improve liver and muscle but not adipose tissue insulin sensitivity in obese men and women. *Diabetes,* 59**,** 1899-905.

KASHIWASE, K., HIGUCHI, Y., HIROTANI, S., YAMAGUCHI, O., HIKOSO, S., TAKEDA, T., WATANABE, T., TANIIKE, M., NAKAI, A., TSUJIMOTO, I., MATSUMURA, Y., UENO, H., NISHIDA, K., HORI, M. & OTSU, K. 2005. CaMKII activates ASK1 and NF-kappaB to induce cardiomyocyte hypertrophy. *Biochem Biophys Res Commun,* 327**,** 136-42.

KASUGA, M., KAHN, C. R., HEDO, J. A., VAN OBBERGHEN, E. & YAMADA, K. M. 1981. Insulin-induced receptor loss in cultured human lymphocytes is due to accelerated receptor degradation. *Proc Natl Acad Sci U S A,* 78**,** 6917-21.

KASUGA, M., KARLSSON, F. A. & KAHN, C. R. 1982. Insulin stimulates the phosphorylation of the 95,000-dalton subunit of its own receptor. *Science,* 215**,** 185-7.

KAWASAKI, N., ASADA, R., SAITO, A., KANEMOTO, S. & IMAIZUMI, K. 2012. Obesity-induced endoplasmic reticulum stress causes chronic inflammation in adipose tissue. *Sci Rep,* 2**,** 799.

KEDERSHA, N. & ANDERSON, P. 2007. Mammalian stress granules and processing bodies. *Methods Enzymol,* 431**,** 61-81.

KELLIHER, M. A., GRIMM, S., ISHIDA, Y., KUO, F., STANGER, B. Z. & LEDER, P. 1998. The death domain kinase RIP mediates the TNF-induced NF-kappaB signal. *Immunity,* 8**,** 297-303.

KIM, A. H., KHURSIGARA, G., SUN, X., FRANKE, T. F. & CHAO, M. V. 2001. Akt phosphorylates and negatively regulates apoptosis signal-regulating kinase 1. *Mol Cell Biol,* 21**,** 893-901.

KIM, D. S., KIM, J. H., LEE, G. H., KIM, H. T., LIM, J. M., CHAE, S. W., CHAE, H. J. & KIM, H. R. 2010. p38 Mitogen-activated protein kinase is involved in endoplasmic reticulum stress-induced cell death and autophagy in human gingival fibroblasts. *Biol Pharm Bull,* 33**,** 545-9.

KIM, I. K., PARK, S. J., PARK, J. H., LEE, S. H., HONG, S. E. & REED, J. C. 2012. Cyclosporine A and bromocriptine attenuate cell death mediated by intracellular calcium mobilization. *BMB Rep,* 45**,** 482-7.

KIM, J. A., YEH, D. C., VER, M., LI, Y., CARRANZA, A., CONRADS, T. P., VEENSTRA, T. D., HARRINGTON, M. A. & QUON, M. J. 2005. Phosphorylation of Ser24 in the pleckstrin homology domain of insulin receptor substrate-1 by Mouse Pelle-like kinase/interleukin-1 receptor-associated kinase: cross-talk between inflammatory signaling and insulin signaling that may contribute to insulin resistance. *J Biol Chem,* 280**,** 23173-83.

KIM, J. W., YANG, J. H., PARK, H. S., SUN, C., LEE, S. H., CHO, J. H., YANG, C. W. & YOON, K. H. 2009. Rosiglitazone protects the pancreatic beta-cell death induced by cyclosporine A. *Biochem Biophys Res Commun,* 390**,** 763-8.

KIM, R. D., DARLING, C. E., CERWENKA, H. & CHARI, R. S. 2000. Hypoosmotic stress activates p38, ERK 1 and 2, and SAPK/JNK in rat hepatocytes. *J Surg Res,* 90**,** 58-66.

KITADA, T., ASAKAWA, S., HATTORI, N., MATSUMINE, H., YAMAMURA, Y., MINOSHIMA, S., YOKOCHI, M., MIZUNO, Y. & SHIMIZU, N. 1998. Mutations in the parkin gene cause autosomal recessive juvenile parkinsonism. *Nature,* 392**,** 605-8.

KLINTWORTH, H., NEWHOUSE, K., LI, T., CHOI, W. S., FAIGLE, R. & XIA, Z. 2007. Activation of c-Jun N-terminal protein kinase is a common mechanism underlying paraquat- and rotenone-induced dopaminergic cell apoptosis. *Toxicol Sci,* 97**,** 149-62.

KNOWLES, B. B., HOWE, C. C. & ADEN, D. P. 1980. Human hepatocellular carcinoma cell lines secrete the major plasma proteins and hepatitis B surface antigen. *Science,* 209**,** 497-9.

KOH, H. J., ARNOLDS, D. E., FUJII, N., TRAN, T. T., ROGERS, M. J., JESSEN, N., LI, Y., LIEW, C. W., HO, R. C., HIRSHMAN, M. F., KULKARNI, R. N., KAHN, C. R. & GOODYEAR, L. J. 2006. Skeletal muscle-selective knockout of LKB1 increases insulin sensitivity, improves glucose homeostasis, and decreases TRB3. *Mol Cell Biol,* 26**,** 8217-27.

KOH, H. J., TOYODA, T., DIDESCH, M. M., LEE, M. Y., SLEEMAN, M. W., KULKARNI, R. N., MUSI, N., HIRSHMAN, M. F. & GOODYEAR, L. J. 2013.

Tribbles 3 mediates endoplasmic reticulum stress-induced insulin resistance in skeletal muscle. *Nat Commun,* 4**,** 1871.

KONO, H. & ROCK, K. L. 2008. How dying cells alert the immune system to danger. *Nat Rev Immunol,* 8**,** 279-89.

KREMERSKOTHEN, J., WENDHOLT, D., TEBER, I. & BARNEKOW, A. 2002. Insulin-induced expression of the activity-regulated cytoskeleton-associated gene (ARC) in human neuroblastoma cells requires p21(ras), mitogen-activated protein kinase/extracellular regulated kinase and src tyrosine kinases but is protein kinase C-independent. *Neurosci Lett,* 321**,** 153-6.

KREUTZBERG, G. W. 1996. Microglia: a sensor for pathological events in the CNS. *Trends Neurosci,* 19**,** 312-8.

KRIGE, D., CARROLL, M. T., COOPER, J. M., MARSDEN, C. D. & SCHAPIRA, A. H. 1992. Platelet mitochondrial function in Parkinson's disease. The Royal Kings and Queens Parkinson Disease Research Group. *Ann Neurol,* 32**,** 782-8.

KUBOTA, K., NIINUMA, Y., KANEKO, M., OKUMA, Y., SUGAI, M., OMURA, T., UESUGI, M., UEHARA, T., HOSOI, T. & NOMURA, Y. 2006. Suppressive effects of 4-phenylbutyrate on the aggregation of Pael receptors and endoplasmic reticulum stress. *J Neurochem,* 97**,** 1259-68.

KUZNETSOV, G., BROSTROM, M. A. & BROSTROM, C. O. 1992. Demonstration of a calcium requirement for secretory protein processing and export. Differential effects of calcium and dithiothreitol. *J Biol Chem,* 267**,** 3932-9.

KWON, D. Y., KIM, Y. S., AHN, I. S., KIM DA, S., KANG, S., HONG, S. M. & PARK, S. 2009. Exendin-4 potentiates insulinotropic action partly via increasing beta-cell proliferation and neogenesis and decreasing apoptosis in association with the attenuation of endoplasmic reticulum stress in islets of diabetic rats. *J Pharmacol Sci,* 111**,** 361-71.

KYRIAKIS, J. M. & AVRUCH, J. 2001. Mammalian mitogen-activated protein kinase signal transduction pathways activated by stress and inflammation. *Physiol Rev,* 81**,** 807-69.

KYRIAKIS, J. M., BANERJEE, P., NIKOLAKAKI, E., DAI, T., RUBIE, E. A., AHMAD, M. F., AVRUCH, J. & WOODGETT, J. R. 1994. The stress-activated protein kinase subfamily of c-Jun kinases. *Nature,* 369**,** 156-60.

LAMB, J. A., VENTURA, J. J., HESS, P., FLAVELL, R. A. & DAVIS, R. J. 2003. JunD mediates survival signaling by the JNK signal transduction pathway. *Mol Cell,* 11**,** 1479-89.

LANE, M. D., RONNETT, G. V., KOHANSKI, R. A. & SIMPSON, T. L. 1985. Posttranslational processing of the insulin proreceptor. *Curr Top Cell Regul,* 27**,** 279-92.

LANG, A. E. & LOZANO, A. M. 1998. Parkinson's disease. First of two parts. *N Engl J Med,* 339**,** 1044-53.

LANGSTON, J. W., BALLARD, P., TETRUD, J. W. & IRWIN, I. 1983. Chronic Parkinsonism in humans due to a product of meperidine-analog synthesis. *Science,* 219**,** 979-80.

LANGSTON, J. W., FORNO, L. S., TETRUD, J., REEVES, A. G., KAPLAN, J. A. & KARLUK, D. 1999. Evidence of active nerve cell degeneration in the substantia nigra of humans years after 1-methyl-4-phenyl-1,2,3,6-tetrahydropyridine exposure. *Ann Neurol,* 46**,** 598-605.

LAWSON, L. J., PERRY, V. H., DRI, P. & GORDON, S. 1990. Heterogeneity in the distribution and morphology of microglia in the normal adult mouse brain. *Neuroscience,* 39**,** 151-70.

LAZARIDES, E. 1982. Intermediate filaments: a chemically heterogeneous, developmentally regulated class of proteins. *Annu Rev Biochem,* 51**,** 219-50.

LEE, F. Y., LI, Y., YANG, E. K., YANG, S. Q., LIN, H. Z., TRUSH, M. A., DANNENBERG, A. J. & DIEHL, A. M. 1999a. Phenotypic abnormalities in macrophages from leptin-deficient, obese mice. *Am J Physiol,* 276**,** C386-94.

LEE, J. C., KASSIS, S., KUMAR, S., BADGER, A. & ADAMS, J. L. 1999b. p38 mitogen-activated protein kinase inhibitors--mechanisms and therapeutic potentials. *Pharmacol Ther,* 82**,** 389-97.

LEE, J. C., LAYDON, J. T., MCDONNELL, P. C., GALLAGHER, T. F., KUMAR, S., GREEN, D., MCNULTY, D., BLUMENTHAL, M. J., HEYS, J. R., LANDVATTER, S. W. & ET AL. 1994. A protein kinase involved in the regulation of inflammatory cytokine biosynthesis. *Nature,* 372**,** 739-46.

LEE, J. C. & YOUNG, P. R. 1996. Role of CSB/p38/RK stress response kinase in LPS and cytokine signaling mechanisms. *J Leukoc Biol,* 59**,** 152-7.

LEE, K., TIRASOPHON, W., SHEN, X., MICHALAK, M., PRYWES, R., OKADA, T., YOSHIDA, H., MORI, K. & KAUFMAN, R. J. 2002. IRE1-mediated unconventional mRNA splicing and S2P-mediated ATF6 cleavage merge to regulate XBP1 in signaling the unfolded protein response. *Genes Dev,* 16**,** 452-66.

LEE, S. Y., REICHLIN, A., SANTANA, A., SOKOL, K. A., NUSSENZWEIG, M. C. & CHOI, Y. 1997. TRAF2 is essential for JNK but not NF-kappaB activation and regulates lymphocyte proliferation and survival. *Immunity,* 7**,** 703-13.

LEI, K. & DAVIS, R. J. 2003. JNK phosphorylation of Bim-related members of the Bcl2 family induces Bax-dependent apoptosis. *Proc Natl Acad Sci U S A,* 100**,** 2432-7.

LERNER, A. G., UPTON, J. P., PRAVEEN, P. V., GHOSH, R., NAKAGAWA, Y., IGBARIA, A., SHEN, S., NGUYEN, V., BACKES, B. J., HEIMAN, M., HEINTZ, N., GREENGARD, P., HUI, S., TANG, Q., TRUSINA, A., OAKES, S. A. & PAPA, F. R. 2012. IRE1alpha induces thioredoxin-interacting protein to activate the NLRP3 inflammasome and promote programmed cell death under irremediable ER stress. *Cell Metab,* 16**,** 250-64.

LEVINE, C. G., MITRA, D., SHARMA, A., SMITH, C. L. & HEGDE, R. S. 2005. The efficiency of protein compartmentalization into the secretory pathway. *Mol Biol Cell,* 16**,** 279-91.

LI, H. M., NIKI, T., TAIRA, T., IGUCHI-ARIGA, S. M. & ARIGA, H. 2005a. Association of DJ-1 with chaperones and enhanced association and colocalization with mitochondrial Hsp70 by oxidative stress. *Free Radic Res,* 39**,** 1091-9.

LI, L. & HOLSCHER, C. 2007. Common pathological processes in Alzheimer disease and type 2 diabetes: a review. *Brain Res Rev,* 56**,** 384-402.

LI, Q. & ENGELHARDT, J. F. 2006. Interleukin-1beta induction of NFkappaB is partially regulated by H2O2-mediated activation of NFkappaB-inducing kinase. *J Biol Chem,* 281**,** 1495-505.

LI, Q., QIAO, Y., WANG, C., ZHANG, G., ZHANG, X. & XU, L. 2016. Associations between two single-nucleotide polymorphisms (rs1801278 and rs2943641) of insulin receptor substrate 1 gene and type 2 diabetes susceptibility: a meta-analysis. *Endocrine,* 51**,** 52-62.

LI, Y., GE, M., CIANI, L., KURIAKOSE, G., WESTOVER, E. J., DURA, M., COVEY, D. F., FREED, J. H., MAXFIELD, F. R., LYTTON, J. & TABAS, I. 2004a. Enrichment of endoplasmic reticulum with cholesterol inhibits sarcoplasmic-endoplasmic reticulum calcium ATPase-2b activity in parallel with increased order of membrane lipids: implications for depletion of endoplasmic reticulum calcium stores and apoptosis in cholesterol-loaded macrophages. *J Biol Chem,* 279**,** 37030-9.

LI, Y., SOOS, T. J., LI, X., WU, J., DEGENNARO, M., SUN, X., LITTMAN, D. R., BIRNBAUM, M. J. & POLAKIEWICZ, R. D. 2004b. Protein kinase C Theta

inhibits insulin signaling by phosphorylating IRS1 at Ser(1101). *J Biol Chem,* 279**,** 45304-7.

LI, Z. Q., HUANG, Y. S., YANG, Z. C. & WANG, J. H. 2005b. [Influence of nuclear factor-kappaB activation on the expression of cytokines in monocytes stimulated by burn serum]. *Zhonghua Shao Shang Za Zhi,* 21**,** 434-7.

LIBERMAN, Z. & ELDAR-FINKELMAN, H. 2005. Serine 332 phosphorylation of insulin receptor substrate-1 by glycogen synthase kinase-3 attenuates insulin signaling. *J Biol Chem,* 280**,** 4422-8.

LIEW, C. W., BOCHENSKI, J., KAWAMORI, D., HU, J., LEECH, C. A., WANIC, K., MALECKI, M., WARRAM, J. H., QI, L., KROLEWSKI, A. S. & KULKARNI, R. N. 2010. The pseudokinase tribbles homolog 3 interacts with ATF4 to negatively regulate insulin exocytosis in human and mouse beta cells. *J Clin Invest,* 120**,** 2876-88.

LIN, A., MINDEN, A., MARTINETTO, H., CLARET, F. X., LANGE-CARTER, C., MERCURIO, F., JOHNSON, G. L. & KARIN, M. 1995. Identification of a dual specificity kinase that activates the Jun kinases and p38-Mpk2. *Science,* 268**,** 286-90.

LINDERSSON, E., BEEDHOLM, R., HOJRUP, P., MOOS, T., GAI, W., HENDIL, K. B. & JENSEN, P. H. 2004. Proteasomal inhibition by alpha-synuclein filaments and oligomers. *J Biol Chem,* 279**,** 12924-34.

LIU, B. & HONG, J. S. 2003. Role of microglia in inflammation-mediated neurodegenerative diseases: mechanisms and strategies for therapeutic intervention. *J Pharmacol Exp Ther,* 304**,** 1-7.

LIU, C. Y., SCHRODER, M. & KAUFMAN, R. J. 2000. Ligand-independent dimerization activates the stress response kinases IRE1 and PERK in the lumen of the endoplasmic reticulum. *J Biol Chem,* 275**,** 24881-5.

LIU, J. & LIN, A. 2005. Role of JNK activation in apoptosis: a double-edged sword. *Cell Res,* 15**,** 36-42.

LIU, J., MINEMOTO, Y. & LIN, A. 2004. c-Jun N-terminal protein kinase 1 (JNK1), but not JNK2, is essential for tumor necrosis factor alpha-induced c-Jun kinase activation and apoptosis. *Mol Cell Biol,* 24**,** 10844-56.

LIU, Y. F., PAZ, K., HERSCHKOVITZ, A., ALT, A., TENNENBAUM, T., SAMPSON, S. R., OHBA, M., KUROKI, T., LEROITH, D. & ZICK, Y. 2001. Insulin stimulates PKCzeta -mediated phosphorylation of insulin receptor substrate-1 (IRS-1). A self-attenuated mechanism to negatively regulate the function of IRS proteins. *J Biol Chem,* 276**,** 14459-65.

LODISH, H. F. & KONG, N. 1990. Perturbation of cellular calcium blocks exit of secretory proteins from the rough endoplasmic reticulum. *J Biol Chem,* 265**,** 10893-9.

LOPES, F. M., SCHRODER, R., DA FROTA, M. L., JR., ZANOTTO-FILHO, A., MULLER, C. B., PIRES, A. S., MEURER, R. T., COLPO, G. D., GELAIN, D. P., KAPCZINSKI, F., MOREIRA, J. C., FERNANDES MDA, C. & KLAMT, F. 2010. Comparison between proliferative and neuron-like SH-SY5Y cells as an in vitro model for Parkinson disease studies. *Brain Res,* 1337**,** 85-94.

LU, M., LAWRENCE, D. A., MARSTERS, S., ACOSTA-ALVEAR, D., KIMMIG, P., MENDEZ, A. S., PATON, A. W., PATON, J. C., WALTER, P. & ASHKENAZI, A. 2014. Cell death. Opposing unfolded-protein-response signals converge on death receptor 5 to control apoptosis. *Science,* 345**,** 98-101.

LUMENG, C. N., BODZIN, J. L. & SALTIEL, A. R. 2007. Obesity induces a phenotypic switch in adipose tissue macrophage polarization. *J Clin Invest,* 117**,** 175-84.

LY, J. D., GRUBB, D. R. & LAWEN, A. 2003. The mitochondrial membrane potential (deltapsi(m)) in apoptosis; an update. *Apoptosis,* 8**,** 115-28.

MACMICKING, J., XIE, Q. W. & NATHAN, C. 1997. Nitric oxide and macrophage function. *Annu Rev Immunol,* 15**,** 323-50.

MAHADEVAN, N. R., RODVOLD, J., SEPULVEDA, H., ROSSI, S., DREW, A. F. & ZANETTI, M. 2011. Transmission of endoplasmic reticulum stress and pro-inflammation from tumor cells to myeloid cells. *Proc Natl Acad Sci U S A,* 108**,** 6561-6.

MALEY, F., TRIMBLE, R. B., TARENTINO, A. L. & PLUMMER, T. H., JR. 1989. Characterization of glycoproteins and their associated oligosaccharides through the use of endoglycosidases. *Anal Biochem,* 180**,** 195-204.

MANDERS, E. M., STAP, J., BRAKENHOFF, G. J., VAN DRIEL, R. & ATEN, J. A. 1992. Dynamics of three-dimensional replication patterns during the S-phase, analysed by double labelling of DNA and confocal microscopy. *J Cell Sci,* 103 (Pt 3)**,** 857-62.

MANDERSON, A. P., KAY, J. G., HAMMOND, L. A., BROWN, D. L. & STOW, J. L. 2007. Subcompartments of the macrophage recycling endosome direct the differential secretion of IL-6 and TNFalpha. *J Cell Biol,* 178**,** 57-69.

MANNING-BOG, A. B., MCCORMACK, A. L., LI, J., UVERSKY, V. N., FINK, A. L. & DI MONTE, D. A. 2002. The herbicide paraquat causes up-regulation and aggregation of alpha-synuclein in mice: paraquat and alpha-synuclein. *J Biol Chem,* 277**,** 1641-4.

MANTHEY, C. L., WANG, S. W., KINNEY, S. D. & YAO, Z. 1998. SB202190, a selective inhibitor of p38 mitogen-activated protein kinase, is a powerful regulator of LPS-induced mRNAs in monocytes. *J Leukoc Biol,* 64**,** 409-17.

MARCHETTI, P., DEL PRATO, S., LUPI, R. & DEL GUERRA, S. 2006. The pancreatic beta-cell in human Type 2 diabetes. *Nutr Metab Cardiovasc Dis,* 16 Suppl 1**,** S3-6.

MARSHALL, C. J. 1995. Specificity of receptor tyrosine kinase signaling: transient versus sustained extracellular signal-regulated kinase activation. *Cell,* 80**,** 179-85.

MARSHALL, R. D. 1974. The nature and metabolism of the carbohydrate-peptide linkages of glycoproteins. *Biochem Soc Symp***,** 17-26.

MARTIN-VILLALBA, A., HERR, I., JEREMIAS, I., HAHNE, M., BRANDT, R., VOGEL, J., SCHENKEL, J., HERDEGEN, T. & DEBATIN, K. M. 1999. CD95 ligand (Fas-L/APO-1L) and tumor necrosis factor-related apoptosis-inducing ligand mediate ischemia-induced apoptosis in neurons. *J Neurosci,* 19**,** 3809-17.

MASSAGUE, J., PILCH, P. F. & CZECH, M. P. 1981. A unique proteolytic cleavage site on the beta subunit of the insulin receptor. *J Biol Chem,* 256**,** 3182-90.

MAURER-STROH, S., EISENHABER, B. & EISENHABER, F. 2002a. N-terminal N-myristoylation of proteins: prediction of substrate proteins from amino acid sequence. *J Mol Biol,* 317**,** 541-57.

MAURER-STROH, S., EISENHABER, B. & EISENHABER, F. 2002b. N-terminal N-myristoylation of proteins: refinement of the sequence motif and its taxon-specific differences. *J Mol Biol,* 317**,** 523-40.

MAURO, C., CRESCENZI, E., DE MATTIA, R., PACIFICO, F., MELLONE, S., SALZANO, S., DE LUCA, C., D'ADAMIO, L., PALUMBO, G., FORMISANO, S., VITO, P. & LEONARDI, A. 2006. Central role of the scaffold protein tumor necrosis factor receptor-associated factor 2 in regulating endoplasmic reticulum stress-induced apoptosis. *J Biol Chem,* 281**,** 2631-8.

MAYTIN, E. V., UBEDA, M., LIN, J. C. & HABENER, J. F. 2001. Stress-inducible transcription factor CHOP/gadd153 induces apoptosis in mammalian cells via p38 kinase-dependent and -independent mechanisms. *Exp Cell Res,* 267**,** 193-204.

MCCORMACK, A. L., THIRUCHELVAM, M., MANNING-BOG, A. B., THIFFAULT, C., LANGSTON, J. W., CORY-SLECHTA, D. A. & DI MONTE, D. A. 2002.

Environmental risk factors and Parkinson's disease: selective degeneration of nigral dopaminergic neurons caused by the herbicide paraquat. *Neurobiol Dis,* 10**,** 119-27.

MCCULLOUGH, K. D., MARTINDALE, J. L., KLOTZ, L. O., AW, T. Y. & HOLBROOK, N. J. 2001. Gadd153 sensitizes cells to endoplasmic reticulum stress by down-regulating Bcl2 and perturbing the cellular redox state. *Mol Cell Biol,* 21**,** 1249-59.

MCGEER, P. L., ITAGAKI, S., BOYES, B. E. & MCGEER, E. G. 1988. Reactive microglia are positive for HLA-DR in the substantia nigra of Parkinson's and Alzheimer's disease brains. *Neurology,* 38**,** 1285-91.

MCGEER, P. L., SCHWAB, C., PARENT, A. & DOUDET, D. 2003. Presence of reactive microglia in monkey substantia nigra years after 1-methyl-4-phenyl-1,2,3,6-tetrahydropyridine administration. *Ann Neurol,* 54**,** 599-604.

MEARES, G. P., LIU, Y., RAJBHANDARI, R., QIN, H., NOZELL, S. E., MOBLEY, J. A., CORBETT, J. A. & BENVENISTE, E. N. 2014. PERK-dependent activation of JAK1 and STAT3 contributes to endoplasmic reticulum stress-induced inflammation. *Mol Cell Biol,* 34**,** 3911-25.

MENNICKEN, F., MAKI, R., DE SOUZA, E. B. & QUIRION, R. 1999. Chemokines and chemokine receptors in the CNS: a possible role in neuroinflammation and patterning. *Trends Pharmacol Sci,* 20**,** 73-8.

MICHEL, P. P., DANDAPANI, B. K., KNUSEL, B., SANCHEZ-RAMOS, J. & HEFTI, F. 1990. Toxicity of 1-methyl-4-phenylpyridinium for rat dopaminergic neurons in culture: selectivity and irreversibility. *J Neurochem,* 54**,** 1102-9.

MICHEL, P. P. & HEFTI, F. 1990. Toxicity of 6-hydroxydopamine and dopamine for dopaminergic neurons in culture. *J Neurosci Res,* 26**,** 428-35.

MIHAI, A. D. & SCHRÖDER, M. 2014. Glucose starvation and hypoxia, but not the saturated fatty acid palmitic acid or cholesterol, activate the unfolded protein response in 3T3-F442A and 3T3-L1 adipocytes. *Adipocyte,* 4**,** 188-202.

MISHRA, R. & KARANDE, A. A. 2014. Endoplasmic reticulum stress-mediated activation of p38 MAPK, Caspase-2 and Caspase-8 leads to abrin-induced apoptosis. *PLoS One,* 9**,** e92586.

MIZRAHI, A., O'MALLEY, J. A., CARTER, W. A., TAKATSUKI, A., TAMURA, G. & SULKOWSKI, E. 1978. Glycosylation of interferons. Effects of tunicamycin on human immune interferon. *J Biol Chem,* 253**,** 7612-5.

MOGI, M., HARADA, M., KONDO, T., RIEDERER, P., INAGAKI, H., MINAMI, M. & NAGATSU, T. 1994. Interleukin-1 beta, interleukin-6, epidermal growth factor and transforming growth factor-alpha are elevated in the brain from parkinsonian patients. *Neurosci Lett,* 180**,** 147-50.

MOLONEY, A. M., GRIFFIN, R. J., TIMMONS, S., O'CONNOR, R., RAVID, R. & O'NEILL, C. 2010. Defects in IGF-1 receptor, insulin receptor and IRS-1/2 in Alzheimer's disease indicate possible resistance to IGF-1 and insulin signalling. *Neurobiol Aging,* 31**,** 224-43.

MOLTON, S. A., TODD, D. E. & COOK, S. J. 2003. Selective activation of the c-Jun N-terminal kinase (JNK) pathway fails to elicit Bax activation or apoptosis unless the phosphoinositide 3'-kinase (PI3K) pathway is inhibited. *Oncogene,* 22**,** 4690-701.

MOLTON, S. A., WESTON, C., BALMANNO, K., NEWSON, C., TODD, D. E., GARNER, A. P. & COOK, S. J. 2005. The conditional kinase DeltaMEKK1:ER* selectively activates the JNK pathway and protects against serum withdrawal-induced cell death. *Cell Signal,* 17**,** 1412-22.

MONDAL, A. K., DAS, S. K., VARMA, V., NOLEN, G. T., MCGEHEE, R. E., ELBEIN, S. C., WEI, J. Y. & RANGANATHAN, G. 2012. Effect of endoplasmic reticulum stress on inflammation and adiponectin regulation in human adipocytes. *Metab Syndr Relat Disord,* 10**,** 297-306.

MONTEFUSCO, O., ASSINI, M. C. & MISSALE, C. 1983. Insulin-mediated effects of glucose on dopamine metabolism. *Acta Diabetol Lat,* 20**,** 71-7.

MOORE, D. J., WEST, A. B., DAWSON, V. L. & DAWSON, T. M. 2005. Molecular pathophysiology of Parkinson's disease. *Annu Rev Neurosci,* 28**,** 57-87.

MOQBEL, R. & COUGHLIN, J. J. 2006. Differential secretion of cytokines. *Sci STKE,* 2006**,** pe26.

MOROO, I., YAMADA, T., MAKINO, H., TOOYAMA, I., MCGEER, P. L., MCGEER, E. G. & HIRAYAMA, K. 1994. Loss of insulin receptor immunoreactivity from the substantia nigra pars compacta neurons in Parkinson's disease. *Acta Neuropathol,* 87**,** 343-8.

MORRIS, J. K., ZHANG, H., GUPTE, A. A., BOMHOFF, G. L., STANFORD, J. A. & GEIGER, P. C. 2008. Measures of striatal insulin resistance in a 6-hydroxydopamine model of Parkinson's disease. *Brain Res,* 1240**,** 185-95.

MOSSER, D. M. 2003. The many faces of macrophage activation. *J Leukoc Biol,* 73**,** 209-12.

MOSSER, D. M. & EDWARDS, J. P. 2008. Exploring the full spectrum of macrophage activation. *Nat Rev Immunol,* 8**,** 958-69.

MUKERJEE, N., MCGINNIS, K. M., PARK, Y. H., GNEGY, M. E. & WANG, K. K. 2000. Caspase-mediated proteolytic activation of calcineurin in thapsigargin-mediated apoptosis in SH-SY5Y neuroblastoma cells. *Arch Biochem Biophys,* 379**,** 337-43.

MURAI, H., HIRAGAMI, F., KAWAMURA, K., MOTODA, H., KOIKE, Y., INOUE, S., KUMAGISHI, K., OHTSUKA, A. & KANO, Y. 2010. Differential response of heat-shock-induced p38 MAPK and JNK activity in PC12 mutant and PC12 parental cells for differentiation and apoptosis. *Acta Med Okayama,* 64**,** 55-62.

MURAKAMI, T., SHOJI, M., IMAI, Y., INOUE, H., KAWARABAYASHI, T., MATSUBARA, E., HARIGAYA, Y., SASAKI, A., TAKAHASHI, R. & ABE, K. 2004. Pael-R is accumulated in Lewy bodies of Parkinson's disease. *Ann Neurol,* 55**,** 439-42.

MURPHY, A. N., BREDESEN, D. E., CORTOPASSI, G., WANG, E. & FISKUM, G. 1996. Bcl-2 potentiates the maximal calcium uptake capacity of neural cell mitochondria. *Proc Natl Acad Sci U S A,* 93**,** 9893-8.

MURZI, E., CONTRERAS, Q., TENEUD, L., VALECILLOS, B., PARADA, M. A., DE PARADA, M. P. & HERNANDEZ, L. 1996. Diabetes decreases limbic extracellular dopamine in rats. *Neurosci Lett,* 202**,** 141-4.

MYERS, M. G., JR. & WHITE, M. F. 1996. Insulin signal transduction and the IRS proteins. *Annu Rev Pharmacol Toxicol,* 36**,** 615-58.

NATHAN, C. 1991. Mechanisms and modulation of macrophage activation. *Behring Inst Mitt***,** 200-7.

NAVONE, F., JAHN, R., DI GIOIA, G., STUKENBROK, H., GREENGARD, P. & DE CAMILLI, P. 1986. Protein p38: an integral membrane protein specific for small vesicles of neurons and neuroendocrine cells. *J Cell Biol,* 103**,** 2511-27.

NGUYEN, M. T., SATOH, H., FAVELYUKIS, S., BABENDURE, J. L., IMAMURA, T., SBODIO, J. I., ZALEVSKY, J., DAHIYAT, B. I., CHI, N. W. & OLEFSKY, J. M. 2005. JNK and tumor necrosis factor-alpha mediate free fatty acid-induced insulin resistance in 3T3-L1 adipocytes. *J Biol Chem,* 280**,** 35361-71.

NISHINA, H., FISCHER, K. D., RADVANYI, L., SHAHINIAN, A., HAKEM, R., RUBIE, E. A., BERNSTEIN, A., MAK, T. W., WOODGETT, J. R. & PENNINGER, J. M. 1997. Stress-signalling kinase Sek1 protects thymocytes from apoptosis mediated by CD95 and CD3. *Nature,* 385**,** 350-3.

NISHITOH, H., MATSUZAWA, A., TOBIUME, K., SAEGUSA, K., TAKEDA, K., INOUE, K., HORI, S., KAKIZUKA, A. & ICHIJO, H. 2002. ASK1 is essential for

endoplasmic reticulum stress-induced neuronal cell death triggered by expanded polyglutamine repeats. *Genes Dev,* 16**,** 1345-55.

NISHITOH, H., SAITOH, M., MOCHIDA, Y., TAKEDA, K., NAKANO, H., ROTHE, M., MIYAZONO, K. & ICHIJO, H. 1998. ASK1 is essential for JNK/SAPK activation by TRAF2. *Mol Cell,* 2**,** 389-95.

NISTICO, R., CAVALLUCCI, V., PICCININ, S., MACRI, S., PIGNATELLI, M., MEHDAWY, B., BLANDINI, F., LAVIOLA, G., LAURO, D., MERCURI, N. B. & D'AMELIO, M. 2012. Insulin receptor beta-subunit haploinsufficiency impairs hippocampal late-phase LTP and recognition memory. *Neuromolecular Med,* 14**,** 262-9.

NUSS, J. E., CHOKSI, K. B., DEFORD, J. H. & PAPACONSTANTINOU, J. 2008. Decreased enzyme activities of chaperones PDI and BiP in aged mouse livers. *Biochem Biophys Res Commun,* 365**,** 355-61.

OHOKA, N., YOSHII, S., HATTORI, T., ONOZAKI, K. & HAYASHI, H. 2005. TRB3, a novel ER stress-inducible gene, is induced via ATF4-CHOP pathway and is involved in cell death. *EMBO J,* 24**,** 1243-55.

OKAMOTO, H., LATRES, E., LIU, R., THABET, K., MURPHY, A., VALENZEULA, D., YANCOPOULOS, G. D., STITT, T. N., GLASS, D. J. & SLEEMAN, M. W. 2007. Genetic deletion of Trb3, the mammalian Drosophila tribbles homolog, displays normal hepatic insulin signaling and glucose homeostasis. *Diabetes,* 56**,** 1350-6.

OLEFSKY, J. M. 1976. Decreased insulin binding to adipocytes and circulating monocytes from obese subjects. *J Clin Invest,* 57**,** 1165-72.

OLEFSKY, J. M. & REAVEN, G. M. 1975. Effects of age and obesity on insulin binding to isolated adipocytes. *Endocrinology,* 96**,** 1486-98.

OLOKOBA, A. B., OBATERU, O. A. & OLOKOBA, L. B. 2012. Type 2 diabetes mellitus: a review of current trends. *Oman Med J,* 27**,** 269-73.

ORD, D. & ORD, T. 2003. Mouse NIPK interacts with ATF4 and affects its transcriptional activity. *Exp Cell Res,* 286**,** 308-20.

OSLOWSKI, C. M., HARA, T., O'SULLIVAN-MURPHY, B., KANEKURA, K., LU, S., HARA, M., ISHIGAKI, S., ZHU, L. J., HAYASHI, E., HUI, S. T., GREINER, D., KAUFMAN, R. J., BORTELL, R. & URANO, F. 2012. Thioredoxin-interacting protein mediates ER stress-induced beta cell death through initiation of the inflammasome. *Cell Metab,* 16**,** 265-73.

OSTREROVA-GOLTS, N., PETRUCELLI, L., HARDY, J., LEE, J. M., FARER, M. & WOLOZIN, B. 2000. The A53T alpha-synuclein mutation increases iron-dependent aggregation and toxicity. *J Neurosci,* 20**,** 6048-54.

OUYANG, M. & SHEN, X. 2006. Critical role of ASK1 in the 6-hydroxydopamine-induced apoptosis in human neuroblastoma SH-SY5Y cells. *J Neurochem,* 97**,** 234-44.

OZCAN, U., CAO, Q., YILMAZ, E., LEE, A. H., IWAKOSHI, N. N., OZDELEN, E., TUNCMAN, G., GORGUN, C., GLIMCHER, L. H. & HOTAMISLIGIL, G. S. 2004. Endoplasmic reticulum stress links obesity, insulin action, and type 2 diabetes. *Science,* 306**,** 457-61.

OZCAN, U., OZCAN, L., YILMAZ, E., DUVEL, K., SAHIN, M., MANNING, B. D. & HOTAMISLIGIL, G. S. 2008. Loss of the tuberous sclerosis complex tumor suppressors triggers the unfolded protein response to regulate insulin signaling and apoptosis. *Mol Cell,* 29**,** 541-51.

OZCAN, U., YILMAZ, E., OZCAN, L., FURUHASHI, M., VAILLANCOURT, E., SMITH, R. O., GORGUN, C. Z. & HOTAMISLIGIL, G. S. 2006. Chemical chaperones reduce ER stress and restore glucose homeostasis in a mouse model of type 2 diabetes. *Science,* 313**,** 1137-40.

OZES, O. N., AKCA, H., MAYO, L. D., GUSTIN, J. A., MAEHAMA, T., DIXON, J. E. & DONNER, D. B. 2001. A phosphatidylinositol 3-kinase/Akt/mTOR pathway mediates and PTEN antagonizes tumor necrosis factor inhibition of insulin signaling through insulin receptor substrate-1. *Proc Natl Acad Sci U S A,* 98**,** 4640-5.

PAETZEL, M., KARLA, A., STRYNADKA, N. C. & DALBEY, R. E. 2002. Signal peptidases. *Chem Rev,* 102**,** 4549-80.

PAHL, H. L. 1999. Activators and target genes of Rel/NF-kappaB transcription factors. *Oncogene,* 18**,** 6853-66.

PALACIOS, N., GAO, X., MCCULLOUGH, M. L., JACOBS, E. J., PATEL, A. V., MAYO, T., SCHWARZSCHILD, M. A. & ASCHERIO, A. 2011. Obesity, diabetes, and risk of Parkinson's disease. *Mov Disord,* 26**,** 2253-9.

PARK, C. W., YOO, K. Y., HWANG, I. K., CHOI, J. H., LEE, C. H., PARK, O. K., CHO, J. H., LEE, Y. L., SHIN, H. C. & WON, M. H. 2009. Age-related changes in the insulin receptor beta in the gerbil hippocampus. *Neurochem Res,* 34**,** 2154-62.

PARKER, W. D., JR., BOYSON, S. J. & PARKS, J. K. 1989. Abnormalities of the electron transport chain in idiopathic Parkinson's disease. *Ann Neurol,* 26**,** 719-23.

PARKINSON, J. 2002. An essay on the shaking palsy. 1817. *J Neuropsychiatry Clin Neurosci,* 14**,** 223-36; discussion 222.

PASCHEN, W. 2003a. Endoplasmic reticulum: a primary target in various acute disorders and degenerative diseases of the brain. *Cell Calcium,* 34**,** 365-383.

PASCHEN, W. 2003b. Endoplasmic reticulum: a primary target in various acute disorders and degenerative diseases of the brain. *Cell Calcium,* 34**,** 365-83.

PASCHEN, W. & DOUTHEIL, J. 1999. Disturbances of the functioning of endoplasmic reticulum: a key mechanism underlying neuronal cell injury? *J Cereb Blood Flow Metab,* 19**,** 1-18.

PATON, A. W., BEDDOE, T., THORPE, C. M., WHISSTOCK, J. C., WILCE, M. C., ROSSJOHN, J., TALBOT, U. M. & PATON, J. C. 2006. AB5 subtilase cytotoxin inactivates the endoplasmic reticulum chaperone BiP. *Nature,* 443**,** 548-52.

PATON, A. W., SRIMANOTE, P., TALBOT, U. M., WANG, H. & PATON, J. C. 2004. A new family of potent AB(5) cytotoxins produced by Shiga toxigenic Escherichia coli. *J Exp Med,* 200**,** 35-46.

PATTI, M. E. & KAHN, B. B. 2004. Nutrient sensor links obesity with diabetes risk. *Nat Med,* 10**,** 1049-50.

PAZ, K., VOLIOVITCH, H., HADARI, Y. R., ROBERTS, C. T., JR., LEROITH, D. & ZICK, Y. 1996. Interaction between the insulin receptor and its downstream effectors. Use of individually expressed receptor domains for structure/function analysis. *J Biol Chem,* 271**,** 6998-7003.

PENDE, M., KOZMA, S. C., JAQUET, M., OORSCHOT, V., BURCELIN, R., LE MARCHAND-BRUSTEL, Y., KLUMPERMAN, J., THORENS, B. & THOMAS, G. 2000. Hypoinsulinaemia, glucose intolerance and diminished beta-cell size in S6K1-deficient mice. *Nature,* 408**,** 994-7.

PERALDI, P., HOTAMISLIGIL, G. S., BUURMAN, W. A., WHITE, M. F. & SPIEGELMAN, B. M. 1996. Tumor necrosis factor (TNF)-alpha inhibits insulin signaling through stimulation of the p55 TNF receptor and activation of sphingomyelinase. *J Biol Chem,* 271**,** 13018-22.

PETER, A., WEIGERT, C., STAIGER, H., MACHICAO, F., SCHICK, F., MACHANN, J., STEFAN, N., THAMER, C., HARING, H. U. & SCHLEICHER, E. 2009. Individual stearoyl-coa desaturase 1 expression modulates endoplasmic reticulum stress and inflammation in human myotubes and is associated with skeletal muscle lipid storage and insulin sensitivity in vivo. *Diabetes,* 58**,** 1757-65.

PLOEGH, H. L., ORR, H. T. & STOMINGER, J. L. 1981. Biosynthesis and cell surface localization of nonglycosylated human histocompatibility antigens. *J Immunol,* 126**,** 270-5.

POLYMEROPOULOS, M. H., LAVEDAN, C., LEROY, E., IDE, S. E., DEHEJIA, A., DUTRA, A., PIKE, B., ROOT, H., RUBENSTEIN, J., BOYER, R., STENROOS, E. S., CHANDRASEKHARAPPA, S., ATHANASSIADOU, A., PAPAPETROPOULOS, T., JOHNSON, W. G., LAZZARINI, A. M., DUVOISIN, R. C., DI IORIO, G., GOLBE, L. I. & NUSSBAUM, R. L. 1997. Mutation in the alpha-synuclein gene identified in families with Parkinson's disease. *Science,* 276**,** 2045-7.

POWELL, W. S. & HEACOCK, R. A. 1973. The oxidation of 6-hydroxydopamine. *J Pharm Pharmacol,* 25**,** 193-200.

PRAGER, D., YAMASAKI, H., WEBER, M. M., GEBREMEDHIN, S. & MELMED, S. 1992. Human insulin-like growth factor I receptor function in pituitary cells is suppressed by a dominant negative mutant. *J Clin Invest,* 90**,** 2117-22.

PRESGRAVES, S. P., AHMED, T., BORWEGE, S. & JOYCE, J. N. 2004. Terminally differentiated SH-SY5Y cells provide a model system for studying neuroprotective effects of dopamine agonists. *Neurotox Res,* 5**,** 579-98.

PRESSLEY, J. C., LOUIS, E. D., TANG, M. X., COTE, L., COHEN, P. D., GLIED, S. & MAYEUX, R. 2003. The impact of comorbid disease and injuries on resource use and expenditures in parkinsonism. *Neurology,* 60**,** 87-93.

PROMLEK, T., ISHIWATA-KIMATA, Y., SHIDO, M., SAKURAMOTO, M., KOHNO, K. & KIMATA, Y. 2011. Membrane aberrancy and unfolded proteins activate the endoplasmic reticulum stress sensor Ire1 in different ways. *Mol Biol Cell,* 22**,** 3520-32.

PURI, P., MIRSHAHI, F., CHEUNG, O., NATARAJAN, R., MAHER, J. W., KELLUM, J. M. & SANYAL, A. J. 2008. Activation and dysregulation of the unfolded protein response in nonalcoholic fatty liver disease. *Gastroenterology,* 134**,** 568-76.

PUTHALAKATH, H., O'REILLY, L. A., GUNN, P., LEE, L., KELLY, P. N., HUNTINGTON, N. D., HUGHES, P. D., MICHALAK, E. M., MCKIMM-BRESCHKIN, J., MOTOYAMA, N., GOTOH, T., AKIRA, S., BOUILLET, P. & STRASSER, A. 2007. ER stress triggers apoptosis by activating BH3-only protein Bim. *Cell,* 129**,** 1337-49.

QI, C. & PEKALA, P. H. 2000. Tumor necrosis factor-alpha-induced insulin resistance in adipocytes. *Proc Soc Exp Biol Med,* 223**,** 128-35.

QIAO, L. Y., GOLDBERG, J. L., RUSSELL, J. C. & SUN, X. J. 1999. Identification of enhanced serine kinase activity in insulin resistance. *J Biol Chem,* 274**,** 10625-32.

QIAO, L. Y., ZHANDE, R., JETTON, T. L., ZHOU, G. & SUN, X. J. 2002. In vivo phosphorylation of insulin receptor substrate 1 at serine 789 by a novel serine kinase in insulin-resistant rodents. *J Biol Chem,* 277**,** 26530-9.

RACITI, M., LOTTI, L. V., VALIA, S., PULCINELLI, F. M. & DI RENZO, L. 2012. JNK2 is activated during ER stress and promotes cell survival. *Cell Death Dis,* 3**,** e429.

RAHMANI, M., PERON, P., WEITZMAN, J., BAKIRI, L., LARDEUX, B. & BERNUAU, D. 2001. Functional cooperation between JunD and NF-kappaB in rat hepatocytes. *Oncogene,* 20**,** 5132-42.

RAINGEAUD, J., GUPTA, S., ROGERS, J. S., DICKENS, M., HAN, J., ULEVITCH, R. J. & DAVIS, R. J. 1995. Pro-inflammatory cytokines and environmental stress cause p38 mitogen-activated protein kinase activation by dual phosphorylation on tyrosine and threonine. *J Biol Chem,* 270**,** 7420-6.

RAINGEAUD, J., WHITMARSH, A. J., BARRETT, T., DERIJARD, B. & DAVIS, R. J. 1996. MKK3- and MKK6-regulated gene expression is mediated by the p38

mitogen-activated protein kinase signal transduction pathway. *Mol Cell Biol,* 16**,** 1247-55.

RAMAN, M., CHEN, W. & COBB, M. H. 2007. Differential regulation and properties of MAPKs. *Oncogene,* 26**,** 3100-12.

RANGANATHAN, A. C., ZHANG, L., ADAM, A. P. & AGUIRRE-GHISO, J. A. 2006. Functional coupling of p38-induced up-regulation of BiP and activation of RNA-dependent protein kinase-like endoplasmic reticulum kinase to drug resistance of dormant carcinoma cells. *Cancer Res,* 66**,** 1702-11.

RAVICHANDRAN, L. V., ESPOSITO, D. L., CHEN, J. & QUON, M. J. 2001. Protein kinase C-zeta phosphorylates insulin receptor substrate-1 and impairs its ability to activate phosphatidylinositol 3-kinase in response to insulin. *J Biol Chem,* 276**,** 3543-9.

RECIO-PINTO, E., RECHLER, M. M. & ISHII, D. N. 1986. Effects of insulin, insulin-like growth factor-II, and nerve growth factor on neurite formation and survival in cultured sympathetic and sensory neurons. *J Neurosci,* 6**,** 1211-9.

REED, B. C. & LANE, M. D. 1980. Insulin receptor synthesis and turnover in differentiating 3T3-L1 preadipocytes. *Proc Natl Acad Sci U S A,* 77**,** 285-9.

REED, B. C., RONNETT, G. V., CLEMENTS, P. R. & LANE, M. D. 1981a. Regulation of insulin receptor metabolism. Differentiation-induced alteration of receptor synthesis and degradation. *J Biol Chem,* 256**,** 3917-25.

REED, B. C., RONNETT, G. V. & LANE, M. D. 1981b. Role of glycosylation and protein synthesis in insulin receptor metabolism by 3T3-L1 mouse adipocytes. *Proc Natl Acad Sci U S A,* 78**,** 2908-12.

REED, S. G. 1999. TGF-beta in infections and infectious diseases. *Microbes Infect,* 1**,** 1313-25.

REERS, M., SMITH, T. W. & CHEN, L. B. 1991. J-aggregate formation of a carbocyanine as a quantitative fluorescent indicator of membrane potential. *Biochemistry,* 30**,** 4480-6.

REN, L. P., CHAN, S. M., ZENG, X. Y., LAYBUTT, D. R., ISELI, T. J., SUN, R. Q., KRAEGEN, E. W., COONEY, G. J., TURNER, N. & YE, J. M. 2012. Differing endoplasmic reticulum stress response to excess lipogenesis versus lipid oversupply in relation to hepatic steatosis and insulin resistance. *PLoS One,* 7**,** e30816.

RHODES, C. J. & WHITE, M. F. 2002. Molecular insights into insulin action and secretion. *Eur J Clin Invest,* 32 Suppl 3**,** 3-13.

RIEUSSET, J., CHAUVIN, M. A., DURAND, A., BRAVARD, A., LAUGERETTE, F., MICHALSKI, M. C. & VIDAL, H. 2012. Reduction of endoplasmic reticulum stress using chemical chaperones or Grp78 overexpression does not protect muscle cells from palmitate-induced insulin resistance. *Biochem Biophys Res Commun,* 417**,** 439-45.

RIUS, J., GUMA, M., SCHACHTRUP, C., AKASSOGLOU, K., ZINKERNAGEL, A. S., NIZET, V., JOHNSON, R. S., HADDAD, G. G. & KARIN, M. 2008. NF-kappaB links innate immunity to the hypoxic response through transcriptional regulation of HIF-1alpha. *Nature,* 453**,** 807-11.

ROBERTSON, B. J., MOEHRING, J. M. & MOEHRING, T. J. 1993. Defective processing of the insulin receptor in an endoprotease-deficient Chinese hamster cell strain is corrected by expression of mouse furin. *J Biol Chem,* 268**,** 24274-7.

ROHRL, C., EIGNER, K., WINTER, K., KORBELIUS, M., OBROWSKY, S., KRATKY, D., KOVACS, W. J. & STANGL, H. 2014. Endoplasmic reticulum stress impairs cholesterol efflux and synthesis in hepatic cells. *J Lipid Res,* 55**,** 94-103.

RON, D. & WALTER, P. 2007. Signal integration in the endoplasmic reticulum unfolded protein response. *Nat Rev Mol Cell Biol,* 8**,** 519-29.

RONNETT, G. V., KNUTSON, V. P., KOHANSKI, R. A., SIMPSON, T. L. & LANE, M. D. 1984. Role of glycosylation in the processing of newly translated insulin proreceptor in 3T3-L1 adipocytes. *J Biol Chem,* 259**,** 4566-75.

ROSS, R. A., SPENGLER, B. A. & BIEDLER, J. L. 1983. Coordinate morphological and biochemical interconversion of human neuroblastoma cells. *J Natl Cancer Inst,* 71**,** 741-7.

ROULSTON, A., REINHARD, C., AMIRI, P. & WILLIAMS, L. T. 1998. Early activation of c-Jun N-terminal kinase and p38 kinase regulate cell survival in response to tumor necrosis factor alpha. *J Biol Chem,* 273**,** 10232-9.

RUBARTELLI, A., COZZOLINO, F., TALIO, M. & SITIA, R. 1990. A novel secretory pathway for interleukin-1 beta, a protein lacking a signal sequence. *EMBO J,* 9**,** 1503-10.

RUBIN, C. S., HIRSCH, A., FUNG, C. & ROSEN, O. M. 1978. Development of hormone receptors and hormonal responsiveness in vitro. Insulin receptors and insulin sensitivity in the preadipocyte and adipocyte forms of 3T3-L1 cells. *J Biol Chem,* 253**,** 7570-8.

RUDDOCK, M. W., STEIN, A., LANDAKER, E., PARK, J., COOKSEY, R. C., MCCLAIN, D. & PATTI, M. E. 2008. Saturated fatty acids inhibit hepatic insulin action by modulating insulin receptor expression and post-receptor signalling. *J Biochem,* 144**,** 599-607.

RUI, L., AGUIRRE, V., KIM, J. K., SHULMAN, G. I., LEE, A., CORBOULD, A., DUNAIF, A. & WHITE, M. F. 2001. Insulin/IGF-1 and TNF-alpha stimulate phosphorylation of IRS-1 at inhibitory Ser307 via distinct pathways. *J Clin Invest,* 107**,** 181-9.

RYU, E. J., HARDING, H. P., ANGELASTRO, J. M., VITOLO, O. V., RON, D. & GREENE, L. A. 2002. Endoplasmic reticulum stress and the unfolded protein response in cellular models of Parkinson's disease. *J Neurosci,* 22**,** 10690-8.

SACCANI, S., PANTANO, S. & NATOLI, G. 2002. p38-Dependent marking of inflammatory genes for increased NF-kappa B recruitment. *Nat Immunol,* 3**,** 69-75.

SAHA, A. R., NINKINA, N. N., HANGER, D. P., ANDERTON, B. H., DAVIES, A. M. & BUCHMAN, V. L. 2000. Induction of neuronal death by alpha-synuclein. *Eur J Neurosci,* 12**,** 3073-7.

SALLER, C. F. & CHIODO, L. A. 1980. Glucose suppresses basal firing and haloperidol-induced increases in the firing rate of central dopaminergic neurons. *Science,* 210**,** 1269-71.

SANCHEZ-PEREZ, I., MURGUIA, J. R. & PERONA, R. 1998. Cisplatin induces a persistent activation of JNK that is related to cell death. *Oncogene,* 16**,** 533-40.

SANDOW, J. J., DORSTYN, L., O'REILLY, L. A., TAILLER, M., KUMAR, S., STRASSER, A. & EKERT, P. G. 2014. ER stress does not cause upregulation and activation of caspase-2 to initiate apoptosis. *Cell Death Differ,* 21**,** 475-80.

SANTIAGO, J. A. & POTASHKIN, J. A. 2013. Shared dysregulated pathways lead to Parkinson's disease and diabetes. *Trends Mol Med,* 19**,** 176-86.

SAVOIE, S., RINDRESS, D., POSNER, B. I. & BERGERON, J. J. 1986. Tunicamycin sensitivity of prolactin, insulin and epidermal growth factor receptors in rat liver plasmalemma. *Mol Cell Endocrinol,* 45**,** 241-6.

SCHAPIRA, A. H., COOPER, J. M., DEXTER, D., CLARK, J. B., JENNER, P. & MARSDEN, C. D. 1990. Mitochondrial complex I deficiency in Parkinson's disease. *J Neurochem,* 54**,** 823-7.

SCHONTHAL, A., SUGARMAN, J., BROWN, J. H., HANLEY, M. R. & FERAMISCO, J. R. 1991. Regulation of c-fos and c-jun protooncogene expression by the Ca(2+)-ATPase inhibitor thapsigargin. *Proc Natl Acad Sci U S A,* 88**,** 7096-100.

SCHRODER, M. 2006. The unfolded protein response. *Mol Biotechnol,* 34**,** 279-90.

SCHRODER, M. & KAUFMAN, R. J. 2005a. ER stress and the unfolded protein response. *Mutat Res,* 569**,** 29-63.

SCHRODER, M. & KAUFMAN, R. J. 2005b. The mammalian unfolded protein response. *Annu Rev Biochem,* 74**,** 739-89.

SCHULINGKAMP, R. J., PAGANO, T. C., HUNG, D. & RAFFA, R. B. 2000. Insulin receptors and insulin action in the brain: review and clinical implications. *Neurosci Biobehav Rev,* 24**,** 855-72.

SCHWAB, R. S. 1960. Progression and prognosis in Parkinson's disease. *J Nerv Ment Dis,* 130**,** 556-66.

SERHAN, C. N. 2010. Novel lipid mediators and resolution mechanisms in acute inflammation: to resolve or not? *Am J Pathol,* 177**,** 1576-91.

SESTI, G., FEDERICI, M., LAURO, D., SBRACCIA, P. & LAURO, R. 2001. Molecular mechanism of insulin resistance in type 2 diabetes mellitus: role of the insulin receptor variant forms. *Diabetes Metab Res Rev,* 17**,** 363-73.

SHAH, O. J., WANG, Z. & HUNTER, T. 2004. Inappropriate activation of the TSC/Rheb/mTOR/S6K cassette induces IRS1/2 depletion, insulin resistance, and cell survival deficiencies. *Curr Biol,* 14**,** 1650-6.

SHARMA, M., URANO, F. & JAESCHKE, A. 2012a. Cdc42 and Rac1 are major contributors to the saturated fatty acid-stimulated JNK pathway in hepatocytes. *J Hepatol,* 56**,** 192-8.

SHARMA, N., BHAT, A. D., KASSA, A. D., XIAO, Y., ARIAS, E. B. & CARTEE, G. D. 2012b. Improved insulin sensitivity with calorie restriction does not require reduced JNK1/2, p38, or ERK1/2 phosphorylation in skeletal muscle of 9-month-old rats. *Am J Physiol Regul Integr Comp Physiol,* 302**,** R126-36.

SHARMA, N. K., DAS, S. K., MONDAL, A. K., HACKNEY, O. G., CHU, W. S., KERN, P. A., RASOULI, N., SPENCER, H. J., YAO-BORENGASSER, A. & ELBEIN, S. C. 2008. Endoplasmic reticulum stress markers are associated with obesity in nondiabetic subjects. *J Clin Endocrinol Metab,* 93**,** 4532-41.

SHENDELMAN, S., JONASON, A., MARTINAT, C., LEETE, T. & ABELIOVICH, A. 2004. DJ-1 is a redox-dependent molecular chaperone that inhibits alpha-synuclein aggregate formation. *PLoS Biol,* 2**,** e362.

SHENG, W., ZONG, Y., MOHAMMAD, A., AJIT, D., CUI, J., HAN, D., HAMILTON, J. L., SIMONYI, A., SUN, A. Y., GU, Z., HONG, J. S., WEISMAN, G. A. & SUN, G. Y. 2011. Pro-inflammatory cytokines and lipopolysaccharide induce changes in cell morphology, and upregulation of ERK1/2, iNOS and sPLA(2)-IIA expression in astrocytes and microglia. *J Neuroinflammation,* 8**,** 121.

SHERER, T. B., BETARBET, R., KIM, J. H. & GREENAMYRE, J. T. 2003a. Selective microglial activation in the rat rotenone model of Parkinson's disease. *Neurosci Lett,* 341**,** 87-90.

SHERER, T. B., KIM, J. H., BETARBET, R. & GREENAMYRE, J. T. 2003b. Subcutaneous rotenone exposure causes highly selective dopaminergic degeneration and alpha-synuclein aggregation. *Exp Neurol,* 179**,** 9-16.

SHIMADA, Y., KOBAYASHI, H., KAWAGOE, S., AOKI, K., KANESHIRO, E., SHIMIZU, H., ETO, Y., IDA, H. & OHASHI, T. 2011. Endoplasmic reticulum stress induces autophagy through activation of p38 MAPK in fibroblasts from Pompe disease patients carrying c.546G>T mutation. *Mol Genet Metab,* 104**,** 566-73.

SHIMURA, H., HATTORI, N., KUBO, S., MIZUNO, Y., ASAKAWA, S., MINOSHIMA, S., SHIMIZU, N., IWAI, K., CHIBA, T., TANAKA, K. & SUZUKI, T. 2000. Familial Parkinson disease gene product, parkin, is a ubiquitin-protein ligase. *Nat Genet,* 25**,** 302-5.

SHULMAN, G. I. 1999. Cellular mechanisms of insulin resistance in humans. *Am J Cardiol,* 84**,** 3J-10J.

SIESJO, B. K. & SIESJO, P. 1996. Mechanisms of secondary brain injury. *Eur J Anaesthesiol,* 13**,** 247-68.

SIRTORI, C. R., BOLME, P. & AZARNOFF, D. L. 1972. Metabolic responses to acute and chronic L-dopa administration in patients with parkinsonism. *N Engl J Med,* 287**,** 729-33.

SLUSS, H. K., BARRETT, T., DERIJARD, B. & DAVIS, R. J. 1994. Signal transduction by tumor necrosis factor mediated by JNK protein kinases. *Mol Cell Biol,* 14**,** 8376-84.

SMILEY, S. T., REERS, M., MOTTOLA-HARTSHORN, C., LIN, M., CHEN, A., SMITH, T. W., STEELE, G. D., JR. & CHEN, L. B. 1991. Intracellular heterogeneity in mitochondrial membrane potentials revealed by a J-aggregate-forming lipophilic cation JC-1. *Proc Natl Acad Sci U S A,* 88**,** 3671-5.

SMITH, M. I. & DESHMUKH, M. 2007. Endoplasmic reticulum stress-induced apoptosis requires bax for commitment and Apaf-1 for execution in primary neurons. *Cell Death Differ,* 14**,** 1011-9.

SMITH, W. W., JIANG, H., PEI, Z., TANAKA, Y., MORITA, H., SAWA, A., DAWSON, V. L., DAWSON, T. M. & ROSS, C. A. 2005. Endoplasmic reticulum stress and mitochondrial cell death pathways mediate A53T mutant alpha-synuclein-induced toxicity. *Hum Mol Genet,* 14**,** 3801-11.

SOKHI, J., SIKKA, R., RAINA, P., KAUR, R., MATHAROO, K., ARORA, P. & BHANWER, A. 2015. Association of genetic variants in INS (rs689), INSR (rs1799816) and PP1G.G (rs1799999) with type 2 diabetes (T2D): a case-control study in three ethnic groups from North-West India. *Mol Genet Genomics*.

SONG, J., WU, L., CHEN, Z., KOHANSKI, R. A. & PICK, L. 2003. Axons guided by insulin receptor in Drosophila visual system. *Science,* 300**,** 502-5.

SPARROW, L. G., MCKERN, N. M., GORMAN, J. J., STRIKE, P. M., ROBINSON, C. P., BENTLEY, J. D. & WARD, C. W. 1997. The disulfide bonds in the C-terminal domains of the human insulin receptor ectodomain. *J Biol Chem,* 272**,** 29460-7.

SPIELMAN, L. J., LITTLE, J. P. & KLEGERIS, A. 2014. Inflammation and insulin/IGF-1 resistance as the possible link between obesity and neurodegeneration. *J Neuroimmunol,* 273**,** 8-21.

SPILLANTINI, M. G., CROWTHER, R. A., JAKES, R., HASEGAWA, M. & GOEDERT, M. 1998. alpha-Synuclein in filamentous inclusions of Lewy bodies from Parkinson's disease and dementia with lewy bodies. *Proc Natl Acad Sci U S A,* 95**,** 6469-73.

SREEJAYAN, N., DONG, F., KANDADI, M. R., YANG, X. & REN, J. 2008. Chromium alleviates glucose intolerance, insulin resistance, and hepatic ER stress in obese mice. *Obesity (Silver Spring),* 16**,** 1331-7.

STANDEN, C. L., KENNEDY, N. J., FLAVELL, R. A. & DAVIS, R. J. 2009. Signal transduction cross talk mediated by Jun N-terminal kinase-interacting protein and insulin receptor substrate scaffold protein complexes. *Mol Cell Biol,* 29**,** 4831-40.

STEHLIK, C., DE MARTIN, R., KUMABASHIRI, I., SCHMID, J. A., BINDER, B. R. & LIPP, J. 1998. Nuclear factor (NF)-kappaB-regulated X-chromosome-linked iap gene expression protects endothelial cells from tumor necrosis factor alpha-induced apoptosis. *J Exp Med,* 188**,** 211-6.

STOLL, G., JANDER, S. & SCHROETER, M. 1998. Inflammation and glial responses in ischemic brain lesions. *Prog Neurobiol,* 56**,** 149-71.

STORCH, A., KAFTAN, A., BURKHARDT, K. & SCHWARZ, J. 2000. 6-Hydroxydopamine toxicity towards human SH-SY5Y dopaminergic neuroblastoma

cells: independent of mitochondrial energy metabolism. *J Neural Transm,* 107**,** 281-93.

SU, X., MAGUIRE-ZEISS, K. A., GIULIANO, R., PRIFTI, L., VENKATESH, K. & FEDEROFF, H. J. 2008. Synuclein activates microglia in a model of Parkinson's disease. *Neurobiol Aging,* 29**,** 1690-701.

SUGENO, N., TAKEDA, A., HASEGAWA, T., KOBAYASHI, M., KIKUCHI, A., MORI, F., WAKABAYASHI, K. & ITOYAMA, Y. 2008. Serine 129 phosphorylation of alpha-synuclein induces unfolded protein response-mediated cell death. *J Biol Chem,* 283**,** 23179-88.

SURI, C., FUNG, B. P., TISCHLER, A. S. & CHIKARAISHI, D. M. 1993. Catecholaminergic cell lines from the brain and adrenal glands of tyrosine hydroxylase-SV40 T antigen transgenic mice. *J Neurosci,* 13**,** 1280-91.

SVENSSON, C., PART, K., KUNNIS-BERES, K., KALDMAE, M., FERNAEUS, S. Z. & LAND, T. 2011. Pro-survival effects of JNK and p38 MAPK pathways in LPS-induced activation of BV-2 cells. *Biochem Biophys Res Commun,* 406**,** 488-92.

TAIRA, T., SAITO, Y., NIKI, T., IGUCHI-ARIGA, S. M., TAKAHASHI, K. & ARIGA, H. 2004. DJ-1 has a role in antioxidative stress to prevent cell death. *EMBO Rep,* 5**,** 213-8.

TAKAHASHI, K., MIZUARAI, S., ARAKI, H., MASHIKO, S., ISHIHARA, A., KANATANI, A., ITADANI, H. & KOTANI, H. 2003. Adiposity elevates plasma MCP-1 levels leading to the increased CD11b-positive monocytes in mice. *J Biol Chem,* 278**,** 46654-60.

TAKAHASHI, M., YAMADA, T., TOOYAMA, I., MOROO, I., KIMURA, H., YAMAMOTO, T. & OKADA, H. 1996. Insulin receptor mRNA in the substantia nigra in Parkinson's disease. *Neurosci Lett,* 204**,** 201-4.

TAKAHASHI, Y., OHOKA, N., HAYASHI, H. & SATO, R. 2008. TRB3 suppresses adipocyte differentiation by negatively regulating PPARgamma transcriptional activity. *J Lipid Res,* 49**,** 880-92.

TALBOT, U. M., PATON, J. C. & PATON, A. W. 2005. Protective immunization of mice with an active-site mutant of subtilase cytotoxin of Shiga toxin-producing Escherichia coli. *Infect Immun,* 73**,** 4432-6.

TANAKA, M., SAWADA, M., YOSHIDA, S., HANAOKA, F. & MARUNOUCHI, T. 1995. Insulin prevents apoptosis of external granular layer neurons in rat cerebellar slice cultures. *Neurosci Lett,* 199**,** 37-40.

TANG, F., TANG, G., XIANG, J., DAI, Q., ROSNER, M. R. & LIN, A. 2002. The absence of NF-kappaB-mediated inhibition of c-Jun N-terminal kinase activation contributes to tumor necrosis factor alpha-induced apoptosis. *Mol Cell Biol,* 22**,** 8571-9.

TANG, X., SHEN, H., CHEN, J., WANG, X., ZHANG, Y., CHEN, L. L., RUKACHAISIRIKUL, V., JIANG, H. L. & SHEN, X. 2011. Activating transcription factor 6 protects insulin receptor from ER stress-stimulated desensitization via p42/44 ERK pathway. *Acta Pharmacol Sin,* 32**,** 1138-47.

TANNER, C. M. 2003. PD or not PD? That is the question. *Neurology,* 61**,** 5-6.

TANSEY, M. G., MCCOY, M. K. & FRANK-CANNON, T. C. 2007. Neuroinflammatory mechanisms in Parkinson's disease: potential environmental triggers, pathways, and targets for early therapeutic intervention. *Exp Neurol,* 208**,** 1-25.

TANTI, J. F., GREMEAUX, T., VAN OBBERGHEN, E. & LE MARCHAND-BRUSTEL, Y. 1994. Serine/threonine phosphorylation of insulin receptor substrate 1 modulates insulin receptor signaling. *J Biol Chem,* 269**,** 6051-7.

TEODORO, T., ODISHO, T., SIDOROVA, E. & VOLCHUK, A. 2012. Pancreatic beta-cells depend on basal expression of active ATF6alpha-p50 for cell survival even under nonstress conditions. *Am J Physiol Cell Physiol,* 302**,** C992-1003.

TETRUD, J. W., LANGSTON, J. W., GARBE, P. L. & RUTTENBER, A. J. 1989. Mild parkinsonism in persons exposed to 1-methyl-4-phenyl-1,2,3,6-tetrahydropyridine (MPTP). *Neurology,* 39**,** 1483-7.

THUERAUF, D. J., ARNOLD, N. D., ZECHNER, D., HANFORD, D. S., DEMARTIN, K. M., MCDONOUGH, P. M., PRYWES, R. & GLEMBOTSKI, C. C. 1998. p38 Mitogen-activated protein kinase mediates the transcriptional induction of the atrial natriuretic factor gene through a serum response element. A potential role for the transcription factor ATF6. *J Biol Chem,* 273**,** 20636-43.

TIWARI, V. K., STADLER, M. B., WIRBELAUER, C., PARO, R., SCHUBELER, D. & BEISEL, C. 2012. A chromatin-modifying function of JNK during stem cell differentiation. *Nat Genet,* 44**,** 94-100.

TOBIUME, K., MATSUZAWA, A., TAKAHASHI, T., NISHITOH, H., MORITA, K., TAKEDA, K., MINOWA, O., MIYAZONO, K., NODA, T. & ICHIJO, H. 2001. ASK1 is required for sustained activations of JNK/p38 MAP kinases and apoptosis. *EMBO Rep,* 2**,** 222-8.

TOBIUME, K., SAITOH, M. & ICHIJO, H. 2002. Activation of apoptosis signal-regulating kinase 1 by the stress-induced activating phosphorylation of pre-formed oligomer. *J Cell Physiol,* 191**,** 95-104.

TOBON-VELASCO, J. C., LIMON-PACHECO, J. H., OROZCO-IBARRA, M., MACIAS-SILVA, M., VAZQUEZ-VICTORIO, G., CUEVAS, E., ALI, S. F., CUADRADO, A., PEDRAZA-CHAVERRI, J. & SANTAMARIA, A. 2013. 6-OHDA-induced apoptosis and mitochondrial dysfunction are mediated by early modulation of intracellular signals and interaction of Nrf2 and NF-kappaB factors. *Toxicology,* 304**,** 109-19.

TONG, M., DONG, M. & DE LA MONTE, S. M. 2009. Brain insulin-like growth factor and neurotrophin resistance in Parkinson's disease and dementia with Lewy bodies: potential role of manganese neurotoxicity. *J Alzheimers Dis,* 16**,** 585-99.

TORNQVIST, H. E. & AVRUCH, J. 1988. Relationship of site-specific beta subunit tyrosine autophosphorylation to insulin activation of the insulin receptor (tyrosine) protein kinase activity. *J Biol Chem,* 263**,** 4593-601.

TORNQVIST, H. E., GUNSALUS, J. R., NEMENOFF, R. A., FRACKELTON, A. R., PIERCE, M. W. & AVRUCH, J. 1988. Identification of the insulin receptor tyrosine residues undergoing insulin-stimulated phosphorylation in intact rat hepatoma cells. *J Biol Chem,* 263**,** 350-9.

TOURNIER, C., HESS, P., YANG, D. D., XU, J., TURNER, T. K., NIMNUAL, A., BAR-SAGI, D., JONES, S. N., FLAVELL, R. A. & DAVIS, R. J. 2000. Requirement of JNK for stress-induced activation of the cytochrome c-mediated death pathway. *Science,* 288**,** 870-4.

TOURNIER, C., WHITMARSH, A. J., CAVANAGH, J., BARRETT, T. & DAVIS, R. J. 1997. Mitogen-activated protein kinase kinase 7 is an activator of the c-Jun NH2-terminal kinase. *Proc Natl Acad Sci U S A,* 94**,** 7337-42.

TOURNIER, C., WHITMARSH, A. J., CAVANAGH, J., BARRETT, T. & DAVIS, R. J. 1999. The MKK7 gene encodes a group of c-Jun NH2-terminal kinase kinases. *Mol Cell Biol,* 19**,** 1569-81.

TOUZANI, O., BOUTIN, H., CHUQUET, J. & ROTHWELL, N. 1999. Potential mechanisms of interleukin-1 involvement in cerebral ischaemia. *J Neuroimmunol,* 100**,** 203-15.

TREMBLAY, F., KREBS, M., DOMBROWSKI, L., BREHM, A., BERNROIDER, E., ROTH, E., NOWOTNY, P., WALDHAUSL, W., MARETTE, A. & RODEN, M. 2005. Overactivation of S6 kinase 1 as a cause of human insulin resistance during increased amino acid availability. *Diabetes,* 54**,** 2674-84.

TROMBETTA, E. S. & PARODI, A. J. 2003. Quality control and protein folding in the secretory pathway. *Annu Rev Cell Dev Biol,* 19**,** 649-76.

TSUNEKAWA, S., YAMAMOTO, N., TSUKAMOTO, K., ITOH, Y., KANEKO, Y., KIMURA, T., ARIYOSHI, Y., MIURA, Y., OISO, Y. & NIKI, I. 2007. Protection of pancreatic beta-cells by exendin-4 may involve the reduction of endoplasmic reticulum stress; in vivo and in vitro studies. *J Endocrinol,* 193**,** 65-74.

UEMURA, K., KITAGAWA, N., KOHNO, R., KUZUYA, A., KAGEYAMA, T., SHIBASAKI, H. & SHIMOHAMA, S. 2003. Presenilin 1 mediates retinoic acid-induced differentiation of SH-SY5Y cells through facilitation of Wnt signaling. *J Neurosci Res,* 73**,** 166-75.

UM, S. H., FRIGERIO, F., WATANABE, M., PICARD, F., JOAQUIN, M., STICKER, M., FUMAGALLI, S., ALLEGRINI, P. R., KOZMA, S. C., AUWERX, J. & THOMAS, G. 2004. Absence of S6K1 protects against age- and diet-induced obesity while enhancing insulin sensitivity. *Nature,* 431**,** 200-5.

UNGER, J. W., MOSS, A. M. & LIVINGSTON, J. N. 1991. Immunohistochemical localization of insulin receptors and phosphotyrosine in the brainstem of the adult rat. *Neuroscience,* 42**,** 853-61.

UPTON, J. P., WANG, L., HAN, D., WANG, E. S., HUSKEY, N. E., LIM, L., TRUITT, M., MCMANUS, M. T., RUGGERO, D., GOGA, A., PAPA, F. R. & OAKES, S. A. 2012. IRE1alpha cleaves select microRNAs during ER stress to derepress translation of proapoptotic Caspase-2. *Science,* 338**,** 818-22.

URANO, F., WANG, X., BERTOLOTTI, A., ZHANG, Y., CHUNG, P., HARDING, H. P. & RON, D. 2000. Coupling of stress in the ER to activation of JNK protein kinases by transmembrane protein kinase IRE1. *Science,* 287**,** 664-6.

UYSAL, K. T., WIESBROCK, S. M., MARINO, M. W. & HOTAMISLIGIL, G. S. 1997. Protection from obesity-induced insulin resistance in mice lacking TNF-alpha function. *Nature,* 389**,** 610-4.

VALDES, P., MERCADO, G., VIDAL, R. L., MOLINA, C., PARSONS, G., COURT, F. A., MARTINEZ, A., GALLEGUILLOS, D., ARMENTANO, D., SCHNEIDER, B. L. & HETZ, C. 2014. Control of dopaminergic neuron survival by the unfolded protein response transcription factor XBP1. *Proc Natl Acad Sci U S A,* 111**,** 6804-9.

VAN WOERT, M. H. & MUELLER, P. S. 1971. Glucose, insulin, and free fatty acid metabolism in Parkinson's disease treated with levodopa. *Clin Pharmacol Ther,* 12**,** 360-7.

VENTURA, J. J., COGSWELL, P., FLAVELL, R. A., BALDWIN, A. S., JR. & DAVIS, R. J. 2004. JNK potentiates TNF-stimulated necrosis by increasing the production of cytotoxic reactive oxygen species. *Genes Dev,* 18**,** 2905-15.

VENTURA, J. J., HUBNER, A., ZHANG, C., FLAVELL, R. A., SHOKAT, K. M. & DAVIS, R. J. 2006. Chemical genetic analysis of the time course of signal transduction by JNK. *Mol Cell,* 21**,** 701-10.

VERFAILLIE, T., GARG, A. D. & AGOSTINIS, P. 2013. Targeting ER stress induced apoptosis and inflammation in cancer. *Cancer Lett,* 332**,** 249-64.

VIRGONE-CARLOTTA, A., UHLRICH, J., AKRAM, M. N., RESSNIKOFF, D., CHRETIEN, F., DOMENGET, C., GHERARDI, R., DESPARS, G., JURDIC, P., HONNORAT, J., NATAF, S. & TOURET, M. 2013. Mapping and kinetics of microglia/neuron cell-to-cell contacts in the 6-OHDA murine model of Parkinson's disease. *Glia,* 61**,** 1645-58.

VITALE, A. & DENECKE, J. 1999. The endoplasmic reticulum-gateway of the secretory pathway. *Plant Cell,* 11**,** 615-28.

WANG, H. G., PATHAN, N., ETHELL, I. M., KRAJEWSKI, S., YAMAGUCHI, Y., SHIBASAKI, F., MCKEON, F., BOBO, T., FRANKE, T. F. & REED, J. C. 1999.

Ca2+-induced apoptosis through calcineurin dephosphorylation of BAD. *Science,* 284**,** 339-43.

WANG, L., ZHAI, Y. Q., XU, L. L., QIAO, C., SUN, X. L., DING, J. H., LU, M. & HU, G. 2014. Metabolic inflammation exacerbates dopaminergic neuronal degeneration in response to acute MPTP challenge in type 2 diabetes mice. *Exp Neurol,* 251**,** 22-9.

WANG, M. C., BOHMANN, D. & JASPER, H. 2003a. JNK signaling confers tolerance to oxidative stress and extends lifespan in Drosophila. *Dev Cell,* 5**,** 811-6.

WANG, N., CHEN, W., LINSEL-NITSCHKE, P., MARTINEZ, L. O., AGERHOLM-LARSEN, B., SILVER, D. L. & TALL, A. R. 2003b. A PEST sequence in ABCA1 regulates degradation by calpain protease and stabilization of ABCA1 by apoA-I. *J Clin Invest,* 111**,** 99-107.

WANG, Q., ZHANG, H., ZHAO, B. & FEI, H. 2009. IL-1beta caused pancreatic beta-cells apoptosis is mediated in part by endoplasmic reticulum stress via the induction of endoplasmic reticulum Ca2+ release through the c-Jun N-terminal kinase pathway. *Mol Cell Biochem,* 324**,** 183-90.

WANG, X. Z., HARDING, H. P., ZHANG, Y., JOLICOEUR, E. M., KURODA, M. & RON, D. 1998. Cloning of mammalian Ire1 reveals diversity in the ER stress responses. *EMBO J,* 17**,** 5708-17.

WANG, X. Z. & RON, D. 1996. Stress-induced phosphorylation and activation of the transcription factor CHOP (GADD153) by p38 MAP Kinase. *Science,* 272**,** 1347-9.

WANG, Y., LIU, W., HE, X. & ZHOU, F. 2013. Parkinson's disease-associated DJ-1 mutations increase abnormal phosphorylation of tau protein through Akt/GSK-3beta pathways. *J Mol Neurosci,* 51**,** 911-8.

WANG, Y. & ORAM, J. F. 2002. Unsaturated fatty acids inhibit cholesterol efflux from macrophages by increasing degradation of ATP-binding cassette transporter A1. *J Biol Chem,* 277**,** 5692-7.

WANG, Z., BUTLER, P., LY, D., SPIOTTO, M., KOONG, A. C. & YANG, G. 2010. Activation of the Unfolded Protein Response in Wound Healing. *Journal of surgical research,* 158**,** 209.

WARNER, T. T. & SCHAPIRA, A. H. 2003. Genetic and environmental factors in the cause of Parkinson's disease. *Ann Neurol,* 53 Suppl 3**,** S16-23; discussion S23-5.

WATANABE, N., KURIYAMA, H., SONE, H., NEDA, H., YAMAUCHI, N., MAEDA, M. & NIITSU, Y. 1988. Continuous internalization of tumor necrosis factor receptors in a human myosarcoma cell line. *J Biol Chem,* 263**,** 10262-6.

WEERAPANA, E. & IMPERIALI, B. 2006. Asparagine-linked protein glycosylation: from eukaryotic to prokaryotic systems. *Glycobiology,* 16**,** 91R-101R.

WELTI, M. 2013. Regulation of dolichol-linked glycosylation. *Glycoconj J,* 30**,** 51-6.

WHITE, M. F. 2002. IRS proteins and the common path to diabetes. *Am J Physiol Endocrinol Metab,* 283**,** E413-22.

WHITE, M. F. 2003. Insulin signaling in health and disease. *Science,* 302**,** 1710-1.

WHITE, M. F., SHOELSON, S. E., KEUTMANN, H. & KAHN, C. R. 1988. A cascade of tyrosine autophosphorylation in the beta-subunit activates the phosphotransferase of the insulin receptor. *J Biol Chem,* 263**,** 2969-80.

WHITMARSH, A. J. & DAVIS, R. J. 1996. Transcription factor AP-1 regulation by mitogen-activated protein kinase signal transduction pathways. *J Mol Med (Berl),* 74**,** 589-607.

WILDEN, P. A., SIDDLE, K., HARING, E., BACKER, J. M., WHITE, M. F. & KAHN, C. R. 1992. The role of insulin receptor kinase domain autophosphorylation in receptor-mediated activities. Analysis with insulin and anti-receptor antibodies. *J Biol Chem,* 267**,** 13719-27.

WU, S., HU, Y., WANG, J. L., CHATTERJEE, M., SHI, Y. & KAUFMAN, R. J. 2002. Ultraviolet light inhibits translation through activation of the unfolded protein response kinase PERK in the lumen of the endoplasmic reticulum. *J Biol Chem,* 277**,** 18077-83.

WU, S., TAN, M., HU, Y., WANG, J. L., SCHEUNER, D. & KAUFMAN, R. J. 2004. Ultraviolet light activates NFkappaB through translational inhibition of IkappaBalpha synthesis. *J Biol Chem,* 279**,** 34898-902.

WU, Y., ZHANG, H., DONG, Y., PARK, Y. M. & IP, C. 2005. Endoplasmic reticulum stress signal mediators are targets of selenium action. *Cancer Res,* 65**,** 9073-9.

WYSS-CORAY, T. & MUCKE, L. 2002. Inflammation in neurodegenerative disease--a double-edged sword. *Neuron,* 35**,** 419-32.

XIE, H. R., HU, L. S. & LI, G. Y. 2010. SH-SY5Y human neuroblastoma cell line: in vitro cell model of dopaminergic neurons in Parkinson's disease. *Chin Med J (Engl),* 123**,** 1086-92.

XU, L., SPINAS, G. A. & NIESSEN, M. 2010. ER stress in adipocytes inhibits insulin signaling, represses lipolysis, and alters the secretion of adipokines without inhibiting glucose transport. *Horm Metab Res,* 42**,** 643-51.

XUE, L. & LUCOCQ, J. M. 1997. Low extracellular pH induces activation of ERK 2, JNK, and p38 in A431 and Swiss 3T3 cells. *Biochem Biophys Res Commun,* 241**,** 236-42.

XUE, X., PIAO, J. H., NAKAJIMA, A., SAKON-KOMAZAWA, S., KOJIMA, Y., MORI, K., YAGITA, H., OKUMURA, K., HARDING, H. & NAKANO, H. 2005. Tumor necrosis factor alpha (TNFalpha) induces the unfolded protein response (UPR) in a reactive oxygen species (ROS)-dependent fashion, and the UPR counteracts ROS accumulation by TNFalpha. *J Biol Chem,* 280**,** 33917-25.

YAMAGUCHI, H. & WANG, H. G. 2004. CHOP is involved in endoplasmic reticulum stress-induced apoptosis by enhancing DR5 expression in human carcinoma cells. *J Biol Chem,* 279**,** 45495-502.

YAMAMURO, A., YOSHIOKA, Y., OGITA, K. & MAEDA, S. 2006. Involvement of endoplasmic reticulum stress on the cell death induced by 6-hydroxydopamine in human neuroblastoma SH-SY5Y cells. *Neurochem Res,* 31**,** 657-64.

YAMAZAKI, H., HIRAMATSU, N., HAYAKAWA, K., TAGAWA, Y., OKAMURA, M., OGATA, R., HUANG, T., NAKAJIMA, S., YAO, J., PATON, A. W., PATON, J. C. & KITAMURA, M. 2009. Activation of the Akt-NF-kappaB pathway by subtilase cytotoxin through the ATF6 branch of the unfolded protein response. *J Immunol,* 183**,** 1480-7.

YANG, D. D., KUAN, C. Y., WHITMARSH, A. J., RINCON, M., ZHENG, T. S., DAVIS, R. J., RAKIC, P. & FLAVELL, R. A. 1997. Absence of excitotoxicity-induced apoptosis in the hippocampus of mice lacking the Jnk3 gene. *Nature,* 389**,** 865-70.

YAZDANI, U., GERMAN, D. C., LIANG, C. L., MANZINO, L., SONSALLA, P. K. & ZEEVALK, G. D. 2006. Rat model of Parkinson's disease: chronic central delivery of 1-methyl-4-phenylpyridinium (MPP+). *Exp Neurol,* 200**,** 172-83.

YE, R., JUNG, D. Y., JUN, J. Y., LI, J., LUO, S., KO, H. J., KIM, J. K. & LEE, A. S. 2010. Grp78 heterozygosity promotes adaptive unfolded protein response and attenuates diet-induced obesity and insulin resistance. *Diabetes,* 59**,** 6-16.

YEH, W. C., SHAHINIAN, A., SPEISER, D., KRAUNUS, J., BILLIA, F., WAKEHAM, A., DE LA POMPA, J. L., FERRICK, D., HUM, B., ISCOVE, N., OHASHI, P., ROTHE, M., GOEDDEL, D. V. & MAK, T. W. 1997. Early lethality, functional NF-kappaB activation, and increased sensitivity to TNF-induced cell death in TRAF2-deficient mice. *Immunity,* 7**,** 715-25.

YOKOTA, T., SUGAWARA, K., ITO, K., TAKAHASHI, R., ARIGA, H. & MIZUSAWA, H. 2003. Down regulation of DJ-1 enhances cell death by oxidative stress, ER stress, and proteasome inhibition. *Biochem Biophys Res Commun,* 312**,** 1342-8.

YOSHIE, O., TADA, K. & ISHIDA, N. 1986. Binding and crosslinking of 125I-labeled recombinant human tumor necrosis factor to cell surface receptors. *J Biochem,* 100**,** 531-41.

YOSHIUCHI, K., KANETO, H., MATSUOKA, T. A., KASAMI, R., KOHNO, K., IWAWAKI, T., NAKATANI, Y., YAMASAKI, Y., SHIMOMURA, I. & MATSUHISA, M. 2009. Pioglitazone reduces ER stress in the liver: direct monitoring of in vivo ER stress using ER stress-activated indicator transgenic mice. *Endocr J,* 56**,** 1103-11.

YU, C., MINEMOTO, Y., ZHANG, J., LIU, J., TANG, F., BUI, T. N., XIANG, J. & LIN, A. 2004. JNK suppresses apoptosis via phosphorylation of the proapoptotic Bcl-2 family protein BAD. *Mol Cell,* 13**,** 329-40.

YUAN, M., KONSTANTOPOULOS, N., LEE, J., HANSEN, L., LI, Z. W., KARIN, M. & SHOELSON, S. E. 2001. Reversal of obesity- and diet-induced insulin resistance with salicylates or targeted disruption of Ikkbeta. *Science,* 293**,** 1673-7.

ZENG, L., LU, M., MORI, K., LUO, S., LEE, A. S., ZHU, Y. & SHYY, J. Y. 2004. ATF6 modulates SREBP2-mediated lipogenesis. *EMBO J,* 23**,** 950-8.

ZEYDA, M. & STULNIG, T. M. 2007. Adipose tissue macrophages. *Immunol Lett,* 112**,** 61-7.

ZHANG, C., KAWAUCHI, J., ADACHI, M. T., HASHIMOTO, Y., OSHIRO, S., ASO, T. & KITAJIMA, S. 2001. Activation of JNK and transcriptional repressor ATF3/LRF1 through the IRE1/TRAF2 pathway is implicated in human vascular endothelial cell death by homocysteine. *Biochem Biophys Res Commun,* 289**,** 718-24.

ZHANG, D. D. 2006. Mechanistic studies of the Nrf2-Keap1 signaling pathway. *Drug Metab Rev,* 38**,** 769-89.

ZHANG, J., TANG, J., CAO, B., ZHANG, Z., LI, J., SCHIMMER, A. D., HE, S. & MAO, X. 2013. The natural pesticide dihydrorotenone induces human plasma cell apoptosis by triggering endoplasmic reticulum stress and activating p38 signaling pathway. *PLoS One,* 8**,** e69911.

ZHANG, K. & KAUFMAN, R. J. 2008. From endoplasmic-reticulum stress to the inflammatory response. *Nature,* 454**,** 455-62.

ZHANG, K., SHEN, X., WU, J., SAKAKI, K., SAUNDERS, T., RUTKOWSKI, D. T., BACK, S. H. & KAUFMAN, R. J. 2006. Endoplasmic reticulum stress activates cleavage of CREBH to induce a systemic inflammatory response. *Cell,* 124**,** 587-99.

ZHANG, L. & WANG, A. 2012. Virus-induced ER stress and the unfolded protein response. *Front Plant Sci,* 3**,** 293.

ZHANG, X. & MOSSER, D. M. 2008. Macrophage activation by endogenous danger signals. *J Pathol,* 214**,** 161-78.

ZHAO, P., XIAO, X., KIM, A. S., LEITE, M. F., XU, J., ZHU, X., REN, J. & LI, J. 2008. c-Jun inhibits thapsigargin-induced ER stress through up-regulation of DSCR1/Adapt78. *Exp Biol Med (Maywood),* 233**,** 1289-300.

ZHOU, L., ZHANG, J., FANG, Q., LIU, M., LIU, X., JIA, W., DONG, L. Q. & LIU, F. 2009. Autophagy-mediated insulin receptor down-regulation contributes to endoplasmic reticulum stress-induced insulin resistance. *Mol Pharmacol,* 76**,** 596-603.

ZINSZNER, H., KURODA, M., WANG, X., BATCHVAROVA, N., LIGHTFOOT, R. T., REMOTTI, H., STEVENS, J. L. & RON, D. 1998. CHOP is implicated in

programmed cell death in response to impaired function of the endoplasmic reticulum. *Genes Dev,* 12**,** 982-95.

INVESTIGATION OF HOW ENDOPLASMIC RETICULUM STRESS CAUSES INSULIN RESISTANCE AND NEUROINFLAMMATION

Volume II

Appendices

Max Adam Brown

This thesis is submitted as part of the requirements for the award of Degree of Doctor of Philosophy

School of Biological and Biomedical Sciences

Durham University

July 2015

TABLE OF CONTENTS

APPENDICES

Appendix A

Representarive melt curves from RT-qPCR performed on a RotorGene machine.

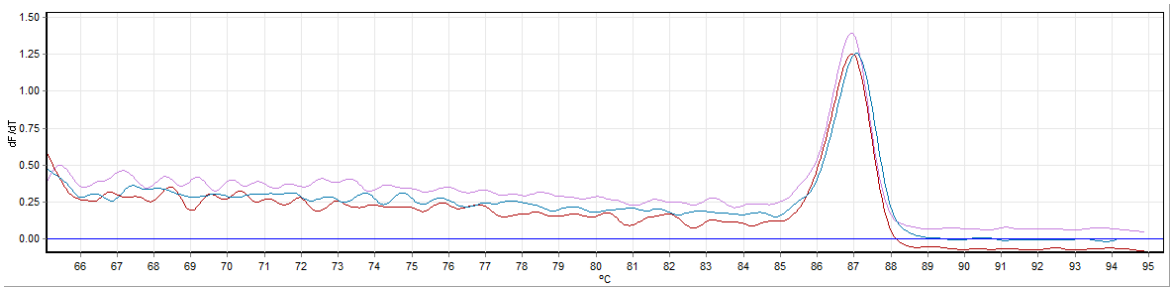

Human *ACTA1*

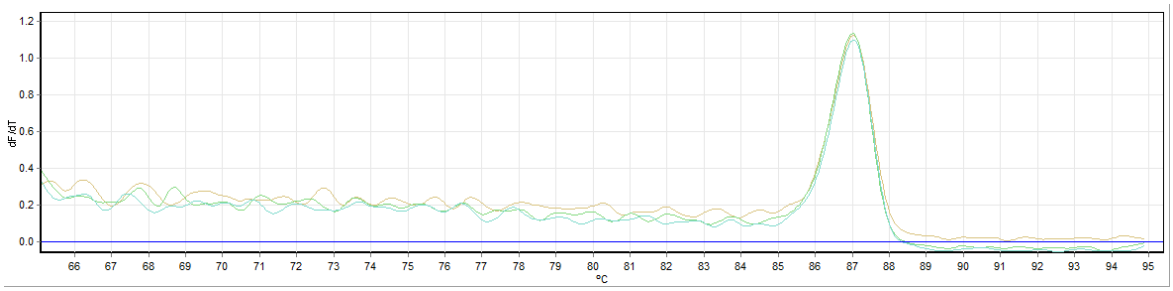

Human *IL-6*

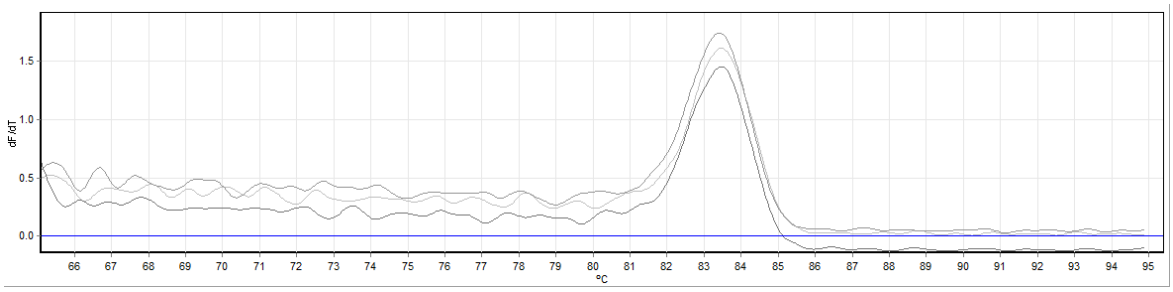

Human *IL-8*

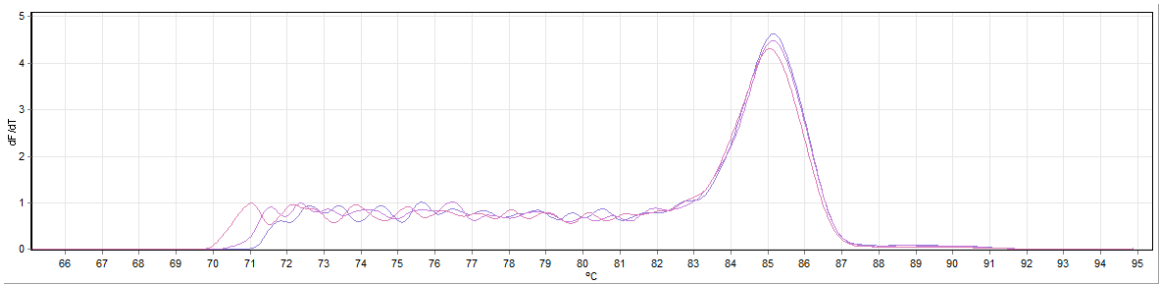

Human *IRE1α*

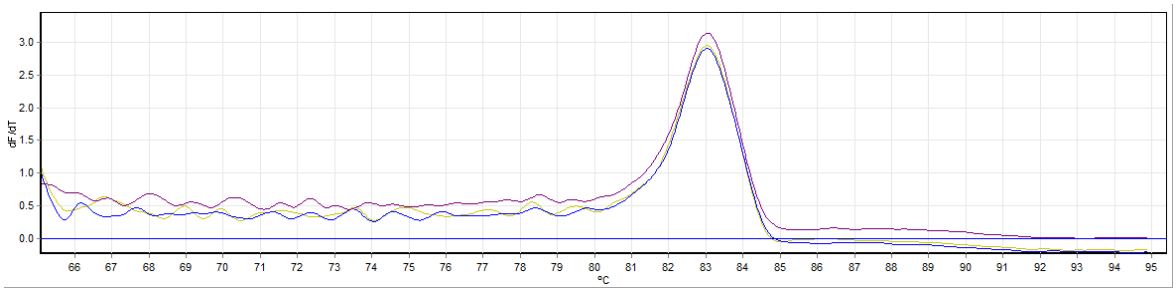

Human *GAPDH*

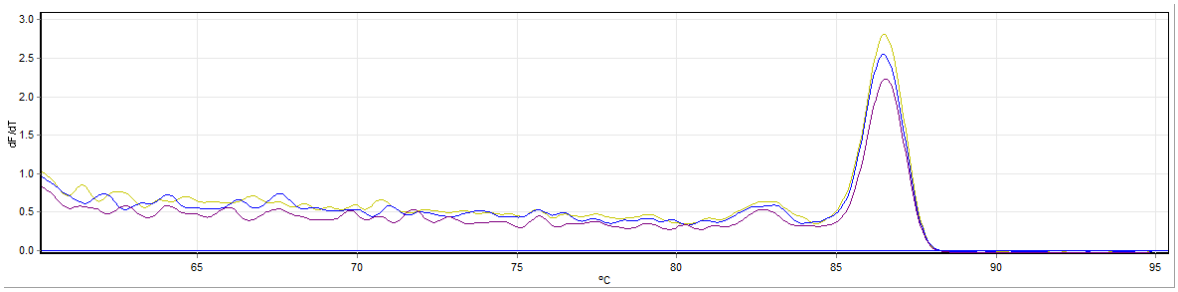

Human *TRAF2*

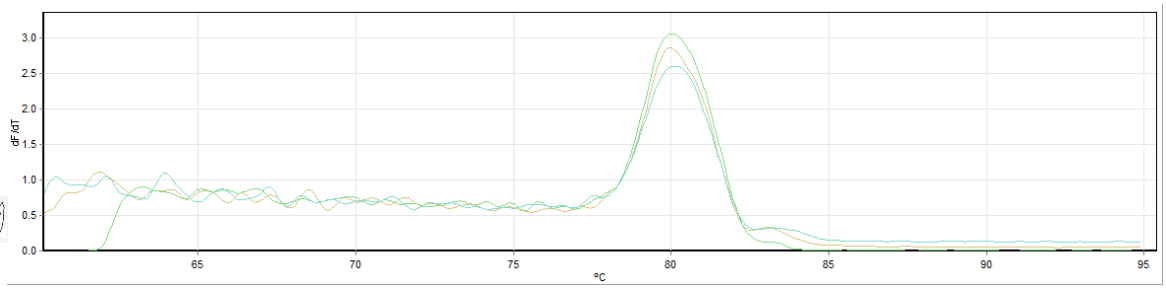

Human *TNFα*

APPENDIX B

The following is the manuscript from which data were used in chapter 3

Transient JNK activation by the endoplasmic reticulum stress sensor IRE1α inhibits cell death early in the endoplasmic reticulum stress response

Max Brown[a-c*], Natalie Strudwick[a-c*], Monika Suwara[a-c*], Louise K. Sutcliffe[a-c], Adina D. Mihai[a-c], Jamie N. Watson[a-c], and Martin Schröder[a-c]

a) Durham University, School of Biological and Biomedical Sciences, Durham DH1 3LE, United Kingdom.

b) Biophysical Sciences Institute, Durham University, Durham DH1 3LE, United Kingdom.

c) North East England Stem Cell Institute (NESCI), Life Bioscience Centre, International Centre for Life, Central Parkway, Newcastle Upon Tyne, NE1 4EP, UK.

* These authors contributed equally to this work.

Address for correspondence: Martin Schröder, Durham University, School of Biological and Biomedical Sciences, Durham DH1 3LE, United Kingdom.

phone: +44 (0) 191-334-1316

FAX: +44 (0) 191-334-9104

email: martin.schroeder@durham.ac.uk

Running Title: JNK is antiapoptotic in the early UPR

Abbreviations: ER – endoplasmic reticulum, JC-1 - 5,5',6,6'-tetrachloro-1,1,3,3'-tetraethylbenzimidazolylcarbocyanine iodide, MEF – mouse embryonic fibroblast, qPCR – quantitative PCR, RT – reverse transcriptase, UPR – unfolded protein response

Abstract

Accumulation of unfolded proteins in the endoplasmic reticulum (ER) activates a signalling network termed the unfolded protein response (UPR). In mammalian cells, UPR signals generated by several ER membrane resident proteins, including the bifunctional protein kinase endoribonuclease IRE1α, control cell survival and the decision to execute apoptosis. Processing of the mRNA for the transcription factor XBP1 by the RNase domain of IRE1α promotes survival of ER stress, while activation of the mitogen-activated protein kinase JNK by IRE1α late in the ER stress response promotes apoptosis. Here we show that immediate and transient activation of JNK by ER stress precedes activation of XBP1. This immediate and transient activation of JNK is dependent on IRE1α and the adaptor protein TRAF2 and coincides with JNK-dependent induction of expression of several antiapoptotic genes, including *cIAP1*, *cIAP2*, *XIAP*, and *BIRC6*. Cell death, as indicated by a decrease in mitochondrial transmembrane potentials, is more pronounced in JNK-deficient mouse embryonic fibroblasts (MEFs) than wild-type MEFs. Hence, JNK-dependent expression of several antiapoptotic genes contributes to delaying the onset of cell death in the early response to ER stress.

Introduction

Perturbation of protein folding homeostasis in the endoplasmic reticulum (ER) activates several signal transduction pathways collectively called the unfolded protein response (UPR) (Ron and Walter, 2007; Walter and Ron, 2011). In mammalian cells, the UPR is initiated by several ER membrane resident proteins, including the protein kinase-endoribonuclease (RNase) IRE1α (Tirasophon *et al.*, 1998; Wang *et al.*, 1998), the protein kinase PERK (Shi *et al.*, 1998; Harding *et al.*, 1999; Shi *et al.*, 1999), and several type II transmembrane transcription factors such as ATF6α (Yoshida *et al.*,

2000) and CREB-H (Zhang *et al.*, 2006). All of these signalling molecules activate prosurvival, but also proapoptotic responses to ER stress.

These opposing signalling outputs are exemplified by IRE1α. The RNase activity of IRE1α initiates non-spliceosomal splicing of the mRNA for the transcription factor XBP1 (Shen *et al.*, 2001; Yoshida *et al.*, 2001; Calfon *et al.*, 2002; Lee *et al.*, 2002), which in turn induces transcription of genes encoding ER-resident molecular chaperones (Lee *et al.*, 2003), components of the ER-associated protein degradation machinery (Yoshida *et al.*, 2003; Oda *et al.*, 2006), and several phospholipid biosynthetic genes (Lee *et al.*, 2003; Lee *et al.*, 2008) to promote cell survival. The IRE1α RNase activity also initiates the decay of several mRNAs encoding proteins targeted to the ER (Hollien and Weissman, 2006; Han *et al.*, 2009; Hollien *et al.*, 2009; Gaddam *et al.*, 2013), which decreases the protein fold load of the stressed ER. Degradation of *DR5* mRNA by IRE1α contributes to establishment of a time window for adaptation to ER stress (Lu *et al.*, 2014). On the other hand, IRE1α promotes apoptosis via both its RNase and protein kinase domains. Cleavage of several miRNAs, including miRNA-17, -34a, -96, and -125b, by the RNase domain of IRE1α stabilizes and promotes translation of *TXNIP* and *caspase-2* mRNAs (Lerner *et al.*, 2012; Oslowski *et al.*, 2012; Upton *et al.*, 2012). TXNIP promotes apoptosis through activation of caspase-1 and secretion of interleukin 1β (Lerner *et al.*, 2012). The role of caspase-2 in ER stress-induced apoptosis has recently been questioned (Lu *et al.*, 2014; Sandow *et al.*, 2014). The kinase domain of IRE1α activates the mitogen-activated protein (MAP) kinase JNK through formation of a complex with the E3 ubiquitin ligase TRAF2 and the MAP kinase kinase kinase (MAPKKK) ASK1 (Nishitoh *et al.*, 2002). Sequestration of TRAF2 by IRE1α may also contribute to activation of caspase-12 in murine cells (Yoneda *et al.*, 2001). Pharmacologic (Zhang

et al., 2001; Smith and Deshmukh, 2007; Chen *et al.*, 2008; Wang *et al.*, 2009; Jung *et al.*, 2012; Teodoro *et al.*, 2012; Huang *et al.*, 2014; Jung *et al.*, 2014) and genetic (Kang *et al.*, 2012; Arshad *et al.*, 2013) studies have provided evidence that activation of JNK 12 h or later after induction of ER stress is proapoptotic.

Much less is known about the role of JNK at earlier time points in the ER stress response. In tumor necrosis factor (TNF)-α-treated cells two phases of JNK activation can be distinguished (Roulston *et al.*, 1998; Lamb *et al.*, 2003), an early and transient antiapoptotic and a later phase, that coincides with activation of caspases (Roulston *et al.*, 1998). In the early phase JNK induces expression of JunD and the antiapoptotic ubiquitin ligase cIAP2/BIRC3 (Lamb *et al.*, 2003). Furthermore, phosphorylation of Bad at T201 and subsequent inhibition of interaction of Bad with Bcl-x_L underlies the antiapoptotic role of JNK in interleukin (IL)-3-dependent hematopoietic cells (Yu *et al.*, 2004), while JNK mediates IL-2-dependent survival of T cells through phosphorylation of MCL1 (Hirata *et al.*, 2013). This functional dichotomy of transient and persistent JNK signalling prompted us to investigate whether immediate and transient activation of JNK occurs in the ER stress response and to characterise the functional significance of such an immediate and transient phase of JNK activation in ER-stressed cells.

Results

ER stress transiently activates JNK before XBP1 splicing reaches maximal levels

To investigate how early JNK is activated in the ER stress response we characterised JNK activation over an 8 h time course by monitoring phosphorylation of JNK in its T-loop on T183 and Y185 by Western blotting with antibodies against phosphorylated and total JNK. In MEFs, phosphorylation increased as early as 10 min after addition of 1 μM thapsigargin (Figure 1, A and C) or 10 μg/ml tunicamycin (Figure 1, D and

F). JNK phosphorylation returned to basal levels 8 h after addition of thapsigargin or 30 min after addition of tunicamycin to cells. The ability of these two mechanistically different ER stressors to elicit rapid and transient activation of JNK suggests that this JNK activation is caused by ER stress invoked by these two chemicals and not a response to secondary effects of these compounds. To compare the kinetics of JNK activation to the kinetics of the *XBP1* splicing reaction we monitored *XBP1* splicing using RT-PCR. Spliced *XBP1* mRNA differs from unspliced *XBP1* mRNA by lacking a 26 nt intron. Hence, the presence of a shorter RT-PCR product on agarose gels is indicative of activation of the IRE1α RNase activity and processing of *XBP1* mRNA. In thapsigargin-treated MEFs ~45% of *XBP1* mRNA was spliced 20 min after addition of thapsigargin (Figure 1, B and C). *XBP1* splicing reached maximal levels only after several hours of thapsigargin treatment, suggesting that activation of JNK precedes maximal activation of XBP1. This kinetic relationship was more evident in tunicamycin-treated MEFs (Figure 1, E and F). In these cells *XBP1* splicing increased only after JNK phosphorylation returned to basal levels.

To investigate whether a similar kinetic relationship between activation of JNK and XBP1 exists in other cell types, we repeated these experiments with Hep G2 hepatoma cells, 3T3-F442A adipocytes, and C_2C_{12} myotubes. In Hep G2 cells, JNK phosphorylation peaked 30 min after addition of 1 μM thapsigargin and then returned to and then below resting levels (Figure 2, A and C). By contrast, 30 min after addition of thapsigargin only ~7% of *XBP1* mRNA were spliced, and after another 15 min *XBP1* splicing was approximately half maximal (Figure 2, B and C). *XBP1* splicing reached maximal levels only after 6 h of thapsigargin treatment. In 3T3-F442A adipocytes phosphorylation of JNK reached a maximum as early as 10 min after application of 1 μM thapsigargin and then returned to basal levels (Figures S1

and S2, A and C). *XBP1* splicing, however, was not detectable until 45 min after addition of thapsigargin, required 4 h to reach maximal levels, and remained at this level for at least another 4 h (Figure S2, B and C). Thus, transient JNK activation also precedes activation of XBP1 in Hep G2 cells and 3T3-F442A adipocytes. The same relationship was observed in C_2C_{12} myotubes. In these cells an increase in JNK phosphorylation was detected as early as 10 min after induction of ER stress with 1 μM thapsigargin (Figure S3, A and C), while the earliest time point at which an increase in *XBP1* splicing was detected was 20 min (Figure S3, B and C). At the same time, activation of JNK diminished over time in C_2C_{12} myotubes, while the level of *XBP1* splicing remained at maximal levels (Figure S3). We conclude that transient activation of JNK preceding induction of *XBP1* splicing in response to ER stress is a phenomenon that can be observed in several murine and human cell types.

Transient JNK activation in ER-stressed cells requires IRE1α and TRAF2

Several different stresses activate JNK (Kyriakis *et al.*, 1994). To examine if the rapid JNK activation seen upon thapsigargin or tunicamycin treatment is in response to ER stress and thus mediated via IRE1α and TRAF2, we characterised whether this JNK activation is IRE1α- and TRAF2-dependent. JNK phosphorylation was induced ~2-3 fold in *ire1α*$^{-/-}$ and *traf2*$^{-/-}$ MEFs compared to an ~8 fold increase in JNK phosphorylation in WT MEFs upon thapsigargin treatment (Figures 1 and 3). JNK activation was also delayed in both *ire1α*$^{-/-}$ and *traf2*$^{-/-}$ MEFs and reached maximal levels in *traf2*$^{-/-}$ MEFs only at the time when spliced *XBP1* mRNA levels had reached steady-state levels (Figure 3F). This delayed activation of JNK in *ire1α*$^{-/-}$ and *traf2*$^{-/-}$ MEFs may be explained by stresses other than and possibly secondary to ER stress, for example oxidative stress (Mauro *et al.*, 2006). To establish if the transient JNK activation is IRE1α- and TRAF2-dependent in cells other than MEFs we characterised

whether small interfering (si)-RNA-mediated knockdown of IRE1α or TRAF2 reduces JNK activation by ER stress. Two IRE1α siRNAs (#2 and #3, Supplemental table 1) reduced IRE1α mRNA levels to ~40% of control eGFP siRNA transfected cells 72 h post-transfection (Figure S4A) and decreased activation of JNK by 37 ± 7% 2 h and by 61 ± 4% 4 h after induction of ER stress (Figure S4, B and C). Likewise, two siRNAs against human or murine TRAF2 blunted the ER stress-dependent JNK activation in Hep G2 cells, 3T3-F442A fibroblasts, and C_2C_{12} myoblasts (Figures S5, S6, and S8). Furthermore, a dominant negative mutant of TRAF2, TRAF2Δ1-86 (Hsu *et al.*, 1996; Reinhard *et al.*, 1997), which lacks the RING domain (Figure S7A) inhibited TNF-α-induced JNK activation (Figure S7B) and blunted the rapid and transient JNK activation in these cells seen upon induction of ER stress with 1 μM thapsigargin in 3T3-F442A preadipocytes (Figure S7, C and D) and C_2C_{12} myoblasts (Figure S9). Taken together, these data demonstrate that the rapid and transient JNK activation upon induction of ER stress is mediated by both IRE1α and TRAF2.

The transient phase of JNK activation in ER stressed cells inhibits cell death

In the early antiapoptotic response to TNF-α JNK is required for expression of the mRNA for the antiapoptotic ubiquitin ligase cIAP2/BIRC3 (Lamb *et al.*, 2003). This motivated us to compare the expression of mRNAs for antiapoptotic genes including *cIAP1*, *cIAP2*, *XIAP*, and *BIRC6* at the onset of activation of JNK with 1 μM thapsigargin (Figure 1A) in WT and *jnk1*$^{-/-}$ *jnk2*$^{-/-}$ MEFs. Expression of the mRNAs for cIAP1, cIAP2, XIAP, and BIRC6 increased in WT cells in the first 45 min of ER stress. By contrast, *cIAP1*, *cIAP2*, and *BIRC6* mRNA levels decreased in *jnk1*$^{-/-}$ *jnk2*$^{-/-}$ cells (Figure 4). The increase in *XIAP* mRNA was more pronounced in WT than in *jnk1*$^{-/-}$ *jnk2*$^{-/-}$ MEFs, suggesting that JNK positively regulates expression of *XIAP* mRNA. These data show that expression of several antiapoptotic genes is induced

early in the ER stress response in a JNK-dependent manner. To investigate the physiologic relevance of the early JNK-dependent induction of antiapoptotic genes we characterised the appearance of dead cells within the first 4 h of thapsigargin treatment by monitoring the depolarization of mitochondrial transmembrane potentials with the fluorescent dye 5,5',6,6'-tetrachloro-1,1,3,3'-tetraethylbenzimidazolylcarbocyanine iodide (JC-1) (Reers *et al.*, 1991; Smiley *et al.*, 1991) (Figure 5A). 45 min after addition of 1 μM thapsigargin cell death was more pronounced in *jnk1*$^{-/-}$ *jnk2*$^{-/-}$ MEFs than in WT MEFs (Figure 5B). This increase susceptibility of *jnk1*$^{-/-}$ *jnk2*$^{-/-}$ MEFs to thapsigargin was also observed after 4 h of exposure to 1 μM thapsigargin (Figure 5B). Hence, JNK-dependent induction of antiapoptotic genes including *cIAP1*, *cIAP2*, *XIAP*, and *BIRC6* delays the onset of cell death early in the ER stress response.

Discussion

We show that JNK is transiently activated early in the mammalian UPR and that this immediate JNK activation is antiapoptotic. Transient activation of JNK early in the UPR by two mechanistically distinct ER stressors, thapsigargin and tunicamycin (Figures 1-2 and S2-S3), and its dependence on IRE1α and TRAF2 (Figures 3, S4-S6, and S8) provides evidence that the early JNK activation is in response to ER stress. Early JNK activation coincides with induction of several antiapoptotic genes (Figures 1 and 4). Maximal expression of the mRNAs for these genes required JNK (Figure 4), while depolarization of mitochondrial transmembrane potentials occurred faster in JNK-deficient MEFs than in WT MEFs upon exposure to 1 μM thapsigargin (Figure 5). Our data arguing that early JNK activation protects ER-stressed cells from executing apoptosis is consistent with reports that show that *traf2*$^{-/-}$ MEFs are more susceptible to ER stress than WT MEFs (Mauro *et al.*, 2006) and that siRNA-

mediated knock-down of JNK1 increased caspase-3 cleavage in tunicamycin-treated neural stem cells (Li *et al.*, 2011).

Mostly pharmacologic data supports that activation of JNK late in the ER stress response promotes cell death (Zhang *et al.*, 2001; Tan *et al.*, 2006; Smith and Deshmukh, 2007; Chen *et al.*, 2008; Wang *et al.*, 2009; Jung *et al.*, 2012; Kang *et al.*, 2012; Teodoro *et al.*, 2012; Arshad *et al.*, 2013; Huang *et al.*, 2014; Jung *et al.*, 2014). Our work suggests that two functionally distinct phases of JNK signalling exist in the ER stress response - an early, transient prosurvival phase and a late phase that promotes cell death. Biphasic JNK signalling with opposing effects on cell viability exists also in other stress responses. Transient activation of JNK in response to several other stresses is anti-apoptotic (Sluss *et al.*, 1994; Traverse *et al.*, 1994; Raingeaud *et al.*, 1995; Chen *et al.*, 1996a; Lee *et al.*, 1997; Nishina *et al.*, 1997), while persistent JNK activation causes cell death (Chen *et al.*, 1996a; Chen *et al.*, 1996b; Guo *et al.*, 1998; Sanchez-Perez *et al.*, 1998). These opposing functional attributes of transient and persistent JNK activation have also been causally established by using JNK-deficient MEFs reconstituted with 1NM-PP1-sensitised alleles of JNK1 and JNK2 (Ventura *et al.*, 2006). Hence, the antiapoptotic function of transiently activated JNK in the ER stress response is another example for the paradigm that the duration of JNK activation controls cell fate. Identification of cIAP1, XIAP, and BIRC6 as genes whose expression required JNK in the early response to ER stress (Figure 4) has allowed us to extend the repertoire of antiapoptotic JNK targets. These, and possibly other, genes may also contribute to how JNK inhibits cell death in other stress responses.

The existence of a transient, anti-apoptotic phase of JNK activation in the ER stress response raises at least two questions: 1) What are the molecular mechanisms

that define the transient phase as anti-apoptotic? 2) What are the mechanisms that restrict JNK activation early in the ER stress response? While future experiments will be necessary to answer these questions, possible explanations may be that the duration of activation affects the subcellular localisation of JNKs, that JNK signalling outputs are controlled by molecular determinants, or that the JNK signalling pathway functionally interacts with the NF-κB signalling pathway.

Opposing signalling outputs of extracellular signal-regulated kinases (ERKs) in PC12 cells have been explained by different subcellular localisations of ERKs (Marshall, 1995). JNK, however, does not appear to relocalise upon stimulation, either in response to transient or persistent activation (Chen *et al.*, 1996a; Sanchez-Perez *et al.*, 1998). This is also the case for JNK transiently activated during the ER stress response (Figure S10). An alternative possibility is that JNK substrates function as molecular determinants of the biological functions of transient and persistent JNK activation, respectively. This is, for example, the case for the ERK substrate c-Fos (Murphy *et al.*, 2002).

In the ER stress response NF-κB activation is transient and displays kinetics in several cell lines that are reminiscent of the transient JNK activation reported in this study (Wu *et al.*, 2002; Jiang *et al.*, 2003; Deng *et al.*, 2004; Wu *et al.*, 2004). In TNF-α signalling JNK functionally interacts with the NF-κB pathway. JNK activation in the absence of NF-κB is apoptotic (Guo *et al.*, 1998; Tang *et al.*, 2002; Deng *et al.*, 2003; Liu *et al.*, 2004) or necrotic (Ventura *et al.*, 2004), while NF-κB transduces an anti-apoptotic response to TNF-α (Kelliher *et al.*, 1998; Devin *et al.*, 2000). At the transcriptional level NF-κB cooperates with JunD (Rahmani *et al.*, 2001), whose phosphorylation is decreased in *jnk1*$^{-/-}$ *jnk2*$^{-/-}$ MEFs (Ventura *et al.*, 2003). NF-κB induces *cIAP1*, *cIAP2*, and *XIAP* (Stehlik *et al.*, 1998). JunD contributes to the

transcriptional induction of *cIAP2* in TNF-α-stimulated cells (Lamb *et al.*, 2003). This collaboration between NF-κB and transcription factors controlled by JNK, such as JunD, may explain the JNK-dependent induction of *cIAP1*, *cIAP2*, *XIAP*, and *BIRC6* (Figure 4), and potentially other anti-apoptotic genes, early in the ER stress response.

Transient activation of NF-κB in the ER stress response may also contribute to control of the duration of JNK activation. NF-κB inhibits JNK activation by TNF-α (De Smaele *et al.*, 2001; Tang *et al.*, 2001; Reuther-Madrid *et al.*, 2002; Tang *et al.*, 2002; Papa *et al.*, 2004) through induction of XIAP (Tang *et al.*, 2001; Tang *et al.*, 2002) and GADD45β (De Smaele *et al.*, 2001; Papa *et al.*, 2004). TNF-α also induces the dual specificity phosphatase MKP1/DUSP1 (Guo *et al.*, 1998). In murine keratinocytes *cis*-platin induced persistent JNK activation but induced MKP1 only weakly, while transient JNK activation by *trans*-platin correlated with strong induction of MKP1 (Sanchez-Perez *et al.*, 1998). Comparison of the ER stress response elicited by 1,4-DL-dithiothreitol (DTT) and tunicamycin suggests that transient activation of JNK in the ER stress response coincides with phosphorylation of MKP1 at S359 and its stabilisation (Li *et al.*, 2011). However, secondary effects or different pharmacokinetics of these two drugs may also contribute to these observations. Additional experimentation is required to resolve whether MKP1 controls JNK activation in the ER stress response.

The duration of JNK activation may also be regulated at the level of the ER stress perceiving protein kinase IRE1α. Activation of JNK by IRE1α requires interaction of TRAF2 with IRE1α (Urano *et al.*, 2000). This interaction has not been observed in cells expressing kinase and RNase-defective K599A-IRE1α (Urano *et al.*, 2000). JNK activation precedes *XBP1* splicing (Figures 1, 2, S2, and S3). *XBP1* splicing by

mammalian IRE1α is stimulated by phosphorylation of IRE1α (Prischi *et al.*, 2014). Hence, overall phosphorylation of IRE1α seems to be an unlikely explanation for the transiency of JNK activation. It is, however, possible that the specific pattern of phosphorylation of the ~10 phosphorylation sites in IRE1α (Itzhak *et al.*, 2014) controls its affinity towards TRAF2 and the activation JNK by IRE1α.

In conclusion, we show that early and transient JNK activation produces antiapoptotic signals early in the ER stress response. Our work also identifies JNK-dependent expression of cIAP1, cIAP2, XIAP, and BIRC6 as a mechanism through which JNK exerts its antiapoptotic functions.

Materials and Methods

Antibodies and reagents. Rabbit anti-caspase-3 (cat. no. 9665), rabbit anti-JNK (cat. no. 9258), rabbit anti-phospho-JNK (cat. no. 4668) antibodies, and human recombinant TNF-α (cat. no. 8902) were purchased from Cell Signaling Technology Inc. (Danvers, MA 01923, USA). The mouse anti-GAPDH antibody (cat. no. G8795) was purchased from Sigma-Aldrich (Gillingham, UK), the rabbit anti-TRAF2 antibody (cat. no. sc-876) from Santa Cruz Biotechnology (Santa Cruz, CA, USA), and the mouse anti-emerin antibody (cat. no. ab49499) from Abcam (Cambridge, UK). siRNAs against TRAF2, IRE1α, and eGFP were obtained from Sigma-Aldrich. siRNA sequences are listed in Supplemental table 1. Tunicamycin was purchased from Merck Chemicals (Beeston, UK) and thapsigargin from Sigma-Aldrich (Gillingham, UK).

Plasmids. Plasmids were maintained in *Escherichia coli* XL10-Gold cells (Agilent Technologies, Stockport, UK, cat. no. 200314). Standard protocols for plasmid constructions were used. Plasmid pMT2T-TRAF2Δ1-86 was generated by amplifying a 1,327 bp fragment from pMT2T-HA-TRAF2 (Leonardi *et al.*, 2000) with primers

H8215 and H8216. The PCR product was cleaved with *Cla*I and *Not*I and cloned into *Cla*I and *Not*I-digested pMT2T-HA-TRAF2 to yield pMT2T-TRAF2Δ1-86. The TRAF2 region in pMT2T-TRAF2Δ1-86 was confirmed by sequencing.

Cell culture. Wild type (WT), *ire1*$\alpha^{-/-}$ (Lee *et al.*, 2002), *jnk1*$^{-/-}$ *jnk2*$^{-/-}$ (Tournier *et al.*, 2000), and *traf2*$^{-/-}$ (Yeh *et al.*, 1997) MEFs were provided by R. J. Kaufman (Sanford Burnham Medical Research Institute, La Jolla, CA, USA), R. Davis (University of Massachusetts, Worchester, MA, USA), and T. Mak (University of Toronto, Ontario Cancer Institute, Toronto, Ontario, Canada). 3T3-F442A preadipocytes (Green and Kehinde, 1976), C_2C_{12} myoblasts (Blau *et al.*, 1985), and Hep G2 cells (Knowles *et al.*, 1980) were obtained from C. Hutchison (Durham University), R. Bashir (Durham University), and A. Benham (Durham University), respectively.

All cell lines were grown at 37 °C in an atmosphere of 95% (v/v) air, 5% (v/v) CO_2, and 95% humidity. Hep G2 cells were grown in minimal essential medium (MEM) (Eagle, 1959) supplemented with 10% (v/v) foetal bovine serum (FBS) and 2 mM L-glutamine. All other cell lines were grown in Dulbecco's modified Eagle's medium (DMEM) containing 4.5 g/l D-glucose (Morton, 1970; Rutzky and Pumper, 1974), 10% (v/v) FBS, and 2 mM L-glutamine. The medium for *ire1*$\alpha^{-/-}$ and corresponding WT MEFs was supplemented with 110 mg/l pyruvate (Lee *et al.*, 2002).

To differentiate C_2C_{12} cells 60-70% confluent cultures were shifted into low mitogen medium consisting of DMEM containing 4.5 g/l D-glucose, 2% (v/v) horse serum, and 2 mM L-glutamine and incubated for another 7-8 d with replacing the low mitogen medium every 2-3 d (Bains *et al.*, 1984). Differentiation of C_2C_{12} cells was assessed by microscopic inspection of cultures, staining of myotubes with rhodamine-labelled phalloidin (Amato *et al.*, 1983), and reverse transcriptase PCR for

transcription of the genes encoding *S*-adenosyl-homocysteine hydrolase (*AHCY*), myosin light chain 1 (*MYL1*), and troponin C (*TNNC1*). To differentiate 3T3-F442A fibroblasts into adipocytes cells were grown to confluency. 2 d postconfluency the medium was changed to DMEM containing 4.5 g/l D-glucose, 10% (v/v) FBS, 2 mM L-glutamine, 1 μg/ml insulin, 0.5 mM 1-methyl-3-isobutylxanthine, 0.25 μM dexamethasone. After 3 d the medium was changed to DMEM containing 4.5 g/l D-glucose, 10% (v/v) FBS, 2 mM L-glutamine, and 1 μg/ml insulin. After another 2 d the medium was changed to DMEM containing 4.5 g/l D-glucose, 10% (v/v) FBS and 2 mM L-glutamine. Cells were incubated another 7 d before the start of experiments (Rubin *et al.*, 1978). Differentiation was assessed by Oil Red O staining (Hansen *et al.*, 1999). ER stress was induced with 1 μM thapsigargin or 10 μg/ml tunicamycin.

Hep G2 cells were transfected with plasmids using jetPRIME (Polyplus Transfection, Illkirch, France, cat. no. 114) and with siRNAs using INTERFERin (Polyplus Transfection, cat. no. 409) transfection reagents. Plasmids and siRNAs were transfected into all other cell lines by electroporation with a Neon electroporator (Life Technologies, Paisley, UK) using a 10 μl tip. Manufacturer-optimised electroporation conditions were used for 3T3-F442A preadipocytes and C_2C_{12} myoblasts. MEFs were electroporated with one pulse of 1200 V and a pulse width of 30 ms. 10-20 nM of each siRNA were transfected. Transfection efficiencies were determined by transfection of 2 μg of pmaxGFP (Lonza Cologne AG, Germany) and detection of GFP-expressing cells with a Zeiss ApoTome fluorescence microscope. Transfection efficiencies were >80%. 24 h after transfection cells were analysed or time courses initiated.

RNA extraction and reverse transcriptase (RT-) PCRs. RNA was extracted with the EZ-RNA total RNA isolation kit (Geneflow, Fradley, UK, cat. no. K1-0120) and

reverse transcribed with oligo-dT primers (Promega, Southampton, cat. no. C1101) and Superscript III reverse transcriptase (Life Technologies, cat. no. 18080044) as described previously (Cox *et al.*, 2011). Protocols for detection of splicing of murine and human *XBP1* have been described previously (Cox *et al.*, 2011). Band intensities were quantitated using ImageJ (Collins, 2007) and the percentage of *XBP1* splicing calculated by dividing the signal for spliced *XBP1* mRNA by the sums of the signals for spliced and unspliced *XBP1* mRNAs. Quantitative PCRs (qPCRs) were run on a Rotorgene 3000 (Qiagen, Crawley, UK). Amplicons were amplified with 0.5 µl 5 U/µl GoTaq® Flexi DNA polymerase (Promega, cat. no. M8305), 2 mM $MgCl_2$, 200 µM dNTPs, and 1 µM of each primer and detected with a 1:2,500 fold dilution of a SybrGreen stock solution (Life Technologies, cat. no. S7563) or the GoTaq qPCR Master Mix from Promega (cat. no. A6002). Primers for qPCR are listed in Supplemental table 2. qPCR using GoTaq DNA polymerase were performed as follows. After denaturation for 2 min at 95°C samples underwent 40 cycles of denaturation at 95°C for 30 s, primer annealing at 58°C for 30 s, and primer extension at 72°C for 30 s. After denaturation at 95°C for 2 min qPCRs with the GoTaq qPCR Master mix were cycled 40 times at 95°C for 15 s, 60°C for 15 s, and 72°C for 15 s for *cIAP1*, *cIAP2*, *XIAP*, and *BRUCE* and 40 times at 95°C for 15 s, 60°C for 60 s for *ACTB*. Fluorescence data were acquired during the annealing or in case of qPCR amplification of *ACTB* with the GoTaq qPCR Master Mix during the first 30 s at 60°C. Amplification of a single PCR product was confirmed by recording the melting curves after each PCR run. Average amplification efficiencies in the exponential phase were calculated using the comparative quantitation analysis in the Rotor Gene Q software and were between 0.6 and 0.7 for all qPCRs. Calculation of C_T values and normalization to *GAPDH, ACTA1*, or *ACTB* mRNA levels as described by Pfaffl

(Pfaffl, 2001) taking the average amplification efficiencies into account. Results represent the average and standard error of three technical repeats. qPCR results were confirmed by at least one other biological replicate. qPCRs for murine *AHCY*, *MYL1*, and *TNNC* were standardised to *GAPDH*, for murine *TRAF*2 and *TRB3* to *ACTB*, and for human and *IRE1*α and *TRAF2* to *ACTA1*.

Cell lysis and Western blotting. Cells were washed three times with ice-cold phosphate-buffered saline (PBS, 4.3 mM Na_2HPO_4, 1.47 mM KH_2PO_4, 27 mM KCl, 137 mM NaCl, pH 7.4) and lysed in RIPA buffer [50 mM Tris-HCl, pH 8.0, 150 mM NaCl, 0.5% (w/v) sodium deoxycholate, 0.1% (v/v) Triton X-100, 0.1% (w/v) SDS] containing Roche complete protease inhibitors (Roche Applied Science, Burgess Hill, UK, cat. no. 11836153001) as described before (Cox *et al.*, 2011).

For isolation of cytosolic and nuclear fractions cells were washed two times with ice-cold PBS and gently lysed in 0.32 M sucrose, 10 mM Tris HCl pH 8.0, 3 mM $CaCl_2$, 2 mM $Mg(OAc)_2$, 0.1 mM EDTA, 0.5% (v/v) NP-40, 1 mM DTT, 0.5 mM PMSF. Nuclei were collected by centrifugation for 5 min at 2,400 g, 4°C. The nuclear pellet were resuspended in 0.32 M sucrose, 10 mM Tris HCl pH 8.0, 3 mM $CaCl_2$, 2 mM $Mg(OAc)_2$, 0.1 mM EDTA, 1 mM DTT, 0.5 mM PMSF by flipping the microcentrifuge tube. The nuclei were collected by centrifugation for 5 min at 2,400 g, 4°C. After aspiration of all of the wash buffer the nuclei were resuspended in 30 μl low salt buffer [20 mM HEPES (pH 7.9), 1.5 mM $MgCl_2$, 20 mM KCl, 0.2 mM EDTA, 25% (v/v) glycerol, 0.5 mM DTT, 0.5 mM PMSF] by flipping the microcentrifuge tube. One volume of high salt buffer [20 mM HEPES (pH 7.9), 1.5 mM $MgCl_2$, 800 mM KCl, 0.2 mM EDTA, 25% glycerol (v/v), 1% NP-40, 0.5 mM DTT, 0.5 mM PMSF] was added drop wise while continuously mixing the contents of the microcentrifuge tube by flipping. The tubes were then incubated for 45 min at 4°C

on an end-over-end rotator. The tubes were centrifuged at 14,000 g for 15 min at 4°C and the supernatant transferred into a fresh microcentrifuge tube to obtain the nuclear extract.

Proteins were separated by SDS-PAGE and transferred to polyvinylidene difluoride (PVDF) membranes (Amersham HyBond^{TM}-P, pore size 0.45 μm, GE Healthcare, Little Chalfont, UK, cat. no. RPN303F) by semi-dry electrotransfer in 0.1 M Tris, 0.192 M glycine, and 5% (v/v) methanol at 2 mA/cm^2 for 60-75 min. Membranes were then blocked for 1 h in 5% (w/v) skimmed milk powder in TBST [20 mM Tris-HCl, pH 7.6, 137 mM NaCl, and 0.1% (v/v) Tween-20] for antibodies against non-phosphorylated proteins and 5% bovine serum albumin (BSA) in TBST for antibodies against phosphorylated proteins and then incubated overnight at 4°C with the primary antibody diluted in blocking solution. Blots were washed three times with TBST and then probed with secondary antibody for 1 hour at room temperature. The anti-JNK, anti-phospho-JNK, and anti-TRAF2 antibodies were used at a 1:1,000 dilution in TBST + 5% (w/v) BSA and the anti-caspase 3 antibody at a dilution of 1:1,000 in TBST + 5% (w/v) skimmed milk powder and incubated with the membranes over night at 4°C with gentle agitation. Membranes were then developed with goat anti-rabbit-IgG (H+L)-horseradish peroxidase (HRP)-conjugated secondary antibody (Cell Signaling, cat. no. 7074S) at a 1:1,000 dilution in TBST + 5% (w/v) skimmed milk powder for 1 h at room temperature. The mouse anti-GAPDH antibody was used at a 1:30,000 dilution in TBST + 5% (w/v) skimmed milk powder over night at 4°C with gentle agitation and developed with goat anti-mouse IgG (H+L)-HRP-conjugated secondary antibody (Thermo Scientific, cat, no. 31432) at a 1:20,000 dilution in TBST 5% (w/v) skimmed milk powder for 1 h at room temperature. For signal detection Pierce ECL Western Blotting Substrate (cat. no. 32209) or Pierce

ECL Plus Western Blotting Substrate (cat. no. 32132) from Thermo Fisher Scientific (Loughborough, UK) were used. Blots were exposed to CL-X Posure™ film (Thermo Fisher Scientific, Loughborough, UK, cat. no. 34091). Exposure times were adjusted on the basis of previous exposures to obtain exposures in the linear range of the film. Signals were quantified using ImageJ (Collins, 2007). To reprobe blots for detection of nonphosphorylated proteins, membranes were stripped using Restore Western Blot Stripping Buffer (Thermo Fisher Scientific, Loughborough, UK, cat. no. 21059) and blocked with 5% (w/v) skimmed milk powder in TBST.

Fluorescence microscopy. For confocal microscopy cells were grown on lumox dishes (Sarstedt, Leichester, UK, cat. no. 94.6077.331). After incubation with 1 μM thapsigargin cells were incubated with 2 μg/ml JC-1 (Life Technologies, cat. no. T3168) at 37°C for 20 min (Reers *et al.*, 1991; Smiley *et al.*, 1991; Cossarizza *et al.*, 1993; Ankarcrona *et al.*, 1995). The cells were washed twice with PBS before addition of fresh medium for live cell imaging on a Leica TCS SP5 II confocal microscope (Leica Microsystems, Mannheim, Germany). JC-1 fluorescence was excited at 488 nm with an argon laser set at 22% of its maximum power. Green fluorescence between 515-545 nm was collected with a photomultiplier tube and orange fluorescence between 590-620 nm with a HyD 5 detector. To determine the percentage of dead cells, cells showing fluorescence emission between 515-545 nm only were counted as dead, while cells showing punctuate fluorescence emission between 590-620 nm were counted as alive.

Error calculations. Experimental data are presented as the average and its standard error. Errors were propagated using the law of error propagation for random, independent errors (Ku, 1966).

Acknowledgements

This work was supported by the European Community's 7th Framework Programme (FP7/2007-2013) under grant agreement no. 201608. We thank A. Benham (Durham University), R. Bashir (Durham University), R. Davis (University of Massachusetts), C. Hutchison (Durham University), R. J. Kaufman (Sanford Burnham Medical Research Institute), and T. Mak (University of Toronto) for providing cell lines. We thank U. Siebenlist (NIAID, NIH) for providing plasmid pMT2T-HA-TRAF2.

References

Amato PA, Unanue ER, and Taylor DL. (1983). Distribution of actin in spreading macrophages: a comparative study on living and fixed cells. J Cell Biol 96, 750-761.

Ankarcrona M, Dypbukt JM, Bonfoco E, Zhivotovsky B, Orrenius S, Lipton SA, and Nicotera P. (1995). Glutamate-induced neuronal death: a succession of necrosis or apoptosis depending on mitochondrial function. Neuron 15, 961-973.

Arshad M, Ye Z, Gu X, Wong CK, Liu Y, Li D, Zhou L, Zhang Y, Bay WP, Yu VC, and Li P. (2013). RNF13, a RING finger protein, mediates endoplasmic reticulum stress-induced apoptosis through the IRE1alpha/JNK pathway. J Biol Chem 288, 8726-8736.

Bains W, Ponte P, Blau H, and Kedes L. (1984). Cardiac actin is the major actin gene product in skeletal muscle cell differentiation in vitro. Mol Cell Biol 4, 1449-1453.

Blau HM, Pavlath GK, Hardeman EC, Chiu CP, Silberstein L, Webster SG, Miller SC, and Webster C. (1985). Plasticity of the differentiated state. Science 230, 758-766.

Calfon M, Zeng H, Urano F, Till JH, Hubbard SR, Harding HP, Clark SG, and Ron D. (2002). IRE1 couples endoplasmic reticulum load to secretory capacity by processing the *XBP-1* mRNA. Nature 415, 92-96.

Chen C-L, Lin C-F, Chang W-T, Huang W-C, Teng C-F, and Lin Y-S. (2008). Ceramide induces p38 MAPK and JNK activation through a mechanism involving a thioredoxin-interacting protein-mediated pathway. Blood 111, 4365-4374.

Chen Y-R, Meyer CF, and Tan T-H. (1996a). Persistent activation of c-Jun N-terminal kinase 1 (JNK1) in γ radiation-induced apoptosis. J Biol Chem 271, 631-634.

Chen YR, Wang X, Templeton D, Davis RJ, and Tan TH. (1996b). The role of c-Jun N-terminal kinase (JNK) in apoptosis induced by ultraviolet C and gamma radiation. Duration of JNK activation may determine cell death and proliferation. J Biol Chem 271, 31929-31936.

Collins TJ. (2007). ImageJ for microscopy. Biotechniques 43, 25-30.

Cossarizza A, Baccarani-Contri M, Kalashnikova G, and Franceschi C. (1993). A new method for the cytofluorimetric analysis of mitochondrial membrane potential using the J-aggregate forming lipophilic cation 5,5',6,6'-tetrachloro-1,1',3,3'-tetraethylbenzimidazolcarbocyanine iodide (JC-1). Biochem Biophys Res Commun 197, 40-45.

Cox DJ, Strudwick N, Ali AA, Paton AW, Paton JC, and Schröder M. (2011). Measuring signaling by the unfolded protein response. Methods Enzymol 491, 261-292.

De Smaele E, Zazzeroni F, Papa S, Nguyen DU, Jin R, Jones J, Cong R, and Franzoso G. (2001). Induction of *gadd45β* by NF-κB downregulates pro-apoptotic JNK signalling. Nature 414, 308-313.

Deng J, Lu PD, Zhang Y, Scheuner D, Kaufman RJ, Sonenberg N, Harding HP, and Ron D. (2004). Translational repression mediates activation of nuclear factor kappa B by phosphorylated translation initiation factor 2. Mol Cell Biol 24, 10161-10168.

494 Deng Y, Ren X, Yang L, Lin Y, and Wu X. (2003). A JNK-dependent pathway is
495 required for TNFα-induced apoptosis. Cell 115, 61-70.
496 Devin A, Cook A, Lin Y, Rodriguez Y, Kelliher M, and Liu Z-g. (2000). The distinct
497 roles of TRAF2 and RIP in IKK activation by TNF-R1: TRAF2 recruits IKK to TNF-
498 R1 while RIP mediates IKK activation. Immunity 12, 419-429.
499 Eagle H. (1959). Amino acid metabolism in mammalian cell cultures. Science 130,
500 432-437.
501 Gaddam D, Stevens N, and Hollien J. (2013). Comparison of mRNA localization and
502 regulation during endoplasmic reticulum stress in *Drosophila* cells. Mol Biol Cell 24,
503 14-20.
504 Green H, and Kehinde O. (1976). Spontaneous heritable changes leading to increased
505 adipose conversion in 3T3 cells. Cell 7, 105-113.
506 Guo Y-L, Baysal K, Kang B, Yang L-J, and Williamson JR. (1998). Correlation
507 between sustained c-Jun N-terminal protein kinase activation and apoptosis induced
508 by tumor necrosis factor-α in rat mesangial cells. J Biol Chem 273, 4027-4034.
509 Han D, Lerner AG, Vande Walle L, Upton J-P, Xu W, Hagen A, Backes BJ, Oakes
510 SA, and Papa FR. (2009). IRE1α kinase activation modes control alternate
511 endoribonuclease outputs to determine divergent cell fates. Cell 138, 562-575.
512 Hansen JB, Petersen RK, Larsen BM, Bartkova J, Alsner J, and Kristiansen K. (1999).
513 Activation of peroxisome proliferator-activated receptor γ bypasses the function of the
514 retinoblastoma protein in adipocyte differentiation. J Biol Chem 274, 2386-2393.
515 Harding HP, Zhang Y, and Ron D. (1999). Protein translation and folding are coupled
516 by an endoplasmic-reticulum-resident kinase. Nature 397, 271-274.

517 Hirata Y, Sugie A, Matsuda A, Matsuda S, and Koyasu S. (2013). TAK1-JNK axis
518 mediates survival signal through Mcl1 stabilization in activated T cells. J Immunol
519 190, 4621-4626.
520 Hollien J, Lin JH, Li H, Stevens N, Walter P, and Weissman JS. (2009). Regulated
521 Ire1-dependent decay of messenger RNAs in mammalian cells. J Cell Biol 186, 323-
522 331.
523 Hollien J, and Weissman JS. (2006). Decay of endoplasmic reticulum-localized
524 mRNAs during the unfolded protein response. Science 313, 104-107.
525 Hsu H, Shu HB, Pan MG, and Goeddel DV. (1996). TRADD-TRAF2 and TRADD-
526 FADD interactions define two distinct TNF receptor 1 signal transduction pathways.
527 Cell 84, 299-308.
528 Huang Y, Li X, Wang Y, Wang H, Huang C, and Li J. (2014). Endoplasmic reticulum
529 stress-induced hepatic stellate cell apoptosis through calcium-mediated JNK/P38
530 MAPK and calpain/caspase-12 pathways. Mol Cell Biochem 394, 1-12.
531 Itzhak D, Bright M, McAndrew P, Mirza A, Newbatt Y, Strover J, Widya M,
532 Thompson A, Morgan G, Collins I, and Davies F. (2014). Multiple
533 autophosphorylations significantly enhance the endoribonuclease activity of human
534 inositol requiring enzyme 1α. BMC Biochem 15, 3.
535 Jiang HY, Wek SA, McGrath BC, Scheuner D, Kaufman RJ, Cavener DR, and Wek
536 RC. (2003). Phosphorylation of the α subunit of eukaryotic initiation factor 2 is
537 required for activation of NF-κB in response to diverse cellular stresses. Mol Cell
538 Biol 23, 5651-5663.
539 Jung TW, Hwang H-J, Hong HC, Choi HY, Yoo HJ, Baik SH, and Choi KM. (2014).
540 Resolvin D1 reduces ER stress-induced apoptosis and triglyceride accumulation
541 through JNK pathway in HepG2 cells. Mol Cell Endocrinol 391, 30-40.

Jung TW, Lee MW, Lee YJ, and Kim SM. (2012). Metformin prevents thapsigargin-induced apoptosis via inhibition of c-Jun NH_2 terminal kinase in NIT-1 cells. Biochem Biophys Res Commun 417, 147-152.

Kang M-J, Chung J, and Ryoo HD. (2012). CDK5 and MEKK1 mediate pro-apoptotic signalling following endoplasmic reticulum stress in an autosomal dominant retinitis pigmentosa model. Nat Cell Biol 14, 409-415.

Kelliher MA, Grimm S, Ishida Y, Kuo F, Stanger BZ, and Leder P. (1998). The death domain kinase RIP mediates the TNF-induced NF-κB signal. Immunity 8, 297-303.

Knowles BB, Howe CC, and Aden DP. (1980). Human hepatocellular carcinoma cell lines secrete the major plasma proteins and hepatitis B surface antigen. Science 209, 497-499.

Ku HH. (1966). Notes on use of propagation of error formulas. J Res Nat Bureau Standards Sect C - Eng Instrumentat 70, 263-273.

Kyriakis JM, Banerjee P, Nikolakaki E, Dai T, Rubie EA, Ahmad MF, Avruch J, and Woodgett JR. (1994). The stress-activated protein kinase subfamily of c-Jun kinases. Nature 369, 156-160.

Lamb JA, Ventura JJ, Hess P, Flavell RA, and Davis RJ. (2003). JunD mediates survival signaling by the JNK signal transduction pathway. Mol Cell 11, 1479-1489.

Lee AH, Iwakoshi NN, and Glimcher LH. (2003). XBP-1 regulates a subset of endoplasmic reticulum resident chaperone genes in the unfolded protein response. Mol Cell Biol 23, 7448-7459.

Lee AH, Scapa EF, Cohen DE, and Glimcher LH. (2008). Regulation of hepatic lipogenesis by the transcription factor XBP1. Science 320, 1492-1496.

Lee K, Tirasophon W, Shen X, Michalak M, Prywes R, Okada T, Yoshida H, Mori K, and Kaufman RJ. (2002). IRE1-mediated unconventional mRNA splicing and S2P-

mediated ATF6 cleavage merge to regulate XBP1 in signaling the unfolded protein response. Genes Dev 16, 452-466.

Lee SY, Reichlin A, Santana A, Sokol KA, Nussenzweig MC, and Choi Y. (1997). TRAF2 is essential for JNK but not NF-κB activation and regulates lymphocyte proliferation and survival. Immunity 7, 703-713.

Leonardi A, Ellinger-Ziegelbauer H, Franzoso G, Brown K, and Siebenlist U. (2000). Physical and functional interaction of filamin (actin-binding protein-280) and tumor necrosis factor receptor-associated factor 2. J Biol Chem 275, 271-278.

Lerner AG, Upton JP, Praveen PV, Ghosh R, Nakagawa Y, Igbaria A, Shen S, Nguyen V, Backes BJ, Heiman M, Heintz N, Greengard P, Hui S, Tang Q, Trusina A, Oakes SA, and Papa FR. (2012). IRE1α induces thioredoxin-interacting protein to activate the NLRP3 inflammasome and promote programmed cell death under irremediable ER stress. Cell Metab 16, 250-264.

Li B, Yi P, Zhang B, Xu C, Liu Q, Pi Z, Xu X, Chevet E, and Liu J. (2011). Differences in endoplasmic reticulum stress signalling kinetics determine cell survival outcome through activation of MKP-1. Cell Signal 23, 35-45.

Liu J, Minemoto Y, and Lin A. (2004). c-Jun N-terminal protein kinase 1 (JNK1), but not JNK2, is essential for tumor necrosis factor alpha-induced c-Jun kinase activation and apoptosis. Mol Cell Biol 24, 10844-10856.

Lu M, Lawrence DA, Marsters S, Acosta-Alvear D, Kimmig P, Mendez AS, Paton AW, Paton JC, Walter P, and Ashkenazi A. (2014). Opposing unfolded-protein-response signals converge on death receptor 5 to control apoptosis. Science 345, 98-101.

Mauro C, Crescenzi E, De Mattia R, Pacifico F, Mellone S, Salzano S, de Luca C, D'Adamio L, Palumbo G, Formisano S, Vito P, and Leonardi A. (2006). Central role

592 of the scaffold protein tumor necrosis factor receptor-associated factor 2 in regulating
593 endoplasmic reticulum stress-induced apoptosis. J Biol Chem 281, 2631-2638.
594 Morton HJ. (1970). A survey of commercially available tissue culture media. In Vitro
595 6, 89-108.
596 Murphy LO, Smith S, Chen RH, Fingar DC, and Blenis J. (2002). Molecular
597 interpretation of ERK signal duration by immediate early gene products. Nat Cell Biol
598 4, 556-564.
599 Nishina H, Fischer KD, Radvanyi L, Shahinian A, Hakem R, Rubie EA, Bernstein A,
600 Mak TW, Woodgett JR, and Penninger JM. (1997). Stress-signalling kinase Sek1
601 protects thymocytes from apoptosis mediated by CD95 and CD3. Nature 385, 350-
602 353.
603 Nishitoh H, Matsuzawa A, Tobiume K, Saegusa K, Takeda K, Inoue K, Hori S,
604 Kakizuka A, and Ichijo H. (2002). ASK1 is essential for endoplasmic reticulum
605 stress-induced neuronal cell death triggered by expanded polyglutamine repeats.
606 Genes Dev 16, 1345-1355.
607 Oda Y, Okada T, Yoshida H, Kaufman RJ, Nagata K, and Mori K. (2006). Derlin-2
608 and Derlin-3 are regulated by the mammalian unfolded protein response and are
609 required for ER-associated degradation. J Cell Biol 172, 383-393.
610 Oslowski CM, Hara T, O'Sullivan-Murphy B, Kanekura K, Lu S, Hara M, Ishigaki S,
611 Zhu LJ, Hayashi E, Hui ST, Greiner D, Kaufman RJ, Bortell R, and Urano F. (2012).
612 Thioredoxin-interacting protein mediates ER stress-induced β cell death through
613 initiation of the inflammasome. Cell Metab 16, 265-273.
614 Papa S, Zazzeroni F, Bubici C, Jayawardena S, Alvarez K, Matsuda S, Nguyen DU,
615 Pham CG, Nelsbach AH, Melis T, De Smaele E, Tang WJ, D'Adamio L, and

Franzoso G. (2004). Gadd45β mediates the NF-κB suppression of JNK signalling by targeting MKK7/JNKK2. Nat Cell Biol 6, 146-153.

Pfaffl MW. (2001). A new mathematical model for relative quantification in real-time RT-PCR. Nucleic Acids Res 29, e45.

Prischi F, Nowak PR, Carrara M, and Ali MM. (2014). Phosphoregulation of Ire1 RNase splicing activity. Nat Commun 5, 3554.

Rahmani M, Peron P, Weitzman J, Bakiri L, Lardeux B, and Bernuau D. (2001). Functional cooperation between JunD and NF-κB in rat hepatocytes. Oncogene 20, 5132-5142.

Raingeaud J, Gupta S, Rogers JS, Dickens M, Han J, Ulevitch RJ, and Davis RJ. (1995). Pro-inflammatory cytokines and environmental stress cause p38 mitogen-activated protein kinase activation by dual phosphorylation on tyrosine and threonine. J Biol Chem 270, 7420-7426.

Reers M, Smith TW, and Chen LB. (1991). J-aggregate formation of a carbocyanine as a quantitative fluorescent indicator of membrane potential. Biochemistry 30, 4480-4486.

Reinhard C, Shamoon B, Shyamala V, and Williams LT. (1997). Tumor necrosis factor α-induced activation of c-jun N-terminal kinase is mediated by TRAF2. EMBO J 16, 1080-1092.

Reuther-Madrid JY, Kashatus D, Chen S, Li X, Westwick J, Davis RJ, Earp HS, Wang C-Y, and Baldwin Jr AS, Jr. (2002). The p65/RelA subunit of NF-κB suppresses the sustained, antiapoptotic activity of Jun kinase induced by tumor necrosis factor. Mol Cell Biol 22, 8175-8183.

Ron D, and Walter P. (2007). Signal integration in the endoplasmic reticulum unfolded protein response. Nat Rev Mol Cell Biol 8, 519-529.

641 Roulston A, Reinhard C, Amiri P, and Williams LT. (1998). Early activation of c-Jun
642 N-terminal kinase and p38 kinase regulate cell survival in response to tumor necrosis
643 factor α. J Biol Chem 273, 10232-10239.
644 Rubin CS, Hirsch A, Fung C, and Rosen OM. (1978). Development of hormone
645 receptors and hormonal responsiveness *in vitro*. Insulin receptors and insulin
646 sensitivity in the preadipocyte and adipocyte forms of 3T3-L1 cells. J Biol Chem 253,
647 7570-7578.
648 Rutzky LP, and Pumper RW. (1974). Supplement to a survey of commercially
649 available tissue culture media (1970). In Vitro 9, 468-469.
650 Sanchez-Perez I, Murguia JR, and Perona R. (1998). Cisplatin induces a persistent
651 activation of JNK that is related to cell death. Oncogene 16, 533-540.
652 Sandow JJ, Dorstyn L, O'Reilly LA, Tailler M, Kumar S, Strasser A, and Ekert PG.
653 (2014). ER stress does not cause upregulation and activation of caspase-2 to initiate
654 apoptosis. Cell death and differentiation 21, 475-480.
655 Shen X, Ellis RE, Lee K, Liu C-Y, Yang K, Solomon A, Yoshida H, Morimoto R,
656 Kurnit DM, Mori K, and Kaufman RJ. (2001). Complementary signaling pathways
657 regulate the unfolded protein response and are required for *C. elegans* development.
658 Cell 107, 893-903.
659 Shi Y, An J, Liang J, Hayes SE, Sandusky GE, Stramm LE, and Yang NN. (1999).
660 Characterization of a mutant pancreatic eIF-2α kinase, PEK, and co-localization with
661 somatostatin in islet delta cells. J Biol Chem 274, 5723-5730.
662 Shi Y, Vattem KM, Sood R, An J, Liang J, Stramm L, and Wek RC. (1998).
663 Identification and characterization of pancreatic eukaryotic initiation factor 2 α-
664 subunit kinase, PEK, involved in translational control. Mol Cell Biol 18, 7499-7509.

665 Sluss HK, Barrett T, Derijard B, and Davis RJ. (1994). Signal transduction by tumor
666 necrosis factor mediated by JNK protein kinases. Mol Cell Biol 14, 8376-8384.
667 Smiley ST, Reers M, Mottola-Hartshorn C, Lin M, Chen A, Smith TW, Steele GD,
668 Jr., and Chen LB. (1991). Intracellular heterogeneity in mitochondrial membrane
669 potentials revealed by a J-aggregate-forming lipophilic cation JC-1. Proc Natl Acad
670 Sci U S A 88, 3671-3675.
671 Smith MI, and Deshmukh M. (2007). Endoplasmic reticulum stress-induced apoptosis
672 requires bax for commitment and Apaf-1 for execution in primary neurons. Cell death
673 and differentiation 14, 1011-1019.
674 Stehlik C, de Martin R, Kumabashiri I, Schmid JA, Binder BR, and Lipp J. (1998).
675 Nuclear factor (NF)-κB-regulated X-chromosome-linked *iap* gene expression protects
676 endothelial cells from tumor necrosis factor α-induced apoptosis. J Exp Med 188,
677 211-216.
678 Tan Y, Dourdin N, Wu C, De Veyra T, Elce JS, and Greer PA. (2006). Ubiquitous
679 calpains promote caspase-12 and JNK activation during endoplasmic reticulum stress-
680 induced apoptosis. J Biol Chem 281, 16016-16024.
681 Tang F, Tang G, Xiang J, Dai Q, Rosner MR, and Lin A. (2002). The absence of NF-
682 κB-mediated inhibition of c-Jun N-terminal kinase activation contributes to tumor
683 necrosis factor alpha-induced apoptosis. Mol Cell Biol 22, 8571-8579.
684 Tang G, Minemoto Y, Dibling B, Purcell NH, Li Z, Karin M, and Lin A. (2001).
685 Inhibition of JNK activation through NF-κB target genes. Nature 414, 313-317.
686 Teodoro T, Odisho T, Sidorova E, and Volchuk A. (2012). Pancreatic β-cells depend
687 on basal expression of active ATF6α-p50 for cell survival even under nonstress
688 conditions. Am J Physiol Cell Physiol 302, C992-C1003.

689 Tirasophon W, Welihinda AA, and Kaufman RJ. (1998). A stress response pathway
690 from the endoplasmic reticulum to the nucleus requires a novel bifunctional protein
691 kinase/endoribonuclease (Ire1p) in mammalian cells. Genes Dev 12, 1812-1824.
692 Tournier C, Hess P, Yang DD, Xu J, Turner TK, Nimnual A, Bar-Sagi D, Jones SN,
693 Flavell RA, and Davis RJ. (2000). Requirement of JNK for stress-induced activation
694 of the cytochrome c-mediated death pathway. Science 288, 870-874.
695 Traverse S, Seedorf K, Paterson H, Marshall CJ, Cohen P, and Ullrich A. (1994).
696 EGF triggers neuronal differentiation of PC12 cells that overexpress the EGF
697 receptor. Curr Biol 4, 694-701.
698 Upton JP, Wang L, Han D, Wang ES, Huskey NE, Lim L, Truitt M, McManus MT,
699 Ruggero D, Goga A, Papa FR, and Oakes SA. (2012). IRE1α cleaves select
700 microRNAs during ER stress to derepress translation of proapoptotic caspase-2.
701 Science 338, 818-822.
702 Urano F, Wang X, Bertolotti A, Zhang Y, Chung P, Harding HP, and Ron D. (2000).
703 Coupling of stress in the ER to activation of JNK protein kinases by transmembrane
704 protein kinase IRE1. Science 287, 664-666.
705 Ventura J-J, Cogswell P, Flavell RA, Baldwin AS, Jr., and Davis RJ. (2004). JNK
706 potentiates TNF-stimulated necrosis by increasing the production of cytotoxic
707 reactive oxygen species. Genes Dev 18, 2905-2915.
708 Ventura J-J, Hubner A, Zhang C, Flavell RA, Shokat KM, and Davis RJ. (2006).
709 Chemical genetic analysis of the time course of signal transduction by JNK. Mol Cell
710 21, 701-710.
711 Ventura JJ, Kennedy NJ, Lamb JA, Flavell RA, and Davis RJ. (2003). c-Jun NH_2-
712 terminal kinase is essential for the regulation of AP-1 by tumor necrosis factor. Mol
713 Cell Biol 23, 2871-2882.

714 Walter P, and Ron D. (2011). The unfolded protein response: from stress pathway to
715 homeostatic regulation. Science 334, 1081-1086.
716 Wang Q, Zhang H, Zhao B, and Fei H. (2009). IL-1β caused pancreatic β-cells
717 apoptosis is mediated in part by endoplasmic reticulum stress via the induction of
718 endoplasmic reticulum Ca^{2+} release through the c-Jun N-terminal kinase pathway.
719 Mol Cell Biochem 324, 183-190.
720 Wang XZ, Harding HP, Zhang Y, Jolicoeur EM, Kuroda M, and Ron D. (1998).
721 Cloning of mammalian Ire1 reveals diversity in the ER stress responses. EMBO J 17,
722 5708-5717.
723 Wu S, Hu Y, Wang JL, Chatterjee M, Shi Y, and Kaufman RJ. (2002). Ultraviolet
724 light inhibits translation through activation of the unfolded protein response kinase
725 PERK in the lumen of the endoplasmic reticulum. J Biol Chem 277, 18077-18083.
726 Wu S, Tan M, Hu Y, Wang JL, Scheuner D, and Kaufman RJ. (2004). Ultraviolet
727 light activates NFκB through translational inhibition of IκBα synthesis. J Biol Chem
728 279, 34898-34902.
729 Yeh W-C, Shahinian A, Speiser D, Kraunus J, Billia F, Wakeham A, de la Pompa JL,
730 Ferrick D, Hum B, Iscove N, Ohashi P, Rothe M, Goeddel DV, and Mak TW. (1997).
731 Early lethality, functional NF-κB activation, and increased sensitivity to TNF-induced
732 cell death in TRAF2-deficient mice. Immunity 7, 715-725.
733 Yoneda T, Imaizumi K, Oono K, Yui D, Gomi F, Katayama T, and Tohyama M.
734 (2001). Activation of caspase-12, an endoplastic reticulum (ER) resident caspase,
735 through tumor necrosis factor receptor-associated factor 2-dependent mechanism in
736 response to the ER stress. J Biol Chem 276, 13935-13940.

737 Yoshida H, Matsui T, Hosokawa N, Kaufman RJ, Nagata K, and Mori K. (2003). A
738 time-dependent phase shift in the mammalian unfolded protein response. Dev Cell 4,
739 265-271.
740 Yoshida H, Matsui T, Yamamoto A, Okada T, and Mori K. (2001). XBP1 mRNA is
741 induced by ATF6 and spliced by IRE1 in response to ER stress to produce a highly
742 active transcription factor. Cell 107, 881-891.
743 Yoshida H, Okada T, Haze K, Yanagi H, Yura T, Negishi M, and Mori K. (2000).
744 ATF6 activated by proteolysis binds in the presence of NF-Y (CBF) directly to the
745 *cis*-acting element responsible for the mammalian unfolded protein response. Mol
746 Cell Biol 20, 6755-6767.
747 Yu C, Minemoto Y, Zhang J, Liu J, Tang F, Bui TN, Xiang J, and Lin A. (2004). JNK
748 suppresses apoptosis via phosphorylation of the proapoptotic Bcl-2 family protein
749 BAD. Mol Cell 13, 329-340.
750 Zhang C, Kawauchi J, Adachi MT, Hashimoto Y, Oshiro S, Aso T, and Kitajima S.
751 (2001). Activation of JNK and transcriptional repressor ATF3/LRF1 through the
752 IRE1/TRAF2 pathway is implicated in human vascular endothelial cell death by
753 homocysteine. Biochem Biophys Res Commun 289, 718-724.
754 Zhang K, Shen X, Wu J, Sakaki K, Saunders T, Rutkowski DT, Back SH, and
755 Kaufman RJ. (2006). Endoplasmic reticulum stress activates cleavage of CREBH to
756 induce a systemic inflammatory response. Cell 124, 587-599.

757 **Figure Legends**

758 **Figure 1.** Transient JNK activation precedes activation of *XBP1* splicing in MEFs.
759 **(A)** Kinetics of JNK activation and **(B)** *XBP1* splicing in MEFs exposed to 1 μM
760 thapsigargin. **(C)** Quantitation of the JNK phosphorylation (white circles, solid line)
761 from panel (A) and *XBP1* splicing (black circles, dashed line) from panel (B). **(D)**

762 Kinetics of JNK activation and **(E)** *XBP1* splicing in MEFs exposed to 10 μg/ml
763 tunicamycin. **(F)** Quantitation of the JNK phosphorylation (white circles, solid line)
764 from panel (D) and *XBP1* splicing (black circles, dashed line) from panel (E).

765 **Figure 2.** Kinetics of JNK activation and of *XBP1* splicing in response to acute ER
766 stress in Hep G2 cells. **(A)** Western blots for phospho-JNK (p-JNK) and total JNK
767 (JNK) of Hep G2 cells exposed to 1 μM thapsigargin for the indicated times. **(B)**
768 Detection of *XBP1* splicing by reverse transcriptase PCR. Hep G2 cells were exposed
769 to 1 μM thapsigargin for the indicated times. **(C)** Quantitation of the JNK
770 phosphorylation (white circles, solid line) from panel (A) and *XBP1* splicing (black
771 circles, dashed line) from panel (B).

772 **Figure 3.** IRE1α and TRAF2 are required for the transient JNK activation in MEFs.
773 **(A)** Kinetics of JNK activation and **(B)** *XBP1* splicing in *ire1α*$^{-/-}$ MEFs exposed to 1
774 μM thapsigargin. **(C)** Quantitation of the JNK phosphorylation (white circles, solid
775 line) from panel (A) and *XBP1* splicing (black circles, dashed line) from panel (B).
776 **(D)** Kinetics of JNK activation and **(E)** *XBP1* splicing in *traf2*$^{-/-}$ MEFs exposed to 1
777 μM thapsigargin. **(F)** Quantitation of the JNK phosphorylation (white circles, solid
778 line) from panel (D) and *XBP1* splicing (black circles, dashed line) from panel (E).

779 **Figure 4.** JNK is required for transcriptional induction of antiapoptotic genes early in
780 the ER stress response. **(A)** *cIAP1* (*BIRC2*), **(B)** *cIAP2* (*BIRC3*), **(C)** *XIAP* (*BIRC4),*
781 and **(D)** *BIRC6* steady-state mRNA levels were quantitated by RT-qPCR in WT and
782 *jnk1*$^{-/-}$ *jnk2*$^{-/-}$ MEFs exposed to 1 μM thapsigargin for the indicated times.

783 **Figure 5.** JNK inhibits cell death early in the ER stress response. **(A)** WT and *jnk1*$^{-/-}$
784 *jnk2*$^{-/-}$ were treated with 1 μM thapsigargin (Tg) for 4 h and stained with JC-1 as
785 described in Materials and Methods. Scale bar – 10 μm. **(B)** Quantitation of the

786 confocal fluorescence microscopy data shown in panel A. At least 600 cells were
787 counted for each sample.

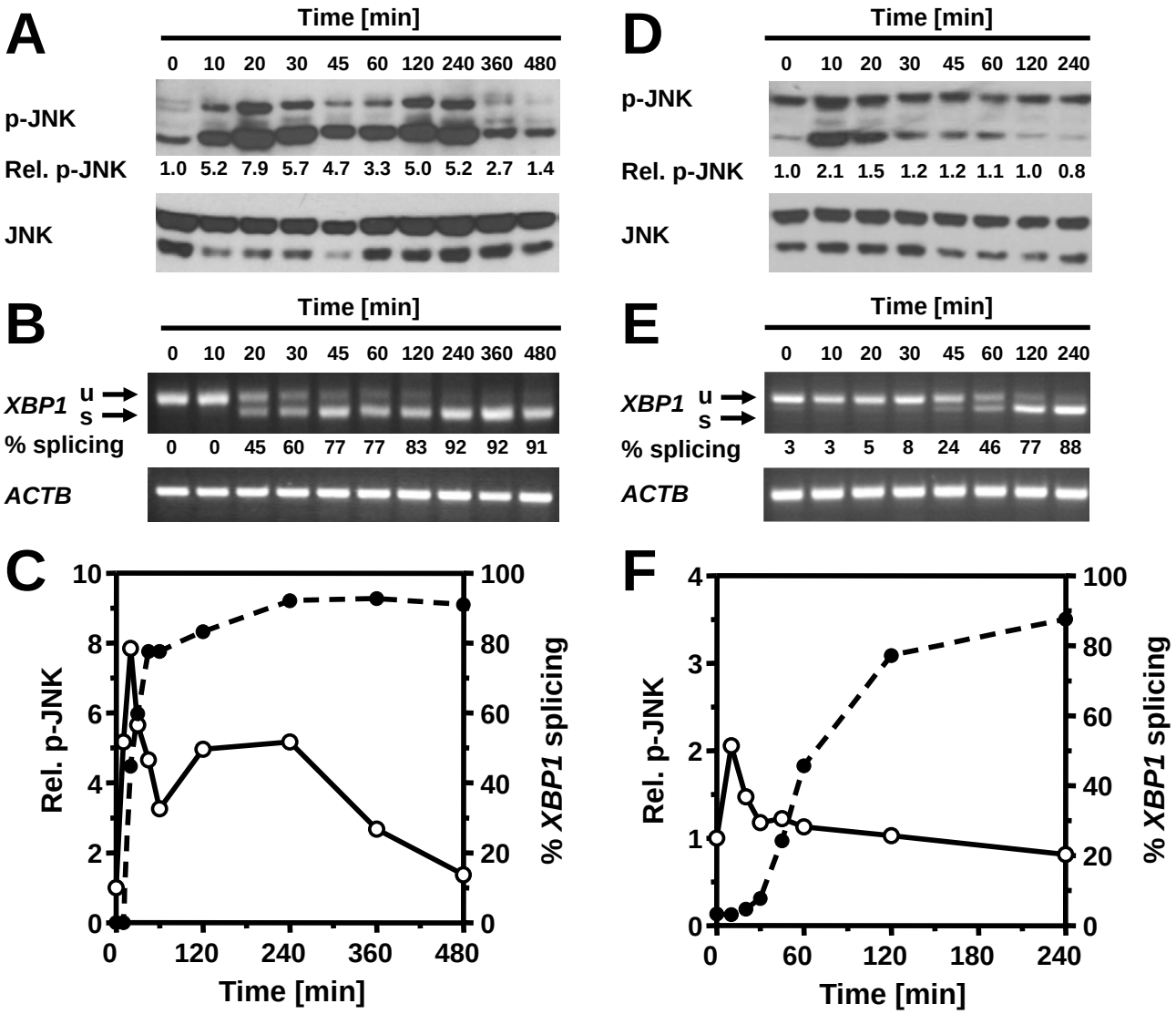

Figure 1. Transient JNK activation precedes activation of *XBP1* splicing in MEFs. **(A)** Kinetics of JNK activation and **(B)** *XBP1* splicing in MEFs exposed to 1 μM thapsigargin. **(C)** Quantitation of the JNK phosphorylation (white circles, solid line) from panel (A) and *XBP1* splicing (black circles, dashed line) from panel (B). **(D)** Kinetics of JNK activation and **(E)** *XBP1* splicing in MEFs exposed to 10 μg/ml tunicamycin. **(F)** Quantitation of the JNK phosphorylation (white circles, solid line) from panel (D) and *XBP1* splicing (black circles, dashed line) from panel (E).

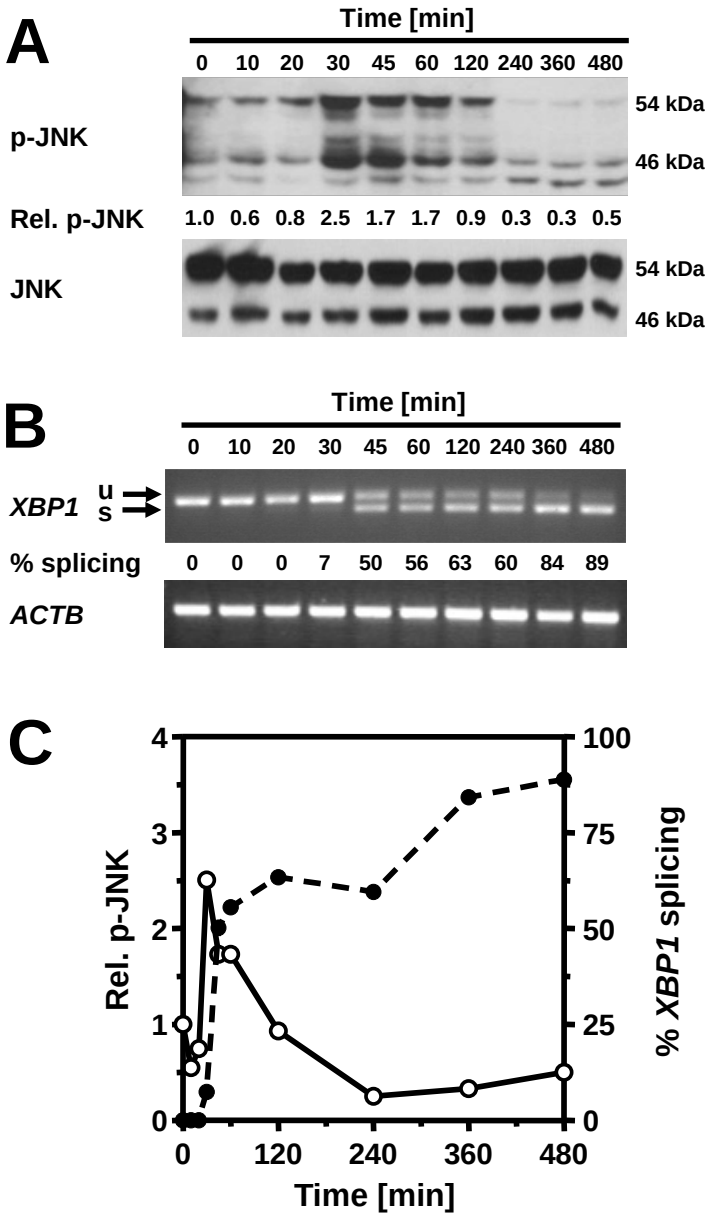

Figure 2. Kinetics of JNK activation and of *XBP1* splicing in response to acute ER stress in Hep G2 cells. **(A)** Western blots for phospho-JNK (p-JNK) and total JNK (JNK) of Hep G2 cells exposed to 1 μM thapsigargin for the indicated times. **(B)** Detection of *XBP1* splicing by reverse transcriptase PCR. Hep G2 cells were exposed to 1 μM thapsigargin for the indicated times. **(C)** Quantitation of the JNK phosphorylation (white circles, solid line) from panel (A) and *XBP1* splicing (black circles, dashed line) from panel (B).

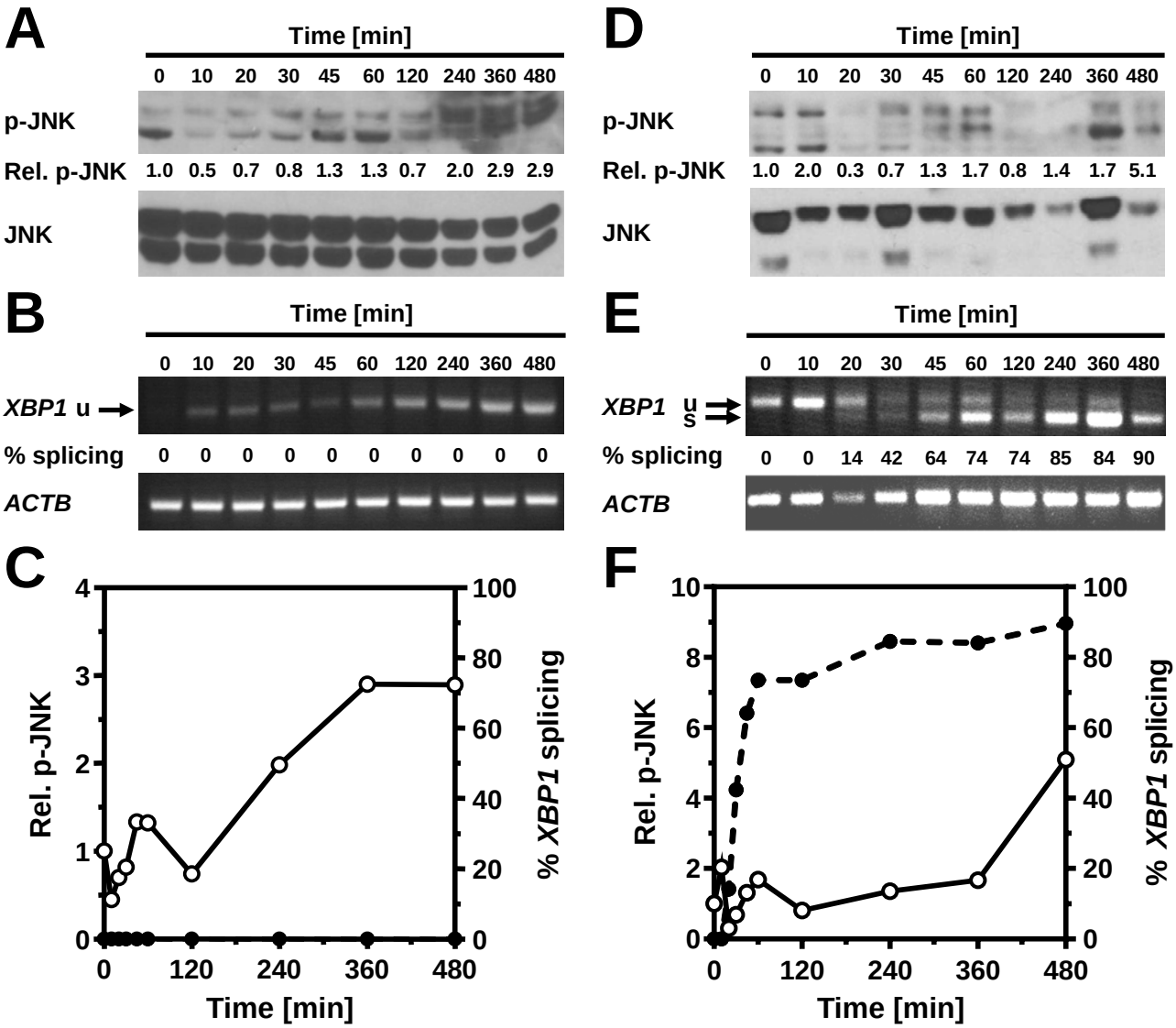

Figure 3. IRE1α and TRAF2 are required for the transient JNK activation in MEFs. **(A)** Kinetics of JNK activation and **(B)** *XBP1* splicing in *ire1α*$^{-/-}$ MEFs exposed to 1 μM thapsigargin. **(C)** Quantitation of the JNK phosphorylation (white circles, solid line) from panel (A) and *XBP1* splicing (black circles, dashed line) from panel (B). **(D)** Kinetics of JNK activation and **(E)** *XBP1* splicing in *traf2*$^{-/-}$ MEFs exposed to 1 μM thapsigargin. **(F)** Quantitation of the JNK phosphorylation (white circles, solid line) from panel (D) and *XBP1* splicing (black circles, dashed line) from panel (E).

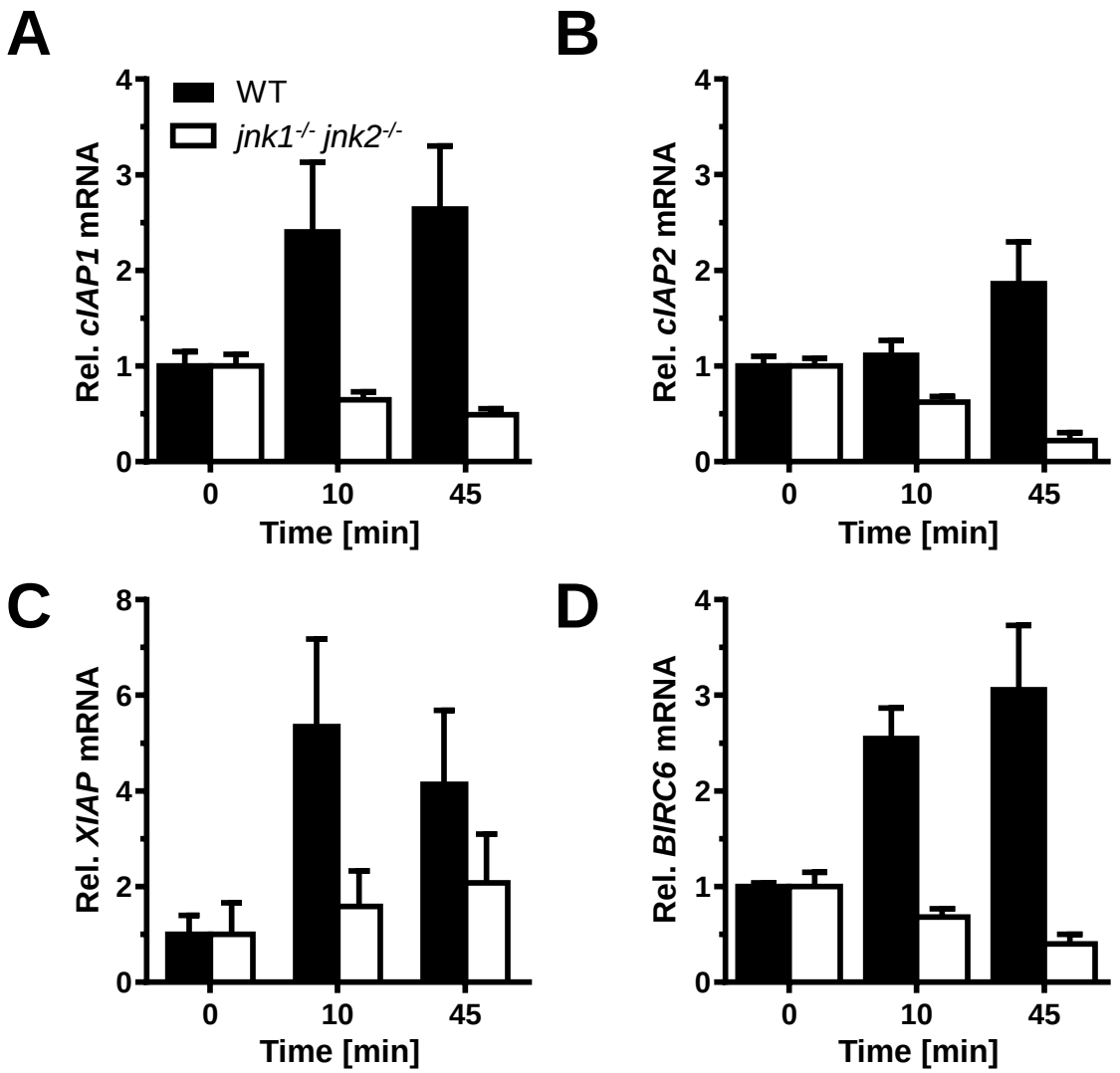

Figure 4. JNK is required for transcriptional induction of antiapoptotic genes early in the ER stress response. **(A)** *cIAP1* (*BIRC2*), **(B)** *cIAP2* (*BIRC3*), **(C)** *XIAP* (*BIRC4),* and **(D)** *BIRC6* (*BRUCE, APOLLON*) steady-state mRNA levels were quantitated by RT-qPCR in WT and *jnk1*$^{-/-}$ *jnk2*$^{-/-}$ MEFs exposed to 1 μM thapsigargin for the indicated times.

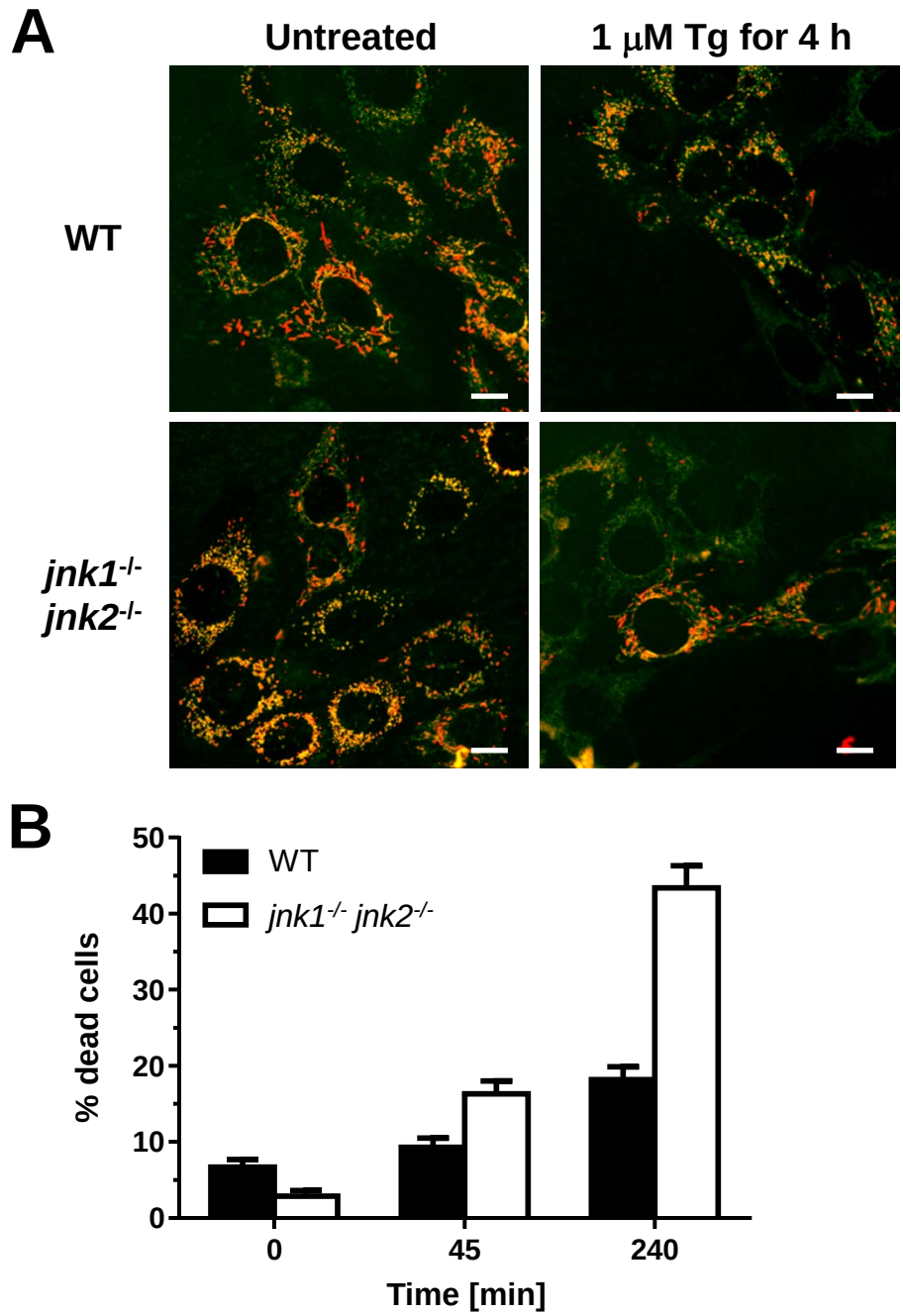

Figure 5. JNK inhibits cell death early in the ER stress response. **(A)** WT and *jnk1*$^{-/-}$ *jnk2*$^{-/-}$ were treated with 1 μM thapsigargin (Tg) for 4 h and stained with JC-1 as described in Materials and Methods. Scale bar – 10 μm. **(B)** Quantitation of the confocal fluorescence microscopy data shown in panel A. At least 600 cells were counted for each sample.

Supplemental Data

Supplemental tables

Supplemental table 1. siRNAs.

Species	Gene	#	Sequence
Homo sapiens	*IRE1α*	1	GCGUAAAUUCAGGACCUAUdTdT
H. sapiens	*IRE1α*	2	GAUAGUCUCUGCCCAUCAAdTdT
H. sapiens	*IRE1α*	3	CAUUGCACGUGAAUUGAUAdTdT
H. sapiens	*TRAF2*	1	CACUCAGAGUGGGAGCACAdTdT
H. sapiens	*TRAF2*	2	GUCAAGACUUGUGGCAAGUdTdT
H. sapiens	*TRAF2*	3	GCCUUCAGGCCCGACGUGAdTdT
Mus musculus	*TRAF2*	1	GAAUUCCUAUGUGCGGGAUdTdT
M. musculus	*TRAF2*	2	GUUAGAGCAUGCAGCAAAUdTdT
M. musculus	*TRAF2*	3	CTATGAAGGCCTGTATGAAdTdT
Aequora victora	eGFP		GCAAGCUGACCCUGAAGUUCAU

Supplemental table 2. Oligodeoxynucleotides. Restriction sites are underlined. The start codon for TRAF2Δ1-86 is shown in bold.

Name	Purpose	Sequence
Oligodeoxynucleotides for *H. sapiens* genes		
H8197	*TRAF2* RT-qPCR for siRNA #3, reverse	AATGGCCTTGATGAAGATGG
H8215	*TRAF2Δ1-86* construction, forward primer	TGCATCGAT**ATG**AGCAGTTCGGCCTTCCCA
H8216	*TRAF2Δ1-86* construction, reverse primer	CGAGCGGCCGCCACTGTGCTGGATATCTGC
H8280	*TRAF2* RT-qPCR for siRNA #1, forward	CTTAGCCAAGGGCTGTGGT
H8281	*TRAF2* RT-qPCR for siRNA #1, reverse	AGGAATGCTCCCTTCTCTCC
H8282	*TRAF2* RT-qPCR for siRNA #2, forward	GTCCGCCTTGGTGAAAAG
H8283	*TRAF2* RT-qPCR for siRNA #2, reverse	TCTCACCCTCTACCGTCTCG
H8284	*TRAF2* RT-qPCR for siRNA #3, forward	ACACCAGCAGGTACGGCTAC
H8287	*ACTA1* RT-qPCR, forward	CTGAGCGTGGCTACTCCTTC
H8288	*ACTA1* RT-qPCR, reverse	GGCATACAGGTCCTTCCTGA
H8289	*XBP1* PCR, forward	GAGTTAAGACAGCGCTTGGG
H8290	*XBP1* PCR, reverse	ACTGGGTCCAAGTTGTCCAG
H8993	*IRE1α* RT-qPCR, forward	TGGGACAGCTAGGCTGAGAT

H8994	*IRE1α* RT-qPCR, reverse	TGGGCACATCTGTGATCAAT

Oligodeoxynucleotides for *M. musculus* genes

H7961	*XBP1* PCR, forward	GATCCTGACGAGGTTCCAGA
H7962	*XBP1* PCR, reverse	ACAGGGTCCAACTTGTCCAG
H7994	*ACTB* PCR, forward	AGCCATGTACGTAGCCATCC
H7995	*ACTB* PCR, reverse	CTCTCAGCTGTGGTGGTGAA
H8237	*TRAF2* RT-qPCR for siRNA #1, forward	GAACTCATCTGTCTCTCTTCTTCG
H8238	*TRAF2* RT-qPCR for siRNA #1, reverse	AGCAGGGGTGGCTAGAGTCC
H8239	*TRAF2* RT-qPCR for siRNA #2, forward	CTGCAGAGCACCCTGTAGC
H8240	*TRAF2* RT-qPCR for siRNA #2, reverse	CCTGCAGGTTCTCAGTCTCC
H8269	*TRAF2* RT-qPCR for siRNA #3, forward	ACTGCTCCTTCTGCCTGACC
H8270	*TRAF2* RT-qPCR for siRNA #3, reverse	TTCTTTCAAGGTCCCCTTCC
H8271	*GAPDH* RT-qPCR, forward	TCGTCCCGTAGACAAAATGG
H8272	*GAPDH* RT-qPCR, reverse	CTCCTGGAAGATGGTGATGG
H8322	*MYL1* 3f RT-qPCR, forward	TGCTGACCAGATTGCCGACTTCA
H8323	*MYL1* 3f RT-qPCR, reverse	CCCGGAGGACGTCTCCCACC
H8326	*AHCY* RT-qPCR, forward	GGTGCTGAGGTGCGGTGGTC
H8327	*AHCY* RT-qPCR, reverse	GGGTCCGTCCTTGAAGTGCAGC
H8328	*TNNC1* RT-qPCR, forward	GCACCAAGGAGCTGGGCAAGG

H8329	*TNNC1* RT-qPCR, reverse	TGTGCCACTGCCATCCTCGT
H9054	*cIAP1* (*BIRC2*) RT-qPCR, forward	TAGTGTTCCTGTTCAGCCCG
H9055	*cIAP1* (*BIRC2*) RT-qPCR, reverse	TCCCAACATCTCAAGCCACC
H9056	*cIAP2* (*BIRC3*) RT-qPCR, forward	ACGATTTAAAGGTATCGCGCC
H9057	*cIAP2*(*BIRC3*) RT-qPCR, reverse	CTGATACCGCAGCCCACTTC
H9076	*XIAP* (*BIRC4*) RT-qPCR, forward	ACGGAGGATGAGTCAAGTCAAA
H9077	*XIAP* (*BIRC4*) RT-qPCR, reverse	AAGTGACCAGATGTCCACAAGG
H9080	*BRUCE* (*BIRC6*) RT-qPCR, forward	CCAGTGTGAGGAGTGGATTGC
H9081	*BRUCE* (*BIRC6*) RT-qPCR, reverse	CCTCAATGTCCGGATCTAAGCC

Supplemental figure legends

Figure S1. Characterization of *in vitro* differentiation of 3T3-F442 adipocytes and C_2C_{12} myotubes. **(A)** Oil red O staining of lipid droplets in 3T3-F442A cells (i) before and (ii) 12 d after differentiation. Magnification: 10 x. **(B)** mRNA levels for the muscle differentiation markers *AHCY* encoding *S*-adenosyl-homocysteine hydrolase, *MYL1* encoding myosin light chain 1, and *TNNC1* encoding troponin C in differentiated C_2C_{12} cells. The fold changes in mRNA abundance relative to undifferentiated cells (day 0) are shown.

Figure S2. Kinetics of JNK activation and of *XBP1* splicing in response to acute ER stress in *in vitro* differentiated 3T3-F442A adipocytes. **(A)** Western blots for phospho-JNK (p-JNK) and total JNK (JNK) and **(B)** *XBP1* splicing in 3T3-F442A cells exposed to 1 μM thapsigargin for the indicated times. **(C)** Quantitation of the JNK phosphorylation (white circles, solid line) from panel (A) and *XBP1* splicing (black circles, dashed line) from panel (B).

Figure S3. Kinetics of JNK activation and of *XBP1* splicing in response to acute ER stress in *in vitro* differentiated C_2C_{12} myotubes. **(A)** Western blots for phospho-JNK (p-JNK) and total JNK (JNK) and **(B)** *XBP1* splicing in C_2C_{12} cells exposed to 1 μM thapsigargin for the indicated times. **(C)** Quantitation of the JNK phosphorylation (white circles, solid line) from panel (A) and *XBP1* splicing (black circles, dashed line) from panel (B).

Figure S4. Acute JNK activation is IRE1α-dependent in Hep G2 cells. **(A)** Hep G2 cells were transfected with 10 nM of the indicated siRNAs. 48 h and 72 h after transfection *IRE1α* mRNA was quantitated by RT-qPCR **(B)** siRNA knock-down of IRE1α impairs ER stress-dependent activation of JNK in Hep G2 cells. 72 h after transfection with the indicated siRNAs Hep G2 cells were stimulated for the indicated times with 1 μM thapsigargin. Cell lysates were analysed by Western blotting. **(C)** Quantitation of JNK phosphorylation in Hep G2 cells treated for the indicated times with 1 μM thapsigargin 72 h after transfection with

the indicated siRNAs. The average and standard error from two independent experiments are shown.

Figure S5. Acute JNK activation in Hep G2 cells is TRAF2 dependent. **(A)** siRNA knock-down of human TRAF2 in Hep G2 cells. Relative *TRAF2* mRNA abundance (to *ACTA1*) was measured by RT-qPCR 24 or 48 h after transfection of Hep G2 cells with the indicated siRNAs. **(B)** Knock-down of TRAF2 expression in Hep G2 cells interferes with ER stress-induced JNK phosphorylation. Hep G2 cells were treated with 1 μM thapsigargin for the times indicated before protein extraction for Western blotting with antibodies against p-JNK, total JNK, TRAF2, and GAPDH. **(C)** Quantitation of the JNK phosphorylation signals in the Western blots of panel (B).

Figure S6. Acute JNK activation is TRAF2-dependent in 3T3-F442A preadipocytes. **(A)** JNK phosphorylation and **(B)** *XBP1* splicing in 3T3-F442A preadipocytes transfected with a siRNA against eGFP. **(C)** Quantitation of the JNK phosphorylation (white circles, solid line) from panel (A) and *XBP1* splicing (black circles, dashed line) from panel (B). **(D)** *TRAF2* mRNA levels measured by real-time PCR in 3T3-F442A preadipocytes after transfection with the indicated siRNAs. **(E)** TRAF2 protein levels relative to GAPDH in 3T3-F442A preadipocytes transfected with the indicated siRNAs against eGFP or murine TRAF2. Cells were treated with 20 ng/ml TNF-α for 20 min where indicated. **(F)** JNK phosphorylation and **(G)** *XBP1* splicing in 3T3-F442A preadipocytes transfected with murine *TRAF2* siRNA #2. **(H)** Quantitation of the JNK phosphorylation (white circles, solid line) from panel (F) and *XBP1* splicing (black circles, dashed line) from panel (G).

Figure S7. Dominant negative TRAF2 blocks JNK activation by acute ER stress in 3T3-F442A preadipocytes. **(A)** Domain structures of WT and dominant-negative TRAF2 (TRAF2Δ1-86). **(B)** Western blots for phospho-JNK, JNK, and TRAF2 in cell lysates prepared from WT MEFs transiently transfected with 8 μg pMT2T-TRAF2Δ1-86 and

stimulated with 50 ng/ml TNF-α for 20 min. **(C)** JNK phosphorylation in 3T3-F442A preadipocytes transfected with pMT2T-TRAF2Δ1-86 to express dominant-negative TRAF2Δ1-86. **(D)** Quantitation of the JNK phosphorylation signals in the Western blots of panel (C).

Figure S8. Acute JNK activation is TRAF2-dependent in C_2C_{12} myoblasts. **(A)** JNK phosphorylation and **(B)** *XBP1* splicing in C_2C_{12} myoblasts transfected with control siRNA against eGFP. (**C)** Quantitation of the JNK phosphorylation (white circles, solid line) from panel (A) and *XBP1* splicing (black circles, dashed line) from panel (B). **(D)** *TRAF2* mRNA levels measured by real-time PCR in C_2C_{12} myoblasts after transfection with the indicated siRNAs. **(E)** JNK phosphorylation and **(F)** *XBP1* splicing in C_2C_{12} myoblasts transfected with murine *TRAF2* siRNA #2. **(G)** Quantitation of the JNK phosphorylation (white circles, solid line) from panel (E) and *XBP1* splicing (black circles, dashed line) from panel (F).

Figure S9. Dominant negative TRAF2 blocks JNK activation by acute ER stress in C_2C_{12} myotubes. **(A)** JNK phosphorylation in C_2C_{12} myoblasts transfected with pMT2T-TRAF2Δ1-86 to express dominant-negative TRAF2Δ1-86. **(B)** Quantitation of the JNK phosphorylation signals.

Figure S10. Immediately activated JNK localizes to the cytosol during ER stress. Serum-starved Hep G2 cells were treated for 45 min with 1 μM thapsigargin or left untreated before isolation of the cytosolic and nuclear fractions. The cytosolic (C) and nuclear (N) fractions were analysed by Western blotting. The asterisk (*) indicates a non-specific band recognised by the anti-emerin antibody. Emerin was used as a nuclear marker and GAPDH as a cytoplasmic marker.

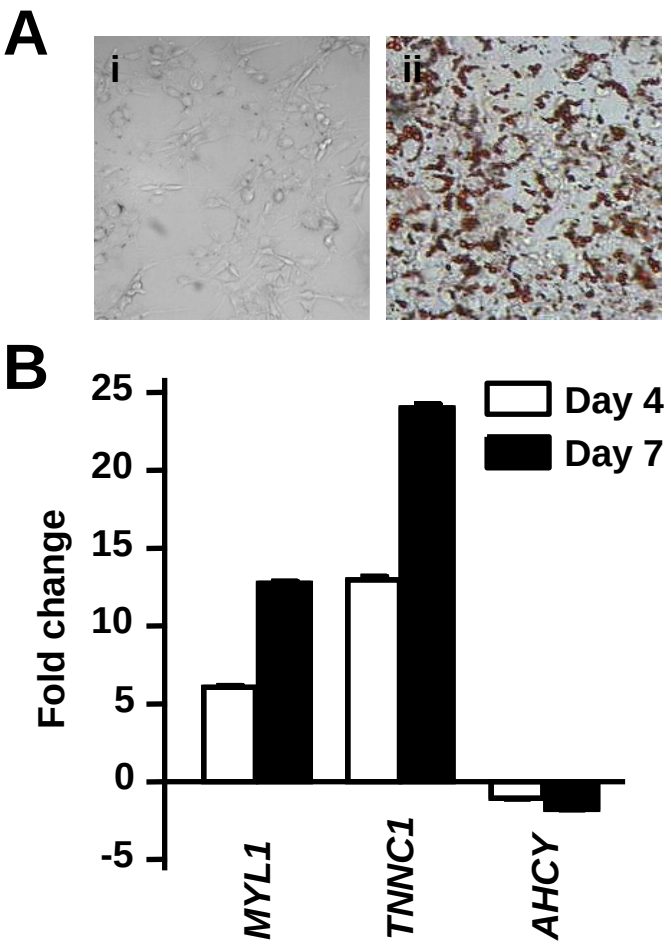

Figure S1. Characterization of *in vitro* differentiation of 3T3-F442 adipocytes and C_2C_{12} myotubes. **(A)** Oil red O staining of lipid droplets in 3T3-F442A cells (i) before and (ii) 12 d after differentiation. Magnification: 10 x. **(B)** mRNA levels for the muscle differentiation markers *AHCY* encoding *S*-adenosyl-homocysteine hydrolase, *MYL1* encoding myosin light chain 1, and *TNNC1* encoding troponin C in differentiated C_2C_{12} cells. The fold changes in mRNA abundance relative to undifferentiated cells (day 0) are shown.

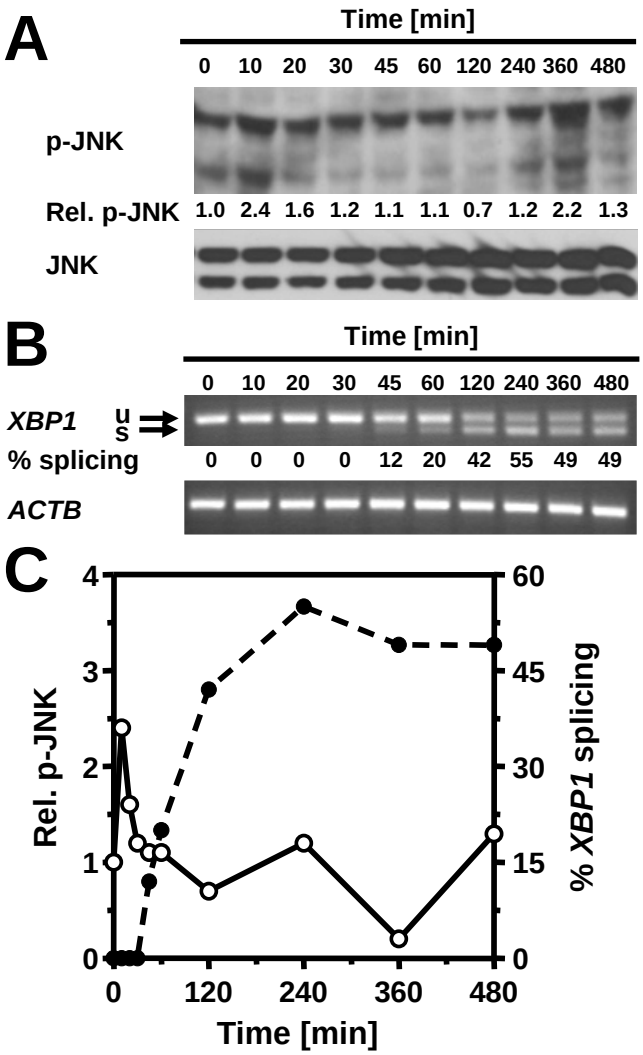

Figure S2. Kinetics of JNK activation and of *XBP1* splicing in response to acute ER stress in *in vitro* differentiated 3T3-F442A adipocytes. **(A)** Western blots for phospho-JNK (p-JNK) and total JNK (JNK) and **(B)** *XBP1* splicing in 3T3-F442A cells exposed to 1 μM thapsigargin for the indicated times. **(C)** Quantitation of the JNK phosphorylation (white circles, solid line) from panel (A) and *XBP1* splicing (black circles, dashed line) from panel (B).

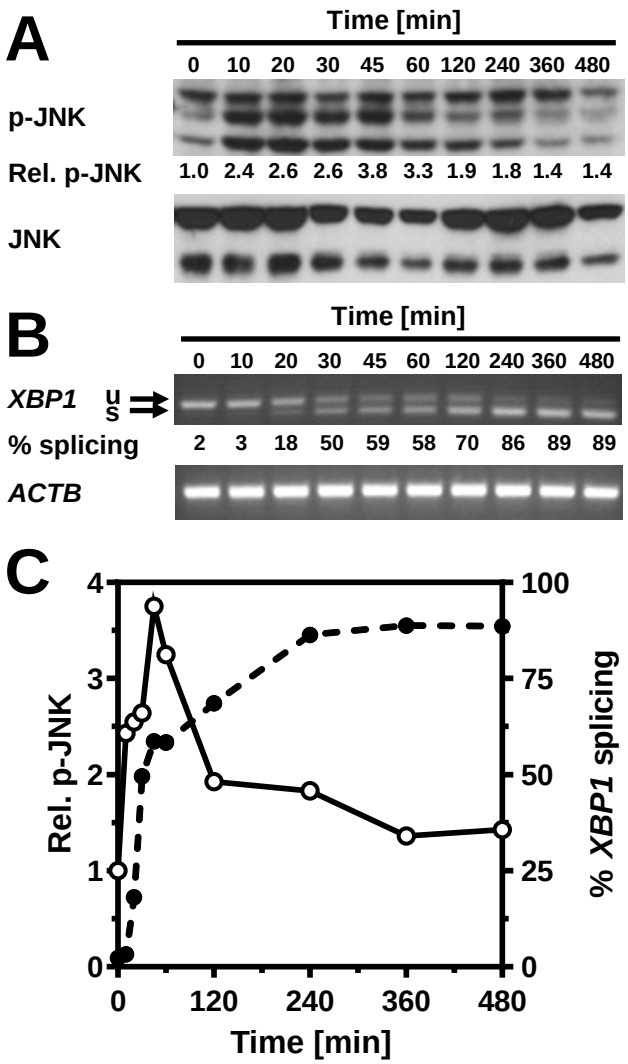

Figure S3. Kinetics of JNK activation and of *XBP1* splicing in response to acute ER stress in *in vitro* differentiated C_2C_{12} myotubes. **(A)** Western blots for phospho-JNK (p-JNK) and total JNK (JNK) and **(B)** *XBP1* splicing in C_2C_{12} cells exposed to 1 μM thapsigargin for the indicated times. **(C)** Quantitation of the JNK phosphorylation (white circles, solid line) from panel (A) and *XBP1* splicing (black circles, dashed line) from panel (B).

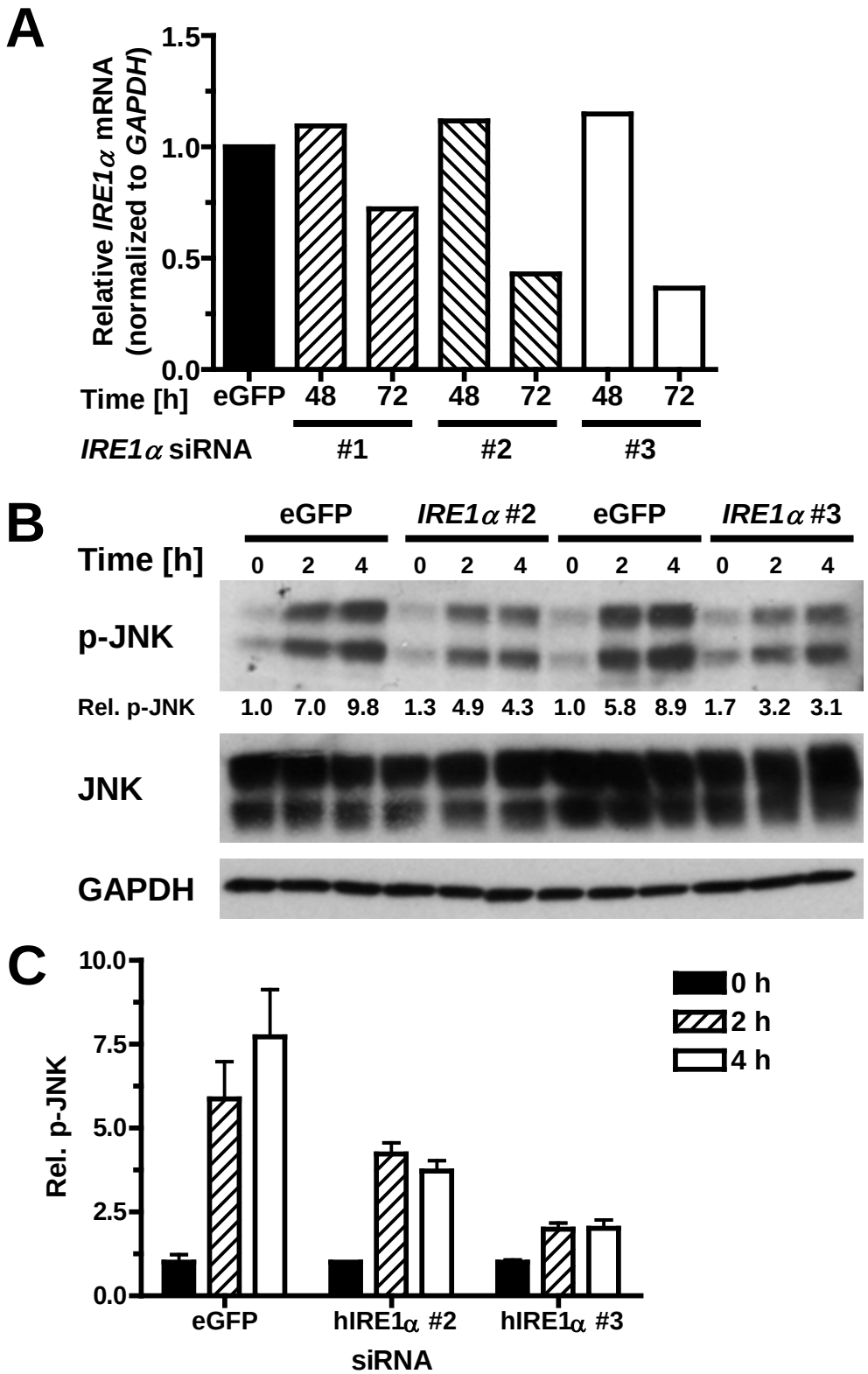

Figure S4. Acute JNK activation is IRE1α-dependent in Hep G2 cells. **(A)** Hep G2 cells were transfected with 10 nM of the indicated siRNAs. 48 h and 72 h after transfection *IRE1α* mRNA was quantitated by quantitative reverse transcriptase (qRT)-PCR located 3' to the siRNA annealing sequences with primers H8993 and H8994. Similar knock-down efficiencies were obtained with a qRT-PCR located 5' to the siRNA annealing sequences (Fig. S4). **(B)** siRNA knock-down of IRE1α impairs ER stress-dependent activation of JNK in Hep G2 cells. 72 h after transfection with the indicated siRNAs Hep G2 cells were stimulated for the indicated times with 1 μM thapsigargin. Cell lysates were analyzed by Western blotting. **(C)** Quantitation of JNK phosphorylation in Hep G2 cells treated for the indicated times with 1 μM thapsigargin 72 h after transfection with the indicated siRNAs. The average and standard error from two independent experiments are shown.

Figure S4, Brown *et al.*

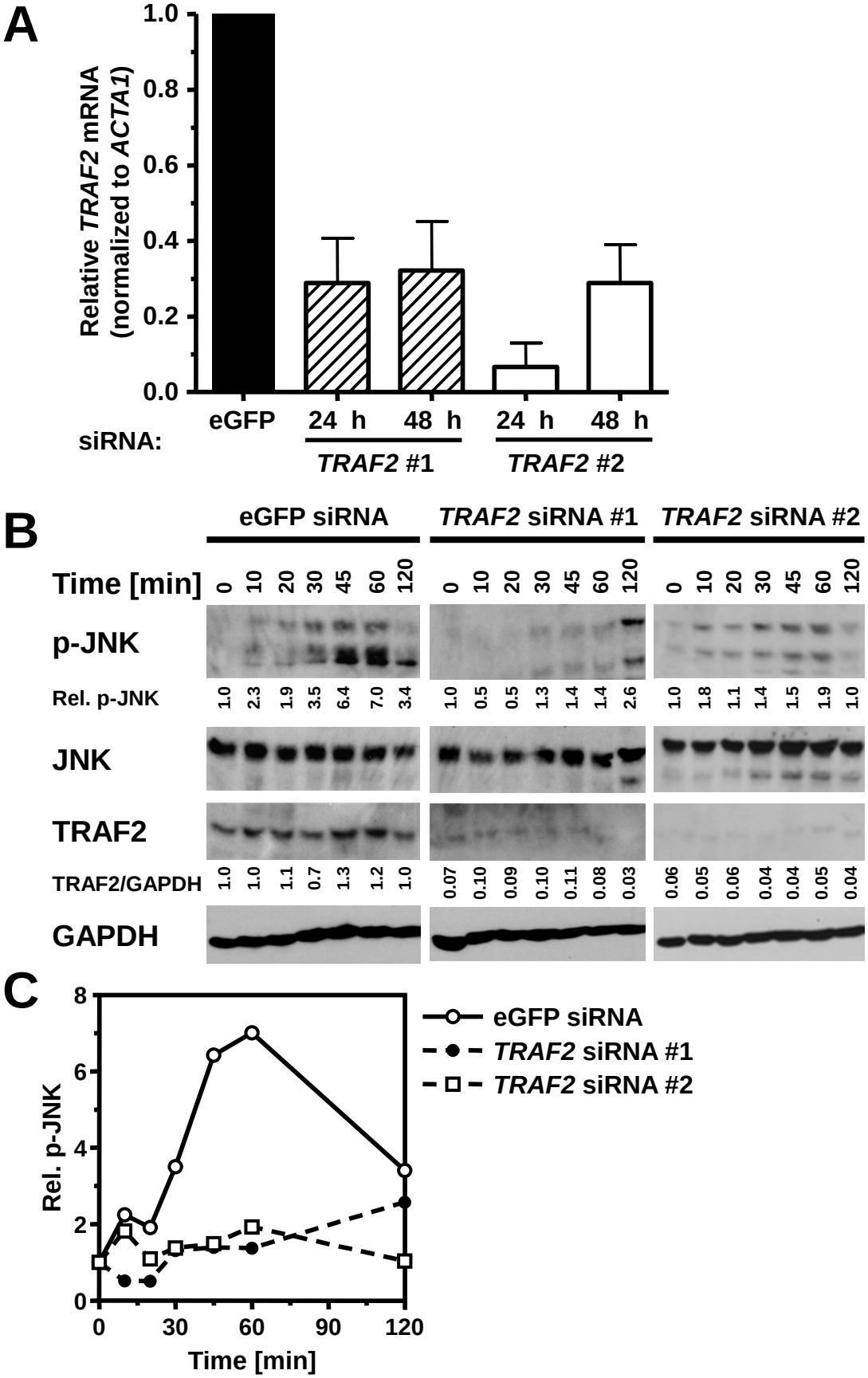

Figure S5. Acute JNK activation in Hep G2 cells is TRAF2 dependent. **(A)** siRNA knock-down of human TRAF2 in Hep G2 cells. Relative *TRAF2* mRNA abundance (to *ACTA1*) was measured by RT-qPCR 24 or 48 h after transfection of Hep G2 cells with the indicated siRNAs. **(B)** Knock-down of TRAF2 expression in Hep G2 cells interferes with ER stress-induced JNK phosphorylation. Hep G2 cells were treated with 1 μM thapsigargin for the times indicated before protein extraction for Western blotting with antibodies against p-JNK, total JNK, TRAF2, and GAPDH. **(C)** Quantitation of the JNK phosphorylation signals in the Western blots of panel (B).

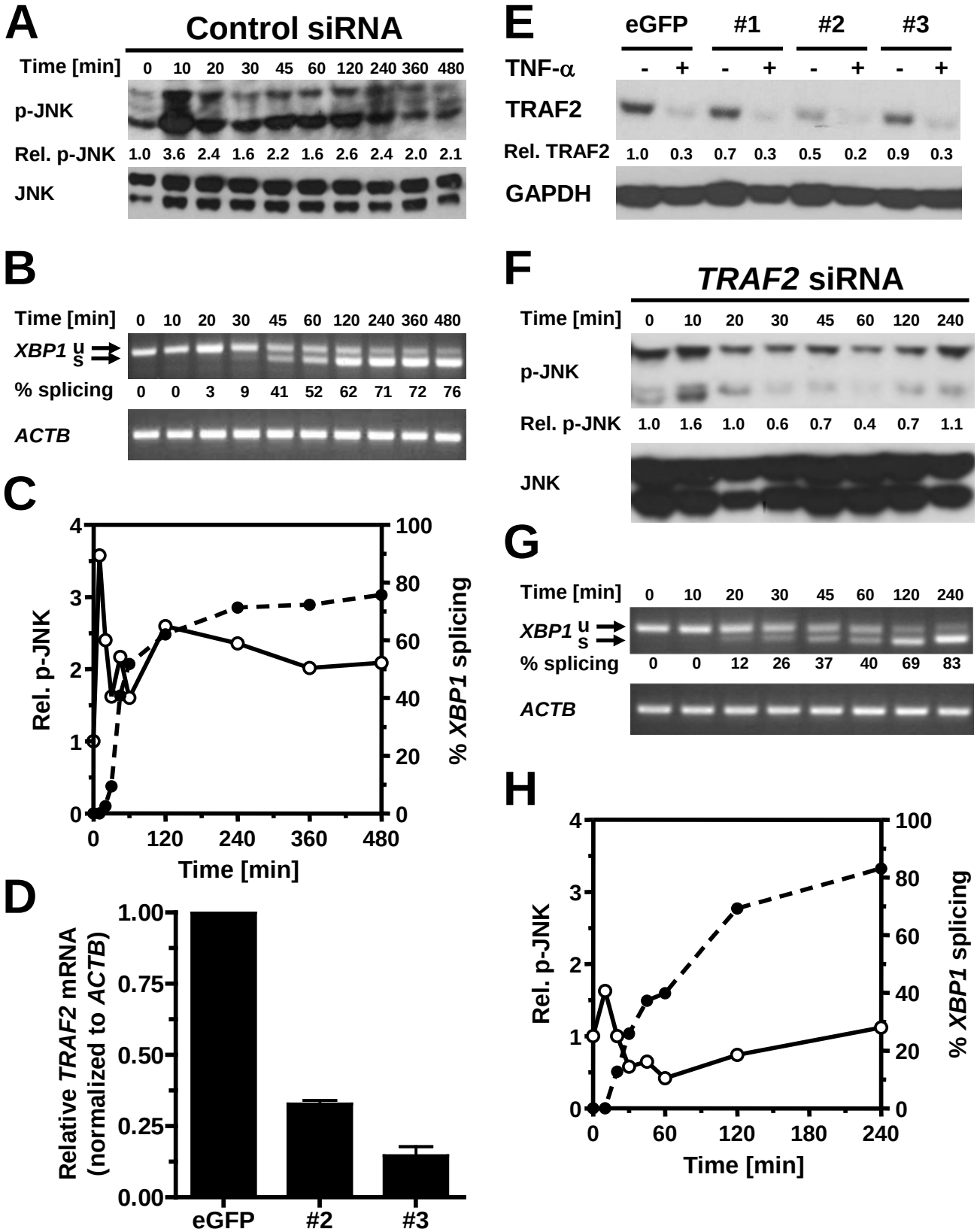

Figure S6. Acute JNK activation is TRAF2-dependent in 3T3-F442A preadipocytes. **(A)** JNK phosphorylation and **(B)** *XBP1* splicing in 3T3-F442A preadipocytes transfected with a siRNA against eGFP. **(C)** Quantitation of the JNK phosphorylation (white circles, solid line) from panel (A) and *XBP1* splicing (black circles, dashed line) from panel (B). **(D)** *TRAF2* mRNA levels measured by real-time PCR in 3T3-F442A preadipocytes after transfection with the indicated siRNAs. **(E)** TRAF2 protein levels relative to GAPDH in 3T3-F442A preadipocytes transfected with the indicated siRNAs against eGFP or murine TRAF2. Cell were treated with 20 ng/ml TNF-α for 20 min where indicated. **(F)** JNK phosphorylation and **(G)** *XBP1* splicing in 3T3-F442A preadipocytes transfected with murine *TRAF2* siRNA #2. **(H)** Quantitation of the JNK phosphorylation (white circles, solid line) from panel (F) and *XBP1* splicing (black circles, dashed line) from panel (G).

Figure S6, Brown *et al.*

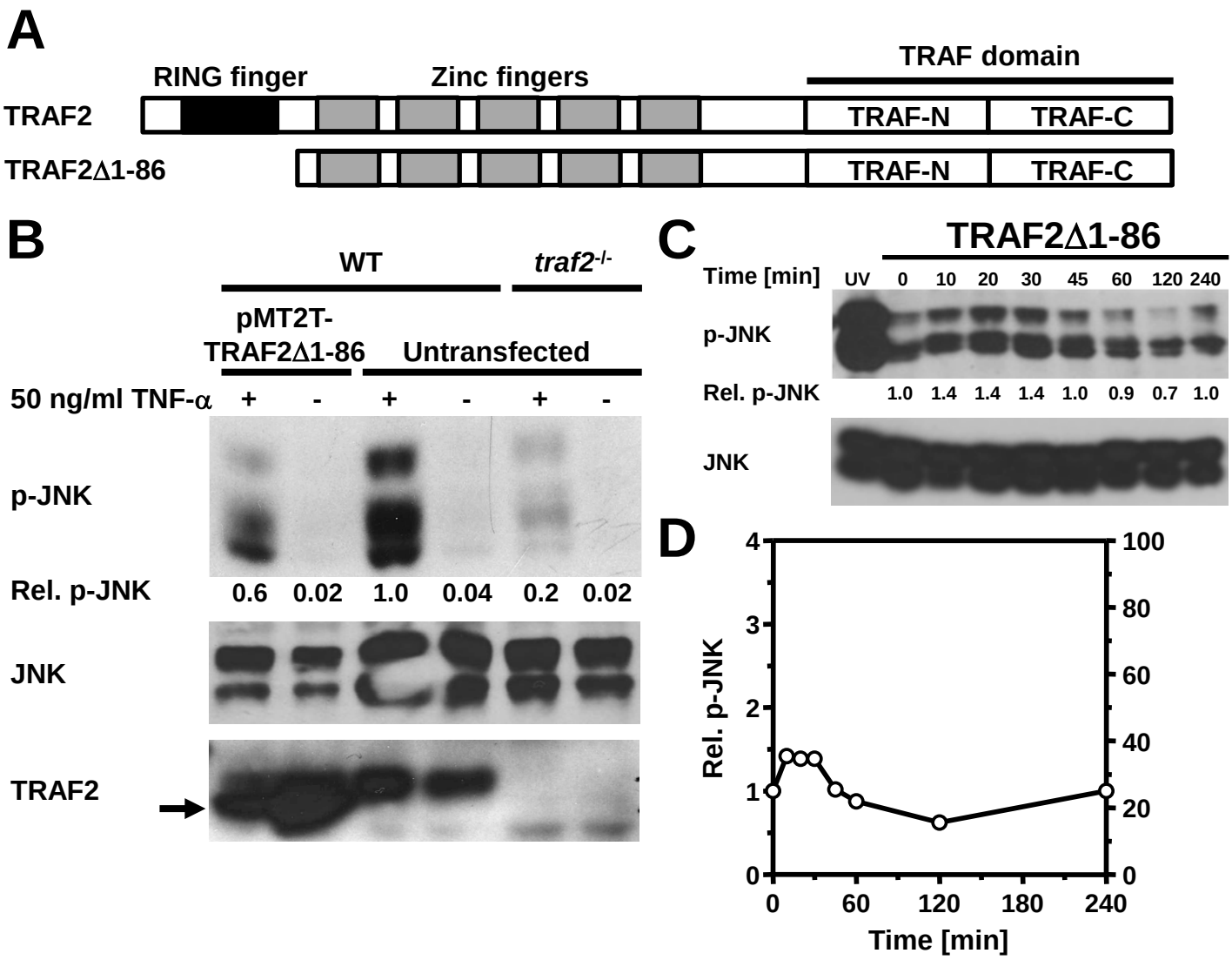

Figure S7. Dominant negative TRAF2 blocks JNK activation by acute ER stress in 3T3-F442A preadipocytes. **(A)** Domain structures of WT and dominant-negative TRAF2 (TRAF2Δ1-86). **(B)** Western blots for phospho-JNK, JNK, and TRAF2 in cell lysates prepared from WT MEFs transiently transfected with 8 μg pMT2T-TRAF2Δ1-86 and stimulated with 50 ng/ml TNF-α for 20 min. **(C)** JNK phosphorylation in 3T3-F442A preadipocytes transfected with pMT2T-TRAF2Δ1-86 to express dominant-negative TRAF2Δ1-86. **(D)** Quantitation of the JNK phosphorylation signals in the Western blots of panel (C).

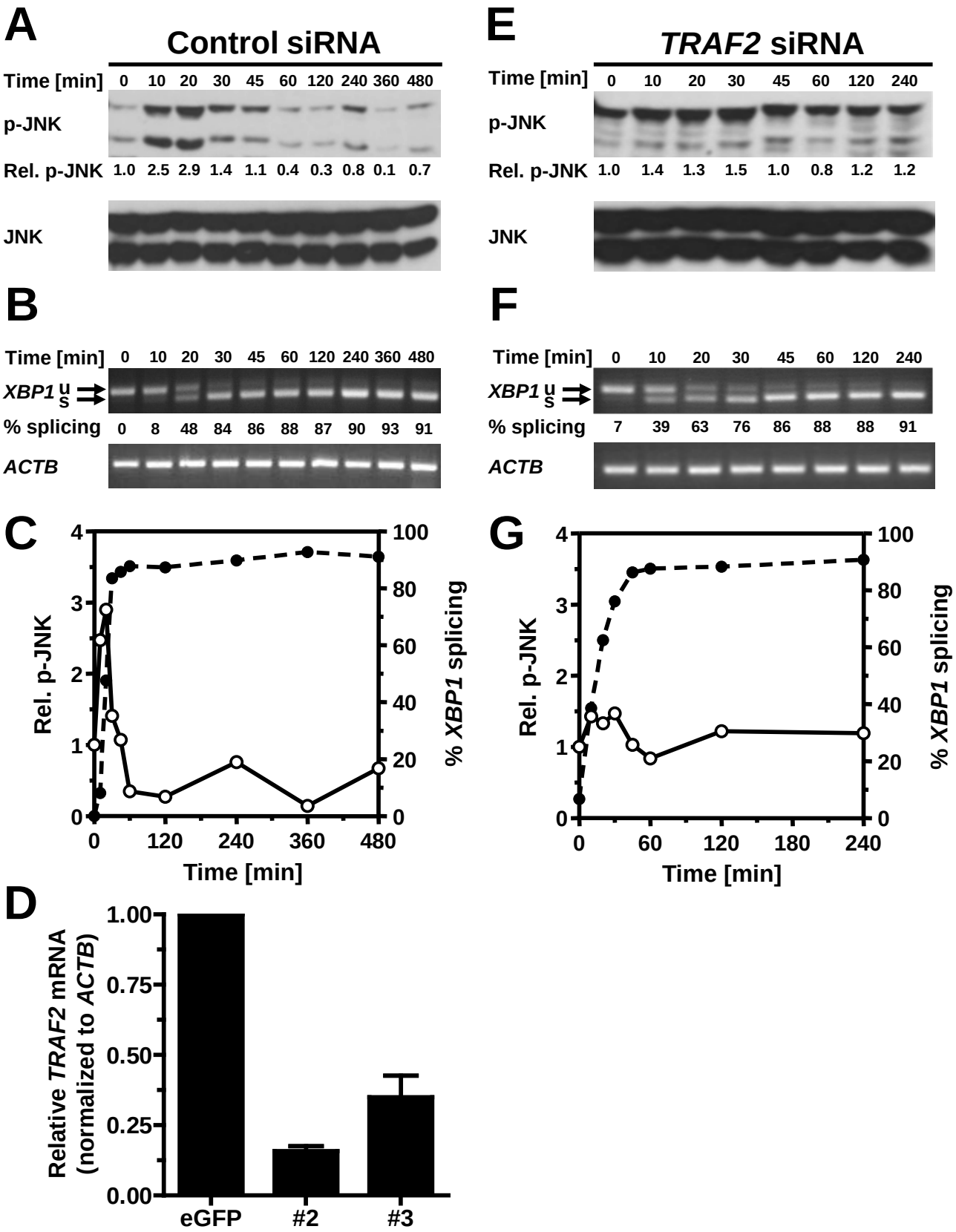

Figure S8. Acute JNK activation is TRAF2-dependent in C_2C_{12} myoblasts. **(A)** JNK phosphorylation and **(B)** *XBP1* splicing in C_2C_{12} myoblasts transfected with control siRNA against eGFP. (**C)** Quantitation of the JNK phosphorylation (white circles, solid line) from panel (A) and *XBP1* splicing (black circles, dashed line) from panel (B). **(D)** *TRAF2* mRNA levels measured by real-time PCR in C_2C_{12} myoblasts after transfection with the indicated siRNAs. **(E)** JNK phosphorylation and **(F)** *XBP1* splicing in C_2C_{12} myoblasts transfected with murine *TRAF2* siRNA #2. **(G)** Quantitation of the JNK phosphorylation (white circles, solid line) from panel (E) and *XBP1* splicing (black circles, dashed line) from panel (F).

Figure S8, Brown *et al.*

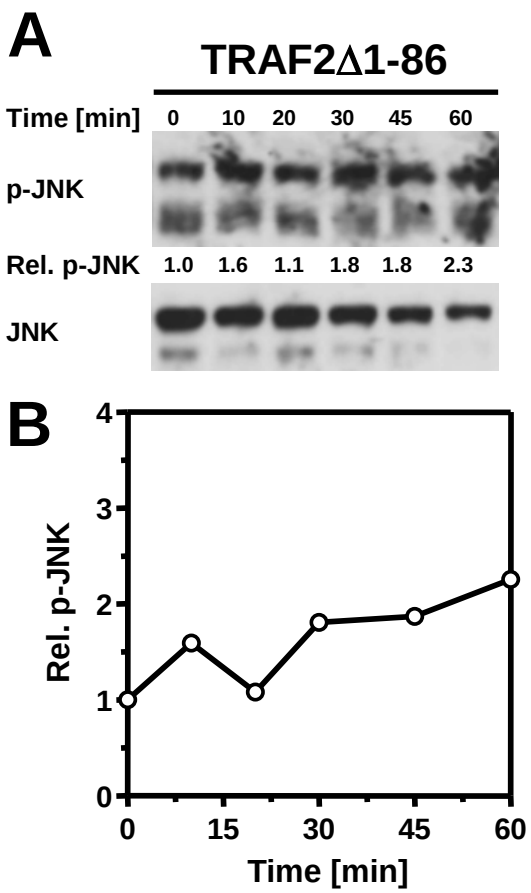

Figure S9. Dominant negative TRAF2 blocks JNK activation by acute ER stress in C_2C_{12} myotubes. **(A)** JNK phosphorylation in C_2C_{12} myoblasts transfected with pMT2T-TRAF2Δ1-86 to express dominant-negative TRAF2Δ1-86. **(B)** Quantitation of the JNK phosphorylation signals.

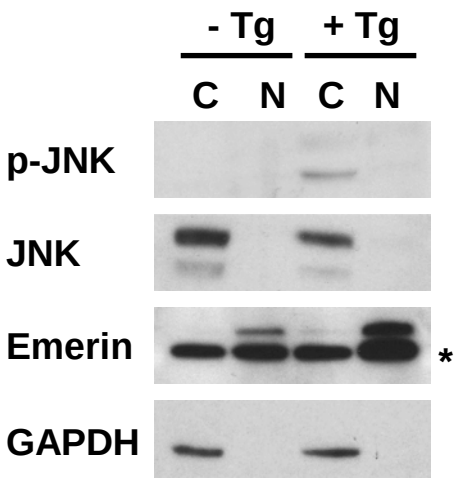

Figure S10. Transiently activated JNK localizes to the cytosol during ER stress. Serum-starved Hep G2 cells were treated for 45 min with 1 μM thapsigargin or left untreated before isolation of the cytosolic and nuclear fractions. The cytosolic (C) and nuclear (N) fractions were analyzed by Western blotting. The asterisk (*) indicates a non-specific band recognized by the anti-emerin antibody. Emerin was used as a nuclear marker and GAPDH as a cytoplasmic marker.

APPENDIX C

The following is the manuscript from which data were used in chapter 4

Acute endoplasmic reticulum stress separates JNK and TRB3 activation from insulin resistance

Max Brown[1-3], Samantha Dainty[1-3], Natalie Strudwick[1-3], Adina D. Mihai[1-3], Jamie N. Watson[1-3], Robina Dendooven[1-3], Adrienne W. Paton[4], James C. Paton[4], and Martin Schröder[1-3,#]

1) Durham University, School of Biological and Biomedical Sciences, Durham DH1 3LE, United Kingdom.

2) Biophysical Sciences Institute, Durham University, Durham DH1 3LE, United Kingdom.

3) North East England Stem Cell Institute (NESCI), Life Bioscience Centre, International Centre for Life, Central Parkway, Newcastle Upon Tyne, NE1 4EP, UK.

4) Research Centre for Infectious Diseases, School of Molecular and Biomedical Science, University of Adelaide, Adelaide, SA 5005, Australia.

Address for correspondence: Martin Schröder, Durham University, School of Biological and Biomedical Sciences, Durham DH1 3LE, United Kingdom.

phone: +44 (0) 191-334-1316

FAX: +44 (0) 191-334-9104

email: martin.schroeder@durham.ac.uk

Running Title: Acute ER stress and insulin resistance

Keywords: endoplasmic reticulum, Ire1, JNK, signal transduction, unfolded protein response, insulin resistance

Abstract

Endoplasmic reticulum (ER) stress has been proposed to cause insulin resistance through two signaling mechanisms, activation of JNK by the ER stress sensor IRE1α and transcriptional induction of the pseudokinase TRB3 downstream of the ER stress sensor PERK. Serine 307 phosphorylation of IRS1 by JNK and formation of a complex between AKT and TRB3 have been implicated in inhibition of insulin action in ER-stressed cells. In contrast to these studies we find that short periods of ER stress do not inhibit activation of AKT by insulin in adipocytes, hepatoma cells, myoblasts, or mouse embryonic fibroblasts, while inducing TRB3 and transiently activating JNK. Short term ER stress did not inhibit insulin-stimulated phosphorylation of AKT at S473 or T308, phosphorylation of glycogen synthase kinase 3α/β or IRS1 tyrosine phosphorylation and did also not induce IRS1 S307 phosphorylation in hepatoma cells or adipocytes. Elevated IRS1 S307 phosphorylation in ER-stressed myotubes did not inhibit IRS1 tyrosine phosphorylation by insulin. Prolonged ER stress extending over several half-lives of the insulin receptor at the plasma membrane, however, caused profound insulin resistance. Our data suggest that insulin resistance develops in ER-stressed cells as a consequence of depletion of insulin receptors at the plasma membrane.

Introduction

Obesity is a major risk factor for development of insulin resistance and type 2 diabetes. Obesity is associated with markers of endoplasmic reticulum (ER) stress in adipose tissue, hypothalamus, and liver of obese mice (1-4), renal cells of obese juvenile sheep (5), and in adipose tissue of obese subjects (6, 7). Weight loss reduces markers of ER stress in adipose tissue and liver (8). The ER is an organelle responsible for the folding and initial posttranslational modification of nearly all

secretory and transmembrane proteins, Ca^{2+} storage, and lipid and sterol synthesis. Perturbation of any of these functions of the ER activates a signaling network termed the unfolded protein response (UPR). The UPR attempts to reestablish homeostasis of the ER through altering several aspects of cellular physiology. The UPR activates expression of genes encoding ER resident molecular chaperones, protein foldases, and phospholipid biosynthetic genes to increase the protein folding capacity of the ER and to dilute its unfolded protein content. Attenuation of general translation, elevation of ER-associated protein degradation, degradation of mRNAs encoding secretory cargo by IRE1α (9, 10), and stimulation of autophagy decreases the unfolded protein load of the ER. The UPR also activates inflammatory signaling pathways which have been proposed to contribute to the onset of insulin resistance in obesity.

Insulin stimulates glucose uptake, cell proliferation, and protein synthesis (11). Binding of insulin to the insulin receptor activates the protein tyrosine kinase domain of the insulin receptor (12-14), leading to tyrosine autophosphorylation of the insulin receptor (15-17) and tyrosine phosphorylation of insulin receptor substrate (IRS)-1, -2, -3, and -4, and of several Shc proteins (18, 19). Tyrosine phosphorylated IRS and Shc proteins are anchoring points for proteins containing Src-homology-2 (SH-2) domains (20), which, for example, can be found in the regulatory subunits of phosphatidylinositol (PI) 3-kinase (21). Activated PI 3-kinase catalyzes the formation of PI-3,4-bisphosphate and PI-3,4,5-trisphosphate (22) and recruitment of phosphoinositide-dependent kinases (PDK) 1 and 2 and several protein kinase B (PKB/AKT) isoforms to the plasma membrane (22). When co-localized at the plasma membrane, PDKs phosphorylate and activate AKT1, -2, and -3. Activated AKT controls many cellular events, including glucose transport, protein and glycogen synthesis, cell proliferation and survival by phosphorylation of numerous substrates

(23-26). Insulin stimulates protein synthesis via activation of the protein serine/threonine kinase mTOR by AKT and PDKs (27, 28). mTOR phosphorylates the serine-threonine protein kinase $p70^{S6K}$ and an inhibitor of translation initiation, eIF-4E binding protein (29-31), to stimulate protein synthesis. Activation of RAS through SHC and IRS1 proteins, RAF, and the mitogen-activated protein kinases ERK1 and ERK2 also mediates the proliferative and mitogenic effects of insulin (32-36).

A major mechanism underlying insulin resistance is inhibition of the insulin signaling pathway by serine phosphorylation of IRS proteins, for example S307 in murine or S312 in human IRS1. IRS serine phosphorylation inhibits recruitment of PI 3-kinase to IRS proteins (37-43), inhibits tyrosine phosphorylation of IRS proteins by the insulin receptor (1, 2), and promotes degradation of IRS1 (44). Several protein kinases have been implicated in serine phosphorylation of IRS proteins including $p70^{S6K}$ (40, 45, 46), IKK (47), and JNK (48-52). JNK increases IRS1 S307 phosphorylation in response to free fatty acids, stress, and inflammation (49, 53-58). IKK also inhibits insulin signaling in response to free fatty acids and inflammation (50, 59-61). Inhibition of insulin signaling by $p70^{S6K}$ may represent a negative feedback loop to fine tune the signaling outputs of the insulin signaling pathway (40) and contributes to tumor necrosis factor (TNF)-α induced insulin resistance (62). Other protein kinases such as ERK (63-65), PKCζ (66-68), PKCθ (50, 69), AKT (70), glycogen synthase kinase (GSK) 3 (71-73), IRAK (74), and mTOR (70, 75) contribute to insulin resistance through IRS1 serine phosphorylation.

UPR signaling is initiated at three ER transmembrane proteins, the membrane-bound transcription factor ATF6, the protein kinase PERK, and the protein kinase endoribonuclease IRE1α. All three arms of the UPR contribute to activation of

inflammatory signaling. ATF6 activates transcription of acute phase response genes (76), while translational arrest mediated by PERK-dependent phosphorylation of the eukaryotic translation initiation factor (eIF) 2 α subunit activates NF-κB (77-80) and expression of the pseudokinase TRB3. Interaction of TRB3 with AKT causes insulin resistance in HEK293 cells (81), cardiac myocytes (82), and muscle cells (83, 84). Its interaction with IRS1 was proposed to inhibit IRS1 tyrosine 612 phosphorylation (84). By contrast, *trb3*$^{-/-}$ mice display normal hepatic insulin signaling and glucose homeostasis (85), while strong overexpression of TRB3 in primary hepatocytes did not affect insulin signaling (86).

IRE1α is thought to be the main player in activation of inflammatory signaling and development of insulin resistance in ER-stressed cells. Through association with the E3 ubiquitin ligase TRAF2 IRE1α activates both JNK (87) and IKK (88). Activation of JNK by IRE1α has been proposed to cause insulin resistance via S307/S312 phosphorylation of IRS1 by JNK (1). IRE1α is a bifunctional protein kinase-endoribonuclease (RNase) (89). The IRE1α RNase activity initiates splicing of *XBP1* mRNA encoding a bZIP transcription factor. Spliced XBP1 (XBP1^{s}) is a more potent transcriptional activator than unspliced XBP1 (XBP1^{u}) for genes encoding ER resident molecular chaperones, phospholipid biosynthetic enzymes, and proteins involved in ER-associated protein degradation (90-93). In addition, relaxed specificity of the RNase activity mediates decay of many mRNAs encoding proteins targeted to the secretory pathway (9, 10, 94).

Here we report that short-term ER stress lasting for up to ~8-12 h does not inhibit insulin-stimulated AKT activation in *in vitro* differentiated 3T3-F442A adipocytes, C_2C_{12} myotubes, two hepatoma cell lines, and mouse embryonic fibroblasts (MEFs). Acute ER stress activates JNK and TRB3, but insulin-stimulated T308 and S473

phosphorylation of AKT as well as insulin-stimulated phosphorylation of GSK3α/β were unaffected by ER stress over a period of ~8 h. Insulin-stimulated IRS1 tyrosine phosphorylation was also unaltered in acutely ER-stressed cells and IRS1 S307 phosphorylation did not increase significantly in ER-stressed 3T3-F442A adipocytes or Hep G2 cells. A ~2 fold increase in IRS1 S307 phosphorylation in *in vitro* differentiated myotubes did not correlate with inhibition of insulin-dependent IRS1 tyrosine phosphorylation. Prolongation of ER stress over several half-lives of the insulin receptor at the plasma membrane, however, caused insulin resistance. Collectively, our data support activation of JNK and TRB3 by ER stress, but also argue that insulin resistance develops independent of both JNK and TRB. By contrast, depletion of insulin receptors may be responsible for the insulin resistance of ER-stressed cells.

Materials and Methods

Antibodies and reagents. Rabbit anti-AKT (cat. no. 4691), rabbit anti-phospho-S473-AKT (cat. no. 4060), rabbit anti-phospho-T308-AKT (cat. no. 4056), rabbit anti-GSK3α/β (cat. no. 5676), rabbit anti-phospho-S21/9-GSK3α/β (cat. no. 9331), rabbit anti-JNK (cat. no. 9258), and rabbit anti-phospho-JNK (cat. no. 4668) antibodies were purchased from Cell Signaling Technology Inc. (Danvers, MA, USA). The mouse anti-GAPDH antibody (cat. no. G8795) was purchased from Sigma-Aldrich (Gillingham, UK). Tunicamycin was purchased from Merck Chemicals (Beeston, UK) and thapsigargin from Sigma-Aldrich (Gillingham, UK).

Cell culture. Wild type (WT) mouse embryonic fibroblasts (MEFs) were provided by T. Mak (University of Toronto, Ontario Cancer Institute, Toronto, Ontario, Canada). 3T3-F442A preadipocytes (95), C_2C_{12} myoblasts (96), and Hep G2 cells (97) were obtained from C. Hutchison (Durham University), R. Bashir (Durham University),

and A. Benham (Durham University), respectively. Fao rat hepatoma cells (98) were obtained from the Health Protection Agency Culture Collection.

All cell lines were grown at 37 °C in an atmosphere of 95% (v/v) air, 5% (v/v) CO_2, and 95% humidity. Fao rat hepatoma cells were grown in Roswell Park Memorial Institute (RPMI) 1640 medium (99) containing 10% (v/v) fetal bovine serum (FBS) and 2 mM L-glutamine and where indicated in Coon's modification of Ham's F12 medium (100) containing 10% (v/v) FBS and 2 mM L-glutamine. All other cell lines were cultured in Dulbecco's minimal essential medium (DMEM) containing 4.5 g/l D-glucose (101, 102), 10% (v/v) FBS, and 2 mM L-glutamine.

To differentiate C_2C_{12} cells 60-70% confluent cultures were shifted into low mitogen medium consisting of DMEM containing 4.5 g/l D-glucose, 2% (v/v) horse serum, and 2 mM L-glutamine. The cells were then incubated for another 7-8 d with replacing the low mitogen medium every 2-3 d (103). Differentiation of C_2C_{12} cells was assessed by microscopic inspection of cultures, staining of myotubes with rhodamine-labeled phalloidin (104), and reverse transcriptase PCR for transcription of the genes encoding *S*-adenosyl-homocysteine hydrolase (*AHCY*), myosin light chain 1 (*MYL1*), and troponin C (*TNNC1*). To differentiate 3T3-F442A fibroblasts into adipocytes cells were grown to confluency. 2 d postconfluency the medium was changed to DMEM containing 4.5 g/l D-glucose, 10% (v/v) FBS, 2 mM L-glutamine, 1 µg/ml insulin, 0.5 mM 1-methyl-3-isobutylxanthine (IBMX), and 0.25 µM dexamethasone. After 3 d the medium was changed to DMEM containing 4.5 g/l D-glucose, 10% (v/v) FBS, 2 mM L-glutamine, and 1 µg/ml insulin. After another 2 d the medium was changed to DMEM containing 4.5 g/l D-glucose, 10% (v/v) FBS, and 2 mM L-glutamine. Cells were incubated another 7 d before the start of experiments (105). Differentiation was assessed by Oil Red O staining (106) and flow

cytometric analysis of $>1 \cdot 10^4$ cells by Nile Red staining as described before (107, 108).

ER stress was induced with 1 µM thapsigargin, 10 µg/ml tunicamycin, or 1 µg/ml subtilase cytotoxin AB (SubAB) if not indicated otherwise. As a control cells were treated with catalytically inactive $SubA_{A272}B$. SubAB and $SubA_{A272}B$ were purified as described before (109, 110). To stimulate cells with insulin, cells were serum-starved for 18 h, followed by addition of fresh serum-free culture medium containing 10 – 100 nM insulin. After 15 min exposure to insulin, cells were harvested for extraction of RNA and protein as described below.

RNA extraction and reverse transcriptase (RT-) PCRs. RNA was extracted with the EZ-RNA total RNA isolation kit (Geneflow, Fradley, UK, cat. no. K1-0120) and reverse transcribed with oligo-dT primers (Promega, Southampton, cat. no. C1101) and Superscript III reverse transcriptase (Life Technologies, Paisley, UK, cat. no. 18080044) as described previously (111). Protocols for detection of splicing of murine and human *XBP1* have been described previously (111). Band intensities were quantitated using ImageJ (112) and the percentage of *XBP1* splicing calculated by dividing the signal for spliced *XBP1* mRNA by the sums of the signals for spliced and unspliced *XBP1* mRNAs. Quantitative PCRs (qPCRs) were run on a Rotorgene 3000 (Qiagen, Crawley, UK). Amplicons were amplified with 0.5 µl 5 U/µl GoTaq® Flexi DNA polymerase (Promega, cat. no. M8305), 2 mM $MgCl_2$, 200 µM dNTPs, and 1 µM of each primer and detected with a 1:2,500 fold dilution of a SybrGreen stock solution (Life Technologies, cat. no. S7563). Primers for qPCRs are listed in Table I. After denaturation for 2 min at 95°C samples underwent 40 cycles of denaturation at 95°C for 30 s, primer annealing at 58°C for 30 s, and primer extension at 72°C for 30 s. Amplification of a single PCR product was confirmed by recording the melting

196 curves after each PCR run. Amplification efficiencies for all qPCRs were ~0.75 ±
197 0.05. Calculation of C_T values and normalization to *GAPDH* or *ACTB* mRNA levels
198 was done using the comparative quantitation function in the Rotorgene software.
199 Results represent the average and standard error of three technical repeats. qPCR
200 results were confirmed by at least one other biological replicate. qPCRs for murine
201 *AHCY*, *MYL1*, and *TNNC* were standardized to *GAPDH*, for murine *TRAF*2 and *TRB3*
202 to *ACTB*, and for human *TRAF2* to *ACTA1*.

203 **Cell lysis and Western blotting.** Cells were washed three times with ice-cold
204 phosphate-buffered saline (PBS, 4.3 mM Na_2HPO_4, 1.47 mM KH_2PO_4, 27 mM KCl,
205 137 mM NaCl, pH 7.4) and lysed in RIPA buffer (50 mM Tris-HCl, pH 8.0, 150 mM
206 NaCl, 0.5% (w/v) sodium deoxycholate, 0.1% (v/v) Triton X-100, 0.1% (w/v) SDS)
207 containing Roche complete protease inhibitors (Roche Applied Science, Burgess Hill,
208 UK, cat. no. 11836153001) as described before (111).

209 Proteins were separated by SDS-PAGE and transferred to polyvinylidene
210 difluoride (PVDF) membranes (Amersham HyBond^{TM}-P, pore size 0.45 μm, GE
211 Healthcare, Little Chalfont, UK, cat. no. RPN303F) by semi-dry electrotransfer in 0.1
212 M Tris, 0.192 M glycine, and 5% (v/v) methanol at 2 mA/cm^2 for 60-75 min.
213 Membranes were blocked for 1 h in 5% (w/v) skimmed milk powder in TBST (20
214 mM Tris-HCl, pH 7.6, 137 mM NaCl, and 0.1% (v/v) Tween-20) for antibodies
215 against non-phosphorylated proteins and 5% bovine serum albumin (BSA) in TBST
216 for antibodies against phosphorylated proteins and incubated overnight at 4°C with
217 the primary antibody diluted in blocking solution. Blots were washed three times with
218 TBST and probed with secondary antibody for 1 hour at room temperature. The anti-
219 AKT, anti-phospho-S473-AKT, anti-phospho-T308-AKT, anti-GSK3α/β, anti-
220 phospho-S21/9-GSK3α/β, anti-JNK, and anti-phospho-JNK antibodies were used at a

1:1,000 dilution in TBST + 5% (w/v) BSA and incubated with the membranes over night at 4°C with gentle agitation. Membranes were then developed with goat anti-rabbit-IgG (H+L)-horseradish peroxidase (HRP)-conjugated secondary antibody (Cell Signaling, cat. no. 7074S) at a 1:1,000 dilution in TBST + 5% (w/v) skimmed milk powder for 1 h at room temperature. The mouse anti-GAPDH antibody was used at a 1:30,000 dilution in TBST + 5% (w/v) skimmed milk powder over night at 4°C with gentle agitation and developed with goat anti-mouse IgG (H+L)-horseradish peroxidase (HRP)-conjugated secondary antibody (Thermo Scientific, cat, no. 31432) at a 1:20,000 dilution in TBST + 5% (w/v) skimmed milk powder for 1 h at room temperature. For signal detection Pierce ECL Western Blotting Substrate (cat. no. 32209) or Pierce ECL Plus Western Blotting Substrate (cat. no. 32132) from Thermo Fisher Scientific (Loughborough, UK) were used. Blots were exposed to CL-X Posure™ film (Thermo Fisher Scientific, Loughborough, UK, cat. no. 34091). Exposure times were adjusted on the basis of previous exposures to obtain exposures in the linear range of the film. Signals were quantified using ImageJ (112). To reprobe blots for detection of nonphosphorylated proteins, membranes were stripped using Restore Western Blot Stripping Buffer (Thermo Fisher Scientific, Loughborough, UK, cat. no. 21059) and blocked with 5% (w/v) skimmed milk powder in TBST.

Immunoprecipitation of IRS1. 50% confluent cultures were serum-starved for 18 h in 100 mm dishes before exposure to thapsigargin, tunicamycin, and insulin as detailed in the figure legends. Cells were washed three times with ice-cold PBS and lysed in 500 µl IP buffer (50 mM Tris-HCl, pH 7.5, 150 mM NaCl, 1 mM EDTA, 0.05% (w/v) SDS) containing 1% (v/v) Nonidet P40 and Roche complete protease inhibitors. Lysates were centrifuged for 10 min at 12,000 g to precipitate cell debris. Supernatants containing 1 mg total protein were pre-cleared with 20 µl 25% protein A

agarose slurry (Santa Cruz Biotechnology, cat. no. sc-2001) for 1 h at 4°C with overhead rotation and then immunoprecipitated with 4 µg rabbit anti-IRS1 (D23G12) antibody (New England Biolabs, Hitchin, UK, cat. no. 3407) at 4°C overnight. Immunoprecipitates were collected by addition of 20 µl 25% protein A agarose for 2 h at 4°C and washed three times with ice-cold IP buffer containing 0.1% (v/v) Nonidet P40 and once with ice-cold IP buffer. Immunoprecipitated proteins were solubilized by boiling in 6 x SDS-PAGE sample buffer (350 mM Tris·HCl, pH 6.8, 30% (v/v) glycerol, 10% (w/v) SDS, 0.5 g/l bromophenol blue, 2% (v/v) β-mercaptoethanol) for 5 min, separated on 4-12% Bis-Tris NuPAGE gels (Life Technologies) and electroblotted onto PVDF membranes as described above. Membranes were blocked with 5% (w/v) skimmed milk powder for 1 h at room temperature. Membranes were incubated with mouse anti-phosphotyrosine 4G10® Platinum (Merck Millipore cat. no. 05-321) at a dilution of 1:1,000 in TBST + 5% (w/v) BSA or anti-IRS1 antibody diluted 1:1,000 in TBST + 5% (w/v) skimmed milk powder for 1 h at room temperature. Membranes were washed extensively with TBST and exposed to horseradish peroxidase-conjugated secondary antibodies against mouse IgG(H+L) or rabbit IgG(H+L) (Thermo Fisher Scientific, cat. no. 31458) at a 1:20,000 dilution in PBST + 5% (w/v) skimmed milk powder for 1 h at room temperature. Blots were extensively washed with TBST, developed with ECL Plus Western blotting detection reagent (GE Healthcare), and exposed to CL-X Posure™ film (Thermo Fisher Scientific, cat. no. 34091) as directed by the manufacturer.

Phospho-S307 IRS1 enzyme-linked immunosorbent assay (ELISA). Hep G2 cells were serum-starved for 18 h, treated with 0.1 to 10 µg/ml tunicamycin for 30 min and stimulated with 100 nM insulin for 15 min. C_2C_{12} or 3T3-F442A cells were treated with 1 µM thapsigargin for 5 to 15 min before stimulation with 100 nM insulin for 5

to 15 min. Cells were washed twice with ice-cold PBS and lysed in RIPA buffer containing Roche protease inhibitors as described above. S307 phosphorylation of IRS1 was measured using the STAR phospho-IRS1 (Ser307 mouse/Ser312 human) ELISA (Millipore, Watford, UK, cat. no. 17-459) following the manufacturer's instructions. S307 phosphorylation is expressed in units relative to a phospho-S307 IRS1 standard provided in the ELISA kit. phospho-S307 IRS1 units were standardized to the amount of total IRS1 in cell lysates determined by Western blotting.

Error calculations. Experimental data are presented as the average and its standard error. Errors were propagated using the law of error propagation for random, independent errors (113).

Results

ER stress for up to ~8 h does not inhibit insulin-stimulated AKT activation

Recent reports have suggested that activation of the MAP kinase JNK and of the pseudokinase TRB3 is responsible for the development of insulin resistance in ER-stressed cells. In the majority of cases, insulin signaling has been examined in cultured cells experiencing long periods of ER stress (82, 114-117). For example, 3T3-L1 adipocytes exposed to the ER stressors thapsigargin and tunicamycin for 16-18 h developed insulin resistance (115), which was partially reversed by the JNK inhibitor SP600125. Likewise, exposure of C_2C_{12} myotubes to tunicamycin for 16 h caused insulin resistance, which correlated with activation of JNK (114). Treatment of cultured HL-1 atrial myocytes for 24 h with 2 μM thapsigargin caused insulin resistance, which could be partially relieved by siRNA-mediated knock-down of TRB3 (82). Two reports, however, described decreased AKT T308 and S473 phosphorylation in Fao rat hepatoma cells and C_2C_{12} myotubes exposed to

296 tunicamycin or thapsigargin for only 4 h (1, 84). Characterization of the JNK
297 activation profile in several cell lines, including 3T3-F442A adipocytes, C_2C_{12}
298 myotubes, Hep G2 cells, and MEFs revealed fast and transient activation of JNK
299 (Brown et al., submitted for publication). Over an 8 h time course all of above cell
300 lines displayed activation of JNK 10 – 60 min after application of ER stressors.
301 Furthermore, JNK activation was transient as evidenced by return of phospho-JNK
302 levels to resting levels toward the end of the time courses. Given the rapid and
303 transient activation of JNK by ER stress we became interested in characterizing
304 whether ER stress-induced insulin resistance can be observed at much earlier time
305 points than previously reported, and whether this insulin resistance is transient in
306 nature.

307 To characterize the kinetics of the onset of insulin resistance in pharmacologically
308 ER-stressed cells we performed time course experiments on *in vitro* differentiated
309 C_2C_{12} myotubes, 3T3-F442A adipocytes, and Hep G2 hepatoma cells. To exclude
310 potential drug specific effects on insulin signaling we used three different ER
311 stressors, the SERCA pump inhibitor thapsigargin (118), the *N*-glycosylation inhibitor
312 tunicamycin (118), and the protease SubAB, which cleaves and inactivates the ER
313 resident HSP70 class molecular chaperone BiP/GRP78 (119). We also titrated the
314 concentrations of thapsigargin and tunicamycin in the culture medium over a 10- or
315 100-fold concentration range, respectively. We monitored activation of the insulin
316 signaling pathway by Western blotting for T308 and S473 phosphorylation of AKT
317 (120) in cells that were serum-starved for 18 h, treated with the ER stressors for the
318 last 1 – 12 h of serum starvation and then stimulated with 100 nM insulin for 15 min
319 in the continued presence of the ER stressors. Surprisingly, these experiments
320 revealed that AKT T308 and S473 phosphorylation were unaffected by any of the

three ER stressors at any concentration for up to ~8 h in C_2C_{12} cells (Fig. 1A). Likewise, thapsigargin-, tunicamycin-, or SubAB-induced ER stress for less than 12 h did not affect insulin-stimulated AKT activation in 3T3-F442A adipocytes or Hep G2 hepatoma cells (Brown et al., submitted for publication). To confirm that treatment of C_2C_{12} cells with the ER stressors induces ER stress we monitored *XBP1* splicing using RT-PCR. The IRE1α-initiated *XBP1* splicing reaction removes a 26 nt intron from *XBP1* mRNA. Therefore, the appearance of a shorter reverse transcriptase (RT)-PCR product on high percentage agarose gels indicates activation of the RNase activity of IRE1α. Upon exposure of serum-starved C_2C_{12} cells to 300 nM thapsigargin, 1 μg/ml tunicamycin, or 1 μg/ml SubAB a shorter RT-PCR product appeared (Fig. 1B), which represents spliced *XBP1* mRNA. Furthermore, serum starvation did not decrease the level of *XBP1* splicing in ER-stressed cells (data not shown), thus ruling out the possibility that induction of ER stress is blunted by decreased protein synthesis rates in serum-starved cells.

A recent report suggested that tunicamycin- or thapsigargin-induced ER stress lasting for 4 h in C_2C_{12} myotubes decreases AKT T308 phosphorylation by 20-50%, while coinciding with induction of TRB3 (84). Because we did not observe any significant changes in insulin-stimulated AKT T308 or S473 phosphorylation in C_2C_{12} cells exposed to various concentrations of tunicamycin or thapsigargin (Fig. 1A), we characterized induction of *TRB3* mRNA by RT-qPCR. All three ER stressors strongly induced *TRB3* (Fig. 1C). Thus, strong transcriptional induction of *TRB3* does not necessarily affect insulin signaling in ER-stressed C_2C_{12} cells.

ER stress does not inhibit insulin-dependent AKT and GSK3α/β phosphorylation in the time window of JNK activation

Early JNK activation in ER-stressed cells is transient. In Hep G2 cells, phosphorylation, and consequently activation, of JNK in its T-loop on T183 and Y185 was induced 30 min after induction of ER stress, but returned to basal levels as early as two hours after induction of ER stress (Brown et al., submitted for publication). JNK activation occurred within 10 min in C_2C_{12} cells, 3T3-F442A cells, or MEFs but also returned to basal levels within several hours in C_2C_{12} cells and MEFs or in less than one hour in 3T3-F442A cells (Brown et al., submitted for publication). Therefore, we decided to characterize whether ER stress inhibits insulin action in cells exposed to various ER stressors for up to 1 h. Exposure of serum-starved MEFs to 1 μM thapsigargin for 10 or 60 min, followed by stimulation with 100 nM insulin for 15 min, caused a strong increase in AKT S473 phosphorylation that was indistinguishable from AKT S473 phosphorylation in untreated MEFs (Fig. 2A). Stimulation with 10 nM insulin for 15 min induced markedly lower levels of AKT S473 phosphorylation, but again ER stress had no effect on phosphorylation of AKT at S473 or phosphorylation of GSK3α at S21 and GSK3β at S9 (Fig. 2A), which are both elevated in response to insulin (121-123). 30 min of thapsigargin-induced ER stress did also have no effect on T308 or S473 phosphorylation of AKT or phosphorylation of GSK3α/β in Hep G2 cells (Fig. 2B), C_2C_{12} myotubes (Fig. 2C), or 3T3-F442A adipocytes (Fig. 2D).

Two other ER stressors, tunicamycin and SubAB did also not significantly affect insulin-induced phosphorylation of AKT or GSK3α/β in any of these three cell lines (Fig. 2B-D). Inhibition of insulin signaling by ER stress within 4 h was originally reported in Fao rat hepatoma cells (1). To address the possibility that the effects of ER stress on insulin signaling are cell type specific, we performed experiments with Fao rat hepatoma cells. All three ER stressors, thapsigargin, tunicamycin, and SubAB,

elicited JNK activation between 30 and 60 min after exposure of Fao cells to these drugs (Fig. 3). However, none of the ER stressors affected insulin-stimulated AKT or GSK3α/β phosphorylation (Fig. 3). Extension of the duration of ER stress to 2, 3, and 4 h and change of the medium from Coon's modification of Ham's F12 medium to RPMI 1640 to fully reflect the original experimental conditions (1) did also not reveal any effect of ER stress on AKT S473 phosphorylation (Fig. 4). Therefore, short periods of ER stress lasting for up to ~8 h, the transient JNK activation, and activation of TRB3 accompanying these short periods of ER stress do not inhibit insulin-dependent AKT and GSK3α/β phosphorylation.

Acute ER stress does not inhibit IRS1 tyrosine phosphorylation

To address the possibility that the dynamics of AKT and GSK3α/β phosphorylation render these measures of insulin signaling insensitive to effects of short periods of ER stress on the insulin signaling pathway, we directly examined the effects of ER stress on IRS1 tyrosine and S307 phosphorylation in the time window of JNK activation. In these experiments serum-starved cells were treated with 1 μM thapsigargin for 10, 20, or 25 min. The cells were stimulated with 100 nM insulin during the final 5 to 15 min of thapsigargin treatment (Figs. 5A-C). Western blotting of IRS1 immunoprecipitates showed that IRS1 tyrosine phosphorylation reached steady-state levels as early as 5 min after addition of insulin (Figs. 5B-D). Treatment of cells with 1 μM thapsigargin before addition of insulin further increased insulin-stimulated IRS1 tyrosine phosphorylation 1.6 ± 0.2 fold in C_2C_{12} and 1.6 ± 0.4 fold in 3T3-F442A cells (Figs. 5B-C). Treatment of Hep G2 cells with various concentrations of tunicamycin for 30 min before stimulation with 100 nM insulin during the final 15 min of tunicamycin treatment did also not affect IRS1 tyrosine phosphorylation (Fig. 5D), but activated JNK (Fig. 5E). Total IRS1 levels appear to increase 5 min after insulin stimulation of

3T3-F442A and Hep G2 cells in the immunoprecipitates (Figs. 5C-D). Human and murine IRS1 primary transcripts are too large (67,474 nt and 58,335 nt, respectively) for this increase to be explained through transcriptional induction, because RNA polymerase II transcribes ~1,000 – 6,000 bp/min (124, 125). Insulin causes strong phosphorylation of IRS1 (126). Phosphorylation-induced conformational changes may increase the immunoreactivity of IRS1, which may lead to more efficient immunoprecipitation of IRS1 from insulin-stimulated cells. In summary, these data show that acute ER stress does not affect insulin-stimulated IRS1 tyrosine phosphorylation.

JNK phosphorylates IRS1 at S307 to inhibit IRS1 tyrosine phosphorylation by the activated insulin receptor (42, 48). Unaltered IRS1 tyrosine phosphorylation in ER-stressed cells suggested that JNK may not phosphorylate S307 under these conditions. To test this hypothesis we measured IRS1 S307 phosphorylation by ELISA and standardized the phospho-S307 IRS1 levels to total IRS1 levels determined by Western blotting (Fig. 6). These experiments revealed that treatment of 3T3-F442A cells for up to 15 min (Fig. 6A) and of Hep G2 cells for up to 2 h with 1 μM thapsigargin (Figs. 6C, D) did not induce IRS1 S307 phosphorylation. By contrast, we noted a 3.2 ± 0.2 fold increase of IRS1 S307 phosphorylation in C_2C_{12} cells (Fig. 6B), which did not negatively affect IRS1 tyrosine phosphorylation in response to insulin (Fig. 5B). To verify that the ELISA can detect changes in IRS1 S307/S312 phosphorylation in all used cell lines, we measured IRS1 S307/S312 phosphorylation in insulin-stimulated cells. Insulin elevated IRS1 S307/S312 phosphorylation in all three cell lines (Fig. 6E), which is consistent with previous reports (42, 64). Thus, the ELISA protocol detects changes in IRS1 S307/S312 phosphorylation. Collectively, these data argue that ER stress does not inhibit IRS1 tyrosine phosphorylation.

The onset of insulin resistance caused by prolonged ER stress coincides with depletion of insulin receptors

Our data argue that ER stress lasting for up to 8 h does not inhibit insulin action in several cell types. To investigate whether ER stress can cause insulin resistance at all, we performed extended time courses lasting up to 36 h. In C_2C_{12} cells, insulin resistance as evidenced by decreased AKT S473 phosphorylation, developed at about 12 h after induction of ER stress (Fig. 7). Similar results were obtained with Hep G2 and 3T3-F442A cells (Brown et al., submitted for publication). The insulin receptor has a half-life of 7-13 h at the plasma membrane (127-133). Therefore, we asked whether the onset of insulin resistance coincides with depletion of insulin receptors in ER-stressed C_2C_{12} cells. The insulin receptor is synthesized as a proreceptor that is cleaved into mature α and β chains in the *trans*-Golgi network by several proprotein convertases (134, 135). Western blotting of cell lysates from C_2C_{12} cells with an antibody against the β chain revealed several bands (Fig. 8A). These can be attributed to two alternatively glycosylated forms of the α-β proreceptor at ~210 kDa (136), two alternatively glycosylated forms of a truncated α-β_1 proreceptor produced by a proteolytic processing event in lysosomes at ~130 kDa (137), and the β chain of ~95 kDa. Quantitation of the blots showed that mature β chains start to deplete after ~12 h of ER stress (Figs. 8B-D). The severity of the decrease in β chains correlates with the extent of insulin resistance observed in C_2C_{12} cells (compare Figs. 7 and 8B-D). We made similar observations in Hep G2 and 3T3-F442A cells (Brown et al., submitted for publication). Hence, it appears that ER stress may cause insulin resistance by depleting mature insulin receptors.

Discussion

444 Recent research has shown that ER stress is associated with insulin resistance in
445 obesity (1-7). The mechanism linking ER stress to insulin resistance is thought to be
446 activation of both JNK and TRB3 by the ER stress sensors IRE1α and PERK (1, 84).
447 Activated JNK phosphorylates IRS1 at S307, which in turn inhibits IRS1 tyrosine
448 phosphorylation by the insulin receptor (1), while interaction of TRB3 with IRS1 and
449 AKT inhibits stimulatory phosphorylation of both proteins (84). Exposure of Fao rat
450 hepatoma cells to 5 μg/ml tunicamycin for 4 h induced IRS1 S307 and inhibited AKT
451 S473 phosphorylation (1). An increase in IRS1 S307 phosphorylation was also
452 detected in Fao cells after induction of ER stress with 300 nM thapsigargin for 1 h (1).
453 Exposure of C_2C_{12} myotubes for 4 h to 1 μg/ml tunicamycin inhibited IRS1 Y612 and
454 AKT T308 phosphorylation by ~50%, while exposure to 2 μM thapsigargin for 4 h
455 resulted in decreases of 20-25% upon stimulation of C_2C_{12} myotubes with 100 nM
456 insulin (84). In contrast to these studies we find no evidence that short-term (≤ 8 h),
457 pharmacologically-induced ER stress inhibits insulin-stimulated AKT activation
458 despite activation of JNK (Fig. 3) and activation of TRB3 (Fig. 1C).

459 We have confirmed our observations by using five different cell lines, including
460 MEFs, human Hep G2 and rat Fao hepatoma cells, C_2C_{12} muscle cells, and 3T3-
461 F442A adipocytes. We obtained essentially the same results with three
462 mechanistically different ER stressors, the *N*-linked glycosylation inhibitor
463 tunicamycin (138), the SERCA Ca^{2+}-ATPase inhibitor thapsigargin (139), and
464 SubAB, a protease that inactivates the ER chaperone BiP (119). Moreover, induction
465 of short-term ER stress with a range of concentrations of tunicamycin or thapsigargin
466 did not lead to insulin resistance (Figs. 1-3) under conditions virtually identical to
467 those used before (1, 84). Short-term ER stress did also not inhibit AKT activation
468 when MEFs were stimulated with 10 nM instead of 100 nM insulin (Fig. 2A).

Stimulation with 10 nM insulin resulted in ~10% of AKT activation compared to stimulation with 100 nM insulin, but short-term ER stress did not affect AKT activation under these conditions (Fig. 2A). Therefore, it is unlikely that too strong stimulation of the insulin signaling pathway masks inhibitory effects of ER stress in experiments in which 100 nM insulin were used. Our observation, that short-term (≤ 8 h) ER stress does not inhibit insulin action is supported by an earlier report showing that induction of ER stress with 2 μg/ml tunicamycin or 150 nM thapsigargin for up to 4 h did not affect repression of glucose-6-phosphatase expression in primary rat hepatocytes by insulin (140).

Short-term, pharmacologically-induced ER stress was also reported to decrease IRS1 tyrosine phosphorylation and to increase IRS1 S307 phosphorylation via activation of JNK (1). We have also not observed any inhibitory effects of tunicamycin- or thapsigargin-induced ER stress on IRS1 tyrosine phosphorylation at time points at which ER stress activates JNK (Fig. 5). Consistent with these results we find no elevation of IRS1 S307 phosphorylation in ER-stressed 3T3-F442A adipocytes or Hep G2 cells. By contrast, IRS1 S307 phosphorylation was elevated ~3 fold in C_2C_{12} muscle cells (Fig. 6B), which did not affect IRS1 tyrosine phosphorylation (Fig. 5B) or Akt activation (Fig. 2C). The difference between these cell lines may be due to larger sarcoplasmic Ca^{2+}-stores in muscle cells, whose release may activate classical protein kinase C isoforms which then phosphorylate IRS1 at S307 (141, 142). Phosphorylation of IRS1 at S302 and S307 inhibits interaction of IRS1 with the insulin receptor in a yeast three hybrid assay (42, 143). Both phosphorylation events are equally important to disrupt this interaction (143). Intact insulin-stimulated IRS1 tyrosine phosphorylation in thapsigargin-treated C_2C_{12} muscle cells that display elevated S307 phosphorylation suggests that S302 may be

494 ineffectively phosphorylated. Classical PKCs have not been reported to phosphorylate
495 S302 (142, 144). Thus, it is plausible that thapsigargin-induced Ca^{2+} release from
496 sarcoplasmic stores is responsible for the increased S307 phosphorylation via
497 activation of classical PKCs in C_2C_{12} cells.

498 Several studies have shown that pharmacologically-induced ER stress causes
499 insulin resistance in primary cells and cultured cell lines (1, 82, 84, 114-117) and that
500 the effect of ER stress on insulin signaling can be reversed by chemical chaperones
501 such as tauroursodeoxycholate (2, 61) or 4-phenylbutyrate (114, 145). In the majority
502 of these studies cells were exposed for relatively long times to ER stressors before
503 examining insulin action. For example, Jung *et al.* report a ~40% decrease in AKT
504 S473 and T308 phosphorylation in primary hepatocytes exposed to 2 μg/ml
505 tunicamycin for 20 h. HL-1 murine cardiomyocytes exposed to 2 μM thapsigargin for
506 24 h displayed decreased insulin-stimulated AKT S473 phosphorylation (82), as did
507 3T3-L1 adipocytes exposed to 2 μg/ml tunicamycin or 300 nM thapsigargin for 16-18
508 h (115), or C_2C_{12} myotubes exposed to 0.5 μg/ml tunicamycin for 16 h (114).
509 Consistent with these reports we also find that prolonged ER stress causes insulin
510 resistance in C_2C_{12} cells (Fig. 7), Hep G2, and 3T3-F442A cells (Brown *et al.*,
511 submitted for publication). Thus, ER stress for more than ~12 h seems to be critical
512 for the development of insulin resistance in ER-stressed cells. Intriguingly, we
513 observe decreased insulin receptor levels when insulin resistance manifests in ER-
514 stressed cells (Fig. 8). Furthermore, the severity of insulin resistance appears to
515 correlate with the decrease in insulin receptor levels. Hence, ER stress may cause
516 insulin resistance by depleting insulin receptors. In support of this hypothesis a
517 decrease in insulin receptor β chains was reported in ER-stressed *in vitro*
518 differentiated 3T3-L1 adipocytes and HEK 293 cells (117). This decrease in insulin

519 receptor β chains was attributed to the PERK-mediated translational arrest or
520 stimulation of autophagy in ER-stressed cells (115, 116). However, restoration of
521 insulin receptor levels by inhibition of autophagy with 3-methyladenine did not
522 restore insulin sensitivity (116). In the accompanying paper we provide evidence that
523 prolonged ER stress causes insulin resistance by inhibiting transport of newly
524 synthesized insulin proreceptors from the ER to the cell surface (Brown *et al.*,
525 submitted for publication).

526 Our results also separate JNK and TRB3 activation by ER stress from insulin
527 resistance. Separation of JNK activation from insulin resistance was also reported in
528 fructose-fed liver-specific *xbp1*$^{-/-}$ and in liver-specific *klf15*$^{-/-}$ mice (146, 147).
529 Furthermore, the protein kinase inhibitor SP600125, which inhibits JNK (148), but
530 also other protein kinases (149), did not restore insulin sensitivity to cells exposed to
531 prolonged ER stress (115, 116). JNK has been shown to interact with and to
532 phosphorylate IRS1 at S307 (48), resulting in inhibition of IRS1 tyrosine
533 phosphorylation by the insulin receptor (42). However, despite activation and
534 continued cytoplasmic localization of JNK in ER-stressed cells (data not shown) IRS1
535 S307 phosphorylation in 3T3-F442A or Hep G2 cells was unaltered (Fig. 7). ER
536 stress causes only relatively weak JNK activation when compared to other stresses
537 such as UV irradiation (Brown et al., submitted for publication). The extent of JNK
538 activation does, however, not correlate with inhibition of insulin action, because
539 several stresses causing very strong JNK activation do not affect insulin action, while
540 weaker JNK elicitors inhibit insulin-stimulated AKT activation (data not shown).
541 Several scaffolding proteins are required for the activation of JNK, for example the
542 JNK-interacting proteins (JIPs) 1-4, and β-arrestin 2 (150, 151). Of these, JIP1 has
543 been linked to insulin resistance (152, 153). Activation of JNK by IRE1α requires

544 TRAF2 (87) and the MAP kinase kinase kinase ASK1 (154, 155). ASK1 is known to
545 interact with JIP3 and JIP4 (156). Therefore, it is possible that JNK activation via
546 ASK1 and specific scaffolding proteins, such as JIP3 and JIP4, may not license JNK
547 for phosphorylation of IRS proteins in ER-stressed cells.

548 *TRB3* mRNA was induced ~20 fold after 4 h of ER stress in C_2C_{12} cells (Fig. 1C).
549 However, no effects of ER stress on insulin-stimulated AKT S473 and T308
550 phosphorylation were observed at this time point (Fig. 1A). Overexpression of TRB3
551 inhibited AKT and IRS1 phosphorylation in several (81, 83, 84, 157, 158), but not all
552 studies (86, 158). TRB3 also co-immunoprecipitated with AKT and IRS1 when
553 overexpressed (81, 83, 84, 157). TRB3 expression levels in ER-stressed cells appear
554 to be lower than in virally transduced cells, for which an overexpression level of 700-
555 1000 fold at the mRNA level has been estimated (86), and thus may not reach the
556 threshold necessary to inhibit IRS1 tyrosine and AKT phosphorylation. TRB3 also
557 interacts with ATF4 (157, 159) and CHOP (160), which are both induced in ER-
558 stressed cells (160, 161). These two proteins, and possibly others induced by ER
559 stress, will compete with AKT for interaction with TRB3, which may explain the lack
560 of an inhibitory effect of TRB3 on insulin-stimulated AKT activation during ER
561 stress. Future studies are necessary to characterize the interaction partners of TRB3
562 during ER stress to more completely understand the role of TRB3 in the ER stress
563 response.

564 In conclusion, we show that short-term ($\leq$ 8 h), pharmacologically-induced ER
565 stress does not affect insulin-stimulated AKT activation, while transiently activating
566 JNK and inducing TRB3. Prolonged ER stress extending over several half-lives of the
567 insulin receptor may cause insulin resistance by depleting mature insulin receptors
568 from the plasma membrane.

Acknowledgements

This work was supported by the European Community's 7th Framework Programme (FP7/2007-2013) under grant agreement no. 201608 and Diabetes UK [BDA 09/0003949]. We thank R. Bashir (Durham University), A. Benham (Durham University), C. Hutchison (Durham University), and T. Mak (University of Toronto) for providing cell lines.

References

1. **Özcan U, Cao Q, Yilmaz E, Lee A-H, Iwakoshi NN, Ozdelen E, Tuncman G, Görgün C, Glimcher LH, Hotamisligil GS.** 2004. Endoplasmic reticulum stress links obesity, insulin action, and type 2 diabetes. Science **306:**457-461.
2. **Özcan U, Yilmaz E, Özcan L, Furuhashi M, Vaillancourt E, Smith RO, Görgün CZ, Hotamisligil GS.** 2006. Chemical chaperones reduce ER stress and restore glucose homeostasis in a mouse model of type 2 diabetes. Science **313:**1137-1140.
3. **Sreejayan N, Dong F, Kandadi MR, Yang X, Ren J.** 2008. Chromium alleviates glucose intolerance, insulin resistance, and hepatic ER stress in obese mice. Obesity (Silver Spring) **16:**1331-1337.
4. **Hosogai N, Fukuhara A, Oshima K, Miyata Y, Tanaka S, Segawa K, Furukawa S, Tochino Y, Komuro R, Matsuda M, Shimomura I.** 2007. Adipose tissue hypoxia in obesity and its impact on adipocytokine dysregulation. Diabetes **56:**901-911.
5. **Sharkey D, Fainberg HP, Wilson V, Harvey E, Gardner DS, Symonds ME, Budge H.** 2009. Impact of early onset obesity and hypertension on the unfolded protein response in renal tissues of juvenile sheep. Hypertension **53:**925-931.

6. **Boden G, Duan X, Homko C, Molina EJ, Song W, Perez O, Cheung P, Merali S.** 2008. Increase in endoplasmic reticulum (ER) stress related proteins and genes in adipose tissue of obese, insulin resistant individuals. Diabetes **57:**2438-2444.
7. **Sharma NK, Das SK, Mondal AK, Hackney OG, Chu WS, Kern PA, Rasouli N, Spencer HJ, Yao-Borengasser A, Elbein SC.** 2008. Endoplasmic reticulum stress markers are associated with obesity in non-diabetic subjects. J Clin Endocrinol Metab **93:**4532-4541.
8. **Gregor MF, Yang L, Fabbrini E, Mohammed BS, Eagon JC, Hotamisligil GS, Klein S.** 2009. Endoplasmic reticulum stress is reduced in tissues of obese subjects after weight loss. Diabetes **58:**693-700.
9. **Hollien J, Lin JH, Li H, Stevens N, Walter P, Weissman JS.** 2009. Regulated Ire1-dependent decay of messenger RNAs in mammalian cells. J Cell Biol **186:**323-331.
10. **Hollien J, Weissman JS.** 2006. Decay of endoplasmic reticulum-localized mRNAs during the unfolded protein response. Science **313:**104-107.
11. **Shulman GI.** 1999. Cellular mechanisms of insulin resistance in humans. Am J Cardiol **84:**3J-10J.
12. **Kasuga M, Karlsson FA, Kahn CR.** 1982. Insulin stimulates the phosphorylation of the 95,000-dalton subunit of its own receptor. Science **215:**185-187.
13. **Wilden PA, Siddle K, Haring E, Backer JM, White MF, Kahn CR.** 1992. The role of insulin receptor kinase domain autophosphorylation in receptor-mediated activities. Analysis with insulin and anti-receptor antibodies. J Biol Chem **267:**13719-13727.

14. **Rhodes CJ, White MF.** 2002. Molecular insights into insulin action and secretion. Eur J Clin Invest **32 Suppl 3:**3-13.

15. **White MF, Shoelson SE, Keutmann H, Kahn CR.** 1988. A cascade of tyrosine autophosphorylation in the beta-subunit activates the phosphotransferase of the insulin receptor. J Biol Chem **263:**2969-2980.

16. **Tornqvist HE, Avruch J.** 1988. Relationship of site-specific β subunit tyrosine autophosphorylation to insulin activation of the insulin receptor (tyrosine) protein kinase activity. J Biol Chem **263:**4593-4601.

17. **Tornqvist HE, Gunsalus JR, Nemenoff RA, Frackelton AR, Pierce MW, Avruch J.** 1988. Identification of the insulin receptor tyrosine residues undergoing insulin-stimulated phosphorylation in intact rat hepatoma cells. J Biol Chem **263:**350-359.

18. **Myers MG, Jr., White MF.** 1996. Insulin signal transduction and the IRS proteins. Annu Rev Pharmacol Toxicol **36:**615-658.

19. **Paz K, Voliovitch H, Hadari YR, Roberts CT, Jr., LeRoith D, Zick Y.** 1996. Interaction between the insulin receptor and its downstream effectors. Use of individually expressed receptor domains for structure/function analysis. J Biol Chem **271:**6998-7003.

20. **Cheatham B, Kahn CR.** 1995. Insulin action and the insulin signaling network. Endocr Rev **16:**117-142.

21. **Backer JM, Myers MG, Jr., Shoelson SE, Chin DJ, Sun XJ, Miralpeix M, Hu P, Margolis B, Skolnik EY, Schlessinger J, White MF.** 1992. Phosphatidylinositol 3'-kinase is activated by association with IRS-1 during insulin stimulation. EMBO J **11:**3469-3479.

642 22. **White MF.** 2002. IRS proteins and the common path to diabetes. Am J Physiol
643 Endocrinol Metab **283:**E413-422.
644 23. **Bandyopadhyay G, Standaert ML, Zhao L, Yu B, Avignon A, Galloway L,**
645 **Karnam P, Moscat J, Farese RV.** 1997. Activation of protein kinase C (α, β, and
646 ζ) by insulin in 3T3/L1 cells. Transfection studies suggest a role for PKC-ζ in
647 glucose transport. J Biol Chem **272:**2551-2558.
648 24. **Alessi DR, Cohen P.** 1998. Mechanism of activation and function of protein
649 kinase B. Curr Opin Genet Dev **8:**55-62.
650 25. **Brunet A, Bonni A, Zigmond MJ, Lin MZ, Juo P, Hu LS, Anderson MJ,**
651 **Arden KC, Blenis J, Greenberg ME.** 1999. Akt promotes cell survival by
652 phosphorylating and inhibiting a Forkhead transcription factor. Cell **96:**857-868.
653 26. **Yenush L, White MF.** 1997. The IRS-signalling system during insulin and
654 cytokine action. Bioessays **19:**491-500.
655 27. **Nave BT, Ouwens M, Withers DJ, Alessi DR, Shepherd PR.** 1999. Mammalian
656 target of rapamycin is a direct target for protein kinase B: Identification of a
657 convergence point for opposing effects of insulin and amino-acid deficiency on
658 protein translation. Biochem J **344:**427-431.
659 28. **Scott PH, Brunn GJ, Kohn AD, Roth RA, Lawrence JC, Jr.** 1998. Evidence of
660 insulin-stimulated phosphorylation and activation of the mammalian target of
661 rapamycin mediated by a protein kinase B signaling pathway. Proc Natl Acad Sci
662 U S A **95:**7772-7777.
663 29. **Burnett PE, Barrow RK, Cohen NA, Snyder SH, Sabatini DM.** 1998. RAFT1
664 phosphorylation of the translational regulators p70 S6 kinase and 4E-BP1. Proc
665 Natl Acad Sci U S A **95:**1432-1437.

30. **Hara K, Yonezawa K, Kozlowski MT, Sugimoto T, Andrabi K, Weng QP, Kasuga M, Nishimoto I, Avruch J.** 1997. Regulation of eIF-4E BP1 phosphorylation by mTOR. J Biol Chem **272:**26457-26463.

31. **Isotani S, Hara K, Tokunaga C, Inoue H, Avruch J, Yonezawa K.** 1999. Immunopurified mammalian target of rapamycin phosphorylates and activates p70 S6 kinase α *in vitro*. J Biol Chem **274:**34493-34498.

32. **Sartipy P, Loskutoff DJ.** 2003. Monocyte chemoattractant protein 1 in obesity and insulin resistance. Proc Natl Acad Sci U S A **100:**7265-7270.

33. **Jiang ZY, Lin YW, Clemont A, Feener EP, Hein KD, Igarashi M, Yamauchi T, White MF, King GL.** 1999. Characterization of selective resistance to insulin signaling in the vasculature of obese Zucker (*fa/fa*) rats. The Journal of clinical investigation **104:**447-457.

34. **Cusi K, Maezono K, Osman A, Pendergrass M, Patti ME, Pratipanawatr T, DeFronzo RA, Kahn CR, Mandarino LJ.** 2000. Insulin resistance differentially affects the PI 3-kinase- and MAP kinase-mediated signaling in human muscle. The Journal of clinical investigation **105:**311-320.

35. **Montagnani M, Golovchenko I, Kim I, Koh GY, Goalstone ML, Mundhekar AN, Johansen M, Kucik DF, Quon MJ, Draznin B.** 2002. Inhibition of phosphatidylinositol 3-kinase enhances mitogenic actions of insulin in endothelial cells. J Biol Chem **277:**1794-1799.

36. **Wang CC, Gurevich I, Draznin B.** 2003. Insulin affects vascular smooth muscle cell phenotype and migration via distinct signaling pathways. Diabetes **52:**2562-2569.

37. **Qiao LY, Goldberg JL, Russell JC, Sun XJ.** 1999. Identification of enhanced serine kinase activity in insulin resistance. J Biol Chem **274:**10625-10632.

691 38. **White MF.** 2003. Insulin signaling in health and disease. Science **302:**1710-1711.
692 39. **Birnbaum MJ.** 2001. Turning down insulin signaling. The Journal of clinical
693 investigation **108:**655-659.
694 40. **Um SH, Frigerio F, Watanabe M, Picard F, Joaquin M, Sticker M, Fumagalli**
695 **S, Allegrini PR, Kozma SC, Auwerx J, Thomas G.** 2004. Absence of S6K1
696 protects against age- and diet-induced obesity while enhancing insulin sensitivity.
697 Nature **431:**200-205.
698 41. **Patti M-E, Kahn BB.** 2004. Nutrient sensor links obesity with diabetes risk. Nat
699 Med **10:**1049-1050.
700 42. **Aguirre V, Werner ED, Giraud J, Lee YH, Shoelson SE, White MF.** 2002.
701 Phosphorylation of Ser307 in insulin receptor substrate-1 blocks interactions with
702 the insulin receptor and inhibits insulin action. J Biol Chem **277:**1531-1537.
703 43. **Qiao LY, Zhande R, Jetton TL, Zhou G, Sun XJ.** 2002. *In vivo* phosphorylation
704 of insulin receptor substrate 1 at serine 789 by a novel serine kinase in insulin-
705 resistant rodents. J Biol Chem **277:**26530-26539.
706 44. **Shah OJ, Wang Z, Hunter T.** 2004. Inappropriate activation of the
707 TSC/Rheb/mTOR/S6K cassette induces IRS1/2 depletion, insulin resistance, and
708 cell survival deficiencies. Curr Biol **14:**1650-1656.
709 45. **Tremblay F, Krebs M, Dombrowski L, Brehm A, Bernroider E, Roth E,**
710 **Nowotny P, Waldhäusl W, Marette A, Roden M.** 2005. Overactivation of S6
711 kinase 1 as a cause of human insulin resistance during increased amino acid
712 availability. Diabetes **54:**2674-2684.
713 46. **Pende M, Kozma SC, Jaquet M, Oorschot V, Burcelin R, Le Marchand-**
714 **Brustel Y, Klumperman J, Thorens B, Thomas G.** 2000. Hypoinsulinaemia,

glucose intolerance and diminished β-cell size in S6K1-deficient mice. Nature **408:**994-997.

47. **Gao Z, Hwang D, Bataille F, Lefevre M, York D, Quon MJ, Ye J.** 2002. Serine phosphorylation of insulin receptor substrate 1 by inhibitor κB kinase complex. J Biol Chem **277:**48115-48121.
48. **Aguirre V, Uchida T, Yenush L, Davis R, White MF.** 2000. The c-Jun NH_2-terminal kinase promotes insulin resistance during association with insulin receptor substrate-1 and phosphorylation of Ser^{307}. J Biol Chem **275:**9047-9054.
49. **Nguyen MTA, Satoh H, Favelyukis S, Babendure JL, Imamura T, Sbodio JI, Zalevsky J, Dahiyat BI, Chi NW, Olefsky JM.** 2005. JNK and tumor necrosis factor-α mediate free fatty acid-induced insulin resistance in 3T3-L1 adipocytes. J Biol Chem **280:**35361-35371.
50. **Gao Z, Zhang X, Zuberi A, Hwang D, Quon MJ, Lefevre M, Ye J.** 2004. Inhibition of insulin sensitivity by free fatty acids requires activation of multiple serine kinases in 3T3-L1 adipocytes. Mol Endocrinol **18:**2024-2034.
51. **Hirosumi J, Tuncman G, Chang L, Görgün CZ, Uysal KT, Maeda K, Karin M, Hotamisligil GS.** 2002. A central role for JNK in obesity and insulin resistance. Nature **420:**333-336.
52. **Bandyopadhyay GK, Yu JG, Ofrecio J, Olefsky JM.** 2005. Increased p85/55/50 expression and decreased phosphotidylinositol 3-kinase activity in insulin-resistant human skeletal muscle. Diabetes **54:**2351-2359.
53. **Hotamisligil GS, Peraldi P, Budavari A, Ellis R, White MF, Spiegelman BM.** 1996. IRS-1-mediated inhibition of insulin receptor tyrosine kinase activity in TNF-α- and obesity-induced insulin resistance. Science **271:**665-668.

739 54. **Hotamisligil GS, Shargill NS, Spiegelman BM.** 1993. Adipose expression of
740 tumor necrosis factor-alpha: Direct role in obesity-linked insulin resistance.
741 Science **259:**87-91.
742 55. **Peraldi P, Hotamisligil GS, Buurman WA, White MF, Spiegelman BM.** 1996.
743 Tumor necrosis factor (TNF)-α inhibits insulin signaling through stimulation of
744 the p55 TNF receptor and activation of sphingomyelinase. J Biol Chem
745 **271:**13018-13022.
746 56. **Uysal KT, Wiesbrock SM, Marino MW, Hotamisligil GS.** 1997. Protection
747 from obesity-induced insulin resistance in mice lacking TNF-α function. Nature
748 **389:**610-614.
749 57. **Qi C, Pekala PH.** 2000. Tumor necrosis factor-α-induced insulin resistance in
750 adipocytes. Proc Soc Exp Biol Med **223:**128-135.
751 58. **Hotamisligil GS, Spiegelman BM.** 1994. Tumor necrosis factor α: A key
752 component of the obesity-diabetes link. Diabetes **43:**1271-1278.
753 59. **Gao Z, Zuberi A, Quon MJ, Dong Z, Ye J.** 2003. Aspirin inhibits serine
754 phosphorylation of insulin receptor substrate 1 in tumor necrosis factor-treated
755 cells through targeting multiple serine kinases. J Biol Chem **278:**24944-24950.
756 60. **de Alvaro C, Teruel T, Hernandez R, Lorenzo M.** 2004. Tumor necrosis factor
757 α produces insulin resistance in skeletal muscle by activation of inhibitor κB
758 kinase in a p38 MAPK-dependent manner. J Biol Chem **279:**17070-17078.
759 61. **Jiao P, Ma J, Feng B, Zhang H, Alan Diehl J, Eugene Chin Y, Yan W, Xu H.**
760 2011. FFA-induced adipocyte inflammation and insulin resistance: Involvement of
761 ER stress and IKKβ pathways. Obesity (Silver Spring) **19:**483-491.

762 62. **Zhang J, Gao Z, Yin J, Quon MJ, Ye J.** 2008. S6K directly phosphorylates IRS-
763 1 on Ser-270 to promote insulin resistance in response to TNF-α signaling through
764 IKK2. J Biol Chem **283:**35375-35382.
765 63. **Engelman JA, Berg AH, Lewis RY, Lisanti MP, Scherer PE.** 2000. Tumor
766 necrosis factor α-mediated insulin resistance, but not dedifferentiation, is
767 abrogated by MEK1/2 inhibitors in 3T3-L1 adipocytes. Mol Endocrinol **14:**1557-
768 1569.
769 64. **Rui L, Aguirre V, Kim JK, Shulman GI, Lee A, Corbould A, Dunaif A, White**
770 **MF.** 2001. Insulin/IGF-1 and TNF-α stimulate phosphorylation of IRS-1 at
771 inhibitory Ser307 via distinct pathways. The Journal of clinical investigation
772 **107:**181-189.
773 65. **De Fea K, Roth RA.** 1997. Modulation of insulin receptor substrate-1 tyrosine
774 phosphorylation and function by mitogen-activated protein kinase. J Biol Chem
775 **272:**31400-31406.
776 66. **Ravichandran LV, Esposito DL, Chen J, Quon MJ.** 2001. Protein kinase C-ζ
777 phosphorylates insulin receptor substrate-1 and impairs its ability to activate
778 phosphatidylinositol 3-kinase in response to insulin. J Biol Chem **276:**3543-3549.
779 67. **Bourbon NA, Sandirasegarane L, Kester M.** 2002. Ceramide-induced inhibition
780 of Akt is mediated through protein kinase Cζ: Implications for growth arrest. J
781 Biol Chem **277:**3286-3292.
782 68. **Liu Y-F, Paz K, Herschkovitz A, Alt A, Tennenbaum T, Sampson SR, Ohba**
783 **M, Kuroki T, LeRoith D, Zick Y.** 2001. Insulin stimulates PKCζ-mediated
784 phosphorylation of insulin receptor substrate-1 (IRS-1). A self-attenuated
785 mechanism to negatively regulate the function of IRS proteins. J Biol Chem
786 **276:**14459-14465.

69. **Li Y, Soos TJ, Li X, Wu J, Degennaro M, Sun X, Littman DR, Birnbaum MJ, Polakiewicz RD.** 2004. Protein kinase C θ inhibits insulin signaling by phosphorylating IRS1 at Ser^{1101}. J Biol Chem **279:**45304-45307.

70. **Ozes ON, Akca H, Mayo LD, Gustin JA, Maehama T, Dixon JE, Donner DB.** 2001. A phosphatidylinositol 3-kinase/Akt/mTOR pathway mediates and PTEN antagonizes tumor necrosis factor inhibition of insulin signaling through insulin receptor substrate-1. Proc Natl Acad Sci U S A **98:**4640-4645.

71. **Eldar-Finkelman H, Krebs EG.** 1997. Phosphorylation of insulin receptor substrate 1 by glycogen synthase kinase 3 impairs insulin action. Proc Natl Acad Sci U S A **94:**9660-9664.

72. **Liberman Z, Eldar-Finkelman H.** 2005. Serine 332 phosphorylation of insulin receptor substrate-1 by glycogen synthase kinase-3 attenuates insulin signaling. J Biol Chem **280:**4422-4428.

73. **Ilouz R, Kowalsman N, Eisenstein M, Eldar-Finkelman H.** 2006. Identification of novel glycogen synthase kinase-3β substrate-interacting residues suggests a common mechanism for substrate recognition. J Biol Chem **281:**30621-30630.

74. **Kim JA, Yeh DC, Ver M, Li Y, Carranza A, Conrads TP, Veenstra TD, Harrington MA, Quon MJ.** 2005. Phosphorylation of Ser^{24} in the pleckstrin homology domain of insulin receptor substrate-1 by mouse Pelle-like kinase/interleukin-1 receptor-associated kinase: cross-talk between inflammatory signaling and insulin signaling that may contribute to insulin resistance. J Biol Chem **280:**23173-23183.

75. **Haruta T, Uno T, Kawahara J, Takano A, Egawa K, Sharma PM, Olefsky JM, Kobayashi M.** 2000. A rapamycin-sensitive pathway down-regulates insulin

811 signaling via phosphorylation and proteasomal degradation of insulin receptor
812 substrate-1. Mol Endocrinol **14:**783-794.
813 76. **Zhang K, Shen X, Wu J, Sakaki K, Saunders T, Rutkowski DT, Back SH,**
814 **Kaufman RJ.** 2006. Endoplasmic reticulum stress activates cleavage of CREBH
815 to induce a systemic inflammatory response. Cell **124:**587-599.
816 77. **Jiang HY, Wek SA, McGrath BC, Scheuner D, Kaufman RJ, Cavener DR,**
817 **Wek RC.** 2003. Phosphorylation of the α subunit of eukaryotic initiation factor 2
818 is required for activation of NF-κB in response to diverse cellular stresses. Mol
819 Cell Biol **23:**5651-5663.
820 78. **Deng J, Lu PD, Zhang Y, Scheuner D, Kaufman RJ, Sonenberg N, Harding**
821 **HP, Ron D.** 2004. Translational repression mediates activation of nuclear factor
822 kappa B by phosphorylated translation initiation factor 2. Mol Cell Biol **24:**10161-
823 10168.
824 79. **Wu S, Hu Y, Wang JL, Chatterjee M, Shi Y, Kaufman RJ.** 2002. Ultraviolet
825 light inhibits translation through activation of the unfolded protein response kinase
826 PERK in the lumen of the endoplasmic reticulum. J Biol Chem **277:**18077-18083.
827 80. **Wu S, Tan M, Hu Y, Wang JL, Scheuner D, Kaufman RJ.** 2004. Ultraviolet
828 light activates NFκB through translational inhibition of IκBα synthesis. J Biol
829 Chem **279:**34898-34902.
830 81. **Du K, Herzig S, Kulkarni RN, Montminy M.** 2003. TRB3: A *tribbles* homolog
831 that inhibits Akt/PKB activation by insulin in liver. Science **300:**1574-1577.
832 82. **Avery J, Etzion S, Debosch BJ, Jin X, Lupu TS, Beitinjaneh B, Grand J,**
833 **Kovacs A, Sambandam N, Muslin AJ.** 2010. TRB3 function in cardiac
834 endoplasmic reticulum stress. Circ Res **106:**1516-1523.

83. **Koh HJ, Arnolds DE, Fujii N, Tran TT, Rogers MJ, Jessen N, Li Y, Liew CW, Ho RC, Hirshman MF, Kulkarni RN, Kahn CR, Goodyear LJ.** 2006. Skeletal muscle-selective knockout of LKB1 increases insulin sensitivity, improves glucose homeostasis, and decreases TRB3. Mol Cell Biol **26:**8217-8227.

84. **Koh HJ, Toyoda T, Didesch MM, Lee MY, Sleeman MW, Kulkarni RN, Musi N, Hirshman MF, Goodyear LJ.** 2013. Tribbles 3 mediates endoplasmic reticulum stress-induced insulin resistance in skeletal muscle. Nat Commun **4:**1871.

85. **Okamoto H, Latres E, Liu R, Thabet K, Murphy A, Valenzeula D, Yancopoulos GD, Stitt TN, Glass DJ, Sleeman MW.** 2007. Genetic deletion of Trb3, the mammalian *Drosophila tribbles* homolog, displays normal hepatic insulin signaling and glucose homeostasis. Diabetes **56:**1350-1356.

86. **Iynedjian PB.** 2005. Lack of evidence for a role of TRB3/NIPK as an inhibitor of PKB-mediated insulin signalling in primary hepatocytes. Biochem J **386:**113-118.

87. **Urano F, Wang X, Bertolotti A, Zhang Y, Chung P, Harding HP, Ron D.** 2000. Coupling of stress in the ER to activation of JNK protein kinases by transmembrane protein kinase IRE1. Science **287:**664-666.

88. **Hu P, Han Z, Couvillon AD, Kaufman RJ, Exton JH.** 2006. Autocrine tumor necrosis factor alpha links endoplasmic reticulum stress to the membrane death receptor pathway through IRE1α-mediated NF-κB activation and down-regulation of TRAF2 expression. Mol Cell Biol **26:**3071-3084.

89. **Sidrauski C, Walter P.** 1997. The transmembrane kinase Ire1p is a site-specific endonuclease that initiates mRNA splicing in the unfolded protein response. Cell **90:**1031-1039.

90. **Calfon M, Zeng H, Urano F, Till JH, Hubbard SR, Harding HP, Clark SG, Ron D.** 2002. IRE1 couples endoplasmic reticulum load to secretory capacity by processing the *XBP-1* mRNA. Nature **415:**92-96.

91. **Yoshida H, Matsui T, Yamamoto A, Okada T, Mori K.** 2001. XBP1 mRNA is induced by ATF6 and spliced by IRE1 in response to ER stress to produce a highly active transcription factor. Cell **107:**881-891.

92. **Shen X, Ellis RE, Lee K, Liu C-Y, Yang K, Solomon A, Yoshida H, Morimoto R, Kurnit DM, Mori K, Kaufman RJ.** 2001. Complementary signaling pathways regulate the unfolded protein response and are required for *C. elegans* development. Cell **107:**893-903.

93. **Lee K, Tirasophon W, Shen X, Michalak M, Prywes R, Okada T, Yoshida H, Mori K, Kaufman RJ.** 2002. IRE1-mediated unconventional mRNA splicing and S2P-mediated ATF6 cleavage merge to regulate XBP1 in signaling the unfolded protein response. Genes Dev **16:**452-466.

94. **Gaddam D, Stevens N, Hollien J.** 2013. Comparison of mRNA localization and regulation during endoplasmic reticulum stress in *Drosophila* cells. Mol Biol Cell **24:**14-20.

95. **Green H, Kehinde O.** 1976. Spontaneous heritable changes leading to increased adipose conversion in 3T3 cells. Cell **7:**105-113.

96. **Blau HM, Pavlath GK, Hardeman EC, Chiu CP, Silberstein L, Webster SG, Miller SC, Webster C.** 1985. Plasticity of the differentiated state. Science **230:**758-766.

97. **Knowles BB, Howe CC, Aden DP.** 1980. Human hepatocellular carcinoma cell lines secrete the major plasma proteins and hepatitis B surface antigen. Science **209:**497-499.

884 98. **Deschatrette J, Weiss MC.** 1974. Characterization of differentiated and
885 dedifferentiated clones from a rat hepatoma. Biochimie **56:**1603-1611.
886 99. **Moore GE, Gerner RE, Franklin HA.** 1967. Culture of normal human
887 leukocytes. JAMA **199:**519-524.
888 100. **Coon HG, Weiss MC.** 1969. A quantitative comparison of formation of
889 spontaneous and virus-produced viable hybrids. Proc Natl Acad Sci U S A
890 **62:**852-859.
891 101. **Morton HJ.** 1970. A survey of commercially available tissue culture media.
892 In Vitro **6:**89-108.
893 102. **Rutzky LP, Pumper RW.** 1974. Supplement to a survey of commercially
894 available tissue culture media (1970). In Vitro **9:**468-469.
895 103. **Bains W, Ponte P, Blau H, Kedes L.** 1984. Cardiac actin is the major actin
896 gene product in skeletal muscle cell differentiation in vitro. Mol Cell Biol **4:**1449-
897 1453.
898 104. **Amato PA, Unanue ER, Taylor DL.** 1983. Distribution of actin in spreading
899 macrophages: a comparative study on living and fixed cells. J Cell Biol **96:**750-
900 761.
901 105. **Rubin CS, Hirsch A, Fung C, Rosen OM.** 1978. Development of hormone
902 receptors and hormonal responsiveness *in vitro*. Insulin receptors and insulin
903 sensitivity in the preadipocyte and adipocyte forms of 3T3-L1 cells. J Biol Chem
904 **253:**7570-7578.
905 106. **Hansen JB, Petersen RK, Larsen BM, Bartkova J, Alsner J, Kristiansen**
906 **K.** 1999. Activation of peroxisome proliferator-activated receptor γ bypasses the
907 function of the retinoblastoma protein in adipocyte differentiation. J Biol Chem
908 **274:**2386-2393.

107. **Greenspan P, Fowler SD.** 1985. Spectrofluorometric studies of the lipid probe, nile red. J Lipid Res **26:**781-789.

108. **Greenspan P, Mayer EP, Fowler SD.** 1985. Nile red: A selective fluorescent stain for intracellular lipid droplets. J Cell Biol **100:**965-973.

109. **Paton AW, Srimanote P, Talbot UM, Wang H, Paton JC.** 2004. A new family of potent AB_5 cytotoxins produced by Shiga toxigenic *Escherichia coli*. J Exp Med **200:**35-46.

110. **Talbot UM, Paton JC, Paton AW.** 2005. Protective immunization of mice with an active-site mutant of subtilase cytotoxin of Shiga toxin-producing *Escherichia coli*. Infect Immun **73:**4432-4436.

111. **Cox DJ, Strudwick N, Ali AA, Paton AW, Paton JC, Schröder M.** 2011. Measuring signaling by the unfolded protein response. Methods Enzymol **491:**261-292.

112. **Collins TJ.** 2007. ImageJ for microscopy. Biotechniques **43:**25-30.

113. **Ku HH.** 1966. Notes on use of propagation of error formulas. J Res Nat Bureau Standards Sect C - Eng Instrumentat **70:**263-273.

114. **Hassan RH, Hainault I, Vilquin J-T, Samama C, Lasnier F, Ferré P, Foufelle F, Hajduch E.** 2012. Endoplasmic reticulum stress does not mediate palmitate-induced insulin resistance in mouse and human muscle cells. Diabetologia **55:**204-214.

115. **Xu L, Spinas GA, Niessen M.** 2010. ER stress in adipocytes inhibits insulin signaling, represses lipolysis, and alters the secretion of adipokines without inhibiting glucose transport. Horm Metab Res **42:**643-651.

116. **Zhou L, Zhang J, Fang Q, Liu M, Liu X, Jia W, Dong LQ, Liu F.** 2009. Autophagy-mediated insulin receptor down-regulation contributes to endoplasmic reticulum stress-induced insulin resistance. Mol Pharmacol **76:**596-603.

117. **Tang X, Shen H, Chen J, Wang X, Zhang Y, Chen LL, Rukachaisirikul V, Jiang H-l, Shen X.** 2011. Activating transcription factor 6 protects insulin receptor from ER stress-stimulated desensitization via p42/44 ERK pathway. Acta Pharmacol Sin **32:**1138-1147.

118. **Back SH, Schröder M, Lee K, Zhang K, Kaufman RJ.** 2005. ER stress signaling by regulated splicing: IRE1/HAC1/XBP1. Methods **35:**395-416.

119. **Paton AW, Beddoe T, Thorpe CM, Whisstock JC, Wilce MC, Rossjohn J, Talbot UM, Paton JC.** 2006. AB5 subtilase cytotoxin inactivates the endoplasmic reticulum chaperone BiP. Nature **443:**548-552.

120. **Alessi DR, Andjelkovic M, Caudwell B, Cron P, Morrice N, Cohen P, Hemmings BA.** 1996. Mechanism of activation of protein kinase B by insulin and IGF-1. EMBO J **15:**6541-6551.

121. **Cross DA, Alessi DR, Cohen P, Andjelkovich M, Hemmings BA.** 1995. Inhibition of glycogen synthase kinase-3 by insulin mediated by protein kinase B. Nature **378:**785-789.

122. **Welsh GI, Proud CG.** 1993. Glycogen synthase kinase-3 is rapidly inactivated in response to insulin and phosphorylates eukaryotic initiation factor eIF-2B. Biochem J **294:**625-629.

123. **Cross DAE, Alessi DR, Vandenheede JR, McDowell HE, Hundal HS, Cohen P.** 1994. The inhibition of glycogen synthase kinase-3 by insulin or insulin-like growth factor 1 in the rat skeletal muscle cell line L6 is blocked by wortmannin, but not by rapamycin: evidence that wortmannin blocks activation of

957 the mitogen-activated protein kinase pathway in L6 cells between Ras and Raf.
958 Biochem J **303:**21-26.
959 124. **Ucker DS, Yamamoto KR.** 1984. Early events in the stimulation of
960 mammary tumor virus RNA synthesis by glucocorticoids. Novel assays of
961 transcription rates. J Biol Chem **259:**7416-7420.
962 125. **Sehgal PB, Derman E, Molloy GR, Tamm I, Darnell JE.** 1976. 5,6-
963 Dichloro-1-β-D-ribofuranosylbenzimidazole inhibits initiation of nuclear
964 heterogeneous RNA chains in HeLa cells. Science **194:**431-433.
965 126. **Fritsche L, Weigert C, Haring HU, Lehmann R.** 2008. How insulin
966 receptor substrate proteins regulate the metabolic capacity of the liver -
967 Implications for health and disease. Curr Med Chem **15:**1316-1329.
968 127. **Reed BC, Lane MD.** 1980. Insulin receptor synthesis and turnover in
969 differentiating 3T3-L1 preadipocytes. Proc Natl Acad Sci U S A **77:**285-289.
970 128. **Kasuga M, Kahn CR, Hedo JA, Van Obberghen E, Yamada KM.** 1981.
971 Insulin-induced receptor loss in cultured human lymphocytes is due to accelerated
972 receptor degradation. Proc Natl Acad Sci U S A **78:**6917-6921.
973 129. **Reed BC, Ronnett GV, Clements PR, Lane MD.** 1981. Regulation of
974 insulin receptor metabolism. Differentiation-induced alteration of receptor
975 synthesis and degradation. J Biol Chem **256:**3917-3925.
976 130. **Reed BC, Ronnett GV, Lane MD.** 1981. Role of glycosylation and protein
977 synthesis in insulin receptor metabolism by 3T3-L1 mouse adipocytes. Proc Natl
978 Acad Sci U S A **78:**2908-2912.
979 131. **Capeau J, Lascols O, Flaig-Staedel C, Blivet MJ, Beck JP, Picard J.** 1985.
980 Degradation of insulin receptors by hepatoma cells: Insulin-induced down-

regulation results from an increase in the rate of basal receptor degradation. Biochimie **67:**1133-1141.

132. **Savoie S, Rindress D, Posner BI, Bergeron JJ.** 1986. Tunicamycin sensitivity of prolactin, insulin and epidermal growth factor receptors in rat liver plasmalemma. Mol Cell Endocrinol **45:**241-246.

133. **Grako KA, Olefsky JM, McClain DA.** 1992. Tyrosine kinase-defective insulin receptors undergo decreased endocytosis but do not affect internalization of normal endogenous insulin receptors. Endocrinology **130:**3441-3452.

134. **Bravo DA, Gleason JB, Sanchez RI, Roth RA, Fuller RS.** 1994. Accurate and efficient cleavage of the human insulin proreceptor by the human proprotein-processing protease furin. Characterization and kinetic parameters using the purified, secreted soluble protease expressed by a recombinant baculovirus. J Biol Chem **269:**25830-25837.

135. **Robertson BJ, Moehring JM, Moehring TJ.** 1993. Defective processing of the insulin receptor in an endoprotease-deficient Chinese hamster cell strain is corrected by expression of mouse furin. J Biol Chem **268:**24274-24277.

136. **Hwang JB, Frost SC.** 1999. Effect of alternative glycosylation on insulin receptor processing. J Biol Chem **274:**22813-22820.

137. **Massague J, Pilch PF, Czech MP.** 1981. A unique proteolytic cleavage site on the beta subunit of the insulin receptor. J Biol Chem **256:**3182-3190.

138. **Tkacz JS, Lampen JO.** 1975. Tunicaymcin inhibition of polyisoprenyl N-acetylglucosaminyl pyrophosphate formation in calf-liver microsomes. Biochem Biophys Res Commun **65:**248-257.

139. **Thastrup O, Cullen PJ, Drøbak BK, Hanley MR, Dawson AP.** 1990. Thapsigargin, a tumor promoter, discharges intracellular Ca^{2+} stores by specific

1006 inhibition of the endoplasmic reticulum Ca^{2+}-ATPase. Proc Natl Acad Sci U S A
1007 **87:**2466-2470.
1008 140. **Wang D, Wei YR, Schmoll D, Maclean KN, Pagliassotti MJ.** 2006.
1009 Endoplasmic reticulum stress increases glucose-6-phosphatase and glucose
1010 cycling in liver cells. Endocrinology **147:**350-358.
1011 141. **Corbalán-García S, Gómez-Fernández JC.** 2006. Protein kinase C
1012 regulatory domains: the art of decoding many different signals in membranes.
1013 Biochim Biophys Acta **1761:**633-654.
1014 142. **Nawaratne R, Gray A, Jørgensen CH, Downes CP, Siddle K, Sethi JK.**
1015 2006. Regulation of insulin receptor substrate 1 pleckstrin homology domain by
1016 protein kinase C: role of serine 24 phosphorylation. Mol Endocrinol **20:**1838-
1017 1852.
1018 143. **Werner ED, Lee J, Hansen L, Yuan M, Shoelson SE.** 2004. Insulin
1019 resistance due to phosphorylation of insulin receptor substrate-1 at serine 302. J
1020 Biol Chem **279:**35298-35305.
1021 144. **Copps KD, White MF.** 2012. Regulation of insulin sensitivity by
1022 serine/threonine phosphorylation of insulin receptor substrate proteins IRS1 and
1023 IRS2. Diabetologia **55:**2565-2582.
1024 145. **Ozcan U, Ozcan L, Yilmaz E, Düvel K, Sahin M, Manning BD,**
1025 **Hotamisligil GS.** 2008. Loss of the tuberous sclerosis complex tumor suppressors
1026 triggers the unfolded protein response to regulate insulin signaling and apoptosis.
1027 Mol Cell **29:**541-551.
1028 146. **Jurczak MJ, Lee AH, Jornayvaz FR, Lee HY, Birkenfeld AL, Guigni BA,**
1029 **Kahn M, Samuel VT, Glimcher LH, Shulman GI.** 2012. Dissociation of
1030 inositol requiring enzyme (IRE1α)-mediated JNK activation from hepatic insulin

1031 resistance in conditional X-box binding protein-1 (XBP1) knockout mice. J Biol
1032 Chem **287:**2558-2567.
1033 147. **Jung DY, Chalasani U, Pan N, Friedline RH, Prosdocimo DA, Nam M,**
1034 **Azuma Y, Maganti R, Yu K, Velagapudi A, O'Sullivan-Murphy B, Sartoretto**
1035 **JL, Jain MK, Cooper MP, Urano F, Kim JK, Gray S.** 2013. KLF15 is a
1036 molecular link between endoplasmic reticulum stress and insulin resistance. PLoS
1037 One **8:**e77851.
1038 148. **Bennett BL, Sasaki DT, Murray BW, O'Leary EC, Sakata ST, Xu W,**
1039 **Leisten JC, Motiwala A, Pierce S, Satoh Y, Bhagwat SS, Manning AM,**
1040 **Anderson DW.** 2001. SP600125, an anthrapyrazolone inhibitor of Jun N-terminal
1041 kinase. Proc Natl Acad Sci U S A **98:**13681-13686.
1042 149. **Bain J, McLauchlan H, Elliott M, Cohen P.** 2003. The specificities of
1043 protein kinase inhibitors: an update. Biochem J **371:**199-204.
1044 150. **Whitmarsh AJ.** 2006. The JIP family of MAPK scaffold proteins. Biochem
1045 Soc Trans **34:**828-832.
1046 151. **Guo C, Whitmarsh AJ.** 2008. The beta-arrestin-2 scaffold protein promotes
1047 c-Jun N-terminal kinase-3 activation by binding to its nonconserved N terminus. J
1048 Biol Chem **283:**15903-15911.
1049 152. **Standen CL, Kennedy NJ, Flavell RA, Davis RJ.** 2009. Signal transduction
1050 cross talk mediated by Jun N-terminal kinase-interacting protein and insulin
1051 receptor substrate scaffold protein complexes. Mol Cell Biol **29:**4831-4840.
1052 153. **Jaeschke A, Czech MP, Davis RJ.** 2004. An essential role of the JIP1
1053 scaffold protein for JNK activation in adipose tissue. Genes Dev **18:**1976-1980.
1054 154. **Nishitoh H, Matsuzawa A, Tobiume K, Saegusa K, Takeda K, Inoue K,**
1055 **Hori S, Kakizuka A, Ichijo H.** 2002. ASK1 is essential for endoplasmic

reticulum stress-induced neuronal cell death triggered by expanded polyglutamine repeats. Genes Dev **16:**1345-1355.

155. **Nishitoh H, Saitoh M, Mochida Y, Takeda K, Nakano H, Rothe M, Miyazono K, Ichijo H.** 1998. ASK1 is essential for JNK/SAPK activation by TRAF2. Mol Cell **2:**389-395.

156. **Kelkar N, Standen CL, Davis RJ.** 2005. Role of the JIP4 scaffold protein in the regulation of mitogen-activated protein kinase signaling pathways. Mol Cell Biol **25:**2733-2743.

157. **Liew CW, Bochenski J, Kawamori D, Hu J, Leech CA, Wanic K, Malecki M, Warram JH, Qi L, Krolewski AS, Kulkarni RN.** 2010. The pseudokinase tribbles homolog 3 interacts with ATF4 to negatively regulate insulin exocytosis in human and mouse β cells. The Journal of clinical investigation **120:**2876-2888.

158. **Takahashi Y, Ohoka N, Hayashi H, Sato R.** 2008. TRB3 suppresses adipocyte differentiation by negatively regulating PPARγ transcriptional activity. J Lipid Res **49:**880-892.

159. **Örd D, Örd T.** 2003. Mouse NIPK interacts with ATF4 and affects its transcriptional activity. Exp Cell Res **286:**308-320.

160. **Ohoka N, Yoshii S, Hattori T, Onozaki K, Hayashi H.** 2005. *TRB3*, a novel ER stress-inducible gene, is induced via ATF4-CHOP pathway and is involved in cell death. EMBO J **24:**1243-1255.

161. **Harding HP, Novoa I, Zhang Y, Zeng H, Wek R, Schapira M, Ron D.** 2000. Regulated translation initiation controls stress-induced gene expression in mammalian cells. Mol Cell **6:**1099-1108.

Figure Legends

Figure 1. Acute ER stress does not inhibit insulin-stimulated AKT T308 or S473 phosphorylation in C_2C_{12} myotubes. (A) C_2C_{12} myotubes were serum-starved for 18 h and treated with the indicated concentrations of thapsigargin (Tg), tunicamycin (Tm), or 1 μg/ml SubAB or catalytically inactive $SubA_{A272}B$ during the last 1-8 h of serum starvation and then stimulated with 100 nM insulin for 15 min where indicated. Cell lysates were analyzed by Western blotting. **(B)** Detection of *XBP1* splicing by RT-PCR. PCR products were separated on a 2% (w/v) agarose gel and visualized with ethidium bromide. PCR products derived from unspliced (u) and spliced (s) *XBP1* mRNA are indicated by arrows. β-Actin (*ACTB*) was used as a loading control. Abbreviations: Tg - 300 nM thapsigargin, Tm - 1 μg/ml tunicamycin. **(C)** Induction of *TRB3* in C_2C_{12} cells by ER stress. C_2C_{12} cells were treated with 300 nM thapsigargin, 1 μg/ml tunicamycin, or 1 μg/ml SubAB or $SubA_{A272}B$ for 4 h. *TRB3* mRNA levels were determined by RT-qPCR and standardized to the loading control *ACTB*.

Figure 2. Acute ER stress does not inhibit insulin-dependent AKT activation. (A) Western blots of serum-starved MEFs treated with 1 μM thapsigargin for the indicated times before stimulation with 10 or 100 nM insulin for 15 min are shown. **(B)** Serum-starved Hep G2 hepatoma cells treated with the indicated concentrations of thapsigargin, tunicamycin or 1 μg/ml SubAB for 30 or 60 min before stimulation with 100 nM insulin for 15 min. **(C)** Serum-starved C_2C_{12} myoblasts and **(D)** serum-starved *in vitro* differentiated 3T3-F442A adipocytes were treated for 30 min with the indicated concentrations of thapsigargin, tunicamycin or 1 μg/ml SubAB before stimulation with 100 nM insulin for 15 min. (B-D) Cells were also treated with 1 μg/ml catalytically inactive $SubA_{A272}B$ where indicated. Cell lysates were analyzed by Western blotting.

Figure 3. Acute ER stress activates JNK, but does not inhibit insulin-dependent AKT activation in Fao rat hepatoma cells. Serum-starved Fao rat hepatoma cells were treated with the indicated concentrations of thapsigargin, tunicamycin or 1 μg/ml SubAB for 30 or 60 min before stimulation with 100 nM insulin for 15 min. Cell lysates were analyzed by Western blotting.

Figure 4. ER stress does not inhibit insulin signalling in Fao rat hepatoma cells. Fao rat hepatoma cells were serum starved for 18 h and treated with 0.1 to 1 μM thapsigargin, 0.1 to 10 μg/ml tunicamycin, 1 μg/ml SubAB or $SubA_{A272}B$ for **(A)** 2, **(B)** and **(C)** 3 h, and **(D)** 4 h. Cells were cultured in RPMI 1640 in panels (A), (B), and (D) and in Coon's modification of Ham's F12 medium in panel (C).

Figure 5. Acute ER stress does not affect tyrosine phosphorylation of IRS1. (A) Experimental set-up. At the start of the experiment (t = 0) serum-starved cells were treated with 1 μM thapsigargin. Cell lysates were prepared in one series of dishes 5, 10, and 15 min after addition of 100 nM insulin. In a second series of dishes cells were treated for 10, 20, or 25 min with 1 μM thapsigargin. 100 nM insulin were added for the last 5, 10, or 15 min of thapsigargin treatment. **(B)** and **(C)** Analysis of the time course described in panel (A) by immunoprecipitation of IRS1 and Western blotting with an anti-phosphotyrosine or anti-IRS1 antibody in (B) C_2C_{12} cells and (C) 3T3-F442A cells. **(D-E)** Serum-starved Hep G2 cells were treated with the indicated concentrations of tunicamycin for 30 min and then stimulated with 100 nM insulin for 15 min. Cell lysates were analyzed by immunoprecipitation of IRS1 and Western blotting with anti-phosphotyrosine and anti-IRS1 antibodies in panel (D) and by Western blotting for phospho-JNK and total JNK in panel (E).

Figure 6. IRS1 S307/S312 phosphorylation during acute ER stress. (A) 3T3-F442A, **(B)** C_2C_{12}, and **(C-D)** Hep G2 cells were treated with 1 μM thapsigargin for

the indicated times. Cell lysates were analyzed by ELISA for phosphorylation of S307 in murine IRS1 and S312 in human IRS1 by using the STAR phospho-IRS1 (Ser307 mouse/Ser312 human) ELISA from Millipore. S307 phosphorylation is expressed in units relative to a phospho-S307 IRS1 standard provided in the ELISA kit. phospho-S307 IRS1 units were standardized to the amount of total IRS1 in cell lysates determined by Western blotting. Equal loading of all lanes in the Western blot was controlled with the GAPDH loading control. **(E)** IRS1 S307/S312 phosphorylation in serum-starved 3T3-F442A, C_2C_{12}, and Hep G2 cells treated with 100 nM insulin for 15 min was determined by ELISA. IRS1 phospho-S307/S312 signals in the ELISA were standardised to total protein levels.

Figure 7. Insulin resistance develops over time in ER-stressed C_2C_{12} myoblasts. Serum-starved C_2C_{12} cells were treated with the indicated concentrations of (A) thapsigargin, (B) tunicamycin, or (C) 1 μg/ml SubAB or $SubA_{A272}B$ for 1-24 h before stimulation with 100 nM insulin for 15 min. Western blots for pS473-AKT and total AKT were analyzed as described in Materials and Methods.

Figure 8. Depletion of insulin receptors (INSR) in ER-stressed cells coincides with development of insulin resistance in C_2C_{12} cells. (A) C_2C_{12} cells were treated with the indicated ER stressors for 12-24 h before serum starvation and stimulation with 100 nM insulin for 15 min. Protein extracts were analyzed by Western blotting. Quantitation of insulin receptor β-chains in **(B)** thapsigargin-, **(C)** tunicamycin-, and **(D)** SubAB-treated C_2C_{12} cells. Bars represent standard errors.

Tables

Table I. Oligodeoxynucleotides. Restriction sites are underlined. The start codon for TRAF2Δ1-86 is shown in bold.

Name	Purpose	Sequence
Oligodeoxynucleotides for *H. sapiens* genes		
H8289	*XBP1* PCR, forward	GAGTTAAGACAGCGCTTGGG
H8290	*XBP1* PCR, reverse	ACTGGGTCCAAGTTGTCCAG
Oligodeoxynucleotides for *M. musculus* genes		
H7961	*XBP1* PCR, forward	GATCCTGACGAGGTTCCAGA
H7962	*XBP1* PCR, reverse	ACAGGGTCCAACTTGTCCAG
H7994	*ACTB* PCR, forward	AGCCATGTACGTAGCCATCC
H7995	*ACTB* PCR, reverse	CTCTCAGCTGTGGTGGTGAA
H8962	*TRB3* real time PCR, forward	TTTGGAACGAGAGCAAGGCA
H8963	*TRB3* real time PCR, reverse	CCACATGCTGGTGGGTAGG

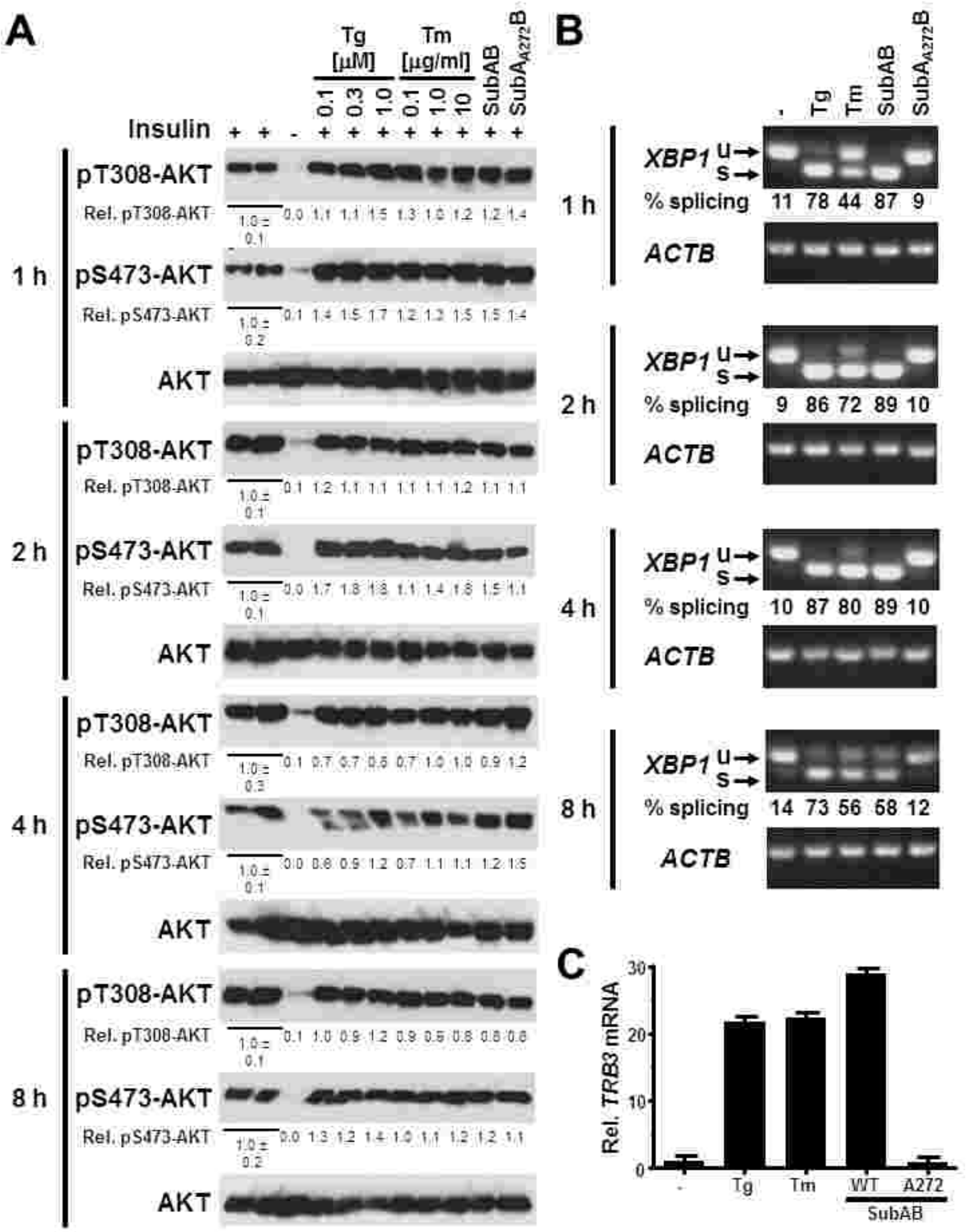

Fig. 1. Acute ER stress does not inhibit insulin-stimulated AKT T308 or S473 phosphorylation in C_2C_{12} myotubes. (A) C_2C_{12} myotubes were serum-starved for 18 h and treated with the indicated concentrations of thapsigargin (Tg), tunicamycin (Tm), or 1 µg/ml SubAB or catalytically inactive $SubA_{A272}B$ during the last 1-8 h of serum starvation and then stimulated with 100 nM insulin for 15 min where indicated. Cell lysates were analyzed by Western blotting. **(B)** Detection of *XBP1* splicing by reverse transcriptase PCR. PCR products were separated on a 2% (w/v) agarose gel and visualized with ethidium bromide. PCR products derived from unspliced (u) and spliced (s) *XBP1* mRNA are indicated by arrows. β-Actin (*ACTB*) was used as a loading control. Abbreviations: Tg - 300 nM thapsigargin, Tm - 1 µg/ml tunicamycin. **(C)** Induction of *TRB3* in C_2C_{12} cells by ER stress. C_2C_{12} cells were treated with 300 nM thapsigargin, 1 µg/ml tunicamycin, or 1 µg/ml SubAB or $SubA_{A272}B$ for 4 h. *TRB3* mRNA levels were determined by RT-qPCR and standardized to the loading control *ACTB*.

Figure 1, Brown *et al.*

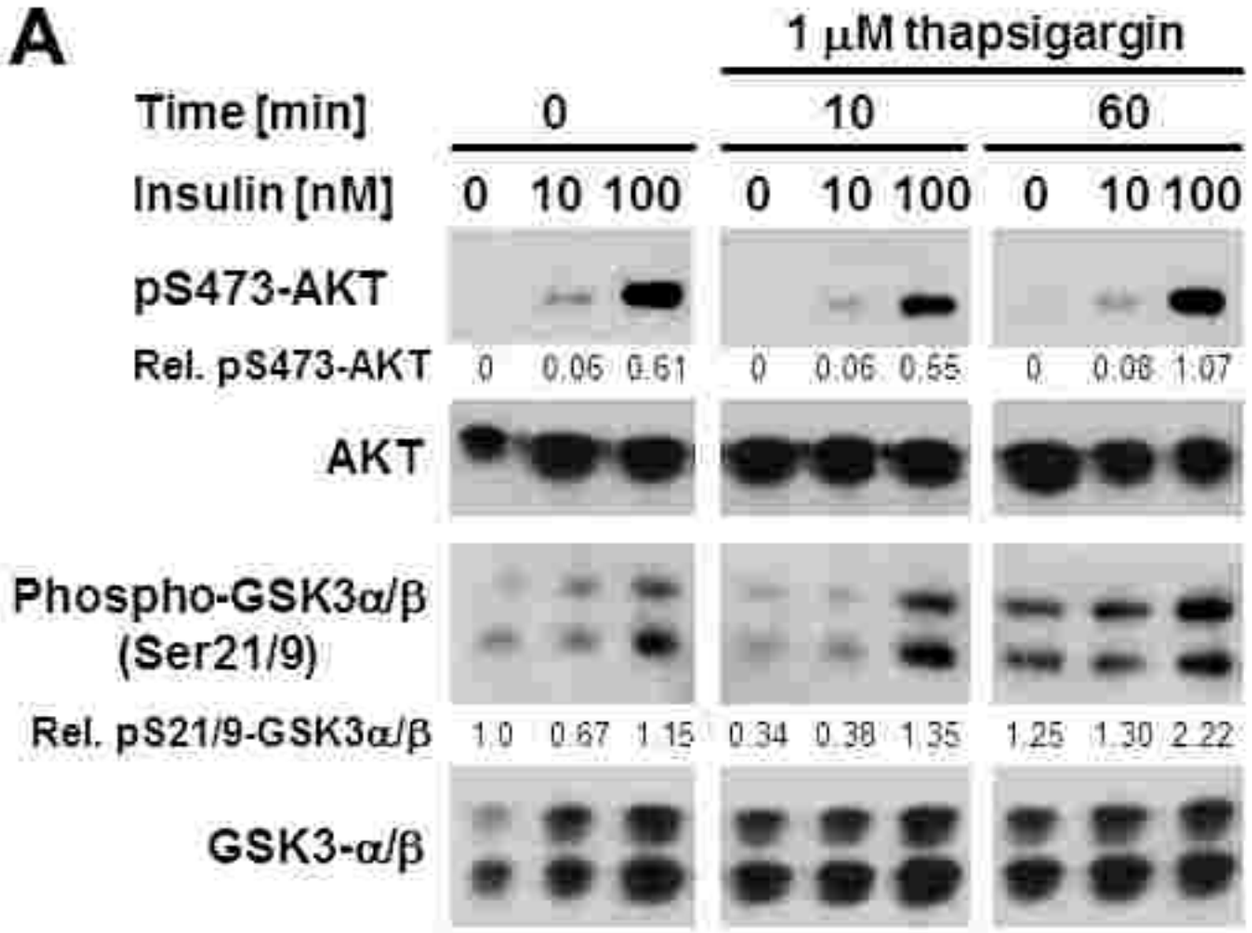

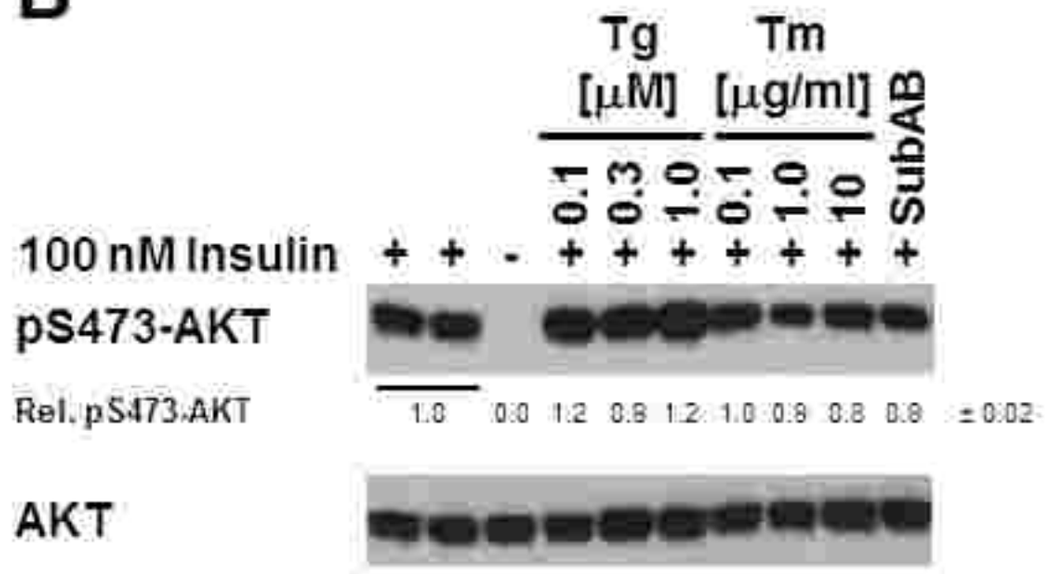

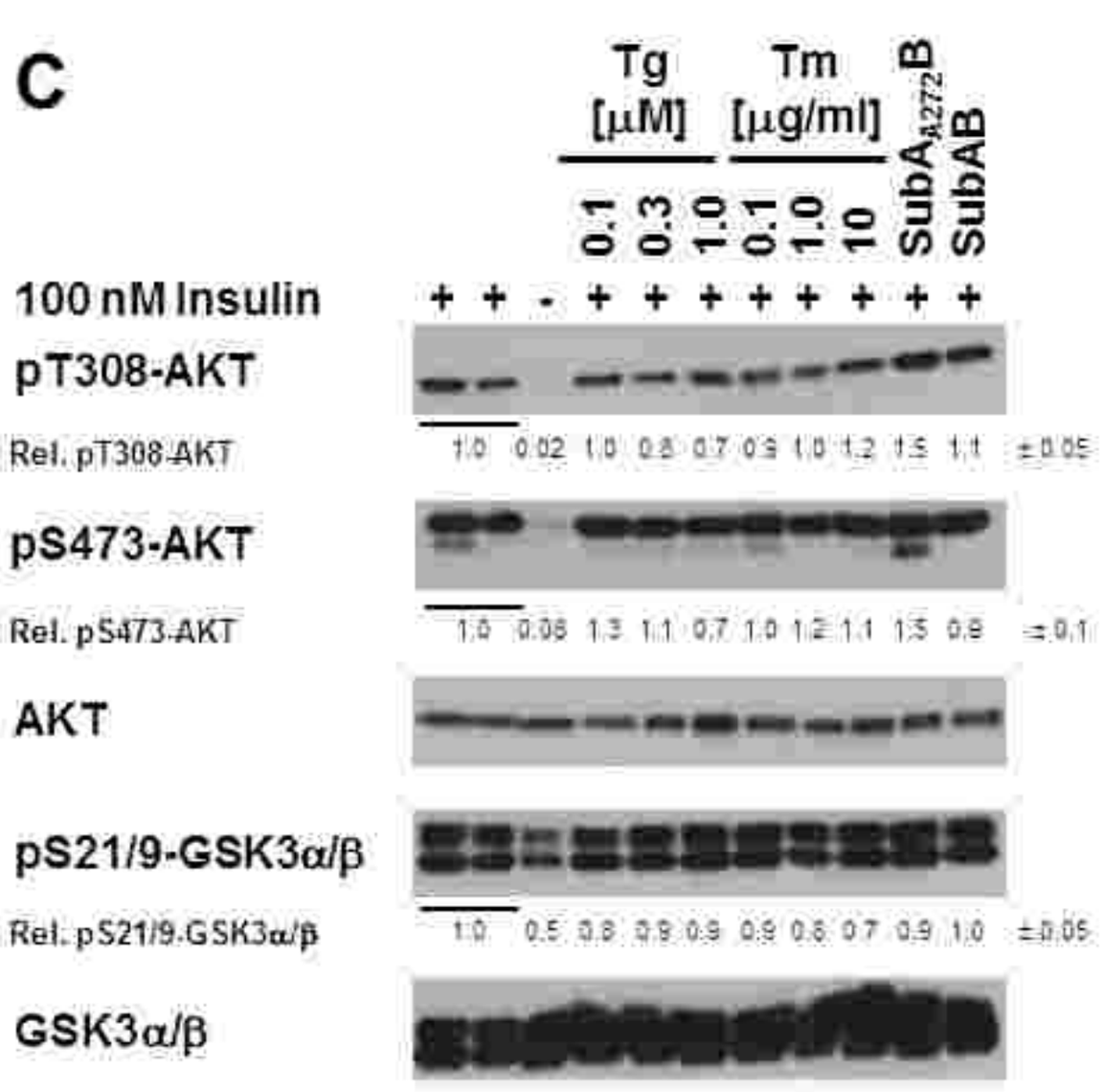

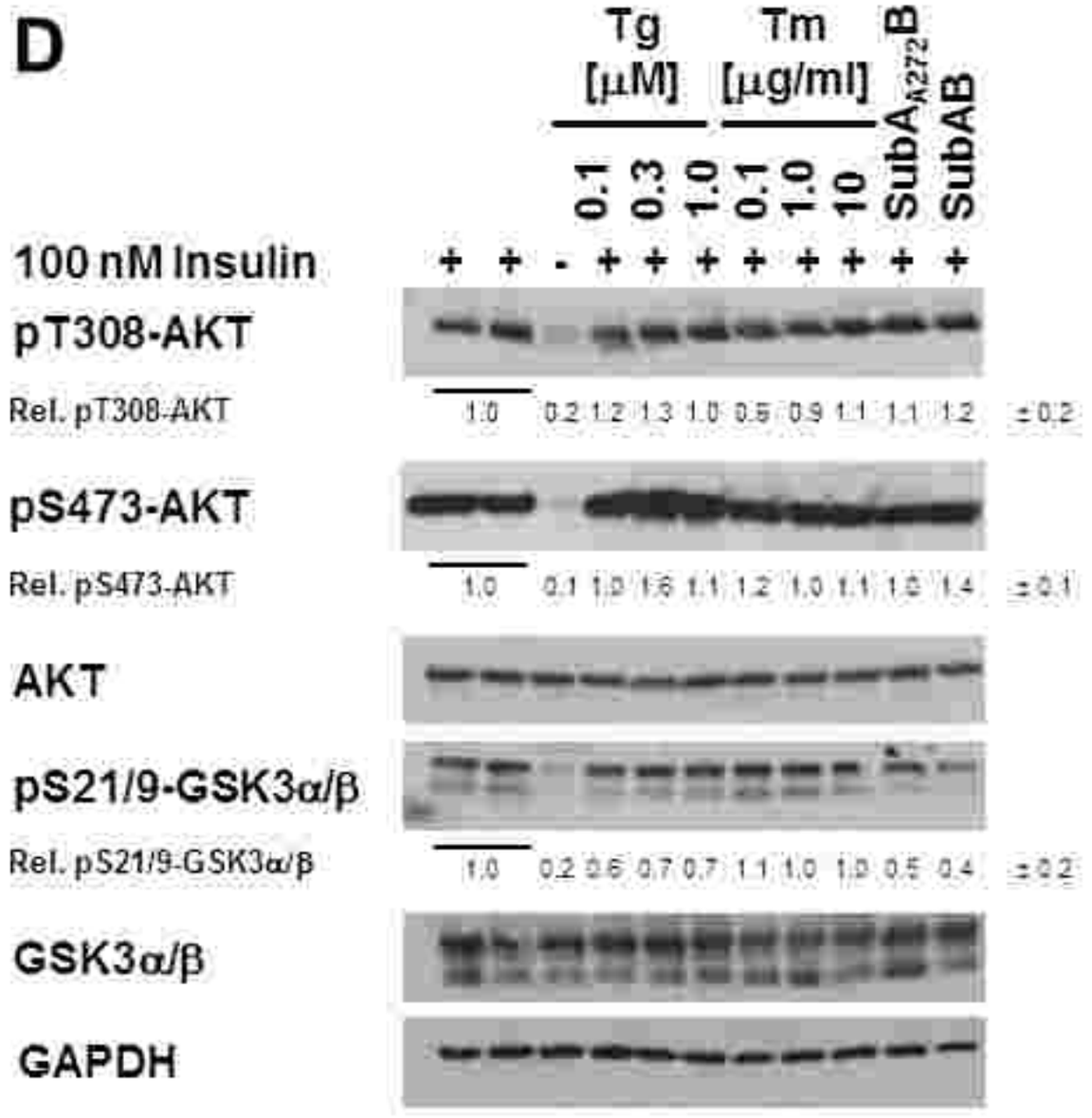

Fig. 2. Acute ER stress does not inhibit insulin-dependent AKT activation. **(A)** Western blots of serum-starved MEFs exposed to 1 μM thapsigargin for the indicated times before stimulation with 10 or 100 nM insulin for 15 min are shown. **(B)** Serum-starved Hep G2 cells treated with the indicated concentrations of thapsigargin, tunicamycin or 1 μg/ml SubAB for 30 min before stimulation with 100 nM insulin for 15 min. **(C)** Serum-starved C_2C_{12} myotubes and **(D)** serum-starved 3T3-F442A adipocytes were treated for 30 min with the indicated concentrations of thapsigargin, tunicamycin or 1 μg/ml SubAB before stimulation with 100 nM insulin for 15 min. Cells were treated with 1 μg/ml catalytically inactive $SubA_{A272}B$ where indicated. Cell lysates were analyzed by Western blotting.

Figure 2, Brown *et al.*

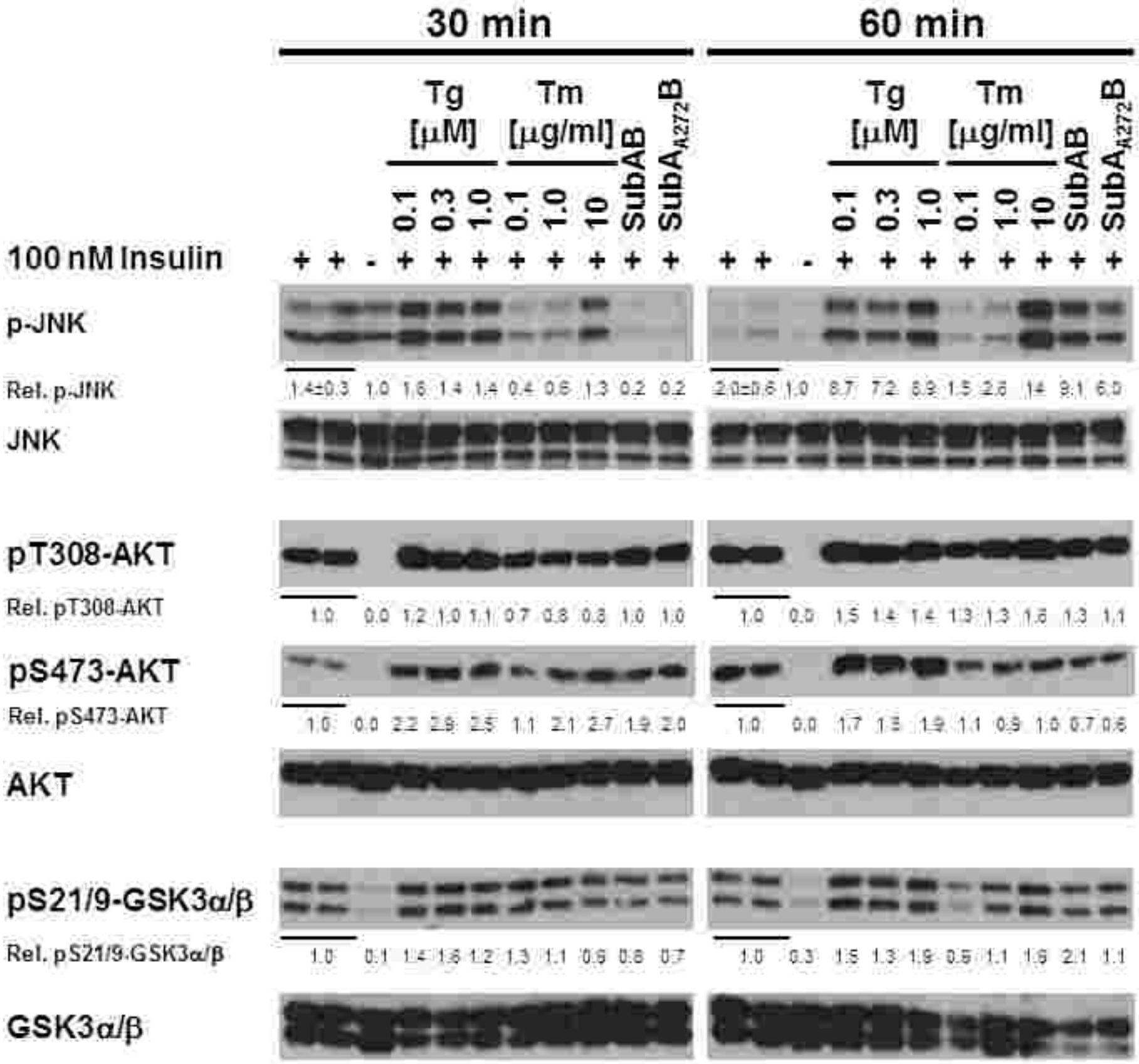

Fig. 3. Acute ER stress activates JNK, but does not inhibit insulin-dependent AKT activation in Fao rat hepatoma cells. Serum-starved Fao rat hepatoma cells were treated with the indicated concentrations of thapsigargin, tunicamycin or 1 μg/ml SubAB for 30 or 60 min before stimulation with 100 nM insulin for 15 min. Cell lysates were analyzed by Western blotting.

Figure 3, Brown *et al.*

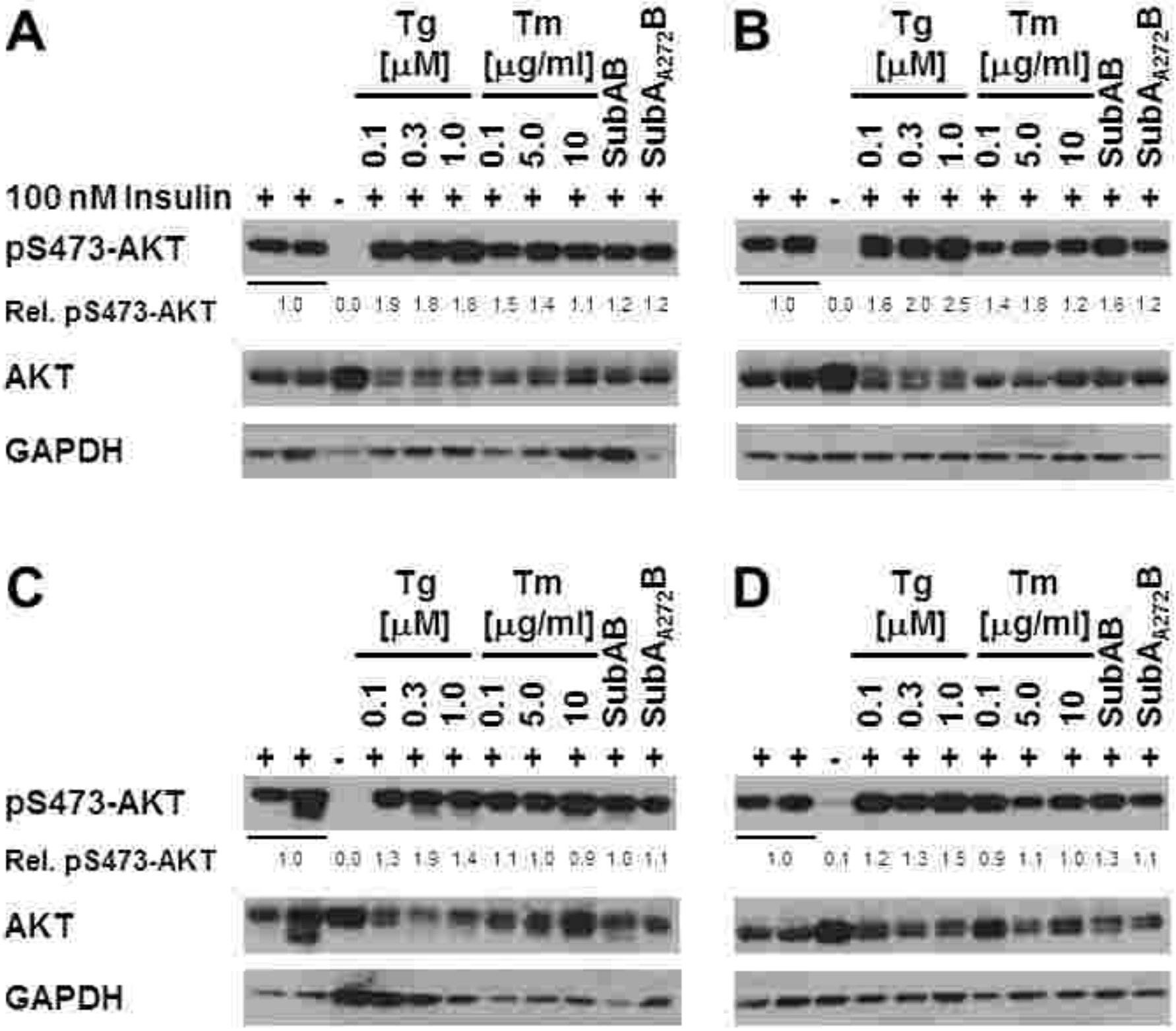

Fig. 4. ER stress does not inhibit insulin signalling in Fao rat hepatoma cells. Fao rat hepatoma cells were serum starved for 18 h and treated with 0.1 to 1 μM thapsigargin, 0.1 to 10 μg/ml tunicamycin, 1 μg/ml SubAB or $SubA_{A272}B$ for **(A)** 2, **(B)** and **(C)** 3 h, and **(D)** 4 h. Cells were cultured in RPMI 1640 in panels (A), (B), and (D) and in Coon's modification of Ham's F12 medium in panel (C).

Figure 4, Brown *et al.*

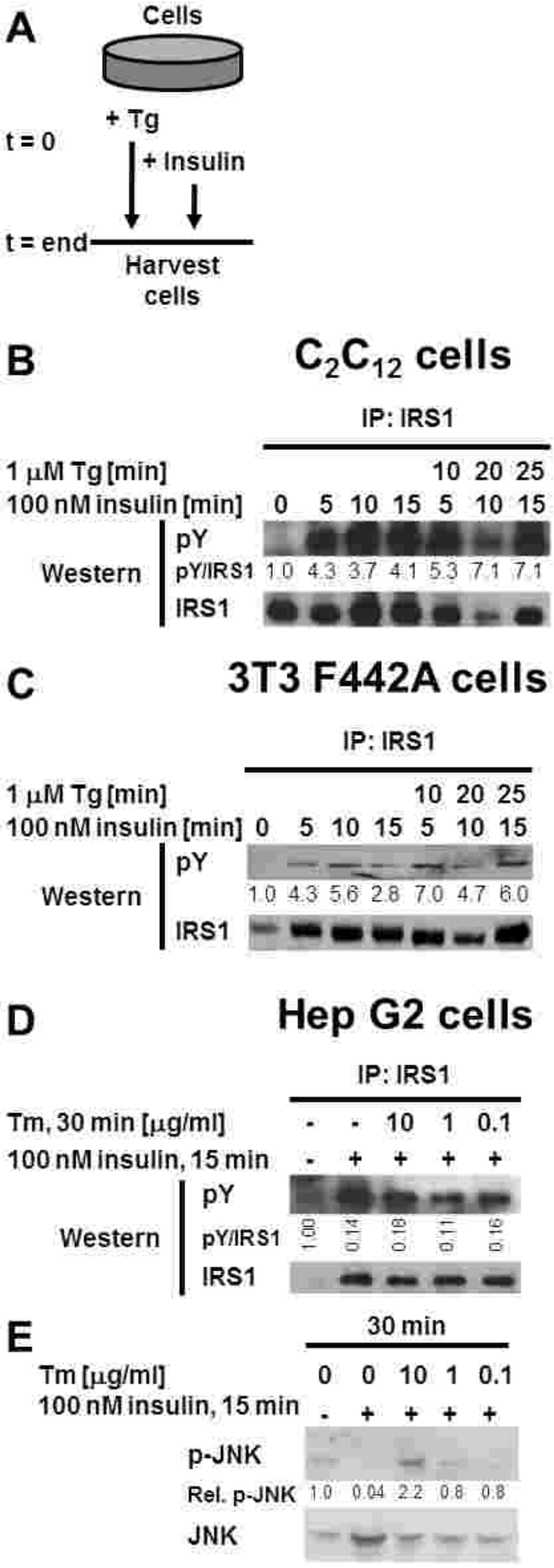

Fig. 5. Acute ER stress does not affect tyrosine phosphorylation of IRS1. (A) Experimental set-up. At the start of the experiment (t = 0) ~50% confluent, serum-starved cells were treated with 1 μM thapsigargin. Cell lysates were prepared in one series of dishes 5, 10, and 15 min after addition of 100 nM insulin. In a second series of dishes cells were treated for 10, 20, or 25 min with 1 μM thapsigargin. 100 nM insulin were added for the last 5, 10, or 15 min of thapsigargin treatment. (B) and (C) Analysis of the time course described in panel (A) by immunoprecipitation of IRS1 and Western blotting with an anti-phosphotyrosine or anti-IRS1 antibody in (B) C_2C_{12} cells and (C) 3T3 F442A cells. (D and E) Serum-starved Hep G2 cells were treated with the indicated concentrations of tunicamycin for 30 min and stimulated with 100 nM insulin during the last 15 min of tunicamycin treatment. Cell lysates were analyzed by immunoprecipitation of IRS1 and Western blotting with anti-phosphotyrosine and anti-IRS1 antibodies in panel (D) and by Western blotting for phospho-JNK and total JNK in panel (E).

Figure 5, Brown *et al.*

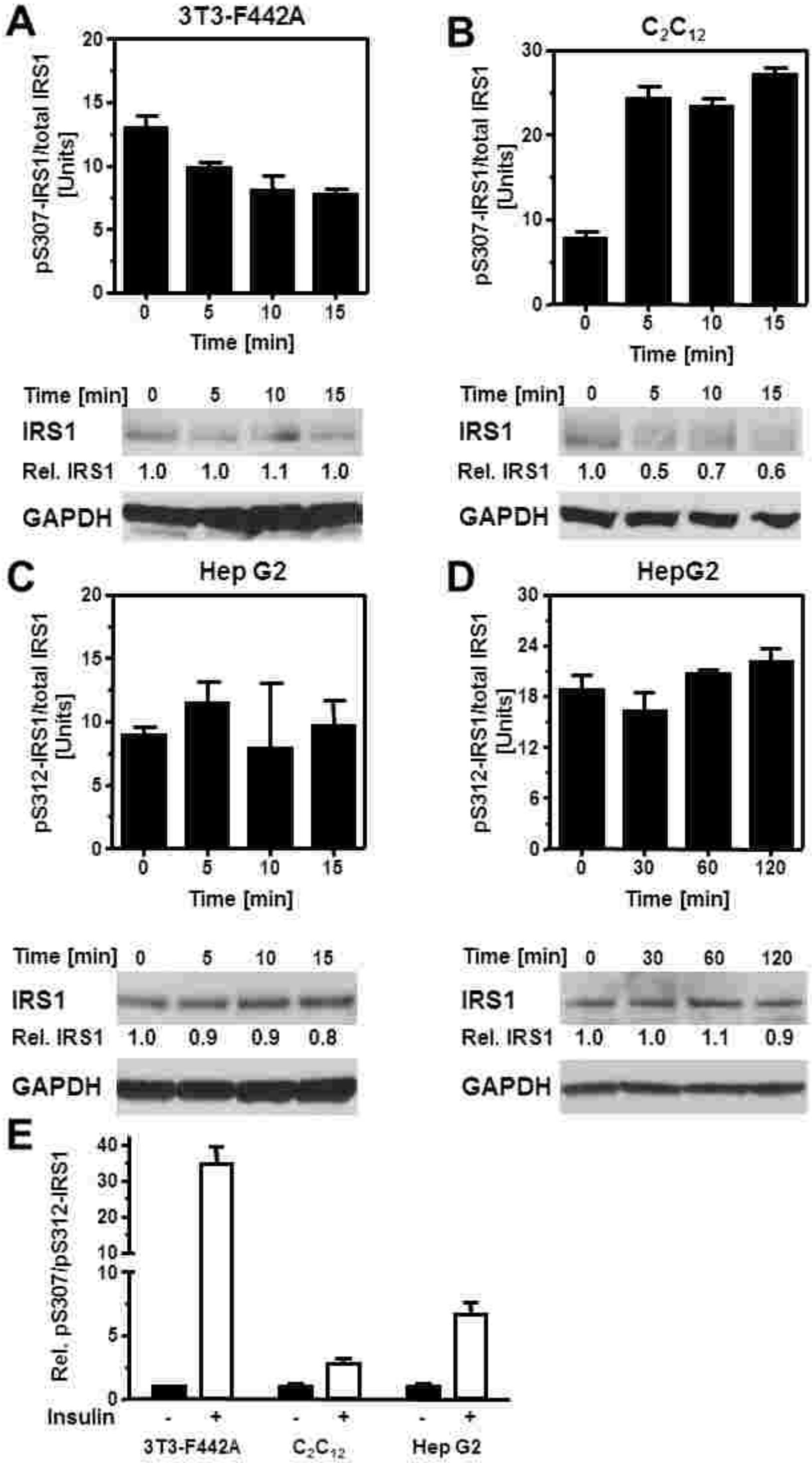

Fig. 6. S307/S312 phosphorylation of IRS1 during acute ER stress. (A) 3T3-F442A, **(B)** C_2C_{12}, and **(C-D)** Hep G2 cells were treated with 1 μM thapsigargin for the indicated times. Cell lysates were analyzed by ELISA for phosphorylation of S307 in murine IRS1 and S312 in human IRS1 by using the STAR phospho-IRS1 (Ser307 mouse/Ser312 human) ELISA from Millipore. S307 phosphorylation is expressed in units relative to a phospho-S307 IRS1 standard provided in the ELISA kit. phospho-S307 IRS1 units were standardized to the amount of total IRS1 in cell lysates determined by Western blotting. Equal loading of all lanes in the Western blot was controlled with the GAPDH loading control. **(E)** IRS1 S307/S312 phosphorylation in serum-starved 3T3-F442A, C_2C_{12}, and Hep G2 cells treated with 100 nM insulin for 15 min was determined by ELISA. IRS1 phospho-S307/S312 signals in the ELISA were standardised to total protein levels.

Figure 6, Brown *et al.*

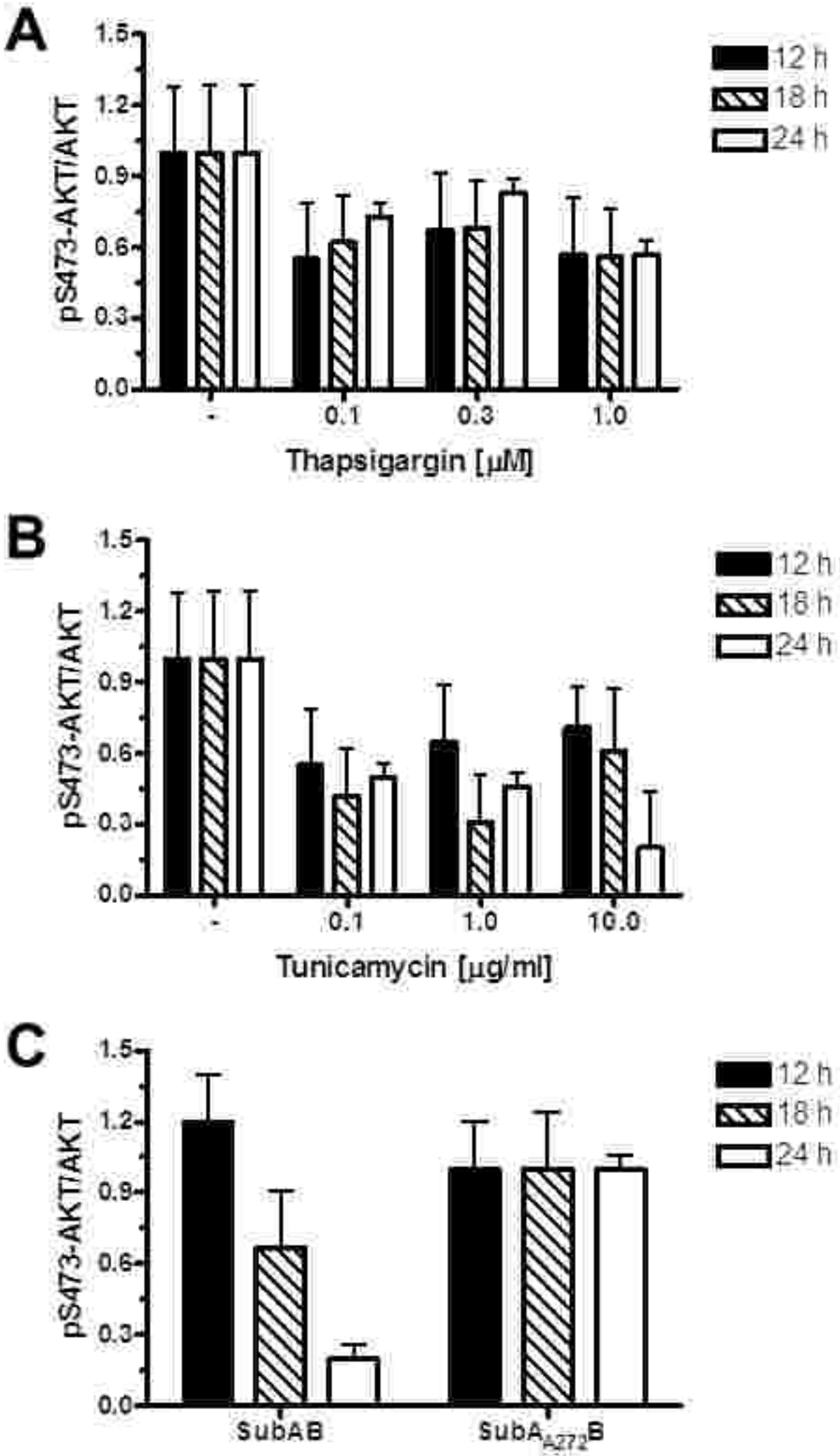

Fig. 7. Insulin resistance develops over time in ER-stressed C_2C_{12} myoblasts. Serum-starved C_2C_{12} cells were treated with the indicated concentrations of (A) thapsigargin, (B) tunicamycin, or (C) 1 μg/ml SubAB or $SubA_{A272}B$ for 1-24 h before stimulation with 100 nM insulin for 15 min. Western blots for pS473-AKT and total AKT were analyzed as described in Materials and Methods.

Figure 7, Brown *et al.*

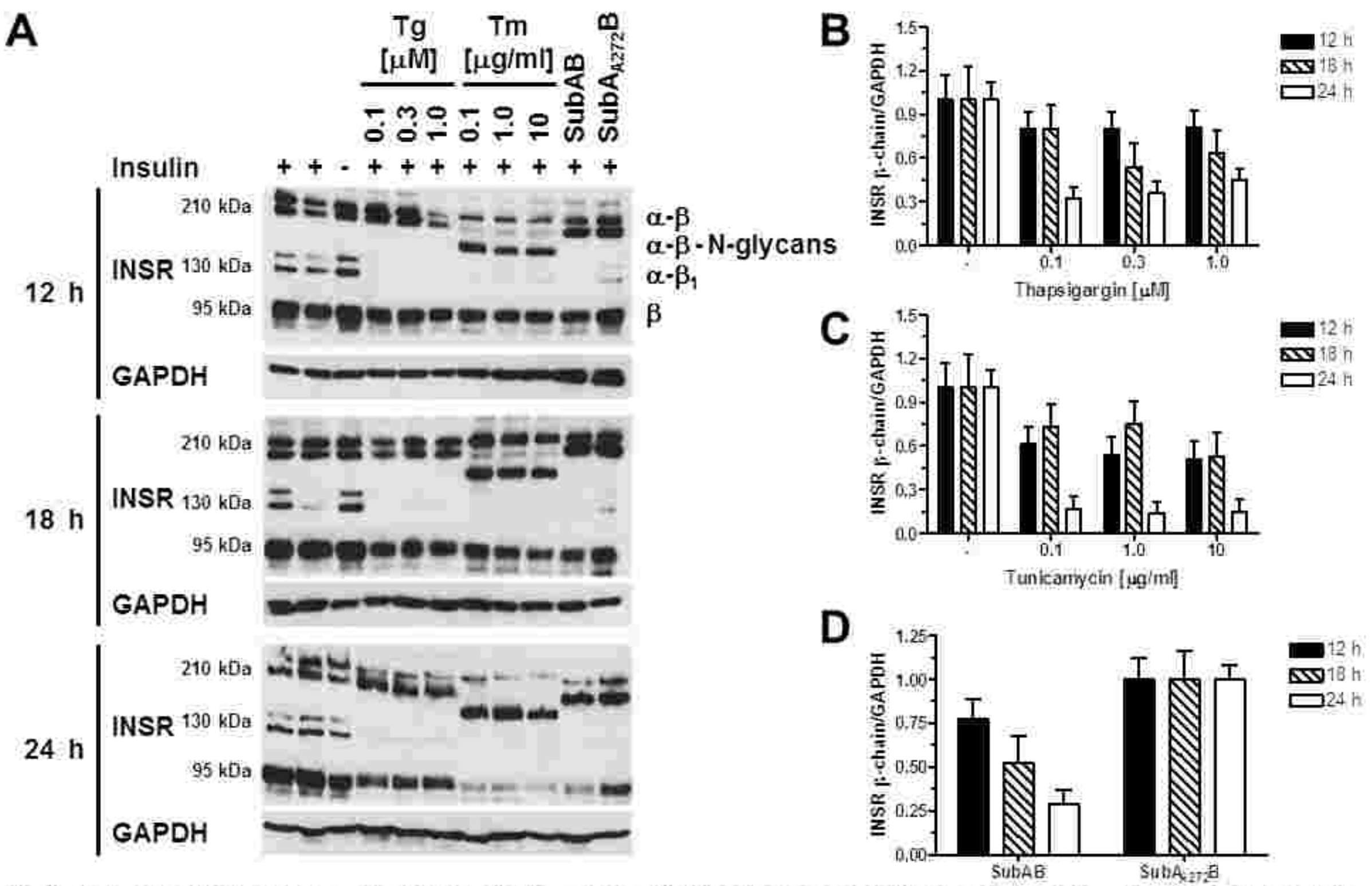

Fig. 8. Depletion of insulin receptors in ER-stressed cells coincides with development of insulin resistance in C_2C_{12} cells. (**A**) C_2C_{12} cells were treated with the indicated ER stressors for 12-24 h before serum starvation and stimulation with 100 nM insulin for 15 min. Protein extracts were analyzed by Western blotting. Quantitation of INSR β-chains in (**B**) thapsigargin-, (**C**) tunicamycin-, and (**D**) SubAB-treated C_2C_{12} cells. Bars represent standard errors.

Figure 8, Brown *et al.*

APPENDIX D

The following is the manuscript from which data were used in Chapter 5

Endoplasmic reticulum stress causes insulin resistance by inhibiting delivery of newly synthesized insulin receptors to the cell surface

Max Brown[1-3], Adina D. Mihai[1-3], Adrienne W. Paton[4], James C. Paton[4], and Martin Schröder[1-3]

1) Durham University, School of Biological and Biomedical Sciences, Durham DH1 3LE, United Kingdom.

2) Biophysical Sciences Institute, Durham University, Durham DH1 3LE, United Kingdom.

3) North East England Stem Cell Institute (NESCI), Life Bioscience Centre, International Centre for Life, Central Parkway, Newcastle Upon Tyne, NE1 4EP, UK.

4) Research Centre for Infectious Diseases, School of Molecular and Biomedical Science, University of Adelaide, Adelaide, SA 5005, Australia.

Address for correspondence: Martin Schröder, Durham University, School of Biological and Biomedical Sciences, Durham DH1 3LE, United Kingdom.

phone: +44 (0) 191-334-1316

FAX: +44 (0) 191-334-9104

email: martin.schroeder@durham.ac.uk

Running Title: ER stress depletes insulin receptors

Keywords: endoplasmic reticulum stress, insulin receptor, signal transduction, unfolded protein response, insulin resistance

Abstract

Endoplasmic reticulum (ER) stress is associated with obesity and insulin resistance. Here we show that ER stress causes insulin resistance by interfering with delivery of newly synthesized insulin receptors to the plasma membrane. Insulin resistance in ER-stressed adipocytes, myotubes, and hepatoma cells develops only after several half-lives of the insulin receptor at the plasma membrane, and coincides with depletion of mature insulin receptors and accumulation of unprocessed proreceptors. Endoglycosidase H digests revealed that unprocessed proreceptors solely carry high mannose N-glycans characteristic or ER-localized proteins. GFP-tagged insulin receptors accumulate in intracellular compartments and deplete at the plasma membrane in ER-stressed cells. siRNA knock-down of insulin receptor expression by ~50% suffices to inhibit insulin signaling by approximately the same degree. Bypass of the secretory pathway by a cytosolic fusion of the tyrosine kinase domain to the drug-inducible F_V2E-dimerisation domain eliminated the effects of ER stress on AKT activation by these insulin receptors. We conclude that ER stress inhibits insulin signaling by interfering with delivery of newly synthesized insulin receptors to the plasma membrane. ER stress also depletes the β chain of the mature insulin-like growth factor I receptor, showing that ER stress affects the abundance of several plasma membrane proteins.

Introduction

Perturbation of protein folding homeostasis in the endoplasmic reticulum (ER) activates the unfolded protein response (UPR). Several ER transmembrane proteins initiate the UPR, including the serine/threonine protein kinase-endoribonuclease (RNase) IRE1α, the serine/threonine protein kinase PERK, and several type II transmembrane basic leucine zipper (bZIP) transcription factors including ATF6α,

ATF6β, BBF2H7, CREB-H, and OASIS [reviewed in (1)]. The RNase domain of IRE1α initiates removal of a 26 nt intron from *XBP1* mRNA resulting in a translational frame-shift and production of a more potent bZIP transcription factor by spliced *XBP1* mRNA. The IRE1α RNase domain also cleaves many mRNAs encoding secretory proteins in a process called regulated-IRE1 dependent decay (RIDD) to ameliorate the unfolded protein burden of the stressed ER (2, 3). Phosphorylation of the α subunit of the trimeric eukaryotic translation initiation factor 2 (eIF2α) attenuates general translation in ER-stressed cells, but also promotes translation of mRNA harboring several short upstream open reading frames (uORFs) in their 5' untranslated regions (5'-UTRs). An example for an mRNA whose translation is increased in ER-stressed cells is the mRNA for the bZIP transcription factor ATF4 (4). ATF6 translocates to the Golgi membrane where its cytosolic bZIP transcription factor domain is proteolytically released from the Golgi membrane by S1P and S2P proteases. These signaling events culminate in transcriptional induction of genes encoding ER resident molecular chaperones and protein foldases, phospholipid biosynthesis, and ER-associated protein degradation (ERAD).

The UPR also activates inflammatory and apoptotic signaling in response to non-resolvable or chronic ER stress (5). Several of these signaling events have been implicated in inhibiting insulin signaling. Insulin signaling is initiated by binding of insulin to the insulin receptor, activation of its tyrosine protein kinase domain, tyrosine autophosphorylation, and tyrosine phosphorylation of insulin receptor substrate (IRS) proteins [reviewed in (6)]. Tyrosine-phosphorylated IRS proteins recruit phosphatidylinositol (PI) 3-kinase (PI3K) to the plasma membrane, followed by formation of PI-3,4-bis- and PI-3,4,5-trisphosphate and recruitment of phosphoinositide-dependent kinases (PDKs) and AKT isoforms to the plasma

membrane. Colocalization of PDKs and AKT to the plasma membrane facilitates phosphorylation of AKT on T308, and on S473 by mTORC2 (7-9), PAK1 (10), and ILK (11) leading to activation of AKT. Activated AKT facilitates glucose transport, protein and glycogen synthesis, and inhibits gluconeogenesis. Activation of mTOR and $p70^{S6K}$ kinase by AKT stimulates protein synthesis, while activation of RAS, RAF, and the mitogen-activated protein kinases ERK1 and ERK2 through GRB2 and IRS proteins mediates the mitogenic effects of insulin.

IRE1α and PERK signaling have been linked to insulin resistance in obesity. ER stress is present in adipose tissue, the hypothalamus, and the liver of obese mice and humans (12-15). Interaction of IRE1α with the E3 ubiquitin ligase TRAF2 activates the mitogen-activated protein (MAP) kinase JNK (16). Activation of JNK by several stimuli, most notably in response to inflammation, causes insulin resistance through phosphorylation of insulin receptor substrate (IRS)-1 on serine 307 which inhibits IRS1 tyrosine phosphorylation by the insulin receptor (17, 18). It was also reported that IRE1α-dependent activation of JNK in ER-stressed cells causes insulin resistance via IRS1 serine 307 phosphorylation (12). However, other work has shown that insulin resistance develops at least partially independent of JNK in ER-stressed cells (19-21). Furthermore, fructose feeding of liver-specific *xbp1*$^{-/-}$ mice caused ER stress and activated JNK, but did not cause insulin resistance (22), arguing that ER stress-dependent JNK activation can be dissociated from insulin resistance. Likewise, *klf15*$^{-/-}$ hepatocytes show increased JNK activation and ER stress, but also improved insulin sensitivity (23). Consistent with these reports, we have observed that short-term, pharmacologically-induced ER stress leads to transient activation of JNK without inhibiting the activity of the insulin signaling pathway (Brown et al., submitted for publication). Thus, the role of JNK in ER-stressed insulin resistance remains unclear.

A transcriptional cascade downstream of PERK induces expression of the pseudokinase TRB3 via activation of the transcription factors ATF4 and CHOP (24). Overexpression of TRB3 inhibits insulin signaling (25-29). TRB3 interacts with AKT (25-28) and IRS1 (29). A Q84R polymorphism in TRB3, which is associated with insulin resistance and type 2 diabetes (30, 31), potentiates its interaction with AKT (28, 30). On a high fat diet *trb3*$^{-/-}$ mice displayed improved glucose tolerance, and improved insulin signaling (29). These results were explained in the context of induction of TRB3 in response to ER stress developing on a high fat diet and inhibition of IRS1 and AKT phosphorylation by TRB3 (29). Hence, TRB3 may be another molecular link between ER stress and insulin resistance.

Another mechanism through which ER stress may cause insulin resistance is by interfering with expression and delivery of insulin receptor molecules to the plasma membrane. The monomers of the dimeric insulin receptor consist of an extracellular α and a β chain harboring a transmembrane and intracellular tyrosine protein kinase domain. Both chains are linked via a disulfide bond between C647 and C872 in the α and β chains (32, 33) (Fig. 1). The α chain carries 14 and the β chain 4 *N*-linked oligosaccharides. The insulin receptor is synthesized as a single polypeptide chain, which, after maturation of the insulin binding domain, dimerization, *N*-linked glycosylation and disulfide formation in the ER, is cleaved by proprotein convertases, including furin, in the *trans*-Golgi network carboxyterminal to the basic sequence RKRR to liberate the mature α and β chains (34, 35). The mature receptor is delivered to the plasma membrane, where it has a half-life of 7-13 h (36-42). Short-term ER stress failed to cause insulin resistance, while prolongation of ER stress over several half-lives of the insulin receptor at the plasma membrane was associated with insulin resistance (Brown et al., submitted for publication). Here we report that insulin

resistance in ER-stressed cells is caused by inhibition of transport of newly synthesized insulin receptors to the plasma membrane. Bypass of the ER in synthesis of functional, cytosolic insulin receptors prevents insulin resistance in ER-stressed cells. Consistent with a trafficking block in the secretory pathway as the underlying cause for insulin resistance in ER-stressed cells we find that ER stress-induced insulin resistance is independent of JNK and that induction of TRB3 by ER stress does not inhibit insulin signaling.

Materials and Methods

Antibodies and reagents. Antibodies against phospho-JNK (cat. no. 4668), JNK (cat. no. 9258), phospho-S473-AKT (cat. no. 4060), phospho-T308-AKT (cat. no. 4056), and AKT (cat. no. 4691) were purchased from Cell Signaling Technology (Danvers, MA, USA). The anti-GAPDH antibody (cat. no. G8795) was purchased from Sigma-Aldrich (Gillingham, UK). The anti-insulin receptor β chain antibody (cat. no. sc-711), anti-insulin-like growth factor (IGF)-I receptor antibody (cat. no. 3018), and normal rabbit IgG (cat. no. sc-2027) were purchased from Santa Cruz Biotechnology (Santa Cruz, CA, USA). Tunicamycin was purchased from Merck Chemicals (Beeston, UK), and bovine insulin (cat. no. I0516), bovine serum albumin (BSA, cat. no. A2153), dexamethasone, 3-isobutyl-1-methylxanthine (IBMX), and thapsigargin from Sigma-Aldrich (Gillingham, UK). Endoglycosidase H (EndoH) and peptide-N-glycosidase (PNGase) F were obtained from New England Biolabs (Hitchin, UK).

Plasmids. Plasmids were maintained in *Escherichia coli* XL10-Gold cells (Agilent Technologies, Stockport, UK, cat. no. 200314). Standard protocols for plasmid constructions were used (43). Plasmid pmaxGFP was obtained from Lonza Cologne AG (Cologne, Germany). Plasmid pEGFP-N2-hINSR encodes a fusion of the human insulin receptor to eGFP (44) and was obtained from Addgene (Cambridge, MA,

146 USA, Addgene ID 22286). Plasmid pcDNA5/FRT/TO-F_V2E-INSRβ was generated
147 by cloning the 1,430 bp *Bsi*WI-*Xma*I fragment of pCLFv2IRE (45) into *Bsi*WI- and
148 *Xma*I-digested pcDNA5/FRT/TO-F_V2E-C'hIRE1α (Cox and Schröder, unpubl.).
149 Plasmid pcDNA5/FRT/TO-MyrF_V2E-INSRβ was generated by cloning the 501 bp
150 *Eco*RI-*Xma*I fragment of pC_4M-F_V2E (Arial Pharmaceuticals, Cambridge, MA, USA)
151 into *Hin*dIII- and *Xma*I-digested pcDNA5/FRT/TO-F_V2E-INSRβ after blunting the
152 *Eco*RI and *Hin*dIII sites with Klenow enzyme.

153 **Cell culture.** WT and *jnk1*$^{-/-}$ *jnk2*$^{-/-}$ (46) mouse embryonic fibroblasts were obtained
154 from R. Davis (University of Massachusetts, Worchester, MA, USA). 3T3-F442A
155 preadipocytes (47), C_2C_{12} myoblasts (48), HEK 293 cells (49-51), and Hep G2 cells
156 (52) were obtained from C. Hutchison (Durham University), R. Bashir (Durham
157 University), M. Cann (Durham University), and A. Benham (Durham University).
158 The Flp-In T-Rex 293 cell line was obtained from Life Technologies (Paisley, UK).

159 All cell lines were grown in an atmosphere of 95% (v/v) air, 5% (v/v) CO_2, and
160 95% humidity and were cultured in Dulbecco's minimal essential medium (DMEM)
161 containing 4.5 g/l D-glucose (53, 54), 10% (v/v) FBS and 2 mM L-glutamine. The
162 medium for the Flp-In T-Rex 293 cells was supplemented with 100 μg/ml zeocin and
163 15 μg/ml blasticidin and the medium for Flp-In T-Rex 293 cells stably expressing the
164 F_V2E-insulin receptor chimeras with 100 μg/ml hygromycin B and 15 μg/ml
165 blasticidin. To differentiate C_2C_{12} cells 60-70% confluent cultures were shifted into
166 low mitogen medium consisting of DMEM containing 4.5 g/l D-glucose, 2% (v/v)
167 horse serum, and 2 mM L-glutamine and incubated for another 7-8 d with replacing
168 the low mitogen medium every 2-3 d (55). Differentiation of C_2C_{12} cells was assessed
169 by microscopic inspection of cultures, staining of myotubes with phalloidin (56), and
170 reverse transcriptase (RT)-PCR for transcription of the genes encoding *S*-adenosyl-

homocysteine hydrolase (*AHCY*), myosin light chain 1 (*MYL1*), and troponin C (*TNC1*). To differentiate 3T3-F442A fibroblasts into adipocytes cells were grown to confluency. 2 d postconfluency the medium was changed to DMEM containing 4.5 g/l D-glucose, 10% (v/v) FBS, 2 mM L-glutamine, 1 µg/ml insulin, 0.5 mM IBMX, 0.25 µM dexamethasone. After 3 d the medium was changed to DMEM containing 4.5 g/l D-glucose, 10% (v/v) FBS, 2 mM L-glutamine, 1 µg/ml insulin for 2 more days and then DMEM containing 4.5 g/l D-glucose, 10% (v/v) FBS, 2 mM L-glutamine until day 12 of differentiation (57). Differentiation was assessed by Oil Red O staining (58) and flow cytometric analysis of $>1 \cdot 10^4$ cells by Nile Red staining as described before (59, 60).

ER stress was induced with 0.1 to 1 µM thapsigargin, 0.1 to 10 µg/ml tunicamycin, or 1 µg/ml subtilase cytotoxin AB (SubAB) or catalytically inactive $SubA_{A272}B$. SubAB and $SubA_{A272}B$ were purified as described before (61, 62). To stimulate cells with insulin cells were starved for serum for 18 h, followed by addition of fresh serum-free culture medium containing 100 nM insulin. Serum starvation for 18 h does not affect activation of the UPR (Brown et al., submitted for publication). After 15 min exposure to insulin cells were harvested and lysed for extraction of RNA and protein as described below. Expression of the F_V2E-insulin receptor chimera was induced for 24 h with 1 µg/ml tetracycline, where indicated. The chimera was dimerized by treating cells with 100 nM AP20187 for the times indicated in the text.

Plasmids were transfected with jetPRIME (Polyplus Transfection, Illkirch, France) and siRNAs with INTERFERin (Polyplus Transfection) following the manufacturer's instructions. siRNAs are listed in Table I. The stably transfected Flp-In T-Rex 293 cell lines expressing a fusion of the F_V2E drug-inducible dimerization domain (43) to the β chain of the human insulin receptor with and without an *N*-

196 terminal myristoylation signal were generated by transfection of the Flp-In T-Rex 293
197 cell line with pOG44 and pcDNA5/FRT/TO-MyrF_V2E-INSRβ. Selection of stably
198 transfected clones was initiated 24 h after transfection by using 50 µg/ml hygromycin
199 B. After two days the hygromycin B concentration was increased to 100 µg/ml.
200 **RNA extraction and RT-PCRs.** RNA was extracted with the EZ-RNA total RNA
201 isolation kit (Geneflow, Fradley, UK, cat. no. K1-0120) and reverse transcribed with
202 oligo-dT primers (Promega, Southampton, UK, cat. no. C1101) and Superscript III
203 reverse transcriptase (Life Technologies, cat. no. 18080044) as described previously
204 (63). Quantitative PCRs (qPCRs) were run on a Rotorgene 3000 (Qiagen, Crawley,
205 UK). Amplicons were amplified with 0.5 µl 5 U/µl GoTaq® Flexi DNA polymerase
206 (Promega, cat. no. M8305), 2 mM $MgCl_2$, 200 µM dNTPs, and 1 µM of each primer
207 and detected with a 1:2,500 fold dilution of a SybrGreen stock solution (Life
208 Technologies, cat. no. S7563). Primers for qPCRs are listed in Table II. After
209 denaturation for 2 min at 95°C samples underwent 40 cycles of denaturation at 95°C
210 for 30 s, primer annealing at 58°C for 30 s, and primer extension at 72°C for 30 s.
211 Amplification of a single PCR product was confirmed by recording the melt curves
212 after each PCR run. Amplification efficiencies for all qPCRs were ~0.75 ± 0.05.
213 Calculation of C_T values and normalization to *ACTB* was done using the comparative
214 quantitation function in the Rotorgene software. Results represent the average and
215 standard error of two biological repeats and three technical repeats within each
216 biological repeat.
217 **Cell lysis and Western blotting.** Cells were washed three times with ice-cold
218 phosphate-buffered saline (PBS, 4.3 mM Na_2HPO_4, 1.47 mM KH_2PO_4, 27 mM KCl,
219 137 mM NaCl, pH 7.4) and lysed in RIPA buffer (50 mM Tris-HCl, pH 8.0, 150 mM
220 NaCl, 0.5% (w/v) sodium deoxycholate, 0.1% (v/v) Triton X-100, 0.1% (w/v) SDS)

containing Roche complete protease inhibitors (Roche Applied Science, Burgess Hill, UK, cat. no. 11836153001) as described before (63). Proteins were separated by SDS-PAGE and transferred to polyvinylidene difluoride (PVDF) membranes (Amersham HyBond^{TM}-P, pore size 0.45 µm, GE Healthcare, cat. no. RPN303F) by semi-dry electrotransfer in 0.1 M Tris, 0.192 M glycine, and 5% (v/v) methanol at 2 mA/cm^2 for 60-75 min. Membranes were blocked for 1 h in 5% (w/v) skimmed milk powder in TBST [20 mM Tris-HCl, pH 7.6, 137 mM NaCl, and 0.1% (v/v) Tween-20] for antibodies against non-phosphorylated proteins and 5% (w/v) BSA in TBST for antibodies against phosphorylated proteins. The anti-AKT, anti-phospho-S473-AKT, anti-phospho-T308-AKT, anti-JNK, and anti-phospho-JNK antibodies were incubated with membranes at a 1:1,000 dilution in TBST + 5% (w/v) BSA over night at 4°C with gentle agitation. Blots were washed three times with TBST and then probed with goat anti-rabbit-IgG (H+L)-horseradish peroxidase (HRP)-conjugated secondary antibody (cat. no. 7074S, Cell Signaling Technology) at a 1:1,000 dilution in TBST + 5% (w/v) skimmed milk powder for 1 h at room temperature. The mouse anti-GAPDH antibody was used at a 1:30,000 dilution in TBST + 5% (w/v) skimmed milk powder over night at 4°C with gentle agitation and was developed with goat anti-mouse IgG (H+L)-horseradish peroxidase (HRP)-conjugated secondary antibody (Thermo Fisher Scientific, Loughborough, UK, cat. no. 31432) at a 1:20,000 dilution in TBST + 5% (w/v) skimmed milk powder for 1 h at room temperature. For signal detection Pierce ECL Western Blotting Substrate (cat. no. 32209) or Pierce ECL Plus Western Blotting Substrate (cat. no. 32132) from Thermo Fisher Scientific were used. Blots were exposed to CL-X Posure^{TM} film (Thermo Fisher Scientific, cat. no. 34091). Exposure times were adjusted on the basis of previous exposures to obtain exposures in the linear range of the film. Signals were quantified using ImageJ (64).

To reprobe blots for detection of nonphosphorylated proteins, membranes were stripped using Restore Western Blot Stripping Buffer (Thermo Fisher Scientific, cat. no. 21059,) and blocked with 5% (w/v) skimmed milk powder in TBST.

Endoglycosidase H (Endo H) and peptide:*N*-glycosidase F (PNGase F) digests. 8 µg of protein were denatured in 0.5% (w/v) SDS, 40 mM DTT at 100°C for 10 min. Samples were then incubated with 1000 U of Endo H in 50 mM sodium citrate, pH 5.5 (at 25°C) at 37°C for 2 h. For PNGase F digests denatured samples were incubated with 1000 U of PNGase F in 50 mM sodium phosphate pH 7.5 (at 25°C), 1% (v/v) NP-40 at 37°C for 2 h.

[^{35}S]-L-methionine/[^{35}S]-L-cysteine pulse labeling experiments. C_2C_{12} myotubes, 3T3-F442A adipocytes, and Hep G2 cells grown to 70-80% confluency were treated with 100 nM thapsigargin, 0.1 µg/ml tunicamycin for 24 h or left untreated for the same period of time. To measure total protein synthesis rates by incorporation of [^{35}S]-L-methionine/[^{35}S]-L-cysteine into newly synthesized protein cells were washed once with PBS prewarmed to 37°C, and incubated with L-cysteine/L-methionine starvation medium (DMEM lacking L-cysteine and L-methionine supplemented with 2 mM L-glutamine) for 20 min at 37°C. The starvation medium was aspirated and replaced with starvation medium containing 50 µCi/ml 70% [^{35}S]-L-methionine, 25% [^{35}S]-L-cysteine (1000 Ci/mmol, Hartmann Analytic, Braunschweig, Germany, cat. no. SCIS-103). After 15 min at 37°C cells were washed three times with ice-cold PBS and then lysed in RIPA buffer as described above. Equal amounts of protein were separated by SDS-PAGE. Gels were fixed and stained with Coomassie Brilliant Blue R250 with 20% (w/v) trichloroacetic acid (TCA) containing 0.1% (w/v) Coomassie Brilliant Blue R250, destained with 10% (v/v) acetic acid, 25% (v/v) methanol and prepared for fluorography by incubation in PBS containing 0.5 M sodium salicylate

and 2% (v/v) glycerol for 15 min. After drying gels were exposed to Kodak BioMax MR film and scanned on a Typhoon 9400 system (GE Healthcare, Little Chalfont, UK). [^{35}S]-L-methionine/[^{35}S]-L-cysteine incorporation of each lane quantitated by phosphorimaging was standardized to the Coomassie Brilliant Blue R250 staining of the lane determined with ImageJ. [^{35}S]-L-methionine/[^{35}S]-L-cysteine incorporation is expressed relative to untreated cells.

To measure [^{35}S]-L-methionine/[^{35}S]-L-cysteine incorporation rates by TCA precipitation equal amounts of protein were precipitated with ice-cold 10% (w/v) TCA on Whatman 3MM papers for 15 min, washed twice with ice-cold 5% (w/v) TCA and once with ethanol. The filter papers were dried and the precipitated radioactivity measured by scintillation counting in a Tri-Carb 1600 Liquid Scintillation Analyzer (Canberra Packard, Pangbourne, UK).

Immunoprecipitation of the insulin receptor. Cells were washed three times with ice-cold PBS and lysed in 250 µl RIPA buffer containing Roche complete protease inhibitors. 1 mg protein lysate was pre-cleared with 20 µl 25% (w/v) protein A agarose beads (Santa Cruz Biotechnology, cat. no. sc-2001) for 1 h at 4°C and then immunoprecipitated with 1 µg anti-insulin receptor β chain antibody at 4°C overnight. Immunoprecipitates were incubated with 20 µl 25% (w/v) protein A agarose beads for 1 h at 4°C and washed three times with ice-cold RIPA buffer containing protease inhibitors and 0.1% (v/v) Nonidet P40 and once with ice-cold RIPA buffer. Immunoprecipitated proteins were solubilized by boiling in 350 mM Tris·HCl, pH 6.8, 30% (v/v) glycerol, 10% (w/v) SDS, 0.5 g/l bromophenol blue, 2% (v/v) β-mercaptoethanol for 5 min and separated by SDS-PAGE. Gels were stained with 20% (w/v) trichloroacetic acid (TCA) containing 0.1% (w/v) Coomassie Brilliant Blue R250, destained with 10% (v/v) acetic acid, 25% (v/v) methanol and prepared for

fluorography by incubation in PBS containing 0.5 M sodium salicylate and 2% (v/v) glycerol for 15 min. After drying the gels were exposed to Kodak BioMax MR film at -80°C.

Fluorescence microscopy. Images of GFP-tagged insulin receptors expressed in HEK 293 cells were taken on a Zeiss ApoTome microscope (Carl Zeiss, Cambridge, UK) 18 h after induction of ER stress with 1 µg/ml tunicamycin or 1 µg/ml $SubAB_5$. The cell membrane was visualized by staining cells for 5 min at room temperature with 5 µg/ml CellMask Deep Red (Life Technologies). GFP fluorescence was observed using a band pass (BP) 450-490 filter (Carl Zeiss, FITC/GFP, filter set 9, cat. no. 488009-000) and a long pass (LP) 515 filter. CellMask Deep red fluorescence was observed using a BP546/12 filter (Carl Zeiss, Rhodamine, filter set 15, cat. no. 488015-0000) and a LP 590 filter. To quantify colocalization of the GFP-tagged insulin receptors and CellMask Deep Red signals, individual cells were defined as regions of interest (ROI) in Image J, and background-corrected for the intracellular fluorescence of CellMask Deep Red using the Background Subtraction from ROI plug-in. The Pearson correlation coefficient between the INSR-GFP and CellMask Deep Red Fluorescence was determined in individual cells using the Colocalization Test plug-in and Costes' image randomization (65) and a point spread function (PSF) width of 0.453 µm as a quantitative measure of colocalization of both fluorescence signals (66, 67).

Error calculations. Experimental data are presented as the average and its standard error. Errors were propagated using the law of error propagation for random, independent errors (68).

Results

Prolonged ER stress extending over several half-lives of the insulin receptor at the plasma membrane causes insulin resistance

Our previous work suggests that short-term ER stress lasting for up to 8 h does not cause insulin resistance, while insulin resistance caused by prolonged ER stress correlates with depletion of insulin receptor β chains in C_2C_{12} myotubes (Brown *et al.*, submitted for publication). Three mechanistically independent ER stressors, the *N*-linked glycosylation inhibitor tunicamycin, the SERCA Ca^{2+} ATPase inhibitor thapsigargin, and SubAB, which cleaves and inactivates the ER HSP70 class molecular chaperone BiP/Grp78 in its hinge region (69), failed to elicit insulin resistance in several different cell lines, including Hep G2 and Fao hepatoma cells, mouse embryonic fibroblasts, *in vitro* differentiated 3T3-F442A adipocytes and C_2C_{12} myotubes when applied to these cells for less than ~8 h. To address whether prolonged ER stress leads to insulin resistance in Hep G2 cells and 3T3-F442A adipocytes, we monitored insulin-stimulated AKT T308 and S473 phosphorylation in extended time courses lasting for up to 36 h. These experiments revealed that ER stress causes insulin resistance after incubation of cells with these drugs lasting for ≥ 12 h (Figs. 2, 3A). Insulin sensitivity, as evidenced by decreased AKT S473 or T308 phosphorylation became gradually worse as time increased. These experiments also confirmed that ER stress for up to ~8 h does not cause insulin resistance even at the highest concentrations of tunicamycin or thapsigargin.

The insulin receptor has a half-life at the plasma membrane of 7-13 h (36-42). Hence, we asked whether the onset of insulin resistance in ER-stressed cells correlates with loss of mature insulin receptors. Western blotting of cell lysates isolated from unstressed cells with an anti-β chain antibody revealed three bands in Hep G2 cells and five bands in 3T3-F442A cells (Figs. 3B, 4A). The two bands migrating at ~210

kDa in SDS-PAGE gels represent the α-β proreceptor and an alternatively glycosylated form (70), whereas the band migrating at 95 kDa represents the mature β chain. The two additional bands seen at ~130 kDa in C_2C_{12} and 3T3-F442A cells arise from a less well characterized lysosomal event (71). Cell extracts from tunicamycin-treated cells displayed an extra band representing the non-glycosylated α-β proreceptor (Figs. 3B, 4A). In thapsigargin-treated Hep G2 cells insulin resistance develops around 36 h (Fig. 2B). Insulin receptor β chains remain largely unchanged for the first 24 h of thapsigargin treatment, but become severely decreased around 36 h (Fig. 4B). Similar results were obtained with tunicamycin and SubAB, where severe insulin resistance and insulin receptor β chain depletion manifested 36 h after application of the drugs (Figs. 2C-D and 4C-D). At the highest tunicamycin concentration insulin resistance developed before 36 h and also correlated with a faster depletion of insulin receptor β chains. These results were further confirmed by using tunicamycin-treated 3T3-F442A adipocytes (Fig. 3). At 1 μg/ml tunicamycin insulin resistance developed at ~12 h at which time there was also a ~50% decrease in insulin receptor β chains. More severe insulin resistance developed with 10 μg/ml tunicamycin, which coincided with a more severe loss of β chains. Furthermore, we observed the same overall correlation between levels of insulin receptor β chains and the degree of insulin-stimulated AKT S473 phosphorylation in C_2C_{12} myotubes (Brown et al., submitted for publication). In summary, these data establish a correlative relationship between loss of mature insulin receptor β chains and insulin resistance in ER-stressed cells.

Unprocessed α-β proreceptors accumulate in the ER of ER-stressed cells

Several mechanisms through which ER stress decreases mature insulin receptors are imaginable: 1) the RIDD activity of IRE1α (2, 3) may degrade the insulin receptor mRNA, 2) transcriptional activity may be repressed (72, 73), 3) phosphorylation of eIF2α by PERK may inhibit translation of the insulin receptor mRNA, and 4) ER stress may interfere with proper folding, maturation, or trafficking of the insulin receptor in the secretory pathway. RT-qPCRs showed that steady-state levels of insulin receptor mRNA increase ~6 fold in ER-stressed C_2C_{12} cells (Fig. 5A), thus making it unlikely that transcriptional effects or RIDD activity of IRE1α can explain loss of insulin receptor β chains in ER-stressed cells. To explore whether a translational arrest can explain the loss of β chains we labeled newly synthesized proteins by pulsing cells for 15 min with a mix of [^{35}S]-L-methionine and [^{35}S]-L-cysteine and measured incorporation of [^{35}S]-L-methionine/[^{35}S]-L-cysteine into protein by scintillation counting of TCA precipitates (Fig. 5B, F, I). These experiments showed that treatment of C_2C_{12} cells and 3T3-F442A cells with 0.1 μM thapsigargin or 0.1 μg/ml tunicamycin for 24 h did not inhibit general protein synthesis (Fig. 5B, F). These mild ER stress conditions inhibit insulin-stimulated AKT S473 phosphorylation and deplete insulin receptor β chains (Figs. 2-4). In Hep G2 cells these conditions decreased total protein synthesis by ~25% (Fig. 5I). We confirmed these results by running equal amounts of [^{35}S]-labeled total protein (10 μg) on SDS-PAGE gels, phosphorimaging of the gels and standardizing the Phosphorimager signals to the intensity of the Coomassie Brilliant Blue R250 staining of the gels (Figs. 5C-D, G-H, J-K). These experiments gave qualitatively the same results as the scintillation counting of TCA-precipitates. Overall, these experiments have identified conditions at which there is no effect of ER stress on translation rates, but at which ER stress inhibits insulin signaling and decreases insulin receptor β

393 chains. Therefore, it is unlikely that a translational arrest can fully explain the
394 depletion of β chains caused by ER stress.

395 To directly establish whether ER stress affects translation of the insulin receptor
396 mRNA we immunoprecipitated insulin receptors with an antibody against the β chain
397 from differentiated 3T3-F442A adipocytes that were pulse-labeled with [^{35}S]-L-
398 methionine/[^{35}S]-L-cysteine for 15 min, ran the immunoprecipitates on SDS-PAGE
399 gels and quantified signals by Phosphorimaging (Fig. 5E). These experiments showed
400 that 0.1 μM thapsigargin did not affect translation of the insulin receptor mRNA.
401 Further evidence that translation of insulin receptors is ongoing in ER-stressed cells is
402 provided by the appearance of non-glycosylated proreceptors in tunicamycin-treated
403 cells (Figs. 3B, 4A, and 6A, C) because tunicamycin does not remove pre-existing *N*-
404 glycans from glycoproteins. In summary, translational arrest mediated by the UPR
405 cannot explain the decrease in insulin receptor β chains in cells exposed to low
406 concentrations of thapsigargin and tunicamycin. Thus another, more generally
407 applicable, explanation for how ER stress decreases insulin receptor β chains exists.

408 Since transcriptional and translational effects cannot fully explain loss of mature
409 insulin receptors in ER-stressed cells, we characterized whether transport of newly
410 synthesized insulin receptors to the plasma membrane is inhibited by ER stress.
411 Consistent with this hypothesis is that while mature β chains decrease in ER-stressed
412 cells, the levels of α-β proreceptors increase relative to the levels of the β chains (Fig.
413 6A-B and data not shown). Cleavage of the proreceptor into α- and β chains by
414 proprotein convertases in the *trans*-Golgi network (34, 35) suggests that α-β
415 proreceptors accumulate in an early compartment of the secretory pathway such as the
416 ER or *cis*-Golgi. To provide additional evidence that proreceptors accumulate in the
417 ER or *cis*-Golgi we digested protein extracts from un- and ER-stressed C_2C_{12} cells

418 with endoglycosidase H (Endo H). Endo H releases high mannose and some hybrid
419 type *N*-linked oligosaccharides from glycoproteins by cleaving between the two *N*-
420 acetylglucosamine units (74). High mannose oligosaccharides are characteristic of
421 proteins that have not been processed by enzymes in the Golgi complex. Endo H-
422 digested α-β proreceptors migrated at the same position in SDS-PAGE as fully
423 deglycosylated proreceptors synthesized in tunicamycin-treated cells (Fig. 6C) or
424 obtained with PNGase F (74) (Fig. 6E). By contrast, β chains carry one Endo H
425 sensitive and several Endo H-resistant *N*-linked oligosaccharides [Figs. 6C, E and
426 (70)]. Thus, these data are consistent with the conclusion that α-β proreceptors
427 accumulate in the ER or *cis*-Golgi of ER-stressed cells.

428 To directly establish whether insulin receptors deplete at the plasma membrane
429 and accumulate in intracellular compartments we compared the localization of *C*-
430 terminally GFP-tagged insulin receptors expressed in HEK 293 cells treated for 18 h
431 with 100 ng/ml tunicamycin or 1 μg/ml SubAB to untreated HEK 293 cells. HEK 293
432 cells were chosen for these experiments because they can be easily transfected and, in
433 contrast to Hep G2 cells, do not grow in clumps. We confirmed that ER stress lasting
434 for 18 h causes insulin resistance and depletes insulin receptor β chains in HEK 293
435 cells (Fig. 6F). Fluorescence microscopy revealed that the GFP-tagged insulin
436 receptor redistributed from the plasma membrane to intracellular compartments in
437 ER-stressed cells (Fig. 6G). To quantitatively assess localization of the insulin
438 receptor to the plasma membrane we determined the Pearson's correlation coefficient,
439 r_{obs}, for the GFP fluorescence and the fluorescence of the CellMask Deep Red plasma
440 membrane stain (Fig. 6H). This analysis confirmed a decrease in colocalization of the
441 GFP and CellMask Deep Red fluorescence in both tunicamycin and SubAB-treated

HEK 293 cells and hence demonstrates that ER stress depletes the population of insulin receptors at the plasma membrane.

AKT activation by a cytosolic F_V2E-insulin receptor chimera is not affected by ER stress

To demonstrate that loss of insulin receptors suffices to cause insulin resistance we silenced expression of the insulin receptor gene in C_2C_{12} cells using three small interfering (si) RNAs and compared insulin-stimulated AKT S473 phosphorylation to cells transfected with a siRNA against eGFP. All three siRNAs decreased insulin receptor mRNA steady-state levels by 50-70% and mature β chains to a similar extent (Figs. 7A-B). Concomitant to the decrease in insulin receptor levels, insulin-stimulated AKT S473 phosphorylation was decreased by 50-80% (Fig. 7B). Thus, an ~50% decrease in insulin receptor levels suffices to decrease insulin-stimulated AKT S473 phosphorylation.

To establish that inhibition of transport of newly synthesized insulin receptors from the ER to the plasma membrane is necessary for ER stress to cause insulin resistance we bypassed the secretory pathway in synthesis of functional insulin receptors by creating a chimera in which the signal peptide, extracellular and transmembrane domains of the insulin receptor are replaced by an *N*-terminal myristoylation signal and the F_V2E domain (Fig. 7C). The myristoylation signal mediates *N*-terminal myristoylation of the protein and its anchoring to intracellular membranes (75, 76). The F_V2E domain contains two binding sites for the macrolide AP20187 and binds AP20187 with subnanomolar affinities (43). Binding of AP20187 to the F_V2E domain induces dimerization of the chimeric protein. Dimerization of the F_V2E-insulin receptor chimera with AP20187 in stably transfected Flp-In T-Rex 293 cells caused an increase in phosphorylation of the chimera at tyrosine 1345, showing

that the chimera possesses tyrosine autophosphorylation activity (Fig. 7D). Addition of AP20187 to serum-starved cells expressing the myristoylated chimera elevated AKT T308 phosphorylation ~2.6 fold (Fig. 7E). We transiently transfected the myristoylated chimera into C_2C_{12} myoblasts to characterize AKT S473 phosphorylation, because AKT S473 phosphorylation was unresponsive to serum starvation in Flp-In T-Rex 293 cells (data not shown). In C_2C_{12} cells AP20187 stimulated AKT S473 phosphorylation ~3 fold (Fig. 7F). Thus, activation of the F_V2E-insulin receptor chimera recapitulates several events in insulin signaling. Induction of ER stress with tunicamycin or SubAB for 24 h in Flp-In T-Rex 293 did not affect AKT activation by the chimera, but depleted β chains of the endogenous receptor by ~40% (Fig. 7E). In transiently transfected C_2C_{12} cells ER stress induced for 24 h with thapsigargin, tunicamycin, or SubAB reduced endogenous β chains by ~50% but again did not affect AKT activation by the chimera (Figs. 7F-G). In both cell lines tunicamycin led to the accumulation of non-glycosylated endogenous proreceptors (Figs. 7E-F). These data are consistent with the conclusion that insulin resistance in ER-stressed cells is caused by blocked passage of newly synthesized insulin receptors through the secretory pathway.

JNK knock-out MEFs are not protected from ER stress-induced insulin resistance

Previous reports have linked UPR signaling to insulin resistance via activation of both JNK by IRE1α (12, 16) and transcriptional induction of TRB3 downstream of PERK (24, 25, 29). To re-evaluate the role of JNK in ER stress-dependent insulin resistance we made use of *jnk1*$^{-/-}$ *jnk2*$^{-/-}$ MEFs, which do not show JNK activation after UV stimulation (46). Induction of ER stress with thapsigargin, tunicamycin, or SubAB for 24 h inhibited insulin-stimulated AKT S473 phosphorylation to the same extent in *jnk1*$^{-/-}$ *jnk2*$^{-/-}$ MEFs as it did in WT MEFs (Figs. 8A-D), while activating JNK 2-4 fold

492 (Figs. 8E-F). These data show that ER stress causes insulin resistance independent of
493 activation of JNK. ER stress conditions that did not affect AKT activation by the
494 F_V2E-insulin receptor chimera induced expression of TRB3 ~6 fold in C_2C_{12} cells
495 (Fig. 8G). Thus, elevated levels of *TRB3* do not inhibit AKT activation in these cells.

496 *ER stress depletes IGF-I receptors*

497 Inhibition of transport of newly synthesized insulin receptors from the ER to the
498 plasma membrane may be a more general phenomenon of ER stress affecting the
499 majority of plasma membrane proteins. To provide evidence that ER stress depletes
500 plasma membrane proteins other than the insulin receptor, we characterized the effect
501 of ER stress on the IGF-I receptor. The IGF-I receptor has a half life of >6 h (77).
502 Processing of the IGF-I proreceptor by proprotein convertases into α and β chains is
503 reminiscent to processing of the insulin receptor (78). ER stress depleted IGF-I
504 receptor β chains in Hep G2 (Figs. 9A-D) and C_2C_{12} cells (Figs. 9F-H) and also led to
505 an accumulation of proreceptors (Figs. 9E, I). These effects of ER stress on IGF-I
506 receptor levels support the conclusion that ER stress not only decreases insulin
507 receptors in the plasma membrane but also other membrane-bound proteins.

508 **Discussion**

509 Several tissues and organs display ER stress in obesity, including adipose tissue,
510 hypothalamus, and the liver of obese mice and of obese patients (12-15). ER stress
511 has been proposed to cause insulin resistance in obesity through activation of UPR
512 signaling pathways leading to IRS1 S307 phosphorylation by JNK and inhibition of
513 AKT phosphorylation by the pseudokinase TRB3. However, insulin resistance still
514 develops in ER-stressed *jnk1*$^{-/-}$ *jnk2*$^{-/-}$ MEFs (Fig. 8), showing that JNK activation is
515 not required for ER stress-induced insulin resistance. In addition, strong
516 transcriptional induction of TRB3 occurs without the manifestation of insulin

517 resistance (Fig. 2 and Brown et al., submitted for publication), which suggests that
518 TRB3 also is not responsible for causing insulin resistance in ER-stressed cells. Here
519 we show that pharmacologically-induced ER stress causes insulin resistance by
520 inhibiting delivery of newly synthesized insulin receptors to the plasma membrane.
521 Constitutive turnover of insulin receptors in the plasma membrane will deplete plasma
522 membrane insulin receptor levels as long as delivery of newly synthesized receptors
523 to the plasma membrane is inhibited. Plasma membrane insulin receptor levels are
524 decreased in obesity (79, 80), while insulin sensitivity and blood glucose homeostasis
525 is restored by chemical chaperones, such as tauroursodeoxycholic acid or 4-
526 phenylbutyrate (13, 81). Our work suggests that less efficient trafficking of newly
527 synthesized insulin receptor molecules to the cell surface due to the presence of ER
528 stress accounts for the decreased insulin receptor abundance in the plasma membrane
529 in obesity. These effects of ER stress on insulin receptor levels may extend to other
530 human diseases associated with ER stress and in which decreases in insulin receptor
531 levels have been reported, for example Parkinson's (82) and Alzheimer's disease (83).
532 Several lines of evidence support the conclusion that ER stress causes insulin
533 resistance by inhibiting transport of newly synthesized insulin receptors to the plasma
534 membrane. Only prolonged ER stress extending over several half-lives of the insulin
535 receptor at the plasma membrane causes insulin resistance (Figs. 2, 3), while short-
536 term ER stress lasting up to 8 h fails to cause ER stress (Brown *et al.*, submitted for
537 publication). The onset of insulin resistance coincides with depletion of mature insulin
538 receptor β chains providing correlative evidence that depletion of insulin receptors is
539 linked to ER stress-induced insulin resistance. A decrease in insulin receptor levels
540 suffices to cause insulin resistance, because siRNA-mediated knock-down of insulin
541 receptor expression by 50-70% decreased insulin-stimulated AKT activation to a

similar degree (Fig. 7A). In ER-stressed cells unprocessed, Endo H sensitive proreceptors accumulate in the ER (Figs. 6A, B). Fluorescence microscopy of GFP-tagged insulin receptors in HEK293 cells shows that receptors are depleted from the plasma membrane (Fig. 6G-H). Finally, bypass of the ER by a functional, myristoylated F_V2E-insulin receptor chimera synthesized on cytosolic ribosomes renders these insulin receptor chimeras insensitive to ER stress (Figs. 7F-G). Thus, ER stress-induced insulin resistance is dependent on transit of newly synthesized insulin receptors through the secretory pathway (Fig. 10).

At the same time, experiments with the myristoylated F_V2E-insulin receptor chimera suggest that ER stress-induced insulin resistance is largely independent of activation of UPR signaling pathways, especially activation of JNK by IRE1α and TRB3 by PERK. Indeed, we find that *jnk1*$^{-/-}$ *jnk2*$^{-/-}$ MEFs are not protected from ER stress-induced insulin resistance (Fig. 8A-F). These data are consistent with other reports showing that the JNK selective inhibitor SP600125 (84) did not restore insulin sensitivity to ER-stressed cells (19, 20). A ~6-fold increase in TRB3 expression also did not decrease AKT activation by the F_V2E-insulin receptor chimera (Figs. 6F-G, 7G). This observation is consistent with our observation in C_2C_{12} cells, in which a ~20-fold increase in steady-state *TRB3* mRNA levels did not affect insulin signaling (Brown *et al.*, submitted for publication). Thus, ER stress signaling pathways do not play a major role in the development of insulin resistance during ER stress.

Processing of the insulin receptor in the secretory pathway has been well characterized (85-87). In these investigations tunicamycin was used to characterize the effects of inhibition of *N*-linked glycosylation on processing of the insulin receptor (39, 40, 88-94). These studies have shown that tunicamycin depletes ^{125}I-insulin binding capacity of cell membranes (40, 90-93, 95), and thus insulin and IGF-I

567 receptors, with a half-live of 7-10 h (39, 89), while having no or relatively small
568 effects on total protein synthesis (39, 89). It was also shown that tunicamycin blocks
569 trafficking of newly synthesized insulin receptors to the plasma membrane (92-94).
570 These effects of tunicamycin have been largely attributed to lack of glycosylation of
571 newly synthesized insulin receptors. Two other ER stressors, thapsigargin and
572 SubAB, which do not directly affect *N*-linked glycosylation, also depleted insulin
573 receptors at the plasma membrane (Fig. 6) and inhibited transport of insulin
574 proreceptors from the ER to the *trans*-Golgi network (Fig. 6A-E). This suggests that
575 accumulation of misfolded and aggregated proteins in the ER underlies the trafficking
576 defects of the insulin receptor in ER-stressed cells. Indirect effects resulting from
577 depletion of proteins functioning in vesicular trafficking and sorting may also account
578 for some of the defects in insulin receptor trafficking, and may, for example, explain
579 an increased half-life of the insulin receptor at the plasma membrane in tunicamycin-
580 treated cells (39) and transient increases in insulin sensitivity in ER-stressed cells
581 (Fig. 2B, 3A).

582 ER stress also depleted IGF-I receptor β chains (Fig. 9) and led to an
583 accumulation of unprocessed IGF-I proreceptors (Fig. 9E, I), which suggests that
584 transport of IGF-I proreceptors from the ER to their site of cleavage in the *trans*-Golgi
585 network is also inhibited by ER stress. Thus, ER stress can inhibit delivery of
586 secretory proteins other than the insulin receptor to the plasma membrane. This effect
587 of ER stress on maturation of secretory and transmembrane proteins may explain
588 several recent observations *without* invoking UPR signaling. For example, inhibition
589 of tumor necrosis factor (TNF)-α-induced reactive oxygen species generation in L929
590 cells by tunicamycin (96) may be due to depletion of TNF receptors. Likewise,
591 inhibition of cholesterol efflux in Hep G2 cells by ER stress (97) may be explained in

part by inhibition of delivery of newly synthesized ATP-binding cassette transporter A1 (ABCA1) to the plasma membrane. Both proteins have short half-lives at the plasma membrane of 1.5-2 h (98-102). However, ER stress may affect delivery of different proteins to the plasma membrane to different degrees. Tunicamycin, the most commonly used ER stressor, inhibits delivery of many proteins to the cell surface, but, for example, does not affect the rate of delivery of HLA-A and HLA-B molecules to the plasma membrane (103) or interferon secretion by human leukocytes (104, 105). Therefore, a case-by-case evaluation will be necessary to address to which extent ER stress reduces delivery of individual proteins to the plasma membrane and/or their secretion.

In conclusion, we show that ER stress causes insulin resistance by inhibiting transport of newly synthesized insulin receptors to the plasma membrane which leads to receptor depletion due to constitutive turnover of plasma membrane proteins. This effect of ER stress may also affect other plasma membrane receptors.

Acknowledgements

This work was supported by the European Community's 7th Framework Programme (FP7/2007-2013) under grant agreement no. 201608 and Diabetes UK [BDA 09/0003949]. We thank R. Davis (University of Massachusetts), A. Benham (Durham University), R. Bashir (Durham University), M. Cann (Durham Unversity), and C. Hutchison (Durham University) for providing cell lines. We thank A. Auricchio (Telethon Institute of Genetics and Medicine, Naples, Italy) for plasmid pCLFv2IRE and Arial Pharmaceuticals for providing plasmid pC_4M-F$_V$2E. We thank A. Benham for assistance with the pulse chase experiments.

References

1. **Schröder M.** 2008. Endoplasmic reticulum stress responses. Cell Mol Life Sci **65:**862-894.

2. **Hollien J, Lin JH, Li H, Stevens N, Walter P, Weissman JS.** 2009. Regulated Ire1-dependent decay of messenger RNAs in mammalian cells. J Cell Biol **186:**323-331.

3. **Hollien J, Weissman JS.** 2006. Decay of endoplasmic reticulum-localized mRNAs during the unfolded protein response. Science **313:**104-107.

4. **Harding HP, Zhang Y, Zeng H, Novoa I, Lu PD, Calfon M, Sadri N, Yun C, Popko B, Paules R, Stojdl DF, Bell JC, Hettmann T, Leiden JM, Ron D.** 2003. An integrated stress response regulates amino acid metabolism and resistance to oxidative stress. Mol Cell **11:**619-633.

5. **Zhang K, Kaufman RJ.** 2008. From endoplasmic-reticulum stress to the inflammatory response. Nature **454:**455-462.

6. **Saltiel AR, Kahn CR.** 2001. Insulin signalling and the regulation of glucose and lipid metabolism. Nature **414:**799-806.

7. **Sarbassov DD, Guertin DA, Ali SM, Sabatini DM.** 2005. Phosphorylation and regulation of Akt/PKB by the rictor-mTOR complex. Science **307:**1098-1101.

8. **Jacinto E, Facchinetti V, Liu D, Soto N, Wei S, Jung SY, Huang Q, Qin J, Su B.** 2006. SIN1/MIP1 maintains rictor-mTOR complex integrity and regulates Akt phosphorylation and substrate specificity. Cell **127:**125-137.

9. **Guertin DA, Stevens DM, Thoreen CC, Burds AA, Kalaany NY, Moffat J, Brown M, Fitzgerald KJ, Sabatini DM.** 2006. Ablation in mice of the mTORC components *raptor*, *rictor*, or *mLST8* reveals that mTORC2 is

required for signaling to Akt-FOXO and PKCα, but not S6K1. Dev Cell **11:**859-871.

10. **Mao K, Kobayashi S, Jaffer ZM, Huang Y, Volden P, Chernoff J, Liang Q.** 2008. Regulation of Akt/PKB activity by P21-activated kinase in cardiomyocytes. J Mol Cell Cardiol **44:**429-434.

11. **McDonald PC, Oloumi A, Mills J, Dobreva I, Maidan M, Gray V, Wederell ED, Bally MB, Foster LJ, Dedhar S.** 2008. Rictor and integrin-linked kinase interact and regulate Akt phosphorylation and cancer cell survival. Cancer Res **68:**1618-1624.

12. **Özcan U, Cao Q, Yilmaz E, Lee A-H, Iwakoshi NN, Ozdelen E, Tuncman G, Görgün C, Glimcher LH, Hotamisligil GS.** 2004. Endoplasmic reticulum stress links obesity, insulin action, and type 2 diabetes. Science **306:**457-461.

13. **Özcan U, Yilmaz E, Özcan L, Furuhashi M, Vaillancourt E, Smith RO, Görgün CZ, Hotamisligil GS.** 2006. Chemical chaperones reduce ER stress and restore glucose homeostasis in a mouse model of type 2 diabetes. Science **313:**1137-1140.

14. **Sreejayan N, Dong F, Kandadi MR, Yang X, Ren J.** 2008. Chromium alleviates glucose intolerance, insulin resistance, and hepatic ER stress in obese mice. Obesity (Silver Spring) **16:**1331-1337.

15. **Hosogai N, Fukuhara A, Oshima K, Miyata Y, Tanaka S, Segawa K, Furukawa S, Tochino Y, Komuro R, Matsuda M, Shimomura I.** 2007. Adipose tissue hypoxia in obesity and its impact on adipocytokine dysregulation. Diabetes **56:**901-911.

16. **Urano F, Wang X, Bertolotti A, Zhang Y, Chung P, Harding HP, Ron D.** 2000. Coupling of stress in the ER to activation of JNK protein kinases by transmembrane protein kinase IRE1. Science **287:**664-666.

17. **Aguirre V, Uchida T, Yenush L, Davis R, White MF.** 2000. The c-Jun NH_2-terminal kinase promotes insulin resistance during association with insulin receptor substrate-1 and phosphorylation of Ser^{307}. J Biol Chem **275:**9047-9054.

18. **Aguirre V, Werner ED, Giraud J, Lee YH, Shoelson SE, White MF.** 2002. Phosphorylation of Ser307 in insulin receptor substrate-1 blocks interactions with the insulin receptor and inhibits insulin action. J Biol Chem **277:**1531-1537.

19. **Xu L, Spinas GA, Niessen M.** 2010. ER stress in adipocytes inhibits insulin signaling, represses lipolysis, and alters the secretion of adipokines without inhibiting glucose transport. Horm Metab Res **42:**643-651.

20. **Zhou L, Zhang J, Fang Q, Liu M, Liu X, Jia W, Dong LQ, Liu F.** 2009. Autophagy-mediated insulin receptor down-regulation contributes to endoplasmic reticulum stress-induced insulin resistance. Mol Pharmacol **76:**596-603.

21. **Achard CS, Laybutt DR.** 2012. Lipid-induced endoplasmic reticulum stress in liver cells results in two distinct outcomes: Adaptation with enhanced insulin signaling or insulin resistance. Endocrinology **153:**2164-2177.

22. **Jurczak MJ, Lee AH, Jornayvaz FR, Lee HY, Birkenfeld AL, Guigni BA, Kahn M, Samuel VT, Glimcher LH, Shulman GI.** 2012. Dissociation of inositol requiring enzyme (IRE1α)-mediated JNK activation from hepatic

insulin resistance in conditional X-box binding protein-1 (XBP1) knockout mice. J Biol Chem **287:**2558-2567.

23. **Jung DY, Chalasani U, Pan N, Friedline RH, Prosdocimo DA, Nam M, Azuma Y, Maganti R, Yu K, Velagapudi A, O'Sullivan-Murphy B, Sartoretto JL, Jain MK, Cooper MP, Urano F, Kim JK, Gray S.** 2013. KLF15 is a molecular link between endoplasmic reticulum stress and insulin resistance. PLoS One **8:**e77851.

24. **Ohoka N, Yoshii S, Hattori T, Onozaki K, Hayashi H.** 2005. *TRB3*, a novel ER stress-inducible gene, is induced via ATF4-CHOP pathway and is involved in cell death. EMBO J **24:**1243-1255.

25. **Du K, Herzig S, Kulkarni RN, Montminy M.** 2003. TRB3: A *tribbles* homolog that inhibits Akt/PKB activation by insulin in liver. Science **300:**1574-1577.

26. **Koh HJ, Arnolds DE, Fujii N, Tran TT, Rogers MJ, Jessen N, Li Y, Liew CW, Ho RC, Hirshman MF, Kulkarni RN, Kahn CR, Goodyear LJ.** 2006. Skeletal muscle-selective knockout of LKB1 increases insulin sensitivity, improves glucose homeostasis, and decreases TRB3. Mol Cell Biol **26:**8217-8227.

27. **He L, Simmen FA, Mehendale HM, Ronis MJ, Badger TM.** 2006. Chronic ethanol intake impairs insulin signaling in rats by disrupting Akt association with the cell membrane. Role of TRB3 in inhibition of Akt/protein kinase B activation. J Biol Chem **281:**11126-11134.

28. **Liew CW, Bochenski J, Kawamori D, Hu J, Leech CA, Wanic K, Malecki M, Warram JH, Qi L, Krolewski AS, Kulkarni RN.** 2010. The

712 pseudokinase tribbles homolog 3 interacts with ATF4 to negatively regulate
713 insulin exocytosis in human and mouse β cells. J Clin Invest **120:**2876-2888.
714 29. **Koh HJ, Toyoda T, Didesch MM, Lee MY, Sleeman MW, Kulkarni RN,**
715 **Musi N, Hirshman MF, Goodyear LJ.** 2013. Tribbles 3 mediates
716 endoplasmic reticulum stress-induced insulin resistance in skeletal muscle. Nat
717 Commun **4:**1871.
718 30. **Prudente S, Hribal ML, Flex E, Turchi F, Morini E, De Cosmo S, Bacci S,**
719 **Tassi V, Cardellini M, Lauro R, Sesti G, Dallapiccola B, Trischitta V.**
720 2005. The functional Q84R polymorphism of mammalian Tribbles homolog
721 TRB3 is associated with insulin resistance and related cardiovascular risk in
722 Caucasians from Italy. Diabetes **54:**2807-2811.
723 31. **Shi Z, Liu J, Guo Q, Ma X, Shen L, Xu S, Gao H, Yuan X, Zhang J.** 2009.
724 Association of TRB3 gene Q84R polymorphism with type 2 diabetes mellitus
725 in Chinese population. Endocrine **35:**414-419.
726 32. **Cheatham B, Kahn CR.** 1992. Cysteine 647 in the insulin receptor is required
727 for normal covalent interaction between α- and β-subunits and signal
728 transduction. J Biol Chem **267:**7108-7115.
729 33. **Sparrow LG, McKern NM, Gorman JJ, Strike PM, Robinson CP, Bentley**
730 **JD, Ward CW.** 1997. The disulfide bonds in the C-terminal domains of the
731 human insulin receptor ectodomain. J Biol Chem **272:**29460-29467.
732 34. **Bravo DA, Gleason JB, Sanchez RI, Roth RA, Fuller RS.** 1994. Accurate
733 and efficient cleavage of the human insulin proreceptor by the human
734 proprotein-processing protease furin. Characterization and kinetic parameters
735 using the purified, secreted soluble protease expressed by a recombinant
736 baculovirus. J Biol Chem **269:**25830-25837.

737 35. **Robertson BJ, Moehring JM, Moehring TJ.** 1993. Defective processing of
738 the insulin receptor in an endoprotease-deficient Chinese hamster cell strain is
739 corrected by expression of mouse furin. J Biol Chem **268:**24274-24277.
740 36. **Reed BC, Lane MD.** 1980. Insulin receptor synthesis and turnover in
741 differentiating 3T3-L1 preadipocytes. Proc Natl Acad Sci U S A **77:**285-289.
742 37. **Kasuga M, Kahn CR, Hedo JA, Van Obberghen E, Yamada KM.** 1981.
743 Insulin-induced receptor loss in cultured human lymphocytes is due to
744 accelerated receptor degradation. Proc Natl Acad Sci U S A **78:**6917-6921.
745 38. **Reed BC, Ronnett GV, Clements PR, Lane MD.** 1981. Regulation of insulin
746 receptor metabolism. Differentiation-induced alteration of receptor synthesis
747 and degradation. J Biol Chem **256:**3917-3925.
748 39. **Reed BC, Ronnett GV, Lane MD.** 1981. Role of glycosylation and protein
749 synthesis in insulin receptor metabolism by 3T3-L1 mouse adipocytes. Proc
750 Natl Acad Sci U S A **78:**2908-2912.
751 40. **Capeau J, Lascols O, Flaig-Staedel C, Blivet MJ, Beck JP, Picard J.** 1985.
752 Degradation of insulin receptors by hepatoma cells: Insulin-induced down-
753 regulation results from an increase in the rate of basal receptor degradation.
754 Biochimie **67:**1133-1141.
755 41. **Savoie S, Rindress D, Posner BI, Bergeron JJ.** 1986. Tunicamycin
756 sensitivity of prolactin, insulin and epidermal growth factor receptors in rat
757 liver plasmalemma. Mol Cell Endocrinol **45:**241-246.
758 42. **Grako KA, Olefsky JM, McClain DA.** 1992. Tyrosine kinase-defective
759 insulin receptors undergo decreased endocytosis but do not affect
760 internalization of normal endogenous insulin receptors. Endocrinology
761 **130:**3441-3452.

762 43. **Clackson T, Yang W, Rozamus LW, Hatada M, Amara JF, Rollins CT,**
763 **Stevenson LF, Magari SR, Wood SA, Courage NL, Lu X, Cerasoli F, Jr.,**
764 **Gilman M, Holt DA.** 1998. Redesigning an FKBP-ligand interface to generate
765 chemical dimerizers with novel specificity. Proc Natl Acad Sci U S A
766 **95:**10437-10442.
767 44. **Bass J, Turck C, Rouard M, Steiner DF.** 2000. Furin-mediated processing in
768 the early secretory pathway: sequential cleavage and degradation of misfolded
769 insulin receptors. Proc Natl Acad Sci U S A **97:**11905-11909.
770 45. **Cotugno G, Pollock R, Formisano P, Linher K, Beguinot F, Auricchio A.**
771 2004. Pharmacological regulation of the insulin receptor signaling pathway
772 mimics insulin action in cells transduced with viral vectors. Hum Gene Ther
773 **15:**1101-1108.
774 46. **Tournier C, Hess P, Yang DD, Xu J, Turner TK, Nimnual A, Bar-Sagi D,**
775 **Jones SN, Flavell RA, Davis RJ.** 2000. Requirement of JNK for stress-
776 induced activation of the cytochrome c-mediated death pathway. Science
777 **288:**870-874.
778 47. **Green H, Kehinde O.** 1976. Spontaneous heritable changes leading to
779 increased adipose conversion in 3T3 cells. Cell **7:**105-113.
780 48. **Blau HM, Pavlath GK, Hardeman EC, Chiu CP, Silberstein L, Webster**
781 **SG, Miller SC, Webster C.** 1985. Plasticity of the differentiated state.
782 Science **230:**758-766.
783 49. **Graham FL, Harrison T, Williams J.** 1978. Defective transforming capacity
784 of adenovirus type 5 host-range mutants. Virology **86:**10-21.

50. **Graham FL, Smiley J, Russell WC, Nairn R.** 1977. Characteristics of a human cell line transformed by DNA from human adenovirus type 5. J Gen Virol **36:**59-74.

51. **Harrison T, Graham F, Williams J.** 1977. Host-range mutants of adenovirus type 5 defective for growth in HeLa cells. Virology **77:**319-329.

52. **Knowles BB, Howe CC, Aden DP.** 1980. Human hepatocellular carcinoma cell lines secrete the major plasma proteins and hepatitis B surface antigen. Science **209:**497-499.

53. **Morton HJ.** 1970. A survey of commercially available tissue culture media. In Vitro **6:**89-108.

54. **Rutzky LP, Pumper RW.** 1974. Supplement to a survey of commercially available tissue culture media (1970). In Vitro **9:**468-469.

55. **Bains W, Ponte P, Blau H, Kedes L.** 1984. Cardiac actin is the major actin gene product in skeletal muscle cell differentiation in vitro. Mol Cell Biol **4:**1449-1453.

56. **Amato PA, Unanue ER, Taylor DL.** 1983. Distribution of actin in spreading macrophages: a comparative study on living and fixed cells. J Cell Biol **96:**750-761.

57. **Rubin CS, Hirsch A, Fung C, Rosen OM.** 1978. Development of hormone receptors and hormonal responsiveness in vitro. Insulin receptors and insulin sensitivity in the preadipocyte and adipocyte forms of 3T3-L1 cells. J Biol Chem **253:**7570-7578.

58. **Hansen JB, Petersen RK, Larsen BM, Bartkova J, Alsner J, Kristiansen K.** 1999. Activation of peroxisome proliferator-activated receptor γ bypasses

809 the function of the retinoblastoma protein in adipocyte differentiation. J Biol
810 Chem **274:**2386-2393.
811 59. **Greenspan P, Fowler SD.** 1985. Spectrofluorometric studies of the lipid
812 probe, nile red. J Lipid Res **26:**781-789.
813 60. **Greenspan P, Mayer EP, Fowler SD.** 1985. Nile red: A selective fluorescent
814 stain for intracellular lipid droplets. J Cell Biol **100:**965-973.
815 61. **Paton AW, Srimanote P, Talbot UM, Wang H, Paton JC.** 2004. A new
816 family of potent AB_5 cytotoxins produced by Shiga toxigenic *Escherichia coli*.
817 J Exp Med **200:**35-46.
818 62. **Talbot UM, Paton JC, Paton AW.** 2005. Protective immunization of mice
819 with an active-site mutant of subtilase cytotoxin of Shiga toxin-producing
820 *Escherichia coli*. Infect Immun **73:**4432-4436.
821 63. **Cox DJ, Strudwick N, Ali AA, Paton AW, Paton JC, Schröder M.** 2011.
822 Measuring signaling by the unfolded protein response. Methods Enzymol
823 **491:**261-292.
824 64. **Collins TJ.** 2007. ImageJ for microscopy. Biotechniques **43:**25-30.
825 65. **Costes SV, Daelemans D, Cho EH, Dobbin Z, Pavlakis G, Lockett S.** 2004.
826 Automatic and quantitative measurement of protein-protein colocalization in
827 live cells. Biophys J **86:**3993-4003.
828 66. **Manders EMM, Stap J, Brakenhoff GJ, van Driel R, Aten JA.** 1992.
829 Dynamics of three-dimensional replication patterns during the S-phase,
830 analysed by double labelling of DNA and confocal microscopy. J Cell Sci
831 **103:**857-862.
832 67. **Manders EMM, Verbeek FJ, Aten JA.** 1993. Measurement of co-
833 localization of objects in dual-colour confocal images. J Microsc **169:**375-382.

68. **Ku HH.** 1966. Notes on use of propagation of error formulas. J Res Nat Bureau Standards Sect C - Eng Instrumentat **70:**263-273.

69. **Paton AW, Beddoe T, Thorpe CM, Whisstock JC, Wilce MC, Rossjohn J, Talbot UM, Paton JC.** 2006. AB5 subtilase cytotoxin inactivates the endoplasmic reticulum chaperone BiP. Nature **443:**548-552.

70. **Hwang JB, Frost SC.** 1999. Effect of alternative glycosylation on insulin receptor processing. J Biol Chem **274:**22813-22820.

71. **Massague J, Pilch PF, Czech MP.** 1981. A unique proteolytic cleavage site on the beta subunit of the insulin receptor. J Biol Chem **256:**3182-3190.

72. **Jang YY, Kim NK, Kim MK, Lee HY, Kim SJ, Kim HS, Seo HY, Lee IK, Park KG.** 2010. The effect of tribbles-related protein 3 on ER stress-suppressed insulin gene expression in INS-1 cells. Korean Diabetes J **34:**312-319.

73. **Örd D, Örd T.** 2003. Mouse NIPK interacts with ATF4 and affects its transcriptional activity. Exp Cell Res **286:**308-320.

74. **Maley F, Trimble RB, Tarentino AL, Plummer TH, Jr.** 1989. Characterization of glycoproteins and their associated oligosaccharides through the use of endoglycosidases. Anal Biochem **180:**195-204.

75. **Maurer-Stroh S, Eisenhaber B, Eisenhaber F.** 2002. N-terminal N-myristoylation of proteins: prediction of substrate proteins from amino acid sequence. J Mol Biol **317:**541-557.

76. **Maurer-Stroh S, Eisenhaber B, Eisenhaber F.** 2002. N-terminal N-myristoylation of proteins: refinement of the sequence motif and its taxon-specific differences. J Mol Biol **317:**523-540.

77. **Prager D, Yamasaki H, Weber MM, Gebremedhin S, Melmed S.** 1992. Human insulin-like growth factor I receptor function in pituitary cells is suppressed by a dominant negative mutant. J Clin Invest **90:**2117-2122.

78. **Duguay SJ, Milewski WM, Young BD, Nakayama K, Steiner DF.** 1997. Processing of wild-type and mutant proinsulin-like growth factor-IA by subtilisin-related proprotein convertases. J Biol Chem **272:**6663-6670.

79. **Olefsky JM, Reaven GM.** 1975. Effects of age and obesity on insulin binding to isolated adipocytes. Endocrinology **96:**1486-1498.

80. **Olefsky JM.** 1976. Decreased insulin binding to adipocytes and circulating monocytes from obese subjects. J Clin Invest **57:**1165-1172.

81. **Ozcan U, Ozcan L, Yilmaz E, Düvel K, Sahin M, Manning BD, Hotamisligil GS.** 2008. Loss of the tuberous sclerosis complex tumor suppressors triggers the unfolded protein response to regulate insulin signaling and apoptosis. Mol Cell **29:**541-551.

82. **Moroo I, Yamada T, Makino H, Tooyama I, McGeer PL, McGeer EG, Hirayama K.** 1994. Loss of insulin receptor immunoreactivity from the substantia nigra pars compacta neurons in Parkinson's disease. Acta Neuropathol **87:**343-348.

83. **Moloney AM, Griffin RJ, Timmons S, O'Connor R, Ravid R, O'Neill C.** 2010. Defects in IGF-1 receptor, insulin receptor and IRS-1/2 in Alzheimer's disease indicate possible resistance to IGF-1 and insulin signalling. Neurobiol Aging **31:**224-243.

84. **Bennett BL, Sasaki DT, Murray BW, O'Leary EC, Sakata ST, Xu W, Leisten JC, Motiwala A, Pierce S, Satoh Y, Bhagwat SS, Manning AM,**

Anderson DW. 2001. SP600125, an anthrapyrazolone inhibitor of Jun N-terminal kinase. Proc Natl Acad Sci U S A **98:**13681-13686.

85. **Lane MD, Ronnett G, Slieker LJ, Kohanski RA, Olson TL.** 1985. Post-translational processing and activation of insulin and EGF proreceptors. Biochimie **67:**1069-1080.

86. **Lane MD, Ronnett GV, Kohanski RA, Simpson TL.** 1985. Posttranslational processing of the insulin proreceptor. Curr Top Cell Regul **27:**279-292.

87. **Hart CB, Roth J, Lesniak MA.** 1988. Post-translational modifications of the insulin receptor. Adv Exp Med Biol **231:**481-494.

88. **Goldstein BJ, Kahn CR.** 1988. Initial processing of the insulin receptor precursor *in vivo* and *in vitro*. J Biol Chem **263:**12809-12812.

89. **Ronnett GV, Lane MD.** 1981. Post-translational glycosylation-induced activation of aglycoinsulin receptor accumulated during tunicamycin treatment. J Biol Chem **256:**4704-4707.

90. **Keefer LM, De Meyts P.** 1981. Glycosylation of cell surface receptors: tunicamycin treatment decreases insulin and growth hormone binding to different levels in cultured lymphocytes. Biochem Biophys Res Commun **101:**22-29.

91. **Boyd FT, Jr., Raizada MK.** 1983. Effects of insulin and tunicamycin on neuronal insulin receptors in culture. Am J Physiol **245:**C283-287.

92. **Kadle R, Fellows RE, Raizada MK.** 1984. The effects of insulin and tunicamycin on insulin receptors of cultured fibroblasts. Exp Cell Res **151:**533-541.

93. **Ercolani L, Brown TJ, Ginsberg BH.** 1984. Tunicamycin blocks the emergence and maintenance of insulin receptors on mitogen-activated human T lymphocytes. Metabolism **33:**309-316.

94. **Ronnett GV, Knutson VP, Kohanski RA, Simpson TL, Lane MD.** 1984. Role of glycosylation in the processing of newly translated insulin proreceptor in 3T3-L1 adipocytes. J Biol Chem **259:**4566-4575.

95. **Wyse BM, Chang AY.** 1981. Insulin binding in cultured Chinese hamster kidney epithelial cells. The effects of glucose concentration in the medium and tunicamycin. Biochim Biophys Acta **677:**57-62.

96. **Xue X, Piao J-H, Nakajima A, Sakon-Komazawa S, Kojima Y, Mori K, Yagita H, Okumura K, Harding H, Nakano H.** 2005. Tumor necrosis factor α (TNFα) induces the unfolded protein response (UPR) in a reactive oxygen species (ROS)-dependent fashion, and the UPR counteracts ROS accumulation by TNFα. J Biol Chem **280:**33917-33925.

97. **Röhrl C, Eigner K, Winter K, Korbelius M, Obrowsky S, Kratky D, Kovacs WJ, Stangl H.** 2014. Endoplasmic reticulum stress impairs cholesterol efflux and synthesis in hepatic cells. J Lipid Res **55:**94-103.

98. **Watanabe N, Kuriyama H, Sone H, Neda H, Yamauchi N, Maeda M, Niitsu Y.** 1988. Continuous internalization of tumor necrosis factor receptors in a human myosarcoma cell line. J Biol Chem **263:**10262-10266.

99. **Yoshie O, Tada K, Ishida N.** 1986. Binding and crosslinking of ^{125}I-labeled recombinant human tumor necrosis factor to cell surface receptors. J Biochem **100:**531-541.

100. **Wang Y, Oram JF.** 2002. Unsaturated fatty acids inhibit cholesterol efflux from macrophages by increasing degradation of ATP-binding cassette transporter A1. J Biol Chem **277:**5692-5697.

101. **Arakawa R, Yokoyama S.** 2002. Helical apolipoproteins stabilize ATP-binding cassette transporter A1 by protecting it from thiol protease-mediated degradation. J Biol Chem **277:**22426-22429.

102. **Wang N, Chen W, Linsel-Nitschke P, Martinez LO, Agerholm-Larsen B, Silver DL, Tall AR.** 2003. A PEST sequence in ABCA1 regulates degradation by calpain protease and stabilization of ABCA1 by apoA-I. J Clin Invest **111:**99-107.

103. **Ploegh HL, Orr HT, Stominger JL.** 1981. Biosynthesis and cell surface localization of nonglycosylated human histocompatibility antigens. J Immunol **126:**270-275.

104. **Mizrahi A, O'Malley JA, Carter WA, Takatsuki A, Tamura G, Sulkowski E.** 1978. Glycosylation of interferons. Effects of tunicamycin on human immune interferon. J Biol Chem **253:**7612-7615.

105. **Fujisawa J, Iwakura Y, Kawade Y.** 1978. Nonglycosylated mouse L cell interferon produced by the action of tunicamycin. J Biol Chem **253:**8677-8679.

Figure Legends

Figure 1. Schematic of trafficking of newly synthesized insulin receptors from the ER to the plasma membrane. In the insulin proreceptor the α and β chains are joined via a peptide bond. The α chain harbors the extracellular, insulin-binding domain, while the β chain harbors the transmembrane (TM) and cytosolic tyrosine

(TYR) protein kinase domain. The α chain carries 14 and the β chain four *N*-linked oligosaccharides (indicated by lines). In the ER the insulin-binding domain matures, disulfide bonds are formed and insulin proreceptor dimers are formed before transport to the *trans*-Golgi network (TGN). In the TGN the proreceptor is cleaved by proprotein convertases including furin to liberate the mature α and β chains carboxyterminal to the basic amino acid sequence RKRR.

Figure 2. Insulin resistance develops over time in ER-stressed Hep G2 cells. (**A**) Serum-starved Hep G2 cells were treated with the indicated concentrations of thapsigargin, tunicamycin or 1 μg/ml SubAB or catalytically-inactive $SubA_{A272}B$ for 12-36 h before stimulation with 100 nM insulin for 15 min. Cell lysates were analyzed by Western blotting. (**B-D**) Quantitation of the results shown in panel (A).

Figure 3. Depletion of insulin receptors in ER-stressed cells coincides with development of insulin resistance in 3T3-F442A cells. (**A**) Serum-starved 3T3-F442A cells were treated with the indicated concentrations of tunicamycin for 1-18 h before stimulation with 100 nM insulin for 15 min. The pT308-AKT signal obtained by Western blotting was standardized to the total AKT signal to obtain the rel. pT308-Akt values. **(B)** 3T3-F442A cells were treated with the indicated concentrations of tunicamycin for 1-18 h before serum starvation and stimulation with 100 nM insulin for 15 min. Protein extracts were analyzed by Western blotting. **(C)** Quantitation of INSR β-chains. Bars represent standard errors.

Figure 4. Depletion of insulin receptors in ER-stressed cells coincides with development of insulin resistance in Hep G2 cells. (A) Hep G2 cells were treated with the indicated ER stressors for 12-36 h before serum starvation and stimulation with 100 nM insulin for 15 min. Protein extracts were analyzed by Western blotting.

977 Quantitation of insulin receptor (INSR) β-chains in **(B)** thapsigargin-, **(C)**
978 tunicamycin-, and **(D)** SubAB-treated Hep G2 cells.

979 **Figure 5. ER stress does not inhibit insulin receptor synthesis at the**
980 **transcriptional or translational level. (A)** *INSR* mRNA levels measured by RT-
981 qPCR in C_2C_{12} cells treated with 300 nM thapsigargin, 1 μg/ml tunicamycin, or 1
982 μg/ml SubAB for 24 h. Protein synthesis rates in C_2C_{12} cells (**B-D**), 3T3 F442A
983 adipocytes (**F-H**), and Hep G2 cells (**I-K**) treated with 0.1 μM thapsigargin or 0.1
984 μg/ml tunicamycin for 24 h measured by incorporation of [^{35}S]-methionine into newly
985 synthesized proteins. (B, F, I) Trichloroacetic acid (TCA)-precipitable [^{35}S] counts
986 standardized to total protein. (C, G, J) SDS-PAGE analysis of 10 μg [^{35}S]-labeled
987 protein. The autoradiogram is shown to the left, Coomassie Brilliant Blue R250
988 staining of the gel to the right. (D, H, K) Quantitation of the gels shown in panels (C,
989 G , J). **(E)** Immunoprecipitation of the insulin receptor after a 15 min pulse with [^{35}S]-
990 methionine. The bands shown represent the α-β proreceptor, the thapsigargin
991 concentration was 0.1 μM.

992 **Figure 6. α-β Proreceptors accumulate in the ER of ER-stressed cells. (A)** Steady-
993 state INSR levels in untreated C_2C_{12} cells or C_2C_{12} cells treated for 24 h with the
994 indicated concentrations of thapsigargin, tunicamycin, 1 μg/ml SubAB, or 1 μg/ml
995 $SubA_{A272}B$ and serum-starved during the last 18 h of drug treatment before
996 stimulation with 100 nM insulin for 15 min. Cell lysates were analyzed by Western
997 blotting. **(B)** Quantitation of the results of insulin-stimulated cells from panel A. **(C)**
998 Cell lysates from panel (A) digested with Endo H. **(D)** Quantitation of the results of
999 insulin-stimulated cells from panel C. **(E)** The mature insulin receptor β chain carries
1000 an Endo H-sensitive *N*-linked oligosaccharide. Endo H and PNGase F digests of

unstressed C_2C_{12} cells were Western blotted for the insulin receptor β chain. **(F)** Steady-state INSR levels in untreated HEK 293 cells or HEK 293 cells treated for 18 h with 0.1 μg/ml tunicamycin, 1 μg/ml SubAB, or 1 μg/ml $SubA_{A272}B$. **(G)** Localization of GFP-tagged INSR in transiently transfected HEK293 cells. HEK 293 were treated for 18 h with 1 μg/ml tunicamycin or 1 μg/ml SubAB were indicated. The scale bar is 10 μm long. **(H)** Average Pearson correlation coefficient r_{obs} between the INSR-GFP and CellMask Deep Red fluorescence determined from 11 randomly chosen cells. The Pearson correlation coefficients for the randomized images are -0.13 ± 0.08, -0.13 ± 0.07, and -0.33 ± 0.07 for the untreated, tunicamycin-, and SubAB-treated cells, respectively.

Figure 7. Bypass of the ER in insulin receptor synthesis abrogates ER stress-induced insulin resistance. (A) siRNA-mediated knock-down of expression of the insulin receptor inhibits insulin-stimulated phosphorylation of AKT. Serum-starved C_2C_{12} cells were stimulated with 100 nM insulin for 15 min 48 h after transfection of 50 nM of the indicated siRNAs. **(B)** Steady-state INSR mRNA levels in C_2C_{12} cells transfected with 50 nM of the indicated siRNAs for 24, 48, or 72 h. **(C)** Schematic of the myristoylated F_V2E-insulin receptor chimera. **(D)** Expression of the F_V2E-insulin receptor chimera was induced in Flp-In T-Rex 293 cells stably transfected with pcDNA5/FRT/TO-MyrF_V2E-INSR for 27 h with 1 mg/ml tetracycline, followed by dimerization with 100 nM AP20187 for the indicated times. **(E)** HEK293 Flip-In T-Rex cells stably transfected with pcDNA5/FRT/TO-MyrF_V2E-INSR were serum-starved during the last 18 h of a 24 h treatment with 10 mg/ml tunicamycin (Tm) or 1 mg/ml SubAB (Sb). Then, expression of the F_V2E-insulin receptor chimera was induced with 1 mg/ml tetracycline for 24 h, followed by dimerization of the construct with 100 nM AP20187 for 4 h . Western blots of total cell lysates are shown. The

arrow indicates the β chain of the mature, endogenous insulin receptor. **(F)** C_2C_{12} cells were transiently transfected with pmaxGFP or pcDNA5/FRT/TO-MyrF_V2E-INSR. 24 h after transfection ER stress was induced for 24 h with 0.1 μM thapsigargin (Tg), 0.1 μg/ml tunicamycin, or 1 μg/ml SubAB followed by dimerization of the receptor with 100 nM AP20187 for 4 h and preparation of cell lysates for Western blotting. **(G)** Quantitation of the results shown in panel (F).

Figure 8. *jnk1*$^{-/-}$ *jnk2*$^{-/-}$ MEFs are not protected from developing insulin resistance when exposed to chronic ER stress. (A) WT and *jnk1*$^{-/-}$ *jnk2*$^{-/-}$ MEFs were treated for 24 h with the indicated concentrations of thapsigargin or tunicamycin, 1 μg/ml SubAB, or 1 μg/ml SubA_{A272}B and serum-starved during the last 18 h of drug treatment before stimulation with 100 nM insulin for 15 min. **(B-D)** Quantitation of AKT S473 phosphorylation relative to total AKT levels in WT and *jnk1*$^{-/-}$ *jnk2*$^{-/-}$ MEFs exposed to (B) thapsigargin, (C) tunicamycin, and (D) SubAB. **(E)** Activation of JNK in WT MEFs exposed to the indicated concentrations of thapsigargin or tunicamycin, 1 μg/ml SubAB, or 1 μg/ml SubA_{A272}B and serum-starved during the last 18 h of drug treatment before stimulation with 100 nM insulin for 15 min. **(F)** Quantitation of the Western blots in panel (E). **(G)** *TRB3* mRNA levels measured by RT-qPCR in C_2C_{12} cells treated with 300 nM thapsigargin, 1 μg/ml tunicamycin, or 1 μg/ml SubAB for 24 h.

Figure 9. Depletion of IGF-I receptors by ER stress. (A) Hep G2 cells were treated for the indicated times with the indicated concentrations of thapsigargin or tunicamycin, 1 μg/ml SubAB, or 1 μg/ml SubA_{A272}B and serum-starved during the last 18 h of drug treatment before stimulation with 100 nM insulin for 15 min. Cell lysates were analyzed by Western blotting. The GAPDH loading control is the same

as the one shown in Figure 2A. **(B-E)** Quantitation of the Western blots shown in panel (A). **(F-I)** Depletion of IGF-I receptors by ER stress induced in C_2C_{12} cells with (F) thapsigargin, (G) tunicamycin, and (H) SubAB. (I) Accumulation of α-β IGF-I proreceptors in C_2C_{12} cells.

Figure 10. ER stress causes insulin resistance by interfering with exit of newly synthesized insulin proreceptors from the ER. The signal peptide sequence targets ribosomes translating the insulin receptor mRNA to the ER, where the newly synthesized polypeptide chain folds into molecules with insulin binding activity. ER stress interferes with folding of newly synthesized insulin receptor molecules, preventing its transport to the Golgi complex. The Myr-F_V2E-insulin receptor chimera is not affected by ER stress because it is translated by cytoplasmic ribosomes and folds in the cytosol into active molecules thus bypassing the ER.

1063 **Tables**

1064 **Table I. siRNAs.**

Species	Gene	#	Sequence, sense strand	Sequence, antisense strand
Mus musculus	*INSR*	1	GAGAUCUCCUGGGAUUCAUdTdT	AUGAAUCCCAGGAGAUCUCdTdT
M. musculus	*INSR*	2	CCUUAUCAAGGCCUGUCUAdTdT	UAGACAGGCCUUGAUAAGGdTdT
M. musculus	*INSR*	3	GAAACUCUGCUUGUCUGAAdTdT	UUCAGACAAGCAGAGUUUCdTdT
Aequora victora	eGFP		GCAAGCUGACCCUGAAGUUCAU	GAACUUCAGGGUCAGCUUGCCG

1065

1066

1067 **Table II. Oligodeoxynucleotides.**

Name	Purpose	Sequence
Oligodeoxynucleotides for *M. musculus* genes		
H7994	*ACTB* real time PCR, forward	AGCCATGTACGTAGCCATCC
H7995	*ACTB* real time PCR, reverse	CTCTCAGCTGTGGTGGTGAA
H8962	*TRB3* real time PCR, forward	TTTGGAACGAGAGCAAGGCA
H8963	*TRB3* real time PCR, reverse	CCACATGCTGGTGGGTAGG
H9044	*INSR* real time PCR, forward	CTTCTCTTCCGTGTCTATGG
H0945	*INSR* real time PCR, reverse	GACCATCTCGAAGATAACCA

1068

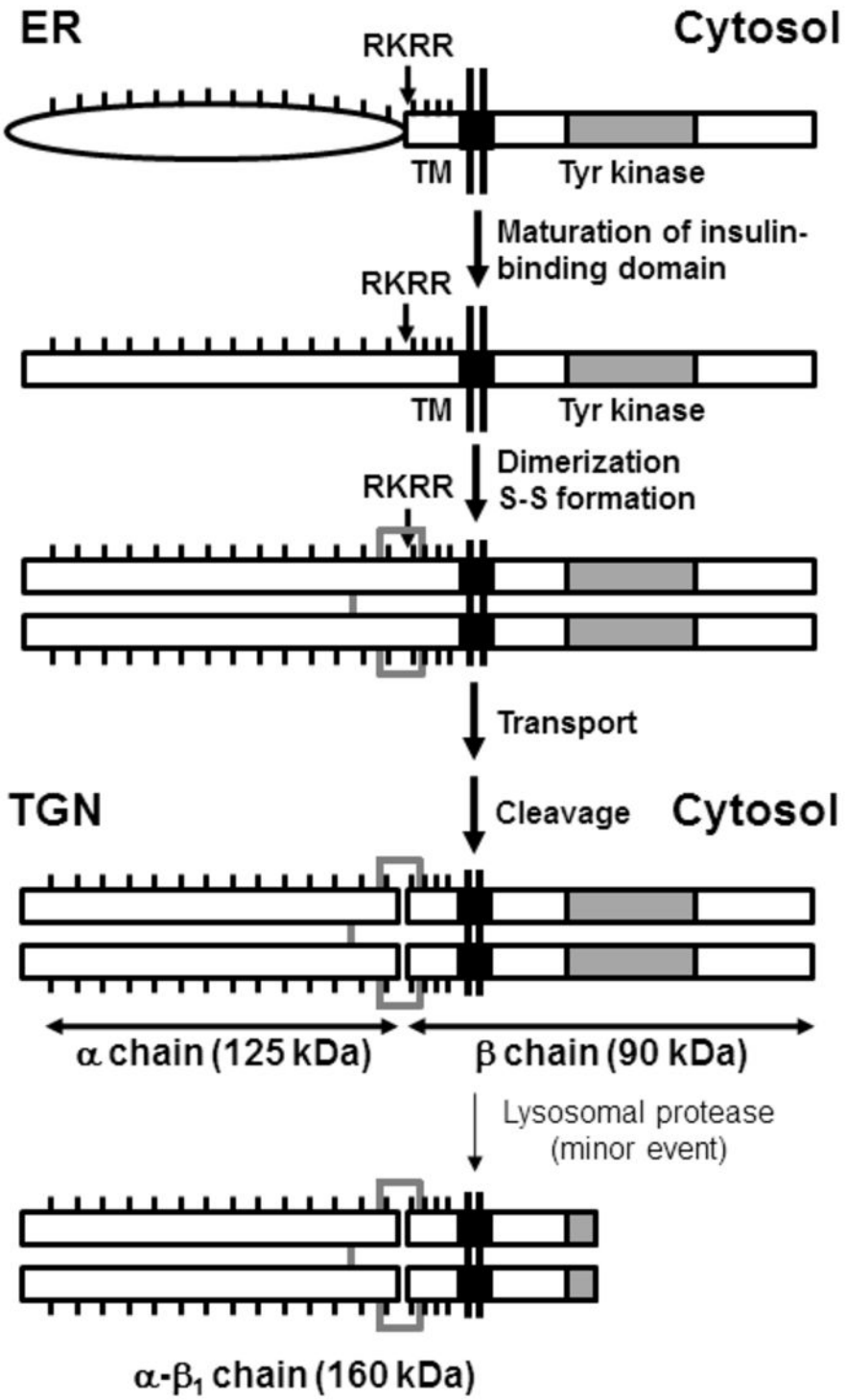

Fig. 1. Schematic of trafficking of newly synthesized insulin receptors from the ER to the plasma membrane. In the insulin proreceptor the α and β chains are joined via a peptide bond. The α chain harbors the extracellular, insulin-binding domain, while the β chain harbors the transmembrane (TM) and cytosolic tyrosine (TYR) protein kinase domain. The α chain carries 14 and the β chain four *N*-linked oligosaccharides (indicated by lines). In the ER the insulin-binding domain matures, disulfide bonds are formed and insulin proreceptor dimers are formed before transport to the *trans*-Golgi network (TGN). In the TGN the proreceptor is cleaved by proprotein convertases including furin to liberate the mature α and β chains carboxyterminal to the basic amino acid sequence RKRR.

Figure 1, Brown *et al.*

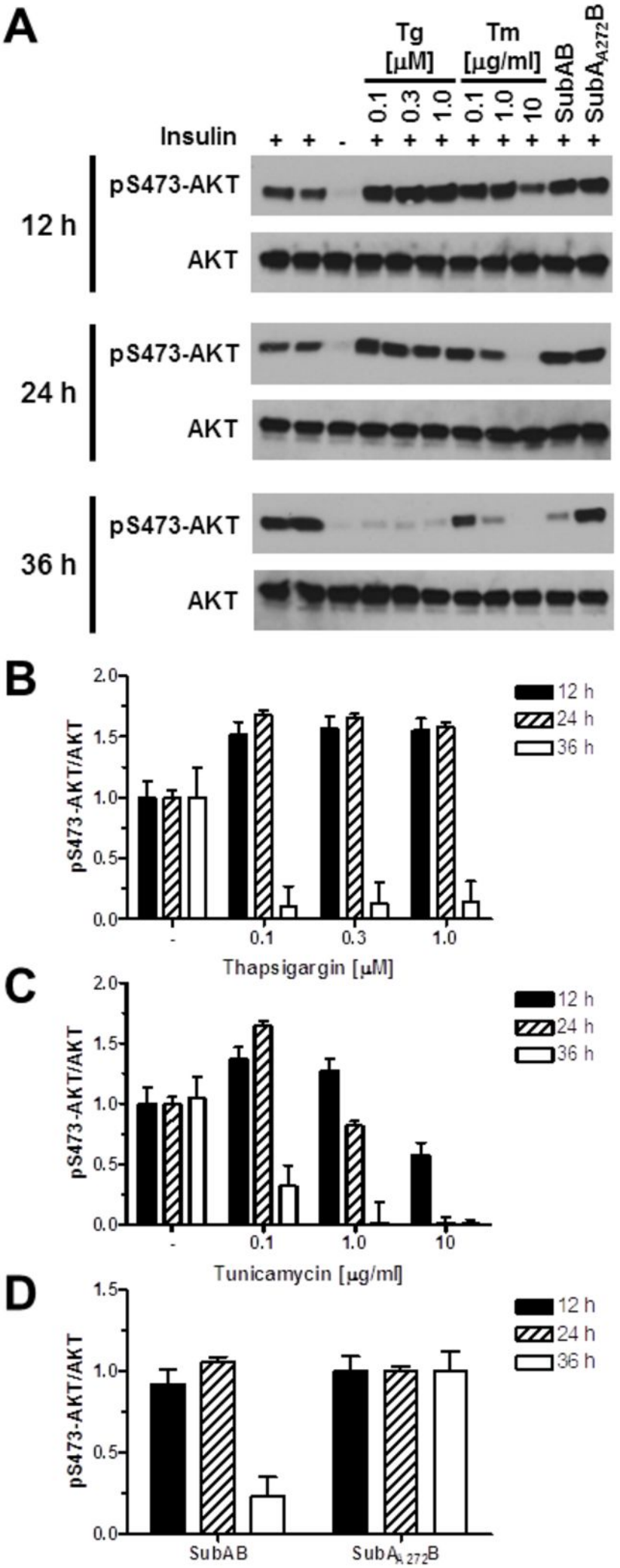

Fig. 2. Insulin resistance develops over time in ER-stressed Hep G2 cells. (**A**) Serum-starved Hep G2 cells were treated with the indicated concentrations of thapsigargin, tunicamycin or 1 μg/ml SubAB or catalytically-inactive $SubA_{A272}B$ for 12-36 h before stimulation with 100 nM insulin for 15 min. Cell lysates were analyzed by Western blotting. (**B**-D) Quantitation of the results shown in panel (A).

Figure 2, Brown *et al.*

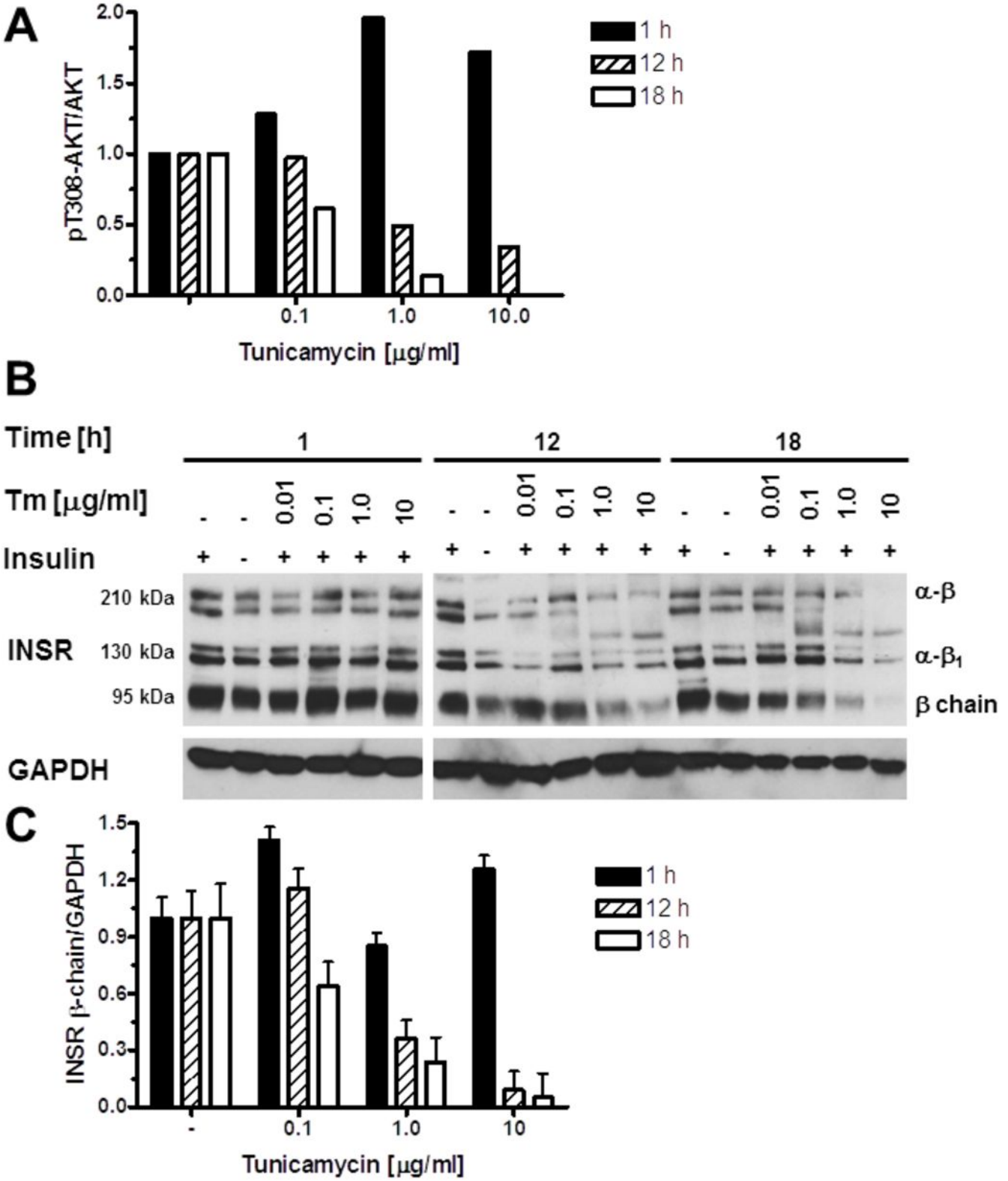

Fig. 3. Depletion of insulin receptors in ER-stressed cells coincides with development of insulin resistance in 3T3-F442A cells. (**A**) Serum-starved 3T3-F442A cells were treated with the indicated concentrations of tunicamycin for 1-18 h before stimulation with 100 nM insulin for 15 min. The pT308-AKT signal obtained by Western blotting was standardized to the total AKT signal to obtain the rel. pT308-Akt values. (**B**) 3T3-F442A cells were treated with the indicated concentrations of tunicamycin for 1-18 h before serum starvation and stimulation with 100 nM insulin for 15 min. Protein extracts were analyzed by Western blotting. (**C**) Quantitation of INSR β-chains. Bars represent standard errors.

Figure 3, Brown *et al.*

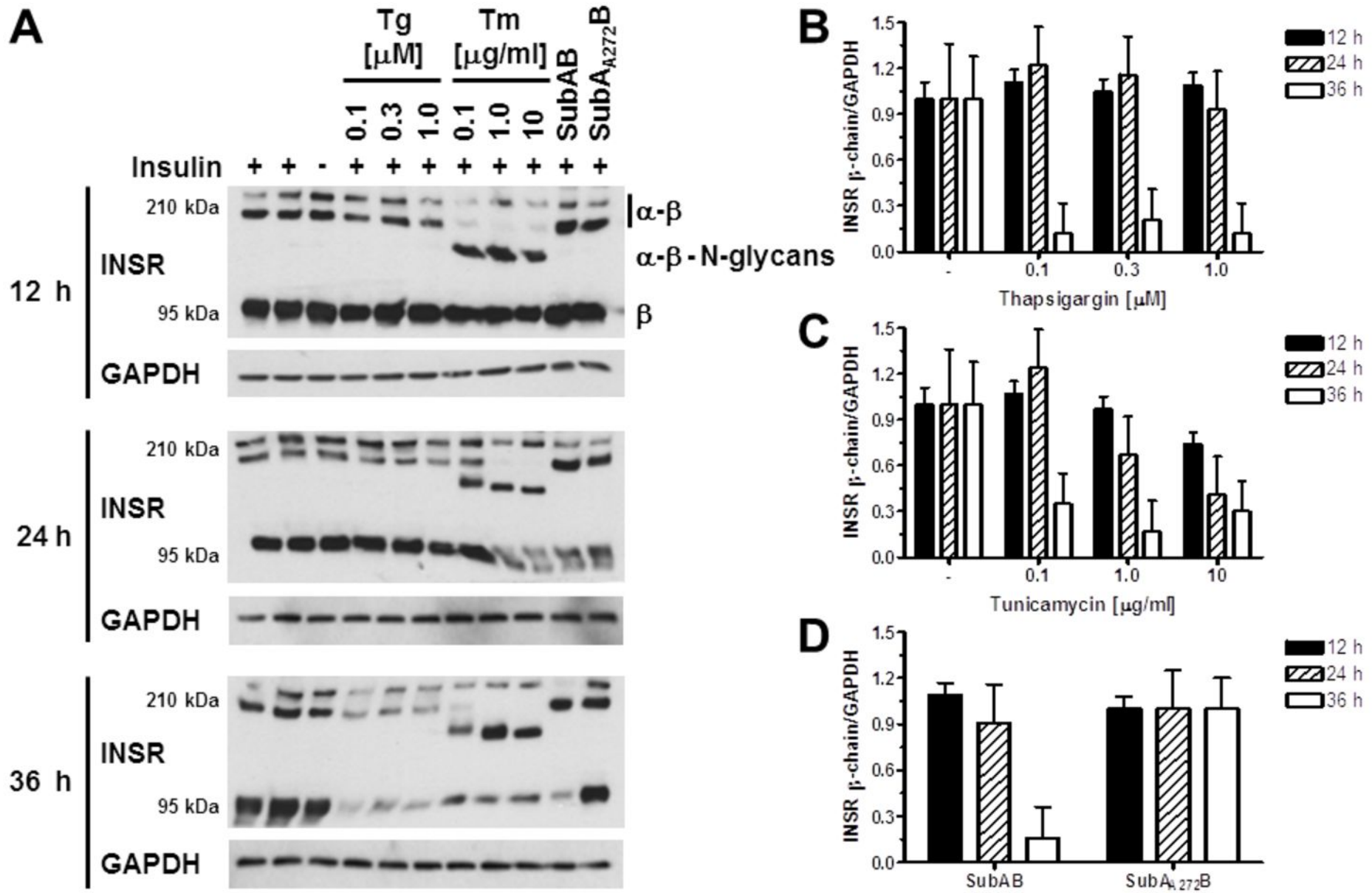

Fig. 4 Depletion of insulin receptors in ER-stressed cells coincides with development of insulin resistance in Hep G2 cells. **(A)** Hep G2 cells were treated with the indicated ER stressors for 12-36 h times before serum starvation and stimulation with 100 nM insulin for 15 min. Protein extracts were analyzed by Western blotting. Quantitation of INSR β-chains in **(B)** thapsigargin-, **(C)** tunicamycin-, and **(D)** SubAB-treated Hep G2 cells.

Figure 4, Brown *et al.*

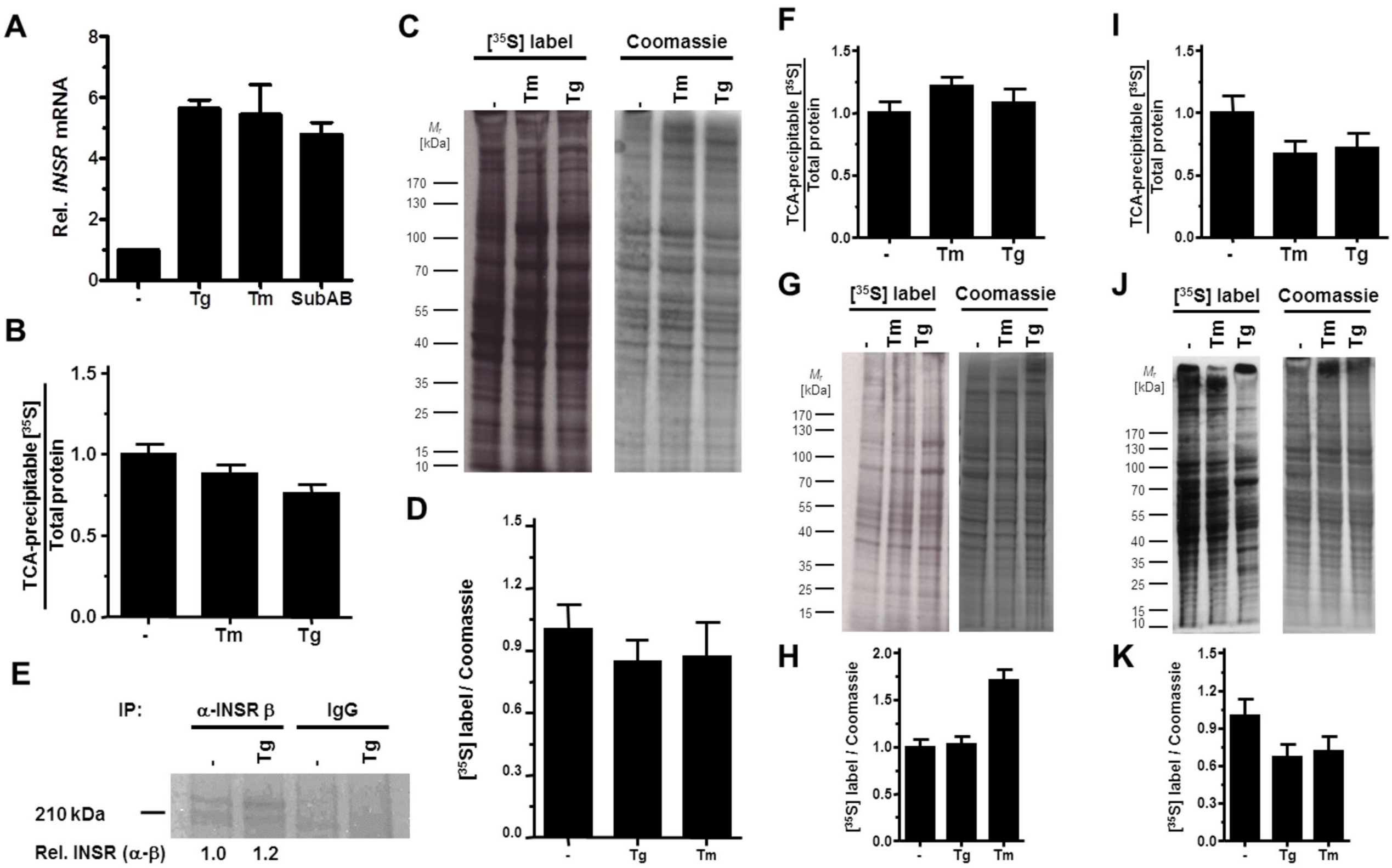

Fig. 5. ER stress does not inhibit insulin receptor synthesis at the transcriptional or translational level. (A) *INSR* mRNA levels measured by RT-qPCR in C_2C_{12} cells treated with 300 nM thapsigargin, 1 μg/ml tunicamycin, or 1 μg/ml SubAB for 24 h. **(B-D)** Protein synthesis rates in C_2C_{12} cells treated with 0.1 μM thapsigargin or 0.1 μg/ml tunicamycin for 24 h measured by incorporation of [^{35}S]-methionine into newly synthesized proteins. (B) Trichloroacetic acid (TCA)-precipitable [^{35}S] counts standardized to total protein . (C) SDS-PAGE analysis of 10 μg [^{35}S]-labeled protein. The autoradiogram is shown to the left, Coomassie Brilliant Blue R250 staining of the gel to the right. (D) Quantitation of the gels shown in panel (C). **(E)** Immunoprecipitation of the INSR after a 15 min pulse with [^{35}S]-methionine. The bands shown represent the α-β proreceptor. Protein synthesis rates in 3T3 F442A adipocytes **(F-H)** and in Hep G2 cells **(I-K)** treated with 0.1 μM thapsigargin or 0.1 μg/ml tunicamycin for 24 h measured by incorporation of [^{35}S]-methionine into newly synthesized proteins. (F, I) Trichloroacetic acid (TCA)-precipitable [^{35}S] counts standardized to total protein . (G, J) SDS-PAGE analysis of 10 μg [^{35}S]-labeled protein. The autoradiogram is shown to the left, Coomassie Brilliant Blue R250 staining of the gel to the right. (H. K) Quantitation of the SDS-PAGE gels in panels (G) and (J).

Figure 5, Brown *et al.*

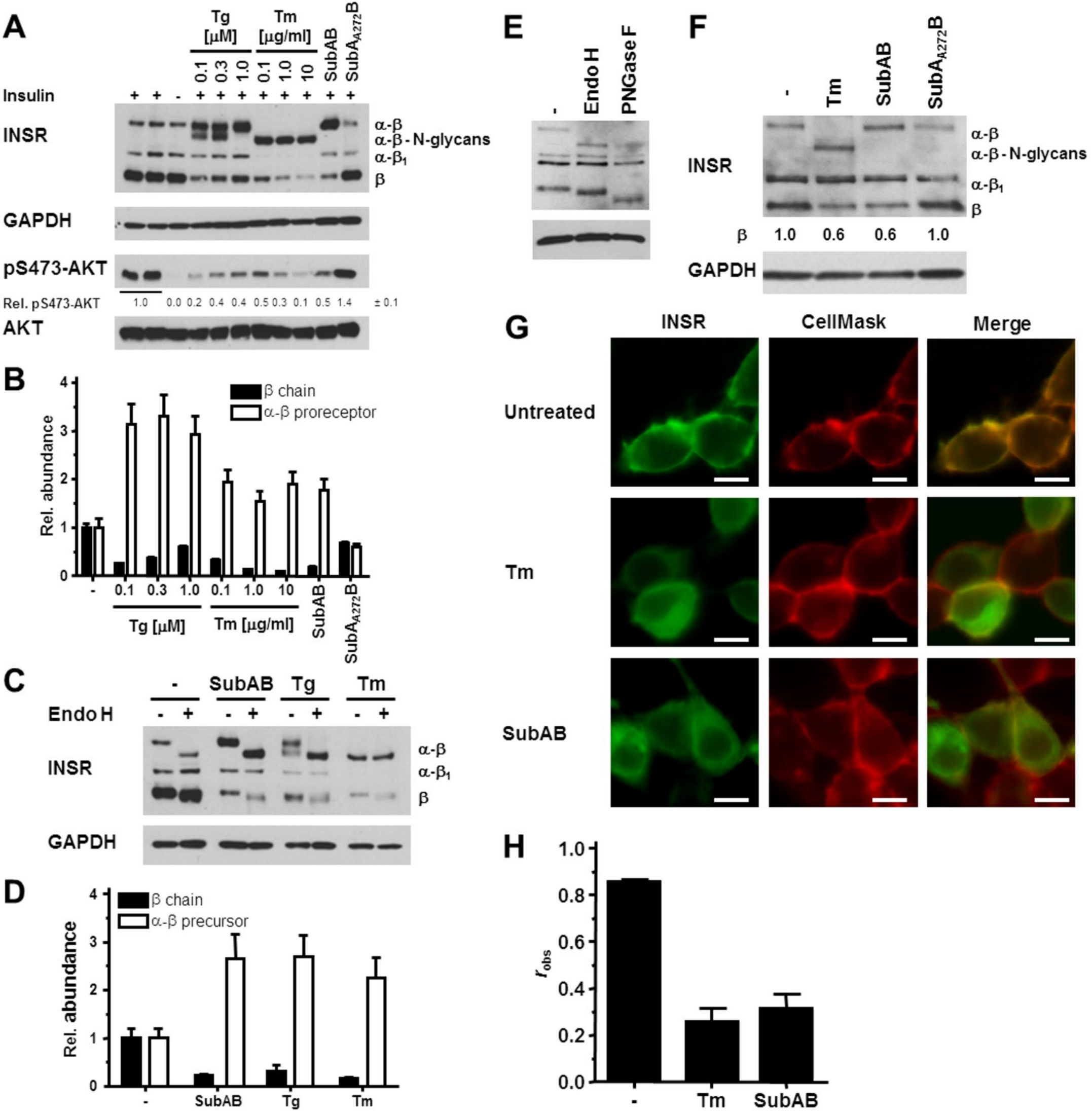

Fig. 6. α-β Proreceptors accumulate in the ER of ER-stressed cells. (A) Steady-state INSR levels in untreated C_2C_{12} cells or C_2C_{12} cells treated for 24 h with the indicated concentrations of thapsigargin, tunicamycin, 1 μg/ml SubAB, or 1 μg/ml SubA$_{A272}$B and serum-starved during the last 18 h of drug treatment before stimulation with 100 nM insulin for 15 min. Cell lysates were analyzed by Western blotting. **(B)** Quantitation of the results of insulin-stimulated cells from panel A. **(C)** Cell lysates from panel (A) digested with Endo H. **(D)** Quantitation of the results of insulin-stimulated cells from panel C. **(E)** The mature insulin receptor β chain carries an Endo H-sensitive *N*-linked oligosaccharide. Endo H and PNGase F digests of unstressed C_2C_{12} cells were Western blotted for the insulin receptor β chain. **(F)** Steady-state INSR levels in untreated HEK 293 cells or HEK 293 cells treated for 18 h with 0.1 μg/ml tunicamycin, 1 μg/ml SubAB, or 1 μg/ml SubA$_{A272}$B. **(G)** Localization of GFP-tagged INSR in transiently transfected HEK 293 cells. HEK 293 were treated for 18 h with 1 μg/ml tunicamycin or 1 μg/ml SubAB were indicated. The scale bar is 10 μm long. **(H)** Average Pearson correlation coefficient r_{obs} between the INSR-GFP and CellMask Deep Red fluorescence determined from 11 randomly chosen cells. The Pearson correlation coefficients for the randomized images are -0.13 ± 0.08, -0.13 ± 0.07, and -0.33 ± 0.07 for the untreated, tunicamycin-, and SubAB-treated cells, respectively.

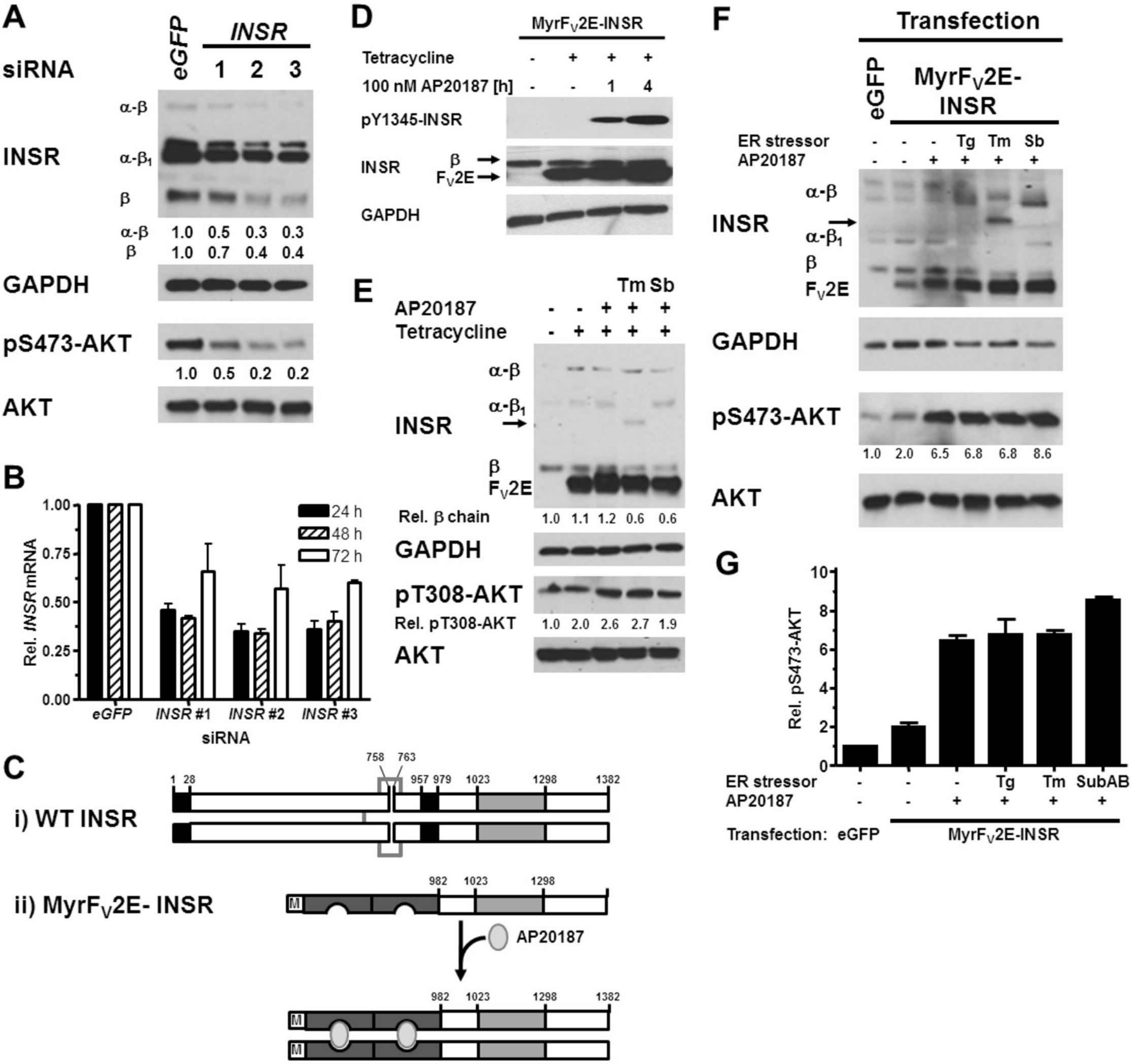

Fig. 7. Bypass of the ER in insulin receptor synthesis abrogates ER stress-induced insulin resistance. (A) siRNA-mediated knock-down of expression of the insulin receptor inhibits insulin-stimulated phosphorylation of AKT. Serum-starved C_2C_{12} cells were stimulated with 100 nM insulin for 15 min 48 h after transfection of 50 nM of the indicated siRNAs. **(B)** Steady-state INSR mRNA levels in C_2C_{12} cells transfected with 50 nM of the indicated siRNAs for 24, 48, or 72 h. qPCR data from three repeats were standardized to *ACTB*. **(C)** Schematic of the myristoylated F_V2E-insulin receptor chimera. **(D)** Expression of the F_V2E-insulin receptor chimera was induced in Flp-In T-Rex 293 cells stably transfected with pcDNA5/FRT/TO-MyrF_V2E-INSR for 27 h with 1 μg/ml tetracycline, followed by dimerization with 100 nM AP20187 for the indicated times. **(E)** HEK293 Flip-In T-Rex cells stably transfected with pcDNA5/FRT/TO-MyrF_V2E-INSR were serum-starved during the last 18 h of a 24 h treatment with 10 μg/ml tunicamycin (Tm) or 1 μg/ml SubAB (Sb). Then, expression of the F_V2E-insulin receptor chimera was induced with 1 μg/ml tetracycline for 24 h, followed by dimerization of the construct with 100 nM AP20187 for 4 h. Western blots of total cell lysates are shown. The arrow indicates the β chain of the mature, endogenous insulin receptor. **(F)** C_2C_{12} cells were transiently transfected with pmaxGFP or pcDNA5/FRT/TO-MyrF_V2E-INSR. 24 h after transfection ER stress was induced for 24 h with 0.1 μM thapsigargin (Tg), 0.1 μg/ml tunicamycin, or 1 μg/ml SubAB followed by dimerization of the receptor with 100 nM AP20187 for 4 h and preparation of cell lysates for Western blotting. **(G)** Quantitation of the results shown in panel (F).

Figure 7, Brown *et al.*

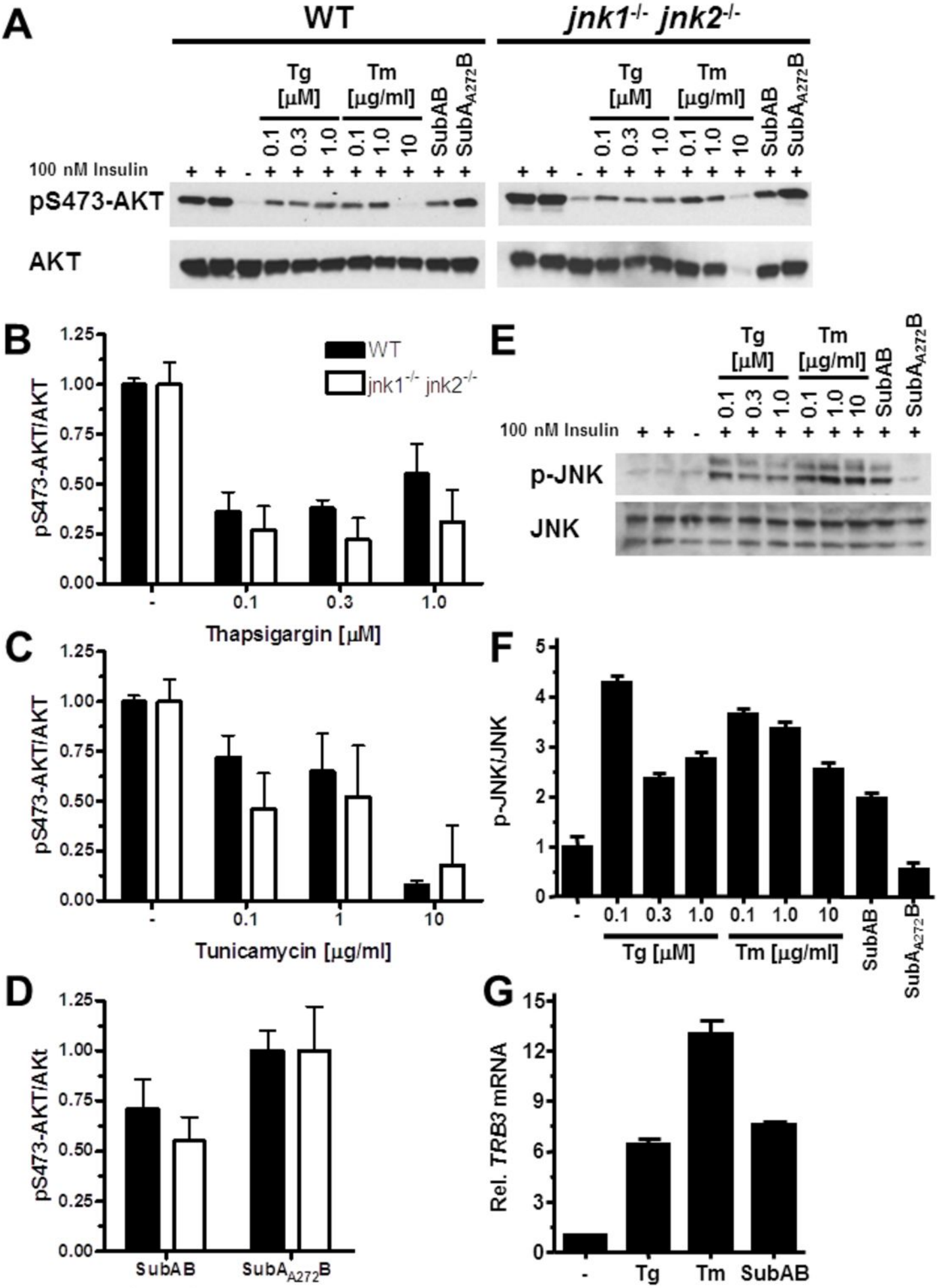

Fig. 8. ***jnk1*$^{-/-}$** ***jnk2*$^{-/-}$** **MEFs are not protected from developing insulin resistance when exposed to chronic ER stress.** **(A)** WT and *jnk1*$^{-/-}$ *jnk2*$^{-/-}$ MEFs were treated for 24 h with the indicated concentrations of thapsigargin or tunicamycin, 1 μg/ml SubAB, or 1 μg/ml $SubA_{A272}B$ and serum-starved during the last 18 h of drug treatment before stimulation with 100 nM insulin for 15 min. **(B-D)** Quantitation of AKT S473 phosphorylation relative to total AKT levels in WT and *jnk1*$^{-/-}$ *jnk2*$^{-/-}$ MEFs exposed to (B) thapsigargin, (C) tunicamycin, and (D) SubAB. **(E)** Activation of JNK in WT MEFs exposed to the indicated concentrations of thapsigargin or tunicamycin, 1 μg/ml SubAB, or 1 μg/ml $SubA_{A272}B$ and serum-starved during the last 18 h of drug treatment before stimulation with 100 nM insulin for 15 min. **(F)** Quantitation of the Western blots in panel (E). **(G)** *TRB3* mRNA levels measured by RT-qPCR in C_2C_{12} cells treated with 300 nM thapsigargin, 1 μg/ml tunicamycin, or 1 μg/ml SubAB for 24 h.

Figure 8, Brown *et al.*

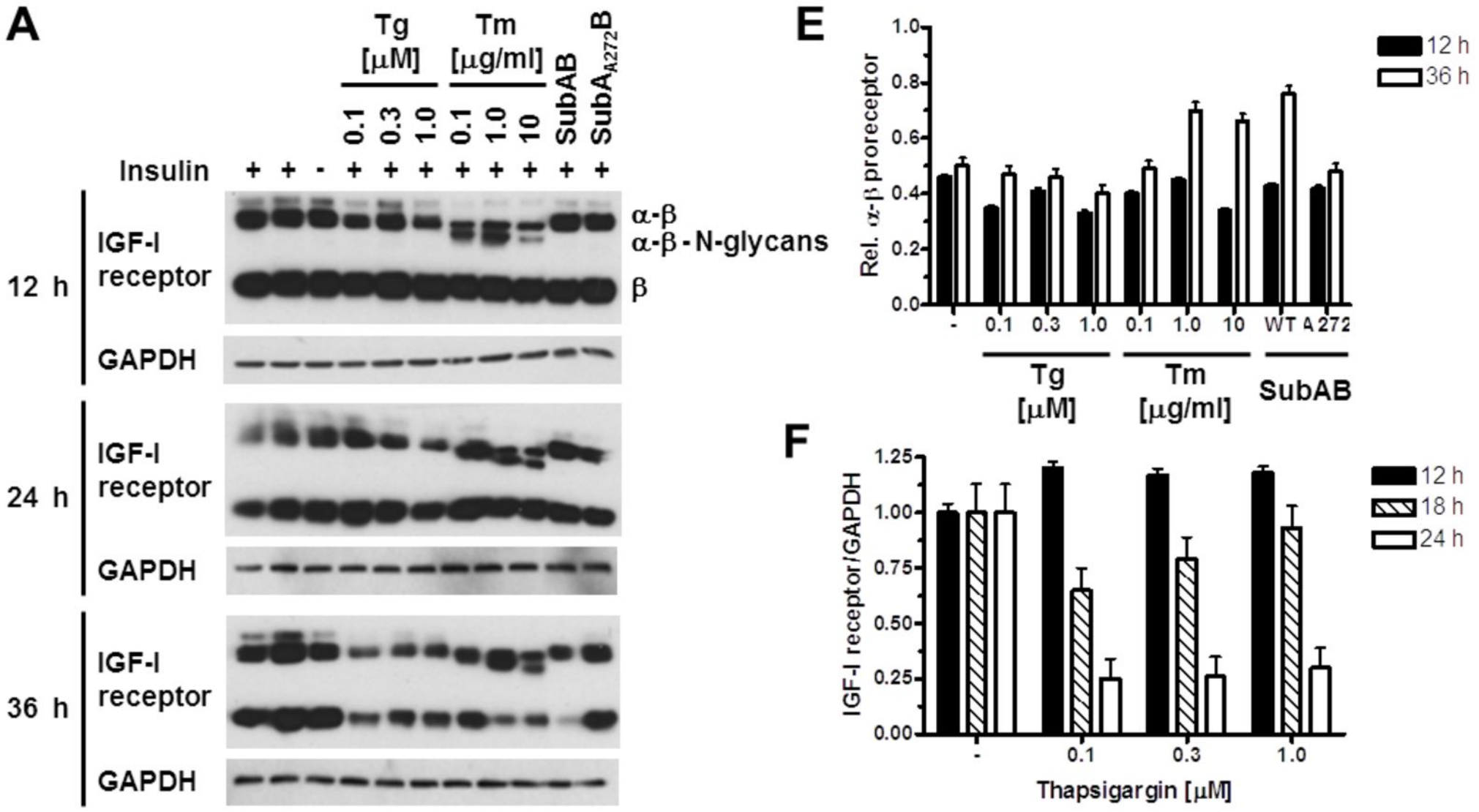

Fig. 9. Depletion of IGF-I receptors by ER stress. (A) Hep G2 cells were treated for the indicated times with the indicated concentrations of thapsigargin or tunicamycin, 1 μg/ml SubAB, or 1 μg/ml SubA$_{A272}$B and serum-starved during the last 18 h of drug treatment before stimulation with 100 nM insulin for 15 min. Cell lysates were analyzed by Western blotting. The GAPDH loading control is the same as the one shown in Figure 4. **(B-E)** Quantitation of the Western blots shown in panel (A). **(F-I)** Depletion of IGF-I receptors by ER stress induced in C_2C_{12} cells with (F) thapsigargin, (G) tunicamycin, and (H) SubAB. (I) Accumulation of α-β IGF-I proreceptors in C_2C_{12} cells.

Figure 9, Brown *et al.*

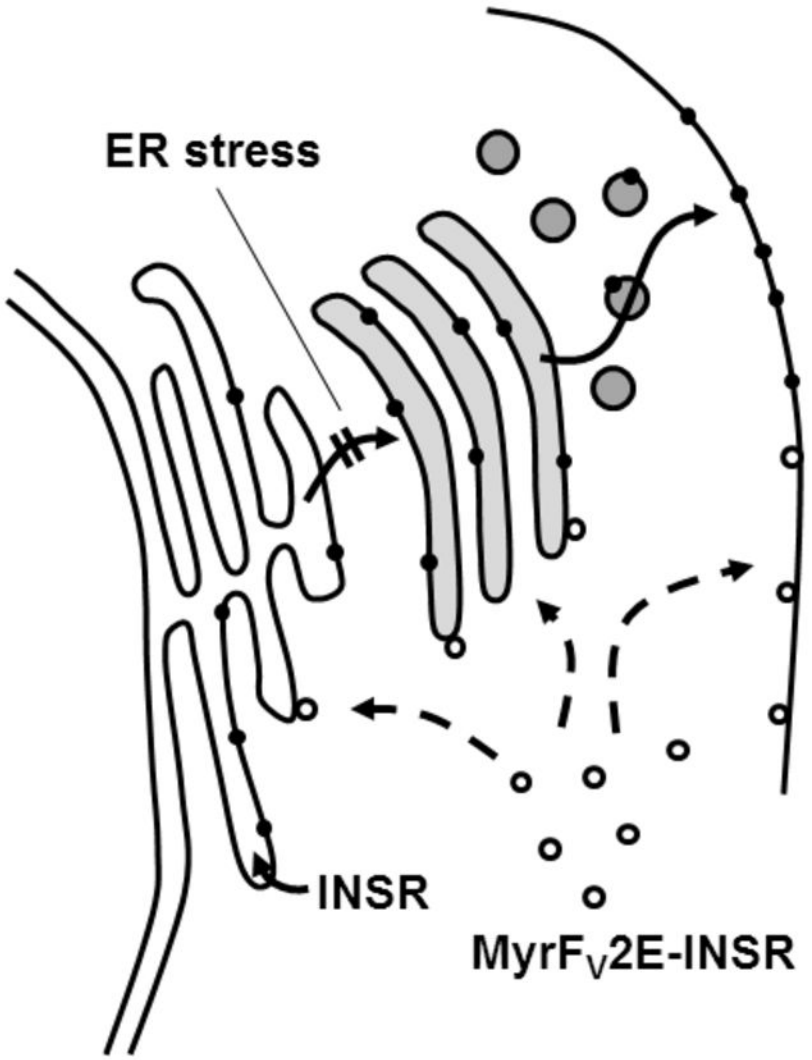

Fig. 10. ER stress causes insulin resistance by interfering with exit of newly synthesized insulin proreceptors from the ER. The signal peptide sequence targets ribosomes translating the insulin receptor mRNA to the ER, where the newly synthesized polypeptide chain folds into molecules with insulin binding activity. ER stress interferes with folding of newly synthesized insulin receptor molecules, preventing its transport to the Golgi complex. The Myr-F$_V$2R-insulin receptor chimera is not effected by ER stress because it is translated by cytoplasmic ribosomes and folds in the cytosol into active molecules thus bypassing the ER.